ADVANCES IN PLANT MEIOSIS: FROM MODEL SPECIES TO CROPS

EDITED BY: Tomás Naranjo, Changbin Chen, Zhukuan Cheng and Mónica Pradillo

PUBLISHED IN: Frontiers in Plant Science

frontiers Research Topics

ISSN 1664-8714
ISBN 978-2-88963-428-6
DOI 10.3389/978-2-88963-428-6

About Frontiers

Frontiers is more than just an open-access publisher of scholarly articles: it is a pioneering approach to the world of academia, radically improving the way scholarly research is managed. The grand vision of Frontiers is a world where all people have an equal opportunity to seek, share and generate knowledge. Frontiers provides immediate and permanent online open access to all its publications, but this alone is not enough to realize our grand goals.

Frontiers Journal Series

The Frontiers Journal Series is a multi-tier and interdisciplinary set of open-access, online journals, promising a paradigm shift from the current review, selection and dissemination processes in academic publishing. All Frontiers journals are driven by researchers for researchers; therefore, they constitute a service to the scholarly community. At the same time, the Frontiers Journal Series operates on a revolutionary invention, the tiered publishing system, initially addressing specific communities of scholars, and gradually climbing up to broader public understanding, thus serving the interests of the lay society, too.

Dedication to Quality

Each Frontiers article is a landmark of the highest quality, thanks to genuinely collaborative interactions between authors and review editors, who include some of the world's best academicians. Research must be certified by peers before entering a stream of knowledge that may eventually reach the public - and shape society; therefore, Frontiers only applies the most rigorous and unbiased reviews.
Frontiers revolutionizes research publishing by freely delivering the most outstanding research, evaluated with no bias from both the academic and social point of view. By applying the most advanced information technologies, Frontiers is catapulting scholarly publishing into a new generation.

What are Frontiers Research Topics?

Frontiers Research Topics are very popular trademarks of the Frontiers Journals Series: they are collections of at least ten articles, all centered on a particular subject. With their unique mix of varied contributions from Original Research to Review Articles, Frontiers Research Topics unify the most influential researchers, the latest key findings and historical advances in a hot research area! Find out more on how to host your own Frontiers Research Topic or contribute to one as an author by contacting the Frontiers Editorial Office: researchtopics@frontiersin.org

ADVANCES IN PLANT MEIOSIS: FROM MODEL SPECIES TO CROPS

Topic Editors:
Tomás Naranjo, Complutense University of Madrid, Spain
Changbin Chen, University of Minnesota Twin Cities, United States
Zhukuan Cheng, University of Chinese Academy of Sciences, China
Mónica Pradillo, Complutense University of Madrid, Spain

Citation: Naranjo, T., Chen, C., Cheng, Z., Pradillo, M., eds. (2020). Advances in Plant Meiosis: From Model Species to Crops. Lausanne: Frontiers Media SA.
doi: 10.3389/978-2-88963-428-6

Table of Contents

frontiers in Plant Science

EDITORIAL
published: 18 December 2019
doi: 10.3389/fpls.2019.01627

Editorial: Advances in Plant Meiosis: From Model Species to Crops

Tomás Naranjo[1]*, *Changbin Chen*[2], *Zhukuan Cheng*[3] and *Mónica Pradillo*[1]

[1] Departamento de Genética, Fisiología y Microbiología, Facultad de Biología, Universidad Complutense de Madrid, Madrid, Spain, [2] Department of Horticultural Science, University of Minnesota, St. Paul, MN, United States, [3] State Key Laboratory of Plant Genomics and Center for Plant Gene Research, Institute of Genetics and Developmental Biology, Chinese Academy of Sciences, Beijing, China

Keywords: chromosome sorting, chromatin organization, telomere dynamics, double-strand breaks, crossovers, homoeologous recombination, *Ph1*

Editorial on the Research Topic

Advances in Plant Meiosis: From Model Species to Crops

Advances in the study of plant meiosis produced in the last three decades were based mainly in the isolation of meiotic mutants and genes in the model species *Arabidopsis thaliana* and in other species such as rice or maize. Chromosome mutants produced in wheat provided also valuable information. Nowadays, many research groups are using translational biology approaches to improve the sustainability of food production in crops based on the manipulation of meiotic recombination. Because many crops are polyploids, complications of the meiotic behavior derived from the polyploid condition are also in the focus of a number of research projects. The purpose of this Research Topic was to provide a platform for the publication of updated information and high-quality research papers, in both model species and crops, which will represent a guide addressing our fundamental knowledge of meiosis as well as its implications for plant breeding. After a large response, which reflects active research being undertaken, we published a total of 21 papers, including 1 Mini-Review, 3 Reviews, 1 Methods, and 16 Original Research. These papers are grouped in the following items: i) new approaches and methods in the study of meiosis; ii) meiotic recombination; iii) meiosis in polyploids; iv) chromosome segregation; and v) other aspects of meiosis.

i) New approaches and methods in the study of meiosis presents one review paper and four technological articles outlining recent advancement of technologies for plant meiosis studies ranging from genomic analysis, single cell sequencing to super-resolution and 3D imaging investigation of chromatin dynamics. All tools available for studying meiosis have been reviewed comprehensively by Lambing and Heckmann, which include super-resolution microscopy and live cell imaging that are extensively used in understanding chromosome dynamics and plant meiosis progression, application of sequencing-based techniques to map crossovers (COs) and their correlation to gene expression landscapes, as well as the proteomic analysis to profile proteins involved in meiosis. Capilla-Perez et al. report a recent development of genetic resources by creating a new homozygous mutant library for researchers to perform functional analysis of meiotic genes. Eight hundred ninety-seven homozygous *Arabidopsis* mutant lines are among this collection, including those targeted 26 previously reported meiotic genes. Dreissig et al. use single pollen nucleus sequencing to study meiotic recombination events and segregation distortion caused by postmeiotic processes. Genome wide distribution of recombination uncovered similarity of recombination landscapes between barley pollen and double haploid plants; but the segregation

OPEN ACCESS

Edited and reviewed by:
Simon Gilroy,
University of Wisconsin-Madison, United States

***Correspondence:**
Tomás Naranjo
toranjo@bio.ucm.es

Specialty section:
This article was submitted to Plant Cell Biology, a section of the journal Frontiers in Plant Science

Received: *09 October 2019*
Accepted: *19 November 2019*
Published: *18 December 2019*

Citation:
Naranjo T, Chen C, Cheng Z and Pradillo M (2019) Editorial: Advances in Plant Meiosis: From Model Species to Crops. Front. Plant Sci. 10:1627. doi: 10.3389/fpls.2019.01627

distortion is high in double haploid population comparing to almost absent in pollen. Sepsi et al. combine immunolabeling, fluorescence *in situ* hybridization, and confocal microscopy to simultaneously detect the nuclear localization of proteins and specific DNA sequences within chromosomes. Construction of 3D images has shown detailed chromosome structures and critical proteins associated with meiosis in rye. Also using rye system, Hesse et al. report a technique combining scanning electronic microscopy and fluorescence microscopy to examine ultrastructure and dynamics of synaptonemal complex (SC) components during meiotic pairing and synapsis. The super high-resolution technique advances the ability of researchers to study chromosome dynamics and configuration during meiosis with great details at the molecular and subcellular levels.

ii) Meiotic recombination is initiated by the formation of DNA double-strand breaks (DSBs). A subset of these DSBs are repaired as COs, reciprocal exchanges of genetic information between homologous chromosomes, allowing the formation of genetically unique gametes. COs are non-randomly distributed along chromosomes, there are regions that recombine more than average (hotspots), while other regions are completely devoid of COs. Okagaki et al. compile historically accumulated evidence to explain that in maize, unlike the situation in other model systems, many recombination hotspots are located within genes. In some of these genes there is a gradient of recombination (polarity) with higher CO rates at the ends (5′ or 3′). As well as in *Arabidopsis*, in maize, the fraction of DSB hotspots resolving as COs is small (less than 4%). The message from this detailed review is that the recombination process of a species does not necessarily fit to those of the model species described. In addition, it is necessary to compile data derived from different methodological approaches in order to have a global view of how the meiotic recombination process takes place. Meiotic recombination is a process highly regulated by specific genes. Among these genes are those involved in processing DSBs. The work by Wang et al. describes the consequences arising from the absence of ZmCOM1 during maize meiosis. They demonstrate that this protein is indispensable to ensure the bouquet formation and the assembly of the SC. In addition, maize plants deficient for this protein display problems during mitosis. According to their observations, the function of COM1 is conserved in plant meiosis. However, during the cell cycle, its function seems to be more important in maize than in plants with smaller genomes. Hu et al. analyze the role of the replication factor C–like protein OsRAD17. This protein, together with the 9-1-1 complex, is essential for DSB repair during rice meiosis, and collaborates with the meiosis-specific ZMM proteins to ensure correct homologous pairing and synapsis. In plant crops, many genes that contribute to agronomically important traits are located within CO suppressed regions. One of the factors that regulate CO frequency is the anti-CO protein Fanconi Anemia Complementation Group M (FANCM). The absence of this protein produces a 3-fold increase in CO formation in *Arabidopsis*, although this increase is not uniform along chromosomes. Blary et al. demonstrate that the anti-CO function of FANCM is also conserved in the crop species *Brassica rapa* and *B. napus*, highlighting the potential application of this gene in plant breeding programs. Zelkowski et al. prove that the meiotic function of the SMC5/6 complex that has been demonstrated in yeasts, worms, and mammals is conserved in plants. Specifically, one δ-kleisin subunit of this complex, AtNSE4A, is essential for the resolution of meiotic recombination intermediates during the first meiotic division in *Arabidopsis*. Furthermore, during prophase I, the NSE4A protein colocalizes with the central element of the SC (ZYP1) in *Arabidopsis*, *B. rapa*, and rye, revealing also a possible role in synapsis.

iii) Meiosis in polyploids includes papers concerning the analysis of preferences on interactions between homologous and identical chromosomes in autotreploids, the identification and mode of action of the wheat *Ph1* gene, the study of the meiotic behavior of alien chromosomes added to wheat, and the identification of homoeologous pairing between wheat and *Elytrigia elonagata* chromosomes. Parra-Núñez et al. report the formation of more multivalents than expected under the assumption of simple random-end pairing in autotetraploids of two accessions of *Arabidopsis*. This suggests more than two autonomous synapsis initiation sites per chromosome and more than one partner switches per tetrasome. The multivalent frequency decreases in the tetraploid obtained after duplication of the hybrid between the two ecotypes, probably because of heterozygosity. Preferences for chiasma formation between homologous versus identical chromosomes in tetrasome 3 but not in tetrasome 2 of the duplicated intraspecific hybrid, reveal the existence of chromosome-specific mechanisms affecting the partner selection. Rey et al. use two TILLING mutants and one CRISPR mutant of the *TaZIP4-B2* gene on chromosome 5B to produce interspecific wheat × *Aegilops variabilis* hybrids whose meiotic phenotype identifies *ZIP4* as the *Ph1* gene. The frequency of interspecific homoeologous recombination induced by the *ZIP4* mutations increases after irrigation of the plants with magnesium of a nutrient solution. Naranjo argues that the meiotic behavior of individual rye chromosomes changes when they are introgressed into a wheat background. The pattern of chromatin organization at early prophase I is affected, especially for chromosome 4R, which increases its length much more than any other rye chromosome at leptotene-zygotene. Telomeres clustering, but not their dispersion, is depending of the chromosome conformation, which has implications on synapsis and recombination. Chiasma formation is affected in some chromosome arms that show complete synapsis. Calderón et al. use addition lines of barley and *Hordeum chilense* chromosomes into wheat to produce double monosomic additions carrying pairs of homoeologous or non-homoeologous *Hordeum* chromosomes. In the presence of *Ph1,* only the *Hordeum* homoeologous pairs recognize each other in subtelomeric regions and complete synapsis. However, they do not form chiasmata suggesting that *Ph1* suppresses homoeologous CO formation. He et al. use genomic *in situ* hybridization to identify the chromosomes of hexaploid wheat and decaploid *E. elongata* in interspecific hybrids and backcrosses of the hybrids with wheat. Some

associations at metaphase I between chromosomes of both species are produced supporting the occurrence of interspecific homoeologous recombination. This agrees the hypothesis that *Ph*-suppressor genes, which promote homoeologous recombination, are present in *E. elongata*.

iv) Chromosome segregation includes three papers focusing on both chromosomal properties and environmental factors that impact on chromosome segregation. Easterling et al. use 3D cytogenetic analysis of meiotic chromosome dynamics in hop (*Humulus lupulus*) pollen mother cells. The configuration of chromosomes in hop male meiosis include multiple, atypical, non-disomic chromosome complexes detected as aneuploidy, segmental aneuploidy, or chromosome rearrangements, which implicate multiple contributing factors to segregation distortion in hop. Through analysis of multiple centromere misdivision derivatives of a translocation between the supernumerary B chromosome and the short arm of chromosome 9 in maize, Han et al. report that the property size of a centromere does not dramatically affect its segregation or its ability to progress to the poles at the end of cell division. The biochemical features of centromeres are likely the factors for the adjustment in response to the cellular conditions. Sudden temperature changes often lead to abnormal chromosome segregation. Liu et al. use the model system *A. thaliana* to explore the mechanisms behind the cold-induced male meiotic restitution. Findings from this research implicate that GA-DELLA signaling is not the critical factor responsible for the cold-induced abnormal chromosome segregation.

v) Other aspects of meiosis include three reviews that individually focus on the influences of exogenous anthropogenic factors in plant meiosis, the effects of recombination regulation on speciation success of polyploidy species, and the technical approaches to engineer key meiotic genes in tropical crops. Plants now grow on environments that are frequently exposed to anthropogenic factors capable of modulating their meiotic processes. In the first review, Fuchs et al. discuss major anthropogenic factors affecting meiosis in plants, including environmental stresses, agricultural inputs, heavy metals, pharmaceuticals and pathogens. In most cases, the anthropogenic impacts on meiosis are altered recombination frequency and distribution, severe chromosomal fragments caused by stickiness and bridges, precocious movements, and unequal separations resulting in micronuclei and aneuploidy, as well as spindle aberrations. Polyploid speciation is closely related to the regulation of meiotic recombination, which is reviewed by Pelé et al. To achieve speciation success of a polyploidy species, three aspects of meiotic recombination should be guaranteed: the regulation of the genetic variability of newly formed polyploids, the maintenance of the allelic combinatorial possibilities in the following generations, and the faithful segregation of multiple homologs or homoeologs in auto- or allopolyploids. During speciation, different patterns of recombination, coupled with different polyploid formation pathways, cause varied level of heterozygosity. The formation of a polyploidy species with high level of heterozygosity will produce more genetically diverse progenies, therefore improving its environmental adaptability through different natural selections. In the third review, Bolaños-Villegas and Argüello-Miranda mainly summarized the possible technical approaches to manipulate meiosis in orphan crop breeding. They proposed that genome haploidization through modified CENH3 or the apomixes-inducing genes could be a rapid option to create new crosses in tropical crops. Moreover, gene editing of some key meiotic genes, such as *ASY1*, *FANCM*, *RECQ4*, and *PH1*, might facilitate produce new varieties that are enriched in desirable wild traits.

AUTHOR CONTRIBUTIONS

TN, CC, ZC, and MP wrote the paper.

FUNDING

Work in the laboratory of TN and MP was supported by grant AGL2015-67349-P from Dirección General de Investigación Científica y Técnica, Ministerio de Economía y Competitividad of Spain. Research in the laboratory of CC is sponsored by the National Science Foundation (NSF-IOS-1546792).

Conflict of Interest: The authors declare that the research was conducted in the absence of any commercial or financial relationships that could be construed as a potential conflict of interest.

frontiers in Plant Science

REVIEW
published: 19 June 2018
doi: 10.3389/fpls.2018.00829

Tackling Plant Meiosis: From Model Research to Crop Improvement

Christophe Lambing[1] and Stefan Heckmann[2]**

[1] Department of Plant Sciences, University of Cambridge, Cambridge, United Kingdom, [2] Independent Research Group Meiosis, Leibniz Institute of Plant Genetics and Crop Plant Research (IPK) Gatersleben, Seeland, Germany

Genetic engineering and traditional plant breeding, which harnesses the natural genetic variation that arises during meiosis, will have key roles to improve crop varieties and thus deliver Food Security in the future. Meiosis, a specialized cell division producing haploid gametes to maintain somatic diploidy following their fusion, assures genetic variation by regulated genetic exchange through homologous recombination. However, meiotic recombination events are restricted in their total number and their distribution along chromosomes limiting allelic variations in breeding programs. Thus, modifying the number and distribution of meiotic recombination events has great potential to improve and accelerate plant breeding. In recent years much progress has been made in understanding meiotic progression and recombination in plants. Many genes and factors involved in these processes have been identified primarily in *Arabidopsis thaliana* but also more recently in crops such as Brassica, rice, barley, maize, or wheat. These advances put researchers in the position to translate acquired knowledge to various crops likely improving and accelerating breeding programs. However, although fundamental aspects of meiotic progression and recombination are conserved between species, differences in genome size and organization (due to repetitive DNA content and ploidy level) exist, particularly among plants, that likely account for differences in meiotic progression and recombination patterns found between species. Thus, tools and approaches are needed to better understand differences and similarities in meiotic progression and recombination among plants, to study fundamental aspects of meiosis in a variety of plants including crops and non-model species, and to transfer knowledge into crop species. In this article, we provide an overview of tools and approaches available to study plant meiosis, highlight new techniques, give examples of areas of future research and review distinct aspects of meiosis in non-model species.

Keywords: meiosis, homologous recombination, crossover, plant breeding, crops, *Arabidopsis thaliana*

OPEN ACCESS

Edited by:
Zhukuan Cheng,
University of Chinese Academy of Sciences (UCAS), China

Reviewed by:
James D. Higgins,
University of Leicester, United Kingdom
Andreas Houben,
Leibniz-Institut für Pflanzengenetik und Kulturpflanzenforschung (IPK), Germany

****Correspondence:***
Christophe Lambing
cal66@cam.ac.uk
Stefan Heckmann
heckmann@ipk-gatersleben.de

Specialty section:
This article was submitted to Plant Cell Biology, a section of the journal Frontiers in Plant Science

Received: *18 April 2018*
Accepted: *28 May 2018*
Published: *19 June 2018*

Citation:
Lambing C and Heckmann S (2018) Tackling Plant Meiosis: From Model Research to Crop Improvement. Front. Plant Sci. 9:829. doi: 10.3389/fpls.2018.00829

BRIEF OVERVIEW OF MEIOSIS

Meiosis is a specialized cell division taking place in most sexually reproducing eukaryotic species. It consists of one round of DNA replication followed by two rounds of nuclear division (**Figures 1A–F**). During meiosis, a large number of DNA double-strand breaks (DSBs) are formed and repaired by the homologous recombination (HR) pathway (Osman et al., 2011) (**Figure 1G**). These recombination events are important to bring homologous chromosomes in close juxtaposition and promote crossover (CO) formation (**Figures 1H,I**). A CO is defined as a

reciprocal exchange of genetic information between chromosomes. When two polymorphic chromosomes recombine, COs create new combinations of alleles. In addition, COs form physical connections between homologous chromosomes and this ensures correct alignment and segregation of homologous chromosomes on the metaphase plate during meiosis I. At meiosis II sister chromatid cohesion is lost and chromatids segregate to form four haploid recombined gametes. Following this, male and female gametes eventually fuse in the event of fertilization and the diploid state is restored (Mercier et al., 2015).

The meiotic recombination pathway is broadly conserved across plant species although differences exist in the progression of recombination events (Lambing et al., 2017). Meiotic recombination initiates with the formation of DSBs catalyzed by SPO11 and accessory proteins (Robert et al., 2016; Vrielynck et al., 2016). Following DSB formation, SPO11 remains covalently attached to the DSB ends (Neale et al., 2005). DSB ends are then nicked and resected to generate 3′-single-stranded DNA molecules (ssDNAs) (Neale et al., 2005). The recombinases RAD51 and DMC1 bind to the ssDNAs and form nucleoprotein filaments that can anneal to the sister chromatid or to a non-sister homologous chromatid to repair the DSBs (Bishop et al., 1992; Shinohara et al., 1992). During meiosis, a bias in DSB repair toward homologous templates exists (Hong et al., 2013). The majority of these inter-homolog (IH) recombination molecules are eventually displaced by a set of anti-CO proteins and only a subset of these recombination molecules matures in COs (Girard et al., 2014, 2015; Seguela-Arnaud et al., 2015). The fate of recombination molecules is thought to be designated early in prophase I and this seems to be correlated with the accumulation of HEI10 at DSB sites (De Muyt et al., 2014; Lambing et al., 2015). HEI10 is an E3 ligase required for formation of class I COs (Chelysheva et al., 2012; Wang K. et al., 2012). Additional proteins (SHOC1, ZIP4, MSH4/5, MER3, PTD, MLH1/3) are involved in class I CO formation and are collectively named ZMM (Mercier et al., 2015). A second class of COs co-exist independently of ZMM proteins. Class II COs are dependent on structure-specific endonucleases including MUS81 (Berchowitz et al., 2007; Higgins et al., 2008). Class I and II COs differ in their sensitivity to CO interference with the former being sensitive and the latter being insensitive. CO interference is a phenomenon whereby the formation of one CO represses the formation of additional COs in adjacent regions with the strength of the inhibitory effect reducing as the distance increases (Zhang et al., 2014b). The presence of two classes of COs has been observed in Arabidopsis (Higgins et al., 2008) and rice (Zhang P. et al., 2017) and inferred in barley (Phillips et al., 2013) and tomato (Anderson et al., 2014). In Arabidopsis and rice, the proportion of class I COs accounts for ∼85–90% of the total COs.

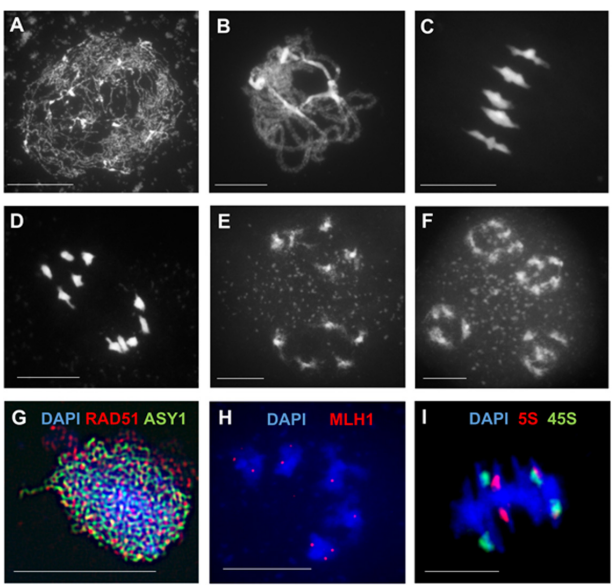

FIGURE 1 | Cytology of male meiosis in *Arabidopsis thaliana*. **(A–F)** Chromosome spreads of Arabidopsis pollen mother cells at different stages during meiosis: **(A)** leptotene, **(B)** pachytene, **(C)** metaphase I, **(D)** anaphase I, **(E)** dyad, **(F)** tetrad. **(G)** Immunolocalization of meiotic-chromosome axis component ASY1 (green) and the recombinase RAD51 (red) at leptotene. **(H)** Immunolocalization of class I CO-marker ZMM protein MLH1 (red) at diakinesis. **(I)** FISH of 45S (green) and 5S (red) rDNA probes at metaphase I discriminates all five pairs of chromosomes forming bivalents. DNA counterstained with DAPI (blue). Scale bar = 10 μM.

CO distribution appears skewed toward the sub-telomeres in tomato (Demirci et al., 2017), maize (Li et al., 2015), wheat (Choulet et al., 2014), and barley (Phillips et al., 2013). At a finer scale, regions of 1–2 kb with higher recombination rates relative to the genome average have been observed in Arabidopsis, maize and wheat (Choi and Henderson, 2015). Several studies suggest that chromatin features could influence recombination. Repressive epigenetic marks such as DNA methylation and H3K9me2 are enriched over heterochromatin which is repressed for COs in Arabidopsis (Yelina et al., 2012; Yelina et al., 2015). In addition, open chromatin features (H3K4me3 and H2A.Z) are found in CO hotspots (Choi et al., 2013) and RNA-directed DNA methylation at two CO hotspots is sufficient to repress CO formation (Yelina et al., 2015).

Meiotic chromatin is organized in loop-base arrays along a proteinaceous chromosome axis (Kleckner, 2006) and yeast DSBs are formed in the chromatin loops tethered to the axis (Panizza et al., 2011). Components of plant chromosome axes comprise HORMA domain containing proteins (Armstrong et al., 2002; Nonomura et al., 2006), coiled-coil proteins (Wang et al., 2011; Ferdous et al., 2012; Lee et al., 2015) and cohesins (Cai et al., 2003; Lam et al., 2005) and axis mutants show defects in CO formation (Wang et al., 2011; Ferdous et al., 2012; Lee et al., 2015). The composition of the chromosome axis is dynamic and axis re-organization correlates with the progression of DSB repair (Lambing et al., 2015). Genome size and organization differ between plant species (Lambing et al., 2017). For instance, the Arabidopsis genome consists of 20% transposons, which are repetitive DNA elements, while the maize genome consists of 85% transposons. These differences in genome size and organization are associated

with changes in chromatin states and epigenetic features and may influence the recombination landscape (Lambing et al., 2017). In addition, findings in Arabidopsis may not be easily transferred to crops. For example, the anti-CO *Atfigl1* Arabidopsis mutant shows increased recombination rates and fertility is unaffected (Girard et al., 2015), while *Osfignl1* rice is infertile (Zhang P. et al., 2017). Therefore, new tools, techniques and approaches are needed to facilitate the investigation of underlying mechanisms and factors responsible for differences between model and crop meiosis, in order to ultimately translate our knowledge into crop breeding programs.

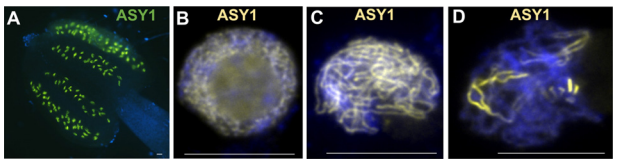

FIGURE 2 | *Arabidopsis thaliana* pollen mother cells expressing FP-TAGged ASY1. **(A)** Squashed anther of *A. thaliana* expressing axis-component ASY1-eGFP (green). **(B–D)** Chromosome spreads of Arabidopsis pollen mother cells expressing ASY1-eYFP (yellow). **(A–D)** No antibody used for detection of ASY1-eYFP. DNA counterstained with DAPI (blue). Scale bar = 10 μM.

IMAGING APPROACHES

Super-Resolution Microscopy

The resolution of fluorescence microscopy is limited to ∼200 nm due to the diffraction limit of light, while EM can resolve cellular structures up to ∼1 nm revealing ultrastructural meiotic chromosome features in various plants (e.g., Albini and Jones, 1987; Albini, 1994; Anderson et al., 2014). However, fluorescence microscopy enables identification and co-localization of labeled cellular structures and molecules. Super-resolution fluorescence microscopy techniques such as SIM (Structured Illumination Microscopy), PALM (Photoactivated Localization Microscopy) or STORM (Stochastic Optical Reconstruction Microscopy) allow analysis of labeled cellular structures and molecules beyond the diffraction limit of light ("subdiffraction" imaging) in plants (Schubert, 2017). Plant cell imaging is challenging when compared to animal tissues due to high levels of autofluorescence and varying tissue refractive indexes leading to light scattering and spherical aberrations (Komis et al., 2015). Tissue-clearing techniques (Kurihara et al., 2015; Musielak et al., 2016; Nagaki et al., 2017) and substances which shift refraction indexes (Littlejohn et al., 2014) may enable "subdiffraction" imaging in intact plant tissues to study meiosis. Currently meiotic chromosome spreads enable high-resolution imaging in various plant species giving new insights into axis, synaptonemal complex (SC) and CO formation as well as meiotic chromosome organization and segregation (Colas et al., 2017; Schubert, 2017). High-resolution microscopic approaches, including single molecule counting and localization by PALM or STORM implemented for non-meiotic plant cells (Schubert and Weisshart, 2015), will likely ensure further insights into meiotic processes in the future.

Live Cell Imaging

Most of our knowledge of plant meiotic progression is based on reconstructions made from fixed materials (Sanchez-Moran and Armstrong, 2014). Meiotic live cell imaging could be an instrumental tool to follow meiotic chromosome and recombination dynamics *in planta* improving our understanding of the spatiotemporal progression of meiotic events. It could, for instance, enable a study of the interplay between axis, SC and HR dynamics or lead to a better understanding of spatiotemporal asymmetric meiotic progression in cereals resulting in CO-heterogeneity (Higgins et al., 2012). However, reports on meiotic live cell imaging are limited. Live cell imaging of isolated and cultured maize meiocytes (Yu et al., 1997, 1999; Nannas et al., 2016) deciphered the dynamics and duration of meiosis I and II chromosome segregation and revealed mechanisms correcting off-centered metaphase spindles. Meiocytes were also analyzed within intact anthers of maize during prophase I (Sheehan and Pawlowski, 2009) and within intact anthers and gynoecia of *Arabidopsis thaliana* (Ingouff et al., 2017). In maize, actin- and tubulin-dependent prophase I chromosome movements are rapid and complex including general chromatin rotations and movements of individual chromosome segments (Sheehan and Pawlowski, 2009). In Arabidopsis, live imaging based on fluorescent protein (FP)-tagged proteins revealed the dynamics of DNA methylation before, during and after meiosis (Ingouff et al., 2017). Although an in-depth analysis of male and female meiotic progression was not performed, highly dynamic chromatin movements during male meiosis were described, suggesting similar prophase Ichromosome movements as in maize. Whether similar prophase I chromatin movements, chromosome segregation dynamics or spindle correction mechanisms occur in other plant species; whether chromosome number or genome size/organization have an impact, and how these processes are interrelated with meiotic progression needs to be established.

In addition to visualizing meiotic proteins based on plants expressing FP-tagged proteins during meiosis (**Figure 2**), the development of CRISPR-imaging (Dreissig et al., 2017b) may enable simultaneous visualization of certain chromosome regions and their dynamics. Tracing single molecule dynamics by CRISPR-PALM in non-plant species (Cho et al., 2016; Khan et al., 2017) as well as live cell SIM imaging and single particle PALM tracking in living plants (Schubert, 2017; Komis et al., 2018) were reported in non-meiotic tissues/cells. Such advanced high-resolution live microscopic imaging applications are challenging for the study of plant meiosis due to the depth of tissue where meiotic cells are embedded, high levels of autofluorescence, light scattering and spherical aberrations. To overcome these plant-specific imaging challenges, the application of multiphoton excitation microscopy (Sheehan and Pawlowski, 2009), two photon excitation microscopy or light sheet fluorescence

microscopy may enable meiotic live cell imaging, although not at high-resolution.

PROTEOMIC APPROACHES

Meiotic Proteomes

Most plant meiotic genes were identified through mutant and genetic suppressor screens or based on sequence conservation with other species. An alternative approach is direct candidate identification by "omics" approaches. To identify proteins present during meiosis, proteomics studies were initially performed using two-dimensional electrophoresis and subsequent "spot" identification by mass spectrometry in various plants (e.g., (Kerim et al., 2003; Sánchez-Morán et al., 2005; Imin et al., 2006; Phillips et al., 2008). Proteomes from flower buds, anthers or isolated meiocytes from Arabidopsis (Lu et al., 2016), tobacco (Ischebeck et al., 2014), *B. oleracea* (Osman et al., 2018), tomato (Chaturvedi et al., 2013), rice (Collado-Romero et al., 2014; Ye et al., 2015), or maize (Wang D. et al., 2012; Zhang et al., 2014a) consist of hundreds or thousands of proteins functionally enriched e.g., for (i) mRNA transcription, stability, and processing, (ii) protein synthesis, translation and splicing and (iii) ubiquitin-proteasome system (UPS) function. While there is evidence implicating transcriptional processes (Nan et al., 2011; Zhang et al., 2015) and UPS function (see section "The Ubiquitin-Proteasome System") in plant meiosis, any direct role of spliceosome or ribosomal proteins in meiotic recombination remains elusive. However, (alternative) splicing is a likely regulatory mechanism during meiosis (Cavallari et al., 2018; Walker et al., 2018).

Meiotic proteome complexity was reduced based on: comparative proteomics combined with transcriptomics in *A. thaliana* (Lu et al., 2016); ASY1 affinity proteomics in *B. oleracea* (Osman et al., 2018); proteomic approaches focusing on the identification of posttranslational protein modifications (PTMs) in rice (Ye et al., 2015; Li et al., 2018). Surprisingly, a comparison of available Arabidopsis flower bud proteomes suggests that protein detection was not saturated (Lu et al., 2016). In addition, proteomes from rice anthers and isolated rice meiocytes identified 6831 and 1316 proteins, respectively (Collado-Romero et al., 2014; Ye et al., 2015). However, only 10 of at least 28 known rice meiotic genes (Luo et al., 2014) were identified, suggesting that even these extensive data sets do not represent the whole meiotic proteome.

Posttranslational Protein Modifications

In non-plant species SC, axis and HR protein dynamics are regulated via PTMs, such as Ubiquitination and SUMOylation (small proteins conjugated to other proteins regulating target stability and localization or their interaction with further proteins) or phosphorylation, coordinately interlinking meiotic chromosome remodeling and HR spatiotemporally during meiosis I (Carballo et al., 2008; Fukuda et al., 2012; Ahuja et al., 2017; Rao et al., 2017). Despite strong evidence for the essential role of PTMs for proper axis, SC and CO formation in budding yeast and mammals, the role of PTMs of corresponding plant homologs are unknown. However, there is growing evidence that in plants too, PTMs of meiotic proteins are essential for meiosis.

Phosphorylation

In non-plant species meiotic chromosome axis proteins undergo phosphorylation critical for their function (Brar et al., 2006; Carballo et al., 2008; Fukuda et al., 2012), e.g., budding yeast Hop1 T318-phosphorylation promotes Hop1-dependent IH bias (Carballo et al., 2008) and S298-phosphorylation promotes stable interaction of Hop1 and Mek1 on chromosomes (Penedos et al., 2015). ASY1 (Hop1) affinity proteomics in *B. oleracea* revealed multiple phosphorylated residues in BoASY1 and BoASY3 (Osman et al., 2018) and OsPAIR2 (homolog of BoASY1) is phosphorylated in rice (Ye et al., 2015). Phosphorylation of BoASY1 at T294 and the flanking residue S300 may functionally correspond to Hop1 T318 and the flanking residue S298 (Osman et al., 2018). In rice anthers phosphoproteomics more than 400 of 3203 identified phosphoproteins are meiotically expressed, including 32 known meiotic genes (Ye et al., 2015). A screen for somatic ATM/ATR (serine/threonine protein kinases triggering the DNA damage response) targets in Arabidopsis identified up- and down-regulated phosphorylation of 108 and 32 candidates, respectively, including various proteins with a role in meiotic DNA damage response (Roitinger et al., 2015). In pollen mother cells, immunolocalization of proteins with phosphorylated [S/T]Q residues, substrate of ATM and ATR kinases, revealed numerous foci associated with the chromosome axis (**Figures 3A–C**). Whether identified phosphorylated residues in meiotic candidate genes in rice and Arabidopsis play a role in meiosis is unclear.

SUMOylation

SUMOylation is a reversible PTM involved in meiotic chromosome axes remodeling, SC formation and HR in budding yeast and nematodes (Zhang et al., 2014c; Nottke et al., 2017). Loss of Arabidopsis SUMO E3 ligase MMS21 results in meiotic chromosome mis-segregation and fragmentation (Liu et al., 2014). Eight SUMO genes (SUMO1-8) are found in Arabidopsis, but only SUMO1/2/3/5 are expressed (Hammoudi et al., 2016). SUMO1/2 are closely related, redundant for plant viability and highly expressed. Immunolocalization of AtSUMO1 on meiotic chromosomes shows abundant signal on chromatin and the chromosome axis (**Figures 3D–I**). In contrast, SUMO3/5 are more divergent and weakly expressed. A SUMO3 mutant shows no obvious plant development phenotype while data on SUMO5 is limited. However, functional data on meiosis are lacking for all expressed SUMOs except SUMO1 which is present on meiotic chromosomes (**Figures 3D–I**). Advances in MS-based detection of SUMO targets (Rytz et al., 2016) and SUMO pathway mutant studies during meiosis should shed further light on whether SUMOylation plays a key role in meiosis in plants.

The Ubiquitin-Proteasome System

In various organisms the UPS is involved in SC and CO formation (Ahuja et al., 2017; Rao et al., 2017). In rice and Arabidopsis, a role for the UPS in meiosis was demonstrated

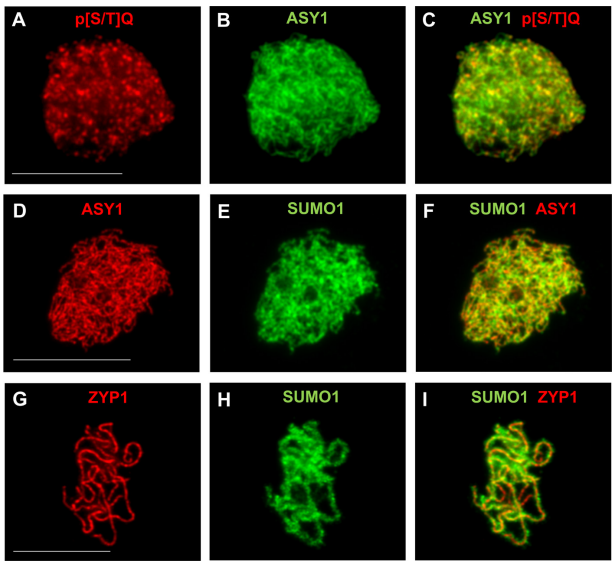

FIGURE 3 | Immunodetection of PTMs on male meiotic *A. thaliana* chromosomes. Immunostaining of ASY1 (green, dilution 1/1000) and phospho-(Ser/Thr) ATM/ATR substrate (p[S/T]Q) (red, Cell Signaling Technology, 2851, dilution 1/2500) at leptotene **(A–C)**, of ASY1 (red, dilution 1/1000) and SUMO1 (green, abcam, ab5316, dilution 1/1000) at leptotene **(D–F)**, and of ZYP1 (red, 1/500) and SUMO1 (green, abcam, ab5316, dilution 1/1000) at pachytene **(G–I)**. Scale bar = 10 μM.

(Yang and McLoud, 2012; He et al., 2016; Zhang F. et al., 2017). In rice, two F-box proteins, MOF and ZYGO1, interact with the rice SKP1-like Protein1 (OSK1), probably as components of the SKP1-CUL1-F-box (SCF) E3 ubiquitin ligase, and are essential for meiosis. MOF regulates male meiotic progression and DSB end-processing and repair (He et al., 2016), whereas ZYGO1 mediates bouquet formation promoting SC and CO formation in both male and female meiosis (Zhang F. et al., 2017). In Arabidopsis, SKP1-like (ASK1) protein (a subunit of the SCF E3 ubiquitin ligase complex) is critical for homologous chromosome pairing, synapsis and nuclear organization during meiosis (Yang and McLoud, 2012) and putative ASK1-substrates include UPS candidates (Lu et al., 2016). Affinity proteomics of the meiotic chromosome axis in *B. oleracea* also identified UPS candidates (Osman et al., 2018).

Additional PTMs

NEDD8, another small protein, is involved in Neddylation that is critical for SC and CO formation in *A. thaliana* (Jahns et al., 2014). Mutation in AXR1, the E3-conjugating NEDD8 ligase, results in a reduced number of bivalents and synapsis defects. The reduced number of bivalents is not due to a general CO decrease, rather due to altered class I CO localization and crossover interference resulting in loss of the obligatory CO. In *arx1 zmm* double mutants barely any CO formation occurs indicating that in *axr1,* MUS81-dependent class II CO are probably abolished. Whether further components of the Neddylation system are critical for meiosis and which meiotic proteins undergo Neddylation needs to be established.

Proteomics from rice anthers identified 357 acetylated proteins including eight rice homologs of known meiotic genes (Li et al., 2018). A positive correlation of simultaneous acetylation and phosphorylation of candidates functionally enriched for ribosome assembly, protein translation, UPS, and RNA degradation was found, further linking these processes to plant meiosis (see section "Meiotic Transcriptome"). Acetylation of histones was abundant, various histone acetyltransferases and deacetylases were detected in rice meiotic transcriptomes (Zhang et al., 2015) and GCN5-related histone N-acetyltransferase alters meiotic recombination in Arabidopsis (Perrella et al., 2010), suggesting a link between histone acetylation and meiosis. Interestingly, in rice H3K9 hyperacetylation correlates with meiotic arrest in *mel1* (Liu and Nonomura, 2016), H3K9 acetylation affects yeast recombination hotspots (Yamada et al., 2013) and H4K12/H4K16 acetylation impacts meiotic chromosome segregation in human and mouse (van den Berg et al., 2011; Ma and Schultz, 2013). All of these sites were acetylated in rice (Li et al., 2018).

GENOMIC AND TRANSCRIPTOMIC APPROACHES

Chromatin Immunoprecipitation of Recombination Proteins

Chromatin immunoprecipitation sequencing (ChIP-seq) of recombination proteins consists of precipitating DNA molecules found in complex with proteins. DNA molecules are then detected using Next-Generation sequencing. In plants, the first genome-wide maps of DSBs were generated in maize using a RAD51 antibody (He et al., 2017) and in Arabidopsis using an epitope-tagged SPO11-1-MYC (Choi et al., 2018). DSB hotspots were located in repetitive and gene regions in both species. Similar to yeast (Pan et al., 2011) and mice (Lange et al., 2016), maize and Arabidopsis DSBs are mostly located in nucleosome depleted regions and in regions of low DNA methylation (He et al., 2017). Genome-wide correlation between DSBs and COs is low while a positive correlation between DSBs located in genic regions and COs was found (He et al., 2017), suggesting that DSB formation is not repressed over repetitive regions but recombination outcome differs depending on local features. Interestingly, removal of the heterochromatin silencing marks H3K9me2 and non-CG methylation in Arabidopsis resulted in an increase in DSBs and COs over the pericentromeres (Underwood et al., 2018). Understanding how DSBs are repaired and acquire a CO fate is essential as it could facilitate the manipulation of CO rate over genes of interest.

Mapping Crossovers

Despite the formation of a large number of meiotic recombination events only a subset of them forms a CO. The remaining recombination molecules are resolved as NCOs (Mercier et al., 2015). NCOs can be accompanied by gene

conversions (GCs) which consist of non-reciprocal exchanges of genetic information causing a non-Mendelian 3:1 segregation ratio of alleles (Sun et al., 2012). Several techniques exist to measure CO rate (**Table 1**). For example, transgenic Arabidopsis lines with genetically linked genes expressing FPs either in pollen (Berchowitz and Copenhaver, 2008) or seeds (Melamed-Bessudo et al., 2005) can be used to measure recombination, based on the segregation ratio of the FP-coding genes, in male meiosis and male/female meiosis, respectively. This technique was also adapted to measure GCs and revealed that GC rate is low and estimated at 3.5×10^{-4} per locus per meiosis and that the majority of these GCs are associated with a CO, while only a few GCs are associated with a NCO in Arabidopsis (Sun et al., 2012). Unfortunately, the generation of FTLs in crops would be laborious, expensive and time-consuming. As an alternative approach single pollen genotyping was developed in barley (Dreissig et al., 2015). The method consists of isolating individual haploid pollen nuclei from F1 hybrids by utilizing fluorescence activated cell sorting (FACS) followed by whole-genome amplification and subsequent multi-locus KASP-genotyping or single-cell genome sequencing (Dreissig et al., 2015; Dreissig et al., 2017a). This technique has the advantage of analyzing the DNA content from gametes before fertilization so that measurement of CO rate is not affected by segregation distortion.

Another technique called genotyping-by-sequencing consists of low-coverage sequencing of the genomes of a large F2 population derived from F1 hybrids providing a genome-wide crossover distribution (Si et al., 2015; Yelina et al., 2015). The position of the COs is inferred by detecting changes in single nucleotide polymorphisms (SNP) positions in the F2 population. However, this technique is expensive, the resolution of CO sites is low (>1 kb) and the number of individuals analyzed is limited (Yelina et al., 2015). Nevertheless, this technique revealed that CO distribution is reduced over the pericentromeric regions in Arabidopsis (Yelina et al., 2015) and rice (Si et al., 2015) and that changes in environmental conditions influence recombination (Si et al., 2015).

TABLE 1 | Comparison between the different methods to detect COs.

Techniques	Principle	Resolution	Species	Reference
Chromosome spreading combined with FISH and immunolocalization of class I CO marker	Detection of chiasmata based on bivalent morphology and detection of class I COs based on immunolocalization of MLH1/HEI10 in Arabidopsis and MLH3 in Barley	Chromosome scale	Bivalent morphology and FISH: variety of plant species; Immunolocalization of class I CO marker: Arabidopsis, barley, brassica, tomato, rice, wheat	e.g., Arabidopsis (Chelysheva et al., 2012), barley (Higgins et al., 2012)
Fluorescent transgenic lines (FTLs)	Measurement of CO rate in pollen (male) or seeds (male/female) based on the segregation ratio of genetically linked genes expressing fluorescent proteins. Measurement of CO interference	Mbs	Arabidopsis	Pollen (Berchowitz and Copenhaver, 2008), seeds (Melamed-Bessudo et al., 2005)
Genotyping-by-sequencing and molecular markers in segregating F2 populations	Measurement of CO rate in F2 population derived from F1 hybrid based on polymorphisms (primarily SNPs) of parental genomes through low-coverage genome sequencing or selected molecular markers. Genome-wide CO distribution and CO interference can be measured. Molecular markers can also be used to study CO rate at a specific region of the chromosome.	∼1 kb depending on SNP density	Arabidopsis, tomato, rice, wheat, and maize	Arabidopsis (Yelina et al., 2015), tomato (Demirci et al., 2017), rice (Si et al., 2015), wheat (Saintenac et al., 2009), maize (Yao and Schnable, 2005)
Microspore (tetrad or pollen nuclei) genotyping or sequencing	Measurement of CO rate in individual microspores (tetrad or pollen nuclei; male meiosis) from F1 hybrid based on polymorphisms (primarily SNPs) of parental genomes through low-coverage genome sequencing or KASP-genotyping. Genome-wide CO distribution and CO interference can also be measured. Detection of gene conversion events if individual nuclei of a tetrad are sequenced. Can differentiate between COs and segregation distortion	∼1 kb depending on SNP density (sequencing). The resolution of COs detected using KASP-genotyping depends on the number of markers used	Barley (pollen: genotyping, sequencing), maize (tetrad: sequencing), Arabidopsis (tetrad: sequencing)	Barley (Dreissig et al., 2015, 2017a), Maize (Li et al., 2015), Arabidopsis (Lu et al., 2012)
Pollen typing	Measurement of CO rate in pollen nuclei (male meiosis) from F1 hybrid at specific loci (hot spots) based on polymorphisms (primarily SNPs) of parental genomes through allele-specific PCRs	<1 kb depending on SNP density	Arabidopsis	Yelina et al., 2012, 2015; Choi et al., 2016

Sequencing the four meiotic products derived from a meiocyte provides additional information on meiotic recombination because the sequence of the four chromatids that were present in meiosis is obtained. This approach was used in Arabidopsis, maize and budding yeast and revealed the presence of complex template switches and GCs (Mancera et al., 2008; Lu et al., 2012; Li et al., 2015). Finally, recombination rate can be measured at fine-scale (<1 kb) using allele specific PCR amplification from F1 hybrid pollen DNA. This approach confirmed the presence of CO hotspots in Arabidopsis and facilitated the study of specific loci (Choi et al., 2016).

Meiotic Transcriptome

Microarray and, later, primarily RNA-seq approaches were used to dissect the male meiotic transcriptome based on flower buds, anthers or even isolated meiocytes in various plants while female meiotic transcriptomes were dissected in Arabidopsis and rice (Dukowic-Schulze and Chen, 2014). All studies revealed a complex picture of the meiotic transcriptome, i.e., a large number of genes are expressed and hundreds to thousands of transcripts are differentially expressed. The picture is even more complex, as a high number of mitochondria-encoded genes possibly constituting a source of energy for meiotic progression (Dukowic-Schulze et al., 2014), transposable elements (Chen et al., 2010; Yang et al., 2011), and (long) non-coding RNAs (Dukowic-Schulze et al., 2016; Flórez-Zapata et al., 2016; Wu et al., 2017) are differentially expressed. Changes in chromatin and chromosome organization may cause a general chromatin de-repression accounting for this complexity including an elevated expression of transposable elements in meiocytes (Chen et al., 2010; Yang et al., 2011; Dukowic-Schulze et al., 2014).

RNA interference (RNAi) machinery components and miRNAs are differentially expressed during meiosis (Dukowic-Schulze et al., 2014, 2016; Flórez-Zapata et al., 2016; Wu et al., 2017) and mutations in RNAi machinery components result in aberrant meiotic progression, chromatin structure or HR (Nonomura et al., 2007; Singh et al., 2011; Oliver et al., 2014, 2017), indicating that the RNAi machinery plays a role in meiosis. In male monocot meiotic transcriptomes phasiRNAs are detected that originate from a few hundred dispersed intergenic, non-repetitive regions (phasiRNA loci) and apparently do not target any genes but instead mediate in *cis* DNA methylation at their loci of origin (Dukowic-Schulze et al., 2016). Various long non-coding RNAs were differentially expressed in meiocytes of three sunflower genotypes differing in meiotic recombination rates (Flórez-Zapata et al., 2016), suggesting a link between long non-coding RNAs and meiosis. What specific roles non-coding RNAs play needs to be elucidated. To decipher their localization and dynamics, single molecule FISH, so far limited to root cells, may be used to visualize and quantify RNA molecules at the single-cell level (Duncan et al., 2016). Down-regulation and/or over-expression of candidate loci may help to dissect their function during meiosis.

To identify key meiotic genes, meiotic transcriptomes from different genetic backgrounds (e.g., mutant vs. wildtype, diploid vs. polyploid, treated vs. untreated) were compared. Comparative meiotic transcriptomics between synthetic tetraploid *B. rapa* with aberrant meiosis and its fertile diploid progenitors identified more than 4500 differentially expressed genes including eleven known meiotic genes (Braynen et al., 2017). ZYP1 and SYN1 expressions were upregulated both of which were also implicated as potential candidates for preventing polyploidy-related chromosome segregation challenges in Arabidopsis (Yant et al., 2013). Maize and rice *am1* meiotic transcriptomes were compared to their respective wild-type (Nan et al., 2011; Zhang et al., 2015). In rice HEI10, MSH5, ZIP4, and PSS1 while in maize SMC3, ATR, ATM, RMI1, and MPA1 were identified among thousands of differentially expressed genes as meiotic candidates, suggesting that AM1 plays a role in modulating the expression of many critical meiotic genes in a species-specific dependent manner. Rice ovule transcriptomes from different wild-type genotypes and various female-sterile lines revealed a high number of differentially expressed genes and miRNAs (Yang et al., 2016, 2017; Zhu et al., 2017). Even by performing comparative meiotic transcriptomics in various plants, the complexity of meiotic transcriptomes is astonishing. Thus, whether all identified genes in meiotic transcriptomes are indeed essential for meiosis or whether the large number of detected transcripts is the result of global de-repression of chromatin during meiosis needs to be elucidated.

Reducing sample complexity could be achieved through single cell-type isolation. Potentially flow-cytometric isolation of meiocytes based on plants expressing meiotic proteins tagged with FPs (**Figure 2**), meiotic protein immunolabelling of meiocytes in solution pre-sorting, or the INTACT method (Deal and Henikoff, 2010) could allow enrichment for distinct meiocyte fractions. However, even isolated meiocytes represent a pool of different cells at various meiotic stages or at least sub stages and so far no studies have reported isolation of meiotic cells or nuclei so it is unclear whether these techniques could be applied to meiocytes.

ENGINEERING PLANTS

Generating Mutants

Reverse genetic approaches are key to identifying genes associated with a phenotype. They are widely used in Arabidopsis and reverse genetic resources, including several targeted induced local lesions in the genome (TILLING) populations, were developed in various crops in recent years (Jacob et al., 2018). The higher level of ploidy and higher gene copy numbers makes polyploid plants such as wheat more tolerant to a high density of mutations than diploid plants such as barley and it reduces the proportion of infertile or embryonic lethal M2 plants. However, the complexity of polyploid genomes renders the detection of the mutation sites challenging. Development of exome capture, that scans the exons to identify mutations disrupting coding regions, has facilitated e.g., the identification of EMS-mediated mutation sites in tetraploid and hexaploid TILLING wheat populations (Krasileva et al., 2017).

However, these mutant populations present several limitations. First, the mutant lines have a high density of mutations and several rounds of backcrosses with a non-mutant line are required before full characterisation of a phenotype. In addition, TILLING approaches have limitations in targeting several copies of a gene of interest and crosses of independent mutant lines are then required to combine mutations. As an alternative, RNAi-based gene silencing and Clustered Regularly Interspaced Short Palindromic Repeats (CRISPR)/Cas9 system are efficient to knockdown or knockout several genes simultaneously. These techniques are promising mutagenesis tools for polyploid species such as wheat and have been used to study meiotic genes e.g., in barley (Fu et al., 2007; Barakate et al., 2014; Wang et al., 2014; Lawrenson et al., 2015). Unfortunately, these techniques typically rely on stable plant transformation and only a few institutions have the technology to transform e.g., cereals with exogenous DNAs.

Several mutations in the meiotic class II CO pathway (Seguela-Arnaud et al., 2015; Fernandes et al., 2017) and overexpression of the E3 ligase HEI10 (Ziolkowski et al., 2017), involved in formation of class I COs, cause an increase in genome-wide CO rate in Arabidopsis. Both class I and II CO pathways are attractive targets to manipulate recombination in crops (Serra et al., 2018). However, several components of the class II CO pathway are also involved in somatic DNA repair and maintenance of genome stability. Thus, targeted delivery systems to modulate activity of specific genes in reproductive tissues are needed. Virus-induced gene silencing (VIGS) has emerged as a rapid and inexpensive transient gene knock-down system in plants by exploiting plant defense mechanism based on RNAi against virus infection (Lee et al., 2012). Barley stripe mosaic virus was successfully engineered to manipulate meiotic genes in the wheat cultivar 'Chinese Spring' and other wheat genotypes (Bennypaul et al., 2012; Bhullar et al., 2014). Additionally, VIGS can transiently knockdown essential genes during development, especially important if the genes to be silenced are involved in epigenetic marks (e.g., DNA methylation) or genome stability, as a stable knockout could otherwise lead to (embryonic) lethality or loss of fertility.

Targeted Recombination

Conventional methods to introduce genetic diversity into plant genomes are laborious and depend on the rate of meiotic recombination. In wheat meiotic recombination is repressed over heterochromatin regions preventing the introduction of genetic diversity into genes present within these regions (Choulet et al., 2014). Therefore, new techniques to engineer the genome and manipulate recombination landscapes are needed. Recent genomic data suggest that DSB rate over genes positively correlates with CO rate in maize (He et al., 2017). It is possible that by influencing the rate of DSBs this will in turn cause a change in COs over targeted regions.

In budding yeast, the formation of artificial DSBs using site specific endonucleases is sufficient to create meiotic recombination in cold spot regions (Sarno et al., 2017). The recombination frequency was variable between employed endonucleases and targeted chromosomal regions suggesting that local factors may influence the conversion rate of DSBs to COs. In plants three classes of site-specific endonucleases, Zinc finger nucleases, transcription activator-like effector nucleases (TALENs) and CRISPR/Cas9 are used to edit the genome of plant species such as Arabidopsis, rice and maize (Sun et al., 2016). These nucleases generate DSBs in the targeted nucleotide sequences and the DSBs are either repaired in an error-prone repair pathway or are repaired and edited by HR using a transgenic donor as DNA repair template (Fauser et al., 2012; Sun et al., 2016). In meiosis, DSBs are preferentially repaired by HR and any additional DSB formed can potentially become a CO. The proven efficiency of these site-specific nucleases to generate somatic DSBs suggests that they may also be used during meiosis to manipulate CO rate. To increase the conversion of artificial DSBs to COs, additional local factors may need to be modified. For example, local nucleosome occupancy can be altered with chromatin remodelers. Pro-CO factors like HEI10 could be site-specific targeted alongside SPO11 to promote both DSB formation and maturation of IH recombination molecules to COs, or artificial DSBs could be triggered in hyper-recombination plants (e.g., *fancm*, *recq4,* and/or *figl1*) increasing the likelihood of a DSB maturing into a CO. Although the potential to target recombination toward genes in crops is significant as it can reduce the cost and time to produce novel plant varieties, several challenges exist and the application of these techniques to plant meiosis remains to be demonstrated.

Making Use of Natural Variation

Arabidopsis thaliana is found in many different natural habitats showing extensive intraspecific variation in measurable traits that differ quantitatively between accessions (Weigel, 2012; The 1001 Genomes Consortium, 2016). The genomes of a total of 1,135 natural inbred *A. thaliana* lines from Eurasia, North Africa and colonized North America and 3010 accessions of Asian cultivated rice were sequenced (The 1001 Genomes Consortium, 2016; Wang et al., 2018). Comparative genomic analysis revealed a high degree of intraspecific genetic divergence with the presence of SNPs, small and large insertions/deletions, copy number variations and structural variations. Interestingly a large number of genes contain SNPs which introduce premature stop codons predicted to form non-functional proteins, SNPs which alter translational start sites or donor/acceptor splicing sites predicted to form alternative transcripts (Cao et al., 2011). Phenotypic differences in Arabidopsis have also been associated with variation in epigenetic marks at specific loci, so-called epialleles (O'Malley and Ecker, 2012; Weigel and Colot, 2012; Dubin et al., 2015). A direct relationship between the phenotypic trait and the extent of DNA methylation was demonstrated for most but not all epialleles suggesting that other epigenetic factors are probably also involved (O'Malley and Ecker, 2012; Weigel and Colot, 2012).

Intraspecific variation in meiotic recombination frequency was found in various plants (Lawrence et al., 2017). For instance, F1 Arabidopsis hybrids from 32 diverse accessions revealed extensive variation in CO rate (Ziolkowski et al., 2015). Several

confounding factors could account for these CO changes. For example, each ecotype has distinct genetic information and the degree of polymorphism represses CO rate (Lawrence et al., 2017). F1 hybrid plants arising from parents with potentially distinct epigenomes could also influence recombination locally (Cortijo et al., 2014; Yelina et al., 2015). In addition, trans-acting factors exerted by polymorphic loci can modulate recombination. The first plant quantitative trait loci for recombination was recently identified as HEI10 and over-expression of HEI10 in Arabidopsis causes a greater than twofold increase in CO formation genome-wide (Ziolkowski et al., 2017). Additional trans-acting factors probably exist. For example, MSH2 presents gene copy number variations among Arabidopsis accessions and represses recombination between divergent genomes (Emmanuel et al., 2006; Zmienko et al., 2016).

NOVEL APPROACHES EXPLOITING NON-MODEL PLANTS

B chromosomes (supernumerary chromosomes) found across a variety of animals, plants and fungi do not recombine with the standard "A" chromosomes (Jones et al., 2008). Numerous reports in plants suggest an impact of B's on meiotic recombination behavior (chiasma frequency and/or distribution) of homologous and homeologous A chromosomes in diploid, polyploid and inter-species hybrids (Jones and Rees, 1982; Jones et al., 2008). Genetic and genotypic A–B interactions seem to impact chiasma number and distribution (Ortiz et al., 1996; Kousaka and Endo, 2012). B chromosomes in rye are transcriptionally active containing several B-enriched transcriptionally active tandem repeats (Martis et al., 2012; Klemme et al., 2013), transcribed transposable elements (Ma et al., 2017), and long non-coding RNAs (Carchilan et al., 2007) all of which are predominantly found in anthers. B-encoded pseudogene-like fragments and genes are transcribed in a tissue-type and genotype-specific manner and can cause down-/upregulation of A-located counterparts (Banaei-Moghaddam et al., 2013; Ma et al., 2017). More than 300 B-encoded anther transcripts show similarity to proteins with functional annotation. Among them are SHOC1, PCH2, or SCC3 known to be involved in meiosis and further candidates relating to DNA methylation, chromatin remodeling, the UPS or DNA repair (Ma et al., 2017). Since the effect of B's on the host recombination landscape seems to have a genetic basis and is often dosage dependent, together with B's encoding non-coding RNAs and various genes including known meiotic genes, it seems likely that B's may have a direct impact on the recombination machinery of its host. Further studies could shed light on meiotic recombination mechanisms in the presence of B's. Despite the potential of B's as tools for manipulating meiotic recombination in breeding processes, there has been limited utilization of this knowledge in crop breeding (Jones et al., 2008). By standard crossing schemes they could be easily introduced and removed without recombining with As.

Although HR is conserved across species (Mercier et al., 2015), differences in progression of meiosis and recombination intermediates are found between plant species (Lambing et al., 2017). In Arabidopsis *figl1* shows an increase in meiotic recombination without affecting fertility (Girard et al., 2015), whereas in rice *figl1* male meiotic chromosomes undergo fragmentation causing male infertility (Zhang P. et al., 2017). In Arabidopsis and barley reduced ZYP1 levels result in reduced CO numbers (Higgins et al., 2005; Barakate et al., 2014), whereas in rice ZEP1 depletion leads to an increase in CO numbers (Wang et al., 2010). Meiotic studies in non-model plant species also revealed differences e.g., in centromere/kinetochore regulation during meiotic divisions leading to altered chromosome segregation patterns (Cabral et al., 2014; Heckmann et al., 2014; Cuacos et al., 2015; Marques and Pedrosa-Harand, 2016). In the European larch, as in most gymnosperms, female meiosis starts and completes during spring whereas male meiosis starts in autumn and finishes in spring and is characterized by a "diffuse stage" during diplotene lasting ∼5 months (Zhang et al., 2008; Kołowerzo-Lubnau et al., 2015). This long male diplotene stage is characterized by microsporocyte growth, synthesis and accumulation of mRNAs and proteins, and changes in chromatin conformation, i.e., condensation cycles of contraction and relaxation correlating with transcriptional activity. Further studies in the European larch or other gymnosperms may reveal additional insights into chromatin dynamics and transcription during meiosis and differences in induction and progression of male vs. female meiosis. Due to slow-paced progression during prophase I, for instance, assembly/disassembly of the bouquet and the SC or formation and dissolution of interlocks could be studied in detail. In numerous plant species, primarily during male prophase I, cytomixis occurs, i.e., migration of whole nuclei, chromosomes and/or chromatin between plant cells through intercellular channels (cytomictic channels) resulting in the formation of unreduced, polyploid, aneuploid or sterile pollen (Mursalimov et al., 2015; Mursalimov and Deineko, 2017). How cytomixis is regulated or interconnected to meiotic progression is unclear. In translocation heterozygote plants CO formation is restricted to distinct chromosome regions commonly leading to long chromosome chains (Stack and Soulliere, 1984; Rauwolf et al., 2011; Golczyk et al., 2014). In Oenothera meiosis, for instance, a spatiotemporal genome compartmentation occurs, i.e., chromosomes are organized in two epigenetically distinct regions, uneven chromosome condensation occurs and COs occur at end-segments of chromosomes roughly at the junction between the two chromatin fractions, resulting in chromosome chains/rings (Rauwolf et al., 2011; Golczyk et al., 2014). How this tightly restricted CO localization is achieved or how balanced chromosome segregation occurs is unclear. Moreover, in closely related species such as Allium differences in recombination patterns are found, i.e., either proximal or interstitial/distal CO (Albini and Jones, 1987), possibly offering models to get a better understand CO patterning control in closely related species.

Thus, although general mechanisms of meiosis and HR are conserved, studies in different species, including non-model species, may widen our knowledge of plant meiosis revealing differences and similarities and possibly enabling a deeper understanding of underlying mechanisms.

CONCLUDING REMARKS AND FUTURE PERSPECTIVES

In recent years studies, mainly in Arabidopsis but also in selected crops and non-model species, have increased our understanding of plant meiotic progression and recombination and many genes and factors involved in these processes were identified. However, much remains to be learned, even though our current knowledge may provide a basic foundation to explore whether meiotic recombination in crops can be manipulated to improve and accelerate plant breeding programs. Differences in plant genome organization (particularly repetitive DNA content and ploidy level) accompanied by differences in chromatin and epigenetic features likely account for differences in meiotic progression and recombination patterns. Thus, available and new approaches are needed to investigate the underlying mechanisms and factors responsible for differences and similarities in meiotic progression and recombination between model, crop and non-model plants to ultimately translate our knowledge into crop breeding programs.

AUTHOR CONTRIBUTIONS

All authors listed have made a substantial, direct and intellectual contribution to the work, and approved it for publication.

FUNDING

CL is funded by the ERA-CAPS/BBSRC (BB/M004937/1). SH and the independent junior research group Meiosis at the IPK Gatersleben are funded by the German Federal Ministry of Education and Research (BMBF – 031B0188) and are further supported by the IPK Gatersleben.

ACKNOWLEDGMENTS

We thank Kim Osman and Maria Cuacos for critical reading of the manuscript.

REFERENCES

Ahuja, J. S., Sandhu, R., Mainpal, R., Lawson, C., Henley, H., Hunt, P. A., et al. (2017). Control of meiotic pairing and recombination by chromosomally tethered 26S proteasome. *Science* 355, 408–411. doi: 10.1126/science.aaf4778

Albini, S. M. (1994). A karyotype of the *Arabidopsis thaliana* genome derived from synaptonemal complex analysis at prophase I of meiosis. *Plant J.* 5, 665–672. doi: 10.1111/j.1365-313X.1994.00665.x

Albini, S. M., and Jones, G. H. (1987). Synaptonemal complex spreading in *Allium cepa* and *A. fistulosum*. *Chromosoma* 95, 324–338. doi: 10.1007/BF00293179

Anderson, L. K., Lohmiller, L. D., Tang, X., Hammond, D. B., Javernick, L., Shearer, L., et al. (2014). Combined fluorescent and electron microscopic imaging unveils the specific properties of two classes of meiotic crossovers. *Proc. Natl. Acad. Sci. U.S.A.* 111, 13415–13420. doi: 10.1073/pnas.1406846111

Armstrong, S. J., Caryl, A. P., Jones, G. H., and Franklin, F. C. H. (2002). Asy1, a protein required for meiotic chromosome synapsis, localizes to axis-associated chromatin in *Arabidopsis* and *Brassica*. *J. Cell Sci.* 115, 3645–3655. doi: 10.1242/jcs.00048

Banaei-Moghaddam, A. M., Meier, K., Karimi-Ashtiyani, R., and Houben, A. (2013). Formation and expression of pseudogenes on the b chromosome of rye. *Plant Cell* 25, 2536–2544. doi: 10.1105/tpc.113.111856

Barakate, A., Higgins, J. D., Vivera, S., Stephens, J., Perry, R. M., Ramsay, L., et al. (2014). The synaptonemal complex protein ZYP1 is required for imposition of meiotic crossovers in barley. *Plant Cell* 26, 729–740. doi: 10.1105/tpc.113.121269

Bennypaul, H. S., Mutti, J. S., Rustgi, S., Kumar, N., Okubara, P. A., and Gill, K. S. (2012). Virus-induced gene silencing (VIGS) of genes expressed in root, leaf, and meiotic tissues of wheat. *Funct. Integr. Genomics* 12, 143–156. doi: 10.1007/s10142-011-0245-0

Berchowitz, L. E., and Copenhaver, G. P. (2008). Fluorescent *Arabidopsis* tetrads: a visual assay for quickly developing large crossover and crossover interference data sets. *Nat. Protoc.* 3, 41–50. doi: 10.1038/nprot.2007.491

Berchowitz, L. E., Francis, K. E., Bey, A. L., and Copenhaver, G. P. (2007). The role of AtMUS81 in interference-insensitive crossovers in *A. thaliana*. *PLoS Genet.* 3:e132. doi: 10.1371/journal.pgen.0030132

Bhullar, R., Nagarajan, R., Bennypaul, H., Sidhu, G. K., Sidhu, G., Rustgi, S., et al. (2014). Silencing of a metaphase I-specific gene results in a phenotype similar to that of the Pairing homeologous 1 (*Ph1*) gene mutations. *Proc. Natl. Acad. Sci. U.S.A.* 111, 14187–14192. doi: 10.1073/pnas.1416241111

Bishop, D. K., Park, D., Xu, L., and Kleckner, N. (1992). DMC1: a meiosis-specific yeast homolog of *E. coli* recA required for recombination, synaptonemal complex formation, and cell cycle progression. *Cell* 69, 439–456. doi: 10.1016/0092-8674(92)90446-J

Brar, G. A., Kiburz, B. M., Zhang, Y., Kim, J.-E., White, F., and Amon, A. (2006). Rec8 phosphorylation and recombination promote the step-wise loss of cohesins in meiosis. *Nature* 441, 532–536. doi: 10.1038/nature04794

Braynen, J., Yang, Y., Wei, F., Cao, G., Shi, G., Tian, B., et al. (2017). Transcriptome analysis of floral buds deciphered an irregular course of meiosis in polyploid *Brassica rapa*. *Front. Plant Sci.* 8:768. doi: 10.3389/fpls.2017.00768

Cabral, G., Marques, A., Schubert, V., Pedrosa-Harand, A., and Schlögelhofer, P. (2014). Chiasmatic and achiasmatic inverted meiosis of plants with holocentric chromosomes. *Nat Commun* 5:5070. doi: 10.1038/ncomms6070

Cai, X., Dong, F., Edelmann, R. E., and Makaroff, C. A. (2003). The *Arabidopsis* SYN1 cohesin protein is required for sister chromatid arm cohesion and homologous chromosome pairing. *J. Cell Sci.* 116, 2999–3007. doi: 10.1242/jcs.00601

Cao, J., Schneeberger, K., Ossowski, S., Gunther, T., Bender, S., Fitz, J., et al. (2011). Whole-genome sequencing of multiple *Arabidopsis thaliana* populations. *Nat. Genet.* 43, 956–963. doi: 10.1038/ng.911

Carballo, J. A., Johnson, A. L., Sedgwick, S. G., and Cha, R. S. (2008). Phosphorylation of the axial element protein Hop1 by Mec1/Tel1 ensures meiotic interhomolog recombination. *Cell* 132, 758–770. doi: 10.1016/j.cell.2008.01.035

Carchilan, M., Delgado, M., Ribeiro, T., Costa-Nunes, P., Caperta, A., Morais-Cecílio, L., et al. (2007). Transcriptionally active heterochromatin in rye B chromosomes. *Plant Cell* 19, 1738–1749. doi: 10.1105/tpc.106.046946

Cavallari, N., Nibau, C., Fuchs, A., Dadarou, D., Barta, A., and Doonan, J. H. (2018). The cyclin-dependent kinase G group defines a thermo-sensitive alternative splicing circuit modulating the expression of Arabidopsis *ATU2AF65A*. *Plant J.* doi: 10.1111/tpj.13914 [Epub ahead of print] .

Chaturvedi, P., Ischebeck, T., Egelhofer, V., Lichtscheidl, I., and Weckwerth, W. (2013). Cell-specific analysis of the tomato pollen proteome from pollen mother cell to mature pollen provides evidence for developmental priming. *J. Proteome Res.* 12, 4892–4903. doi: 10.1021/pr400197p

Chelysheva, L., Vezon, D., Chambon, A., Gendrot, G., Pereira, L., Lemhemdi, A., et al. (2012). The *Arabidopsis* HEI10 is a new ZMM protein related to Zip3. *PLoS Genet.* 8:e1002799. doi: 10.1371/journal.pgen.1002799

Chen, C., Farmer, A. D., Langley, R. J., Mudge, J., Crow, J. A., May, G. D., et al. (2010). Meiosis-specific gene discovery in plants: RNA-Seq applied to isolated

Arabidopsis male meiocytes. *BMC Plant Biol.* 10:280. doi: 10.1186/1471-2229-10-280

Cho, W.-K., Jayanth, N., Mullen, S., Tan, T. H., Jung, Y. J., and Cissé, I. I. (2016). Super-resolution imaging of fluorescently labeled, endogenous RNA Polymerase II in living cells with CRISPR/Cas9-mediated gene editing. *Sci. Rep.* 6:35949. doi: 10.1038/srep35949

Choi, K., and Henderson, I. R. (2015). Meiotic recombination hotspots – a comparative view. *Plant J.* 83, 52–61. doi: 10.1111/tpj.12870

Choi, K., Reinhard, C., Serra, H., Ziolkowski, P. A., Underwood, C. J., Zhao, X., et al. (2016). Recombination rate heterogeneity within Arabidopsis disease resistance genes. *PLoS Genet.* 12:e1006179. doi: 10.1371/journal.pgen.1006179

Choi, K., Zhao, X., Kelly, K. A., Venn, O., Higgins, J. D., Yelina, N. E., et al. (2013). *Arabidopsis* meiotic crossover hot spots overlap with H2A.Z nucleosomes at gene promoters. *Nat. Genet.* 45, 1327–1336. doi: 10.1038/ng.2766

Choi, K., Zhao, X., Tock, A. J., Lambing, C., Underwood, C. J., Hardcastle, T. J., et al. (2018). Nucleosomes and DNA methylation shape meiotic DSB frequency in *Arabidopsis thaliana* transposons and gene regulatory regions. *Genome Res.* 28, 532–546. doi: 10.1101/gr.225599.117

Choulet, F., Alberti, A., Theil, S., Glover, N., Barbe, V., Daron, J., et al. (2014). Structural and functional partitioning of bread wheat chromosome 3B. *Science* 345:1249721. doi: 10.1126/science.1249721

Colas, I., Darrier, B., Arrieta, M., Mittmann, S. U., Ramsay, L., Sourdille, P., et al. (2017). Observation of extensive chromosome axis remodeling during the "diffuse-phase" of meiosis in large genome cereals. *Front. Plant Sci.* 8:1235. doi: 10.3389/fpls.2017.01235

Collado-Romero, M., Alós, E., and Prieto, P. (2014). Unravelling the proteomic profile of rice meiocytes during early meiosis. *Front. Plant Sci.* 5:356. doi: 10.3389/fpls.2014.00356

Cortijo, S., Wardenaar, R., Colome-Tatche, M., Gilly, A., Etcheverry, M., Labadie, K., et al. (2014). Mapping the epigenetic basis of complex traits. *Science* 343, 1145–1148. doi: 10.1126/science.1248127

Cuacos, M. H., Franklin, F. C., and Heckmann, S. (2015). Atypical centromeres in plants—what they can tell us. *Front. Plant Sci.* 6:913. doi: 10.3389/fpls.2015.00913

De Muyt, A., Zhang, L., Piolot, T., Kleckner, N., Espagne, E., and Zickler, D. (2014). E3 ligase Hei10: a multifaceted structure-based signaling molecule with roles within and beyond meiosis. *Genes Dev.* 28, 1111–1123. doi: 10.1101/gad.240408.114

Deal, R. B., and Henikoff, S. (2010). The INTACT method for cell type–specific gene expression and chromatin profiling in *Arabidopsis thaliana*. *Nat. Protoc.* 6, 56–68. doi: 10.1038/nprot.2010.175

Demirci, S., Dijk Aalt, D. J., Sanchez Perez, G., Aflitos, S. A., Ridder, D., and Peters, S. A. (2017). Distribution, position and genomic characteristics of crossovers in tomato recombinant inbred lines derived from an interspecific cross between *Solanum lycopersicum* and *Solanum pimpinellifolium*. *Plant J.* 89, 554–564. doi: 10.1111/tpj.13406

Dreissig, S., Fuchs, J., Cápal, P., Kettles, N., Byrne, E., and Houben, A. (2015). Measuring meiotic crossovers via multi-locus genotyping of single pollen grains in barley. *PLoS One* 10:e0137677. doi: 10.1371/journal.pone.0137677

Dreissig, S., Fuchs, J., Himmelbach, A., Mascher, M., and Houben, A. (2017a). Sequencing of single pollen nuclei reveals meiotic recombination events at megabase resolution and circumvents segregation distortion caused by postmeiotic processes. *Front. Plant Sci.* 8:1620. doi: 10.3389/fpls.2017.01620

Dreissig, S., Schiml, S., Schindele, P., Weiss, O., Rutten, T., Schubert, V., et al. (2017b). Live-cell CRISPR imaging in plants reveals dynamic telomere movements. *Plant J.* 91, 565–573. doi: 10.1111/tpj.13601

Dubin, M. J., Zhang, P., Meng, D., Remigereau, M. S., Osborne, E. J., Paolo Casale, F., et al. (2015). DNA methylation in *Arabidopsis* has a genetic basis and shows evidence of local adaptation. *eLife* 4:e05255. doi: 10.7554/eLife.05255

Dukowic-Schulze, S., and Chen, C. (2014). The meiotic transcriptome architecture of plants. *Front. Plant Sci.* 5:220. doi: 10.3389/fpls.2014.00220

Dukowic-Schulze, S., Sundararajan, A., Mudge, J., Ramaraj, T., Farmer, A. D., Wang, M., et al. (2014). The transcriptome landscape of early maize meiosis. *BMC Plant Biol.* 14:118. doi: 10.1186/1471-2229-14-118

Dukowic-Schulze, S., Sundararajan, A., Ramaraj, T., Kianian, S., Pawlowski, W. P., Mudge, J., et al. (2016). Novel meiotic miRNAs and indications for a role of PhasiRNAs in meiosis. *Front. Plant Sci.* 7:762. doi: 10.3389/fpls.2016.00762

Duncan, S., Olsson, T. S. G., Hartley, M., Dean, C., and Rosa, S. (2016). A method for detecting single mRNA molecules in *Arabidopsis thaliana*. *Plant Methods* 12:13. doi: 10.1186/s13007-016-0114-x

Emmanuel, E., Yehuda, E., Melamed-Bessudo, C., Avivi-Ragolsky, N., and Levy, A. A. (2006). The role of AtMSH2 in homologous recombination in *Arabidopsis thaliana*. *EMBO Rep.* 7, 100–105. doi: 10.1038/sj.embor.7400577

Fauser, F., Roth, N., Pacher, M., Ilg, G., Sanchez-Fernandez, R., Biesgen, C., et al. (2012). In planta gene targeting. *Proc. Natl. Acad. Sci. U.S.A.* 109, 7535–7540. doi: 10.1073/pnas.1202191109

Ferdous, M., Higgins, J. D., Osman, K., Lambing, C., Roitinger, E., Mechtler, K., et al. (2012). Inter-homolog crossing-over and synapsis in *Arabidopsis* meiosis are dependent on the chromosome axis protein AtASY3. *PLoS Genet.* 8:e1002507. doi: 10.1371/journal.pgen.1002507

Fernandes, J. B., Seguela-Arnaud, M., Larcheveque, C., Lloyd, A. H., and Mercier, R. (2017). Unleashing meiotic crossovers in hybrid plants. *Proc. Natl. Acad. Sci. U.S.A.* 115, 2431–2436. doi: 10.1073/pnas.1713078114

Flórez-Zapata, N. M. V., Reyes-Valdés, M. H., and Martínez, O. (2016). Long non-coding RNAs are major contributors to transcriptome changes in sunflower meiocytes with different recombination rates. *BMC Genomics* 17:490. doi: 10.1186/s12864-016-2776-1

Fu, D., Uauy, C., Blechl, A., and Dubcovsky, J. (2007). RNA interference for wheat functional gene analysis. *Transgenic Res.* 16, 689–701. doi: 10.1007/s11248-007-9150-7

Fukuda, T., Pratto, F., Schimenti, J. C., Turner, J. M. A., Camerini-Otero, R. D., and Höög, C. (2012). Phosphorylation of chromosome core components may serve as axis marks for the status of chromosomal events during mammalian meiosis. *PLoS Genet.* 8:e1002485. doi: 10.1371/journal.pgen.1002485

Girard, C., Chelysheva, L., Choinard, S., Froger, N., Macaisne, N., Lehmemdi, A., et al. (2015). AAA-ATPase FIDGETIN-LIKE 1 and helicase FANCM antagonize meiotic crossovers by distinct mechanisms. *PLoS Genet.* 11:e1005369. doi: 10.1371/journal.pgen.1005369

Girard, C., Crismani, W., Froger, N., Mazel, J., Lemhemdi, A., Horlow, C., et al. (2014). FANCM-associated proteins MHF1 and MHF2, but not the other Fanconi anemia factors, limit meiotic crossovers. *Nucleic Acids Res.* 42, 9087–9095. doi: 10.1093/nar/gku614

Golczyk, H., Massouh, A., and Greiner, S. (2014). Translocations of chromosome end-segments and facultative heterochromatin promote meiotic ring formation in evening primroses. *Plant Cell* 26, 1280–1293. doi: 10.1105/tpc.114.122655

Hammoudi, V., Vlachakis, G., Schranz, M. E., and Van Den Burg, H. A. (2016). Whole-genome duplications followed by tandem duplications drive diversification of the protein modifier SUMO in Angiosperms. *New Phytol.* 211, 172–185. doi: 10.1111/nph.13911

He, Y., Wang, C., Higgins, J. D., Yu, J., Zong, J., Lu, P., et al. (2016). MEIOTIC F-BOX is essential for male meiotic DNA double-strand break repair in rice. *Plant Cell* 28, 1879–1893. doi: 10.1105/tpc.16.00108

He, Y., Wang, M., Dukowic-Schulze, S., Zhou, A., Tiang, C. L., Shilo, S., et al. (2017). Genomic features shaping the landscape of meiotic double-strand-break hotspots in maize. *Proc. Natl. Acad. Sci. U.S.A.* 114, 12231–12236. doi: 10.1073/pnas.1713225114

Heckmann, S., Jankowska, M., Schubert, V., Kumke, K., Ma, W., and Houben, A. (2014). Alternative meiotic chromatid segregation in the holocentric plant *Luzula elegans*. *Nat. Commun.* 5:4979. doi: 10.1038/ncomms5979

Higgins, J. D., Buckling, E. F., Franklin, F. C., and Jones, G. H. (2008). Expression and functional analysis of *AtMUS81* in Arabidopsis meiosis reveals a role in the second pathway of crossing-over. *Plant J.* 54, 152–162. doi: 10.1111/j.1365-313X.2008.03403.x

Higgins, J. D., Perry, R. M., Barakate, A., Ramsay, L., Waugh, R., Halpin, C., et al. (2012). Spatiotemporal asymmetry of the meiotic program underlies the predominantly distal distribution of meiotic crossovers in barley. *Plant Cell* 24, 4096–4109. doi: 10.1105/tpc.112.102483

Higgins, J. D., Sanchez-Moran, E., Armstrong, S. J., Jones, G. H., and Franklin, F. C. (2005). The *Arabidopsis* synaptonemal complex protein *ZYP1* is required

for chromosome synapsis and normal fidelity of crossing over. *Genes Dev.* 19, 2488–2500. doi: 10.1101/gad.354705

Hong, S., Sung, Y., Yu, M., Lee, M., Kleckner, N., and Kim, K. P. (2013). The logic and mechanism of homologous recombination partner choice. *Mol. Cell.* 51, 440–453. doi: 10.1016/j.molcel.2013.08.008

Imin, N., Kerim, T., Weinman, J. J., and Rolfe, B. G. (2006). Low temperature treatment at the young microspore stage induces protein changes in rice anthers. *Mol. Cell. Proteom.* 5, 274–292. doi: 10.1074/mcp.M500242-MCP200

Ingouff, M., Selles, B., Michaud, C., Vu, T. M., Berger, F., Schorn, A. J., et al. (2017). Live-cell analysis of DNA methylation during sexual reproduction in *Arabidopsis* reveals context and sex-specific dynamics controlled by noncanonical RdDM. *Genes Dev.* 31, 72–83. doi: 10.1101/gad.289397.116

Ischebeck, T., Valledor, L., Lyon, D., Gingl, S., Nagler, M., Meijón, M., et al. (2014). Comprehensive Cell-specific protein analysis in early and late pollen development from diploid microsporocytes to pollen tube growth. *Mol. Cell. Proteom.* 13, 295–310. doi: 10.1074/mcp.M113.028100

Jacob, P., Avni, A., and Bendahmane, A. (2018). Translational research: exploring and creating genetic diversity. *Trends Plant Sci.* 23, 42–52. doi: 10.1016/j.tplants.2017.10.002

Jahns, M. T., Vezon, D., Chambon, A., Pereira, L., Falque, M., Martin, O. C., et al. (2014). Crossover localisation is regulated by the neddylation posttranslational regulatory pathway. *PLoS Biol.* 12:e1001930. doi: 10.1371/journal.pbio.1001930

Jones, R. N., and Rees, H. (1982). *B Chromosomes*. London: Academic Press.

Jones, R. N., Viegas, W., and Houben, A. (2008). A century of B chromosomes in plants: so what? *Ann. Bot.* 101, 767–775. doi: 10.1093/aob/mcm167

Kerim, T., Imin, N., Weinman, J. J., and Rolfe, B. G. (2003). Proteome analysis of male gametophyte development in rice anthers. *Proteomics* 3, 738–751. doi: 10.1002/pmic.200300424

Khan, A. O., Simms, V. A., Pike, J. A., Thomas, S. G., and Morgan, N. V. (2017). CRISPR-Cas9 mediated labelling allows for single molecule imaging and resolution. *Sci. Rep.* 7:8450. doi: 10.1038/s41598-017-08493-x

Kleckner, N. (2006). Chiasma formation: chromatin/axis interplay and the role(s) of the synaptonemal complex. *Chromosoma* 115, 175–194. doi: 10.1007/s00412-006-0055-7

Klemme, S., Banaei-Moghaddam, A. M., Macas, J., Wicker, T., Novák, P., and Houben, A. (2013). High-copy sequences reveal distinct evolution of the rye B chromosome. *New Phytol.* 199, 550–558. doi: 10.1111/nph.12289

Kołowerzo-Lubnau, A., Niedojadło, J., Świdziński, M., Bednarska-Kozakiewicz, E., and Smoliński, D. J. (2015). Transcriptional activity in diplotene larch microsporocytes, with emphasis on the diffuse stage. *PLoS One* 10:e0117337. doi: 10.1371/journal.pone.0117337

Komis, G., Novák, D., Ovečka, M., Šamajová, O., and Šamaj, J. (2018). Advances in imaging plant cell dynamics. *Plant Physiol.* 176, 80–93. doi: 10.1104/pp.17.00962

Komis, G., Šamajová, O., Ovečka, M., and Šamaj, J. (2015). Super-resolution microscopy in plant cell imaging. *Trends Plant Sci.* 20, 834–843. doi: 10.1016/j.tplants.2015.08.013

Kousaka, R., and Endo, T. R. (2012). Effect of a rye B chromosome and its segments on homoeologous pairing in hybrids between common wheat and *Aegilops variabilis*. *Genes Genet. Syst.* 87, 1–7. doi: 10.1266/ggs.87.1

Krasileva, K. V., Vasquez-Gross, H. A., Howell, T., Bailey, P., Paraiso, F., Clissold, L., et al. (2017). Uncovering hidden variation in polyploid wheat. *Proc. Natl. Acad. Sci. U.S.A.* 114, E913–E921. doi: 10.1073/pnas.1619268114

Kurihara, D., Mizuta, Y., Sato, Y., and Higashiyama, T. (2015). ClearSee: a rapid optical clearing reagent for whole-plant fluorescence imaging. *Development* 142, 4168–4179. doi: 10.1242/dev.127613

Lam, W. S., Yang, X., and Makaroff, C. A. (2005). Characterization of *Arabidopsis thaliana* SMC1 and SMC3: evidence that AtSMC3 may function beyond chromosome cohesion. *J. Cell Sci.* 118, 3037–3048. doi: 10.1242/jcs.02443

Lambing, C., Franklin, F. C. H., and Wang, C.-J. R. (2017). Understanding and manipulating meiotic recombination in plants. *Plant Physiol.* 173, 1530–1542. doi: 10.1104/pp.16.01530

Lambing, C., Osman, K., Nuntasoontorn, K., West, A., Higgins, J. D., Copenhaver, G. P., et al. (2015). Arabidopsis PCH2 mediates meiotic chromosome remodeling and maturation of crossovers. *PLoS Genet.* 11:e1005372. doi: 10.1371/journal.pgen.1005372

Lange, J., Yamada, S., Tischfield, S. E., Pan, J., Kim, S., Zhu, X., et al. (2016). The landscape of mouse meiotic double-strand break formation, processing, and repair. *Cell* 167, 695–708e16. doi: 10.1016/j.cell.2016.09.035

Lawrence, E. J., Griffin, C. H., and Henderson, I. R. (2017). Modification of meiotic recombination by natural variation in plants. *J. Exp. Bot.* 68, 5471–5483. doi: 10.1093/jxb/erx306

Lawrenson, T., Shorinola, O., Stacey, N., Li, C., Ostergaard, L., Patron, N., et al. (2015). Induction of targeted, heritable mutations in barley and *Brassica oleracea* using RNA-guided Cas9 nuclease. *Genome Biol.* 16:258. doi: 10.1186/s13059-015-0826-7

Lee, D. H., Kao, Y. H., Ku, J. C., Lin, C. Y., Meeley, R., Jan, Y. S., et al. (2015). The axial element protein DESYNAPTIC2 mediates meiotic double-strand break formation and synaptonemal complex assembly in maize. *Plant Cell* 27, 2516–2529. doi: 10.1105/tpc.15.00434

Lee, W. S., Hammond-Kosack, K. E., and Kanyuka, K. (2012). Barley stripe mosaic virus-mediated tools for investigating gene function in cereal plants and their pathogens: virus-induced gene silencing, host-mediated gene silencing, and virus-mediated overexpression of heterologous protein. *Plant Physiol.* 160, 582–590. doi: 10.1104/pp.112.203489

Li, X., Li, L., and Yan, J. (2015). Dissecting meiotic recombination based on tetrad analysis by single-microspore sequencing in maize. *Nat. Commun.* 6:6648. doi: 10.1038/ncomms7648

Li, X., Ye, J., Ma, H., and Lu, P. (2018). Proteomic analysis of lysine acetylation provides strong evidence for involvement of acetylated proteins in plant meiosis and tapetum function. *Plant J.* 93, 142–154. doi: 10.1111/tpj.13766

Littlejohn, G. R., Mansfield, J. C., Christmas, J. T., Witterick, E., Fricker, M. D., Grant, M. R., et al. (2014). An update: improvements in imaging perfluorocarbon-mounted plant leaves with implications for studies of plant pathology, physiology, development and cell biology. *Front. Plant Sci.* 5:140. doi: 10.3389/fpls.2014.00140

Liu, H., and Nonomura, K.-I. (2016). A wide reprogramming of histone H3 modifications during male meiosis I in rice is dependent on the Argonaute protein MEL1. *J. Cell Sci.* 129, 3553–3561. doi: 10.1242/jcs.184937

Liu, M., Shi, S., Zhang, S., Xu, P., Lai, J., Liu, Y., et al. (2014). SUMO E3 ligase AtMMS21 is required for normal meiosis and gametophyte development in *Arabidopsis*. *BMC Plant Biol.* 14:153. doi: 10.1186/1471-2229-14-153

Lu, D., Ni, W., Stanley, B. A., and Ma, H. (2016). Proteomics and transcriptomics analyses of Arabidopsis floral buds uncover important functions of ARABIDOPSIS SKP1-LIKE1. *BMC Plant Biol.* 16:61. doi: 10.1186/s12870-015-0571-9

Lu, P., Han, X., Qi, J., Yang, J., Wijeratne, A. J., Li, T., et al. (2012). Analysis of *Arabidopsis* genome-wide variations before and after meiosis and meiotic recombination by resequencing Landsberg *erecta* and all four products of a single meiosis. *Genome Res.* 22, 508–518. doi: 10.1101/gr.127522.111

Luo, Q., Li, Y., Shen, Y., and Cheng, Z. (2014). Ten years of gene discovery for meiotic event control in rice. *J. Genet. Genomics* 41, 125–137. doi: 10.1016/j.jgg.2014.02.002

Ma, P., and Schultz, R. M. (2013). Histone deacetylase 2 (HDAC2) regulates chromosome segregation and kinetochore function via H4K16 deacetylation during oocyte maturation in mouse. *PLoS Genet.* 9:e1003377. doi: 10.1371/journal.pgen.1003377

Ma, W., Gabriel, T. S., Martis, M. M., Gursinsky, T., Schubert, V., Vrána, J., et al. (2017). Rye B chromosomes encode a functional Argonaute-like protein with in vitro slicer activities similar to its A chromosome paralog. *New Phytol.* 213, 916–928. doi: 10.1111/nph.14110

Mancera, E., Bourgon, R., Brozzi, A., Huber, W., and Steinmetz, L. M. (2008). High-resolution mapping of meiotic crossovers and non-crossovers in yeast. *Nature* 454, 479–485. doi: 10.1038/nature07135

Marques, A., and Pedrosa-Harand, A. (2016). Holocentromere identity: from the typical mitotic linear structure to the great plasticity of meiotic holocentromeres. *Chromosoma* 125, 669–681. doi: 10.1007/s00412-016-0612-7

Martis, M. M., Klemme, S., Banaei-Moghaddam, A. M., Blattner, F. R., Macas, J., Schmutzer, T., et al. (2012). Selfish supernumerary chromosome reveals its

origin as a mosaic of host genome and organellar sequences. *Proc. Natl. Acad. Sci. U.S.A.* 109, 13343–13346. doi: 10.1073/pnas.1204237109

Melamed-Bessudo, C., Yehuda, E., Stuitje, A. R., and Levy, A. A. (2005). A new seed-based assay for meiotic recombination in *Arabidopsis thaliana*. *Plant J.* 43, 458–466. doi: 10.1111/j.1365-313X.2005.02466.x

Mercier, R., Mézard, C., Jenczewski, E., Macaisne, N., and Grelon, M. (2015). The molecular biology of meiosis in plants. *Annu. Rev. Plant Biol.* 66, 297–327. doi: 10.1146/annurev-arplant-050213-035923

Mursalimov, S., and Deineko, E. (2017). Cytomixis in plants: facts and doubts. *Protoplasma* 255, 719–731. doi: 10.1007/s00709-017-1188-7

Mursalimov, S., Permyakova, N., Deineko, E., Houben, A., and Demidov, D. (2015). Cytomixis doesn't induce obvious changes in chromatin modifications and programmed cell death in tobacco male meiocytes. *Front. Plant Sci.* 6:846. doi: 10.3389/fpls.2015.00846

Musielak, T. J., Slane, D., Liebig, C., and Bayer, M. (2016). A versatile optical clearing protocol for deep tissue imaging of fluorescent proteins in *Arabidopsis thaliana*. *PLoS One* 11:e0161107. doi: 10.1371/journal.pone.0161107

Nagaki, K., Yamaji, N., and Murata, M. (2017). ePro-ClearSee: a simple immunohistochemical method that does not require sectioning of plant samples. *Sci. Rep.* 7:42203. doi: 10.1038/srep42203

Nan, G.-L., Ronceret, A., Wang, R. C., Fernandes, J. F., Cande, W. Z., and Walbot, V. (2011). Global transcriptome analysis of two ameiotic1alleles in maize anthers: defining steps in meiotic entry and progression through prophase I. *BMC Plant Biol.* 11:120. doi: 10.1186/1471-2229-11-120

Nannas, N. J., Higgins, D. M., and Dawe, R. K. (2016). Anaphase asymmetry and dynamic repositioning of the division plane during maize meiosis. *J. Cell Sci.* 129, 4014–4024. doi: 10.1242/jcs.194860

Neale, M. J., Pan, J., and Keeney, S. (2005). Endonucleolytic processing of covalent protein-linked DNA double-strand breaks. *Nature* 436, 1053–1057. doi: 10.1038/nature03872

Nonomura, K., Nakano, M., Eiguchi, M., Suzuki, T., and Kurata, N. (2006). PAIR2 is essential for homologous chromosome synapsis in rice meiosis I. *J. Cell Sci.* 119, 217–225. doi: 10.1242/jcs.02736

Nonomura, K.-I., Morohoshi, A., Nakano, M., Eiguchi, M., Miyao, A., Hirochika, H., et al. (2007). A germ cell–specific gene of the ARGONAUTE family is essential for the progression of premeiotic mitosis and meiosis during sporogenesis in rice. *Plant Cell* 19, 2583–2594. doi: 10.1105/tpc.107.053199

Nottke, A. C., Kim, H.-M., and Colaiácovo, M. P. (2017). "Wrestling with chromosomes: the roles of SUMO during meiosis," in *SUMO Regulation of Cellular Processes*, ed. V. G. Wilson (Cham: Springer International Publishing), 185–196. doi: 10.1007/978-3-319-50044-7_11

Oliver, C., Pradillo, M., Jover-Gil, S., Cuñado, N., Ponce, M. R., and Santos, J. L. (2017). Loss of function of Arabidopsis microRNA-machinery genes impairs fertility, and has effects on homologous recombination and meiotic chromatin dynamics. *Sci. Rep.* 7:9280. doi: 10.1038/s41598-017-07702-x

Oliver, C., Santos, J., and Pradillo, M. (2014). On the role of some ARGONAUTE proteins in meiosis and DNA repair in *Arabidopsis thaliana*. *Front. Plant Sci.* 5:177. doi: 10.3389/fpls.2014.00177

O'Malley, R. C., and Ecker, J. R. (2012). Epiallelic variation in *Arabidopsis thaliana*. *Cold Spring Harb. Symp. Quant. Biol.* 77, 135–145. doi: 10.1101/sqb.2012.77.014571

Ortiz, M., Puertas, M. J., Jiménez, M. M., Romera, F., and Jones, R. N. (1996). B-chromosomes in inbred lines of rye (*Secale cereale* L.). *Genetica* 97, 65–72. doi: 10.1007/BF00132582

Osman, K., Higgins, J. D., Sanchez-Moran, E., Armstrong, S. J., and Franklin, F. C. H. (2011). Pathways to meiotic recombination in *Arabidopsis thaliana*. *New Phytol.* 190, 523–544. doi: 10.1111/j.1469-8137.2011.03665.x

Osman, K., Yang, J., Roitinger, E., Lambing, C., Heckmann, S., Howell, E., et al. (2018). Affinity proteomics reveals extensive phosphorylation of the Brassica chromosome axis protein ASY1 and a network of associated proteins at prophase I of meiosis. *Plant J.* 93, 17–33. doi: 10.1111/tpj.13752

Pan, J., Sasaki, M., Kniewel, R., Murakami, H., Blitzblau, H. G., Tischfield, S. E., et al. (2011). A hierarchical combination of factors shapes the genome-wide topography of yeast meiotic recombination initiation. *Cell* 144, 719–731. doi: 10.1016/j.cell.2011.02.009

Panizza, S., Mendoza, M. A., Berlinger, M., Huang, L., Nicolas, A., Shirahige, K., et al. (2011). Spo11-accessory proteins link double-strand break sites to the chromosome axis in early meiotic recombination. *Cell* 146, 372–383. doi: 10.1016/j.cell.2011.07.003

Penedos, A., Johnson, A. L., Strong, E., Goldman, A. S., Carballo, J. A., and Cha, R. S. (2015). Essential and checkpoint functions of budding yeast ATM and ATR during meiotic prophase are facilitated by differential phosphorylation of a meiotic adaptor protein, Hop1. *PLoS One* 10:e0134297. doi: 10.1371/journal.pone.0134297

Perrella, G., Consiglio, M. F., Aiese-Cigliano, R., Cremona, G., Sanchez-Moran, E., Barra, L., et al. (2010). Histone hyperacetylation affects meiotic recombination and chromosome segregation in Arabidopsis. *Plant J.* 62, 796–806. doi: 10.1111/j.1365-313X.2010.04191.x

Phillips, D., Mikhailova, E. I., Timofejeva, L., Mitchell, J. L., Osina, O., Sosnikhina, S. P., et al. (2008). Dissecting meiosis of rye using translational proteomics. *Ann. Bot.* 101, 873–880. doi: 10.1093/aob/mcm202

Phillips, D., Wnetrzak, J., Nibau, C., Barakate, A., Ramsay, L., Wright, F., et al. (2013). Quantitative high resolution mapping of HvMLH3 foci in barley pachytene nuclei reveals a strong distal bias and weak interference. *J. Exp. Bot.* 64, 2139–2154. doi: 10.1093/jxb/ert079

Rao, H. B., Qiao, H., Bhatt, S. K., Bailey, L. R. J., Tran, H. D., Bourne, S. L., et al. (2017). A SUMO-ubiquitin relay recruits proteasomes to chromosome axes to regulate meiotic recombination. *Science* 355, 403–407. doi: 10.1126/science.aaf6407

Rauwolf, U., Greiner, S., Mráèek, J., Rauwolf, M., Golczyk, H., Mohler, V., et al. (2011). Uncoupling of sexual reproduction from homologous recombination in homozygous *Oenothera* species. *Heredity* 107, 87–94. doi: 10.1038/hdy.2010.171

Robert, T., Nore, A., Brun, C., Maffre, C., Crimi, B., Bourbon, H. M., et al. (2016). The TopoVIB-Like protein family is required for meiotic DNA double-strand break formation. *Science* 351, 943–949. doi: 10.1126/science.aad5309

Roitinger, E., Hofer, M., Köcher, T., Pichler, P., Novatchkova, M., Yang, J., et al. (2015). Quantitative phosphoproteomics of the ataxia telangiectasia-mutated (ATM) and ataxia telangiectasia-mutated and Rad3-related (ATR) dependent DNA damage response in *Arabidopsis thaliana*. *Mol. Cell. Proteom.* 14, 556–571. doi: 10.1074/mcp.M114.040352

Rytz, T. C., Miller, M. J., and Vierstra, R. D. (2016). "Purification of SUMO conjugates from Arabidopsis for mass spectrometry analysis," in *SUMO: Methods and Protocols*, ed. M. S. Rodriguez (New York, NY: Springer), 257–281. doi: 10.1007/978-1-4939-6358-4_18

Saintenac, C., Falque, M., Martin, O. C., Paux, E., Feuillet, C., and Sourdille, P. (2009). Detailed recombination studies along chromosome 3B provide new insights on crossover distribution in wheat (*Triticum aestivum*L.). *Genetics* 181, 393–403. doi: 10.1534/genetics.108.097469

Sanchez-Moran, E., and Armstrong, S. J. (2014). Meiotic chromosome synapsis and recombination in *Arabidopsis thaliana*: new ways of integrating cytological and molecular approaches. *Chromosome Res.* 22, 179–190. doi: 10.1007/s10577-014-9426-8

Sánchez-Morán, E., Mercier, R., Higgins, J. D., Armstrong, S. J., Jones, G. H., and Franklin, F. C. H. (2005). A strategy to investigate the plant meiotic proteome. *Cytogenet. Genome Res.* 109, 181–189. doi: 10.1159/000082398

Sarno, R., Vicq, Y., Uematsu, N., Luka, M., Lapierre, C., Carroll, D., et al. (2017). Programming sites of meiotic crossovers using Spo11 fusion proteins. *Nucleic Acids Res.* 45:e164. doi: 10.1093/nar/gkx739

Schubert, V. (2017). Super-resolution microscopy–applications in plant cell research. *Front. Plant Sci.* 8:531. doi: 10.3389/fpls.2017.00531

Schubert, V., and Weisshart, K. (2015). Abundance and distribution of RNA polymerase II in *Arabidopsis* interphase nuclei. *J. Exp. Bot.* 66, 1687–1698. doi: 10.1093/jxb/erv091

Seguela-Arnaud, M., Crismani, W., Larcheveque, C., Mazel, J., Froger, N., Choinard, S., et al. (2015). Multiple mechanisms limit meiotic crossovers: TOP3alpha and two BLM homologs antagonize crossovers in parallel to FANCM. *Proc. Natl. Acad. Sci. U.S.A.* 112, 4713–4718. doi: 10.1073/pnas.1423107112

Serra, H., Lambing, C., Griffin, C. H., Topp, S. D., Nageswaran, D. C., Underwood, C. J., et al. (2018). Massive crossover elevation via combination of *HEI10* and *recq4a recq4b* during *Arabidopsis* meiosis. *Proc. Natl. Acad. Sci. U.S.A.* 115, 2437–2442. doi: 10.1073/pnas.1713071115

Sheehan, M. J., and Pawlowski, W. P. (2009). Live imaging of rapid chromosome movements in meiotic prophase I in maize. *Proc. Natl. Acad. Sci. U.S.A.* 106, 20989–20994. doi: 10.1073/pnas.0906498106

Shinohara, A., Ogawa, H., and Ogawa, T. (1992). Rad51 protein involved in repair and recombination in *S. cerevisiae* is a RecA-like protein. *Cell* 69, 457–470. doi: 10.1016/0092-8674(92)90447-K

Si, W., Yuan, Y., Huang, J., Zhang, X., Zhang, Y., Zhang, Y., et al. (2015). Widely distributed hot and cold spots in meiotic recombination as shown by the sequencing of rice F2 plants. *New Phytol.* 206, 1491–1502. doi: 10.1111/nph.13319

Singh, M., Goel, S., Meeley, R. B., Dantec, C., Parrinello, H., Michaud, C., et al. (2011). Production of viable gametes without meiosis in maize deficient for an ARGONAUTE protein. *Plant Cell* 23, 443–458. doi: 10.1105/tpc.110.079020

Stack, S. M., and Soulliere, D. L. (1984). The relation between synapsis and Chiasma formation in *Rhoeo spathacea*. *Chromosoma* 90, 72–83. doi: 10.1007/BF00352281

Sun, Y., Ambrose, J. H., Haughey, B. S., Webster, T. D., Pierrie, S. N., Munoz, D. F., et al. (2012). Deep genome-wide measurement of meiotic gene conversion using tetrad analysis in *Arabidopsis thaliana*. *PLoS Genet.* 8:e1002968. doi: 10.1371/journal.pgen.1002968

Sun, Y., Li, J., and Xia, L. (2016). Precise genome modification via sequence-specific nucleases-mediated gene targeting for crop improvement. *Front. Plant Sci.* 7:1928. doi: 10.3389/fpls.2016.01928

The 1001 Genomes Consortium (2016). 1,135 genomes reveal the global pattern of polymorphism in *Arabidopsis thaliana*. *Cell* 166, 481–491. doi: 10.1016/j.cell.2016.05.063

Underwood, C. J., Choi, K., Lambing, C., Zhao, X., Serra, H., Borges, F., et al. (2018). Epigenetic activation of meiotic recombination near *Arabidopsis thaliana* centromeres via loss of H3K9me2 and non-CG DNA methylation. *Genome Res.* 28, 519–531. doi: 10.1101/gr.227116.117

van den Berg, I. M., Eleveld, C., Van Der Hoeven, M., Birnie, E., Steegers, E. A. P., Galjaard, R. J., et al. (2011). Defective deacetylation of histone 4 K12 in human oocytes is associated with advanced maternal age and chromosome misalignment. *Hum. Reprod.* 26, 1181–1190. doi: 10.1093/humrep/der030

Vrielynck, N., Chambon, A., Vezon, D., Pereira, L., Chelysheva, L., De Muyt, A., et al. (2016). A DNA topoisomerase VI-like complex initiates meiotic recombination. *Science* 351, 939–943. doi: 10.1126/science.aad5196

Walker, J., Gao, H., Zhang, J., Aldridge, B., Vickers, M., Higgins, J. D., et al. (2018). Sexual-lineage-specific DNA methylation regulates meiosis in *Arabidopsis*. *Nat. Genet.* 50, 130–137. doi: 10.1038/s41588-017-0008-5

Wang, D., Adams, C. M., Fernandes, J. F., Egger, R. L., and Walbot, V. (2012). A low molecular weight proteome comparison of fertile and male sterile 8 anthers of Zea mays. *Plant Biotechnol. J.* 10, 925–935. doi: 10.1111/j.1467-7652.2012.00721.x

Wang, K., Wang, M., Tang, D., Shen, Y., Miao, C., Hu, Q., et al. (2012). The role of rice HEI10 in the formation of meiotic crossovers. *PLoS Genet.* 8:e1002809. doi: 10.1371/journal.pgen.1002809

Wang, K., Wang, M., Tang, D., Shen, Y., Qin, B., Li, M., et al. (2011). PAIR3, an axis-associated protein, is essential for the recruitment of recombination elements onto meiotic chromosomes in rice. *Mol. Biol. Cell* 22, 12–19. doi: 10.1091/mbc.E10-08-0667

Wang, M., Wang, K., Tang, D., Wei, C., Li, M., Shen, Y., et al. (2010). The central element protein ZEP1 of the synaptonemal complex regulates the number of crossovers during meiosis in rice. *Plant Cell* 22, 417–430. doi: 10.1105/tpc.109.070789

Wang, W., Mauleon, R., Hu, Z., Chebotarov, D., Tai, S., Wu, Z., et al. (2018). Genomic variation in 3,010 diverse accessions of Asian cultivated rice. *Nature* 557, 43–49. doi: 10.1038/s41586-018-0063-9

Wang, Y., Cheng, X., Shan, Q., Zhang, Y., Liu, J., Gao, C., et al. (2014). Simultaneous editing of three homoeoalleles in hexaploid bread wheat confers heritable resistance to powdery mildew. *Nat. Biotechnol.* 32, 947–951. doi: 10.1038/nbt.2969

Weigel, D. (2012). Natural variation in Arabidopsis: from molecular genetics to ecological genomics. *Plant Physiol.* 158, 2–22. doi: 10.1104/pp.111.189845

Weigel, D., and Colot, V. (2012). Epialleles in plant evolution. *Genome Biol.* 13:249. doi: 10.1186/gb-2012-13-10-249

Wu, Y., Yang, L., Yu, M., and Wang, J. (2017). Identification and expression analysis of microRNAs during ovule development in rice (*Oryza sativa*) by deep sequencing. *Plant Cell Rep.* 36, 1815–1827. doi: 10.1007/s00299-017-2196-y

Yamada, S., Ohta, K., and Yamada, T. (2013). Acetylated histone H3K9 is associated with meiotic recombination hotspots, and plays a role in recombination redundantly with other factors including the H3K4 methylase Set1 in fission yeast. *Nucleic Acids Res.* 41, 3504–3517. doi: 10.1093/nar/gkt049

Yang, H., Lu, P., Wang, Y., and Ma, H. (2011). The transcriptome landscape of Arabidopsis male meiocytes from high-throughput sequencing: the complexity and evolution of the meiotic process. *Plant J.* 65, 503–516. doi: 10.1111/j.1365-313X.2010.04439.x

Yang, L., Wu, Y., Wang, W., Mao, B., Zhao, B., and Wang, J. (2017). Genetic subtraction profiling identifies candidate miRNAs involved in rice female gametophyte abortion. *G3* 7, 2281–2293. doi: 10.1534/g3.117.040808

Yang, L., Wu, Y., Yu, M., Mao, B., Zhao, B., and Wang, J. (2016). Genome-wide transcriptome analysis of female-sterile rice ovule shed light on its abortive mechanism. *Planta* 244, 1011–1028. doi: 10.1007/s00425-016-2563-x

Yang, M., and McLoud, J. (2012). The conserved function of Skp1 in meiosis. *Front. Genet.* 3:179. doi: 10.3389/fgene.2012.00179

Yant, L., Hollister, J. D., Wright, K. M., Arnold, B. J., Higgins, J. D., Franklin, F. C. H., et al. (2013). Meiotic adaptation to genome duplication in *Arabidopsis arenosa*. *Curr. Biol.* 23, 2151–2156. doi: 10.1016/j.cub.2013.08.059

Yao, H., and Schnable, P. S. (2005). Cis -effects on meiotic recombination across distinct a1-sh2 intervals in a common zea genetic background. *Genetics* 170, 1929–1944. doi: 10.1534/genetics.104.034454

Ye, J., Zhang, Z., Long, H., Zhang, Z., Hong, Y., Zhang, X., et al. (2015). Proteomic and phosphoproteomic analyses reveal extensive phosphorylation of regulatory proteins in developing rice anthers. *Plant J.* 84, 527–544. doi: 10.1111/tpj.13019

Yelina, N. E., Choi, K., Chelysheva, L., Macaulay, M., De Snoo, B., Wijnker, E., et al. (2012). Epigenetic remodeling of meiotic crossover frequency in *Arabidopsis thaliana* DNA methyltransferase mutants. *PLoS Genet.* 8:e1002844. doi: 10.1371/journal.pgen.1002844

Yelina, N. E., Lambing, C., Hardcastle, T. J., Zhao, X., Santos, B., and Henderson, I. R. (2015). DNA methylation epigenetically silences crossover hot spots and controls chromosomal domains of meiotic recombination in *Arabidopsis*. *Genes Dev.* 29, 2183–2202. doi: 10.1101/gad.270876.115

Yu, H.-G., Hiatt, E. N., Chan, A., Sweeney, M., and Dawe, R. K. (1997). Neocentromere-mediated chromosome movement in maize. *J. Cell Biol.* 139, 831–840. doi: 10.1083/jcb.139.4.831

Yu, H.-G., Muszynski, M. G., and Kelly Dawe, R. (1999). The maize homologue of the cell cycle checkpoint protein MAD2 reveals kinetochore substructure and contrasting mitotic and meiotic localization patterns. *J. Cell Biol.* 145, 425–435. doi: 10.1083/jcb.145.3.425

Zhang, B., Xu, M., Bian, S., Hou, L., Tang, D., Li, Y., et al. (2015). Global identification of genes specific for rice meiosis. *PLoS One* 10:e0137399. doi: 10.1371/journal.pone.0137399

Zhang, F., Tang, D., Shen, Y., Xue, Z., Shi, W., Ren, L., et al. (2017). The F-box protein ZYGO1 mediates bouquet formation to promote homologous pairing, synapsis, and recombination in rice meiosis. *Plant Cell* 29, 2597–2609. doi: 10.1105/tpc.17.00287

Zhang, P., Zhang, Y., Sun, L., Sinumporn, S., Yang, Z., Sun, B., et al. (2017). The rice AAA-ATPase OsFIGNL1 is essential for male meiosis. *Front. Plant Sci.* 8:1639. doi: 10.3389/fpls.2017.01639

Zhang, H., Egger, R. L., Kelliher, T., Morrow, D., Fernandes, J., Nan, G.-L., et al. (2014a). Transcriptomes and proteomes define gene expression progression in pre-meiotic maize anthers. *G3* 4, 993–1010. doi: 10.1534/g3.113.009738

Zhang, L., Liang, Z., Hutchinson, J., and Kleckner, N. (2014b). Crossover patterning by the beam-film model: analysis and implications. *PLoS Genet.* 10:e1004042. doi: 10.1371/journal.pgen.1004042

Zhang, L., Wang, S., Yin, S., Hong, S., Kim, K. P., and Kleckner, N. (2014c). Topoisomerase II mediates meiotic crossover interference. *Nature* 511, 551–556. doi: 10.1038/nature13442

Zhang, S.-G., Yang, W.-H., Qi, Y.-C., Li, M.-X., Wang, J.-H., Sun, X.-M., et al. (2008). Development of male gametophyte of *Larix leptolepis* Gord. with emphasis on diffuse stage of meiosis. *Plant Cell Rep.* 27:1687. doi: 10.1007/s00299-008-0579-9

Zhu, Y., Yu, Y., Cheng, K., Ouyang, Y., Wang, J., Gong, L., et al. (2017). Processes underlying a reproductive barrier in indica-japonica rice hybrids revealed by transcriptome analysis. *Plant Physiol.* 174, 1683–1696. doi: 10.1104/pp.17.00093

Ziolkowski, P. A., Berchowitz, L. E., Lambing, C., Yelina, N. E., Zhao, X., Kelly, K. A., et al. (2015). Juxtaposition of heterozygous and homozygous regions causes reciprocal crossover remodelling via interference during Arabidopsis meiosis. *eLife* 4:e03708. doi: 10.7554/eLife.03708

Ziolkowski, P. A., Underwood, C. J., Lambing, C., Martinez-Garcia, M., Lawrence, E. J., Ziolkowska, L., et al. (2017). Natural variation and dosage of the HEI10 meiotic E3 ligase control *Arabidopsis* crossover recombination. *Genes Dev.* 31, 306–317. doi: 10.1101/gad.295501.116

Zmienko, A., Samelak-Czajka, A., Kozlowski, P., Szymanska, M., and Figlerowicz, M. (2016). *Arabidopsis thaliana* population analysis reveals high plasticity of the genomic region spanning *MSH2*, *AT3G18530* and *AT3G18535* genes and provides evidence for NAHR-driven recurrent CNV events occurring in this location. *BMC Genomics* 17:893. doi: 10.1186/s12864-016-3221-1

Conflict of Interest Statement: The authors declare that the research was conducted in the absence of any commercial or financial relationships that could be construed as a potential conflict of interest.

The reviewer AH declared a shared affiliation, though no other collaboration, with one of the authors SH to the handling Editor.

frontiers in Plant Science

ORIGINAL RESEARCH
published: 19 September 2018
doi: 10.3389/fpls.2018.01339

The HEM Lines: A New Library of Homozygous *Arabidopsis thaliana* EMS Mutants and its Potential to Detect Meiotic Phenotypes

*Laia Capilla-Perez, Victor Solier, Virginie Portemer, Aurelie Chambon, Aurelie Hurel, Alexia Guillebaux, Daniel Vezon, Laurence Cromer, Mathilde Grelon and Raphael Mercier**

CNRS, Institut Jean-Pierre Bourgin, INRA, AgroParisTech, Université Paris-Saclay, Versailles, France

Genetic screens have been crucial for deciphering many important biological processes, including meiosis. In *Arabidopsis thaliana*, previous forward screens have likely identified almost all the meiotic genes that when mutated lead to a pronounced decrease in fertility. However, the increasing number of genes identified in reverse genetics studies that play crucial roles in meiosis, but do not exhibit strong phenotypes when mutated, suggests that there are still many genes with meiotic function waiting to be discovered. In this study, we produced 897 *A. thaliana* homozygous mutant lines using Ethyl Methyl Sulfonate (EMS) mutagenesis followed by either single seed descent or haploid doubling. Whole genome sequencing of a subset of lines showed an average of 696 homozygous mutations per line, 195 of which (28%) modify a protein sequence. To test the power of this library, we carried out a forward screen looking for meiotic defects by observing chromosomes at metaphase I of male meiosis. Among the 649 lines analyzed, we identified 43 lines with meiotic defects. Of these, 21 lines had an obvious candidate causal mutation, namely a STOP or splicing site mutation in a gene previously shown to play a role in meiosis (*ATM, MLH3, MLH1, MER3, HEI10, FLIP, ASY4, FLIP, PRD2, REC8, FANCL,* and *PSS1*). Interestingly, this was the first time that six of these genes were identified in a forward screen in *Arabidopsis* (*MLH3, MLH1, SGO1, PSS1*, *FANCL,* and *ASY4*). These results illustrate the potential of this mutant population for screening for any qualitative or quantitative phenotype. Thus, this new mutant library is a powerful tool for functional genomics in *A. thaliana*. The HEM (Homozygote EMS Mutants) lines are available at the Versailles *Arabidopsis* stock center.

Keywords: forward screens, mutagenesis, meiosis, EMS, mutant collection, *Arabidopsis*

OPEN ACCESS

Edited by:
Changbin Chen,
University of Minnesota Twin Cities, United States

Reviewed by:
Junhua Li,
Henan Normal University, China
Bradlee Nelms,
Stanford University, United States

***Correspondence:**
Raphael Mercier
raphael.mercier@inra.fr

Specialty section:
This article was submitted to Plant Cell Biology, a section of the journal Frontiers in Plant Science

Received: *28 June 2018*
Accepted: *24 August 2018*
Published: *19 September 2018*

Citation:
Capilla-Perez L, Solier V, Portemer V, Chambon A, Hurel A, Guillebaux A, Vezon D, Cromer L, Grelon M and Mercier R (2018) The HEM Lines: A New Library of Homozygous Arabidopsis thaliana EMS Mutants and its Potential to Detect Meiotic Phenotypes. Front. Plant Sci. 9:1339. doi: 10.3389/fpls.2018.01339

INTRODUCTION

Genetic screens have improved our knowledge of the genetic basis of biological processes. However, to identify all the genes involved in a biological pathway screening strategies must be sensitive, specific and feasible. In this context, the two classic approaches, which are still widely used, are forward and reverse genetics. On one hand, forward genetics can be used to decipher specific pathways without *a priori* knowledge of the genes involved. This is achieved by screening the

phenotype of a population with random mutations throughout the genome, which alter gene function and thus give an identifiable phenotype. On the other hand, the principle of reverse genetics is to test the function of a specific candidate gene by analysing the consequences of its disruption on the process of interest.

Different types of chemical, biological and physical mutagens have been used to generate mutant collections for forward and reverse genetics (reviewed in Page and Grossniklaus, 2002; Nawaz and Shu, 2014). Ethyl Methyl Sulfonate (EMS) is the most common mutagen as it is very easy to use and can produce very high mutagenesis rates compared with other methods (reviewed in Sikora et al., 2011). EMS has an alkylating effect that mainly induces point mutations with G/C to T/A transitions, as seen for example in rice (Till et al., 2007), maize (Till et al., 2004), and *Arabidopsis* (McCallum et al., 2000; Martín et al., 2009). Point mutations have the potential to not only produce loss-of-function mutants but also weak or separation-of-function alleles (e.g., Séguéla-Arnaud et al., 2015). Thus analysis of these mutants can be used to functionally characterize essential genes.

Meiosis is a specialized cell division where two rounds of chromosome segregation follow one round of DNA replication leading to the production of haploid cells that are essential for sexual reproduction. The list of genes described to be involved in meiosis has steadily increased as a result of various genetic screens (see Mercier et al., 2015 and references therein, 2015). *Arabidopsis* first emerged as a model in the late 90s when T-DNA insertion lines with meiotic defects were first characterized (Peirson et al., 1997). Subsequently, large-scale forward screens in *Arabidopsis* (e.g., De Muyt et al., 2009) identified meiotic mutants by looking for mutant lines with reduced fertility as a result of meiotic defects. This strategy led to the description of a number of genes involved in meiosis, however, it was also biased toward genes whose disruption produces very pronounced meiotic defects. More recently, meiotic genes were identified in suppressor screens, for example by observing fertility restoration in *zmm* mutants (Crismani et al., 2012; Girard et al., 2014; Séguéla-Arnaud et al., 2015; Fernandes et al., 2018). The phenotypes of these mutants consist of an increase in crossover number, which is not easily observable at a macroscopic level, preventing identification in forward screens.

In parallel, an increasing number of important meiotic genes have been identified from reverse genetics screens such as *MLH1* (Dion et al., 2007), *MLH3* (Jackson et al., 2006), *SGO1* (Cromer et al., 2013; Zamariola et al., 2013), *PSS1* (Duroc et al., 2014), *PCH2* (Lambing et al., 2015), and *RPA1* (Osman et al., 2009), among others. These mutants are characterized by subtle fertility defects and have not yet been identified in any forward screens. This therefore suggests that a number of meiotic genes, whose inactivation leads to subtle meiotic defects, could have been missed in previous forward screens based on reduced fertility observable at a macroscopic level.

Here, we produced a total of 897 homozygous *Arabidopsis thaliana* EMS mutant lines with >170,000 mutations leading to changes in protein sequences and identified meiotic defects in 43 lines. These results demonstrate the usefulness of these HEM (Homozygote EMS Mutant) lines that can be used to detect either qualitative or quantitative phenotypes. Thus this new mutant collection is a very useful resource for functional genomics and applied research in *A. thaliana.*

RESULTS

Generation of the HEM Lines: Two Collections of Homozygous *Arabidopsis thaliana* EMS Mutants

To produce the HEM lines we generated two collections of almost fully homozygous lines using two different strategies: (i) single seed descent (SSD) and (ii) doubled haploids (DH) (**Figures 1A,B**).

For the SSD subset we applied EMS to wild type Col-0 seeds and produced four successive generations by self-fertilization using a single seed in each generation (SSD) (**Figure 1A**). Six parallel rounds of mutagenesis followed by SSD were carried out, giving a total of 698 independent mutant lines (**Table 1**). With this approach, we expected to obtain a level of homozygosity of 87% in the 4th generation (M4) that was screened (see below). The M5 seeds are available at the Versailles *Arabidopsis* stock center.

For the second population, the strategy was to generate homozygous mutagenized lines by haploidization followed by genome doubling (Doubled haploid, DH) (**Figure 1B**). We applied EMS to Col-0 seeds with a homozygous mutation in the *GALBRA-1* gene (*GL1)*, which is characterized by the absence of trichomes (Marks and Feldmann, 1989). The first generation plants (M1) were selfed and the next generation (M2) was crossed to a haploid inducing strain (the CENH3 Tailswap line) to obtain haploid descendants (Ravi and Chan, 2010). M3 haploid plants were visually identified due to the absence of trichomes conferred by the *gl1* mutation (Portemer et al., 2015) and reproduced by self-fertilization, which spontaneously produced diploid seeds (M4). Using this approach, we expected to obtain virtually completely homozygous mutant lines. Finally, M4 seeds were propagated to obtain a total of 199 M5 independent lines (**Figure1B**).

Analysis of Mutation Frequencies in the HEM Lines

To estimate the number of mutations in the HEM populations, we sequenced 47 mutant lines using Illumina: 25 SSD lines (series 10) and 22 DH lines. Among these, 41 lines showed a meiotic defect (see section below) and 6 lines without meiotic defects were randomly chosen among the DH lines.

The HEM populations showed a total mean number of 897 mutations per line, ranging from 500 to 1,500, with a normal distribution (**Figure 2A**). Of these 897 mutations, 99% were G > A or C > T transitions. When this value was compared for each of the subsets obtained, the SSD lines had more mutations (1,003 mutations per line) than the DHs (with 776 mutations per line; *T*-test, $p < 0.05$*; **Figure 2B** and **Table 2**).

The percentage of fixed mutations, was different for each of the subsets due to the different approaches used (SSD and DH;

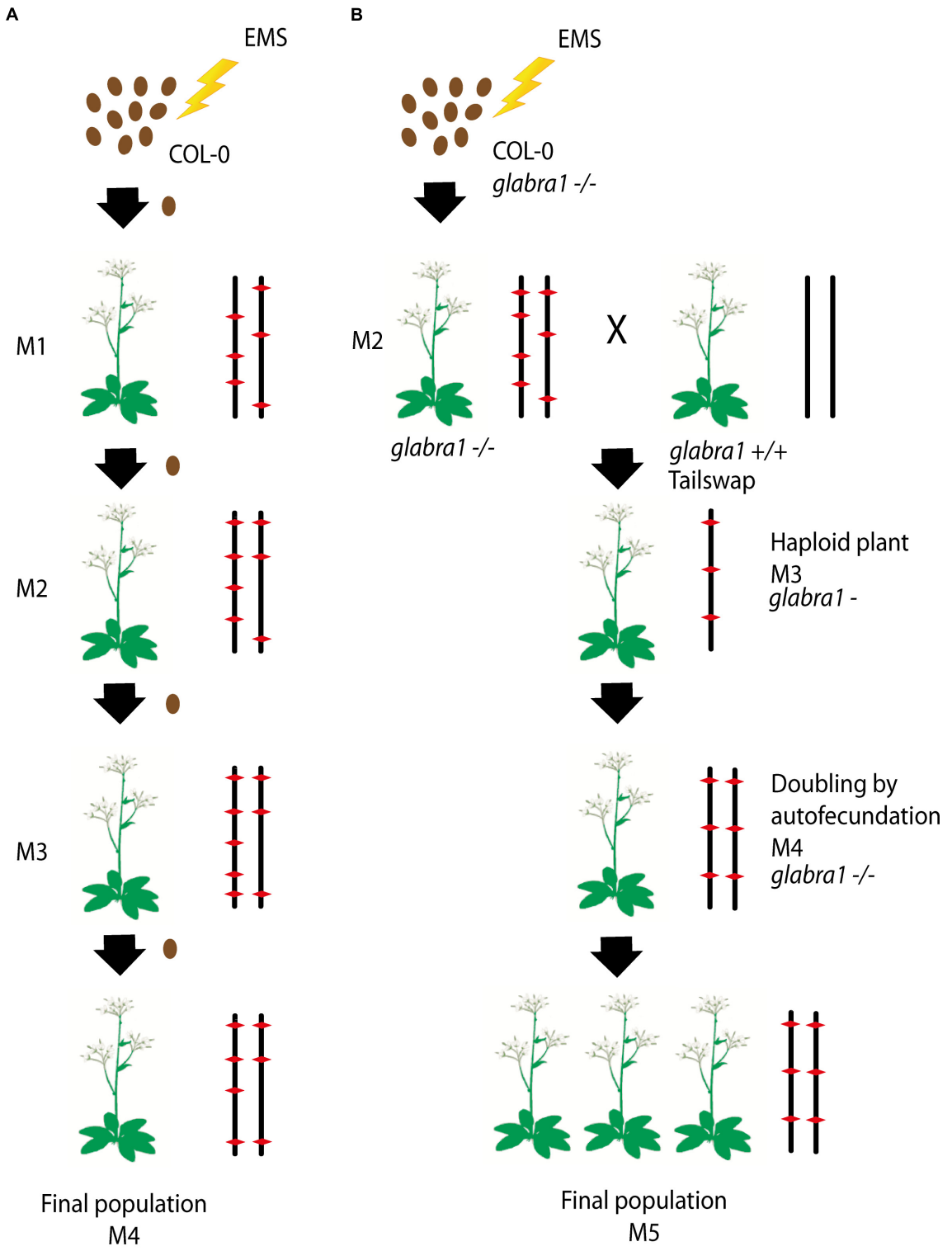

FIGURE 1 | (A,B) Schematic diagram of the approaches used to generate each subset of the homozygous EMS mutant lines: (i) Single seed descent (SSD) **(A)** and (ii) doubled haploids (DH) **(B)**. **(A)** For the SSD population, a set of Col-0 seeds were mutagenized by EMS and four different generations were grown from them by selecting a single seed in each generation. **(B)** The DH lines were obtained by mutagenizing a set of Col-0 GALBRA-1 seeds. M2 were then crossed to the Tailswap strain and the haploids of the next generation were selected by the absence of trichomes produced by the GLABRA- 1 mutation. Diploids were then obtained by spontaneous doubling from self-fertilization of the M3 plants. Chromosomes representing the genetic constitution (EMS mutations represented by a red diamond) are displayed for each generation.

TABLE 1 | The different series of independent mutagenesis carried out to generate each of the HEM subsets.

	SSD collection			DH collection		
Series	**Lines in the collection**	**Lines screened**	**Meiotic mutants**	**Lines in the collection**	**Lines screened**	**Meiotic mutants**
1	60	58	0	199	199	18
2	90	55	0			
3	47	43	0			
6	140	–	–			
10	302	261	25			
11	59	26	0			

The number of mutant lines produced for each subset of the HEM lines (SSD and DH) is shown with the different independent mutagenesis series produced, the number of lines screened for subtle meiotic phenotypes at metaphase I and the number of meiotic mutants found in each subset.

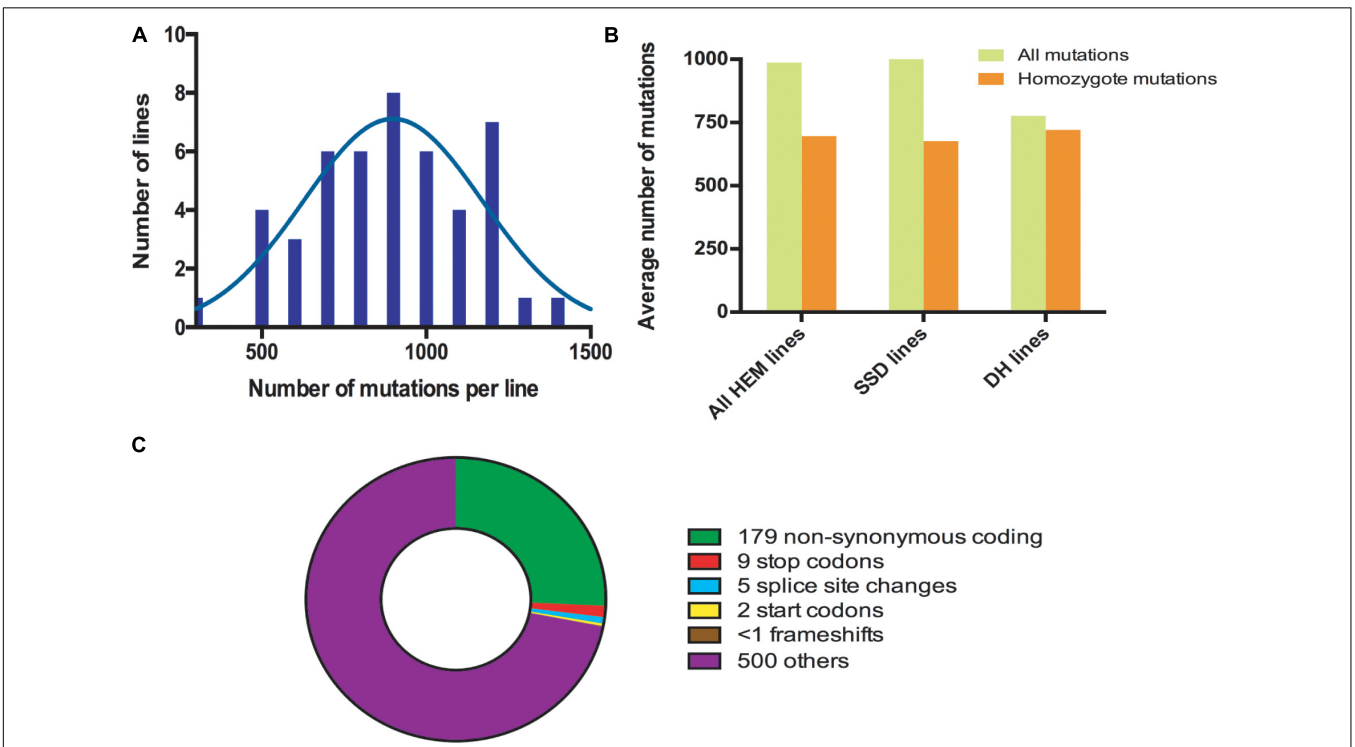

FIGURE 2 | (A) Distribution frequencies of the total number of mutations per HEM line. **(B)** The average total number of and homozygous mutations per line, comparing the HEM lines and each of the subsets (SSDs and DHs). **(C)** Average number of each type of mutation predicted to change the sequence and/or knockout a protein in one HEM line. "Others" category includes: synonymous coding, intergenic, intragenic, intron, and synonymous stop mutations.

Figure 2B and **Table 2**): in the SSD lines 70% of the mutations were fixed (676 mutations per line on average), which was lower than the 87% expected for those lines, perhaps due to counter-selection. In the case of the DH lines, we obtained an average of 94% homozygous mutations (720 mutations per line on average). The six randomly chosen lines had a similar number of mutations than the lines having a meiotic phenotype (690 vs. 697 mutations per line, respectively).

Considering that the DH lines were produced by doubling the genome of haploid plants, we expected complete fixation of the mutations and this is what we observed in 16 of the 22 lines analyzed (>95% of detected mutation). However, in six lines the percentage of homozygous mutations was 80% (on average) suggesting that the haploidization was not successful or that cross-pollination occurred during their production. Regardless, these lines still show a very high level of homozygosity, equivalent to that in the SSD lines.

In all the HEM lines (SSD and DH), 28% of the fixed mutations (an average of 195 mutations per line) modified a protein sequence (**Figure 2C** and **Table 2**). This category includes: non-synonymous coding mutations that change a single AA (179 mutations per line, on average); small indels leading to frame shifts (<1 per line, on average); new stop codons (nine per line, on average); new start codons (two per line, on average) and splice site changes (five per line, on average). Considering only the mutations resulting in frameshifts, new stop codons or splice

TABLE 2 | Number of mutations detected in the HEM lines and in the SSD and DH subsets.

	HEM (*n* = 47)	SSD (*n* = 25)	DH (*n* = 22)
All Mutations	897	1,003	776
Homozygous mutations	696 (81%)	676 (70%)	720 (94%)
Homozygous mutations that change protein sequences	195	193	199
Homozygous non synonymous coding mutations	179	177	182
Homozygous mutations that may affect protein function*	14	15	14

**This category includes premature stops, splice site changes, and frameshifts.*

site changes, 14 mutations per line should severely disrupt gene functions (**Figure 2C** and **Table 2**).

In summary, when a single line of the HEM library is screened, the effect of 195 homozygous mutations causing an amino acid change can be examined, at least 14 of which are predicted to knock out the function of the protein.

A Screen for Subtle Meiotic Defects

The HEM populations were then tested in a forward genetic screen targeting subtle meiotic phenotypes with the aim of identifying new genes involved in the meiotic process. For this we used two different approaches: (i) Alexander staining to detect dead pollen grains (Alexander, 1969) and then observations of meiotic chromosomal behavior (using chromosome spreads) in the selected lines, or (ii) direct observation of meiotic chromosomal spreads without a pre-screen.

All of the 199 M5 mutant lines from the DH subset were first pre-screened by Alexander staining. The meiotic chromosomal behavior was then examined in lines with more than 10% dead pollen grains. In the case of the SSD lines, we screened 539 M4 mutants (77% of the total 698 lines produced) by directly observing meiotic chromosomal behavior at metaphase I. Of these, the lines with a minimum of 20 cells at metaphase I captured were considered as screened, which resulted in a total of 450 mutant lines. For each of the mutants with a meiotic defect at metaphase I, we verified that the same phenotype was observed in the next generation. To optimize the screening procedure, we focused on metaphase I: (i) cells at that stage are relatively easy to find and (ii) most meiotic defects can be detected at metaphase I (e.g., modifications in crossover number or distribution, chromosome alignment defects and DSB repair defects). A drawback is that some defects cannot be observed at that stage (e.g., premature loss of cohesion, meiosis II spindle defects, cell cycle defects) and would be missed in this screen. However, we occasionally detected meiosis II defects that were included in the study.

We identified a total of 43 lines with various meiotic defects (18 DH lines and 25 SSD lines), representing 9% (18/199) of the screened DH lines and 6% (25/450) of the SSD lines. However, we observed an important difference among the six different series of mutagenesis used to produce the SSD subset (**Table 1**): 10% of the lines (25/261; **Table 1**) had meiotic defects in series 10, whereas no meiotic defects were observed in the other series produced (1–3, 6 and 11; 0/189). This variability could reflect differences in the efficiency of the mutagenesis due to slight variations in experimental conditions (e.g., room temperature, age of the seeds. . .) that may influence the final outcome of EMS mutagenesis. Therefore, the high number of meiotic mutants observed in the SSD series 10 and the HD lines suggests that these series are especially suitable for carrying out other forward genetic screens.

Overall, after screening 80% of the HEM lines the rate of meiotic mutant was high, with 9.4% of the lines showing different types of meiotic phenotypes in the DH and SSD series 10 (43 mutants with a robust meiotic phenotype among 199 DH lines + 261 series 10 SSD lines). The phenotypes described in the 43 HEM lines identified cover a variety of meiotic defects at metaphase I, compared to wild type (**Figure 3A**): (i) Different levels of fragmentation (suggesting a failure to complete the recombination process and leading in some cases to reduced fertility; observed in 10 lines; **Figure 3B**), (ii) bivalent shape defects (observed in five lines; **Figure 3C**), (iii) the presence of univalent chromosomes at different frequencies suggesting a lack of crossovers (ranging from 0.1 to 6 pair of univalent chromosomes per cell; observed in 26 lines; **Figures 3D,E**), and (iv) bivalent alignment abnormalities (observed in 2 lines; **Figure 3F**).

Identification of Candidate Causal Mutations

Of the 41 lines sequenced with meiotic defects, 18 had an obvious candidate mutation (**Table 3**). We considered a candidate mutation to be causal when the mutation was predicted to strongly affect a protein (i.e., stop codon, frame shift or a splice site change) with a described role in meiosis. Additionally, the observed phenotype had to be consistent with the previously described phenotype. An additional missense mutation in *ATM* was shown to be causal by genetic mapping (**Table 3**). In all these lines, the presence of the candidate mutation was confirmed by Sanger sequencing. In addition, Sanger sequencing of the candidate gene *SGO1* in two lines that showed premature loss of sister chromatid cohesion identified a stop and a splice site mutation (lines HDGem3 and HD479; **Table 3**).

The genes described in the 21 lines are involved in a wide range of meiotic mechanisms: *ATM* (found in five different mutant lines) plays a role in DSBs repair (Garcia et al., 2000, 2003); *MLH1*, *MLH3*, *MER3* (each identified in two different mutant lines), and *HEI10* are involved in class I crossover formation (Mercier et al., 2005; Jackson et al., 2006; Dion et al., 2007; Chelysheva et al., 2012), *FLIP* is both an anti- and pro-crossover factor (Fernandes et al., 2018); *FANCL* promotes crossover formation (Girard et al., 2014); *PRD2* is required for DSBs formation (De Muyt et al., 2009); *REC8* and *SGO1* (found in 3 different mutant lines) are both involved in sister chromatid cohesion (Chelysheva et al., 2004; Cromer et al., 2013); *ASY4* is involved in crossover and synaptonemal complex formation (Chambon et al., 2018); and *PSS1* plays a role in chromosome

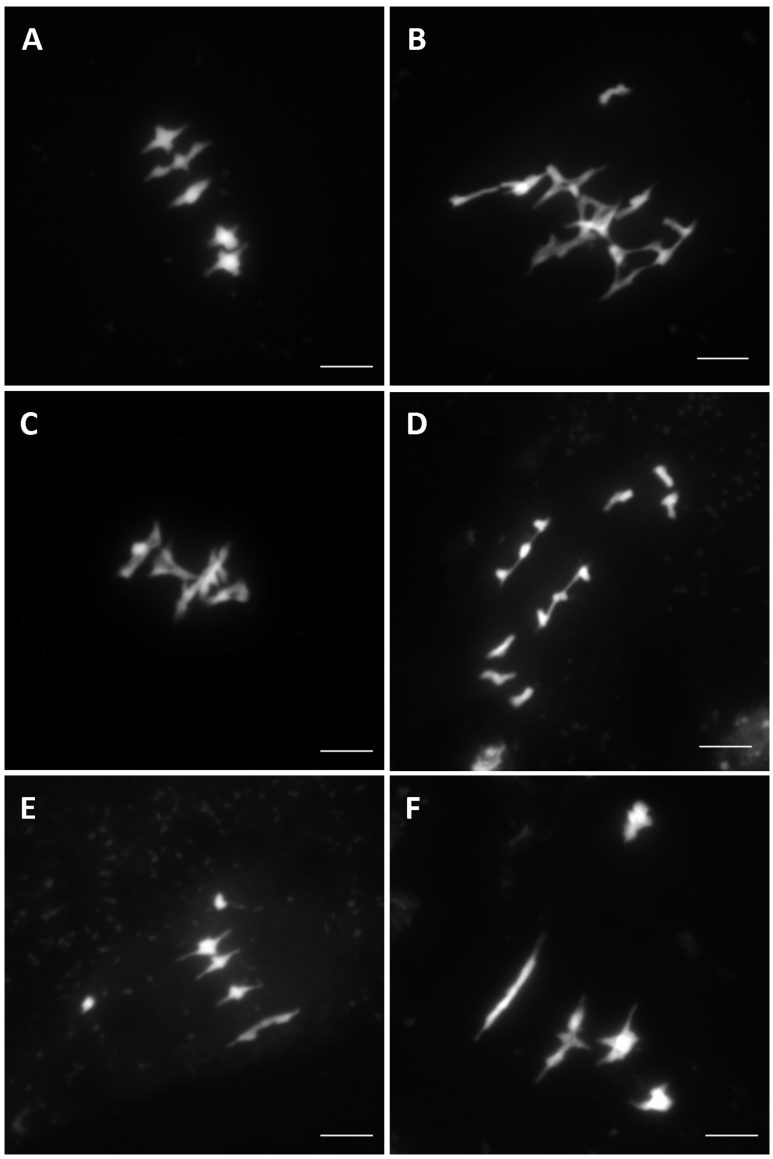

FIGURE 3 | Different meiotic phenotypes observed in the HEM lines at metaphase I showing: **(A)** Wild type meiosis **(B)** Chromosome fragmentation, **(C)** Bivalent shape defects, **(D,E)** Different levels of univalent chromosomes (ranging from a mean of 6 to 0.1 per cell) and **(F)** Bivalent alignment defects.

synapsis and crossover distribution (Duroc et al., 2014; **Table 3**). Interestingly, most of these mutations have only a mild impact on fertility (e.g., *MLH1, MLH3, ASY4, FANCL,* or *PSS1*).

In addition, among the 43 lines identified with meiotic phenotypes, in 22 there was no obvious candidate mutation, according to the criteria described above. These lines displayed different meiotic phenotypes and further work is needed to identify their causal mutation.

DISCUSSION

We have described the HEM collections, two libraries of almost fully homozygous *Arabidopsis* EMS mutants. These mutants show a high mutation rate per line, 897 mutations per line on average, of which most are fixed. Thus, due to the fixed nature of the mutations, these libraries can be used to repeatedly screen for a specific phenotype and therefore, to analyze either quantitative or qualitative traits.

Of all the mutations produced, we estimate that the HEM lines contain, >170,000 mutations (195 per line, on average) with an effect in the protein sequence. Among these >12,000 (14 per line, on average) are mutations that likely knock out the protein's function (new stop codons, splice site changes and frameshifts).

In this study, the HEM lines were used in a forward screen targeting subtle meiotic phenotypes as a new approach to identify novel meiotic mutants. Nine Percent of the mutant lines screened in the DH and SSD series 10 collections showed defects in

TABLE 3 | List of the genes identified as candidate causal mutations in the HEM lines.

Gene	Function	Position in bp (TAIR 10)	Mutant line	Change	Mutation effect	Phenotype	References
ATM (AT3G48190) Chr3	DSBs repair	17807938	ES1M5S10236	G > A	Premature stop	Fragmentation	Garcia et al., 2000, 2003
		17827101	ES1M5S10017	G > A	Splice change	Fragmentation	
		17824467	ES1M5S10070	G > A	Missense	Fragmentation	
		17812658	HD776	G > A	Splice change	Fragmentation	
		17823207	HD790	G > A	Splice change	Fragmentation	
MLH3 (AT4G35520) Chr4	class I COs	16868001	ES1M5S10052	C > T	Premature stop	Univalent chromosomes	Jackson et al., 2006
		16868745	HD662	C > T	Premature stop	Univalent chromosomes	
Mer3 (AT3G27730) Chr3	class I COs	10277172	ES1M5S10068	C > T	Splice change	Univalent chromosomes	Chen et al., 2005; Mercier et al., 2005
		10278220	HD577	C > T	Splice change	Univalent chromosomes	
Hei10 (AT1G53490) Chr1	Class I COs	19964116	HD768	G > A	Start gained	Univalent chromosomes	Chelysheva et al., 2012
FLIP (AT1G04650) Chr1	Pro and anti- CO	1298121	ES1M5S10083	C > T	Splice change	Univalent chromosomes	Fernandes et al., 2018
FANCL (AT5G65740) Chr5	Class II COs	26302687	ES1M5S10195	G > A	Premature stop	Univalent chromosomes	Girard et al., 2014
PRD2 (AT5G57880) Chr5	DSBs formation	23446256	ES1M5S10108	G > A	Premature stop	All univalent chromosomes	De Muyt et al., 2009
Rec8 (AT5G05490) Chr5	Cohesin subunit	1625685	ES1M5S10121	G > A	Splice change	Fragmentation	Chelysheva et al., 2005
ASY4 (AT2G33793) Chr2	CO formation and synapsis	14297325	HD721	G > A	Splice change	Univalent chromosomes	Chambon et al., 2018
PSS1 (AT3G63480) Chr3	Synapsis and CO regulation	23443192	HD783	C > T	Splice change	Univalent chromosomes	Duroc et al., 2014
MLH1 (AT4G09140) Chr4	COs class I	5820399	HD803	C > T	Splice change	Univalent chromosomes	Dion et al., 2007
	COs class I	5820399	HD853	C > T	Splice change	Univalent chromosomes	
SGO1 (AT3G10440) Chr3	Chromosome cohesion	3246274	HDsach17	G > A	Splice change	Univalent chromosomes	Cromer et al., 2013
		3246364	HDGem3	G > A	Splice change	Univalent chromosomes	
		3248339	HD479	C > T	Premature stop	Univalent chromosomes	

The table includes information on the name of the gene, meiotic function, position of the mutation, the nucleotide change resulting from the mutation, the effect of the mutation, the phenotype showed by the mutant and the literature describing these mutants.

meiosis (43 lines), which is a direct evidence of the efficiency of mutagenesis in the HEM lines.

Within these mutants, there are 12 clear candidate genes (*ATM, MLH3, MLH1, MER3, HEI10, SGO1, ASY4, FLIP, FANCL, PRD2, REC8,* and *PSS1*) involved in different meiotic mechanisms. Interestingly, six of these identified genes (*MLH3, MLH1, SGO1 PSS1, FANCL,* and *ASY4*) have been found here for the first time in a forward genetic screen. These mutants have only moderate defects in chromosome distribution at meiosis, leading to a subtle reduction in fertility, which is under the threshold of detection by visual examination of fruit length.

In addition, the finding that in 22 mutant lines there is no obvious causal mutation among the previously described meiotic genes, suggests that these lines may be mutated in novel meiotic genes that will require genetic mapping to be identified. Thus, these results are a proof of concept and support the usefulness of the HEM lines to decipher various biological processes. The two collections are available at the Versailles *Arabidopsis* stock center.

MATERIALS AND METHODS

EMS Mutagenesis and Plant Growth

To generate the single seed descent (SSD) collection, we applied ethyl methanesulfonate (EMS) to wild type *A. thaliana* accession Col-0 as described in (Portemer et al., 2015). Seeds were incubated for 17 h at room temperature with gentle agitation in 5 mL of 0.3% (v/v) EMS. Neutralization was performed by adding

5 mL of sodium thiosulfate 1 M for 5 min. Three milliliter of water was added to make the seeds sink. The supernatant was removed and the seeds were washed three times for 20 min with 15 mL of water. Mutagenized seeds were grown and carried through to the fourth generation using only one seed each time. The M4 seeds were used to screen for meiotic defects.

To generate the DH collection, mutagenesis was performed as in the SSD in Col-0 plants with an existing T-DNA insertion in *GLABRA1* (*GL1*). Mutagenized seeds were grown and then crossed as male to the tailswap line (TS) to obtain haploid plants that could be identified due to their lack of trichomes. Diploids were obtained by self-fertilization. M4 seeds were multiplied to obtain the final mutant population of the collection. All plants were cultivated in greenhouses with a 16 h/day and 8 h/night photoperiod, at 20°C and 70% humidity.

Plant Phenotyping

Alexander staining for pollen viability was performed as described in Alexander (1969). Meiotic chromosomal spreads were prepared and stained with DAPI as described in Ross et al. (1996). Observations were made using a Zeiss Axio Observer epifluorescence microscope and photographs were taken using an AxioCam MRm (Zeiss) camera driven by ZEN 2 Software (Carl Zeiss Microscopy, GmbH). Plots and statistical analysis were made using the GraphPad software Prism6[1].

Whole Genome Sequencing and Mutation Analysis

Genome sequencing was performed with Illumina Hiseq3000 HWIJ00115 with > 8X coverage. The resulting fastq files were analyzed using the Mutdetect pipeline (version 0.0.6-e3ef10e) (Girard et al., 2015) using TAIR10 COL-0 genome as the reference genome. The FileMatch package was used to eliminate false positives by comparing each mutant line with another two mutant lines as controls. Mutations were considered after quality filtering (>80) and the presence of 0 or only one read with wild type allele was considered to indicate a homozygous mutations. Additionally, to differentiate real mutations from false positives, we compared the total number of reads with the coverage, discarding mutations that showed unmapped reads as a proxy for repetitive regions. The sequencing raw data of fully characterized lines is available in the sequence read archive at NCBI SRA accession: SRP156100) and we encourage future users of the collection to do the same.

[1] http://www.graphpad.com

AUTHOR CONTRIBUTIONS

LC-P, VP, MG, and RM contributed to the conception and design of the study. LC-P, VS, AC, AH, AG, VP, DV, and LC performed the experiments. LC and RM analyzed the sequencing data. LC-P wrote the first draft of the manuscript.

FUNDING

The authors thank Rijk Zwaan for funding this study (Xmas project). The IJPB benefits from the support of the LabEx Saclay Plant Sciences-SPS (ANR-10-LABX-0040-SPS).

ACKNOWLEDGMENTS

We thank the Versailles Arabidopsis Resource center for technical support.

REFERENCES

Alexander, M. P. (1969). Differential staining of aborted and nonaborted pollen. *Stain Technol.* 44, 117–122. doi: 10.3109/10520296909063335

Chambon, A., West, A., Vezon, D., Horlow, C., De Muyt, A., Chelysheva, L., et al. (2018). Identification of ASYNAPTIC$_4$, a component of the meiotic chromosome axis. *Plant Physiol.* 178, 233–246. doi: 10.1104/pp.17.01725

Chelysheva, L., Diallo, S., Vezon, D., Gendrot, G., Vrielynck, N., Belcram, K., et al. (2004). AtREC8 and AtSCC3 are essential to the monopolar orientation of the kinetochores during meiosis. *J. Cell Sci.* 117, 4017–4023. doi: 10.1242/jcs.01352

Chelysheva, L., Diallo, S., Vezon, D., Gendrot, G., Vrielynck, N., Belcram, K., et al. (2005). AtREC8 and AtSCC3 are essential to the monopolar orientation of the kinetochores during meiosis. *J. Cell Sci.* 118, 4621–32. doi: 10.1242/jcs.02583

Chelysheva, L., Vezon, D., Chambon, A., Gendrot, G., Pereira, L., Lemhemdi, A., et al. (2012). The *Arabidopsis* HEI10 is a new ZMM protein related to Zip3. *PLoS Genet.* 8:e1002799. doi: 10.1371/journal.pgen.1002799

Chen, C., Zhang, W., Timofejeva, L., Gerardin, Y., and Ma, H. (2005). The Arabidopsis *ROCK-N-ROLLERS* gene encodes a homolog of the yeast ATP-dependent DNA helicase MER3 and is required for normal meiotic crossover formation. *Plant J.* 43, 321–334. doi: 10.1111/j.1365-313X.2005.02461.x

Crismani, W., Girard, C., Froger, N., Pradillo, M., Santos, J. L., Chelysheva, L., et al. (2012). FANCM limits meiotic crossovers. *Science* 336, 1588–1590. doi: 10.1126/science.1220381

Cromer, L., Jolivet, S., Horlow, C., Chelysheva, L., Heyman, J., De Jaeger, G., et al. (2013). Centromeric cohesion is protected twice at meiosis, by SHUGOSHINs at anaphase i and by PATRONUS at interkinesis. *Curr. Biol.* 23, 2090–2099. doi: 10.1016/j.cub.2013.08.036

De Muyt, A., Pereira, L., Vezon, D., Chelysheva, L., Gendrot, G., Chambon, A., et al. (2009). A high throughput genetic screen identifies new early meiotic recombination functions in *Arabidopsis thaliana*. *PLoS Genet.* 5:e1000654. doi: 10.1371/journal.pgen.1000654

Dion, E., Li, L., Jean, M., and Belzile, F. (2007). An *Arabidopsis MLH1* mutant exhibits reproductive defects and reveals a dual role for this gene in mitotic recombination. *Plant J.* 51, 431–40. doi: 10.1111/j.1365-313X.2007.03145.x

Duroc, Y., Lemhemdi, A., Larchevêque, C., Hurel, A., Cuacos, M., Cromer, L., et al. (2014). The kinesin AtPSS1 promotes synapsis and is required for proper crossover distribution in meiosis. *PLoS Genet.* 10:e1004674. doi: 10.1371/journal.pgen.1004674

Fernandes, J. B., Duhamel, M., Seguéla-Arnaud, M., Froger, N., Girard, C., Choinard, S., et al. (2018). FIGL1 and its novel partner FLIP form a conserved complex that regulates homologous recombination. *PLoS Genet.* 14:e1007317. doi: 10.1371/journal.pgen.1007317

Garcia, V., Bruchet, H., Camescasse, D., Granier, F., Bouchez, D., and Tissier, A. (2003). *AtATM* Is essential for meiosis and the somatic response to dna damage in plants. *Plant Cell* 15, 119–132. doi: 10.1105/tpc.006577

Garcia, V., Salanoubat, M., Choisne, N., and Tissier, A. (2000). An *ATM* homologue from *Arabidopsis thaliana*: complete genomic organisation and expression analysis. *Nucleic Acids Res.* 28, 1692–1699. doi: 10.1093/nar/28.8.1692

Girard, C., Chelysheva, L., Choinard, S., Froger, N., Macaisne, N., Lemhemdi, A., et al. (2015). AAA-ATPase FIDGETIN-LIKE 1 and helicase FANCM antagonize meiotic crossovers by distinct mechanisms. *PLoS Genet.* 11:e1005369. doi: 10.1371/journal.pgen.1005369

Girard, C., Crismani, W., Froger, N., Mazel, J., Lemhemdi, A., Horlow, C., et al. (2014). FANCM-associated proteins MHF1 and MHF2, but not the other fanconi anemia factors, limit meiotic crossovers. *Nucleic Acids Res.* 42, 9087–9095. doi: 10.1093/nar/gku614

Jackson, N. P., Sanchez-Moran, E., Buckling, E., Armstrong, S. J., Jones, G. H., and Franklin, F. C. H. (2006). Reduced meiotic crossovers and delayed prophase I progression in AtMLH3-deficient *Arabidopsis*. *EMBO J.* 25, 1315–23. doi: 10.1038/sj.emboj.7600992

Lambing, C., Osman, K., Nuntasoontorn, K., West, A., Higgins, J. D., Copenhaver, G. P., et al. (2015). Arabidopsis PCH2 Mediates Meiotic Chromosome Remodeling and Maturation of Crossovers. *PLoS Genet.* 11:e1005372. doi: 10.1371/journal.pgen.1005372

Marks, M. D., and Feldmann, K. A. (1989). Trichome development in *Arabidopsis thaliana*. I. T-DNA tagging of the GLABROUS1 gene. *Plant Cell* 1, 1043–1050. doi: 10.1105/tpc.1.11.1043

Martín, B., Ramiro, M., Martínez-Zapater, J. M., and Alonso-Blanco, C. (2009). A high-density collection of EMS-induced mutations for TILLING in Landsberg *erecta* genetic background of *Arabidopsis*. *BMC Plant Biol.* 9:147. doi: 10.1186/1471-2229-9-147

McCallum, C. M., Comai, L., Greene, E. A., and Henikoff, S. (2000). Targeted screening for induced mutations. *Nat. Biotechnol.* 18, 455–457. doi: 10.1038/74542

Mercier, R., Jolivet, S., Vezon, D., Huppe, E., Chelysheva, L., Giovanni, M., et al. (2005). Two meiotic crossover classes cohabit in *Arabidopsis*: one is dependent on *MER3*,whereas the other one is not. *Curr. Biol.* 15, 692–701. doi: 10.1016/j.cub.2005.02.056

Mercier, R., Mezard, C., Jenczewski, E., Macaisne, N., and Grelon, M. (2015). The molecular biology of meiosis in plants. *Annu. Rev. Plant Biol.* 66, 297–327. doi: 10.1146/annurev-arplant-050213-035923

Nawaz, Z., and Shu, Q. (2014). Molecular nature of chemically and physically induced mutants in plants: a review. *Plant Genet. Res.* 12, S74–S78. doi: 10.1017/S1479262114000318

Osman, K., Sanchez-Moran, E., Mann, S. C., Jones, G. H., and Franklin, F. C. H. (2009). Replication protein A (AtRPA1a) is required for class I crossover formation but is dispensable for meiotic DNA break repair. *EMBO J.* 28, 394–404. doi: 10.1038/emboj.2008.295

Page, D. R., and Grossniklaus, U. (2002). The art and design of genetic screens: *Arabidopsis thaliana*. *Nat. Rev. Genet.* 3, 124–136. doi: 10.1038/nrg730

Peirson, B. N., Bowling, S. E., and Makaroff, C. A. (1997). A defect in synapsis causes male sterility in a T-DNA-tagged *Arabidopsis thaliana* mutant. *Plant J.* 11, 659–669. doi: 10.1046/j.1365-313X.1997.11040659.x

Portemer, V., Renne, C., Guillebaux, A., and Mercier, R. (2015). Large genetic screens for gynogenesis and androgenesis haploid inducers in *Arabidopsis thaliana* failed to identify mutants. *Front. Plant Sci.* 6:147. doi: 10.3389/fpls.2015.00147

Ravi, M., and Chan, S. W. L. (2010). Haploid plants produced by centromere-mediated genome elimination. *Nature* 464, 615–618. doi: 10.1038/nature08842

Ross, K. J., Fransz, P., and Jones, G. H. (1996). A light microscopic atlas of meiosis in *Arabidopsis thaliana*. *Chromosom Res.* 4, 507–516. doi: 10.1007/BF02261778

Séguéla-Arnaud, M., Crismani, W., Larchevêque, C., Mazel, J., Froger, N., Choinard, S., et al. (2015). Multiple mechanisms limit meiotic crossovers: TOP3α and two BLM homologs antagonize crossovers in parallel to FANCM. *Proc. Natl. Acad. Sci. U.S.A.* 112, 4713–4718. doi: 10.1073/pnas.1423107112

Sikora, P., Chawade, A., Larsson, M., Olsson, J., and Olsson, O. (2011). Mutagenesis as a tool in plant genetics, functional genomics, and breeding. *Int. J. Plant Genomics* 2011:314829. doi: 10.1155/2011/314829

Till, B. J., Cooper, J., Tai, T. H., Colowit, P., Greene, E. A., Henikoff, S., et al. (2007). Discovery of chemically induced mutations in rice by TILLING. *BMC Plant Biol.* 7:19. doi: 10.1186/1471-2229-7-19

Till, B. J., Reynolds, S. H., Weil, C., Springer, N., Burtner, C., Young, K., et al. (2004). Discovery of induced point mutations in maize genes by TILLING. *BMC Plant Biol.* 4:12. doi: 10.1186/1471-2229-4-12

Zamariola, L., De Storme, N., Tiang, C. L., Armstrong, S. J., Franklin, F. C. H., and Geelen, D. (2013). SGO1 but not SGO2 is required for maintenance of centromere cohesion in *Arabidopsis thaliana* meiosis. *Plant Reprod.* 26, 197–208. doi: 10.1007/s00497-013-0231-x

Conflict of Interest Statement: The authors declare that the research was conducted in the absence of any commercial or financial relationships that could be construed as a potential conflict of interest.

frontiers in Plant Science

ORIGINAL RESEARCH
published: 26 September 2017
doi: 10.3389/fpls.2017.01620

Sequencing of Single Pollen Nuclei Reveals Meiotic Recombination Events at Megabase Resolution and Circumvents Segregation Distortion Caused by Postmeiotic Processes

Steven Dreissig[1], *Jörg Fuchs*[1], *Axel Himmelbach*[2], *Martin Mascher*[3,4]* and *Andreas Houben*[1]*

[1] Department of Breeding Research, Leibniz Institute of Plant Genetics and Crop Plant Research (IPK) Gatersleben, Seeland, Germany, [2] Department of Genebank, Leibniz Institute of Plant Genetics and Crop Plant Research (IPK) Gatersleben, Seeland, Germany, [3] Domestication Genomics, Leibniz Institute of Plant Genetics and Crop Plant Research (IPK) Gatersleben, Seeland, Germany, [4] German Centre for Integrative Biodiversity Research (iDiv) Halle-Jena-Leipzig, Leipzig, Germany

OPEN ACCESS

Edited by:
Tomás Naranjo, Complutense University of Madrid, Spain

Reviewed by:
James D. Higgins, University of Leicester, United Kingdom
Yingxiang Wang, Fudan University, China

***Correspondence:**
Martin Mascher
mascher@ipk-gatersleben.de
Andreas Houben
houben@ipk-gatersleben.de

Specialty section:
This article was submitted to Plant Genetics and Genomics, a section of the journal Frontiers in Plant Science

Received: *05 July 2017*
Accepted: *04 September 2017*
Published: *26 September 2017*

Citation:
Dreissig S, Fuchs J, Himmelbach A, Mascher M and Houben A (2017) Sequencing of Single Pollen Nuclei Reveals Meiotic Recombination Events at Megabase Resolution and Circumvents Segregation Distortion Caused by Postmeiotic Processes. Front. Plant Sci. 8:1620. doi: 10.3389/fpls.2017.01620

Meiotic recombination is a fundamental mechanism to generate novel allelic combinations which can be harnessed by breeders to achieve crop improvement. The recombination landscape of many crop species, including the major crop barley, is characterized by a dearth of recombination in 65% of the genome. In addition, segregation distortion caused by selection on genetically linked loci is a frequent and undesirable phenomenon in double haploid populations which hampers genetic mapping and breeding. Here, we present an approach to directly investigate recombination at the DNA sequence level by combining flow-sorting of haploid pollen nuclei of barley with single-cell genome sequencing. We confirm the skewed distribution of recombination events toward distal chromosomal regions at megabase resolution and show that segregation distortion is almost absent if directly measured in pollen. Furthermore, we show a bimodal distribution of inter-crossover distances, which supports the existence of two classes of crossovers which are sensitive or less sensitive to physical interference. We conclude that single pollen nuclei sequencing is an approach capable of revealing recombination patterns in the absence of segregation distortion.

Keywords: single-cell genomics, pollen, meiosis, homologous recombination, crossover, crossover interference, segregation distortion

INTRODUCTION

Meiotic recombination is a key mechanism in eukaryotic reproduction which enables novel combinations of alleles and provides a mechanism for plant breeders to achieve crop improvement. Recombination patterns are shaped by genetic, epigenetic and environmental factors (Melamed-Bessudo and Levy, 2012; Mirouze et al., 2012; Yelina et al., 2012; Ziolkowski et al., 2015, 2017; Ritz et al., 2017). In many crops, including barley, recombination events occur predominantly in distal regions of the chromosomes where gene density is high. In contrast, interstitial and centromere-proximal regions containing 12–24% of the barley gene complement are marked by strongly reduced recombination rates (Baker et al., 2014). Although genetic diversity is reduced

in low-recombining regions, they nevertheless contain genes and thus represent a resource that is hardly accessible to plant breeders. Therefore, significant efforts are being directed toward the manipulation of recombination frequency and distribution. Several approaches were shown to be successful, including the increase of crossovers via mutation of an anti-crossover factor (Crismani et al., 2012), epigenetic remodeling of crossover frequency via reduced DNA methylation (Melamed-Bessudo and Levy, 2012; Mirouze et al., 2012; Yelina et al., 2012; Habu et al., 2015), and shifting of crossover positions via increased or decreased temperatures (Higgins et al., 2012; Phillips et al., 2015; Martin et al., 2017). Furthermore, natural diversity of recombination patterns was shown to exist in *Arabidopsis*, maize, and *Hordeum* (Gale et al., 1970; Sall, 1990; Sall et al., 1990; Nilsson and Pelger, 1991; Sidhu et al., 2015; Ziolkowski et al., 2015, 2017).

In addition to low recombining regions limiting crop improvement, segregation distortion (SD) is another undesirable phenomenon as it reduces the chance of combining certain alleles. SD is defined as a deviation of the segregation ratio of alleles from the expected Mendelian segregation ratio. In barley double haploid (DH) populations, large proportions of the genome can show segregation distortion (Bélanger et al., 2016a). A frequent cause of segregation distortion is selection acting on genetically linked loci which results in entire chromosomal regions showing segregation distortion (hereafter termed SDR for segregation distortion region) (Hiraizumi et al., 1960; Hill and Robertson, 1966).

Taken together, tight genetic linkage of large proportions of the genome and distorted segregation resulting in a linkage drag of alleles hamper the advance of plant breeding. Future attempts to overcome these restrictions will require efficient methods to assay such effects. There are numerous methods to measure meiotic recombination in plants, including molecular markers (Salome et al., 2012), cytological visualization of crossovers (Sybenga, 1966; Anderson et al., 2003; Phillips et al., 2013), tetrad analysis (Copenhaver et al., 2000), fluorescent protein-tagged loci expressed in pollen (Yelina et al., 2013), and several pollen genotyping approaches (Drouaud and Mezard, 2011; Khademian et al., 2013; Dreissig et al., 2015). Although these methods have been successfully used to characterize recombination patterns and improve our understanding of meiosis, each of them has its specific advantages and disadvantages. The analysis of recombination by molecular markers requires the generation of a segregating population, which is laborious and very challenging for some plant species. Cytological analysis of recombination is more widespread and applicable to many plant species, yet its resolution is lower compared to sequence-based approaches and the analysis is demanding in terms of time and experience. Tetrad analysis combined with fluorescence markers is a very powerful high-throughput approach but requires the integration of reporter transgenes and is so far limited to the model species *Arabidopsis*.

Single-cell sequencing is a new technology that holds the promise to directly measure the outcome of meiosis in individual cells, e.g., microspores (Li et al., 2015) or pollen grains. We have previously developed a single pollen genotyping approach based on flow-sorting of haploid nuclei followed by whole genome amplification via multiple-displacement-amplification (MDA) of DNA and multi-locus competitive allele specific PCR (KASP) genotyping (Dreissig et al., 2015). This approach has shown the potential of single-cell analyses to measure recombination, but was limited by the number of KASP markers that could be assayed. To overcome this restriction, we took advantage of representative whole-genome amplification combined with next-generation-sequencing (NGS) library preparation and sequencing in the current study.

Here we present a new approach to directly investigate meiotic recombination at the DNA sequence level by combining flow-sorting of pollen nuclei with PicoPLEX single-cell sequencing (Rubicon Genomics). This sequencing approach is based on quasi-random PCR amplification of single-cell genomic DNA and yields a library with dual indexes for limited coverage sequencing. We show that this approach is capable of measuring meiotic recombination and segregation ratios throughout the whole genome of the large genome species barley at megabase resolution by comparing our results obtained through pollen sequencing to genotyping-by-sequencing (GBS) data of a barley DH population.

MATERIALS AND METHODS

Plant Material and Isolation of Single Pollen Nuclei

Pollen grains were collected from a *Hordeum vulgare* L. F_1 plant derived from a cross between the cultivars "Morex" (♂) and "Barke" (♀) and grown at 20°C during the day (7:00–20:00) and 16°C during the night. Pollen nuclei were isolated and stained as described previously (Dreissig et al., 2015) and sorted using a BD Influx cell sorter (BD Biosciences) into a 384 microwell plate (Applied Biosystems) using the "1.0 drop single" sort mode of the BD FACS software. As a control, we sorted three individual pollen nuclei from the parental genotype "Barke."

Single Nuclei Library Preparation and Illumina Sequencing

Illumina NGS libraries were prepared from 43 individual nuclei using the PicoPLEX DNA-seq kit essentially following the manufacturer's instructions (Rubicon Genomics). After the final amplification reaction with primers containing unique dual barcodes suitable for Illumina NGS, 10 µl aliquots of each library were pooled. The pooled DNA sample was purified using AMPure XP beads (Beckman Coulter Inc.) as described (Rubicon Genomics). The pool was eluted in 30 µl TE (pH 8.0) and size-fractionated using a SYBR-Gold stained 2% agarose gel (Himmelbach et al., 2014). The region of interest (350–1,000 bp) was excised, and the DNA was extracted using the Qiagen MinElute Kit (Himmelbach et al., 2014). The library was characterized using an Agilent 2100 Bioanalyzer (Himmelbach et al., 2014) and quantified by Real-Time PCR as described (Mascher et al., 2013b). After the addition of 8% PhiX DNA as a control, the pooled library was sequenced using the Illumina HiSeq2500 device (rapid run, 1 lane, cBot clustering, 2x 100 cycles paired-end, dual-indexing with 8 cycles per index) according to

the manufacturer's instructions. Sequence raw data are available under EMBL ENA accession PRJEB21630.

Sequence Read Mapping and Genotype Analysis

Illumina adapters were trimmed using Cutadapt version 1.12 (Martin, 2011). Trimmed reads were aligned to the barley cv. "Morex" reference genome sequence assembly (Mascher et al., 2017) using BWA-MEM version 0.7.15 (Li, 2013) with default parameters. The resulting SAM files were converted to BAM format with SAMtools (Li et al., 2009). Sorting and detection of optical and PCR duplicates was done with Novosort (http://www.novocraft.com/products/novosort/). SAMtools version 1.3 (Li, 2011) was used for multiple-sample genotype calling at single-nucleotide polymorphism (SNP) sites which were previously ascertained in the "Morex" × "Barke" RIL population using the POPSEQ method (Mascher et al., 2013a). VCF files were imported into the R statistical environment (R Core Team, https://www.r-project.org/contributors.html). Consensus genotypes were derived by aggregating information in 1 Mb bins using functionalities of the R package "data.table" (https://cran.r-project.org/package=data.table). This resulted in a genotype file containing allele information at 1 megabase pair (Mbp) resolution which was used to analyse recombination frequency and segregation distortion.

We used GBS data derived from a "Morex" × "Barke" DH population which was described previously (IBGSC, 2012) for comparison. GBS data were retrieved from https://wheat.pw.usda.gov/ggpages/MxB/. GBS tags were mapped onto the most recent version of the barley reference genome sequence (Mascher et al., 2017) an aggregated in 1 Mbp intervals.

Recombination Analysis Based on Pollen and a Double Haploid Population

To identify meiotic recombination events in the pollen and double haploid (DH) population, we searched for recombination patterns in each genotype matrix which were indicated by changes from "0" ("Barke" allele) to "2" ("Morex" allele) or vice versa. To count recombination events, we conducted a text search for patterns indicating recombination events (e.g., 0→0→0→2→2→2). We manually curated the genotype files by removing markers showing a high frequency of double crossovers (e.g., 0→2→0), which were considered genotyping errors (Salome et al., 2012). To map the approximate position of recombination events onto the physical map of the barley genome, a 5-Mbp sliding window approach was used to scan along each chromosome searching for allele changes from "0" to "2" and vice versa. We then calculated recombination frequency in cM/Mbp [cM = 100*(# of recombinations/#total)] along each chromosome by counting the number of recombination events in 5-Mbp sliding windows relative to the total number of samples. To analyse crossover interference, we extracted all samples showing more than two recombination events on a given chromosome and calculated the physical distance (Mbp) between nearby recombination events. To determine the effect of crossover interference, we used the crossover distribution analyser (CODA) software (Gauthier et al., 2011) which compares observed inter-crossover distances against a simulated gamma model to calculate *nu*. A value of $nu = 1$ indicates no interference, $nu < 1$ indicates negative interference, and $nu > 1$ indicates positive interference. Genotype data are available as Supplementary File 1.

Analysis of Segregation Distortion in Pollen and Double Haploid Population

Segregation distortion was analyzed by calculating average allele frequencies in 10 Mbp sliding windows along each chromosome of both populations. Markers with >50% missing data were removed from the analysis. To test for significant deviation from the expected segregation ratio of 1:1 of each parental allele, we conducted a χ^2-test between expected and observed allele frequencies. Segregation distortion regions (SDR) were identified by a significant deviation from the expected ratio of 1:1 ($P < 0.05$).

RESULTS

Sequencing of Individual Pollen Nuclei

To identify recombination events, we first sequenced the genomes of individual haploid pollen nuclei. Toward this purpose, we utilized our previously established approach for pollen nuclei isolation (Dreissig et al., 2015) combined with PicoPLEX single-cell DNA amplification and NGS library preparation. A total of 40 pollen nuclei derived from a single "Morex" (♂) x "Barke" (♀) F_1 plant were subjected to PicoPLEX sequencing. As a control, pollen nuclei obtained from the parental genotype "Barke" were used. The initial DNA amplification via quasi-random priming yielded an average fragment size of 933 bp. No amplification was detected in the negative control which indicates that the amount of DNA contamination was below the level of detection. Sequencing the 40 pollen nuclei on the Illumina HiSeq 2500 platform yielded between 2.7 million and 11.6 million (mean: 5.9 million) reads per sample, corresponding to an average read depth of 0.1x per haploid nucleus. Reads were mapped to the reference genome assembly of cv. "Morex" (Mascher et al., 2017) and genotypes were called at single-nucleotide polymorphism (SNP) sites known to segregate in the "Morex" × "Barke" population (Mascher et al., 2013a). Consensus genotypes were derived by aggregating SNP information in 1 Mbp bins based on the reference genome. **Figure 1** shows the graphical genotypes of the 40 pollen nuclei at 1 Mbp resolution.

Comparing the Recombination Landscape of Barley Pollen and DH Plants

Based on cytological analyses (Sybenga, 1966; Phillips et al., 2013; Aliyeva-Schnorr et al., 2015) and molecular analyses of segregating populations (Künzel et al., 2000; IBGSC, 2012; Phillips et al., 2015), the recombination landscape of barley is characterized by elevated recombination frequencies in distal chromosome regions and strongly reduced recombination in (peri-)centromeric regions. In order to overcome the resolution limit of cytological analyses, we attempted to investigate the

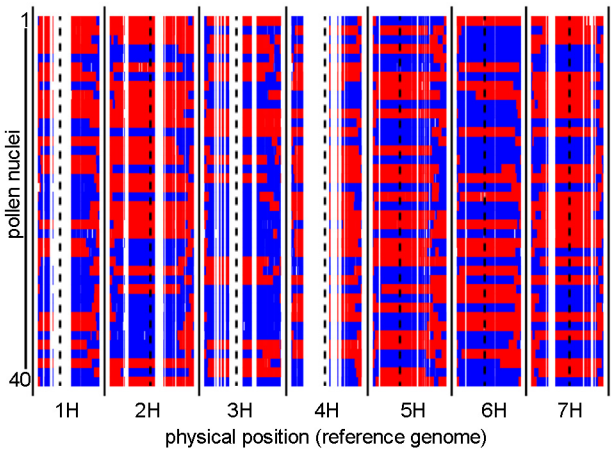

FIGURE 1 | Graphical genotypes of individual pollen nuclei revealed by single-cell genome sequencing. Recombination events were detected in 40 individual pollen nuclei. The two parental barley genotypes are shown in red ("Morex") and blue ("Barke"). Consensus genotypes were mapped to the physical reference genome of barley at 1 Mbp resolution. Centromere positions are indicated by dashed black lines. White gaps which consistently occur in all samples are regions where no genetic polymorphisms exist between "Morex" and "Barke."

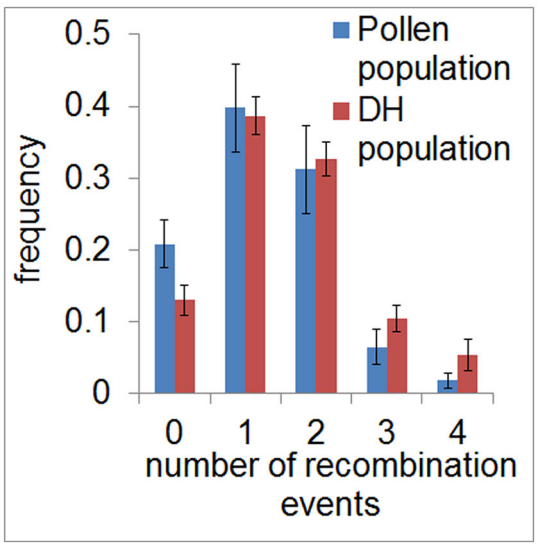

FIGURE 2 | Frequency of recombination events in pollen and DH plants. Relative frequency of the average number of recombination events per chromosome is shown for the pollen (blue) and DH population (red) in classes ranging from 0 to 4. Error bars represent the standard deviations based on measurements conducted on all seven barley chromosomes.

recombination landscape of barley directly at the DNA sequence level by sequencing individual pollen nuclei.

To assess the recombination landscape of barley pollen compared to DH plants, we first counted the number of recombination events in each sample in both populations. We measured a total of 380 recombination events in the population of 40 haploid pollen nuclei (average of 9.5 per pollen nucleus, SE = 0.38) and 974 recombination events in the DH population composed of 89 plants (average of 10.9 per DH plant, SE = 0.3). Predominantly, we detected one or two recombination events per chromosome in both populations with 38.7–39.8% of samples showing one recombination event and 31.1–32.6% of samples showing two recombination events. The number of recombination events, which was ranging from zero to four per chromosome, was found to be similar between pollen and DH population (χ^2-goodness of fit test, $P > 0.99978$) (**Figure 2**). The occurrence of chromatids apparently lacking any recombination event detected by SNPs (13–20%) seems to be the same as in an *Arabidopsis* data set described by Salome et al. (2012). Consequently, recombination frequency was found to be similar in barley pollen compared to whole DH plants.

Since the number of recombination events per chromosome was highly similar between the pollen population and the DH population, we then examined whether the genome wide distribution of recombination events differed between both populations. We measured recombination frequencies along all chromosomes of barley using a 5 Mbp sliding window approach. In both populations, we found elevated recombination frequencies in distal regions of all chromosomes and almost no recombination in (peri-)centromeric regions (**Figure 3**, Supplementary files 2–7). This observation is in agreement with

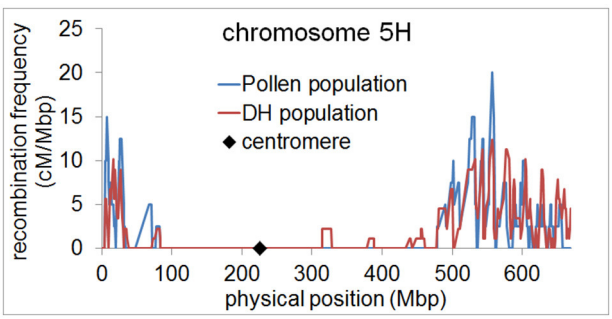

FIGURE 3 | Elevated recombination frequencies in distal regions of barley chromosome 5H. Recombination frequency in pollen (blue) and DH plants (red) was calculated in 5 Mbp sliding windows along chromosome 5H and plotted along the physical map. The position of the centromere is marked by a black diamond.

previous studies showing a skewed distribution of recombination events toward distal chromosome regions in barley (Künzel, 1982; Linde-Laursen, 1982; Künzel et al., 2000; Phillips et al., 2013; Baker et al., 2014; Dreissig et al., 2015). It also shows that there is no different positioning of recombination events in pollen, i.e., in (peri-)centromeric regions. These regions were shown to harbor essential genes encoding proteins for basic cellular functions such as translation and photosynthesis (Mascher et al., 2017). It could therefore be reasoned that (peri-)centromeric recombination events could theoretically be absent in DH plants due to selection against housekeeping gene-encoding (peri-)centromeric sites of recombination which would disrupt linkage between essential genes.

In agreement with the predominantly distal positioning of recombination events in both populations, we found positive crossover interference indicated by 48.9–59.8% of recombination events being separated by more than 400 Mbp (range = 402–729 Mbp) over a chromosome size ranging from 558 to 767 Mbp. Interestingly, 35.6–39.6% of recombination events were separated by less than 100 Mbp (range = 10–98 Mbp) (**Figure 4**). The smallest distance between two recombination events was 10 Mbp which corresponds to ∼1.5% of the chromosome. We conducted a crossover interference analysis (gamma model; measured in *nu*) to determine the strength of interference (Gauthier et al., 2011). A value of $nu = 1$ indicates no interference, $nu < 1$ indicates negative interference, and $nu > 1$ indicates positive interference. Due to the low number of chromosomes showing at least two recombination events, we did not analyse chromosomes separately, but pooled data from all seven barley chromosomes. Positive interference values of $nu = 4.76$ and 3.02 were detected in DH and pollen populations, respectively. In addition, we split all recombination events into two groups with <100 or >400 Mbp distance between two events. When both groups were analyzed separately, we found weaker interference values for recombination events less than 100 Mbp apart ($nu = 2.336$ for pollen and $nu = 2.202$ for DH population) and stronger interference values when more than 400 Mbp apart ($nu = 8.511$ for pollen and $nu = 8.199$ for DH population). These patterns might be attributed to interference sensitive and less sensitive crossovers, i.e., class I and class II crossover. We then tested whether recombination events separated by less than 100 Mbp were confined to specific chromosomal regions or distributed randomly by plotting the physical positions of multiple recombination events on the same chromosome against themselves (**Figure 5**). All recombination events separated by less than 100 Mbp were strictly confined to distal regions, which corresponds to the accumulation of dots in the bottom left and top right quarters of **Figure 5**. Recombination events separated by more than 400 Mbp were located on different arms (dots in the top left quarter of **Figure 5**). Our data show that crossover interference is positive in barley. However, a substantial proportion of recombination events is separated by less than 100 Mbp which supports the existence of class I and class II crossovers in barley.

Segregation Distortion Is High in DH Plants, But Almost Absent in Pollen

Segregation distortion is defined as the preferential transmission of one allele over the other, which results in a statistically significant deviation from an expected Mendelian segregation ratio of 1:1. We asked whether the extent of segregation distortion differs between pollen and DH plants. Our hypothesis was that segregation distortion would be substantially lower in pollen because of the absence of any selective pressure which might arise during pollen tube growth, fertilization, hybrid compatibility, and plant development. We expected the opposite in the DH population because of selective pressure during microspore culture, embryo development, plant regeneration, and spontaneous diploidization. It is important to note that the DH population which was genotyped and provided by the IBGSC (2012) consisted of spontaneously diploidized plants only.

In the pollen population, we found normal segregation ratios for almost all chromosomal regions (Supplementary files 8–12). The exceptions were one region on chromosome 2H located at

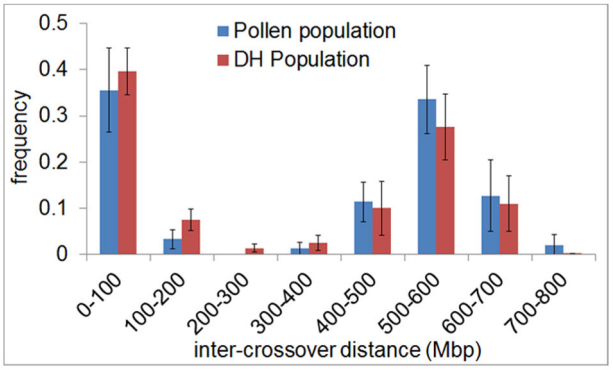

FIGURE 4 | Inter-crossover distance reveals positive crossover interference and supports the existence of two crossover classes in barley. The frequency of the distance between crossovers on the same chromatid (inter-crossover distance) in pollen (blue) and DH plants (red) was determined in 100 Mbp classes ranging from <100 to >700 Mbp. The relative frequency of nearby crossovers present in each class was plotted. Error bars represent the standard deviation based on measurements conducted on all seven barley chromosomes.

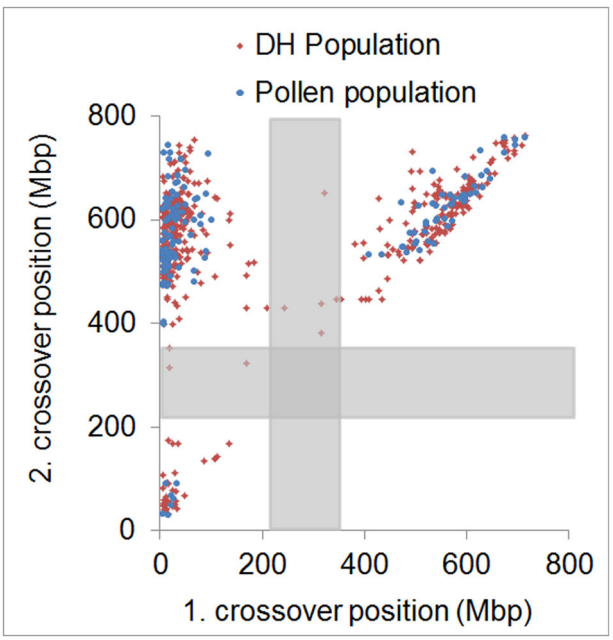

FIGURE 5 | Physical distribution of first and second crossover positions. Physical positions of first and second crossover event for all samples showing more than two crossovers in the pollen (blue) and DH (red) population. Approximate centromeric regions are marked by gray boxes. Strong physical interference is shown by dots accumulated in the top left quarter. Weak physical interference is shown by dots accumulated in the bottom left and top right quarter.

736–752 Mbp and two regions on chromosome 3H located at 634–642 Mbp and 682–695 Mbp (**Figure 6**). These regions only amount to 2 and 3% of chromosome 2H and 3H, respectively. In both cases, these SDRs were located in high recombining regions of the chromosome allowing them to remain small and not cause distorted segregation of a larger part of the chromosome through linkage (Supplementary file 13). In contrast, in the DH population, a high proportion of large chromosomal regions were affected by segregation distortion. We detected a total of 15 SDRs distributed across all chromosomes which varied in size ranging from 0.01 up to 87.3% of the chromosome. Major SDRs, varying from 72.6 up to 87.3% of the chromosome, were found on chromosome 1H, 2H, 5H, and 7H (**Figure 6A**, Supplementary files 8, 10, 12). In addition to these major SDRs, we detected 11 minor SDRs which varied in size ranging from 0.01 up to 5% of the chromosome (**Figure 6B**, Supplementary files 8, 10–12). Interestingly, we did not detect the same SDRs on chromosome 2H and 3H in the pollen population as in the DH population which indicates different selective pressures acting on these loci. For example, in the DH population, two regions of chromosome 3H (571.6–606.6 Mbp and 672.2–698.3 Mbp) exhibited higher transmission of the "Morex" allele whereas, in the pollen population, two regions of the chromosome (634–642 Mbp and 682–695 Mbp) exhibited higher transmission of the "Barke" allele (**Figure 6B**). This example shows that under varying conditions (e.g., pollen development vs. DH production) not only different regions can be selected, but also different parental alleles can be preferentially transmitted.

Hence, our results show that segregation distortion is almost absent in pollen grains which supports the conclusion that meiosis alone is not the main cause of this phenomenon. On the contrary, segregation distortion was found for nearly half of the entire genome (49.9%) in barley DH plants. We conclude that selective pressure during microspore culture, embryo development, plant regeneration, and diploidization is the most likely cause for segregation distortion in DH plants.

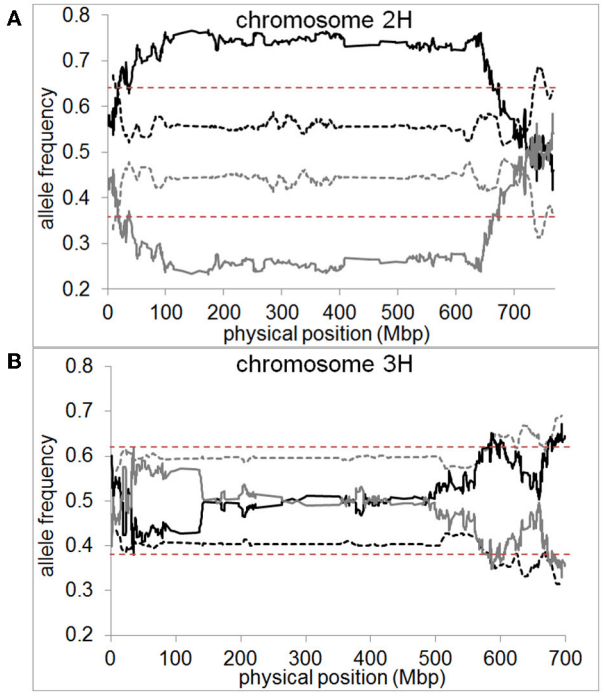

FIGURE 6 | Segregation distortion is almost absent if measured in pollen but abundant in DH plants. Allele frequencies for "Morex" (black) and "Barke" (gray) measured in pollen (dashed line) and DH plants (straight line) are shown as 10 Mbp moving averages for **(A)** chromosome 2H and **(B)** chromosome 3H of barley. Dashed red lines represent the significance threshold of distorted segregation ratios (χ^2-test, $P < 0.05$). Pollen or DH allele frequencies above the significance threshold mark genomic regions of distorted segregation ratios.

DISCUSSION

The main conclusion of the present study is that the recombination landscape of barley pollen and DH plants does not differ in frequency or positioning of recombination events, yet segregation distortion is almost absent in pollen grains whereas it is detectable to a large extent in DH plants likely caused by selection during DH production. In addition, we present recombination measurements which support the existence of class I and class II crossovers in barley. We demonstrate that our approach for single pollen nuclei sequencing is suitable to directly investigate the recombination landscape of barley at the molecular level in an unbiased way.

Pollen Sequencing as a Robust Approach to Directly Measure Recombination at Megabase Resolution in Barley

We sought to analyse recombination in pollen and DH plants separately to test if the typical recombination pattern found in segregating populations of barley, characterized by a predominantly distal positioning of recombination events, is caused by selection against (peri-)centromeric recombination events or reflects the real outcome of meiosis. The low recombining regions of the barley genome were previously shown to constrain gene diversity (IBGSC, 2012; Baker et al., 2014). This phenomenon is widespread in nature and is most likely caused by a combination of selective sweeps via fixation of advantageous alleles and background selection against deleterious mutations (Hill and Robertson, 1966; Smith and Haigh, 1974; Hudson, 1994; Wright et al., 2006). Furthermore, it was recently shown that essential genes involved in translation and photosynthesis reside in (peri-)centromeric low-recombining regions of the barley genome (Mascher et al., 2017). It could thus be argued that recombination events in low-recombining regions would break linkage between advantageous alleles and therefore be selected against. In pollen, however, these recombination events could still be present due to the absence of selective pressure which certainly arises during pollen tube growth, fertilization, and plant development (Pedersen, 1988; Sarigorla et al., 1992; Walsh and Charlesworth, 1992).

Our data show that the recombination landscape of barley, characterized by elevated recombination frequencies in distal regions (**Figure 3**), is truly the outcome of meiosis and not

a result of postmeiotic selection against (peri-)centromeric recombination events. This is in agreement with previous cytogenetic studies taking direct recombination measurements by means of scoring MHL3 immunostaining foci or chiasmata (Bennett et al., 1973; Phillips et al., 2013). However, it was of interest for us to test if these observations reveal the same recombination landscape as by sequencing of pollen nuclei. The direct sequencing of pollen nuclei, through the approach presented in this study, offers a much higher resolution in detecting the positions of recombination events (i.e., 1 Mbp, approximately 0.2% of the smallest barley chromosome) compared to the mapping of MLH3 fluorescence foci during meiotic prophase by structured illumination microscopy (Phillips et al., 2013). Compared to chiasmata counts performed in a variety of barley genotypes, the average number of recombination events detected in our study seems to be lower (Gale et al., 1970; Bennett et al., 1973; Colas et al., 2016). If it holds true that all cytologically defined chiasmata represent genetic exchanges between homologous chromosomes, we cannot exclude that certain recombination events are missing in our data sets. On the other hand, we measured similar recombination frequencies in pollen and DH plants while both populations were genotyped by two different methods, i.e., single-cell sequencing vs. genotyping-by-sequencing of DH plants. Furthermore, both approaches are based on haploid male gametes where only one of the four possible meiotic products, i.e., chromatids, is present. Hence, as evident from *Arabidopsis* tetrad analysis where all four chromatids are analyzed (Lu et al., 2012; Wijnker et al., 2013), it is possible for a haploid pollen nucleus to contain the exact chromatid that did not undergo meiotic recombination. It is therefore unlikely that single cell sequencing accounts for missing recombination events. It could also be argued that these differences reflect genotypic variations or environmental effects as such were shown in many cases (Sall et al., 1990; Bauer et al., 2013; Phillips et al., 2015; Sidhu et al., 2015; Ziolkowski et al., 2015, 2017).

We detected positive crossover interference in both pollen and DH plants, which is in agreement with the primarily distal positioning of recombination events. Previously, Phillips et al. (2013) reported for barley that 34–38% of crossovers are <20% of chromosome length apart and the majority of crossovers are >70% apart which results in a bimodal distribution of inter-crossover distances. Here, we found 36.8–40.4% of crossovers separated by less than 100 Mbp (approximately 15% of chromosome length) and 48.3–57.4% separated by more than 400 Mbp (approximately 60% of chromosome length) reflecting a similar bimodal distribution of inter-crossover distances (**Figure 4**). The minimum inter-crossover distance found in our study was 10 Mbp which refers to 1.5% of the corresponding chromosome. We quantified crossover interference strength (gamma model; measured in *nu*) in the pollen and DH population. We detected positive physical interference between crossovers in both pollen ($nu = 3.02$) and DH population ($nu = 4.76$). These interference values are higher than those previously reported for the barley cultivar "Morex," which was at $nu = 1.58$ (Phillips et al., 2013). However, Higgins et al. (2014) argued that crossover interference might actually be stronger than estimated by Phillips et al. (2013) because the relative separation of MLH3 foci was measured when synapsis of chromosomes was completed and not at the exact time point when crossover designation took place during synapsis. Our data, which are based on scoring crossovers at the sequence level, support this hypothesis by showing stronger crossover interference values for barley.

The existence of two crossover classes, namely class I for interference-sensitive crossovers and class II for interference-insensitive crossovers, was shown in *S. cerevisiae* and *A. thaliana* mutants being defective for core components involved in class I crossover formation (Börner et al., 2004; Higgins et al., 2004). In these mutants, 15% of crossovers of the wild-type level were still formed, which indicates the existence of an alternative class II pathway. However, the presence of two crossover classes has not been confirmed experimentally in barley yet although increasing evidence supports their existence (Phillips et al., 2013, 2015). In our study, the occurrence of recombination events separated by <100 or >400 Mbp supports the existence of interference-sensitive and less sensitive crossovers, i.e., class I and class II. However, it remains a matter of speculation why nearby crossovers are strictly confined to distal regions and do not span (peri-)centromeric regions. There is a well-known correlation between low-recombining (peri-)centromeric regions and certain histone modifications in barley, i.e., histone H3K9me2, H3K9me3, H3K27me1, and H3K27me2, as shown by chromatin immunoprecipitation (ChIP) sequencing in barley seedlings (Baker et al., 2015). Furthermore, it was shown in *Arabidopsis* that DNA methylation restricts crossovers in centromeric regions and that crossover hot spots are associated with active chromatin modifications such as H2A.Z and H3K4me3 (Yelina et al., 2012; Choi et al., 2013). It could therefore be argued that by changing specific DNA or histone modifications, crossover positioning could be manipulated to increase genetic recombination in (peri-)centromeric regions in crops such as barley.

Comparison of Segregation Distortion in Pollen and DH Plants

Segregation distortion is a widespread phenomenon in plant populations characterized by a deviation from the expected Mendelian segregation ratio. For plant breeders, it presents a problem as it has an effect on allele frequencies and can reduce the chances of obtaining specific combinations of alleles. Double haploid technology has developed into one of the most important methods for plant breeders to accelerate the otherwise lengthy process of obtaining homozygous genotypes (Germana, 2011). The disadvantage of this technology is that it is accompanied by segregation distortion to a very high extent in many genotypes and species (Xu et al., 1997; Taylor and Ingvarsson, 2003; Bélanger et al., 2016a). Segregation distortion during DH production appears to be caused by selective pressure acting upon certain loci or genomic regions. Selective pressure might arise during microspore culture, embryogenesis, plant regeneration, and spontaneous diploidization of haploid plants. Bélanger et al. (2016b) have shown that segregation distortion in barley arises predominantly during embryogenesis and plant regeneration.

In the current study, we hypothesized that segregation distortion would be low if measured in pollen grains due to the absence of selective pressure. Our data show that only three small chromosomal regions show distorted segregation ratios in pollen, amounting to 0.8% of the genome, whereas nearly 50% of the genome shows distorted segregation ratios in DH plants. This suggests that segregation distortion is not a direct outcome of meiosis but a product of selection acting at different developmental stages. Compared to Bélanger et al. (2016b) who detected no segregation distortion in immature pollen, we found one region on chromosome 2H and two regions on chromosome 3H with distorted segregation rations in mature pollen. It can be speculated that these regions might play a role in pollen development and therefore show distorted segregation. Furthermore, environmental conditions, e.g., heat stress (Frova and Sari-Gorla, 1994) or higher nutrient levels in the soil (Martin et al., 2017) can have an effect on segregation ratios in pollen, although our experiment did not involve any stress treatment.

Further improvements in protocols and decreases in the price of sequencing should enable the application of single pollen sequencing as a novel prediction tool in research and plant breeding in a wide range of species.

AUTHOR CONTRIBUTIONS

SD isolated pollen nuclei, conducted flow-sorting, analyzed the data, and wrote the manuscript. JF conducted flow-sorting, contributed to the manuscript and edited the manuscript. AHi conducted PicoPLEX single-cell sequencing, contributed to the manuscript and edited the manuscript. MM processed all raw data, analyzed the data, contributed to the manuscript and edited the manuscript. AHo conceptualized the experiments, supervised the analyses, contributed to the manuscript and edited the manuscript. All authors read and approved the final version of this manuscript.

ACKNOWLEDGMENTS

We thankfully acknowledge Nils Stein (IPK, Gatersleben) for providing us with "Morex" × "Barke" F1 seeds. We also gratefully acknowledge the excellent technical assistance by Sandra Driesslein and Ines Walde (IPK, Gatersleben, NGS Sequencing Laboratory). We are thankful to Anne Fiebig (IPK, Gatersleben) for data submission. Finally, we would like to thank Stefan Heckmann (IPK, Gatersleben) for critical reading of this manuscript. This work was supported by the IPK Gatersleben.

SUPPLEMENTARY MATERIAL

The Supplementary Material for this article can be found online at: http://journal.frontiersin.org/article/10.3389/fpls.2017.01620/full#supplementary-material

REFERENCES

Aliyeva-Schnorr, L., Beier, S., Karafiatova, M., Schmutzer, T., Scholz, U., Dolezel, J., et al. (2015). Cytogenetic mapping with centromeric bacterial artificial chromosomes contigs shows that this recombination-poor region comprises more than half of barley chromosome 3H. *Plant J.* 84, 385–394. doi: 10.1111/tpj.13006

Anderson, L. K., Doyle, G. G., Brigham, B., Carter, J., Hooker, K. D., Lai, A., et al. (2003). High-resolution crossover maps for each bivalent of *Zea mays* using recombination nodules. *Genetics* 165, 849–865.

Baker, K., Bayer, M., Cook, N., Dreissig, S., Dhillon, T., Russell, J., et al. (2014). The low-recombining pericentromeric region of barley restricts gene diversity and evolution but not gene expression. *Plant J.* 79, 981–992. doi: 10.1111/tpj.12600

Baker, K., Dhillon, T., Colas, I., Cook, N., Milne, I., Milne, L., et al. (2015). Chromatin state analysis of the barley epigenome reveals a higher-order structure defined by H3K27me1 and H3K27me3 abundance. *Plant J.* 84, 111–124. doi: 10.1111/tpj.12963

Bauer, E., Falque, M., Walter, H., Bauland, C., Camisan, C., Campo, L., et al. (2013). Intraspecific variation of recombination rate in maize. *Genome Biol.* 14:R103. doi: 10.1186/gb-2013-14-9-r103

Bélanger, S., Clermont, I., Esteves, P., and Belzile, F. (2016a). Extent and overlap of segregation distortion regions in 12 barley crosses determined via a pool-GBS approach. *Theor. Appl. Genet.* 129, 1393–1404. doi: 10.1007/s00122-016-2711-5

Bélanger, S., Esteves, P., Clermont, I., Jean, M., and Belzile, F. (2016b). Genotyping-by-sequencing on pooled samples and its use in measuring segregation bias during the course of androgenesis in barley. *Plant Genome* 9. doi: 10.3835/plantgenome2014.10.0073

Bennett, M. D., Finch, R. A., Smith, J. B., and Rao, M. K. (1973). Time and duration of female meiosis in wheat, rye and barley. *Proceed. Royal Soc. B Biol. Sci.* 183, 301–319. doi: 10.1098/rspb.1973.0019

Börner, G. V., Kleckner, N., and Hunter, N. (2004). Crossover/noncrossover differentiation, synaptonemal complex formation, and regulatory surveillance at the leptotene/zygotene transition of meiosis. *Cell* 117, 29–45. doi: 10.1016/S0092-8674(04)00292-2

Choi, K., Zhao, X., Kelly, K. A., Venn, O., Higgins, J. D., Yelina, N. E., et al. (2013). *Arabidopsis* meiotic crossover hot spots overlap with H2A.Z nucleosomes at gene promoters. *Nat. Genet.* 45, 1327–1336. doi: 10.1038/ng.2766

Colas, I., Macaulay, M., Higgins, J. D., Phillips, D., Barakate, A., Posch, M., et al. (2016). A spontaneous mutation in MutL-Homolog 3 (HvMLH3) affects synapsis and crossover resolution in the barley desynaptic mutant des10. *New Phytol.* 212, 693–707. doi: 10.1111/nph.14061

Copenhaver, G. P., Keith, K. C., and Preuss, D. (2000). Tetrad analysis in higher plants. A budding technology. *Plant Physiol.* 124, 7–16. doi: 10.1104/pp.124.1.7

Crismani, W., Girard, C., Froger, N., Pradillo, M., Santos, J. L., Chelysheva, L., et al. (2012). FANCM limits meiotic crossovers. *Science* 336, 1588–1590. doi: 10.1126/science.1220381

Dreissig, S., Fuchs, J., Capal, P., Kettles, N., Byrne, E., and Houben, A. (2015). Measuring meiotic crossovers via multi-locus genotyping of single pollen grains in barley. *PLoS ONE* 10:e0137677. doi: 10.1371/journal.pone.0137677

Drouaud, J., and Mezard, C. (2011). Characterization of meiotic crossovers in pollen from *Arabidopsis thaliana*. *Methods Mol. Biol.* 745, 223–249. doi: 10.1007/978-1-61779-129-1_14

Frova, C., and Sari-Gorla, M. (1994). Quantitative trait loci (QTLs) for pollen thermotolerance detected in maize. *Mol. Gen. Genet.* 245, 424–430. doi: 10.1007/BF00302254

Gale, M. D., Rees, H., and Others (1970). Genes controlling chiasma frequency in *Hordeum*. *Heredity (Edinb).* 25, 393–410. doi: 10.1038/hdy.1970.40

Gauthier, F., Martin, O. C., and Falque, M. (2011). CODA (crossover distribution analyzer): quantitative characterization of crossover position patterns along chromosomes. *BMC Bioinform.* 12:27. doi: 10.1186/1471-2105-12-27

Germana, M. A. (2011). Gametic embryogenesis and haploid technology as valuable support to plant breeding. *Plant Cell Rep.* 30, 839–857. doi: 10.1007/s00299-011-1061-7

Habu, Y., Ando, T., Ito, S., Nagaki, K., Kishimoto, N., Taguchi-Shiobara, F., et al. (2015). Epigenomic modification in rice controls meiotic recombination and segregation distortion. *Mol. Breed.* 35:103. doi: 10.1007/s11032-015-0299-0

Higgins, J. D., Armstrong, S. J., Franklin, F. C., and Jones, G. H. (2004). The *Arabidopsis* MutS homolog AtMSH4 functions at an early step in recombination: evidence for two classes of recombination in *Arabidopsis*. *Genes. Dev.* 18, 2557–2570. doi: 10.1101/gad.317504

Higgins, J. D., Osman, K., Jones, G. H., and Franklin, F. C. (2014). Factors underlying restricted crossover localization in barley meiosis. *Annu. Rev. Genet.* 48, 29–47. doi: 10.1146/annurev-genet-120213-092509

Higgins, J. D., Perry, R. M., Barakate, A., Ramsay, L., Waugh, R., Halpin, C., et al. (2012). Spatiotemporal asymmetry of the meiotic program underlies the predominantly distal distribution of meiotic crossovers in Barley. *Plant Cell* 24, 4096–4109. doi: 10.1105/tpc.112.102483

Hill, W. G., and Robertson, A. (1966). The effect of linkage on limits to artificial selection. *Genet. Res.* 8, 269–294. doi: 10.1017/S0016672300010156

Himmelbach, A., Knauft, M., and Stein, N. (2014). Plant sequence capture optimised for Illumina sequencing. *Bio. Protocol.* 4:e1166. doi: 10.21769/BioProtoc.1166

Hiraizumi, Y., Sandler, L., and Crow, J. E. (1960). Meiotic drive in natural populations of *Drosophila melanogaster*.3. Populational implications of the segregation-distorter locus. *Evolution* 14, 433–444.

Hudson, R. R. (1994). How can the low levels of DNA sequence variation in regions of the *Drosophila* genome with low recombination rates be explained? *Proc. Natl. Acad. Sci. U.S.A* 91, 6815–6818. doi: 10.1073/pnas.91.15.6815

IBGSC (2012). A physical, genetic and functional sequence assembly of the barley genome. *Nature* 491, 711–716. doi: 10.1038/nature11543

Khademian, H., Giraut, L., Drouaud, J., and Mezard, C. (2013). Characterization of meiotic non-crossover molecules from *Arabidopsis thaliana* pollen. *Methods Mol. Biol.* 990, 177–190. doi: 10.1007/978-1-62703-333-6_18

Künzel, G. (1982). Differences between genetic and physical centromere distances in the case of two genes for male sterility in barley. *Theor. Appl. Genet.* 64, 25–29. doi: 10.1007/BF00303645

Künzel, G., Korzun, L., and Meister, A. (2000). Cytologically integrated physical restriction fragment length polymorphism maps for the barley genome based on translocation breakpoints. *Genetics* 154, 397–412.

Li, H. (2011). A statistical framework for SNP calling, mutation discovery, association mapping and population genetical parameter estimation from sequencing data. *Bioinformatics* 27, 2987–2993. doi: 10.1093/bioinformatics/btr509

Li, H. (2013). Aligning sequence reads, clone sequences and assembly contigs with BWA-MEM. *arXiv*. arXiv:1303.3997v2.

Li, H., Handsaker, B., Wysoker, A., Fennell, T., Ruan, J., Homer, N., et al. (2009). The sequence alignment/map format and SAMtools. *Bioinformatics* 25, 2078–2079. doi: 10.1093/bioinformatics/btp352

Li, X., Li, L., and Yan, J. (2015). Dissecting meiotic recombination based on tetrad analysis by single-microspore sequencing in maize. *Nat. Commun.* 6:6648. doi: 10.1038/ncomms7648

Linde-Laursen, I. (1982). Linkage map of the long arm of barley chromosome-3 using C-bands and marker genes. *Heredity (Edinb).* 49, 27–35. doi: 10.1038/hdy.1982.62

Lu, P. L., Han, X. W., Qi, J., Yang, J. G., Wijeratne, A. J., Li, T., et al. (2012). Analysis of *Arabidopsis* genome-wide variations before and after meiosis and meiotic recombination by resequencing Landsberg erecta and all four products of a single meiosis. *Genome Res.* 22, 508–518. doi: 10.1101/gr.127522.111

Martin, A. C., Rey, M. D., Shaw, P., and Moore, G. (2017). Dual effect of the wheat Ph1 locus on chromosome synapsis and crossover. *Chromosoma* doi: 10.1007/s00412-017-0630-0. [Epub ahead of print].

Martin, M. (2011). Cutadapt removes adapter sequences from high-throughput sequencing reads. *EMBnet. J.* 17, 10–12. doi: 10.14806/ej.17.1.200

Mascher, M., Gundlach, H., Himmelbach, A., Beier, S., Twardziok, S. O., Wicker, T., et al. (2017). A chromosome conformation capture ordered sequence of the barley genome. *Nature* 544, 427–433. doi: 10.1038/nature22043

Mascher, M., Muehlbauer, G. J., Rokhsar, D. S., Chapman, J., Schmutz, J., Barry, K., et al. (2013a). Anchoring and ordering NGS contig assemblies by population sequencing (POPSEQ). *Plant J.* 76, 718–727. doi: 10.1111/tpj.12319

Mascher, M., Richmond, T. A., Gerhardt, D. J., Himmelbach, A., Clissold, L., Sampath, D., et al. (2013b). Barley whole exome capture: a tool for genomic research in the genus *Hordeum* and beyond. *Plant J.* 76, 494–505. doi: 10.1111/tpj.12294

Melamed-Bessudo, C., and Levy, A. A. (2012). Deficiency in DNA methylation increases meiotic crossover rates in euchromatic but not in heterochromatic regions in *Arabidopsis*. *Proc. Natl. Acad. Sci. U.S.A.* 109, E981–E988. doi: 10.1073/pnas.1120742109

Mirouze, M., Lieberman-Lazarovich, M., Aversano, R., Bucher, E., Nicolet, J., Reinders, J., et al. (2012). Loss of DNA methylation affects the recombination landscape in *Arabidopsis*. *Proc. Natl. Acad. Sci. U.S.A.* 109, 5880–5885. doi: 10.1073/pnas.1120841109

Nilsson, N. O., and Pelger, S. (1991). The relationship between natural variation in chiasma frequencies and recombination frequencies in barley. *Hereditas* 115, 121–126. doi: 10.1111/j.1601-5223.1991.tb03545.x

Pedersen, S. (1988). Pollen competition in barley. *Hereditas* 109, 75–81. doi: 10.1111/j.1601-5223.1988.tb00185.x

Phillips, D., Jenkins, G., Macaulay, M., Nibau, C., Wnetrzak, J., Fallding, D., et al. (2015). The effect of temperature on the male and female recombination landscape of barley. *New Phytol.* 208, 421–429. doi: 10.1111/nph.13548

Phillips, D., Wnetrzak, J., Nibau, C., Barakate, A., Ramsay, L., Wright, F., et al. (2013). Quantitative high resolution mapping of HvMLH3 foci in barley pachytene nuclei reveals a strong distal bias and weak interference. *J. Exp. Bot.* 64, 2139–2154. doi: 10.1093/jxb/ert079

Ritz, K. R., Noor, M. A. F., and Singh, N. D. (2017). Variation in recombination rate: adaptive or not? *Trends Genet.* 33, 364–374. doi: 10.1016/j.tig.2017.03.003

Sall, T. (1990). Genetic control of recombination in barley. 2. Variation in linkage between marker genes. *Hereditas* 112, 171–178. doi: 10.1111/j.1601-5223.1990.tb00054.x

Sall, T., Flink, J., and Bengtsson, B. O. (1990). Genetic control of recombination in barley. 1. Variation in recombination frequency measured with inversion heterozygotes. *Hereditas* 112, 157–170. doi: 10.1111/j.1601-5223.1990.tb00053.x

Salome, P. A., Bomblies, K., Fitz, J., Laitinen, R. A., Warthmann, N., Yant, L., et al. (2012). The recombination landscape in *Arabidopsis thaliana* F2 populations. *Heredity (Edinb).* 108, 447–455. doi: 10.1038/hdy.2011.95

Sarigorla, M., Pe, M. E., Mulcahy, D. L., and Ottaviano, E. (1992). Genetic dissection of pollen competitive ability in maize. *Heredity (Edinb).* 69, 423–430. doi: 10.1038/hdy.1992.146

Sidhu, G. K., Fang, C., Olson, M. A., Falque, M., Martin, O. C., and Pawlowski, W. P. (2015). Recombination patterns in maize reveal limits to crossover homeostasis. *Proc. Natl. Acad. Sci. U.S.A.* 112, 15982–15987. doi: 10.1073/pnas.1514265112

Smith, J. M., and Haigh, J. (1974). The hitch-hiking effect of a favourable gene. *Genet. Res.* 23, 23–35. doi: 10.1017/S0016672300014634

Sybenga, J. (1966). Quantitative analysis of chromosome pairing and chiasma formation based on relative frequencies of M I configurations. 4. Interchange heterozygotes. *Genetica* 37, 199–206. doi: 10.1007/BF01547131

Taylor, D. R., and Ingvarsson, P. K. (2003). Common features of segregation distortion in plants and animals. *Genetica* 117, 27–35. doi: 10.1023/A:1022308414864

Walsh, N. E., and Charlesworth, D. (1992). Evolutionary interpretations of differences in pollen tube growth rates. *Q. Rev. Biol.* 67, 19–37. doi: 10.1086/417446

Wijnker, E., Velikkakam James, G., Ding, J., Becker, F., Klasen, J. R., Rawat, V., et al. (2013). The genomic landscape of meiotic crossovers and gene conversions in *Arabidopsis thaliana*. *eLife* 2:e01426. doi: 10.7554/eLife.01426

Wright, S. I., Foxe, J. P., DeRose-Wilson, L., Kawabe, A., Looseley, M., Gaut, B. S., et al. (2006). Testing for effects of recombination rate on nucleotide diversity in natural populations of *Arabidopsis* lyrata. *Genetics* 174, 1421–1430. doi: 10.1534/genetics.106.062588

Xu, Y., Zhu, L., Xiao, J., Huang, N., and McCouch, S. R. (1997). Chromosomal regions associated with segregation distortion of molecular markers in F2, backcross, doubled haploid, and recombinant inbred populations in rice (*Oryza sativa* L.). *Mol. Gen. Genet.* 253, 535–545. doi: 10.1007/s004380050355

Yelina, N. E., Choi, K., Chelysheva, L., Macaulay, M., de Snoo, B., Wijnker, E., et al. (2012). Epigenetic remodeling of meiotic crossover frequency in *Arabidopsis thaliana* DNA methyltransferase mutants. *PLoS Genet.* 8:e1002844. doi: 10.1371/journal.pgen.1002844

Yelina, N. E., Ziolkowski, P. A., Miller, N., Zhao, X., Kelly, K. A., Munoz, D. F., et al. (2013). High-throughput analysis of meiotic crossover

frequency and interference via flow cytometry of fluorescent pollen in *Arabidopsis thaliana*. *Nat. Protoc.* 8, 2119–2134. doi: 10.1038/nprot.2013.131

Ziolkowski, P. A., Berchowitz, L. E., Lambing, C., Yelina, N. E., Zhao, X., Kelly, K. A., et al. (2015). Juxtaposition of heterozygous and homozygous regions causes reciprocal crossover remodelling via interference during *Arabidopsis* meiosis. *eLife* 4:e03708. doi: 10.7554/eLife.03708

Ziolkowski, P. A., Underwood, C. J., Lambing, C., Martinez-Garcia, M., Lawrence, E. J., Ziolkowska, L., et al. (2017). Natural variation and dosage of the HEI10 meiotic E3 ligase control *Arabidopsis* crossover recombination. *Genes Dev.* 31, 306–317. doi: 10.1101/gad.295501.116

Conflict of Interest Statement: The authors declare that the research was conducted in the absence of any commercial or financial relationships that could be construed as a potential conflict of interest.

frontiers in Plant Science

METHODS
published: 14 August 2018
doi: 10.3389/fpls.2018.01193

ImmunoFISH: Simultaneous Visualisation of Proteins and DNA Sequences Gives Insight Into Meiotic Processes in Nuclei of Grasses

Adél Sepsi[1], Attila Fábián[1], Katalin Jäger[1], J. S. Heslop-Harrison[2] and Trude Schwarzacher[2]*

[1] Department of Plant Cell Biology, Centre for Agricultural Research, Hungarian Academy of Sciences, Martonvásár, Hungary, [2] Department of Genetics and Genome Biology, University of Leicester, Leicester, United Kingdom

ImmunoFISH is a method combining immunolabelling (IL) with fluorescent *in situ* hybridisation (FISH) to simultaneously detect the nuclear distribution of proteins and specific DNA sequences within chromosomes. This approach is particularly important when analysing meiotic cell division where morphogenesis of individual proteins follows stage-specific changes and is accompanied by a noticeable chromatin dynamism. The method presented here is simple and provides reliable results of high quality signal, low background staining and can be completed within 2 days following preparation. Conventional widefield epifluorescent or laser scanning microscopy can be used for high resolution and three-dimensional analysis. Fixation and preparation techniques were optimised to best preserve nuclear morphology and protein epitopes without the need for any antigen retrieval. Preparation of plant material involved short cross-linking fixation of meiotic tissues with paraformaldehyde (PFA) followed by enzyme digestion and slide-mounting. In order to avoid rapid sample degradation typical of shortly fixed plant materials, and to be able to perform IL later, slides were snap-frozen and stored at −80°C. Ultra-freezing produced a remarkable degree of structural preservation for up to 12 months, whereby sample quality was similar to that of fresh material. Harsh chemicals and sample dehydration were avoided throughout the procedure and permeability was ensured by a 0.1–0.3% detergent treatment. The ImmunoFISH method was developed specifically for studying meiosis in *Triticeae*, but should also be applicable to other grass and plant species.

Keywords: meiosis, cytology, chromatin dynamics, immunolabelling, ImmunoFISH, chromatin morphology

OPEN ACCESS

Edited by:
Tomás Naranjo, Complutense University of Madrid, Spain

Reviewed by:
Stefan Heckmann, University of Birmingham, United Kingdom
Pilar Prieto, Instituto de Agricultura Sostenible (IAS), Spain

****Correspondence:***
Adél Sepsi
sepsi.adel@agrar.mta.hu;
sepsiadele@yahoo.fr

Specialty section:
This article was submitted to Plant Cell Biology, a section of the journal Frontiers in Plant Science

Received: *15 May 2018*
Accepted: *25 July 2018*
Published: *14 August 2018*

Citation:
Sepsi A, Fábián A, Jäger K, Heslop-Harrison JS and Schwarzacher T (2018) ImmunoFISH: Simultaneous Visualisation of Proteins and DNA Sequences Gives Insight Into Meiotic Processes in Nuclei of Grasses. Front. Plant Sci. 9:1193. doi: 10.3389/fpls.2018.01193

INTRODUCTION

Chromosome–chromosome interactions leading to homologous pairing at meiosis are accompanied by programmed changes in chromatin organisation and structure. Distinct stages of chromatin remodelling and movement with association of landmark chromosomal regions imprint the period of early meiosis and result in a distinctive nuclear polarisation (Colas et al., 2008; Heslop-Harrison and Schwarzacher, 2011; Sepsi et al., 2017). These chromatin dynamics

are facilitated by meiosis-specific functional protein complexes, whose presence and localisation at particular chromosomal regions reflect the progression through meiosis (Schwarzacher, 2003; Cahoon and Hawley, 2016). To understand regulation and interdependence of these complex events, and to evaluate possible effects on plant fertility, the morphogenesis of specific proteins needs to be visualised in the context of chromatin organisation and movement.

Isolation of the *Arabidopsis thaliana* genes involved in synapsis, recombination and meiotic chromatin movement and the production of polyclonal antibodies against meiotic proteins led to a more accurate deciphering of the meiotic processes in higher plants (Osman et al., 2011; Pradillo et al., 2014; Mercier et al., 2015; Naranjo, 2015; Varas et al., 2015). Methods are available to track meiotic proteins in *Arabidopsis* (Chelysheva et al., 2010; Higgins et al., 2014) but optimal tissue preservation and achievement of high-quality immunosignal in grasses with their large chromosomes (30–100 times the size of *Arabidopsis*; Choulet et al., 2010; Heslop-Harrison and Schwarzacher, 2011) requires modifications of fixation, preparation and labelling techniques.

Analysis of meiosis of crop plants such as the *Triticeae*, where the crop is the seed, is particularly important as any meiotic aberrations directly affect fertility and grain yield and thus have major economic impacts. Cytogenetic techniques including conventional staining, chromosome banding and fluorescent *in situ* hybridisation (FISH) had been used earlier to study meiosis in bread wheat (*Triticum aestivum*, 2n = 6x = 42) and provided valuable knowledge on the pairing of the hexaploid chromosome set. However, a precise timing of chromosome behaviour at early meiosis could not be determined using these techniques alone. Cytological and anatomical criteria (chromatin morphology, anther length and position of the floret within the ear) are only indicative for differentiating stages of prophase I (Aragón-Alcaide et al., 1997; Schwarzacher, 1997; Maestra et al., 2002). On the other hand, whilst electron microscopy can detect lateral and central elements of the synaptonemal complex providing an accurate sequence of chromosome synapsis – thus accurately defining the meiotic sub-stages – the complex preparation reveals only the SC and it is not possible to identify the individual chromosomes (Holm, 1977; Jenkins, 1983; Wang and Holm, 1988).

ImmunoFISH combines FISH to label chromosomes and chromosome regions with immunohistochemistry and high-resolution microscopy, to study chromatin dynamics and specific meiotic proteins simultaneously, providing a precise timing of prophase I (Martín et al., 2017; Sepsi et al., 2017). The protocol presented here was developed for the analysis of meiotic cells of *Triticeae* and focused on the three-dimensional (3D) preservation of nuclei and long-term storage without the need for time-consuming embedding and tissue sectioning. Our protocol, is an all in one method and does not need relocating photographed nuclei with the first procedure [e.g., immunolabelling (IL)] after the second procedure (e.g., FISH) as reported by Martín et al. (2017). It addresses challenges presented when nuclear proteins, often difficult to preserve and requiring careful balanced conditions during IL, are to be detected at the same time as specific DNA sequences using *in situ* hybridisation that require different procedures to open up chromatin to allow penetration of the probe.

Here, we also give details of growing plants in growth cabinets to provide plentiful developmentally homogenous material with healthy ears undergoing meiosis. We followed the chromosome axis component ASY1 and the SC transverse filament protein ZYP1 with respect to active centromeres (CENH3 labelling) and telomeric repeat sequences (TRS-FISH) within male meiotic nuclei of hexaploid wheat (Armstrong et al., 2002; Houben and Schubert, 2003; Higgins et al., 2005) the procedure has been proven on barley and wheat–barley hybrid lines when studying alien centromere activity and chromosome elimination at meiosis. Our method will also be applicable to other *Triticeae* and grass species and to generic FISH protocols (Schwarzacher and Heslop-Harrison, 2000) that we developed in wheat relevant to all plant species with little modification.

The presented fixation and IL method can be used alone to detect proteins. However when combining IL with FISH (ImmunoFISH) it is challenging to balance fixation and permeabilisation treatments to preserve protein antigenicity and 3D nuclear architecture while ensuring cell permeability. We used a non-denaturing fixative (4% paraformaldehyde, PFA), which preserved chromatin and nuclear proteins but hindered penetration of antibodies and labelled FISH probes. Permeabilisation steps were subsequently adjusted by testing several treatments. One of the major limitations of non-denaturing fixation of plant tissues is that samples need to be subject to IL promptly (a few days after fixation) otherwise nuclear integrity would be compromised. Meiotic experiments in wheat as well as other plants, involve processing of a large amount of flowers, spikes, spikelets, and anthers within a short period of time (generally 1–2 weeks for a set of plants), quickly resulting in a large number of preparations and the need to proceed to IL limits the number of plants that can be analysed. We therefore focused on methods for the long-term storage of meiotic preparations prior to the ImmunoFISH procedure in order to facilitate work planning and to increase the number of plants processed.

MATERIALS AND METHODS

Plant Materials

Seeds of spring wheat cv. "Chinese Spring" were sown in Jiffy pellet pots and grown at room temperature (RT) for 10 days or until they were 10 cm high. Plants were replanted in soil in 20 cm diameter pots and transferred to a greenhouse or growth cabinet and maintained at 20°C (±1°C) with 12 h light/day. Winter cultivars that require a period of cold treatment (vernalisation) in order to avoid a delay in ear initiation, were transferred to a vernalisation cabinet ahead of potting up and kept at 4°C with 12 h light/day for 6 weeks. Shorter days (8 h) with slightly higher temperatures (up to 8°C) can also be used.

Potted plants should be ideally grown in growth cabinets where environmental conditions (temperature, day length, humidity, light intensity) can be adjusted to their specific needs.

Alternatively, plants can be grown in a glasshouse or outdoors during spring exploiting the natural increase in day length and temperature, but time interval to flowering will not be as predicable using these methods due to changing weather patterns. A standard cabinet program for wheat consists of 15°C day/10°C night (12 h/day) for an initial 4 weeks period. Day length and temperature should then be increased by 2 h and 2°C, respectively, every 3 weeks until the day-temperature reaches 19°C and the day length 16 h/day. For faster growing wheat varieties and other cereals these time intervals might need to be adjusted as reaching 19°C before meiosis is important for full fertility. Depending on the variety, wheat enters meiosis ∼8–10 weeks after vernalisation. Compared to wheat, barley genotypes reach meiosis earlier, while rye usually enters meiosis 1–2 weeks later.

ImmunoFISH Experimental Procedures

For the following experimental procedures, different reagents and conditions were tested (**Supplementary Table 1**), but only those yielding the best results are given here.

Collection of Meiotic Tissue and Fixation

Meiotic division follows a circadian cycle, and meiocytes are arrested in early meiotic prophase during the night; in order to have stages around or in meiotic metaphase, spikes need to be collected in the morning ∼3 h after the light comes on. Developing ears within leaf sheaths can be felt by gently running the ear between the finger and thumb while squeezing slightly; their position in respect to internodes and the emergence of the flag leaf can be used for estimating ear development (**Figure 1**). Tillers estimated to enter meiosis were collected and placed in water to avoid desiccation. Spikes were then dissected from the leaf sheaths and transferred to a Petri dish containing a wet filter paper.

Spikes composed of a series of spikelets alternating on opposite sides of the rachis were numbered for reference starting at the bottom. Spikelets of hexaploid wheats carry at least three fertile florets (**Figure 1**), however, only the first two florets are used in most studies, since they are the best developed and most uniform. The most developed spikelets are located in the middle of the ear while spikelets towards the top and the base carry florets at successively earlier stages with the top and bottom spikelet, respectively, being the earliest. Anthers of the same floret carry meiocytes in the same developmental stage (Bennett, 1971). Starting with the spikelet positioned at the middle of the ear, one anther was excised from the first two florets (termed as floret A and B) and squashed in 45% (v/v) acetic acid to determine the approximate meiotic stage. Anther lengths were also carefully noted down for future reference. The two remaining anthers of each floret were placed into a 14-mm cell culture insert (8 μm membrane pore size, Thermo Fisher Scientific, Waltham, MA, United States, No. 140656) in a 12-well tissue culture plate containing ice-cold 4% PFA.

Isotonic microfiltered PFA (Agar Scientific, Stansted, United Kingdom; No. R1026, 16%) was diluted to 4% in 1× PBS (phosphate buffered saline, 137 mM NaCl, 2.68 mM KCl, 10 mM Na_2HPO_4, 1.76 mM KH_2PO_4, pH 7.4). 4% PFA can alternatively be freshly prepared by dissolving PFA powder (Sigma-Aldrich, Darmstadt, Germany, No. P6148) in 1× PBS by heating to 75–80°C while stirring. A 48-μM NaOH/100 ml of fluid should be added (e.g., 6 μl of 8 M NaOH/100 ml) after which the mix will immediately clear. To avoid thermal decomposition, care should be taken not to overheat the solution. Sampling continued towards the bottom of the ear and anthers were consequently checked and fixed from the first two florets of each spikelet. In order to allow the penetration of PFA into the inner layers of the tissues, anthers were fixed for 1 h while kept on ice. Washing consisted of two times 5 min at RT in 1× PBS by keeping the anthers in the inserts and exchanging the fluids with a fine tip Pasteur pipette. Fixed and washed anthers were kept in a final change of fresh 1× PBS in the inserts of the plate that was covered with a lid and placed on ice into an icebox and left at 4°C overnight (**Figure 2**).

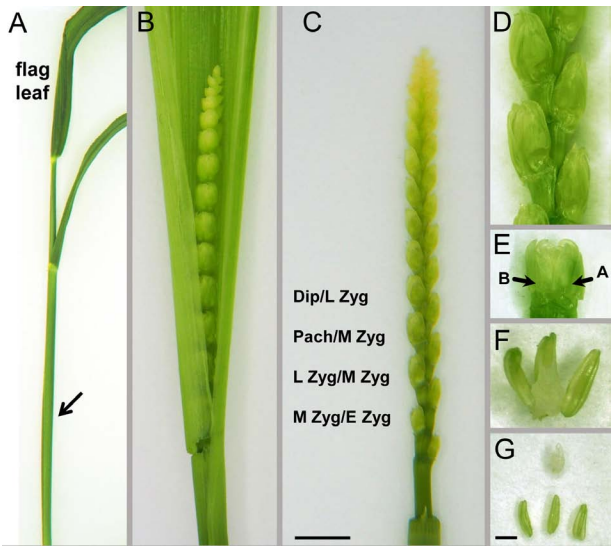

FIGURE 1 | Dissection of anthers from the developing wheat spike. **(A)** An intact spike entering meiotic prophase I with the flag leave emerged and the ear enclosed within the sheaths of leaves (arrow). **(B)** The developing wheat ear within the manually opened leaf sheaths. **(C)** Dissected ear with a series of spikelets; each spikelet has a series of florets with decreasing developmental stages, example of stages as indicated. Dipl, diplotene; Pach, pachytene; Zyg, zygotene, L, late; M, middle; E, early. Bar = 1.5 cm in **(A)**, 1 cm in **(B)**, and 0.5 cm in **(C)**. **(D)** Alternating pattern of spikelets at the middle of the ear. **(E)** An individual spikelet with the two most developed florets termed as floret "A" and floret "B" (arrows). **(F,G)** Three anthers and the ovary dissected from an individual floret within a spikelet. Bar = 1 mm in **(D,E,G)**, 0.5 mm in **(F)**.

Preparation of Cell Nuclei for ImmunoFISH

1× PBS washing buffer was removed carefully and replaced by 300 μl of enzyme solution prepared according to Houben and Schubert (2003). Final concentrations were as follows: 2.5% (w/v) pectinase (from *Aspergillus niger*, 1 U/mg protein Sigma-Aldrich, 17389) 2.5% (w/v) pectolyase (from *Aspergillus japonicus*, 0.3 U/mg protein, Sigma-Aldrich, P3026), 2.5% (w/v) cellulase

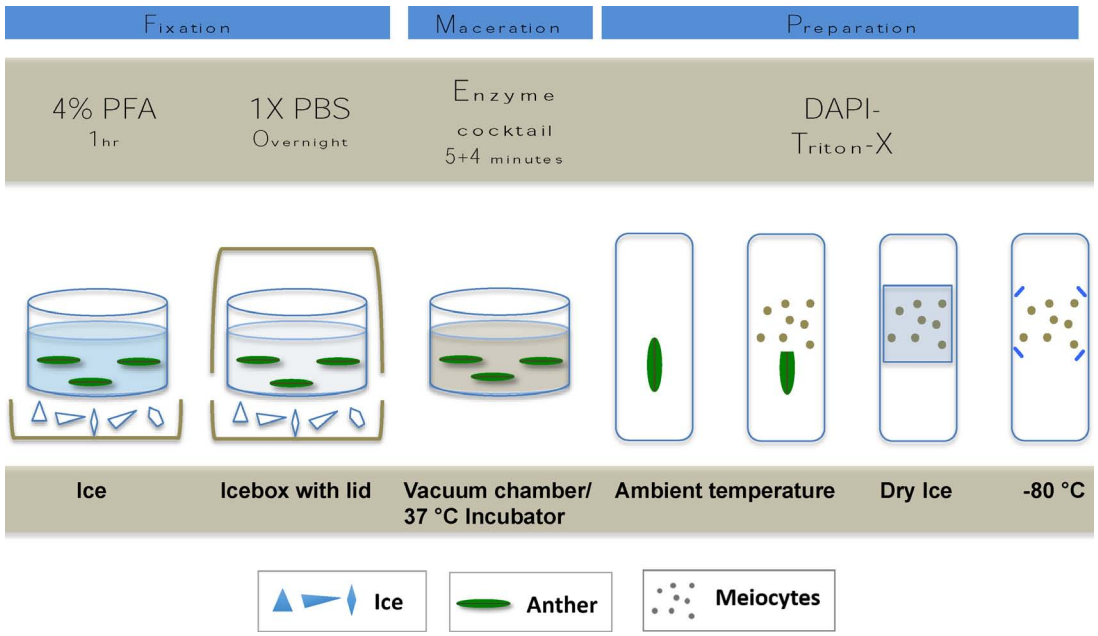

FIGURE 2 | Cartoon showing the main steps of tissue fixation maceration and slide mounting of meiotic nuclei preparation.

(from *A. niger*, 0.3 U/mg protein, Sigma-Aldrich, C1184) and 1.5% (w/v) cytohelicase (extracted from *Helix pomatia*, Sigma-Aldrich, No. C8274); enzyme mixture can be stored frozen at −20°C for several months and can be used repeatedly. Five minutes of vacuum infiltration was used to facilitate enzyme penetration. Samples were subsequently incubated at 37°C for an additional 5 min. Anthers were kept on ice and subsequent sample preparation was made to judge the extent of digestion. Incubation with the enzyme mix could be extended for a further 5 min at 37°C if needed. The enzyme solution was then immediately taken off and replaced with ice-cold 1× PBS (two times for 5 min).

Preparations were made promptly after the enzyme treatment on Superfrost Plus Adhesion slides (Thermo Fisher Scientific). The anther tip was cut with a razor blade and using fine tungsten needles, pollen mother cell loculi were squeezed out into a drop of DAPI-Triton-X (2 μg/ml 4′,6-diamidino-2-phenylindole, Sigma-Aldrich, No. 10236276001; diluted from 100 μg/ml stock in water with 0.05% Triton-X in 1× PBS). A coverslip was carefully placed on the top of the cell mixture and tapped lightly to produce a single layer of meiotic cells then pressed gently between filter papers. The quality of preparations was examined by using an epifluorescent microscope and slides suitable for ImmunoFISH were snap-frozen on dry ice. Coverslips were removed by a razor blade and slides were either used immediately or quickly transferred to −80°C to avoid preparations drying out (**Figure 2**). Samples were stored for up to 12 months.

FISH Probe Preparation

The universal plant TRS were amplified by PCR using the oligomer primers T1 (5′-TTTAGGG-3′)$_5$ and T2 (5′-CCCTAAA-3′)$_5$ (Schwarzacher and Heslop-Harrison, 1991). For preparing the barley genomic probe, total genomic DNA of barley was sheared and labelled by nick translation with biotin-14-dATP as described (Sepsi et al., 2008).

Permeabilisation, Post-fixation, and *in situ* Hybridisation

Before *in situ* hybridisation, nuclei were permeabilised so that the FISH probes could access the chromatin threads. Several conditions and different detergents were tested (see section "Results") before settling on the most successful as follows. Slide-mounted preparations were taken out from the ultra-freezer and immediately put into cold (4°C) 1× PBS buffer for 5 min. Slides were then transferred to 0.1% Triton-X and 0.3% CHAPS (3-[(3-cholamidopropyl)dimethylammonio]-1-propanesulfonate) hydrate (Sigma-Aldrich, No C3023) in 1× PBS and incubated at RT for 10–15 min and washed twice in 1× PBS. Subsequently, preparations were incubated in 10 mM HCl for 1 min at RT and 50 μl pepsin solution (100 μg/ml pepsin in 1 mM HCl, Sigma-Aldrich, No P6887 3,200-4,500 U/mg protein) was applied to each slide, covered with a parafilm cover slip and incubated at 37°C for 5 min. Slides were rinsed in distilled water followed by a quick post-fixation step in 4% PFA in 1× PBS (3 min at RT under a fume hood) and washed in 1× PBS.

Slides first underwent the FISH protocol (see Schwarzacher and Heslop-Harrison, 2000; Sepsi et al., 2008). Briefly, the probe mixture was prepared for each slide by adding 60 ng labelled TRS probe to 30 μl hybridisation mix consisting of 60% (v/v) deionised formamide (Sigma-Aldrich, No. F9037) and 10% (w/v) dextran sulphate (Sigma-Aldrich, No. 67578) in 2× SSC. The probe mixture was denatured at 85°C for 8 min 30 s in a PCR machine and immediately transferred to ice for at least 5 min.

The ice-cold mixture was carefully pipetted on the surface of the preparations and covered with a 22 × 32 glass coverslip. The slides were denatured together with the probe mix at 75°C for 4 min on a PCR machine equipped with a stainless steel plate (see Sepsi et al., 2008). The slides were then transferred to a plastic box with a fitted lid containing moist tissue paper, and incubated at 37°C overnight. Post-hybridisation washes consisted washing slides four times in 1× PBS at 37°C 5 min each taking care that slides do not dry out between steps.

Immunolabelling of Meiotic Proteins

Nuclei preparations were blocked immediately after the post-hybridisation washes by adding 50–100 μl of IS blocking buffer consisting of 1× TNB (0.1 M Tris–HCl, pH 7.5, 0.15 M NaCl, 0.5% Blocking Reagent, Roche, No. 11096176001) and 0.3 M Glycine (Sigma-Aldrich, G8898). A parafilm coverslip was applied and slides were replaced in the plastic box for 30–60 min at RT. Rabbit anti-CENH3 primary antibody was prepared as described by Sepsi et al. (2017). Guinea pig anti-ASY1 antibody was developed by an immunisation program using a recombinant protein including the Horma-domain of *A. thaliana* ASY1 protein while the ZYP1 antibody was produced against a recombinant protein matching the C-terminal region of the *A. thaliana* ZYP1B protein (Osman et al., 2018). Primary antibodies were diluted in a ratio of 1:300 in IS blocking buffer. A 50 μl of the diluted solution was added to each slide covered with a plastic coverslip and put back into the moist plastic box. Preparations were incubated for 3 h at 37°C then washed twice in 1× PBS at RT 5 min each again avoiding any drying out between steps.

In order to detect the localisation of the primary antibodies and that of the biotin FISH signal we used appropriate secondary antibodies depending on the animal that the primary antibodies were raised with and are as follows: goat anti-rabbit IgG, Alexa 594 or 488 (Invitrogen, CA, United States No. A-11072, A-11008), donkey anti-rat IgG, Alexa 488 or goat anti-rat IgG Alexa 594 (Invitrogen No. A-21208 and Abcam, Cambridge, United Kingdom, No. ab150160), goat anti-guinea-pig IgG, Alexa 647 (Abcam, No. ab150187) and streptavidin, Alexa 488 or Alexa 594 conjugates (Invitrogen, Nos. S11223, S11227). The working solution was prepared in IS blocking buffer with a final concentration of 1:300 for the secondary antibodies and a 4 μg/ml final concentration for the streptavidin. A 50 μl of the working solution was added to each slide, covered with a plastic coverslip and incubated for 30–45 min at 37°C. After washing the slides twice in 1× PBS, 12 μl of Vectashield Antifade Mounting Medium with DAPI (Vector Laboratories, Burlingame, CA, United States, No. H-1200) was applied per slide and covered with a thin 22 or 24 × 32 No. 0 glass coverslip.

Image Collection

Confocal microscopy was carried out using a Leica TCS SP8 confocal laser-scanning microscope (Leica Microsystems GmbH, Wetzlar, Germany). Series of confocal images ("*z* stacks") with a lateral (*x* and *y*) resolution of 45 nm and an axial (*z*) resolution of 200 nm were acquired by a HC PL APO CS2 63×/1.40 oil immersion objective (Leica Microsystems GmbH). Size of confocal aperture was set to 1.35 Airy Unit (128.9 μm). Image acquisition was carried out by bidirectional scanning along the *x*-axis, and images were averaged from three distinct image frames in order to reduce image noise. Image stack deconvolution was performed using a Huygens Essential software v17.10 (Scientific Volume Imaging, Hilversum, Netherlands). 3D reconstructions were obtained using a Leica Application Suite Advanced Fluorescence software v3.1.5.1638 (Leica Microsystems GmbH).

ImmunoFISH images of wheat–barley introgression lines were captured by widefield microscopy on a Nikon Eclipse 80i epifluorescent microscope equipped with DS-QiMc monochromatic camera (Nikon, Tokyo, Japan). Series of grey-scale images for each colour were captured along the *Z*-axis, taking 15–20 stacks per colour. Single channel images were pseudocoloured and merged in NIS elements (Nikon). All-in-focus images were created using the extended depth of focus (EDF) module.

RESULTS

By using our method, chromatin dynamics could be mapped in high resolution within the meiotic nuclei of bread wheat. We were able to visualise nuclear structures (telomeres, centromeres, SC axial and central element related proteins) simultaneously with the bulk chromatin (DAPI contrast staining) and followed changes in organisation and structure throughout meiotic prophase I (**Figures 3–5**). Proteins and landmark chromosome regions can be detected together at 2D or 3D by conventional epifluorescence microscopy, however, resolution, especially along the *z*-axis will be low. As nuclei were only squashed lightly during preparation, this allowed us to observe meiotic nuclei in 3D by using optical sectioning reaching a resolution of 45 nm in the *x*- and *y*-directions, and 150–200 nm in the *z*-direction. By sampling nuclei of different developmental stages from anthers of florets at defined positions within the ears (**Figure 1**), a sequence of meiotic chromatin events could be developed.

Preservation of Nuclei and Proteins

Good spatial visualisation of cellular structures, such as we were able to observe (**Figures 3**, **4**), assumes meiotic cells to be adequately preserved, stored and handled during the staining procedures. Cells fixed with PFA have a superior cellular architecture and proteins are preserved in their 3D relationships within the nucleus (Kiernan, 2000). However, in order to access nuclear structures during IL and FISH, only a very short PFA fixation (1–2 h) at 4°C with immediate transfer to buffer can be undertaken (**Supplementary Table 1**) and therefore keeping those fixed plant tissues at RT or 4°C would shortly lead to sample degradation and quality loss. Similarly, keeping ready prepared slides at RT also showed sample degradation.

In order to store slides and plan experiments with large number of samples, we investigated the effect of deep-freezing on the preservation of preparations. Storage of slides at −20°C saw a rapid decrease in quality, however, snap freezing followed by storage at −80°C preserved the 3D structure for up to 12 months

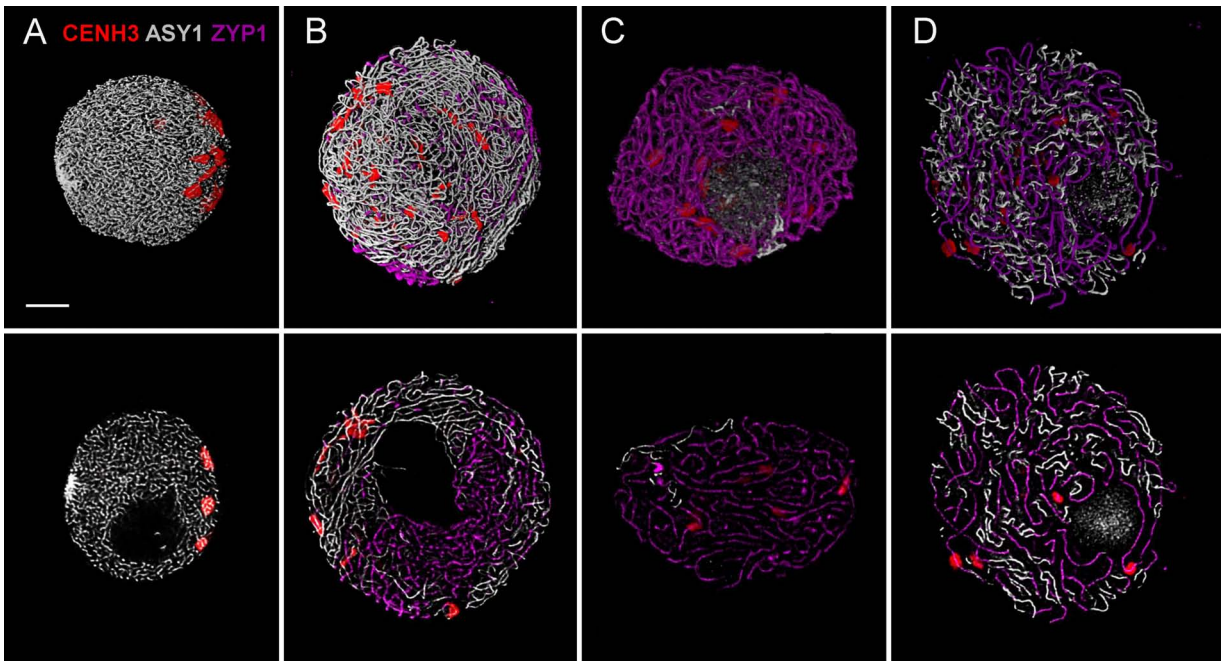

FIGURE 3 | Three-colour immunolabelling on meiotic prophase I (leptotene to diplotene) nuclei of wheat. CENH3 centromeric protein is visualised by a rabbit anti-CENH3 antibody and is shown in red, SC axial element protein ASY1 is visualised by a guinea pig anti-ASY1 antibody and is shown in grey and SC central element protein is visualised by a rat anti-ZYP1 antibody and is pseudo-coloured in purple. Three-dimensionally reconstructed confocal image stacks are shown in the top row while a single *z* stack of the image is presented in the bottom row. Images show substages of meiotic prophase I: **(A)** leptotene, **(B)** mid-zygotene, **(C)** pachytene, **(D)** diplotene. Bar = 5 μm.

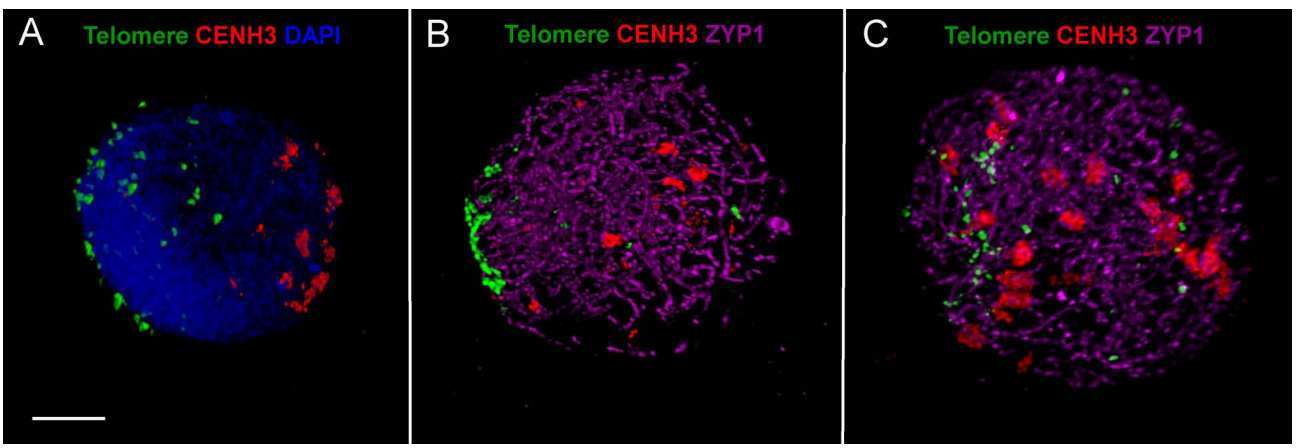

FIGURE 4 | ImmunoFISH showing progression of synapsis and simultaneous centromere–telomere dynamics through three successive stages of meiotic prophase I in wheat. **(A)** Early leptotene, **(B)** early-mid zygotene, **(C)** late zygotene. Active centromeres and the SC central element protein are visualised by immunolabelling with anti-CENH3 (rabbit, red) and anti-ZYP1 (rat, purple) antibodies while telomeres are detected by TRS-FISH (green). Bar = 5 μm.

(**Supplementary Table 1**) and the quality of the stored slides was comparable to those of the fresh samples. For a good structural preservation, it is important to avoid preparations drying out throughout all steps of the procedure.

Permeabilisation of Tissue

This fixation method can be used to detect proteins using IL. However, when combined with FISH one needs to balance fixation and permeabilisation treatments in order to preserve protein antigenicity and 3D nuclear architecture, whilst ensuring cell permeability. We used a non-denaturing fixative (4% PFA), which preserved chromatin and nuclear proteins but hindered penetration of antibodies and labelled FISH probes. We tested several concentrations and combinations of permeabilisation agents (cold methanol, Proteinase-K, RNase, Tween-20, Triton-X-100, CHAPS-hydrate, repeated freeze-thaw

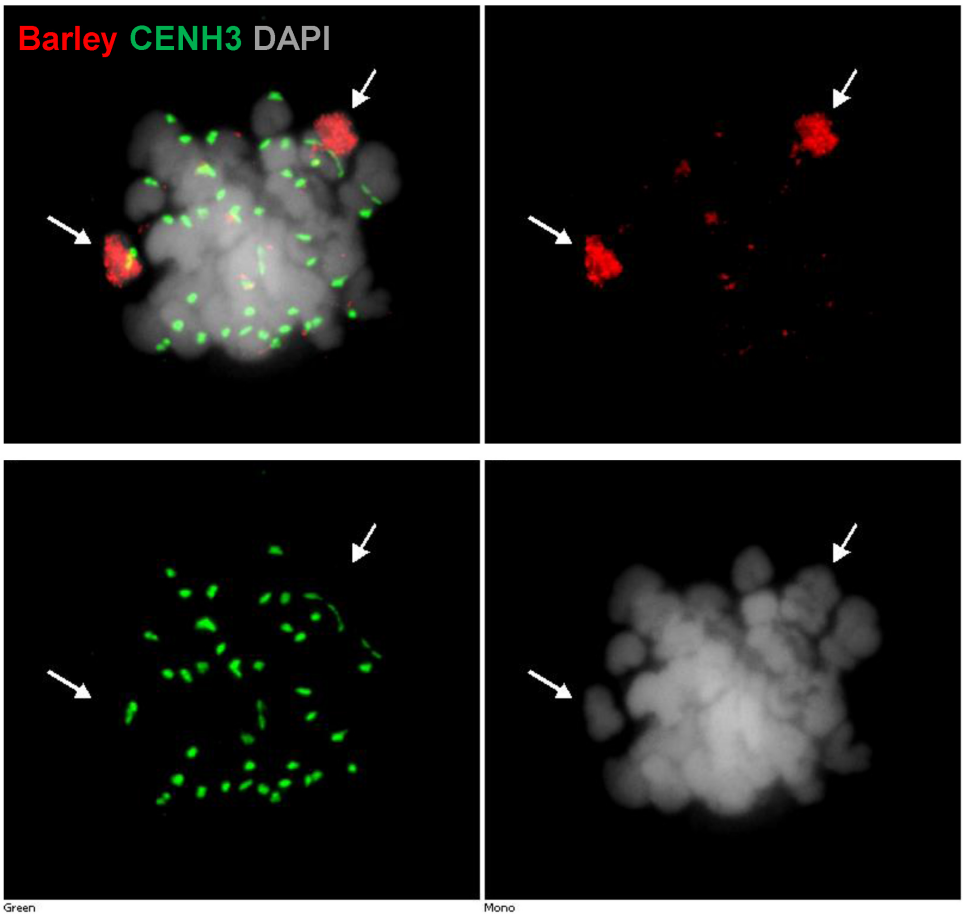

FIGURE 5 | Detection of barley chromatin and CENH3 centromeric histone protein within the metaphase chromosomes of a wheat–barley addition line (2n = 6x = 44) carrying a pair of 3H chromosome and the complete chromosome complement of wheat. Barley chromatin is shown in red (arrows) and CENH3 is visualised in green colour labelled by a rabbit-anti CENH3 antibody. Chromosomes are counterstained by DAPI (grey signal). Bar = 5 μm.

cycles; see **Supplementary Table 1**) for various times prior to ImmunoFISH to achieve an optimal accessibility of DNA and proteins whilst maintaining nuclear structure. The best results were obtained with a low concentration of Triton-X-100 and CHAPS hydrate-solution (0.1 and 0.3%, respectively, in 1× PBS) followed by a short pepsin digestion and a quick PFA post-fixation step applied before FISH (**Supplementary Table 1**). NICK-Translation *in situ* probe labelling was chosen in order to control probe-length (the longer the Nick-translation procedure the shorter the probe) and thus further facilitate penetration, but assume that short directly labelled oligonucleotides or those labelled with random priming will also be suitable.

Precise Protein Immunolocalisation During Meiosis

Following adequate fixation and permeabilisation treatments we obtained well-preserved meiotic nuclei and were able to label the following nuclear structures with IL: CENH3 protein (showing active centromeres) together with SC axial and central element proteins ASY and ZYP1. Subsequently, in separate experiments we performed ImmunoFISH to show telomeres and centromeres concurrently with SC central elements (ZYP1): telomeres were visualised by FISH (TRS-FISH) while centromeres and the ZYP1 proteins were stained by IL. The bulk chromatin was labelled by DAPI in both cases. This enabled us to correlate centromere–telomere dynamics and that of the bulk chromatin to the development of the synaptonemal complex (Sepsi et al., 2017; **Figures 3**, **4**).

Samples were scanned by confocal laser scanning microscopy (CLSM) and 2D images were collected every 200 nm in depth (*Z*-direction) from each channel resulting in *z* stack series covering the whole 3D volume of the nucleus (**Figures 7A–D**, **8A,B,F,G**). Consequently, merged 2D images of the four channels collected from the same focal plane represented localisation of the nuclear structures within the *x*- and *y*-axis (**Figures 3** bottom row, **6**, **7E**, **8C–E**) while 3D reconstruction of the whole *Z*-series allowed modelling of spatial relationships within the nucleus (**Figures 3** top row, **7A–D**, **8**).

As a single ear of a cereal plant contains a sequence of meiotic stages, sampling spikelets/anthers from the middle towards the bottom or top of the ear revealed dynamics of

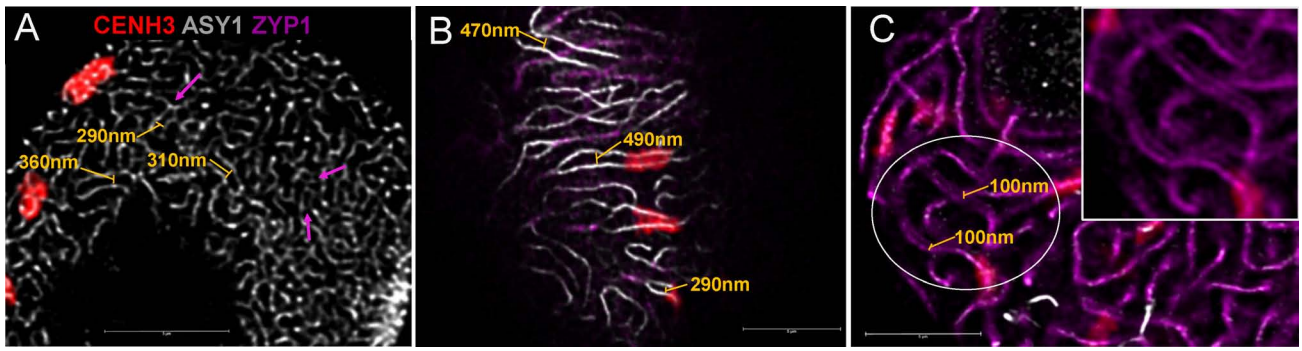

FIGURE 6 | Axis distances during early meiotic prophase I in hexaploid wheat. **(A)** Leptotene and **(B)** zygotene images are single stack enlargements from samples presented in **Figures 3A,B**. Panel **(C)** is from a pachytene nucleus. Unsynapsed chromosome axes (later lateral elements) are shown as white threads (guinea pig anti-ASY1 antibody, detected by Alexa 647), the central element protein of the synaptonemal complex (rat anti-ZYP1 antibody, is pseudocoloured in purple and active centromeres (rabbit anti-CENH3 antibody) are displayed in red. Axis distances are indicated by yellow bars on **(A)** and **(B)** and purple arrows highlight closely aligned, coalescing chromosome axes. Pachytene double structures **(C)** seen with the anti-ZYP1 antibody are highlighted by yellow bars; a region of interest is enlarged and inserted to the upper right of the figure). Bar = 5 μm.

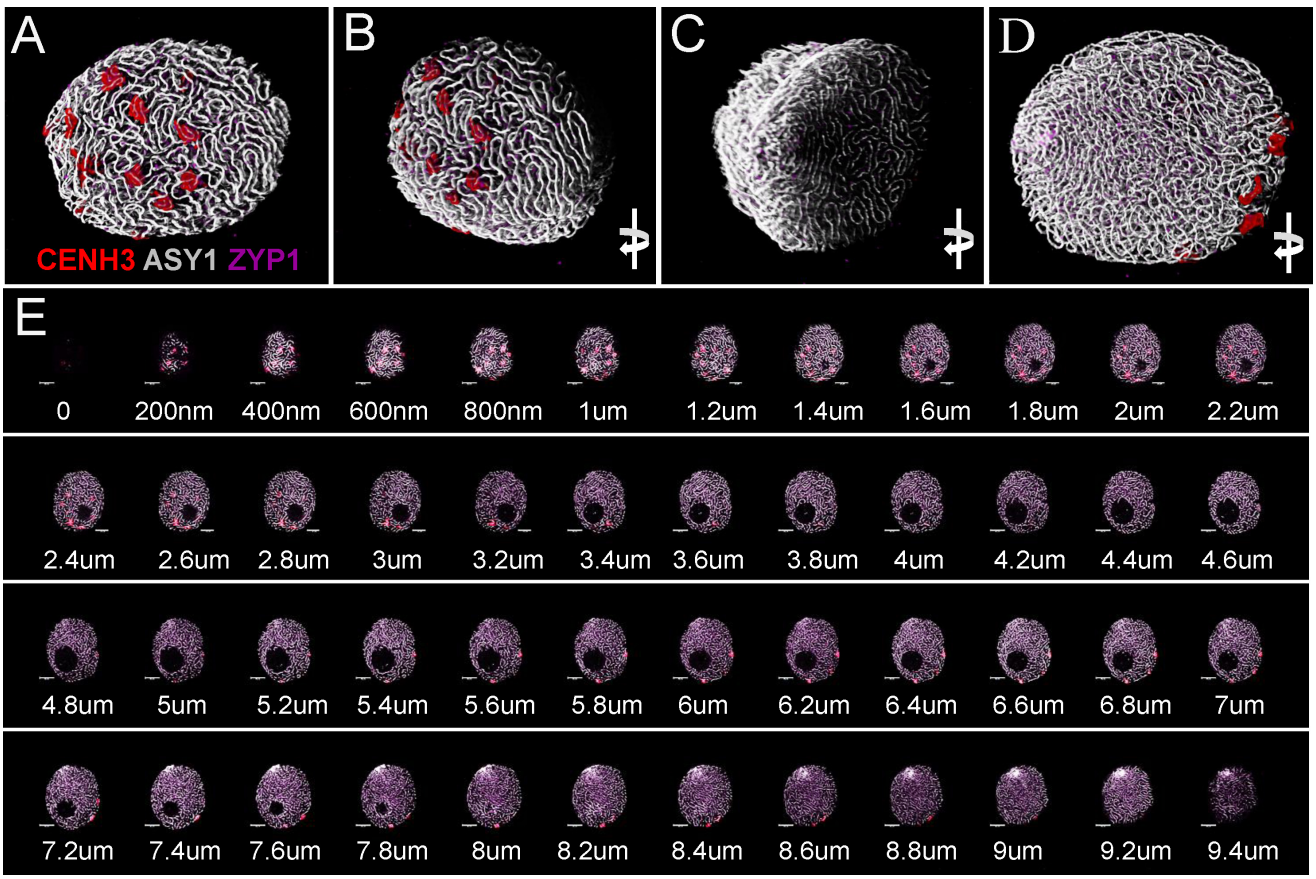

FIGURE 7 | Three-dimensional rendering of 2D confocal images collected from sequential focal planes of an early zygotene nucleus. Different channels represent signals from anti-CENH3 (red), anti-ASY1 (white), and anti-ZYP1 (purple) antibodies. The 3D image is turned to be observable from different angles. **(A)** Centromeric pole, **(B)** side view of the centromeric pole, **(C)** telomeric pole with the telomere bouquet, **(D)** projection turned 180° compared to the centromeric pole. **(E)** Optical sections collected by confocal laser scanning microscopy showing sequential focal planes of **(A–D)**. ΔZ = 200 nm. Bar = 5 μm.

nuclear structures during meiotic prophase I. Centromere- and telomere associations, their position with respect to the nuclear envelope and the state of SC formation are reliable indicators of meiotic progression and can be referred to

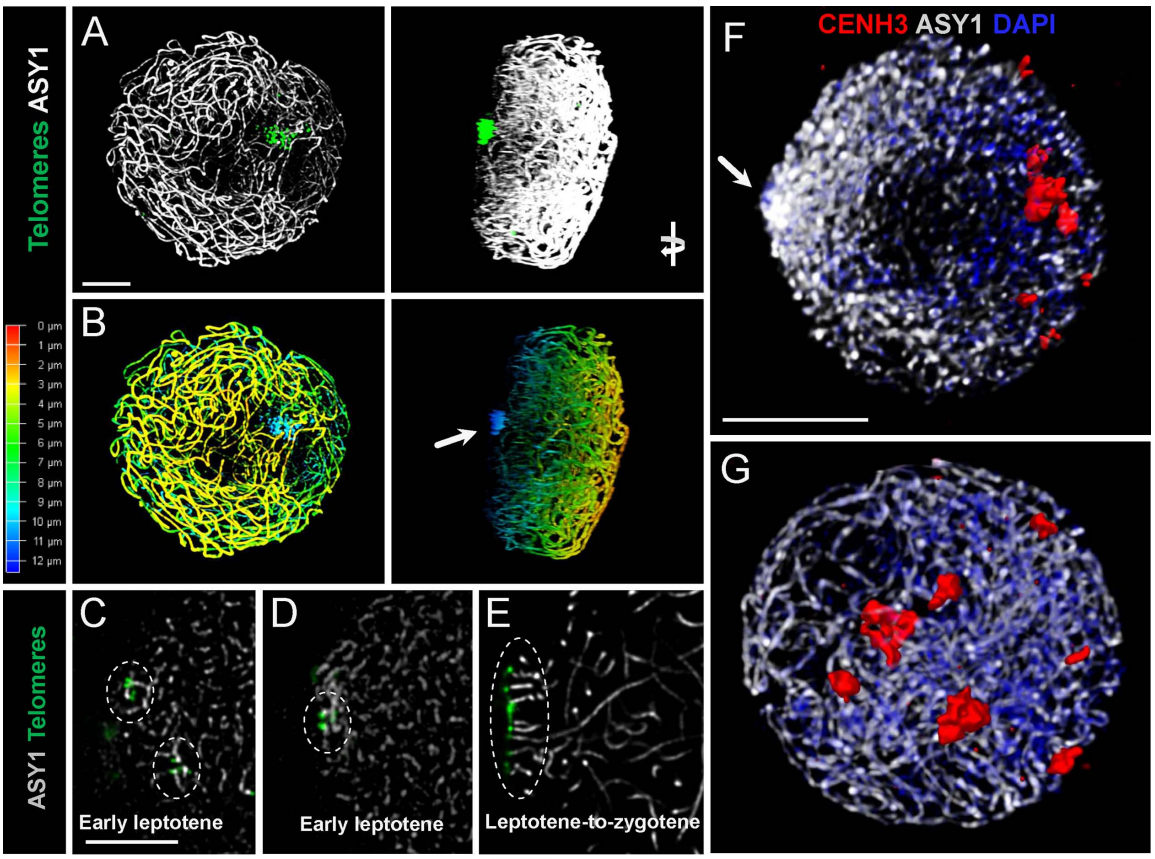

FIGURE 8 | Spatial relationships of telomeres, centromeres, and chromosome axes in early meiosis of a diploid and a synthetic tetraploid barley (2n = 4x = 28, originating from a cross between two autotetraploid *Hordeum vulgare* cultivars: Morex × Golden Promise). Axial elements are visualised by an anti-ASY1 antibody (white signal), centromeres are stained with an anti-CENH3 antibody and shown in red, while telomeres are detected by FISH (green signal in **A,C–E**). Chromatin is contrast stained with DAPI (blue) on **(F,G)**. **(A)** Snapshot of a 3D rendered early zygotene nucleus with continuous chromosome axes and fully formed telomere bouquet in the tetraploid barley. The nucleus is turned to show the side view. **(B)** Conversion of the 3D rendered stack into a 2D image by *z*-depth-coding, whereby consecutive *z*-slices are represented by a specific colour (colour coding on the left). Note the extreme peripheral localisation of the telomeres perceived in deep blue (= 12 µm in depth, arrow). **(C,D)** Single stack images showing early telomere behaviour in tetraploid barley with small telomere groups (encircled) scattered within the nucleus in early leptotene while chromosome axes are yet uncontinuous (white signal). **(E)** At the leptotene-to-zygotene transition telomeres become gathered within a small peripheral area of the nucleus to form the bouquet while subtelomeric chromosome axes align in anticipation of pairing (white parallel threads, encircled). **(F)** Uncontinuous chromosome axes within a polarised leptotene nucleus and small centromere groups located close to the nuclear periphery while the telomere bouquet is formed at the opposite pole (arrow). **(G)** Axial elements are linear and centromeres become released from the nuclear periphery during zygotene.

as meiotic markers showing sub-stages of prophase I (Sepsi et al., 2017). Leptotene nuclei, defined by the formation of major polarised centromere associations and the linearisation of axial elements along chromosomes, showed in addition to our previous results (Sepsi et al., 2017) a notable nuclear compaction (**Figure 3A**). Chromosome axes were compressed against each-other frequently forming parallel alignments of less than 300 nm while some regions showed two separate chromosome axes coming near each other and coalescing through protein bridges (**Figure 6A**). During zygotene, when synapsis elongates in two stages (first from the telomeres and second from the chromosome arms), nuclei became enlarged and parallel alignments between the unsynapsed axes measured 300–500 nm, exceeding axis distances observed at leptotene (**Figures 3B**, **6B**). At pachytene, bivalents show perfect synapsis and when labelled with anti-ZYP1 antibody juxtaposed axes were discerned as double-structures 100 nm apart (**Figure 6C**). Asymmetric arrangement typical of early prophase nuclei resolved at late zygotene when the telomere bouquet dispersed (Sepsi et al., 2017; **Figure 4**) and during desynapsis in diplotene landmark chromosomal regions showed random distribution (**Figures 3C,D**).

We also used ImmunoFISH detected by widefield fluorescence microscopy to follow centromere activity of alien chromosomes in wheat–barley introgression lines (**Figure 5**). Labelled total genomic DNA of barley and CENH3 antibody showed active centromeres demonstrating that barley centromeres successfully load wheat CENH3, (**Figure 5**).

We analysed early meiosis in diploid barley cv. Golden Promise (2n = 2x = 14) and in a synthetic tetraploid barley (2n = 4x = 28) and showed association of telomeres in small groups scattered within the nucleus during the period of axis

extension in early leptotene which was followed by telomere bouquet formation (**Figures 8C–E**). Leptotene was marked by a polarised chromatin organisation whereby telomeres were gathered close to the nuclear envelope and centromeres were associated in small groups at the periphery opposite to the telomere bouquet (**Figures 8A,B,F,G**).

DISCUSSION

Here we present a simple and reliable protocol for the IL of meiotic proteins within higher plants, combining IL with FISH, offering the advantage of simultaneously tracking multiple proteins and specific DNA sequences. Previous methods providing visualisation of high quality 3D nuclear structures in plants required laborious tissue fixation, embedding and sectioning (Holm, 1977; Murphy and Bass, 2012) and have limited possibilities for the identification of specific proteins and DNA sequences. Sectioning of the material after short fixation using a vibratome can take several days despite the need for processing plant material promptly following a brief fixation (Aragon-Alcaide et al., 1998; Prieto et al., 2007) risking the degradation of material. Our technique produces a single layer of well-preserved, cytoplasm-free nuclei embedded in antifade, an ideal situation for high resolution imaging with CLSM. Good resolution using CLSM on thick sections is only possible within the upper 15–20 μm of the preparations because of the light scattering effect of the cytoplasm and the cell walls, reducing the efficiency of both fluorochrome excitation and emitted signal detection. Although point spread function of the imaging system can be corrected using a deconvolution software, signal-reducing effect of the thick tissue surrounding the nuclei results in lower quality compared to the single-layer preparations. Our method does not depend upon specialised sectioning equipment and can be completed within two working days following slide preparation. Moreover, meiotic preparations can be stored for several months in an ultra-freezer without any effect on nuclear morphology, allowing a better project planning and processing of a significantly higher number of plants.

ImmunoFISH was used earlier to follow chromatin dynamism during SC formation in hexaploid wheat and revealed that major centromere associations followed by the formation of the telomere bouquet create a highly polarised nuclear environment that immediately precedes synapsis initiation from the telomeres. We showed that centromere dynamics (notably depolarisation and scattering of centromere clusters) correlates with a second wave of SC elongation from multiple nucleation sites within the euchromatic chromosome arms (Sepsi et al., 2017).

In the present work, we were able to increase the resolution of our analysis, and to measure axis distances through meiotic prophase I and showed alignments of 200–300 nm at leptotene. In contrast, parallel configurations of unsynapsed regions at mid-zygotene spanned 300–500 nm indicating that the tight chromatin arrangement observed in early meiosis is relaxed upon SC initiation. Presynaptic alignments of 400 nm typical of leptotene nuclei are known to be mediated by recombination initiation through the interactions of homologous duplexes (Henderson and Keeney, 2005). A detailed investigation in the filamentous fungus *Sordaria macrospora* (Storlazzi et al., 2010) indicated that homologous juxtapositions at leptotene are promoted by proteins of the recombination machinery (Mer3, Msh4, and Mlh1) with Msh4 identified as the first factor specifically determining presynaptic inter-axis distances. Thus, specific recombination complex proteins support homologous pairing well before their action in the recombination process. Double strand break (DSB)-mediated homologue interactions also define spatial patterns of SC nucleation sites, a subset of which carry embedded crossover interactions (Zhang et al., 2014). Larger axis distances as we showed at mid-zygotene, when a great proportion of the chromosome arms were synapsed, are most likely indicative of synapsis elongating from earlier nucleation sites rather than new SC initiation sites.

Protein morphogenesis can reflect initiation and progression of recombination, strategy of synapsis construction in wild and mutant backgrounds and thus is a major indicator of the fate of meiosis. Alteration in chromatin organisation and dynamics are essential to generate chromosome–chromosome interactions during the critical period of homologue recognition and pairing, so the timing and fidelity of synapsis and recombination relies on these processes (Lambing et al., 2015; Székvölgyi et al., 2015). Meiosis is influenced by environmental factors so it is increasingly relevant to reveal meiotic progression under stress conditions in crops and highlight the variable exposures influencing recombination, fertility and ultimately yield (Jackson et al., 2015; Phillips et al., 2015; Modliszewski and Copenhaver, 2017). To understand the control and interdependence of key meiotic events in higher plants it is critical to simultaneously study DNA processes and chromatin organisation. Our method has allowed us to analyse chromatin dynamics at meiosis with high resolution and will be applicable to plant species in general to gain insight into this critical stage of plant reproduction.

DATA AVAILABILITY

All datasets generated for this study are included in the manuscript.

AUTHOR CONTRIBUTIONS

TS, JH-H, and AS conceived and designed the project. AS made the chromosome preparations and performed the cytological experiments. AF and KJ designed the settings and carried out the confocal microscopy analysis. AS and TS wrote the paper. All authors contributed to the manuscript revision, and read and approved the submitted version.

FUNDING

The present work was funded by the European Union's Seventh Framework Programme "People," Marie Curie Actions (FP7/2007-2013) under REA grant agreement no. 625835, by

the Hungarian Academy of Sciences (János Bolyai Research Scholarship, GENPROF IF 18/2012 and KEP-5/2017), and by the Hungarian Scientific Research Fund (OTKA, proposal ID 124266).

ACKNOWLEDGMENTS

We thank Dr. John Bailey for revising the manuscript and for his advice and help with meiotic chromosome preparation. We are grateful to Drs. James Higgins and Stuart Desjardin for providing support during recombinant protein production used for the generation of the ASY1 antibody. We thank Dr. James Higgins for the gift of the anti-ZYP1 antibody and Drs. László Sági and Dávid Polgári for providing the plants of tetraploid and diploid barleys. Erika Gondos and Ramesh Patel are gratefully acknowledged for their technical assistance.

SUPPLEMENTARY MATERIAL

The Supplementary Material for this article can be found online at: https://www.frontiersin.org/articles/10.3389/fpls.2018.01193/full#supplementary-material

REFERENCES

Aragon-Alcaide, L., Beven, A., Moore, G., and Shaw, P. (1998). The use of vibratome sections of cereal spikelets to study anther development and meiosis. *Plant J.* 14, 503–508. doi: 10.1046/j.1365-313X.1998.00148.x

Aragón-Alcaide, L., Reader, S., Beven, A., Shaw, P., Miller, T., and Moore, G. (1997). Association of homologous chromosomes during floral development. *Curr. Biol.* 7, 905–908. doi: 10.1016/S0960-9822(06)00383-6

Armstrong, S. J., Caryl, A. P., Jones, G. H., and Franklin, F. C. (2002). Asy1, a protein required for meiotic chromosome synapsis, localizes to axis-associated chromatin in Arabidopsis and Brassica. *J. Cell Sci.* 115, 3645–3655. doi: 10.1242/jcs.00048

Bennett, M. D. (1971). The duration of meiosis. *Proc. R. Soc. Lond.* 178, 277–299. doi: 10.1098/rspb.1971.0066

Cahoon, C. K., and Hawley, R. S. (2016). Regulating the construction and demolition of the synaptonemal complex. *Nat. Struct. Mol. Biol.* 23, 369–377. doi: 10.1038/nsmb.3208

Chelysheva, L., Grandont, L., Vrielynck, N., Le Guin, S., Mercier, R., and Grelon, M. (2010). An easy protocol for studying chromatin and recombination protein dynamics during *Arabidopsisthaliana* meiosis: immunodetection of cohesins, histones and MLH1. *Cytogenet. Genome Res.* 129, 143–153. doi: 10.1159/000314096

Choulet, F., Wicker, T., Rustenholz, C., Paux, E., Salse, J., Leroy, P., et al. (2010). Megabase level sequencing reveals contrasted organization and evolution patterns of the wheat gene and transposable element spaces. *Plant Cell* 22, 1686–1701. doi: 10.1105/tpc.110.074187

Colas, I., Shaw, P., Prieto, P., Wanous, M., Spielmeyer, W., Mago, R., et al. (2008). Effective chromosome pairing requires chromatin remodeling at the onset of meiosis. *Proc. Natl. Acad. Sci. U.S.A.* 105, 6075–6080. doi: 10.1073/pnas.0801521105

Henderson, K. A., and Keeney, S. (2005). Synaptonemal complex formation: where does it start? *Bioessays* 27, 995–998. doi: 10.1002/bies.20310

Heslop-Harrison, J. S. (2000). comparative genome organization in plants: from sequence and markers to chromatin and chromosomes. *Plant Cell Online* 12, 617–636. doi: 10.1105/tpc.12.5.617

Heslop-Harrison, J. S., and Schwarzacher, T. (2011). Organisation of the plant genome in chromosomes. *Plant J.* 66, 18–33. doi: 10.1111/j.1365-313X.2011.04544.x

Higgins, J. D., Sanchez-Moran, E., Armstrong, S. J., Jones, G. H., and Franklin, F. C. (2005). The Arabidopsis synaptonemal complex protein ZYP1 is required for chromosome synapsis and normal fidelity of crossing over. *Genes Dev.* 19, 2488–2500. doi: 10.1101/gad.354705

Higgins, J. D., Wright, K. M., Bomblies, K., and Franklin, F. C. (2014). Cytological techniques to analyze meiosis in *Arabidopsis arenosa* for investigating adaptation to polyploidy. *Front. Plant Sci.* 4:546. doi: 10.3389/fpls.2013.00546

Holm, P. B. (1977). Three-dimensional reconstruction of chromosome pairing during the zygotene stage of meiosis in *Lilium longiflorum* (thunb.). *Carlsberg Res. Commun.* 42, 103–151. doi: 10.1007/BF02906489

Houben, A., and Schubert, I. (2003). DNA and proteins of plant centromeres. *Curr. Opin. Plant Biol.* 6, 554–560. doi: 10.1016/j.pbi.2003.09.007

Jackson, S., Nielsen, D. M., and Singh, N. D. (2015). Increased exposure to acute thermal stress is associated with a non-linear increase in recombination frequency and an independent linear decrease in fitness in Drosophila. *BMC Evol. Biol.* 15:175. doi: 10.1186/s12862-015-0452-8

Jenkins, G. (1983). Chromosome pairing in triticum aestivum cv. *Chin. Spring. Carlsberg Res. Commun.* 48, 255–283. doi: 10.1007/BF02907772

Kiernan, J. A. (2000). Formaldehyde, formalin, paraformaldehyde and glutaraldehyde: what they are and what they do. *Micros. Today* 8, 8–13. doi: 10.1017/S1551929500057060

Lambing, C., Osman, K., Nuntasoontorn, K., West, A., Higgins, J. D., Copenhaver, G. P., et al. (2015). Arabidopsis PCH2 mediates meiotic chromosome remodeling and maturation of crossovers. *PLoS Genet.* 11:e1005372. doi: 10.1371/journal.pgen.1005372

Maestra, B., Hans de Jong, J., Shepherd, K., and Naranjo, T. (2002). Chromosome arrangement and behaviour of two rye homologous telosomes at the onset of meiosis in disomic wheat-5RL addition lines with and without the Ph1 locus. *Chromosome Res.* 10, 655–667. doi: 10.1023/A:1021564327226

Martín, A. C., Rey, M.-D., Shaw, P., and Moore, G. (2017). Dual effect of the wheat Ph1 locus on chromosome synapsis and crossover. *Chromosoma* 126, 669–680. doi: 10.1007/s00412-017-0630-0

Mercier, R., Mézard, C., Jenczewski, E., Macaisne, N., and Grelon, M. (2015). The molecular biology of meiosis in plants. *Annu. Rev. Plant Biol.* 66, 297–327. doi: 10.1146/annurev-arplant-050213-035923

Modliszewski, J. L., and Copenhaver, G. P. (2017). Meiotic recombination gets stressed out: CO frequency is plastic under pressure. *Curr. Opin. Plant Biol.* 36, 95–102. doi: 10.1016/j.pbi.2016.11.019

Murphy, S. P., and Bass, H. W. (2012). The maize (Zea mays) desynaptic (dy) mutation defines a pathway for meiotic chromosome segregation, linking nuclear morphology, telomere distribution and synapsis. *J. Cell Sci.* 125, 3681–3690. doi: 10.1242/jcs.108290

Naranjo, T. (2015). Contribution of structural chromosome mutants to the study of meiosis in plants. *Cytogenet. Genome Res.* 147, 55–69. doi: 10.1159/000442219

Osman, K., Higgins, J. D., Sanchez-Moran, E., Armstrong, S. J., and Franklin, F. C. (2011). Pathways to meiotic recombination in *Arabidopsis thaliana*. *New Phytol.* 190, 523–544. doi: 10.1111/j.1469-8137.2011.03665.x

Osman, K., Yang, J., Roitinger, E., Lambing, C., Heckmann, S., Howell, E., et al. (2018). Affinity proteomics reveals extensive phosphorylation of the Brassica chromosome axis protein ASY1 and a network of associated proteins at prophase I of meiosis. *Plant J.* 93, 17–33. doi: 10.1111/tpj.13752

Phillips, D., Jenkins, G., Macaulay, M., Nibau, C., Wnetrzak, J., Fallding, D., et al. (2015). The effect of temperature on the male and female recombination landscape of barley. *New Phytol.* 208, 421–429. doi: 10.1111/nph.13548

Pradillo, M., Varas, J., Oliver, C., and Santos, J. L. (2014). On the role of AtDMC1, AtRAD51 and its paralogs during Arabidopsis meiosis. *Front. Plant Sci.* 5:23. doi: 10.3389/Fpls.2014.00023

Prieto, P., Moore, G., and Shaw, P. (2007). Fluorescence in situ hybridization on vibratome sections of plant tissues. *Nat. Protoc.* 2, 1831–1838. doi: 10.1038/nprot.2007.265

Schwarzacher, T. (1997). Three stages of meiotic homologous chromosome pairing in wheat: cognition, alignment and synapsis. *Sex. Plant Reprod.* 10, 324–331. doi: 10.1007/s004970050106

Schwarzacher, T. (2003). Meiosis, recombination and chromosomes: a review of gene isolation and fluorescent in situ hybridization data in plants. *J. Exp. Bot.* 54, 11–23. doi: 10.1093/jxb/

Schwarzacher, T., and Heslop-Harrison, J. S. (1991). *In situ* hybridization to plant telomeres using synthetic oligomers. *Genome* 34, 317–323. doi: 10.1139/g91-052

Schwarzacher, T., and Heslop-Harrison, J. S. (2000). *Practical in Situ Hybridization*. Oxford: BIOS, 90–124.

Sepsi, A., Higgins, J. D., Heslop-Harrison, J. S., and Schwarzacher, T. (2017). CENH3 morphogenesis reveals dynamic centromere associations during synaptonemal complex formation and the progression through male meiosis in hexaploid wheat. *Plant J.* 89, 235–249. doi: 10.1111/tpj.13379

Sepsi, A., Molnár, I., Szalay, D., and Molnár-Láng, M. (2008). Characterization of a leaf rust-resistant wheat-*Thinopyrum ponticum* partial amphiploid BE-1, using sequential multicolor GISH and FISH. *Theor. Appl. Genet.* 116, 825–834. doi: 10.1007/s00122-008-0716-4

Storlazzi, A., Gargano, S., Ruprich-Robert, G., Falque, M., David, M., Kleckner, N., et al. (2010). Recombination proteins mediate meiotic spatial chromosome organization and pairing. *Cell* 141, 94–106. doi: 10.1016/j.cell.2010.02.041

Székvölgyi, L., Ohta, K., and Nicolas, A. (2015). Initiation of meiotic homologous recombination: flexibility, impact of histone modifications, and chromatin remodeling. *Cold Spring Harb. Perspect. Biol.* 7:a016527. doi: 10.1101/cshperspect.a016527

Varas, J., Graumann, K., Osman, K., Pradillo, M., Evans, D. E., Santos, J. L., et al. (2015). Absence of SUN1 and SUN2 proteins in *Arabidopsis thaliana* leads to a delay in meiotic progression and defects in synapsis and recombination. *Plant J.* 81, 329–346. doi: 10.1111/tpj.12730

Wang, X., and Holm, P. B. (1988). Chromosome pairing and synaptonemal complex formation in wheat-rye hybrids. *Carlsberg Res. Commun.* 53, 167–190. doi: 10.1007/BF02907178

Zhang, L., Espagne, E., de Muyt, A., Zickler, D., and Kleckner, N. E. (2014). Interference-mediated synaptonemal complex formation with embedded crossover designation. *Proc. Natl. Acad. Sci. U.S.A.* 111, E5059–E5068. doi: 10.1073/pnas.1416411111

Conflict of Interest Statement: The authors declare that the research was conducted in the absence of any commercial or financial relationships that could be construed as a potential conflict of interest.

frontiers in Plant Science

ORIGINAL RESEARCH
published: 20 June 2019
doi: 10.3389/fpls.2019.00773

Ultrastructure and Dynamics of Synaptonemal Complex Components During Meiotic Pairing and Synapsis of Standard (A) and Accessory (B) Rye Chromosomes

Susann Hesse[1], *Mateusz Zelkowski*[1†], *Elena I. Mikhailova*[2], *Christian J. Keijzer*[3], *Andreas Houben*[1] *and Veit Schubert*[1*]

[1] Leibniz Institute of Plant Genetics and Crop Plant Research (IPK) Gatersleben, Seeland, Germany, [2] N.I.Vavilov Institute of General Genetics, Russian Academy of Sciences, Saint-Petersburg State University, Saint-Petersburg, Russia, [3] Innovert GBVM, Vlierden, Netherlands

During prophase I a meiosis-specific proteinaceous tripartite structure, the synaptonemal complex (SC), forms a scaffold to connect homologous chromosomes along their lengths. This process, called synapsis, is required in most organisms to promote recombination between homologs facilitating genetic variability and correct chromosome segregations during anaphase I. Recent studies in various organisms ranging from yeast to mammals identified several proteins involved in SC formation. However, the process of SC disassembly remains largely enigmatic. In this study we determined the structural changes during SC formation and disassembly in rye meiocytes containing accessory (B) chromosomes. The use of electron and super-resolution microscopy (3D-SIM) combined with immunohistochemistry and FISH allowed us to monitor the structural changes during prophase I. Visualization of the proteins ASY1, ZYP1, NSE4A, and HEI10 revealed an extensive SC remodeling during prophase I. The ultrastructural investigations of the dynamics of these four proteins showed that the SC disassembly is accompanied by the retraction of the lateral and axial elements from the central region of the SC. In addition, SC fragmentation and the formation of ball-like SC structures occur at late diakinesis. Moreover, we show that the SC composition of rye B chromosomes does not differ from that of the standard (A) chromosome complement. Our ultrastructural investigations indicate that the dynamic behavior of the studied proteins is involved in SC formation and synapsis. In addition, they fulfill also functions during desynapsis and chromosome condensation to realize proper recombination and homolog separation. We propose a model for the homologous chromosome behavior during prophase I based on the observed dynamics of ASY1, ZYP1, NSE4A, and HEI10.

Keywords: B chromosomes, CENH3, meiosis, recombination, *Secale cereale*, scanning electron microscopy, super-resolution microscopy, synaptonemal complex

OPEN ACCESS

Edited by:
Mónica Pradillo, Complutense University of Madrid, Spain

Reviewed by:
Kim Osman, University of Birmingham, United Kingdom
Juan Luis Santos, Complutense University of Madrid, Spain

***Correspondence:**
Veit Schubert
schubertv@ipk-gatersleben.de

†Present Address:
Mateusz Zelkowski, Plant Biology Section, School of Integrative Plant Science, Cornell University, Ithaca, NY, United States

Specialty section:
This article was submitted to Plant Cell Biology, a section of the journal Frontiers in Plant Science

Received: *24 May 2019*
Accepted: *28 May 2019*
Published: *20 June 2019*

Citation:
Hesse S, Zelkowski M, Mikhailova EI, Keijzer CJ, Houben A and Schubert V (2019) Ultrastructure and Dynamics of Synaptonemal Complex Components During Meiotic Pairing and Synapsis of Standard (A) and Accessory (B) Rye Chromosomes. Front. Plant Sci. 10:773. doi: 10.3389/fpls.2019.00773

INTRODUCTION

Meiosis is a type of cell division that reduces the chromosome number by half, and creates haploid cells. This type of cell division is a fundamental and evolutionary conserved process in all sexually reproducing eukaryotes and is characterized by four main chromosomal processes. First, sister chromatid cohesion becomes established during S phase by cohesin complexes. Second, the chromosome axis condenses and pairing of homologous chromosomes takes place. Third, the synaptonemal complex (SC) is formed via synapsis and fourth, recombination occurs eventually leading to crossover formation (Sanchez-Moran et al., 2008). In addition, homology-dependent or -independent interactions, e.g., centromere and/or telomere clustering can prelude and/or complement these processes (Zickler and Kleckner, 2015). The segregation of homologous chromosomes to the opposite poles of the spindle during meiosis I is followed by the second part of meiosis (meiosis II), which leads to the formation of four daughter cells. In species with monocentric chromosomes meiosis II resembles a mitotic division in terms of sister chromatid separation.

Only few organisms exhibit a deviating program of prophase I events. In most species SC formation depends on double strand break (DSB) formation and strand invasion. However, in e.g., *Caenorhabditis elegans* and *Drosophila* females SC formation occurs without DSB formation (Zickler and Kleckner, 2015). In *Schizosaccharomyces pombe* and *Aspergillus nidulans* no SCs become established and pairing occurs recombination-independent and recombination-mediated, respectively (Olson et al., 1978; Egel-Mitani et al., 1982; Bahler et al., 1993).

Studies across yeast, mammals and plants indicate that the SC structure is as highly conserved as meiosis itself (Zickler and Kleckner, 1999, 2015; Page and Hawley, 2004). Early transmission electron microscopy revealed the basic SC organization as a tripartite structure consisting of two lateral elements (LEs) flanking a ∼100 nm wide central region (CR) (Fawcett, 1956; Moses, 1956, 1968). Prior to SC formation, axial element (AE) components assemble alongside the cohesin-based chromosome axis mediating sister chromatid cohesion, to establish the meiotic chromatin loop-axis structure (Zickler and Kleckner, 1999). During synapsis, homologous AEs are linked in a zipper-like manner by CR components along their entire length. With a diameter of about 50 nm, the AEs are called lateral elements (LEs) within the SC (Moses, 1968; Westergaard and von Wettstein, 1972). The CR consists of two functional units, namely the transverse filament (TF) proteins that span the CR to link both homologous chromosomes, as well as central region proteins acting tentatively to stabilize the CR (De Vries et al., 2005; Bolcun-Filas et al., 2007, 2009; Hamer et al., 2008; Page et al., 2008; Schramm et al., 2011; Humphryes et al., 2013; Collins et al., 2014; Hernandez-Hernandez et al., 2016).

Genomic and proteomic approaches, e.g., in budding yeast, identified multiple genes and proteins involved in SC formation and meiotic processes that appear to have orthologs across various eukaryotes (Zickler and Kleckner, 1999, 2015; Page and Hawley, 2004; Gerton and Hawley, 2005). Despite the common basic structural similarity between SCs, primary amino acid sequence comparisons of orthologs components show a substantial dissimilarity. For example the TF protein ZYP1 of *Arabidopsis thaliana* (L.) Heynh shares only 18–20% sequence identity and 36–40% similarity with the corresponding proteins of budding yeast (ZIP1), *Drosophila* (C(3)G) and rat (SCP1) (Meuwissen et al., 1992; Sym et al., 1993; Page and Hawley, 2001; Higgins et al., 2005). Furthermore, orthologous genes do not necessarily encode proteins with equivalent functions. For instance, electron microscopy confirmed that the ASY1 protein of *A. thaliana* belongs to the axis-associated proteins, whereas its ortholog of budding yeast (HOP1) is crucial for AE formation (Hollingsworth and Ponte, 1997; Armstrong et al., 2002). In summary, the studies of SC components suggest that their evolution was driven by the need to fulfill a structural role, rather than conserving a catalytic one (Zickler and Kleckner, 2015).

Beside ASY1 and ZYP1, additional components, such as subunits of the structural maintenance of chromosome (SMC)5/6 complex and human enhancer of invasion-10 (HEI10) proteins associated with the chromosome axis (axial/lateral element) have been identified. Components of the plant chromosome axis comprise in addition HORMA domain containing proteins (Armstrong et al., 2002; Nonomura et al., 2006), coiled-coil proteins (Wang et al., 2011; Ferdous et al., 2012; Lee et al., 2015) and cohesins (Cai et al., 2003; Lam et al., 2005).

The conserved SMC5/6 complex belongs to the SMC family which is formed via the interaction of the hinge domains of the SMC5 and SMC6 subunits resulting in a heterodimer connected by the δ-kleisin NSE4 (NON-SMC ELEMENT 4) at the head domains of SMC5 and SMC6 (Lehmann et al., 1995; Fousteri and Lehmann, 2000; Palecek et al., 2006; Taylor et al., 2008). In addition to functions of SMC5/6 in somatic tissues, various essential roles during meiosis were found in yeasts, worm, mouse and human. SMC5/6 subunits were proven to play a role in meiotic processes such as in response to double strand breaks (DSBs), meiotic recombination, heterochromatin maintenance, centromere cohesion, homologous chromosome synapsis and meiotic sex chromosome inactivation (Verver et al., 2016). In *A. thaliana*, due to the presence of two alternative SMC6 (SMC6A and SMC6B) and NSE4 (NSE4A and NSE4B) subunits, different SMC5/6 complexes may be composed (Schubert, 2009; Zelkowski et al., 2019).

HEI10 is a member of the ZMM (ZIP1/ZIP2/ZIP3/ZIP4, MSH4/MSH5, and MER3) protein family, originally identified as a growth regulator and essential for meiotic recombination in different eukaryotes (Toby et al., 2003; Whitby, 2005; Osman et al., 2011; Chelysheva et al., 2012; Wang et al., 2012). Possessing a RING-finger motif, coiled-coil and tail domains, HEI10 functions as an E3 ligase catalyzing post-translational protein modification by ubiquitin-like proteins and thereby integrates different meiotic processes for successful recombination (De Muyt et al., 2014; Qiao et al., 2014).

In the past, in plants such as *A. thaliana* as well as large-genome cereals important meiotic studies were performed. The cereal species rye (*Secale cereale* L.) contains, in addition to the standard A chromosome (As) complement, dispensable accessory chromosomes, also called B chromosomes (Bs). The number of Bs varies between individuals of a population. Bs were

reported in thousands of eukaryotic species, but so far remain an evolutionary mystery. Apart from other peculiarities, Bs do not pair or recombine with As at meiosis and often exhibit a non-Mendelian inheritance (Houben et al., 2014). Previous studies by electron microscopy showed that the synaptic behavior of rye Bs differs from that of As. In addition to bivalent formation, Bs may also perform intrachromosomal synapsis and form multivalents (Santos et al., 1993, 1995; Jiménez et al., 1994). However, the SC protein composition of As and Bs has not yet been investigated in detail.

Despite extensive studies on the assembly of SCs, much less is known about the process of SC disassembly, which is essential for correct chromosome segregation (Cahoon and Hawley, 2016). In this study, we used super-resolution and electron microscopy to monitor the dynamics of ultrastructural changes during the assembly and disassembly of SCs in rye plants containing Bs at a resolution beyond widefield microscopy. Immunohistochemistry allowed us to track the four meiotic proteins ASY1 (a marker for AE/LE), ZYP1 (a transverse filament protein), HEI10 (a structure-based signal transduction protein involved in recombination), and NSE4A (a δ-kleisin of the SMC5/6 complex) during prophase I. Until the complete disassembly, all four proteins were present at the SC. Their spatio-temporal distribution revealed extensive chromatin structure changes.

MATERIALS AND METHODS

Plant Material

Rye (*Secale cereale* L. cv. Paldang) plants carrying B chromosomes ($2n = 14 + 0 - 4$ supernumerary Bs) (Romera et al., 1989) were grown under greenhouse conditions (22°C, 16 h light/8 h dark) to obtain anthers containing pollen mother cells (PMCs) during prophase I. The number of Bs in individual plants was determined by FISH using rye B chromosome-specific probes.

FISH Probe Preparation

The retrotransposon Bilby (Francki, 2001) was used as centromere-specific probe, and the repeats Sc11, Sc55c1, Sc63c34, D1100, E3900, and Sc36c82 were employed as rye B chromosome-specific probes (Sandery et al., 1990; Blunden et al., 1993; Klemme et al., 2013). Labeling was done by nick translation using a NT Labeling Kit (Jena Bioscience GmbH, Jena Germany).

Identification of B Chromosome Number

Root tips of each rye plant were cut and in fixed in ethanol/acetic acid (3:1) for 48 h at room temperature. The fixed roots were stained in 1% acetocarmine solution (1% carmine in 45% acetic acid, 12–24 h at room temperature). For slide preparation the roots were carefully heated up in the acetocarmine solution over an open flame until they became soft. Then, the soft roots were placed on a slide, the root tip cap was cut off with a razor blade and the meristem was carefully extracted on the slide by use of a preparation needle. The extracted meristem was squashed in 45% acetic acid using a coverslip. After coverslip removal using liquid nitrogen, the slides were stored in 100% ethanol (4°C). Subsequently, the slides were air-dried and the FISH probe-containing hybridization mix (FISH probes diluted in 20% dextran sulfate, Sigma-Aldrich, cat. no. D 8906, 50% deionized formamide, 300 mM NaCl, 30 mM tri-sodium citrate dehydrate, 50 mM phosphate buffer, pH 7.0) was applied. Then, the slides were incubated for denaturation for 2 min at 80°C in darkness. FISH was performed at 37°C overnight. Slides were washed 3 × 5 min in 1 × PBS and afterwards mounted and counterstained with 4′,6-diamidine-2′-phenylindole dihydrochloride (DAPI, 1 mg/ml) in Vectashield (Vector Laboratories). To determine the number and type of B chromosomes (Endo et al., 2008), FISH probes directed against the pericentromeric repeat Sc11 and a subtelomeric repeat (E3900 or D1100) were used in parallel. In case of standard rye B chromosomes the detected number of both repeats is equal. Plants containing standard Bs were cultivated further under greenhouse conditions (22°C, 16 h light/8 h dark) for this study.

Immunostaining and FISH on Meiotic Chromosomes

Rye anthers with meiocytes at prophase I were fixed 25 min under vacuum in 4% ice-cold paraformaldehyde in 1 × PBS (phosphate buffer saline, pH 7.4), washed 3 × 5 min in ice-cold 1 × PBS and 20 min digested at 37°C in an enzyme cocktail (0.1% cellulose, Calbiochem, cat. no. 219466; 0.1% pectolyase Y-23, Sigma-Aldrich, cat. no. P3026; 0.1% cytohelicase, Sigma-Aldrich, cat. no. C8274) in 1 × PBS. After washing 3 × 5 min in ice-cold 1 × PBS, single anthers were transferred to slides and squashed in 1 × PBS + 0.001% Tween-20 using coverslips. After coverslip removal using liquid nitrogen, the slides were stored in 1 × PBS. For longer storage they were transferred to 100% glycerol (Carl Roth, cat. no. 3783) and kept at 4°C. The following primary antibodies were applied at 37°C for 90 min: rabbit anti-*Zea mays* ASY1 (1:200), guinea pig anti-*Zea mays* ZYP1 (1:200; Golubovskaya et al., 2011), rabbit anti-*A. thaliana* NSE4A (1:200; Zelkowski et al., 2019), mouse anti-*Oryza sativa* HEI10 (1:200; Wang et al., 2012), and rabbit anti-grass CENH3 (1:1,000; Sanei et al., 2011). For detection, the following secondary antibodies were applied at 37°C for 60 min: goat anti-rabbit Dylight488 (1:200; Dianova cat. no. 111-485-144), goat anti-guinea pig Alexa Fluor594 (1:400; Molecular Probes cat. no. A11076), goat anti-mouse Cy3 (1:400; Dianova cat. no. 115-166-146), and donkey anti-guinea pig Alexa Fluor647 (1:200; Dianova cat. no. 706-605-148). Afterwards, the slides were washed in 3 × 5 min 1 × PBS, dehydrated (2 min each step; 70, 90, and 100% ethanol), air-dried and fixed in ethanol/acetic acid (3:1; 24–48 h in darkness at room temperature). Subsequently, the slides were air-dried and incubated with the FISH probe-free hybridization mix (see above) for 12 h at 37°C. After short washing for 5 min in 2 × SSC containing 0.1% Triton X100, the slides were dehydrated and air-dried. Then, for DNA denaturation, slides were incubated in 0.2 N NaOH (in 70% ethanol; 10 min at room temperature), dehydrated and air-dried. Subsequently, the FISH probes were diluted and denatured for 5 min at 95°C in the hybridization mix before application on

slides. FISH was performed at 37°C overnight using Bilby or the B-specific probes. Slides were washed 3 × 5 min in 1 × PBS and afterwards mounted and counterstained with DAPI, (1 mg/ml) in Vectashield (Vector Laboratories).

Determination of Meiotic B Chromosome Pairing Configurations

To determine the meiotic pairing behavior of rye B chromosomes, immunostaining using the primary antibodies directed against *Zea mays* ASY1 and *Z. mays* ZYP1, and subsequent FISH using a cocktail of the rye B chromosome-specific probes Sc11, Sc55c1, Sc63c34, D1100, E3900, and Sc36c82 was performed on meiocytes as described above. The determination of pairing configurations was done using a BX61 microscope (Olympus) equipped with an ORCA-CCD camera (Hamamatsu) or by super-resolution microscopy. For quantification only meiocytes with completed synapsis were considered.

Super-Resolution Microscopy

To analyse the ultrastructure of immunosignals and chromatin beyond the classical Abbe/Raleigh limit at a lateral resolution of ∼120 nm (super-resolution, achieved with a 488 nm laser) spatial structured illumination microscopy (3D-SIM) was applied using a 63×/1.4 Oil Plan-Apochromat objective of an Elyra PS.1 microscope system and the software ZENblack (Carl Zeiss GmbH). Images were captured separately for each fluorochrome using the 642, 561, 488, and 405 nm laser lines for excitation and appropriate emission filters (Weisshart et al., 2016). Maximum intensity projections of whole meiocytes were calculated via the ZEN software. Zoom in sections were presented as single slices to indicate the subnuclear chromatin and protein structures at the super-resolution level. 3D rendering and CENH3 volume measurements based on SIM image stacks was done using the Imaris 8.0 (Bitplane) software.

Scanning Electron Microscopy

Anthers of *S. cereale* were cut into equal halves. In order to determine the meiotic stage, one half was fixed in ethanol-acetic acid (3:1). Then, spread preparations of the fixed anthers containing PMCs at different meiotic stages were made according to Zhong et al. (1996). The preparations were air-dried, mounted in DAPI-Vectashield and observed using fluorescence microscopy. Alternatively, they were fixed in ethanol-acetic acid (3:1), stained with acetocarmine and observed with bright field microscopy. The complementary half was fixed in 70% ethanol, frozen by plunging into liquid propane at −180°C, cryo-fractured using a nitrogen-cooled razor blade and thawed to room temperature in 70% ethanol. This complementary half was dehydrated in 100% ethanol and critical point dried over carbon dioxide. Subsequently, it was mounted on a stub with the fractured plane up, coated with 2 nm platinum and observed in a JEOL 6300F field emission scanning electron microscope (SEM) at 5 kV.

After extensive trials looking for the best fixative for this purpose, 70% ethanol proved to produce the best images in SEM compared to the more advanced fixatives as glutaraldehyde and osmium tetroxide which are generally used for observing phospholipid- and protein-related structures in electron microscopy.

RESULTS

Compared to widefield microscopy, electron and super-resolution microscopy provide a significantly increased resolution, thus offering the analysis of plant chromatin and protein structures at the nanoscopic level (Baroux and Schubert, 2018). Here we used scanning electron microscopy (SEM; **Figure 1**) to obtain new insights in the structure of paired homologous chromosomes in prophase I meiocytes of rye. Although electron microscopy allows visualizing cell structures at a resolution of 1–2 nm it is challenging to label and localize DNA and proteins specifically (Baroux and Schubert, 2018). Therefore, we additionally applied fluorescence-based 3D-SIM to investigate chromatin and protein substructures in more detail (**Figures 2–8**). Compared to widefield microscopy a clearly increased resolution and the removal of out-of-focus blur has been achieved by SIM (**Supplementary Figure 1**). The localization and dynamics of the specifically stained SC components ASY1 and ZYP1, as well as the associated proteins NSE4A and HEI10 were monitored during prophase I at rye A and B chromosomes (**Figures 3–8**; **Supplementary Figure 2**; **Supplementary Movies 2–4**).

To identify centromeres and to conclude on the orientation of uni- and bivalents the A and B centromeres were labeled by the centromere-specific FISH probe Bilby (Francki, 2001) and CENH3 antibodies (**Figures 2**, **4B**, **5B,E**; **Supplementary Figure 2**; **Supplementary Movies 1**, **2**).

SEM Identifies the Organization of Synapsed Homologs

Cross-sections of meiocytes were analyzed by SEM. Similar to what was observed earlier on somatic barley metaphase chromosomes (Zoller et al., 2004a,b; Wanner et al., 2005) several chromatin clusters (chromomeres) were identified at the surface of the synapsed rye homologs (**Figure 1A**). During zygotene-pachytene the paired homologs are connected via a structure presumably representing the SC. Similar to lily, maize and human (Holm, 1977; Scherthan et al., 1998; Franklin et al., 1999) the SC of rye is located laterally to the chromatin of both homologs (**Figure 1B**).

ASY1 and ZYP1 Form Typical Structures During SC Assembly and Disassembly

The dynamics of the synaptonemal complex during prophase I was monitored by immunolocalization of ASY1 and ZYP1 (**Figures 3**, **5A,D**, **6–8**; **Supplementary Figure 1**; **Supplementary Movies 2–4**). At zygotene, synapsis is initiated at several sites along both homologs. During the SC assembly, ASY1 is partially released from synapsed chromosomes resulting in substantially lower fluorescence intensity and diffuse ASY1 signals in the nucleoplasm at pachytene. Notably, apart from linear tracts disperse ZYP1 signals can also be detected, likely

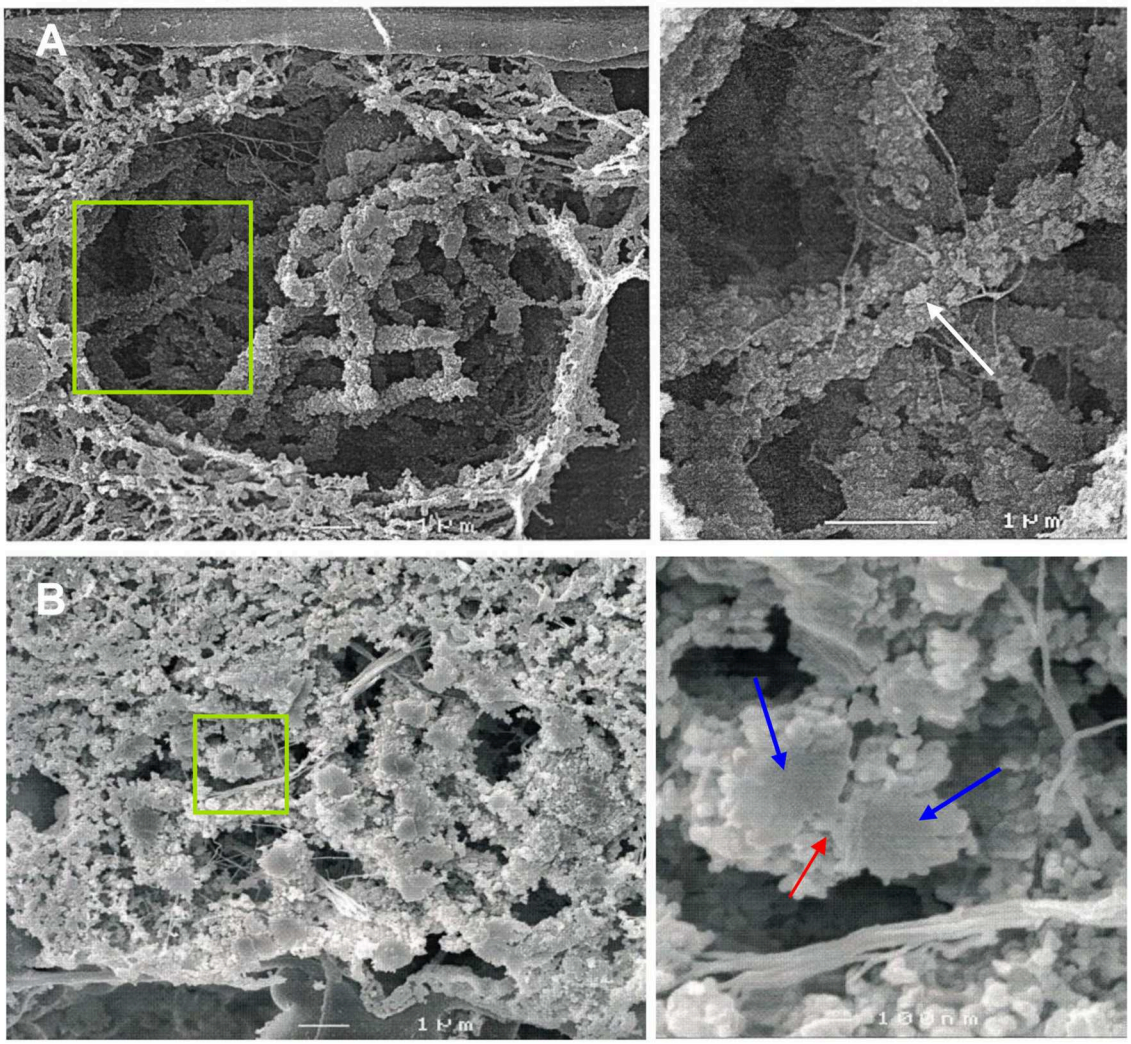

FIGURE 1 | SEM imaging reveals the ultrastructure of rye bivalents during prophase I. The images of the right column show the regions of interest enlarged. **(A)** Top view of aligned homologous chromosomes inside a meiocyte at zygotene. Chromatin clusters (chromomeres) are clearly visible at the chromosome surface (arrow). **(B)** Cross section of a bivalent inside a meiocyte during zygotene-pachytene. The bivalent in the green rectangle is composed of two paired homologs (blue arrows) both containing two chromatids. The red arrow indicates the SC.

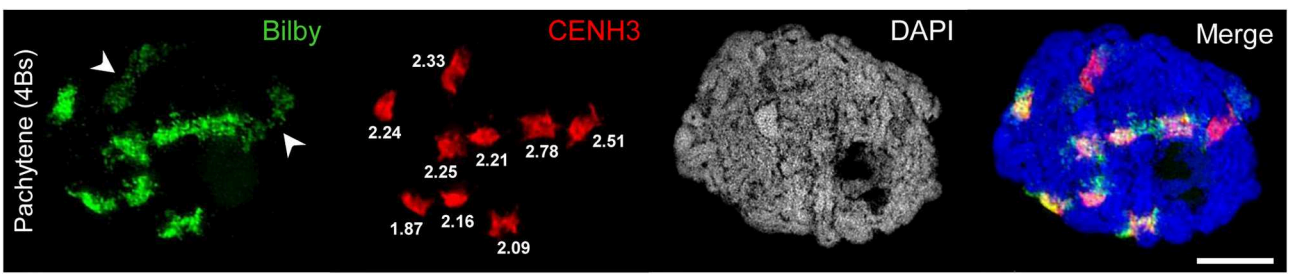

FIGURE 2 | Bilby repeats and CENH3 identify the centromeres of A and B chromosomes. A rye meiocyte containing four Bs at pachytene shows the pairing of all centromeres labeled with Bilby and CENH3 at the centromeric regions. The brighter Bilby signals reflect the seven (peri)centromeric regions of the A bivalents. In contrast, the Bilby signals of the Bs (arrowheads) appear darker and less condensed. Interestingly, this difference is not revealed by means of the CENH3 labeling implying that the actual size of active centromeres does not differ between A and B chromosomes. The similar CENH3 volumes (μm^3) are indicated at the signals. The global chromatin staining with DAPI dicerns the chromatin-free SC structures. Bar = 5 μm.

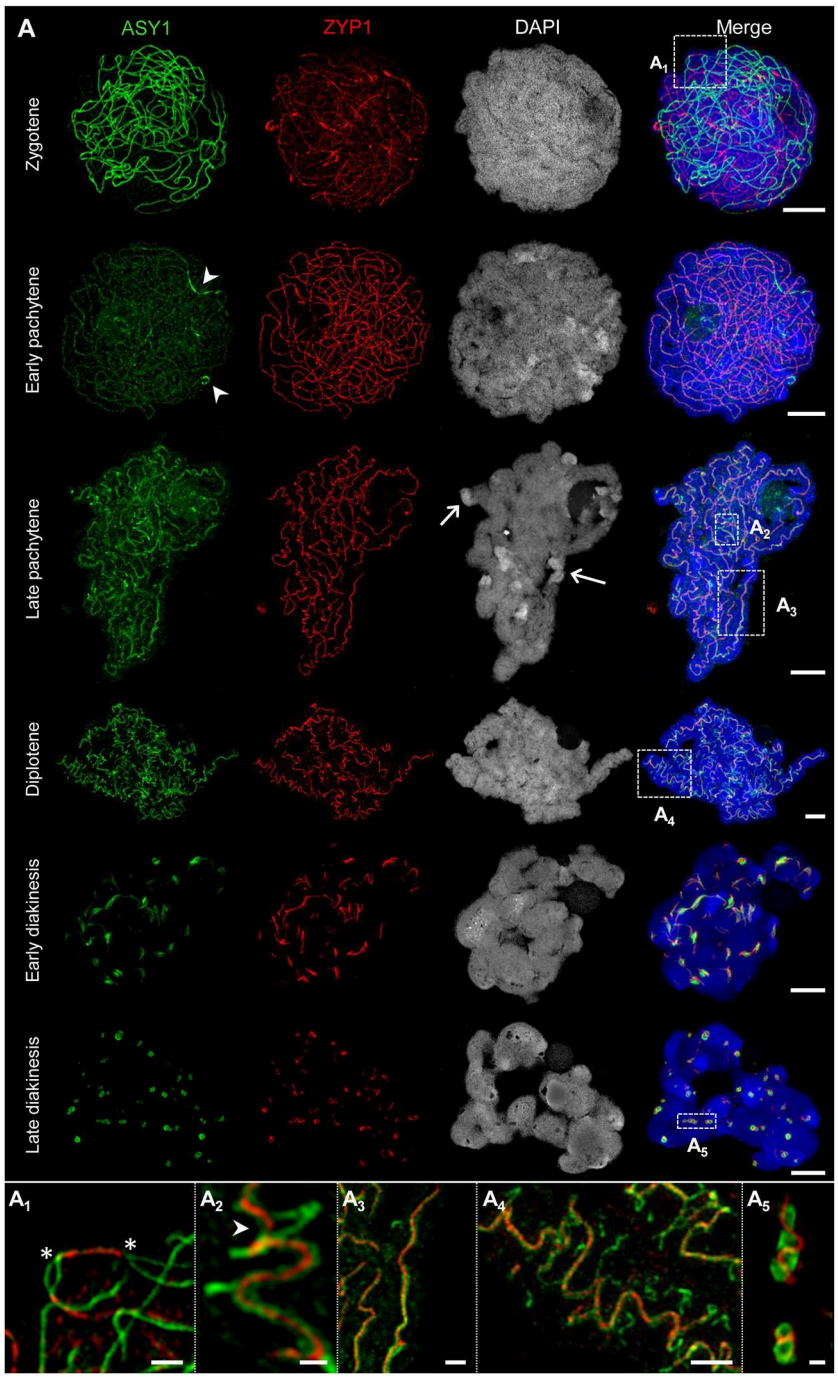

FIGURE 3 | The behavior of ASY1 and ZYP1 during prophase I. The images **A_1-A_5** show enlarged regions delimited by dashed boxes. Chromatin was stained with DAPI. **(A)** Representative examples of immunostaining of ASY1, a marker for chromosome axis, and ZYP1, a SC transverse filament protein. At zygotene, intense ASY1 signals are visible along not yet synapsed chromatin axes. When synapsis proceeds in early pachytene, the SCs assemble at multiple sites of the chromatin and the ZYP1 signals become more prominent. The ASY1 signal intensity strongly decreases at synapsed regions, but never vanishes completely. At early pachytene, all homologs are synapsed. The last separated regions can be identified by brighter ASY1 signals (arrowheads). At late pachytene, the ongoing chromatin condensation causes a twisted SC structure. ASY1 starts separating from ZYP1, reflecting the initiation of SC disintegration **(A_2,A_3)**. Note the regions with a substantially higher DAPI staining intensity at the telomeric heterochromatin (arrows) corresponding to increased chromatin condensation. At diplotene, the SCs form spiral-like structures with ASY1 strands retracting from the SC at multiple positions **(A_4)**, which reflects proceeding SC disassembly and further chromatin condensation. At early diakinesis, ZYP1 staining detects only short SC fragments enwrapped by ASY1. At late diakinesis, only compact ball-like ASY1 structures with embedded ZYP1 remain **(A_5)**, **Figure 5E**; **Supplementary Movie 2**). They disappear completely until the end of diakinesis (**Figure 6E**). Bars = 5 μm. **(A_1)** An interstitial synapsis

(Continued)

FIGURE 3 | initiation site showing ZYP1 signals flanked by still separated ASY1 strands (asterisks, see also **Supplementary Movie 3**). Bar = 1 μm. **(A_2)** Initiation of SC disintegration at late pachytene. ASY1 strands dissociate from single SC sites via loop formation. At positions where both ASY1 strands become retracted from the SC, ZYP1 disappears (arrowhead). Bar = 0.5 μm. **(A_3)** ZYP1 enwinded in two ASY1 strands during late pachytene. Bar = 1 μm. **(A_4)** At diplotene, the ASY1 structures dissociate from the SC and start to dissolve at various positions indicating multiple desynapsis sites. Bar = 2 μm. **(A_5)** At late diakinesis, short ZYP1 fragments are embedded in ball-like ASY1 structures. Bar = 0.5 μm.

indicating yet unassembled proteins (**Figure 3A$_1$**). At the beginning of pachytene synapsis completes and the SC tripartite structure is clearly visible (**Figure 3A$_3$**). ASY1 signals appear as discontinuous stretches and spots with varying intensities. At late pachytene the ongoing chromatin condensation is accompanied by SC coiling, showing the most compact twisted structure at diplotene. The compaction of chromosomes also results in a more contiguous staining of ASY1. The first initiation of SC disassembly can be detected at late pachytene by the re-organization of ASY1 at single SC sites to form transient loop-like structures. At positions where both ASY1 strands dissociate from the SC, ZYP1 signals are no longer detectable indicating the local release of synapsis (**Figures 3A$_{2-4}$, 5A,D**). During progression of SC disassembly at diplotene, ASY1 undergoes partial degradation resulting in fragmented ASY1 threads (**Figures 3A$_4$, 5D, 6A3,C**; **Supplementary Movie 4**). At early diakinesis the SC fragments continue condensing, at which ASY1 winds up around residual ZYP1 fragments. Further shortening of these fragmented SCs progresses until 2–3 compact ball-like structures per bivalent remain at late diakinesis among the centromeres and at potential recombination sites (**Figure 3**, **Supplementary Movie 2**). The SC structures marked by ASY1 and ZYP1 disappear completely at the end of diakinesis (**Figures 6A$_4$,E**).

In summary, we conclude that the SC structures composed by ASY1 and ZYP1 are involved not only in the establishment of synapsis. Obviously, they are also required to organize and stabilize the paired homologs during chromatin condensation until prophase I terminates.

The SMC5/6 Complex δ-kleisin NSE4 Colocalizes to ZYP1 Within the SC During Synapsis

The SMC5/6 complex has been implicated to have versatile functions in meiotic processes, i.e. in recombination as well as in SC assembly and stability (Verver et al., 2016). To investigate the role of SMC5/6 complex subunits during prophase I we analyzed the distribution and dynamics of δ-kleisin NSE4. To confirm the specificity of the *A. thaliana* NSE4A antibodies (Zelkowski et al., 2019) and to exclude unspecific signal detection which could be induced by fluorescence crosstalk of ZYP1, we labeled rye meiocytes with NSE4A antibodies only. The detected twisted NSE4A labeling corresponds to the typical SC labeling visible at synapsed homologs during diplotene. Thereby, a color crosstalk caused by ZYP1 immunolabelling can be excluded (**Figures 4B**, **5B**; **Supplementary Figure 2**). Concurrently, chromosomes were labeled by the centromere-specific FISH probe Bilby to identify centromeres, and the orientation of paired homologs (**Figures 4B**, **5B,E**, **7**; **Supplementary Figure 2**; **Supplementary Movies 1**, **2**).

The simultaneous labeling of NSE4A and ZYP1 revealed a strong co-localization of both proteins at the central region of the SC (**Figure 4A**). At zygotene, NSE4A is present only along the synapsed homologs. When chromatin condensation progresses, the twisted structure of NSE4A follows the SC structure typically seen at diplotene. During SC disassembly at early diakinesis, NSE4A signals match to the spatial distribution of ZYP1 and can be detected exclusively on the remaining ZYP1-positive SC fragments (**Figure 4A$_1$**). At late diakinesis typical co-localized ball-like structures of NSE4A and ZYP1 are evident (**Figures 4A$_2$,A$_3$, 5C**).

Our findings suggest that NSE4, together with ZYP1, is involved in the organization and stabilization of synapsis during prophase I in rye.

The SC Is a Protein Structure Embedded in Chromatin

The immunolozalisation of ASY1, ZYP1, and NSE4A at the SCs and the absence of DNA-specific DAPI staining indicate that the inner SC is mainly a chromatin-free protein structure during prophase I (**Figures 5A–C**). This structure becomes visible at zygotene (**Figure 3**), and is present until late diakinesis (**Figure 5C**).

The resolution achieved by SIM allows measuring the width of the ASY1 and ZYP1 structures at different prophase I stages (**Figures 5D,E**). At diplotene the width of single ASY1 loops is approximately half of that of synapsed regions. This reflects the retraction of individual chromosome axes regions during the SC disintegration at diplotene. At diakinesis, ASY1 signal measurements indicate that the ball-like structures are established by the accumulation of separate ASY1 threads around a ZYP1 core (**Figure 5E**).

HEI10 Localizes to the SC During Synapsis and Indicates Likely the Location of Recombination Sites at Late Diakinesis

Recently it has been shown, that the ZMM protein family member HEI10 is involved in homologous recombination, and that it marks class I crossover loci in a number of organisms such as rice, *Arabidopsis* and mouse (Ward et al., 2007; Chelysheva et al., 2012; Wang et al., 2012; Qiao et al., 2014). To examine whether HEI10 exercises the same function in rye, we labeled different stages of prophase I with ASY1, ZYP1, and HEI10 antibodies simultaneously (**Figure 6**).

At zygotene, distinct HEI10 foci were detected exclusively at the central region of the SC marked by ZYP1 (**Figure 6A$_1$**). When synapsis is completed at pachytene, single HEI10 foci become more prominent and clearly distinguishable (**Figure 6A$_2$**). At diplotene, when the progression of the SC disassembly results

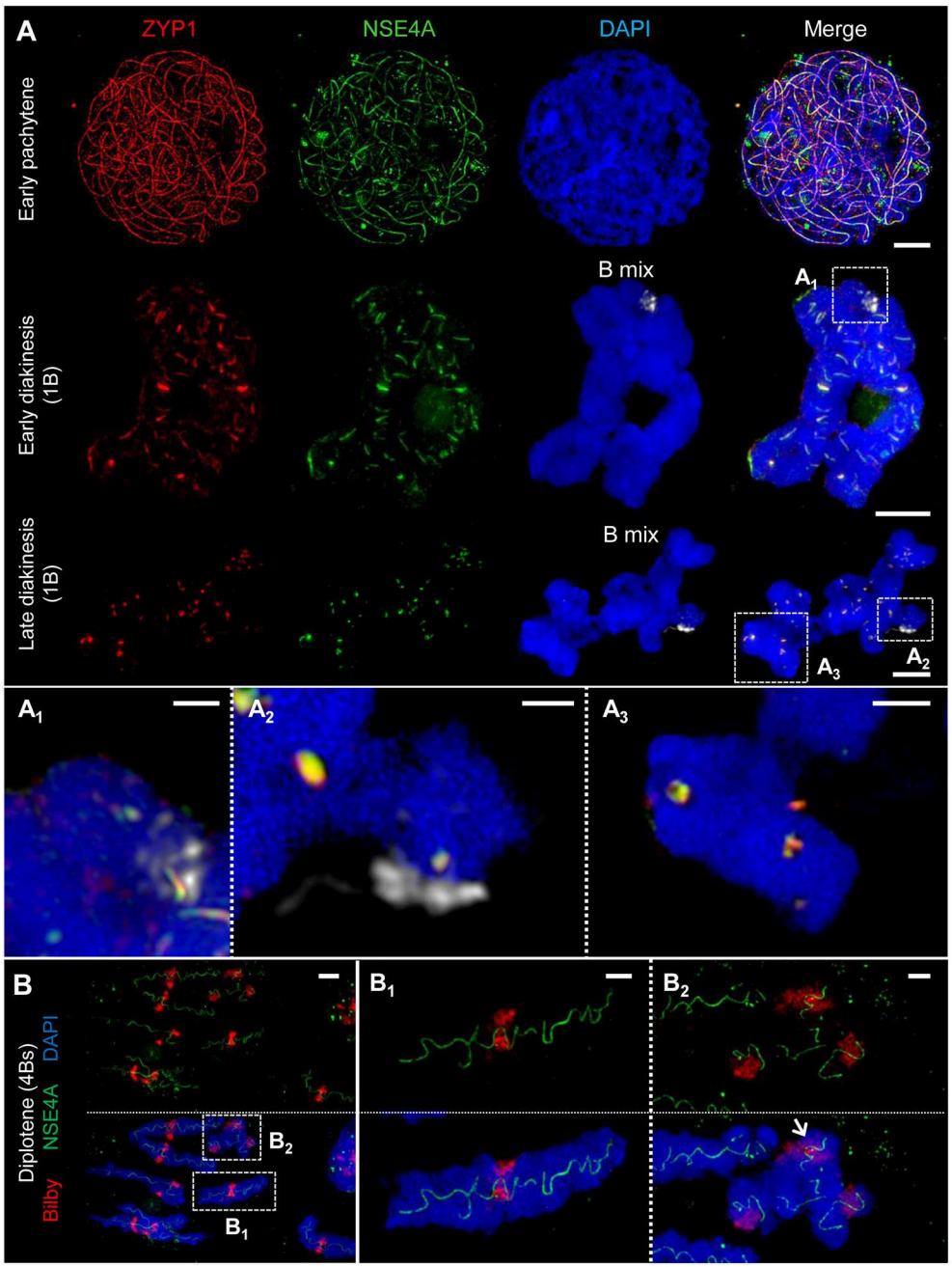

FIGURE 4 | ZYP1 and NSE4A colocalize at the SCs of rye A and B chromosomes. The images **(A_1-A_3,B_1,B_2)** show enlarged regions delimited by dashed boxes. The B chromosomes were detected by a B-specific FISH probe mix, centromeres by the specific repeat Bilby. The global chromatin was stained with DAPI. **(A)** Simultaneous immunolocalization of NSE4A and ZYP1 shows clearly their co-localization at the central region of the SC throughout prophase I. At pachytene, the NSE4A signals are present along the synapsed homologs. When degradation proceeds during diakinesis, NSE4A can be detected only at the ZYP1-positive SC fragments. A and B chromosomes behave similar **(A_1-A_3)**. Bars = 5 μm. **(A_1)** A self-pairing rye B chromosome manifests the co-localization of NSA4A and ZYP1 at early diakinesis. Bar = 1 μm. **(A_2)** At late diakinesis, a self-paired rye B chromosome displays typical ball-like residual structures of the SC complex identical to those present on A chromosomes. NSE4A and ZYP1 colocalize. Bar = 2 μm. **(A_3)** An A chromosome bivalent showing ball-like structures of the remaining SC at late diakinesis. Note the colocalisation of NSE4A and ZYP1. Bar = 2 μm. **(B)** A meiocyte with seven A homologs and four B chromosomes (4Bs) at diplotene. The twisted NSE4A signals follow the SC structure typically present at diplotene. Bilby identifies the centromeres of the bivalents. The NSE4A structures are identical at A and B chromosomes **(B_1,B_2)**. Bars = 5 μm. **(B_1)** Typical twisted NSA4A structure of an A bivalent. Bar = 2 μm. **(B_2)** Twisted NSE4A structures indicate the SCs at four B chromosomes forming a multivalent. The Bs can be distinguished from As by their smaller size and the increased Bilby signal dispersion. Two of the B centromeres are associated (arrow). Bar = 2 μm.

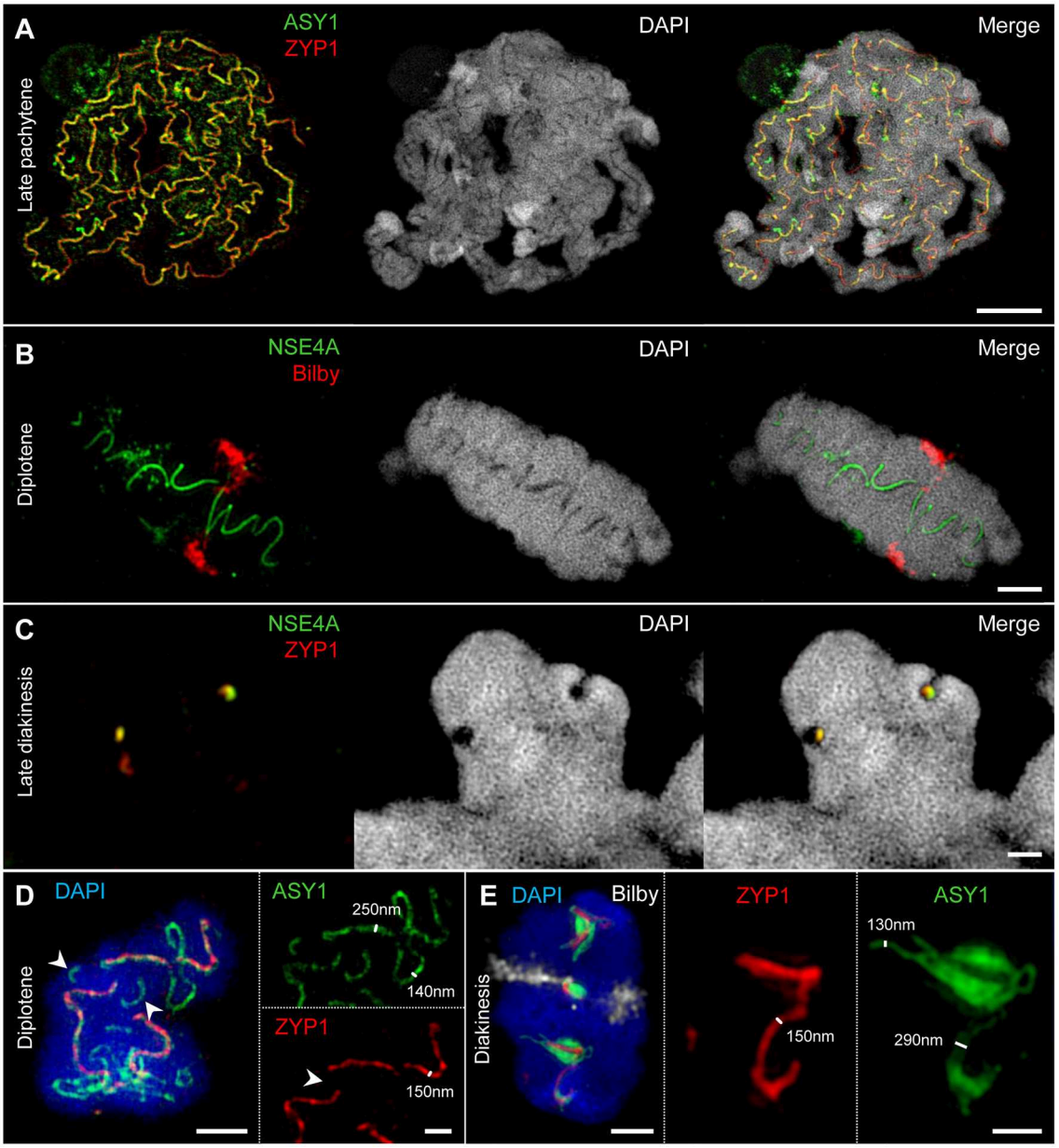

FIGURE 5 | SIM identifies the SC as a complex protein structure embedded in chromatin. Chromatin was stained with DAPI. **(A–C)** At different stages of prophase I, chromatin-free structures can be visualized within paired homologs. They comprise co-localized ASY1, ZYP1, and NSE4A proteins indicating the inner SC as chromatin-free. Bars = 5 μm **(A)**, 2 μm **(B)**, 1 μm **(C)**. **(D)** An A chromosome bivalent at diplotene showing SC disintegration accompanied by the retraction of ASY1 from the SC. While ASY1 forms loop structures at early desynapsis, ZYP1 disappears at positions were synapsis is already resolved (arrowheads). Bars = 2 μm (bivalent), 1 μm (enlarged region). **(E)** At diakinesis ASY1 winds up around the short residual ZYP1 strands at few positions suggesting a special role of these emerging ball-like structures. The centromeres were labeled with Bilby (see also **Supplementary Movie 2**). Bars = 2 μm (bivalent), 1 μm (enlarged region). The SIM resolution allows to measure the relative width of the ASY1 and ZYP1 structures at different prophase I stages. Single ASY1 strand have about the same width as ZYP1 strands **(D,E)**.

in SC fragmentation, HEI10 can be detected as numerous low-intensity foci located along the central element of the SC. Additionally, a few prominent foci slightly apart from ZYP1 were present. The localization of such foci toward the bivalent termini suggests a staining of potential crossover sites (**Figures 6C,D**; **Supplementary Movie 4**). At late diakinesis, ASY1 and ZYP1 signals disappear completely, but distinct HEI10 puncta remain at potential crossover loci. The quantification of HEI10 signals in 50 meiocytes at this stage resulted in a mean of 13.1 signals per cell ($SD = 1.57$). This value reflects the expected number of chiasmata observed in diploid rye by Jones (1967) and strongly suggests a detection of crossover sites by anti-HEI10.

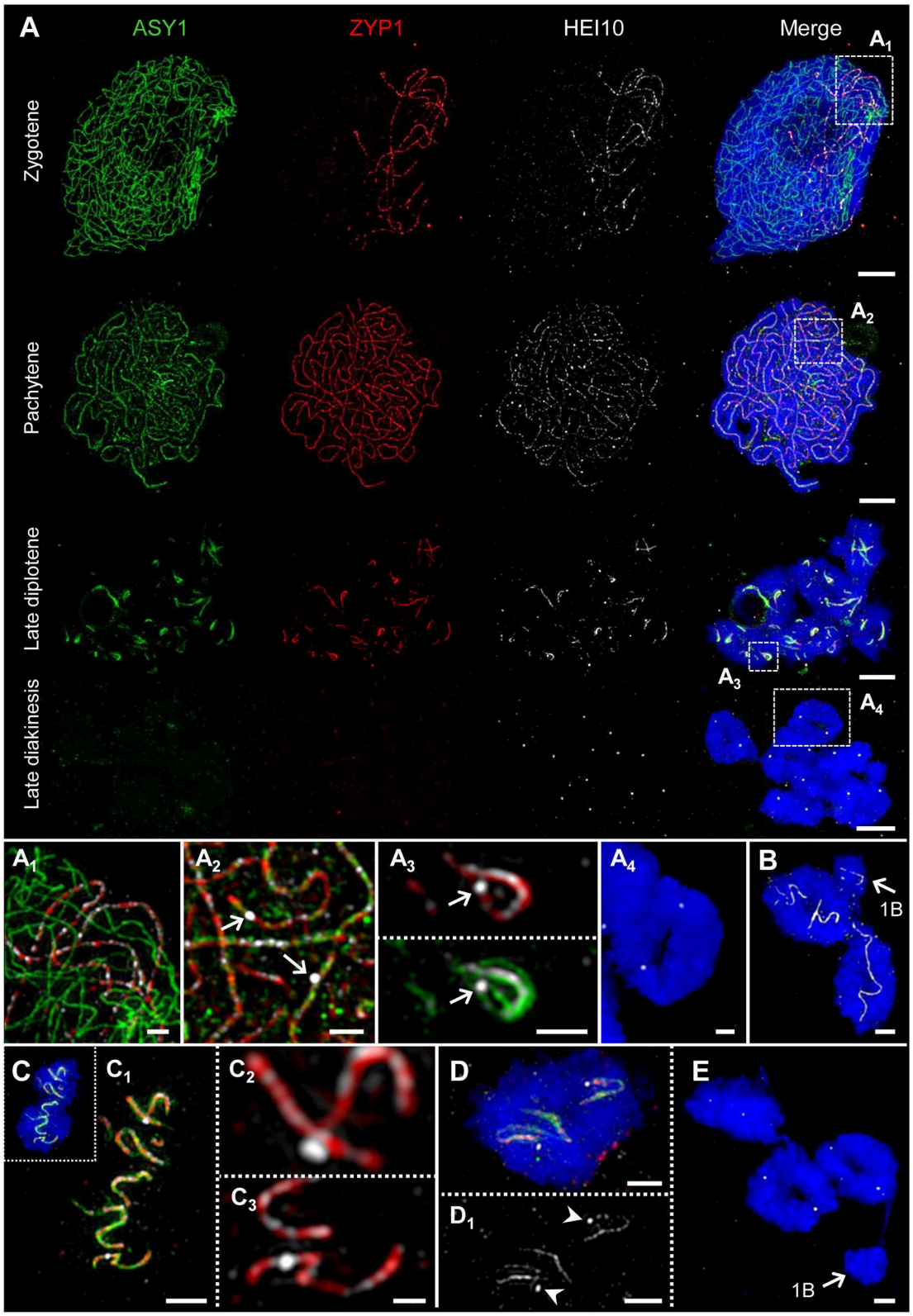

FIGURE 6 | HEI10 behavior compared to ASY1 and ZYP1 dynamics during prophase I. The images **(A_1-A_4)** show enlarged regions delimited by dashed boxes. Chromatin was counterstained with DAPI. **(A)** Throughout prophase I until late diplotene, HEI10 foci follow the dynamics of ZYP1. At zygotene, HEI10 foci are present

(Continued)

FIGURE 6 | at the central region of the SC marked by ZYP1. At the end of synapsis during pachytene single HEI10 foci become more prominent. At diplotene, the progression of SC disassembly causes the fragmentation of the SC, and HEI10 can be detected either as numerous low-intensity foci organized along the central element, or as a few prominent foci most likely corresponding to crossover- fated recombination sites. At late diakinesis, ASY1 and ZYP1 disappear, but HEI10 proteins remain as distinct spots at the potential recombination sites. Bars = 5 μm. **(A_1)** At zygotene, HEI10 foci occur exclusively in SCs marked by ZYP1. Bar = 1 μm. **(A_2)** At pachytene, individual HEI10 foci become more pronounced and clearly distinguishable (arrows). Bar = 1 μm. **(A_3)** Low-intensity HEI10 foci along the residual central region of the SC exist in parallel to a pronounced HEI10 focus (arrow) indicating a recombination site at late diplotene. ASY1 threads coil up at this position. Bar = 1 μm. **(A_4)** An A chromosome ring bivalent at late diakinesis with two HEI10 spots marking the potential sites of crossovers. ASY1 and ZYP1 signals are no longer detectable. Bar = 1 μm. **(B)** Two A chromosome ring bivalents accompanied by a single B chromosome (arrow) at diplotene. Similar as on the A chromosomes HEI10 threads are evident on the self-paired B chromosome. Bar = 2 μm. **(C)** Typical twisted SC structures marked by ASY1, ZYP1, and HEI10 on an A bivalent at diplotene. **(C_1)** The enlarged view of **(C)** shows the co-localization of the three proteins at the fragmented SC and indicates the ongoing desynapsis. Bar = 2 μm. **(C_2,C_3)** Besides weak HEI10 foci along ZYP1, two pronounced HEI10 spots are visible at higher magnification. The localization of such foci toward the bivalent connection sites at late diakinesis **(A_4,D)** suggests the staining of crossovers. Note, the HEI10 spot in **(C_2)** is localized slightly apart from the central element of the SC marked by ZYP1. Bar = 2 μm. **(D,D_1)** Distinct HEI10 spots (arrowheads) on an A chromosome ring bivalent at late diplotene. Both spots are not located on SC residues and likely correspond to the HEI10 signals exclusively evident at late diakinesis **(A_4)**. Bar = 2 μm. **(E)** Three A bivalents at late diakinesis show two HEI10 foci each. Instead, the single B chromosome (arrow) does not contain any HEI10 spots. Bar = 2 μm.

Active Centromeres and the SC Structure of Rye A and B Chromosomes Do Not Differ

FISH using the centromere-specific probe Bilby showed, as previously described by Banaei-Moghaddam et al. (2012), that the meiotic B centromeres exhibit an extended and diffuse Bilby signal distribution compared to those of A chromosome centromeres. Taking the signal size of an antibody recognizing the centromere-specific histone H3 variant CENH3 as a means to determine centromere activity (Wang and Dawe, 2018), the simultaneous labeling of meiocytes by Bilby and anti-CENH3 revealed that the actual size of active centromeres is similar between A and B chromosomes (**Figure 2**).

Rye Bs may occur in even or odd numbers ranging from 1 to 8 (Jones and Rees, 1982). Analysis of the SC structure revealed that ASY1 becomes loaded onto the B chromosome axis at early prophase I irrespective of the presence of a homologous partner (**Figures 7A**, **8**). In case of 2Bs, a normal SC assembly accompanied by the incorporation of ZYP1 occurs at pachytene. However, the SC formation of Bs present in odd numbers may be impaired. Beside the absence of ZYP1 and/or ASY1 loading (**Figures 8A_1,B_1**), the intrachromosomal SC formation ranging from small clusters (**Figure 8D_1**) to long SC stretches (**Figures 7C**, **8C_1**) was observed on univalent Bs. When prophase I progresses, B chromosome SCs show the same twisted structure evident on As (**Figures 4B_2**, **7C,D**). No differences between inter- and intrachromosomal SCs were observed. At diplotene, the SC disintegration, indicated by the retraction of ASY1, results in transient ASY1 threads, SC fragmentation and the subsequent formation of residual ball-like SC structures (**Figures 4A_{1-2}**, **7D,E**). The immunolocalization of NSE4A and HEI10 on Bs showed the co-localization of both proteins with ZYP1, and followed the above-mentioned SC dynamics (**Figures 4**, **6**; **Supplementary Movie 4**). Nevertheless, HEI10 disappeared completely at the end of diakinesis (**Figure 6E**) and was absent on univalent Bs.

In general, we conclude that Bs form similar SCs as As. In addition, the SC formation of Bs may be impaired depending on the B chromosome number per meiocyte.

Prophase I Pairing Configurations of B Chromosomes Depend on Their Number

The quantification of the meiotic pairing within PMCs of rye plants containing different Bs allowed revealing various types of B chromosome behavior. In case of one B chromosome, ASY1/ZYP1-positive SC fragments reflecting self-synapsis were detected on all univalents examined ($n = 10$ meiocytes). Plants with 2Bs ($n = 12$ meiocytes) showed regular SC assembly and bivalent formation. Only in one case two univalents were formed in such plants and fragmented SCs were observed on those univalents. Plants carrying 3Bs ($n = 94$ meiocytes) revealed three modes of SC formation during prophase I. Namely, 84% of their meiocytes had one bivalent and one univalent (**Figures 8A–C**), in 12.8% a clusters of all 3Bs was formed, and only 3.2% of the cells contained three univalents (**Figure 8D**). In case of plants carrying 4Bs ($n = 121$ meiocytes) the following configurations were observed: 64.5% of meiocytes contained only bivalents, in 29.7% multivalents joining up all Bs were formed, and 5.8% had one bivalent plus two univalents.

Altogether, the data indicate the influence of the B chromosome number on the pairing configurations of Bs.

DISCUSSION

Synapsed Homologs Form Chromomeres and a Chromatin-Free SC

SEM has been proven to be a suitable tool to investigate the architecture of plant chromosomes at the nanoscopic level (Wanner et al., 1991; Iwano et al., 2003; Wanner and Schroeder-Reiter, 2008). Studies on somatic plant metaphase chromosomes based on protein and DNA staining followed by SEM allowed to establish the so-called "dynamic matrix model" (Wanner and Formanek, 2000; Wanner et al., 2005). The model proposes that the chromosomes are mainly composed of DNA packed in chromomeres (coiled solenoides) around a dynamic matrix formed by parallel protein fibers. This protein matrix may also contribute to form the chromatin-free axes/SCs during synapsis. The model was also shown to be applicable to meiotic chromatin of rye (Zoller et al., 2004a,b). In line with these reports, we observed tightly packed chromomeres at the surface of chromosomes from zygotene to diplotene in rye. Furthermore,

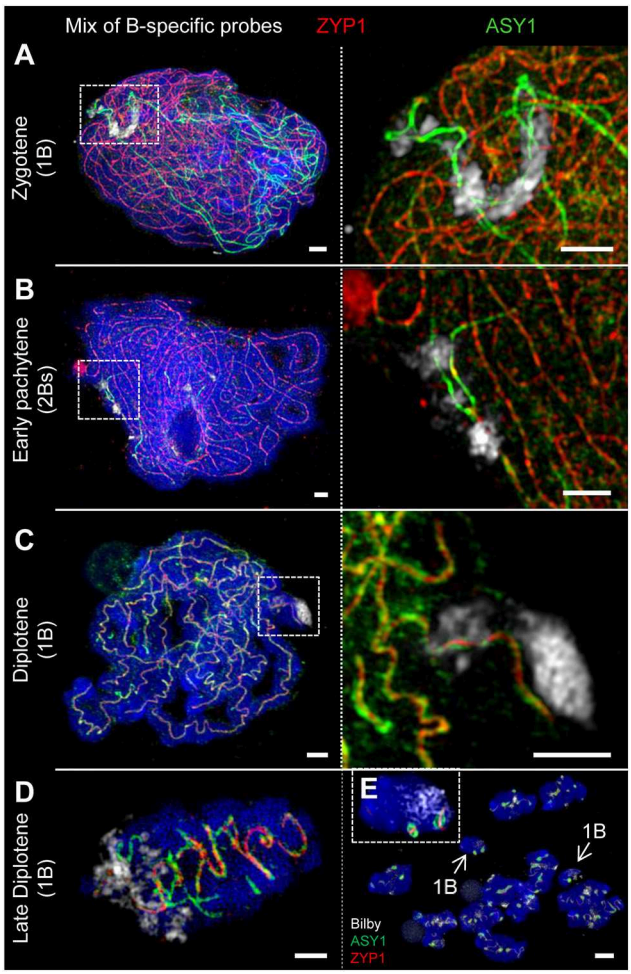

FIGURE 7 | The SC structure of B chromosomes does not differ from that of As. Bs were detected by means of a B-specific FISH probe mix. The global chromatin was counterstained with DAPI. **(A)** At zygotene, ASY1 is associated with the B chromosome axis similar to that on As. The loading of ASY1 is independent of the B chromosome number, thus also occurring at single Bs performing intrachromosomal synapsis. Bars = 2 μm. **(B)** In case of 2 Bs, normal synapsis of both occurs. The enlargement shows a not yet synapsed B chromosome region indicated by two separate ASY1 strands with brighter fluorescence at early pachytene. Bars = 5 μm. **(C)** In absence of a homologous pairing partner, intrachromosomal synapsis of single B chromosomes takes place. The ASY1 and ZYP1 staining is identical to that of A bivalents during diplotene. Bars = 2 μm. **(D)** Similar to that of A bivalents at late diplotene (**Figure 3A$_4$**) B bivalents show the retraction of ASY1 strands from the SC during desynapsis. Bar = 2 μm. **(E)** Two meiocytes (mixed by squashing) of rye carrying 1B chromosome each at diakinesis. Both Bs (arrows) can be distinguished from As by smaller size. The inset shows one of the B chromosomes with two typical ball-like residual structures of the SC complex. Bar = 5 μm.

our finding that the SC is localized outside and not enclosed by chromatin, suggests a lateral co-orientation of the chromatid axes prior to SC formation. Such a chromatin configuration can facilitate an unhindered loading of the AE proteins and the SC assembly. As a consequence, this results in a mainly chromatin-free proteinaceous SC structure that was previously documented in other organisms such as lily and maize (Holm, 1977; Dawe et al., 1994). Due to the high degree of compactness of meiotic chromosomes, the detection of matrix fibers would require an additional application of enzymes, such as proteinase K to loosen the chromatin (Zoller et al., 2004b).

The Dynamics of ASY1 and ZYP1 Indicate an Assembly and Disassembly of the SC During Prophase I

Previous studies demonstrated that antibodies raised against the two SC proteins ASY1 and ZYP1 of *A. thaliana* are suitable for the detection of orthologous proteins in other plant species, e.g., in barley and rye (Mikhailova et al., 2006; Phillips et al., 2008, 2010). Here, we utilized ASY1 and ZYP1 to investigate homologous pairing events during prophase I in rye utilizing SIM. Synapsis is initiated in rye at telomeres and interstitial sites as previously reported (Abirached-Darmency et al., 1983). When synapsis occurs, the ASY1 signal intensity decreases severely. It cannot be excluded, that this observation results from a decreased accessibility of the ASY1 antibodies to the epitopes as a consequence of the SC assembly and chromatin compaction (Golubovskaya et al., 2006). However, a weak ASY1 staining in the nucleoplasm is detectable at early pachytene suggesting that ASY1 is partially removed from the AEs/LEs during synapsis. Similar observations were reported for various species. In rice, maize and budding yeast the signal intensity for the orthologs PAIR2, ASY1, and HOP1, respectively, also significantly decrease during synapsis (Smith and Roeder, 1997; Nonomura et al., 2006). However, in contrast to these species, rye ASY1 is not removed from the axes during pachytene. It remains at the SC until its disintegration, comparable to the orthologous proteins of barley and *Arabidopsis* (Armstrong et al., 2002; Phillips et al., 2012). Previous studies, using rye synaptic mutants as experimental material, reported that ASY1 and ZYP1 pre-assemble. It was hypothesized that these double layer tracts could be formed in wild-type rye as well before synapsis and later could interact to form the SC (Mikhailova et al., 2006; Phillips et al., 2008). In our study, we did not observe such a pre-alignment of SC fragments in wild-type rye meiocytes carrying accessory B chromosomes, but ASY1 located exclusively to the AE/LE elements in As and Bs. At zygotene, ZYP1 was incorporated at the CR of the SC in a zipper-like manner. Moreover, a diffuse staining of yet unassembled ZYP1 within the nucleoplasm was found, which decreased when synapsis has finished. These deviating observations could be due to the different rye genotypes studied, as well as the specificity of the different antibodies used, i.e., anti-maize in this study vs. anti-*Arabidopsis* ASY1 and ZYP1 in the previous one. Different slide preparation techniques, especially the fixation in 4 vs. 2% paraformaldehyde, as well as the increased resolution and detection sensitivity achieved by SIM, which allows more precise observations compared to confocal laser scanning microscopy, could also be crucial. During the progression of prophase I, we observed remarkable structural chromatin changes. At the end of pachytene, the SC adopts a twisted structure, consistent with previous studies (Fedotova et al., 1989; Mikhailova et al.,

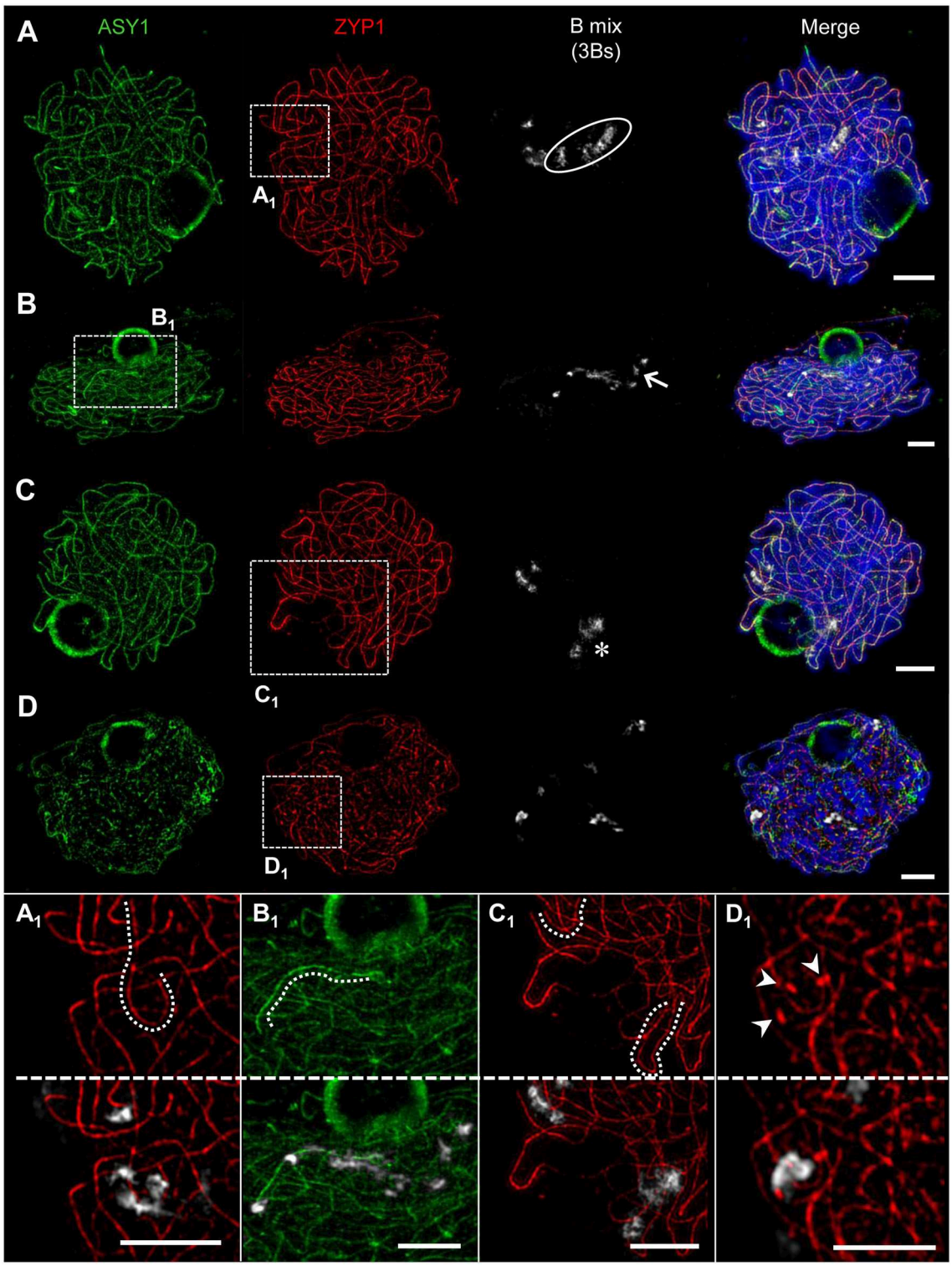

FIGURE 8 | Pairing configurations of B chromosomes at pachytene. 3Bs were detected by means of a B-specific FISH probe mix, SCs with ASY1- and ZYP1-specific antibodies. Three different types of B chromosome arrangement were observed. Chromatin was counterstained with DAPI. **(A)** The Bs form one bivalent and one univalent. The bivalent **(A_1)** shows normal synapsis, whereas the univalent B (circle) did not show any labeling by ASY1 or ZYP1 indicating the absence of a SC. **(B)** One B univalent and one B bivalent associate. While the bivalent (arrow) performs normal synapsis indicated by ZYP1, the univalent **(B_1)** was exclusively loaded with ASY1. **(C)** Formation of one B bivalent and one B univalent. The bivalent (asterisk) performs normal synapsis, while the univalent B shows intrachromosomal synapsis revealed by ZYP1 labeling **(C_1)**. **(D)** Three B univalents show a fragmented SC formation [**(D_1)**, arrow heads]. Bars = 5 μm.

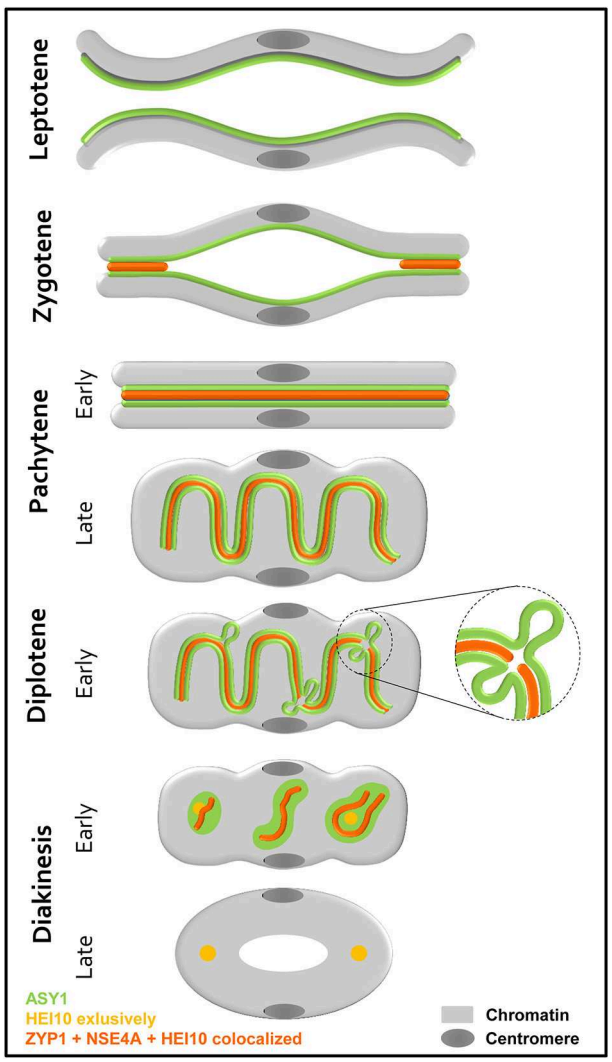

FIGURE 9 | Scheme showing the behavior of two homologous chromosomes, together with the localization of the SC proteins ASY1, ZYP1, NSE4A, and HEI10 during prophase I. Before synapsis, ASY1 is loaded along each chromosome axis at leptotene. During zygotene, the assembly of the SC occurs at multiple sites of the homologs. Thereby, ZYP1, NSE4A, and HEI10 are incorporated at the central region. Synapsis completes at the beginning of pachytene visible by the tripartite structure consisting of two lateral elements enclosing the central region. The ongoing degree of condensation observed throughout prophase I, is accompanied by a coiling of the SC at late pachytene. At diplotene, the onset of SC disintegration is accompanied by the retraction of ASY1 forming transient loops. At positions, where both ASY1 threads are retracted from the SC, ZYP1, NSE4A, and HEI10 disappear (enlarged). The progression of the SC degradation results in fragmented ball-like SC structures at early diakinesis. In addition to the ZYP1 and NSE4A labeling at the crossover sites and in between the centromeres, distinct HEI10 foci marking crossover sites are evident. At late diakinesis, the SC disassembly is completed, and ASY1, ZYP1, and NSE4A disappeared completely. Only the sites of crossovers remain clearly marked by HEI10.

2006; Simanovsky et al., 2014). This coiling was not the result of helical winding of the chromosomes, because the SC structures did not form symmetrical spirals. Instead, it was a result of contracting chromatin.

According to the "dynamic matrix model" (see above) coiled solenoids bind to interconnected matrix fibers. During condensation, the matrix fibers may act in an actin/myosin-like manner, whereby the parallel arrangement of the matrix favors shortening and thickening of the chromosomes. We propose that a similar mechanism could occur in meiotic chromosomes. But in contrast to mitosis, meiotic chromosomes need to condense and separate two paired homologs. Therefore, it is plausible, that the SC does not only provide the platform for recombination but it may also link both homologs to synchronize the condensation process. By tethering chromomeres of all chromatids to a common axis a random chromatin organization may be prohibited. Given that chromosomes condense during complete prophase I, a successive compaction of the chromomeres is reached. As a consequence of the sterical restrictions the tension along the paired homologs increases and thus, causes the bending of the SC at pachytene. At late pachytene/diplotene when the tension increases further, a local repulsion of single LE occurs, apparent by the retraction of ASY1 threads, which form transient loops. Similar dynamic structures of ASY1 were recently described in meiotic chromosomes of wheat and barley (Colas et al., 2017). During these processes ZYP1 disappears from the CR and disintegration of the SCs emerges. By disassembly of the SC, both homologs become separated piecewise. Possibly, the ball-like SC structures of ZYP1 and ASY1 are formed and remain to counteract the tension throughout diakinesis. Thus, a stabilization of the bivalents is achieved and the premature separation of recombination sites and centromeres may be prevented. Last traces of the SC are lost at the end of diakinesis, when chiasmata and centromere formation are fully accomplished.

The persistence of SC components at centromeres, additionally to the recombination sites during their disassembly in late prophase I, has also been described in budding yeast, *Drosophila*, mouse and human (Bisig et al., 2012; Qiao et al., 2012; Kurdzo and Dawson, 2015). Our finding, that SC components accumulate also at centromeres during the SC disassembly in plants indicates a conserved phenomenon, important to perform proper meiotic chromosome segregation.

In many organisms, including protists, fungi, animals, and plants the aggregation of SC-related material to form so-called polycomplexes was reported (Zickler and Kleckner, 1999). Because our study shows that the ball-like structures result directly from SC disassembly, we conclude that they are not SC-independent aggregations of SC-related proteins as present in polycomplexes (Zickler and Kleckner, 1999). Despite intense studies, polycomplexes have never been reported in prophase I stages of rye. Therefore, we exclude this sort of interpretation.

The SMC5/6 Complex δ-kleisin NSE4 Seems to Be Required for Synapsis and Recombination

NSE4 is the crucial non-SMC δ-kleisin component of the SMC5/6 complex, and therefore can be considered as a reliable marker for its localization (Palecek et al., 2006). In *A. thaliana*, two orthologs, *Nse4A* and *Nse4B*, were identified. Both genes

are expressed in different tissues and are required to realize complete fertility. However, *Nse4A* is the more essential gene (Watanabe et al., 2009; Zelkowski et al., 2019). Despite the increasing knowledge about SMC5/6 of non-plant eukaryotes (Verver et al., 2016), the immunohistochemical analysis of the NSE4 distribution and its dynamics during meiosis in plants was challenging so far due to the lack of specific antibodies. In the present study, we localized for the first time the SMC5/6 complex subunit NSE4 in prophase I of rye, using antibodies raised against NSE4A of *A. thaliana* (Zelkowski et al., 2019). The detection of NSE4 from early zygotene until late diakinesis is similar to the localization pattern found in mammalian meiosis (Verver et al., 2016). In rye, NSE4 co-localizes with the TF protein ZYP1, indicating the restriction of NSE4 to synapsed chromosomes. Consistent observations were described in mice, where a SYCP1-dependent loading of SMC6 occurs (Gomez et al., 2013), and in human, where SMC5/6 localizes to synapsed chromosome axes (Verver et al., 2014). By its recruitment to synapsed axes, the SMC5/6 complexes might facilitate the formation and/or stabilization of synapsis in rye. Moreover, in *C. elegans*, fission and budding yeasts the SMC5/6 complexes are involved in homologous recombination and proper chromosome segregation (Pebernard et al., 2004; Bickel et al., 2010; Wehrkamp-Richter et al., 2012; Copsey et al., 2013; Lilienthal et al., 2013; Xaver et al., 2013). Our observed localization pattern of NSE4, especially at the late ball-like SC structures during diakinesis, might also indicate a function of SMC5/6 complexes in homologous recombination of rye.

The involvement in synapsis has also been proven for the meiotic α-kleisin of the SMC family complex cohesin. Its presence in prophase I was shown in plants such as *Arabidopsis* (Cai et al., 2003), tomato (Qiao et al., 2011), rice (Zhang et al., 2006; Shao et al., 2011), and in addition its co-localization to ZYP1 was proven in *Luzula* (Ma et al., 2016). These findings support the importance of SMC complex proteins for proper meiosis.

HEI10, a Marker for Class I Crossovers in Rye?

In mice, the two RING-family E3 ligases HEI10 and RNF212 were shown to be essential for recombination (Reynolds et al., 2013; Qiao et al., 2014). In contrast to mammals, plants possess only one member of the broad RNF212/HEI10 protein family (Toby et al., 2003; Ward et al., 2007; Chelysheva et al., 2012; Wang et al., 2012; Rao et al., 2017). During meiosis of *A. thaliana* and rice, HEI10 proteins label the sites of class I crossovers (Chelysheva et al., 2012; Wang et al., 2012; Ziolkowski et al., 2017).

Our study provides evidence that antibodies raised against HEI10 of *O. sativa* (Wang et al., 2012) detect the corresponding proteins in rye. In rice, a punctate pattern of HEI10 occurs in early leptotene. Importantly, a linear distribution of signals alongside of ZEP1 (ZYP1 ortholog of rice) can be observed during synapsis, but disappears at diplotene. From late pachytene to diakinesis, additional prominent HEI10 foci were localized at the chromosomes, presumably marking class I crossover sites (Wang et al., 2012). Similar results were obtained in *A. thaliana* (Chelysheva et al., 2012). The localization of the orthologous rye protein found in our study differs from those reports, as HEI10 foci were not detectable before the onset of ZYP1 installation/loading. Thus, a crucial role of HEI10 at pre-synaptic events of recombination seems to be unlikely in rye.

Recent studies in *Sordaria* and mice revealed a similar localization pattern of HEI10 as seen in rye, by being associated only with SCs, although HEI10 is not a SC component. In both species, it was shown that HEI10 becomes engaged after the Mer3/MLH- and/or DMC1-mediated homolog pairing, and seems to regulate post-synapsis steps of meiotic recombination via a SUMO-ubiquitin switch (Storlazzi et al., 2010; De Muyt et al., 2014; Qiao et al., 2014). In *Sordaria*, HEI10/MSH4 foci were classified by morphology and dynamics, and proposed to mark three different types of recombination complexes: early and late SC-associated nodules, as well as non-nodule associated interactions (De Muyt et al., 2014). Previous TEM studies characterized two morphologically different types of recombination nodules: one at early and the second at late pachytene of rye (Abirached-Darmency et al., 1983). Given the lower resolution of SIM, the differentiation of these nodule types during pachytene of rye is not feasible. Nevertheless, it is tempting to assume that our observation of high fluorescence intensity HEI10 foci from pachytene on correspond to such recombination nodules, whereas the weak foci represent axis-associated HEI10 involved in the SUMO-ubiquitin switch. This assumption is supported by the distinct HEI10 foci present at late prophase I. During SC disassembly at diplotene, both types of HEI10 foci are clearly distinguishable, i.e. week signals associated with the remaining SC fragments, as well as prominent foci located toward the end of the bivalents either on or in close proximity to the SC. HEI10 foci apart from the SC may indicate recombination sites no longer connected to the SC due the proceeding chromosome condensation. After the complete disintegration of the SC at the end of diakinesis, only prominent HEI10 foci still persist. The mean number of those foci (13.1; $SD = 1.57$; $n = 50$ cells) matches the observed number of chiasmata in rye (Jones, 1967; Naranjo and Lacadena, 1980).

In short, we assume that HEI10 may be the first recombination marker identified in rye, most likely labeling class I crossovers.

A Model for the Behavior of Rye Chromosomes During Prophase I

Despite extensive studies on the mechanisms of SC establishment and disassembly in various organisms, it is still challenging to decipher the complex events underlying the SC formation and recombination.

Based on our findings, we propose a model for the homologous chromosome behavior during prophase I based on the observed dynamics of ASY1, ZYP1, NSE4A, and HEI10 (**Figure 9**). At leptotene, the AE/LE-associated protein ASY1 is loaded onto the chromosome axes prior to SC formation. As synapsis occurs, ZYP1, NSE4A, and HEI10 become incorporated at the central region of the SC. Further, the ongoing condensation of the chromatin throughout prophase I leads to the coiling of the SC at late pachytene. The following disintegration of the SC is

accompanied by the retraction of ASY1 from the central region, most likely as a result of the increasing tension on chromatin caused by condensation. At positions where both ASY1 threads are retracted, the CR is dissolved and ZYP1, NSE4A, and HEI10 are no longer detectable (**Figure 9**, enlarged). As a consequence, SC fragmentation and the formation of ball-like structures can be observed at early diakinesis. Additionally to weak HEI10 signals on the remaining SC, distinct foci at both ends of the bivalent reflecting the sites of crossover are detectable. Colocalizing ASY1, ZYP1, and NSE4A proteins are also present in between the homologous centromeres. But here, HEI10 is missing indicating the absence of crossovers. At late diakinesis, the SC disassembly is completed as indicated by the disappearance of ASY1, ZYP1, and NSE4A at the crossover sites as well as at the centromeres. Only the class I crossovers remain marked by HEI10.

During Prophase I Bs Behave Like A Chromosomes

For decades the origin of rye B chromosomes remained enigmatic. The application of next generation sequencing revealed that Bs originate from several A chromosome fragments and an accumulation of various repeats and insertions of organellar DNA (Martis et al., 2012). Moreover it was shown, that Bs possess their own evolutionary pathways and that they accumulate high copy sequences, allowing to identify rye Bs during prophase I by FISH (Klemme et al., 2013). By combination of antibodies directed against ASY1, ZYP1, NSE4A and HEI10 with B-specific FISH probes, we analyzed the SC composition of Bs. Previous EM studies of the SC formation in various species revealed substantial differences between the meiotic pairing of As and Bs dependent on their number (Jenkins, 1985; Switonski et al., 1987; Kolomiets et al., 1988; Shi et al., 1988; Santos et al., 1993). Moreover, studies of the Chinese racoon dog demonstrated diverging SC structures of As and Bs. Namely during pachytene the SC axes of the B chromosomes are significantly denser than those of the As. Depending on the number of Bs, bivalents and multivalents could be formed. If three Bs were present in parallel, the alignment of all three SC axes might occur (Shi et al., 1988). For rye Bs it was shown, that in contrast to 2Bs, univalents and higher B chromosome numbers form either intrachromosomal SCs, or perform the segmental pairing in multivalents. In contrast to the Chinese racoon dog, SCs of Bs formed by more than two AEs/LEs have never been observed (Santos et al., 1993). In rye with increasing B numbers altered SC formation occurs unrelated to the mean number of A-located chiasmata (Diez et al., 1993), while in *Crepis capillaris* SC irregularities of As correlate with defective A chromosome pairing when 4 Bs are present (Jones et al., 1991). Our study revealed that in general the SC composition of Bs does not differ from that of As, as proven on meiocytes containing 2Bs. All four proteins investigated localize to the SCs of Bs and manifest the same dynamics as described for As. Despite their different nature compared to As, rye Bs utilize obviously the same protein structures to ensure meiotic pairing and proper chromosome condensation. Rye plants comprising less or more than 2Bs show also a similar SC composition independent of segmental or intrachromosomal pairing. Obviously, by producing the same SC structures the Bs try to fulfill the pairing requirements. Similar observations were described also for univalent A chromosomes, e.g., in barley, lily, wheat, and maize (Gillies, 1974, 1981; Holm, 1977; Hobolth, 1981). Only in very rare cases, the formation of SCs fails and either ASY1 only or none of the proteins were detectable. Previous studies suggested that the intrachromosomal pairing is a non-homologous process and has no genetic consequences due to the lack of recombination (Santos et al., 1993).

The prophase I meiotic pairing configurations of rye Bs were found to be genotype-dependent and are linked to the efficiency of B chromosome transmission to the next generation. Whereas bivalent formation secures the successful transmission of Bs, uni-, and multivalents have a much lower transmission rate (Jiménez et al., 2000). The rye variety "Paldang" we analyzed has a B transmission rate of about 20% (Romera et al., 1989).

In summary, we conclude that despite the deviating chromatin composition A and B chromosomes establish similar SC structures to perform pairing in prophase I.

DATA AVAILABILITY

All datasets for this study are included in the manuscript and the **Supplementary Files**.

AUTHOR CONTRIBUTIONS

SH, AH, VS, and EM conceived the study and designed the experiments. SH, VS, MZ, EM, and CK performed the experiments. SH and VS wrote the manuscript. All authors read and approved the final manuscript.

FUNDING

This study has been funded by the European Union project Marie-Curie COMREC network FP7 ITN-606956.

ACKNOWLEDGMENTS

We thank Katrin Kumke for excellent technical assistance, Karin Lipfert for help with artwork, Stefan Heckmann for critical reading of the manuscript and Graham Moore for helpful discussions. The rabbit anti *Z. mays* ASY1 and ZYP1 antibodies were kindly provided by W. Zacheus Cande (University of California, Berkeley), and the *O. sativa* HEI10 antibodies by Zhukuan Cheng (Chinese Academy of Science, Beijing).

SUPPLEMENTARY MATERIAL

The Supplementary Material for this article can be found online at: https://www.frontiersin.org/articles/10.3389/fpls.2019.00773/full#supplementary-material

Supplementary Figure 1 | SIM improves the resolution, and thus the identification of SC nanostructures significantly. Chromatin was stained with DAPI.

(A) Comparison of ASY1 and ZYP1 immunosignals at zygotene acquired by conventional widefield microscopy and SIM. The increased resolution of SIM reveals more nanostructures and improves the co-localization analysis by higher precision. Bar = 2 μm. **(A_1)** Enlarged region showing clearly interstitial synapsis (arrows) by SIM. Bar = 1 μm. **(B)** Widefield imaging of the ball-like ASY1 and ZYP1 structures at late diakinesis. Bar = 5 μm. **(B_1)** SIM delivers a clearly increased substructural information compared to widefield microscopy. ZYP1 is embedded into a ball of ASY1. Bar = 0.5 μm.

Supplementary Figure 2 | The exclusive NSE4A antibody application to meiocytes proves that the detected signals are not a result of fluorescence crosstalk. NSE4A co-localizing to ZYP1 (**Figure 4**) shows without a ZYP1 labeling the typical twisted NSE4A signals during diplotene, thus excluding a fluorescent crosstalk possible via double labeling. (Peri)centromeric regions of the homologs are marked by Bilby FISH probes. Chromatin was stained with DAPI. Bar = 5 μm.

Supplementary Movie 1 | Meiocyte at zygotene containing seven A and two B bivalents labeled with the centromere-specific markers Bilby (green) and CENH3 (red). The B bivalents can be identified by their increased Bilby dispersion (below). See also **Figure 2**.

Supplementary Movie 2 | At diakinesis ZYP1 threads (red) are embedded in three ball-like ASY1 (green) structures possibly stabilizing the centromeric region (white, marked by Bilby) and the two recombination sites at both chromosome arms (see also **Figure 5E**). The movie shows a single bivalent.

Supplementary Movie 3 | Image stack of a meiocyte showing the distribution of ASY1 (green) and ZYP1 (red) at the SCs during zygotene (see also **Figure 4A**).

Supplementary Movie 4 | ASY1 (green), ZYP1 (red), and HEI10 (white) colocalize at the SCs of two A bivalents and a smaller self-paired B chromosome (below) at diplotene (see also **Figure 6B**).

REFERENCES

Abirached-Darmency, M., Zickler, D., and Cauderon, Y. (1983). Synaptonemal complex and recombination nodules in rye (*Secale cereale*). *Chromosoma* 88, 299–306. doi: 10.1007/bf00292907

Armstrong, S. J., Caryl, A. P., Jones, G. H., and Franklin, F. C. (2002). Asy1, a protein required for meiotic chromosome synapsis, localizes to axis-associated chromatin in *Arabidopsis* and *Brassica*. *J. Cell Sci*. 115, 3645–3655. doi: 10.1242/jcs.00048

Bahler, J., Wyler, T., Loidl, J., and Kohli, J. (1993). Unusual nuclear structures in meiotic prophase of fission yeast: a cytological analysis. *J. Cell Biol.* 121, 241–256. doi: 10.1083/jcb.121.2.241

Banaei-Moghaddam, A. M., Schubert, V., Kumke, K., Weibeta, O., Klemme, S., Nagaki, K., et al. (2012). Nondisjunction in favor of a chromosome: the mechanism of rye B chromosome drive during pollen mitosis. *Plant Cell* 24, 4124–4134. doi: 10.1105/tpc.112.105270

Baroux, C., and Schubert, V. (2018). Technical review: microscopy and image processing tools to analyze plant chromatin: practical considerations. In *Plant Chromatin Dynamics: Methods and Protocols*, eds. M. Bemer and C. Baroux (New York, NY: Springer), 537–589. doi: 10.1007/978-1-4939-7318-7_31

Bickel, J. S., Chen, L., Hayward, J., Yeap, S. L., Alkers, A. E., and Chan, R. C. (2010). Structural maintenance of chromosomes (SMC) proteins promote homolog-independent recombination repair in meiosis crucial for germ cell genomic stability. *PLoS Genet*. 6:e1001028. doi: 10.1371/journal.pgen.1001028

Bisig, C. G., Guiraldelli, M. F., Kouznetsova, A., Scherthan, H., Hoog, C., Dawson, D. S., et al. (2012). Synaptonemal complex components persist at centromeres and are required for homologous centromere pairing in mouse spermatocytes. *PLoS Genet*. 8:e1002701. doi: 10.1371/journal.pgen.1002701

Blunden, R., Wilkes, T. J., Forster, J. W., Jiménez, M. M., Sandery, M. J., Karp, A., et al. (1993). Identification of the E3900 family, a 2nd family of rye chromosome-B specific repeated sequences. *Genome* 36, 706–711. doi: 10.1139/g93-095

Bolcun-Filas, E., Costa, Y., Speed, R., Taggart, M., Benavente, R., De Rooij, D. G., et al. (2007). SYCE2 is required for synaptonemal complex assembly, double strand break repair, and homologous recombination. *J. Cell Biol*. 176, 741–747. doi: 10.1083/jcb.200610027

Bolcun-Filas, E., Hall, E., Speed, R., Taggart, M., Grey, C., de Massy, B., et al. (2009). Mutation of the mouse Syce1 gene disrupts synapsis and suggests a link between synaptonemal complex structural components and DNA repair. *PLoS Genet*. 5:e1000393. doi: 10.1371/journal.pgen.1000393

Cahoon, C. K., and Hawley, R. S. (2016). Regulating the construction and demolition of the synaptonemal complex. *Nat. Struct. Mol. Biol.* 23, 369–377. doi: 10.1038/nsmb.3208

Cai, X., Dong, F., Edelmann, R. E., and Makaroff, C. A. (2003). The *Arabidopsis* SYN1 cohesin protein is required for sister chromatid arm cohesion and homologous chromosome pairing. *J. Cell Sci*. 116, 2999–3007. doi: 10.1242/jcs.00601

Chelysheva, L., Vezon, D., Chambon, A., Gendrot, G., Pereira, L., Lemhemdi, A., et al. (2012). The *Arabidopsis* HEI10 is a new ZMM protein related to Zip3. *PLoS Genet*. 8:e1002799. doi: 10.1371/journal.pgen.1002799

Colas, I., Darrier, B., Arrieta, M., Mittmann, S. U., Ramsay, L., Sourdille, P., et al. (2017). Observation of extensive chromosome axis remodeling during the "diffuse-phase" of meiosis in large genome cereals. *Front. Plant Sci*. 8:1235. doi: 10.3389/fpls.2017.01235

Collins, K. A., Unruh, J. R., Slaughter, B. D., Yu, Z., Lake, C. M., Nielsen, R. J., et al. (2014). Corolla is a novel protein that contributes to the architecture of the synaptonemal complex of *Drosophila*. *Genetics* 198, 219–228. doi: 10.1534/genetics.114.165290

Copsey, A., Tang, S., Jordan, P. W., Blitzblau, H. G., Newcombe, S., Chan, A. C., et al. (2013). Smc5/6 coordinates formation and resolution of joint molecules with chromosome morphology to ensure meiotic divisions. *PLoS Genet*. 9:e1004071. doi: 10.1371/journal.pgen.1004071

Dawe, R. K., Sedat, J. W., Agard, D. A., and Cande, W. Z. (1994). Meiotic chromosome pairing in maize is associated with a novel chromatin organization. *Cell* 76, 901–912. doi: 10.1016/0092-8674(94)90364-6

De Muyt, A., Zhang, L., Piolot, T., Kleckner, N., Espagne, E., and Zickler, D. (2014). E3 ligase Hei10: a multifaceted structure-based signaling molecule with roles within and beyond meiosis. *Genes Dev*. 28, 1111–1123. doi: 10.1101/gad.240408.114

De Vries, F. A., de Boer, E., van den Bosch, M., Baarends, W. M., Ooms, M., Yuan, L., et al. (2005). Mouse Sycp1 functions in synaptonemal complex assembly, meiotic recombination, and XY body formation. *Genes Dev*. 19, 1376–1389. doi: 10.1101/gad.329705

Diez, M., Jiménez, M. M., and Santos, J. L. (1993). Synaptic patterns of rye B-Chromosomes. II. The effect of the standard B-chromosomes on the pairing of the A set. *Theor. Appl. Genet.* 87, 17–21. doi: 10.10007/BF00223737

Egel-Mitani, M., Olson, L. W., and Egel, R. (1982). Meiosis in *Aspergillus nidulans*: another example for lacking synaptonemal complexes in the absence of crossover interference. *Hereditas* 97, 179–187. doi: 10.1111/j.1601-5223.1982.tb00870.x

Endo, T. R., Nasuda, S., Jones, N., Dou, Q., Akahori, A., Wakimoto, M., et al. (2008). Dissection of rye B chromosomes, and nondisjunction properties of the dissected segments in a common wheat background. *Genes Genet. Syst*. 83, 23–30. doi: 10.1266/ggs.83.23

Fawcett, D. W. (1956). The fine structure of chromosomes in the meiotic prophase of vertebrate spermatocytes. *J. Biophys. Biochem. Cytol.* 2, 403–406. doi: 10.1083/jcb.2.4.403

Fedotova, Y. S., Kolomiets, O. L., and Bogdanov, Y. F. (1989). Synaptonemal complex transformations in rye microsporocytes at the diplotene stage of meiosis. *Genome* 32, 816–823. doi: 10.1139/g89-516

Ferdous, M., Higgins, J. D., Osman, K., Lambing, C., Roitinger, E., Mechtler, K., et al. (2012). Inter-homolog crossing-over and synapsis in *Arabidopsis* meiosis are dependent on the chromosome axis protein AtASY3. *PLoS Genet*. 8:e1002507. doi: 10.1371/journal.pgen.1002507

Fousteri, M. I., and Lehmann, A. R. (2000). A novel SMC protein complex in *Schizosaccharomyces pombe* contains the Rad18 DNA repair protein. *EMBO J.* 19, 1691–1702. doi: 10.1093/emboj/19.7.1691

Francki, M. G. (2001). Identification of Bilby, a diverged centromeric Ty1-copia retrotransposon family from cereal rye (*Secale cereale* L.). *Genome* 44, 266–274. doi: 10.1139/g00-112

Franklin, A. E., McElver, J., Sunjevaric, I., Rothstein, R., Bowen, B., and Cande, W. Z. (1999). Three-dimensional microscopy of the Rad51 recombination protein during meiotic prophase. *Plant Cell* 11, 809–824. doi: 10.1105/tpc.11.5.809

Gerton, J. L., and Hawley, R. S. (2005). Homologous chromosome interactions in meiosis: diversity amidst conservation. *Nat. Rev. Genet*. 6, 477–487. doi: 10.1038/nrg1614

Gillies, C. B. (1974). The nature and extent of synaptonemal complex formation in haploid barley. *Chromosoma* 48, 441–453. doi: 10.1007/bf00290998

Gillies, C. B. (1981). Electron microscopy of spread maize pachytene synaptonemal complexes. *Chromosoma* 83, 575–591. doi: 10.1007/bf00328521

Golubovskaya, I. N., Hamant, O., Timofejeva, L., Wang, C. J., Braun, D., Meeley, R., et al. (2006). Alleles of afd1 dissect REC8 functions during meiotic prophase I. *J. Cell Sci*. 119, 3306–3315. doi: 10.1242/jcs.03054

Golubovskaya, I. N., Wang, C. J., Timofejeva, L., and Cande, W. Z. (2011). Maize meiotic mutants with improper or non-homologous synapsis due to problems in pairing or synaptonemal complex formation. *J. Exp. Bot*. 62, 1533–1544. doi: 10.1093/jxb/erq292

Gomez, R., Jordan, P. W., Viera, A., Alsheimer, M., Fukuda, T., Jessberger, R., et al. (2013). Dynamic localization of SMC5/6 complex proteins during mammalian meiosis and mitosis suggests functions in distinct chromosome processes. *J. Cell Sci*. 126, 4239–4252. doi: 10.1242/jcs.130195

Hamer, G., Wang, H., Bolcun-Filas, E., Cooke, H. J., Benavente, R., and Hoog, C. (2008). Progression of meiotic recombination requires structural maturation of the central element of the synaptonemal complex. *J. Cell Sci*. 121, 2445–2451. doi: 10.1242/jcs.033233

Hernandez-Hernandez, A., Masich, S., Fukuda, T., Kouznetsova, A., Sandin, S., Daneholt, B., et al. (2016). The central element of the synaptonemal complex in mice is organized as a bilayered junction structure. *J. Cell Sci*. 129, 2239–2249. doi: 10.1242/jcs.182477

Higgins, J. D., Sanchez-Moran, E., Armstrong, S. J., Jones, G. H., and Franklin, F. C. (2005). The *Arabidopsis* synaptonemal complex protein ZYP1 is required for chromosome synapsis and normal fidelity of crossing over. *Genes Dev*. 19, 2488–2500. doi: 10.1101/gad.354705

Hobolth, P. (1981). Chromosome pairing in allohexaploid wheat var. *Chinese Spring. Transformation of multivalents into bivalents, a mechanism for exclusive bivalent formation. Carlsberg Res. Commun*. 46, 129–173. doi: 10.1007/bf02910465

Hollingsworth, N. M., and Ponte, L. (1997). Genetic interactions between HOP1, RED1 and MEK1 suggest that MEK1 regulates assembly of axial element components during meiosis in the yeast *Saccharomyces cerevisiae*. *Genetics* 147, 33–42.

Holm, P. B. (1977). Three-dimensional reconstruction of chromosome pairing during the zygotene stage of meiosis in *Lilium longiflorum* (Thunb.). *Carlsberg Res. Commun*. 42, 103–151. doi: 10.1007/bf02906489

Houben, A., Banaei-Moghaddam, A. M., Klemme, S., and Timmis, J. N. (2014). Evolution and biology of supernumerary B chromosomes. *Cell Mol. Life Sci*. 71, 467–478. doi: 10.1007/s00018-013-1437-7

Humphryes, N., Leung, W. K., Argunhan, B., Terentyev, Y., Dvorackova, M., and Tsubouchi, H. (2013). The Ecm11-Gmc2 complex promotes synaptonemal complex formation through assembly of transverse filaments in budding yeast. *PLoS Genet*. 9:e1003194. doi: 10.1371/journal.pgen.1003194

Iwano, M., Che, F. S., Takayama, S., Fukui, K., and Isogai, A. (2003). Three-dimensional architecture of ribosomal DNA within barley nucleoli revealed with electron microscopy. *Scanning* 25, 257–263. doi: 10.1002/sca.4950250507

Jenkins, G. (1985). Synaptonemal complex formation in hybrids of *Lolium temulentum* × *Lolium perenne* (L.). *Chromosoma* 92, 81–88. doi: 10.1007/bf00328459

Jiménez, G., Manzanero, S., and Puertas, M. J. (2000). Relationship between pachytene synapsis, metaphase I associations, and transmission of 2B and 4B chromosomes in rye. *Genome* 43, 232–239. doi: 10.1139/g99-110

Jiménez, M., Diez, M., and Santos, J. L. (1994). Synaptic patterns of rye B chromosomes. III. The deficient B. *Chromosome Res.* 2, 93–98. doi: 10.1007/BF01553488

Jones, G. H. (1967). Control of chiasma distribution in rye. Chromosoma 22, 69-90. doi: 10.1007/Bf00291287

Jones, G. H., Albini, S. M., and Whitewhorn, J. F. (1991). Ultrastructure of meiotic pairing in B chromosomes of *Crepis capillaris*. *Chromosoma* 100, 193–202. doi: 10.1007/BF00337248

Jones, R. N., and Rees, H. (1982). B Chromosomes. 1st Edn. New York, NY: Academic Press.

Klemme, S., Banaei-Moghaddam, A. M., Macas, J., Wicker, T., Novak, P., and Houben, A. (2013). High-copy sequences reveal distinct evolution of the rye B chromosome. *New Phytol*. 199, 550–558. doi: 10.1111/nph.12289

Kolomiets, O. L., Borbiev, T. E., Safronova, L. D., Borisov, Y. M., and Bogdanov, Y. F. (1988). Synaptonemal complex analysis of B-chromosome behavior in meiotic prophase I in the East-Asiatic mouse (*Apodemus peninsulae*) (*Muridae, Rodentia*). *Cytogenet. Genome Res*. 48, 183–187. doi: 10.1159/000132621

Kurdzo, E. L., and Dawson, D. S. (2015). Centromere pairing—tethering partner chromosomes in meiosis I. *FEBS J*. 282, 2445–2457. doi: 10.1111/febs.13280

Lam, W. S., Yang, X., and Makaroff, C. A. (2005). Characterization of *Arabidopsis thaliana* SMC1 and SMC3: evidence that AtSMC3 may function beyond chromosome cohesion. *J. Cell Sci*. 118, 3037–3048. doi: 10.1242/jcs.02443

Lee, D. H., Kao, Y. H., Ku, J. C., Lin, C. Y., Meeley, R., Jan, Y. S., et al. (2015). The axial element protein DESYNAPTIC2 mediates meiotic double-strand break formation and synaptonemal complex assembly in maize. *Plant Cell* 27, 2516–2529. doi: 10.1105/tpc.15.00434

Lehmann, A. R., Walicka, M., Griffiths, D. J., Murray, J. M., Watts, F. Z., McCready, S., et al. (1995). The rad18 gene of *Schizosaccharomyces pombe* defines a new subgroup of the SMC superfamily involved in DNA repair. *Mol. Cell Biol*. 15, 7067–7080. doi: 10.1128/MCB.15.12.7067

Lilienthal, I., Kanno, T., and Sjogren, C. (2013). Inhibition of the Smc5/6 complex during meiosis perturbs joint molecule formation and resolution without significantly changing crossover or non-crossover levels. *PLoS Genet*. 9:e1003898. doi: 10.1371/journal.pgen.1003898

Ma, W., Schubert, V., Martis, M. M., Hause, G., Liu, Z., Shen, Y., et al. (2016). The distribution of alpha-kleisin during meiosis in the holocentromeric plant *Luzula elegans*. *Chromosome Res*. 24, 393–405. doi: 10.1007/s10577-016-9529-5

Martis, M. M., Klemme, S., Banaei-Moghaddam, A. M., Blattner, F. R., Macas, J., Schmutzer, T., et al. (2012). Selfish supernumerary chromosome reveals its origin as a mosaic of host genome and organellar sequences. *Proc. Natl. Acad. Sci. U.S.A*. 109, 13343–13346. doi: 10.1073/pnas.1204237109

Meuwissen, R. L., Offenberg, H. H., Dietrich, A. J., Riesewijk, A., van Iersel, M., and Heyting, C. (1992). A coiled-coil related protein specific for synapsed regions of meiotic prophase chromosomes. *EMBO J*. 11, 5091–5100.

Mikhailova, E. I., Phillips, D., Sosnikhina, S. P., Lovtsyus, A. V., Jones, R. N., and Jenkins, G. (2006). Molecular assembly of meiotic proteins Asy1 and Zyp1 and pairing promiscuity in rye (*Secale cereale* L.) and its synaptic mutant sy10. *Genetics* 174, 1247–1258. doi: 10.1534/genetics.106.064105

Moses, M. J. (1956). Chromosomal structures in crayfish spermatocytes. *J. Biophys. Biochem. Cytol*. 2, 215–218. doi: 10.1083/jcb.2.2.215

Moses, M. J. (1968). Synaptonemal complex. *Annu. Rev. Genet*. 2, 363–412. doi: 10.1146/annurev.ge.02.120168.002051

Naranjo, T., and Lacadena, J. R. (1980). Interaction between wheat chromosomes and rye telomeric heterochromatin on meiotic pairing of chromosome pair 1R of rye in wheat-rye derivatives. *Chromosoma* 81, 249–261. doi: 10.1007/BF00285951

Nonomura, K., Nakano, M., Eiguchi, M., Suzuki, T., and Kurata, N. (2006). PAIR2 is essential for homologous chromosome synapsis in rice meiosis I. *J. Cell Sci*. 119, 217–225. doi: 10.1242/jcs.02736

Olson, L. W., Eden, U., Egelmitani, M., and Egel, R. (1978). Asynaptic meiosis in fission yeast. *Hereditas* 89, 189–199. doi: 10.1111/j.1601-5223.1978.tb01275.x

Osman, K., Higgins, J. D., Sanchez-Moran, E., Armstrong, S. J., and Franklin, F. C. (2011). Pathways to meiotic recombination in *Arabidopsis thaliana*. *New Phytol*. 190, 523–544. doi: 10.1111/j.1469-8137.2011.03665.x

Page, S. L., and Hawley, R. S. (2001). c(3)G encodes a *Drosophila* synaptonemal complex protein. *Genes Dev*. 15, 3130–3143. doi: 10.1101/gad.935001

Page, S. L., and Hawley, R. S. (2004). The genetics and molecular biology of the synaptonemal complex. *Ann. Rev. Cell Dev. Biol*. 20, 525–558. doi: 10.1146/annurev.cellbio.19.111301.155141

Page, S. L., Khetani, R. S., Lake, C. M., Nielsen, R. J., Jeffress, J. K., Warren, W. D., et al. (2008). Corona is required for higher-order assembly of transverse filaments into full-length synaptonemal complex in *Drosophila* oocytes. *PLoS Genet*. 4:e1000194. doi: 10.1371/journal.pgen.1000194

Palecek, J., Vidot, S., Feng, M., Doherty, A. J., and Lehmann, A. R. (2006). The Smc5-Smc6 DNA repair complex. bridging of the Smc5-Smc6 heads by the

KLEISIN, Nse4, and non-Kleisin subunits. J. Biol. Chem. 281, 36952-36959. doi: 10.1074/jbc.M608004200

Pebernard, S., McDonald, W. H., Pavlova, Y., Yates, J. R. III., and Boddy, M. N. (2004). Nse1, Nse2, and a novel subunit of the Smc5-Smc6 complex, Nse3, play a crucial role in meiosis. *Mol. Biol. Cell* 15, 4866–4876. doi: 10.1091/mbc.E04-05-0436

Phillips, D., Mikhailova, E. I., Timofejeva, L., Mitchell, J. L., Osina, O., Sosnikhina, S. P., et al. (2008). Dissecting meiosis of rye using translational proteomics. *Ann. Bot*. 101, 873–880. doi: 10.1093/aob/mcm202

Phillips, D., Nibau, C., Ramsay, L., Waugh, R., and Jenkins, G. (2010). Development of a molecular cytogenetic recombination assay for barley. *Cytogenet. Genome Res*. 129, 154–161. doi: 10.1159/000314335

Phillips, D., Nibau, C., Wnetrzak, J., and Jenkins, G. (2012). High resolution analysis of meiotic chromosome structure and behaviour in barley (*Hordeum vulgare* L.). *PLoS ONE* 7:e39539. doi: 10.1371/journal.pone.0039539

Qiao, H., Lohmiller, L. D., and Anderson, L. K. (2011). Cohesin proteins load sequentially during prophase I in tomato primary microsporocytes. *Chromosome Res*. 19, 193–207. doi: 10.1007/s10577-010-9184-1

Qiao, H., Prasada Rao, H. B., Yang, Y., Fong, J. H., Cloutier, J. M., Deacon, D. C., et al. (2014). Antagonistic roles of ubiquitin ligase HEI10 and SUMO ligase RNF212 regulate meiotic recombination. *Nat. Genet*. 46, 194–199. doi: 10.1038/ng.2858

Qiao, H. Y., Chen, J. K., Reynolds, A., Hoog, C., Paddy, M., and Hunter, N. (2012). Interplay between synaptonemal complex, homologous recombination, and centromeres during mammalian meiosis. *PLoS Genet*. 8:e1002790. doi: 10.1371/journal.pgen.1002790

Rao, H. B., Qiao, H., Bhatt, S. K., Bailey, L. R., Tran, H. D., Bourne, S. L., et al. (2017). A SUMO-ubiquitin relay recruits proteasomes to chromosome axes to regulate meiotic recombination. *Science* 355, 403–407. doi: 10.1126/science.aaf6407

Reynolds, A., Qiao, H., Yang, Y., Chen, J. K., Jackson, N., Biswas, K., et al. (2013). RNF212 is a dosage-sensitive regulator of crossing-over during mammalian meiosis. *Nat. Genet*. 45, 269–278. doi: 10.1038/ng.2541

Romera, F., Vega, J. M., Diez, M., and Puertas, M. J. (1989). B chromosome polymorphism in Korean rye populations. *Heredity* 62:117. doi: 10.1038/hdy.1989.16

Sanchez-Moran, E., Osman, K., Higgins, J. D., Pradillo, M., Cunado, N., Jones, G. H., et al. (2008). ASY1 coordinates early events in the plant meiotic recombination pathway. *Cytogenet. Genome. Res*. 120, 302–312. doi: 10.1159/000121079

Sandery, M. J., Forster, J. W., Blunden, R., and Jones, R. N. (1990). Identification of a family of repeated sequences on the rye B-chromosome. *Genome* 33, 908–913. doi: 10.1139/g90-137

Sanei, M., Pickering, R., Kumke, K., Nasuda, S., and Houben, A. (2011). Loss of centromeric histone H3 (CENH3) from centromeres precedes uniparental chromosome elimination in interspecific barley hybrids. *Proc. Nat. Acad. Sci. U.S.A*. 108, 498–505. doi: 10.1073/pnas.1103190108

Santos, J. L., Jiménez, M. M., and Diez, M. (1993). Synaptic patterns of rye B chromosomes. I: The standard type. *Chromosome Res*. 1, 145–152. doi: 10.1007/BF00710768

Santos, J. L., Jiménez, M. M., and Diez, M. (1995). Synaptic patterns of rye B chromosomes. IV. The B isochromosomes. *Heredity* 74 (Pt 1), 100–107. doi: 10.1038/hdy.1995.12

Scherthan, H., Eils, R., Trelles-Sticken, E., Dietzel, S., Cremer, T., Walt, H., et al. (1998). Aspects of three-dimensional chromosome reorganization during the onset of human male meiotic prophase. *J. Cell Sci.* 111 (Pt 16), 2337–2351.

Schramm, S., Fraune, J., Naumann, R., Hernandez-Hernandez, A., Hoog, C., Cooke, H. J., et al. (2011). A novel mouse synaptonemal complex protein is essential for loading of central element proteins, recombination, and fertility. *PLoS Genet*. 7:e1002088. doi: 10.1371/journal.pgen.1002088

Schubert, V. (2009). SMC proteins and their multiple functions in higher plants. *Cytogenet. Genome Res*. 124, 202–214. doi: 10.1159/000218126

Shao, T., Tang, D., Wang, K., Wang, M., Che, L., Qin, B., et al. (2011). OsREC8 is essential for chromatid cohesion and metaphase I monopolar orientation in rice meiosis. *Plant Physiol*. 156, 1386–1396. doi: 10.1104/pp.111.177428

Shi, L., Tang, L., Ma, K., and Ma, C. (1988). Synaptonemal complex formation among supernumerary B chromosomes: an electron microscopic study on spermatocytes of Chinese raccoon dogs. *Chromosoma* 97, 178–183. doi: 10.1007/bf00327376

Simanovsky, S. A., Matveevsky, S. N., Iordanskaya, I. V., Spangenberg, V. E., Kolomiets, O. L., and Bogdanov, Y. F. (2014). Spiral cores of synaptonemal complex lateral elements at the diplotene stage in rye include the ASY1 protein. *Russ. J. Genet*. 50, 1250–1253. doi: 10.1134/s1022795414100111

Smith, A. V., and Roeder, G. S. (1997). The yeast Red1 protein localizes to the cores of meiotic chromosomes. *J. Cell Biol*. 136, 957–967. doi: 10.1083/jcb.136.5.957

Storlazzi, A., Gargano, S., Ruprich-Robert, G., Falque, M., David, M., Kleckner, N., et al. (2010). Recombination proteins mediate meiotic spatial chromosome organization and pairing. *Cell* 141, 94–106. doi: 10.1016/j.cell.2010.02.041

Switonski, M., Gustavsson, I., Höjer, K., and Plöen, L. (1987). Synaptonemal complex analysis of the B-chromosomes in spermatocytes of the silver fox (*Vulpes fulvus* Desm.). *Cytogenet. Cell Genet*. 45, 84–92. doi: 10.1159/000132435

Sym, M., Engebrecht, J. A., and Roeder, G. S. (1993). ZIP1 is a synaptonemal complex protein required for meiotic chromosome synapsis. *Cell* 72, 365–378. doi: 10.1016/0092-8674(93)90114-6

Taylor, E. M., Copsey, A. C., Hudson, J. J., Vidot, S., and Lehmann, A. R. (2008). Identification of the proteins, including MAGEG1, that make up the human SMC5-6 protein complex. *Mol. Cell Biol*. 28, 1197–1206. doi: 10.1128/MCB.00767-07

Toby, G. G., Gherraby, W., Coleman, T. R., and Golemis, E. A. (2003). A novel RING finger protein, human enhancer of invasion 10, alters mitotic progression through regulation of cyclin B levels. *Mol. Cell Biol*. 23, 2109–2122. doi: 10.1128/MCB.23.6.2109-2122.2003

Verver, D. E., Hwang, G. H., Jordan, P. W., and Hamer, G. (2016). Resolving complex chromosome structures during meiosis: versatile deployment of Smc5/6. *Chromosoma* 125, 15–27. doi: 10.1007/s00412-015-0518-9

Verver, D. E., Langedijk, N. S., Jordan, P. W., Repping, S., and Hamer, G. (2014). The SMC5/6 complex is involved in crucial processes during human spermatogenesis. *Biol. Reprod*. 91:22. doi: 10.1095/biolreprod.114.118596

Wang, K., Wang, M., Tang, D., Shen, Y., Miao, C., Hu, Q., et al. (2012). The role of rice HEI10 in the formation of meiotic crossovers. *PLoS Genet*. 8:e1002809. doi: 10.1371/journal.pgen.1002809

Wang, K., Wang, M., Tang, D., Shen, Y., Qin, B., Li, M., et al. (2011). PAIR3, an axis-associated protein, is essential for the recruitment of recombination elements onto meiotic chromosomes in rice. *Mol. Biol. Cell* 22, 12–19. doi: 10.1091/mbc.E10-08-0667

Wang, N., and Dawe, R. K. (2018). Centromere size and its relationship to haploid formation in plants. *Mol. Plant* 11, 398–406. doi: 10.1016/j.molp.2017.12.009

Wanner, G., and Formanek, H. (2000). A new chromosome model. *J. Struct. Biol*. 132, 147–161. doi: 10.1006/jsbi.2000.4310

Wanner, G., Formanek, H., Martin, R., and Herrmann, R. G. (1991). High resolution scanning electron microscopy of plant chromosomes. *Chromosoma* 100, 103–109. doi: 10.1007/bf00418243

Wanner, G., and Schroeder-Reiter, E. (2008). Scanning electron microscopy of chromosomes. *Methods Cell Biol*. 88, 451–474. doi: 10.1016/S0091-679X(08)00423-8

Wanner, G., Schroeder-Reiter, E., and Formanek, H. (2005). 3D analysis of chromosome architecture: advantages and limitations with SEM. *Cytogenet. Genome Res*. 109, 70–78. doi: 10.1159/000082384

Ward, J. O., Reinholdt, L. G., Motley, W. W., Niswander, L. M., Deacon, D. C., Griffin, L. B., et al. (2007). Mutation in mouse hei10, an e3 ubiquitin ligase, disrupts meiotic crossing over. *PLoS Genet*. 3:e139. doi: 10.1371/journal.pgen.0030139

Watanabe, K., Pacher, M., Dukowic, S., Schubert, V., Puchta, H., and Schubert, I. (2009). The structural maintenance of chromosomes 5/6 complex promotes sister chromatid alignment and homologous recombination after DNA damage in *Arabidopsis thaliana*. *Plant Cell* 21, 2688–2699. doi: 10.1105/tpc.108.060525

Wehrkamp-Richter, S., Hyppa, R. W., Prudden, J., Smith, G. R., and Boddy, M. N. (2012). Meiotic DNA joint molecule resolution depends on Nse5-Nse6 of the Smc5-Smc6 holocomplex. *Nucleic Acids Res*. 40, 9633–9646. doi: 10.1093/nar/gks713

Weisshart, K., Fuchs, J., and Schubert, V. (2016). Structured illumination microscopy (SIM) and photoactivated localization microscopy (PALM) to analyze the abundance and distribution of RNA polymerase II molecules in flow-sorted *Arabidopsis* nuclei. *Bio-protocol* 6:e1725. doi: 10.21769/bioprotoc.1725

Westergaard, M., and von Wettstein, D. (1972). The synaptonemal complex. *Annu. Rev. Genet*. 6, 71–110. doi: 10.1146/annurev.ge.06.120172.000443

Whitby, M. C. (2005). Making crossovers during meiosis. *Biochem. Soc. Trans*. 33, 1451–1455. doi: 10.1042/BST20051451

Xaver, M., Huang, L., Chen, D., and Klein, F. (2013). Smc5/6-Mms21 prevents and eliminates inappropriate recombination intermediates in meiosis. *PLoS Genet*. 9:e1004067. doi: 10.1371/journal.pgen.1004067

Zelkowski, M., Zelkowska, K., Pradillo, M., Santos, J. L., Marzec, M., Meister, A., et al. (2019). *Arabidopsis* NSE4 proteins act in somatic nuclei and meiosis to ensure plant viability and fertility. *Front. Plant Sci.* doi: 10.3389/fpls.2019.00774. [Epub ahead of print].

Zhang, L., Tao, J., Wang, S., Chong, K., and Wang, T. (2006). The rice OsRad21-4, an orthologue of yeast Rec8 protein, is required for efficient meiosis. *Plant Mol. Biol*. 60, 533–554. doi: 10.1007/s11103-005-4922-z

Zhong, X., Fransz, P. F., Wennekes van Eden, J., Zabel, P., van Kammen, A., and de Jong, J. H. (1996). High-resolution mapping on pachytene chromosomes and extended DNA fibres by fluorescent in situ hybridisation. *Plant Mol. Biol. Rep*. 14, 232–242. doi: 10.1007/bf02671658

Zickler, D., and Kleckner, N. (1999). Meiotic chromosomes: integrating structure and function. *Annu. Rev. Genet*. 33, 603–754. doi: 10.1146/annurev.genet.33.1.603

Zickler, D., and Kleckner, N. (2015). Recombination, pairing, and synapsis of homologs during meiosis. *Cold Spring Harb. Perspect. Biol*. 7:a016626. doi: 10.1101/cshperspect.a016626

Ziolkowski, P. A., Underwood, C. J., Lambing, C., Martinez-Garcia, M., Lawrence, E. J., Ziolkowska, L., et al. (2017). Natural variation and dosage of the HEI10 meiotic E3 ligase control *Arabidopsis* crossover recombination. *Genes Dev*. 31, 306–317. doi: 10.1101/gad.295501.116

Zoller, J. F., Herrmann, R. G., and Wanner, G. (2004a). Chromosome condensation in mitosis and meiosis of rye (*Secale cereale* L.). *Cytogenet. Genome Res*. 105, 134–144. doi: 10.1159/000078020

Zoller, J. F., Hohmann, U., Herrmann, R. G., and Wanner, G. (2004b). Ultrastructural analysis of chromatin in meiosis I + II of rye (*Secale cereale* L.). *Cytogenet. Genome Res*. 105, 145–156. doi: 10.1159/000078021

Conflict of Interest Statement: The authors declare that the research was conducted in the absence of any commercial or financial relationships that could be construed as a potential conflict of interest.

frontiers in Plant Science

REVIEW
published: 29 October 2018
doi: 10.3389/fpls.2018.01560

A Critical Assessment of 60 Years of Maize Intragenic Recombination

Ron J. Okagaki[1†], Stefanie Dukowic-Schulze[2†], William B. Eggleston[3] and Gary J. Muehlbauer[1,4]*

[1] Department of Agronomy and Plant Genetics, University of Minnesota, St. Paul, MN, United States, [2] Department of Horticultural Science, University of Minnesota, St. Paul, MN, United States, [3] Department of Biology, Virginia Commonwealth University, St. Paul, MN, United States, [4] Department of Plant and Microbial Biology, University of Minnesota, St. Paul, MN, United States

Until the mid-1950s, it was believed that genetic crossovers did not occur within genes. Crossovers occurred between genes, the "beads on a string" model. Then in 1956, Seymour Benzer published his classic paper describing crossing over within a gene, intragenic recombination. This result from a bacteriophage gene prompted Oliver Nelson to study intragenic recombination in the maize *Waxy* locus. His studies along with subsequent work by others working with maize and other organisms described the outcomes of intragenic recombination and provided some of the earliest evidence that genes, not intergenic regions, were recombination hotspots. High-throughput genotyping approaches have since replaced single gene intragenic studies for characterizing the outcomes of recombination. These large-scale studies confirm that genes, or more generally genic regions, are the most active recombinogenic regions, and suggested a pattern of crossovers similar to the budding yeast *Saccharomyces cerevisiae*. In *S. cerevisiae* recombination is initiated by double-strand breaks (DSBs) near transcription start sites (TSSs) of genes producing a polarity gradient where crossovers preferentially resolve at the 5′ end of genes. Intragenic studies in maize yielded less evidence for either polarity or for DSBs near TSSs initiating recombination and in certain respects resembled *Schizosaccharomyces pombe* or mouse. These different perspectives highlight the need to draw upon the strengths of different approaches and caution against relying on a single model system or approach for understanding recombination.

Keywords: recombination, hotspots, intragenic, polarity, double-strand breaks, maize

OPEN ACCESS

Edited by:
Mónica Pradillo, Complutense University of Madrid, Spain

Reviewed by:
Kyuha Choi, Pohang University of Science and Technology, South Korea
Piotr Andrzej Ziolkowski, Adam Mickiewicz University in Poznań, Poland

***Correspondence:**
Gary J. Muehlbauer
muehl003@umn.edu

† These authors have contributed equally to this work

Specialty section:
This article was submitted to Plant Cell Biology, a section of the journal Frontiers in Plant Science

Received: *25 July 2018*
Accepted: *04 October 2018*
Published: *29 October 2018*

Citation:
Okagaki RJ, Dukowic-Schulze S, Eggleston WB and Muehlbauer GJ (2018) A Critical Assessment of 60 Years of Maize Intragenic Recombination. Front. Plant Sci. 9:1560. doi: 10.3389/fpls.2018.01560

INTRODUCTION

Recombination is the exchange of genetic information between chromosomes. Meiotic recombination is a major contributor to genetic diversity and facilitates selection by nature and breeders. A large share of our current understanding of recombination is based on work studying intragenic recombination (recombination within genes) in model fungal species, especially the budding yeast (*Saccharomyces cerevisiae*). Conclusions from genetic fungal studies have been supported by recent molecular and genomic approaches, providing a relatively detailed, although still incomplete, picture of recombination (reviewed in Keeney et al., 2014; Gray and Cohen, 2016). Beginning in the early 2000s, studies in the plant model system *Arabidopsis thaliana* have supported

a similar picture of recombination (Wang and Copenhaver, 2018). Maize has been a genetic model organism since the early 1900s, and there is an extensive history of intragenic recombination studies in maize. Maize studies identified genes as recombination hotspots with crossovers distributed approximately evenly across many genes, which conflicts with the discrete hotspots and polarity found in *S. cerevisiae*. Our purpose here is to review the maize intragenic recombination work, and place this work in context with results from genomic studies of maize recombination and work in fungal and animal model systems.

To fully comprehend what intragenic as well as large-scale genomics studies can tell us about recombination, we recapitulate and reconcile knowledge from historic and more recent studies. **Figure 1** depicts the approaches for gene-scale and genomic-scale to illustrate their data origins and differences. To facilitate a smooth and easy understanding of the information in this review, we first clarify the following terms which are frequently used:

- **"Recombination"** is a term used for mechanisms of somatic DNA repair as well as for exchange of genetic information during meiosis. While underlying mechanisms and involved proteins overlap, there are profound differences between somatic and meiotic recombination. Meiotic recombination can refer to **crossovers (COs)** which are due to exchange of whole chromosome parts, to **non-crossovers (NCOs)** which are locally restricted, or to both. Both COs and NCOs can result in local genetic changes via gene conversion.
- **"Gene conversion" (GC)** is the non-reciprocal transfer of information. Resolution of double Holliday structures into COs produces a gene conversion tract, as do pathways leading to NCOs. The latter is often used interchangeably with GC although it does not cover all GC instances.
- **"Intragenic recombination"** refers to both NCOs and COs within genes. Some intragenic recombination studies look at short regions containing several genes, albeit mostly with emphasis on the outcome within genes. These loci or genes are often recombination hotspots.
- **"Hotspots"** are genomic regions with elevated levels of recombination-related events, and can refer to the meiotic **double-strand breaks (DSBs)** initiating recombination, **COs** or **general recombination** including both COs and NCOs. There is no standard definition of hotspots regarding their strength or size. The amount of events distinguishing hotspots from cold regions is arbitrary, and the definition and identification depends strongly on the respective study.
- **"Polarity"** exists when there is a gradient of recombination, e.g., higher recombination rates at the 5′ or 3′ end of a gene. The 5′ end is defined here as the transcription start site (TSS), and the 3′ end as the transcription termination site (TTS). Other definitions have been used such as the promoter region for the 5′ end. However, in practice, COs are localized to intervals defined by available sequence polymorphisms which may not coincide with the defined 5′ and 3′ ends.

We have two goals for this review. First, we hope to show how the study of individual genes may influence our interpretation of genomic studies of recombination. Second, we describe characteristics in several model systems to illustrate the variation present in nature, and to argue that recombination in maize shares some, but not all, properties of each of these systems.

A HISTORY OF MAIZE INTRAGENIC RECOMBINATION

The classical conception of genes posited that genes were indivisible units and recombination occurs between genes (reviewed in Green, 1955; Portin, 1993). Recombination within genes, intragenic recombination, was not believed to exist, especially since several apparent exceptions turned out to be recombination between duplicated gene copies in a complex locus. An alternative position was supported by several prominent geneticists who viewed genes as having multiple sites where crossing over could occur (Pontecorvo, 1955). Arthur Chovnick's Perspectives article in Genetics provides a historical overview (Chovnick, 1989).

Today, Seymour Benzer's papers demonstrating intragenic recombination in bacteriophage are often seen as the experimental work changing our understanding of recombination and genes (Benzer, 1955). At that time however, it was not clear. Several explanations for the contrasting results from bacteriophage versus *Drosophila melanogaster* and other familiar genetic systems were proposed (Green, 1955). One possibility was that recombination was different in bacteriophage and eukaryotes. Alternatively, detecting intragenic recombination might require screening very large populations.

Nelson (1957) proposed testing intragenic recombination at the maize *Waxy* (*Wx*) locus. *Wx* encodes a starch synthase required for amylose in the kernel endosperm and pollen. A recombination event between two mutant alleles would create a non-mutant *Wx* allele giving a revertant *Wx* pollen grain. Non-mutant *Wx* pollen contains a mixture of amylose and amylopectin starches and is stained a dark black by potassium iodine, while mutant *wx* pollen contains only amylose and stains reddish. This pollen phenotype is readily scored under a microscope and allows screening of very large numbers of meiotic products. Using this pollen assay, Nelson was able to detect intragenic recombination in a higher eukaryote (Nelson, 1959). A second study incorporated genetic markers flanking the *Wx* locus to connect recombination within the *Wx* locus with the exchange of flanking markers (Nelson, 1962).

After the initial observation of intragenic recombination in maize, the *Wx* locus was used for further studies focusing on exploring the recombination process. Nelson's studies provided early evidence for a non-crossover recombination pathway, by using lines where the *wx-C* allele was located inside a chromosome inversion or a complex chromosomal rearrangement (Nelson, 1975). Single-crossovers between these *wx-C* alleles on a rearranged chromosome and the *wx-90* allele on a normal chromosome produce inviable gametes unless there was a second crossover within the inversion (**Figure 2**).

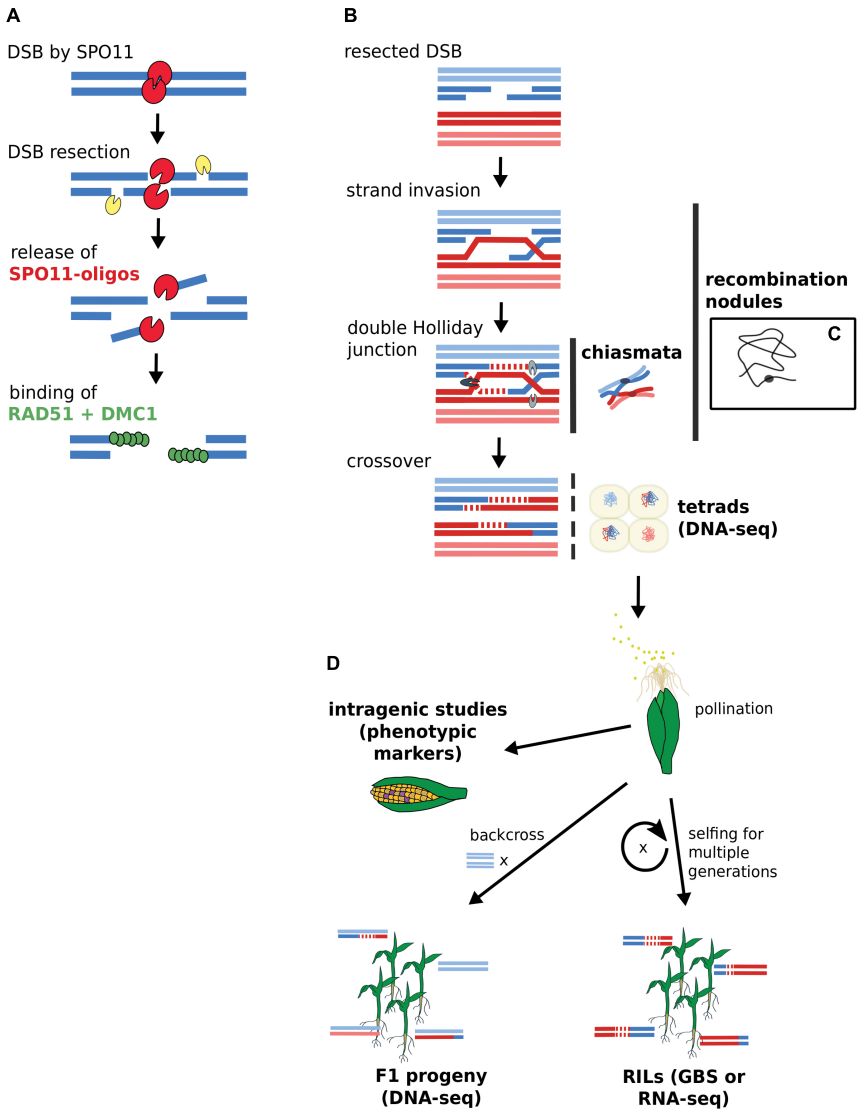

FIGURE 1 | Acquisition of DSB and CO data by gene-scale and genome-scale approaches. **(A)** DSB generation by SPO11 with subsequent binding of RAD51 and DMC1. DSB data derives from SPO11-oligos or RAD51-bound fragments via ChIP-seq. **(B)** CO generation via double Holliday junction. **(C)** Chiasmata and recombination nodules are visible via microscopy. A single recombination nodule on a chromosome is illustrated. **(D)** Mapping recombinants. Sequencing approaches rely on isolated microspores from tetrads or progeny lines. Intragenic studies directly score recombination via visible kernel markers. Terms in bold indicate data source options. RILs, recombinant inbred lines; GBS, genotyping by sequencing.

When both *wx-C* and *wx-90* were on normal chromosomes crossover events accounted for approximately 65% of the *Wx* revertants based on the segregation of flanking markers. There was crossing over between the flanking markers in 35% of the *Wx* revertants when *wx-C* was located within a pericentric inversion. A portion of these crossovers occurred outside of the inversion and accompanied a NCO event between the *wx* alleles. When *wx-C* was within a complex rearrangement the few revertants arose through non-crossover events.

The *Wx* pollen system was also used to explore whether the distance of a locus from the centromere altered recombination frequency (Yu and Peterson, 1973). Using chromosome translocation lines with *wx* alleles at different distances from the centromere they showed that distance of a locus from the centromere is correlated with recombination frequency. Other studies by Peterson examined the effects of chemical treatments on recombination and noted the effect of environment on recombination at the *Wx* locus (Sukhapinda and Peterson, 1980).

Pollen phenotyping procedures were developed for other genes to study intragenic recombination. Mike Freeling described an odd situation where *alcohol dehydrogenase1* (*adh1*) alleles derived from the same progenitor allele showed intragenic recombination, but *adh1* alleles derived from different progenitor alleles did not recombine (Freeling, 1978). One possibility suggested at the time was that local structural differences between progenitor alleles inhibited synapsis and recombination. This

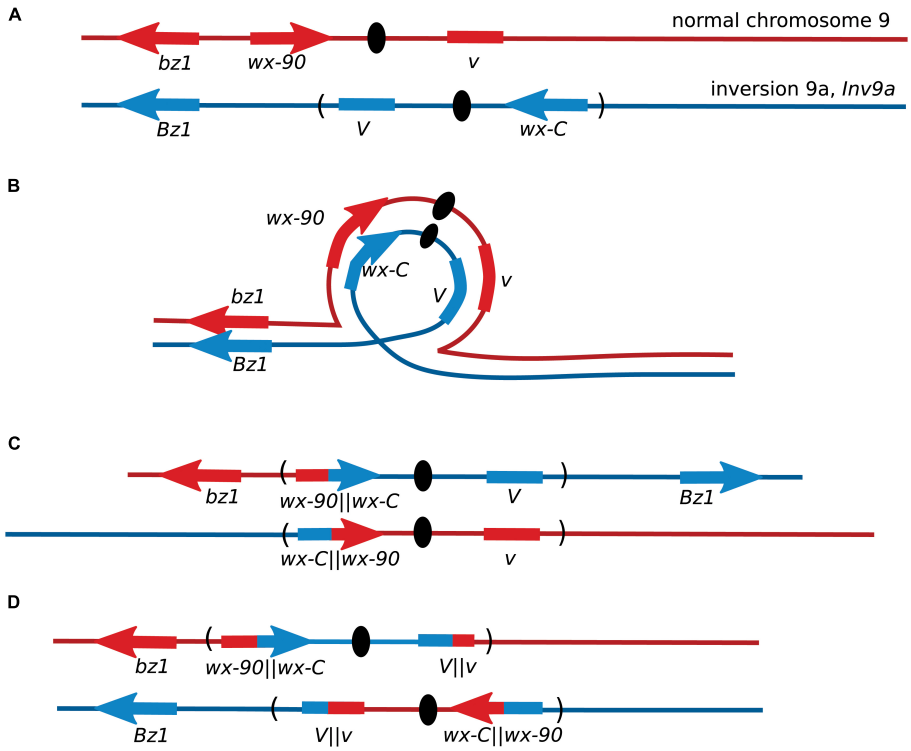

FIGURE 2 | Recovery of maize *Wx* recombinants from an inversion heterozygote. **(A)** Locations of the *Wx* locus and the flanking markers *Bronze1* (*Bz1*) and *Virescent* (*V*) on the normal chromosome 9, and their locations on the pericentric inversion chromosome 9. The orientation of *V* is not known. **(B)** Chromosome pairing during meiosis. **(C)** Gametes from meiosis with crossovers within a pericentric inversion are generally inviable because one centromere carries with it both short arms and the other centromere carries both long arms. Non-crossover events may produce non-mutant *Wx* kernels. **(D)** Crossovers between *wx-C* and *wx-90* will produce inviable pollen unless there is a second crossover within the inversion. Most *Wx* revertant pollen will be from non-crossover events as double crossovers are rare in short genetic intervals. This illustration shows the second crossover occurring within *V*.

conjecture was supported by subsequent molecular findings of little similarity between regions flanking most, but not all, parental *Adh1* alleles (Johns et al., 1983; Sachs et al., 1986). In general, maize intragenic studies focused on genes with an easily scored phenotype, and most genes studied proved to be hotspots. A partial list of key results from intragenic studies is presented in **Table 1**.

With the cloning and sequencing of maize genes, it became possible to compare the frequency of recombination within genes to the genome average. Hugo Dooner, studying the *Bronze1* (*Bz1*) gene estimated that the ratio of genetic to physical distance within *Bz1* was 100-fold higher than the genome average (Dooner, 1986). This result was consistent with the conjecture that recombination is restricted to genes (Thuriaux, 1977), and stands in complete contrast to the initial view of recombination occurring only between genes.

CROSSING OVER AND POLARITY

Lessons From *S. cerevisiae* and *A. thaliana*

The foundation for our understanding of recombination is built upon intragenic recombination studies in fungal systems, particularly the budding yeast, *S. cerevisiae* (Nicolas and Petes, 1994; Gray and Cohen, 2016). These studies established a picture of recombination initiating at DSB hotspots which were usually found near TSSs (Petes, 2001). Later, this model was confirmed by genomic studies on the genome wide distribution of DSBs and meiotic recombination (**Figure 1**). DSB break maps, produced by capturing and sequencing SPO11-bound oligonucleotides released during initial DSB resection, confirmed that DSBs occur mainly near TSSs in *S. cerevisiae* (Pan et al., 2011). High resolution mapping of COs and NCOs placed 84% of recombination hotpots overlapping promoters near TSSs (Mancera et al., 2008). The agreement of genome-wide DSB maps and high-resolution recombination maps provides a clear picture of the general recombination pattern in *S. cerevisiae* (**Table 2**).

In Arabidopsis, DSB hotspots also localize to gene promoters, additionally to terminators, as well as introns (Choi et al., 2018). Though only a fraction of DSBs is resolved into COs in Arabidopsis, DSB and CO levels were shown to correlate strongly at the chromosome scale, though varying along arms (Choi et al., 2018) (**Table 2**).

The recombination machinery has been extensively described and reviewed in general as well as in plants (Pradillo et al., 2014; Lambing et al., 2017). Briefly, recombination initiates with a DSB. Resection creates a 3′-overhang that invades a homologous

TABLE 1 | Landmark maize intragenic recombination studies.

Authors	Locus	Notable results
Stadler and Emmerling, 1956	*R1*	Recombination between genes in a complex locus
Nelson, 1959	*Wx*	Demonstration of intragenic recombination in a higher eukaryote
Nelson, 1968	*Wx*	Mapping transposable elements within a gene
Yu and Peterson, 1973	*Wx*	Physical distance from centromere affects recombination rates
Nelson, 1975	*Wx*	Evidence for crossover and non-crossover mechanisms
Freeling, 1978	*Adh1*	Role of flanking sequences in crossing-over
Dooner et al., 1985	*Bz1*	*Bz1* is a recombination hotspot, 100-fold higher than the genome average
Brown and Sundaresan, 1991	*A1*	Crossover hotspot in the 5′ coding region
Civardi et al., 1994	*A1-Sh2*	Fine mapping crossovers in a chromosomal region
Patterson et al., 1995	*B1*	Crossover hotspot in the 5′ coding region
Eggleston et al., 1995	*R1*	Unequal crossing-over within the complex *R-st* allele fractionates its epigenetic potential
Dooner and Martínez-Férez, 1997	*Bz1*	Recombination is uniform across the *Bz1* gene
Okagaki and Weil, 1997	*Wx*	The promoter region is not required for recombination at *Wx*
Yao et al., 2002	*A1-Sh2*	Hotspots and cold regions in a 140 kb region; a non-genic low-copy sequence can be a recombination hotspot
Dooner, 2002	*Bz1*	Low sequence diversity between alleles favors NCO pathway
Yao and Schnable, 2005	*A1-Sh2*	Sequence polymorphisms partially explain crossover distributions in hotspots
Yandeau-Nelson et al., 2006	*A1*	Choice of template in a tandem duplication, rare use of sister chromatid
Dooner and He, 2008	*Bz1* region	Impact of adjacent retrotransposon polymorphisms on recombination
Wang et al., 2011	278 kb region on chromosome 10	Gene density and recombination
Dooner and He, 2014	*Bz1*	NCO events show polarity at the 5′ and 3′ ends of the gene

DNA region and pairs with its complementary sequence, binding it as a repair template. DNA synthesis can then proceed from the exposed 3′-end. From here, the invading strand plus newly synthesized sequence may dissociate from the complementary strand giving non-crossover events through SDSA (synthesis-dependent strand annealing). Alternatively, a double Holliday junction structure may form which can resolve into a crossover.

Both COs and NCOs give rise to a short region with non-reciprocal transfer of genetic information known as a gene conversion tract. The length of gene conversion tracts depends on DSB resection, synthesis from the exposed 3′-end, and migration of Holliday junctions. Median gene conversion tract lengths in *S. cerevisiae* have been measured at 2.0 kb for COs and 1.8 kb for NCOs (Mancera et al., 2008). NCO conversion tracts reached up to 40.8 kb in length, but 97% were less than 5 kb in length. Some CO and NCO conversion tracts had complex tracts arising via template switching between the parental alleles (Marsolier-Kergoat et al., 2018). In general, crossovers in *S. cerevisiae* are located close to the position of initiating DSBs.

Gene conversion tracts in Arabidopsis wild type have been far more difficult to detect and characterize, and are in general fewer and shorter than in budding yeast. For COs, gene conversion tracts were detected first at a maximal median length of ∼1.1 kb, for NCOs in the range of 1 bp to ∼6.6 kb (Lu et al., 2012). In another study, Arabidopsis NCO gene conversion ranged from mean tracts of 1 bp to ∼0.5 kb, the longest at ∼3.0 kb (Drouaud et al., 2013). The marker resolution underlies the precision at which gene conversion tracts can be defined, and might explain the even shorter estimates of CO-associated tracts of ∼0.3–0.4 kb and NCO-associated tracts of 25–50 bp (Wijnker et al., 2013).

Polarity for recombination is seen in many *S. cerevisiae* genes. The small discrete DSB hotspots located near TSSs concentrate recombination events at the 5′ end of many genes. A DSB hotspot at the 5′ end of a gene can give polarity near the 3′ end of a neighboring gene. Variation in gene conversion tract length and mismatch repair both contribute to polarity (Nicolas and Petes, 1994). Polarity can also be seen in Arabidopsis genes where recombination peaks near TSS, then decreases toward the end of genes (Hellsten et al., 2013; Choi et al., 2016). In maize, the relative importance of polarity in recombination is one of the questions arising between intragenic recombination studies and high-throughput genotyping studies.

Distribution of Crossovers in Maize Intragenic Studies

In a series of studies beginning in 1985, and continuing today, Hugo Dooner described a number of properties of maize recombination using the *Bz1* locus (**Table 1**). For genetic crossovers, there is no polarity within *Bz1*. The ratio of physical distance to genetic distance (kb/cM) at the 5′ and 3′ ends of *Bz1* are similar (Dooner and Martínez-Férez, 1997). This absence of polarity extends beyond *Bz1* into adjacent sequences. Upstream, the genetic distance from a marker within *Bz1* to the upstream gene *Mkk1* 100 kb away was less than the genetic length of *Bz1* (Dooner, 1986; Fu et al., 2002). Similarly, no crossovers were detected in the downstream interval between *Bz1* and the adjacent gene, *Stc1* (He and Dooner, 2009). There is, however, polarity for NCOs at both ends of the *Bz1* gene. Point mutations at both ends of *Bz1* are converted more frequently than point mutations in the middle of the gene. 5′ flanking sequences are required for polarity at the 5′ end; the requirement for 3′ flanking sequences have not been tested (Dooner and He, 2014). To summarize, the number of NCOs peak at the ends of *Bz1*, but COs are evenly distributed across the entire *Bz1* coding region and are rare in upstream and downstream regions.

TABLE 2 | Comparative characteristics of DSB hotspots.

	S. cerevisiae	*S. pombe*	*Mus musculus*	*Arabidopsis thaliana*	*Zea mays*
Number of DSB breaks/meiosis	~160[1]	~58[2]	230–350[3]	~235[4]; 120[5]	~500[6]
Number of DSB hotspots	3604[1]	603[2]	13,960[7]	5914[8]	3126[9]
	SPO11	SPO11 homolog	SPO11 homolog	SPO11 homolog	RAD51 homolog
DSBs mapped by:					
Hotspot width	189 bp median	965 bp median	143 bp median 99.8% < 2001 bp[7]	823 bp mean width[8]	1.2 kb; use of RAD51 may inflate hotspot width[9,10]
	73.4% between 50 and 300 bp, single peak[1]				
			Has secondary peaks[7]		
		range ~50 bp – 7 kb[2]			
Location of DSBs	DSBs near TSS[1,11]	19% of DSBs within 200 bp of TSS[2,11]	3% of DSBs near TSS[11,12]	DSBs high at TSS and TTS[8,11]	DSBs high at TSS and TTS[9,11]
Importance of DSBs for COs	89% of DSBs in DSB hotspots. Recombination and DSBs are tightly linked[1]	72% of DSBs in hotspots. DSBs in cold regions account for almost half of COs [2]	59.6% DSBs in DSB hotspots[7]. Account for ~75% COs	Levels of DSBs and COs correlate at large scale, but no direct relation at fine scale[8]	Correlation of DSBs and COs only in genic regions[9]
DSBs in repetitive sequence?	Strongly under-represented[1]	Few[2]	Estimated 32.8% reads mapped to multiple sites[7]	Abundant, >50% of DSBs[8]	73.9% DSB in repetitive sequence[9]
Open chromatin, micrococcal nuclease sensitivity	DSBs mainly in NDR[1] NDR provides access, other factors more important for determining if DSB occurs	DSBs are not concentrated in NDRs[2]	Most hotspots have a central NDR[8]	DSBs directly at NDRs[8]	Open chromatin[9]
H3K4me3	Association with hotspots may be indirect[12]	Low level of H3K4me3 at *ade6-M26* hotspot[13]	Presence at hotspots, serves to direct DSBs away from TSS[14]	Close to H3K4me3 sites at genes, but no correlation[8]	20% of all hotspots
					55% of genic hotspots[9]
DNA sequence motif				AT-richer[8]	G's at 3 nt-periodicity[9]

[1]*Pan et al., 2011*; [2]*Fowler et al., 2014*; [3]*Plug et al., 1996*; [4]*Chelysheva et al., 2007*; [5]*Varas et al., 2015*; [6]*Franklin et al., 1999*; [7]*Lange et al., 2016*; [8]*Choi et al., 2018*; [9]*He et al., 2017*; [10]*DSB mapping with SPO11 provides higher precision than with RAD51 (Pan et al., 2011)*; [11]*TSS, transcription start site and TTS, transcription termination site*; [12]*Tischfield and Keeney, 2012*; [13]*Yamada et al., 2013*; [14]*Brick et al., 2012*.

Outside of *Bz1* the most extensive intragenic recombination data comes from the *Wx* locus. Here too there is no evidence for polarity of COs. Nelson fine-mapped 29 *wx* alleles, and a number of these mutations were sequenced in Sue Wessler's lab. Looking at recombination between pairs of alleles with a variety of genetic backgrounds and mutational lesions found no indication of polarity at *Wx* (Okagaki and Weil, 1997). Though limited to only four alleles, results at the rice *Wx* locus are in agreement (Inukai et al., 2000). Similarly, at the maize *Stc1* locus, COs are found across the length of the gene with similar numbers of crossovers at the 5′ and 3′ ends of the gene (Dooner and He, 2008; He and Dooner, 2009).

Contrasting with the absence of polarity at the *Wx* locus is the strong polarity for COs at the maize *A1*, *B1,* and *R1* genes. 5′-polarity was seen at *A1* and *B1*. Thirty-three of 35 crossovers in *B1* mapped to a 620 bp interval overlapping the start codon (Patterson et al., 1995. The *A1* gene has a 377 bp hotspot beginning in exon 1 and spanning exon 2 (Xu et al., 1995). Recombination at *R1* showed a polarity gradient with highest levels of recombination at the 3′-end of *R1* that declined to low levels in the middle of the gene, a distance of approximately 3.5 kb (Eggleston et al., 1995; Dietrich, 1998; Kermicle, personal communication).

Intragenic recombination studies have also looked at recombination within small genetic intervals. Since high recombination rates measured within genes suggests that little recombination happens in intergenic regions this work directly asks whether crossing over can take place outside of genes. Studying recombination in the *Al – Sh2* interval, Patrick Schnable's group identified three CO hotspots in the 130–140 kb interval (Yao et al., 2002; Yao and Schnable, 2005). Two of the four genes in the region were CO hotspots, and the third hotspot was in a unique non-genic sequence. Only four of the 101 COs mapped outside of the three hotspots (Yao et al., 2002). The genic region surrounding *Bz1* presents a similar pattern with a majority of the genes in the region functioning as CO hotspots (Fu et al., 2002; He and Dooner, 2009). The large block of repetitive sequence upstream of *Bz1* is heavily methylated consistent with methylation suppressing recombination as has been seen in Arabidopsis (Melamed-Bessudo and Levy, 2012;

Mirouze et al., 2012; Yelina et al., 2015). Haplotype structure and local sequence differences locally suppressing recombination provides an additional mechanism for modifying crossover frequencies (Yao and Schnable, 2005; Dooner and He, 2008).

In summary, the key results from intragenic recombination studies in maize are as follows: (1) both crossover and non-crossover events are detected; (2) many maize genes are recombination hotspots; (3) some but not all genes show polarity that may be punctate or have a gradient; (4) some recombination hotspots are in non-genic low-copy sequences; (5) sequence differences between parental chromosomes affect the distribution of recombination events. However, the number of studies with adequate data is small and conclusions about relative frequency of genes showing polarity should not be drawn.

Distribution of Maize Crossovers by High-Throughput Genotyping

At the genome-wide scale, maize COs form a particular U-shape pattern, with COs increasing strongly toward chromosome ends (Anderson et al., 2003; Li et al., 2015; Rodgers-Melnick et al., 2015; Kianian et al., 2018). Maize chromosomes have rather big pericentromeric heterochromatin regions that cover more than half of them (Baucom et al., 2009; Wei et al., 2009). Heterochromatin is thus negatively correlated with COs at large scale, but we want to keep the focus on the gene-scale data to allow comparison between traditional intragenic studies in maize and the newer cohort of sequencing-technology-driven studies.

Four studies based on next-generation sequencing have mapped recombination events in maize (**Table 3**). Three studies have been published (Li et al., 2015; Rodgers-Melnick et al., 2015; Kianian et al., 2018). Data from the fourth study was reported in Alina Ott's Ph.D. dissertation, and a manuscript is in preparation (Ott, 2017). High marker density is critical for studying polarity and other questions. Three maize genome-wide studies reported polarity for crossovers, with COs most frequent in the 5′ region of genes and low in the central region of genes (Li et al., 2015; Ott, 2017; Kianian et al., 2018). The resolution of one study was generally not sufficient to address this question (Rodgers-Melnick et al., 2015). Crossovers were mapped with sufficient precision to identify polarity for approximately 50% (Kianian et al., 2018) and approximately 10% of crossovers placed (Li et al., 2015; Ott, 2017). Two of the studies reported evidence for high crossover frequency at the 3′ end of the gene (Li et al., 2015; Kianian et al., 2018). Recombination polarity at the 5′ and often 3′ ends of genes has been reported to be the common pattern in several plant species (reviewed in Choi and Henderson, 2015).

Crossover hotspots were identified in three studies (Rodgers-Melnick et al., 2015; Ott, 2017; Kianian et al., 2018). Kianian's study defined hotspots as 5 kb regions with CO rates fivefold higher than the genome average; there were 282 and 257 hotspots in the male and female parents of the population respectively (Kianian et al., 2018). Using the 793 COs mapped within a gene, Ott identified 158 genes with more than one CO event in her population; many of these genes are statistically likely to be CO hotspots (Ott, 2017). These two studies relied on relatively small populations. Using a much larger population, Rodgers-Melnick's study found 410 hotspots (Rodgers-Melnick et al., 2015). Not all of the genic hotspots described by intragenic recombination studies were identified in these studies. Sampling depth may be a limiting factor in detecting CO hotspots, but the variable number and locations of CO hotspots suggests we need to think carefully about the meaning of hotspots.

TABLE 3 | Maize sequencing based CO studies.

Study	Li et al., 2015	Rodgers-Melnick et al., 2015	Kianian et al., 2018	Ott, 2017
Crossover measurement	DNA-seq of tetrads after WGA	GBS of RILs	DNA-seq of backcrossed F1 plants	RNA-seq of RILs
Coverage	Low (∼1.4x)		Low (∼1.5–5x)	
COs per meiosis	19.2	Most between 20 and 25	17.2 (male), 18.6 (female)	
Marker density	Median 1 SNP/ 235 bp		Median 1 SNP/44 bp	1.3 SNPs/kb of gene
Number of individuals	96 (24 tetrads)	4714 (US-NAM), 1382 (China-NAM)	135 (male), 122 female	105
Crossover intervals	∼63% ≤ 100 kb	Median 127 kb (10% ≤ 10 kb)	∼50% ≤ 2 kb	Median 104.6 kb
Hotspot definition	n.d.	Regions containing a concentration of narrow crossover intervals. Estimated FDR of 0.5%	5 kb region with ≥5x genome average	Genes with ≥2 crossovers
Number of crossovers	924	103,459 (US-NAM) 32,536 (China-NAM)	1164 (male) 1139 (female)	7574
Number of crossovers mapped short interval	234 ≤ 10 kb	10% ≤ 10 kb	∼50% ≤ 2 kb	793 mapped within a gene
Number of hotspots	n.d.	410	282 (male) 257 (female)	158
Percent of crossovers outside of hotspots	n.d.	Estimated 70%	n.d.	n.d.
Percent of genome with crossover hotspot	n.d.	≤0.2%	∼0.05%	n.d.

Conclusions drawn from high-throughput genotyping studies emphasized polarity with COs concentrated at 5′ and 3′ ends of genes (Li et al., 2015; Ott, 2017; Kianian et al., 2018). Although this differs at first glance from intragenic studies which reported genes with and without polarity, the data actually agrees. Intragenic studies reporting on individual genes found a mix of genes showing polarity and others that do not. What is reported in genome-wide studies is an accumulated pattern from 100s of genes. The polarity found in these studies could be a result of a generalized polarity at most genes or the result of a mix of genes with and without CO polarity as seen in intragenic studies. While high-throughput studies emphasize increased CO rates at 5′ and 3′ ends of genes, intragenic studies report on individual genes, exposing the mix of genes with large diffuse hotspots or localized hotspots (**Figure 3**). Similarly, in Arabidopsis, it has been shown that the level of polarity-underlying DSBs at the TSS and TTS are independent from each other (Choi et al., 2018).

DOUBLE-STRAND BREAK HOTSPOTS

Lessons From *S. cerevisiae* and *A. thaliana*

In *S. cerevisiae*, most meiotic DSBs resolve into COs and NCOs. The 140–170 DSBs observed per yeast meiosis (Buhler et al., 2007) closely match the 90.5 COs and 46.5 NCOs counted per meiosis (Mancera et al., 2008). Precise mapping of DSB hotspots via SPO11-bound nucleotides released at resection revealed that almost 90% of DSBs occurred in a described hotspot (Pan et al., 2011) (**Table 2**). DSBs were underrepresented in repetitive sequences with repetitive DNA comprising 14% of the genome while accounting for only 1.16% of DSB breaks defined by SPO11 reads (Pan et al., 2011). Overall, 95% of DSBs identified by SPO11 oligonucleotides were confined to just 15% of the yeast genome (Marsolier-Kergoat et al., 2018). In Arabidopsis, mapping of SPO11-oligonucleotides also revealed that DSBs are preferentially located in regions with high gene density, and underrepresented in TE dense regions (Choi et al., 2018).

Although there was no consensus target sequence for the SPO11 nuclease responsible for meiotic DSBs, the DNA sequence was non-random with preferred nucleotides at certain positions, and a central AT-rich sequence surrounded by modestly GC-rich sequence. AT-rich motifs were also found at Arabidopsis DSB sites (Choi et al., 2018), likely due to those motifs generally excluding nucleosomes (Segal and Widom, 2009).

Saccharomyces cerevisiae DSBs map preferentially to nucleosome depleted regions (NDRs) around the TSS, a hallmark of open chromatin (Pan et al., 2011). The trimethylated histone H3 lysine 4 (H3K4me3) is a histone modification promoting an open chromatin structure that is found at DSB hotspots (Borde et al., 2009). Noteworthy, however, is that not all NDRs are DSB hotspots and H3K4me3 is absent at some DSB hotspots (Pan et al., 2011; Tischfield and Keeney, 2012). This picture of open chromatin being favored by the DSB machinery is also true in Arabidopsis: here, DSBs were shown to correlate with H3K4me3 and low nucleosome density (Choi et al., 2018).

In summary, the correlation of DSBs and recombination in *S. cerevisiae* is clear as almost all DSBs lead to recombination and both the initiating DSBs and resolving recombination hotspots are mainly found near TSSs. The picture is different in other systems, including Arabidopsis, where a few 100 DSBs get resolved into only ∼6–12 COs (Giraut et al., 2011; Lu et al., 2012; Salomé et al., 2012; see **Table 2**).

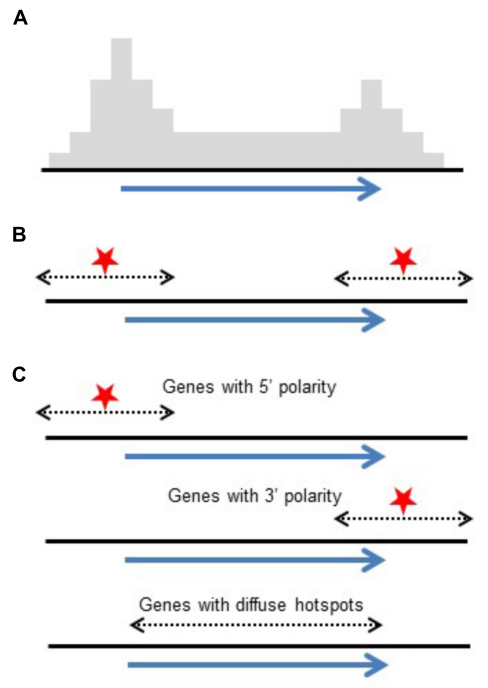

FIGURE 3 | Reconciling polarity gradients as seen in high-throughput genotyping versus intragenic studies. **(A)** Histogram representing crossover polarity seen in high-throughput genotyping studies. **(B)** DSB hotspots at both ends of genes could produce this distribution. **(C)** Alternatively, a mix of genes having DSB hotspots at their 5′ ends, their 3′ ends, and genes that are diffuse hotspots give the same pattern of crossovers.

Location and Distribution of Maize Double-Strand Breaks

Double-strand breaks cannot be directly mapped by intragenic studies, but their possible positions may be deduced by examining recombination in deletion mutations. Homozygous deletions of DSB hotspots reduce recombination and eliminate polarity at the *S. cerevisiae HIS4* locus (Detloff et al., 1992). The maize *wx-B* allele is a 1 kb deletion around the TSS from −459 to +505, while *wx-C4* has a smaller deletion within the transcribed region from +257 to +454 (Wessler et al., 1990; Okagaki and Weil, 1997). If DSBs near the TSS contribute substantially to recombination, then more recombinants should be recovered between alleles with intact TSS regions than with alleles containing TSS region deletions. This, however, was not seen when Oliver Nelson measured recombination between *wx-B* and *wx-C4* with downstream alleles (**Supplementary Table 1**). Second, there is directionality to the repair of meiotic DSBs since DSBs are repaired using sequences on the homologous

chromosome. Thus in a line where one allele contains a deletion of its DSB hotspot and the other allele retains its DSB hotspot, recombination preferentially deletes the previously non-mutant sequence (Nicolas et al., 1989). The *wx-B1* allele has a deletion from −655 to +299 (Wessler et al., 1990). Recombination between *wx-B1* and the *wx-I* allele, containing a large insertion in the 3′ region, also argued against a single DSB hotspot near the TSS (Okagaki and Weil, 1997). Here, 28 of 29 recombinants were crossovers between *wx-B1* and *wx-I*. The DSBs in this experiment most likely were in the region between *wx-B1* and *wx-I* rather than in the 5′ region.

Indirect evidence against a yeast-like concentration of DSBs near TSSs in maize comes from one whole genome study. A high-throughput recombination study via the maize transcriptome mapped 2634 NCO conversion tracts in a maize RIL population (Ott, 2017). Non-crossover conversion tracts in the 5′, the central, and 3′ regions of maize genes were roughly equally distributed, with a slightly higher number in the middle region of genes (Ott, 2017). According to the original canonical DSB model, gene conversion tracts produced at NCOs and COs will flank or encompass the position of initiating DSBs, thus indirectly mapping DSBs (Szostak et al., 1983). More recent data in *S. cerevisiae* shows that NCO conversion tracts can be located a short distance from the DSB (Marsolier-Kergoat et al., 2018). The even distribution of NCO conversion tracts across maize genes argues against the concentration of DSBs at the ends of maize genes.

A recent maize genomic DSB study using a genome-wide approach similar to the one used in *S. cerevisiae* and other model species captured and sequenced single-stranded DNA bound to RAD51 (He et al., 2017). In total, the maize DSB mapping effort identified 3126 hotspots (He et al., 2017), similar to the 3604 DSB hotspots in *S. cerevisiae* (Pan et al., 2011). The number of defined maize DSB hotspots is conservative. With relaxed stringency and controls the number is considerably larger (He et al., 2017). Although maize DSB hotspots shared some characteristics with their *S. cerevisiae* counterparts and DSB hotspots from Arabidopsis and other model systems, there are some clear differences (**Table 2**). The almost 73% of maize DSB hotspots in repetitive sequence contrasts with the under-representation of DSB hotspots in *S. cerevisiae* repetitive sequences. Maize DSB hotspots were also wider than *S. cerevisiae* DSB hotspots, 1.2 kb versus 189 bp. This difference might be a consequence of the precision of the SPO11 based approach used in *S. cerevisiae* versus the lower resolution possible with the RAD51 based approach used in maize, or it could represent physical differences in their DSB hotspots. Perhaps of greater interest is the close relationship between DSB hotspots and COs found in *S. cerevisiae* may not hold in maize (see section "The Role of Double-Strand Breaks in Maize and Other Model Organisms"). One mapped DSB hotspot was immediately upstream of *Bz1*. However, as we have seen from intragenic studies, COs at *Bz1* do not show polarity, although NCOs show polarity at the 5′ and 3′ ends of *Bz1* (Dooner and Martínez-Férez, 1997; Dooner and He, 2014). Thus the importance of a DSB hotspot flanking *Bz1* for recombination is unclear.

Approximately, 85% of the maize genome is composed of families of repetitive elements widely distributed in the maize genome (Schnable et al., 2009). Ty1-gypsy-like elements are the most abundant families (Meyers et al., 2001). Over 50% of maize DSB hotspots are in gypsy-like elements (He et al., 2017). Both DNA methylation and sequence polymorphisms are suggested mechanisms for suppressing COs in maize repetitive sequences (Fu et al., 2002; Yao and Schnable, 2005). Repetitive elements are commonly found in blocks separating individual genes or small clusters of genes (Haberer et al., 2005). These blocks are not conserved between maize lines, and two genes may be separated by a short stretch of low-copy sequence in one line and by significant stretches of repetitive sequence resulting from multiple repetitive elements in another line (He and Dooner, 2009). This absence of sequence homology will strongly inhibit recombination. Even when the overall structure of a repetitive block is preserved, nucleotide polymorphisms could locally inhibit crossing over, as seen in the a1-sh2 region (Yao and Schnable, 2005). However, results from one intragenic recombination study argues against sequence polymorphism as the primary mechanism suppressing crossing over in repetitive sequences (Fu et al., 2002). In this study using the Bz1 region, crossing over was compared between a short genic region and a block of repetitive sequence flanking the genes. Because the haplotypes used in this experiment were derived from the same progenitor, there was little if any sequence difference in the region except for the genetic markers. In this region, at least, sequence differences cannot account for the lack of crossing over in repetitive sequence.

The Role of Double-Strand Breaks in Maize and Other Model Organisms

Meiotic DSBs serve two functions, first to promote chromosome pairing and second to produce the crossovers necessary to ensure proper segregation of chromosomes at anaphase (Page and Hawley, 2003). Meiotic DSBs can be visualized on chromosomes as RAD51 foci (Franklin et al., 1999). In mid-zygotene when chromosomes are pairing, there are approximately 500 RAD51 foci decreasing to about 12 RAD51 foci in pachytene (Franklin et al., 1999; Pawlowski et al., 2003). The zygotene foci are distributed across the chromosomes where single-stranded DNA ends produced by DSBs and resection promote chromosome alignment (Smithies and Powers, 1986; Peoples-Holst and Burgess, 2005). The pachytene foci, also known as late recombination nodules when viewed with electron microscopy, represent the sites of crossing-over (Stack and Anderson, 2002). Control of the number of COs and which DSBs are channeled into the crossover pathway is tightly regulated (Lake and Hawley, 2016). There are two types of COs, with interference-sensitive COs (type I) constituting the majority of COs, and a few additionally interspersed interference-insensitive COs (type II) in many species (Gray and Cohen, 2016). Some species lack the type I interference-sensitive pathway (Gray and Cohen, 2016). Though their mechanisms are distinct, their outcomes are treated equally in intragenic as well as whole genome studies.

Double-strand breaks are necessary for recombination, but the importance of DSB hotspots for genetic crossovers is less clear. Compared with *S. cerevisiae*, the fraction of maize DSBs resolving as crossovers is small. Mapping crossovers using *S. cerevisiae* tetrads gave an average of 90.5 crossovers per meiosis, with an estimated 160 DSBs per meiosis (Mancera et al., 2008; Pan et al., 2011). In contrast, only a fraction (∼5–10%) of DSBs get resolved into COs in Arabidopsis (Giraut et al., 2011; Lu et al., 2012; Salomé et al., 2012; also see **Table 2**). Mapping crossovers from maize tetrads determined an average of 19 crossovers per meiosis (Li et al., 2015), similar to the range of cytologically determined CO in maize inbreeds (Sidhu et al., 2015). Thus, less than 4% of maize DSBs resulted in COs versus 56% in *S. cerevisiae* tetrads. In fact, the majority of DSB hotspots appear unlikely to contribute much to crossing over as almost 73% of hotspots are in repetitive sequence where crossovers are believed to be suppressed (He et al., 2017). It seems reasonable to conclude that a majority of maize DSBs promote chromosome alignment (Peoples-Holst and Burgess, 2005).

The genome-wide maize DSB data identified 3126 high-confidence DSB hotspots, about one-fourth of them in genes. This is a conservative estimate of the number of hotspots based on very stringent criteria (He et al., 2017). What the genomic maize DSB study shows clearly, however, is the concentration of DSBs around TSS and TTS of many genes (He et al., 2017). This is mirrored in other model systems, for example Arabidopsis, with highest DSB levels at TSS and TTS (Choi et al., 2018), and is in general a prerequisite for recombination polarity along a gene body.

Though the concept is enticing, enrichment of maize DSB hotspots around the TSS and TTS of genes may not exist at all genes, with or without producing polarity. On average, DSBs have an increased tendency to peak at TSS and on both sides of TTS (He et al., 2017), agreeing with CO peaks close to TSS and TTS (Kianian et al., 2018). However, polarity for CO is not seen at *Bz1* despite the adjacent DSB hotspot (Dooner and Martínez-Férez, 1997; He et al., 2017). In *S. cerevisiae*, the tight connection between DSB hotspots and recombination is well-established (Pan et al., 2011; Marsolier-Kergoat et al., 2018), but there are large differences between eukaryotes (Fowler et al., 2014; Stapley et al., 2017). Results from similar studies in the fission yeast *Schizosaccharomyces pombe* (*S. pombe*) present a very different picture (**Table 2**). Less than 20% of *S. pombe* DSB hotspots are near the TSS. Furthermore, DSBs in *S. pombe* hotspots are preferentially repaired from the sister chromatid; these events do not contribute to crossing-over. A large fraction of COs are initiated at non-hotspot DSBs in *S. pombe* (Fowler et al., 2014).

On the other hand, *S. pombe* DSB hotspots are not strongly correlated with NDRs (Fowler et al., 2014). This contrasts with *S. cerevisiae*, Arabidopsis and maize.

Mouse DSB hotspots share characteristics of both *S. cerevisiae* and *S. pombe* and hint at the complexities underlying hotspots. DSB hotspot widths are similar to *S. cerevisiae* (Lange et al., 2016). Unlike *S. cerevisiae*, these hotspots are over-represented within the genic region defined by the start and stop codons, and only 3% are located near the TSS (Smagulova et al., 2011; Brick et al., 2012). The H3K4me3 modification at mouse DSB hotspots is produced by the *Prdm9* histone methyltransferase (Baudat et al., 2010). H3K4me3 is present at other sites along mouse chromosomes including TSS. Removing H3K4me3 at DSB hotspots using *prdm9* mutant mice blocks DSBs from forming at these hotspots. Instead, DSBs occur at other H3K4me3 sites on the chromosome; many of these are near the TSS (Brick et al., 2012). Of critical importance here is the observation that these mice are defective in DSB repair and chromosome pairing (Hayashi et al., 2005).

Open chromatin is so far the only universal criteria for DSBs and CO locations across different model systems, though caution is needed regarding the scale (Tischfield and Keeney, 2012). The active chromatin mark H3K4me3 for example can be found near DSBs, but overlaps COs even more, arguing that it promotes recombination downstream of DSBs, in yeast and Arabidopsis, while DSB association is merely due to location to promoters (Tischfield and Keeney, 2012; Choi et al., 2018). Rather, chromosomal context and the relationship between the DSB and the synaptonemal complex are important (Medhi et al., 2016). DNA methylation is yet another component underlying the structure of the chromosome, but details on its association with DSB and COs are beyond the scope of this review, which focused on intragenic recombination.

NO MODEL SYSTEM EXPLAINS ALL

As described here, there are aspects of systems other than *S. cerevisiae* that provide insight into maize. For example, in *S. pombe,* DSBs in hotspots contribute far less to COs than expected – most DSBs in hotspots do not resolve as COs. Might this be similar to maize where three-fourths of DSB hotspots are in repetitive sequence? Does the absence of class I COs in *S. pombe* disqualify *S. pombe* as a model system for maize recombination, any more than the under-representation of DSB hotspots in *S. cerevisiae* repetitive sequence disqualifies *S. cerevisiae* as a model for maize where three-fourths of DSB hotspots are in repetitive sequence? Is there a clear reason why class I versus class II COs are a more important criteria for choosing a reference model system than the weak association between DSB hotspots and COs in maize and *S. pombe* versus the tight association in *S. cerevisiae*?

Deleting the promoter region in a yeast gene strongly reduces recombination at the gene (De Massy and Nicolas, 1993; Porter et al., 1993). Deleting the promoter region in maize *Bz1* and *Wx* does not strongly reduce recombination at the gene (see section "Lessons From *S. cerevisiae* and *A. thaliana*," **Supplementary Table 1**).

Mouse provides the valuable lesson that open chromatin in promoters is not necessarily a target for DSBs. On the other hand, mouse DSB hotspots are mediated by PRDM9 which does not seem to exist in plants. Are plants as the mostly related species not the best system to compare with maize? In spite of different genome architecture of Arabidopsis and maize, many commonalities of DSB and CO hotspots can indeed be found. The agreement of recombination distribution is even better when comparing other large-genome crops with each other, as for

example maize, wheat, and barley (Higgins et al., 2012; Darrier et al., 2017). Only when integrating information learned from different model organisms and different approaches do we have a chance of resolving the whole story on DSBs, recombination, polarity, and underlying genome features.

SUMMARY

Maize has been a genetic model genetic system for almost 100 years, and has been used to address questions regarding recombination as fundamental as the connection between cytological crossing over and genetic crossing over (Creighton and McClintock, 1931). However, there is a chasm between what we know based on extensive data, what we think we know, and what is known in other model systems used for studying recombination. Intragenic studies on small genetic regions have characterized most genes as recombination hotspots, but some genes are coldspots and some non-genic regions are recombination hotspots (Yao et al., 2002; He and Dooner, 2009; Wang et al., 2011). Issues may arise when extrapolating results from the handful of maize genes where intragenic recombination has been studied in depth. On the other hand, high-throughput genotyping studies suffer from a lack of resolution or depth, and small sample sizes. The median interval defining crossovers in three of the four studies was over 100 kb (Li et al., 2015; Rodgers-Melnick et al., 2015; Ott, 2017). Greater precision is necessary to minimize the misleading correlations possible with low-resolution mapping (Tischfield and Keeney, 2012).

Where do crossovers occur in maize? At the chromosomal level, intragenic and genome-wide studies identified an association between gene-density and elevated crossover rates (Yao et al., 2002; Wang et al., 2011; Pan et al., 2017). Looking at single genes or small genetic intervals, intragenic studies conclude that most crossovers take place within genes. Genes appear to fall into two categories with crossovers either concentrated at one end of the gene, either 5′ or 3′ polarity, or distributed evenly across the gene (Eggleston et al., 1995; Patterson et al., 1995; Dooner and Martínez-Férez, 1997; Okagaki and Weil, 1997; Yao and Schnable, 2005). High-throughput genotyping studies, drawing parallels with the polarity found in *S. cerevisiae* genes, emphasize polarity at the 5′ and 3′ ends of genes (Li et al., 2015; Ott, 2017; Kianian et al., 2018). But two of these studies determined that about one-fourth of the crossovers mapped within a gene were in the central region (Li et al., 2015; Ott, 2017). In the third study, 50% of the crossovers did not map to either the 5′ or 3′ regions (Kianian et al., 2018). Intragenic studies look at many recombination events at a few genes while genomic approaches average over many genes with few recombination events each. The two approaches give different snapshots and interpretations of crossing over and point to their relative strengths and weaknesses.

Due to the underlying literature we have focused this review on hotspots for crossover and DSBs. This perspective may be problematic. It seems that hotspots are not the best means to describe crossovers in maize which could be better described as following a chromosome-wide polarity gradient toward the chromosome ends coupled with an avoidance of repetitive sequence in the case of COs. This wider perspective encompasses additional questions including the importance of trans-acting modifiers, frequently genes from recombination pathways (Pan et al., 2017).

In addition, the fraction of crossovers attributed to recombination hotspots is not high. The 410 CO hotspots defined by Rodgers-Melnick accounted for 30.6% crossovers defined to a narrow interval (Rodgers-Melnick et al., 2015). Our interest in hotspots seems to be focusing our attention on local determinants of recombination as a functional unity and away from the larger and possibly more important chromosomal context (Pan et al., 2011). Where a DSB occurs along a chromosome may be just as important in determining the DSB fate as local hotspot features (Serrentino and Borde, 2012). There is now an intense interest and effort in understanding the roles of chromatin features including the synaptonemal axis, loops, and cohesin proteins, which will help refine our views on meiotic recombination mechanisms and patterns (Barrington et al., 2017).

AUTHOR'S NOTE

Results from Alina Ott's Ph.D. dissertation have now been published in Liu et al. (2018).

AUTHOR CONTRIBUTIONS

RO: conception of this project. SD-S: re-analyzing recombination data. WE: *R1* recombination data. RO and SD-S: drafting of manuscript. RO, SD-S, WBE, and GM: editing of manuscript. All authors approved the final version of the manuscript.

FUNDING

SD-S thanks Changbin Chen for all his support and the opportunity to work on maize meiosis, supported by the National Science Foundation (IOS-1025881 and IOS-1546792), and a grant-in-aid fund from the University of Minnesota. GM received funding from Endowed Chair in Molecular Genetics Applied to Crop Improvement.

ACKNOWLEDGMENTS

This paper is dedicated to Oliver E. Nelson in recognition for his many contributions to the study of genetics.

SUPPLEMENTARY MATERIAL

The Supplementary Material for this article can be found online at: https://www.frontiersin.org/articles/10.3389/fpls.2018.01560/full#supplementary-material

REFERENCES

Anderson, L. K., Doyle, G. G., Brigham, B., Carter, J., Hooker, K. D., Lai, A., et al. (2003). High-resolution crossover maps for each bivalent of *Zea mays* using recombination nodules. *Genetics* 165, 849–865.

Barrington, C., Pezic, D., and Hadjur, S. (2017). Chromosome structure dynamics during the cell cycle: a structure to fit every phase. *EMBO J.* 36, 2661–2663. doi: 10.15252/embj.201798014

Baucom, R. S., Estill, J. C., Chaparro, C., Upshaw, N., Jogi, A., Deragon, J.-M., et al. (2009). Exceptional diversity, non-random distribution, and rapid evolution of retroelements in the B73 maize genome. *PLoS Genet.* 5:e1000732. doi: 10.1371/journal.pgen.1000732

Baudat, R., Buard, J., Grey, C., Fledel-Alon, A., Ober, C., Przeworski, M., et al. (2010). PRDM9 is a major determinant of meiotic recombination hotspots in humans and mice. *Science* 327, 836–840. doi: 10.1126/science.1183439

Benzer, S. (1955). Fine structure of a genetic region in bacteriophage. *Proc. Natl. Acad. Sci. U.S.A.* 41, 344–354. doi: 10.1073/pnas.41.6.344

Borde, V., Robine, N., Lin, W., Bonfils, S., Géli, V., and Nicolas, A. (2009). Histone H3 lysine 4 trimethylation marks meiotic recombination initiation sites. *EMBO J.* 28, 99–111. doi: 10.1038/emboj.2008.257

Brick, K., Smagulova, F., Khil, P., Camerini-Otero, R. D., and Petukhova, G. V. (2012). Genetic recombination is directed away from functional genomic elements in mice. *Nature* 485, 642–645. doi: 10.1038/nature11089

Brown, J. W. S., and Sundaresan, V. (1991). A recombination hotspot in the maize A1 intragenic region. *Theor. Appl. Genet.* 81, 185–188. doi: 10.1007/BF00215721

Buhler, C., Borde, V., and Lichten, M. (2007). Mapping meiotic single-strand DNA reveals a new landscape of DNA double-strand breaks in *Saccharomyces cerevisiae*. *PLoS Biol.* 5:e324. doi: 10.1371/journal.pbio.0050324

Chelysheva, L., Gendrot, G., Vezon, D., Doutriaux, M.-P., Mercier, R., and Grelon, M. (2007). Zip4/Spo22 is required for Class I CO formation but not for synapsis completion in *Arabidopsis thaliana*. *PLoS Genet.* 3:e83. doi: 10.1371/journal.pgen.0030083

Choi, K., and Henderson, I. R. (2015). Meiotic recombination hotspots – a comparative view. *Plant J.* 83, 52–61. doi: 10.1111/tpj.12870

Choi, K., Reinhard, C., Serra, H., Ziolkowski, P. A., Underwood, C. J., Zhao, X., et al. (2016). Recombination rate heterogeneity within Arabidopsis disease resistance genes. *PLoS Genet.* 12:e1006179. doi: 10.1371/journal.pgen.1006179

Choi, K., Zhao, X., Tock, A. J., Lambing, C., Underwood, C. J., Hardcastle, T. J., et al. (2018). Nucleosomes and DNA methylation shape meiotic DSB frequency in *Arabidopsis thaliana* transposons and gene regulatory regions. *Genome Res.* 28, 532–546. doi: 10.1101/gr.225599.117

Chovnick, A. (1989). Intragenic recombination in Drosophila: the *rosy* locus. *Genetics* 123, 621–624.

Civardi, L., Xia, Y., Edwards, K. J., Schnable, P. S., and Nikolau, B. F. (1994). The relationship between genetic and physical distances in the cloned *a1-sh2* interval of the *Zea mays* L. genome. *Proc. Natl. Acad. Sci. U.S.A.* 91, 8268–8272. doi: 10.1073/pnas.91.17.8268

Creighton, H. B., and McClintock, B. (1931). A correlation of cytological and genetical crossing-over in *Zea mays*. *Proc. Natl. Acad. Sci. U.S.A.* 17, 492–497. doi: 10.1073/pnas.17.8.492

Darrier, B., Rimbert, H., Balfourier, F., Pingault, L., Josselin, A.-A., Servin, B., et al. (2017). High-resolution mapping of crossover events in the hexaploid wheat genome suggests a universal recombination mechanism. *Genetics* 206, 1373–1388. doi: 10.1534/genetics.116.196014

De Massy, B., and Nicolas, A. (1993). The control *in cis* of the position and amount of the *ARG4* meiotic double-strand break of *Saccharomyces cerevisiae*. *EMBO J.* 12, 1459–1466. doi: 10.1002/j.1460-2075.1993.tb05789.x

Detloff, P., White, M. A., and Petes, T. D. (1992). Analysis of a gene conversion gradient at the HIS4 locus in *Saccharomyces cerevisiae*. *Genetics* 132, 113–123.

Dietrich, W. R. (1998). *Determination of Rates and Patterns of Recombination at the Maize Red Color (r1) Locus*. MS thesis, Richmond, VA, Virginia Commonwealth University.

Dooner, H. K. (1986). Genetic fine structure of the bronze locus in maize. *Genetics* 113, 1021–1036.

Dooner, H. K. (2002). Extensive interallelic polymorphisms drive meiotic recombination into a crossover pathway. *Plant Cell* 14, 1173–1183. doi: 10.1105/tpc.001271

Dooner, H. K., and He, L. (2008). Maize genome structure variation: interplay between retrotransposon polymorphisms and genic recombination. *Plant Cell* 20, 249–258. doi: 10.1105/tpc.107.057596

Dooner, H. K., and He, L. (2014). Polarized gene conversion at the *bz* locus of maize. *Proc. Natl. Acad. Sci. U.S.A.* 111, 13918–13923. doi: 10.1073/pnas.1415482111

Dooner, H. K., and Martínez-Férez, I. M. (1997). Recombination occurs uniformly within the bronze gene, a meiotic recombination hotspot in the maize genome. *Plant Cell* 9, 1633–1646. doi: 10.1105/tpc.9.9.1633

Dooner, H. K., Weck, E., Adams, S., Ralston, E., Favreau, M., and English, J. (1985). A molecular genetic analysis of insertions in the bronze locus in maize. *Mol. Gen. Genet.* 200, 240–246. doi: 10.1007/BF00425430

Drouaud, J., Khademian, H., Giraut, L., Zanni, V., Bellalou, S., Henderson, I. R., et al. (2013). Contrasted patterns of crossover and non-crossover at *Arabidopsis thaliana* meiotic recombination hotspots. *PLoS Genet.* 9:e1003922. doi: 10.1371/journal.pgen.1003922

Eggleston, W. B., Alleman, M., and Kermicle, J. L. (1995). Molecular organization and germinal instability of R-stippled maize. *Genetics* 141, 347–360.

Fowler, K. R., Sasaki, M., Milman, N., Keeney, S., and Smith, G. R. (2014). Evolutionarily diverse determinants of meiotic DNA break and recombination landscapes across the genome. *Genome Res.* 24, 1650–1664. doi: 10.1101/gr.172122.114

Franklin, A. E., McElver, J., Sunjevaric, I., Rothstein, R., Bowen, B., and Cande, W. Z. (1999). Three-dimensional microscopy of the Rad51 recombination protein during meiotic prophase. *Plant Cell* 11, 809–824. doi: 10.2307/3870816

Freeling, M. (1978). Allelic variation at the level of intragenic recombination. *Genetics* 89, 211–224.

Fu, H., Zheng, Z., and Dooner, H. K. (2002). Recombination rates between adjacent genic and retrotransposon regions in maize vary by 2 orders of magnitude. *Proc. Natl. Acad. Sci. U.S.A.* 99, 1082–1087. doi: 10.1073/pnas.022635499

Giraut, L., Falque, M., Drouaud, J., Pereira, L., Martin, O. C., and Mézard, C. (2011). Genome-wide crossover distribution in *Arabidopsis thaliana* meiosis reveals sex-specific patterns along chromosomes. *PLoS Genet.* 7:e1002354. doi: 10.1371/journal.pgen.1002354

Gray, S., and Cohen, P. E. (2016). Control of meiotic crossovers: from double-strand break formation to designation. *Ann. Rev. Genet.* 50, 175–210. doi: 10.1146/annurev-genet-120215-035111

Green, M. M. (1955). Pseudoallelism and the gene concept. *Am. Nat.* 89, 65–71. doi: 10.1086/281866

Haberer, G., Young, S., Bharti, A. K., Gundlach, H., Raymond, C., Fuks, G., et al. (2005). Structure and Architecture of the Maize Genome. *Plant Physiol.* 139, 1612–1624. doi: 10.1104/pp.105.068718

Hayashi, K., Yoshida, K., and Matsui, Y. (2005). A histone H3 methyltransferase controls epigenetic events required for meiotic prophase. *Nature* 438, 374–378. doi: 10.1038/nature04112

He, L., and Dooner, H. K. (2009). Haplotype structure strongly affects recombination in a maize genetic interval polymorphic for Helitron and retrotransposon insertions. *Proc. Natl. Acad. Sci. U.S.A.* 106, 8410–8416. doi: 10.1073/pnas.0902972106

He, Y., Wang, M., Dukowic-Schulze, S., Zhou, A., Tiang, C.-L., Shilo, S., et al. (2017). Genomic features shaping the landscape of meiotic double-strand-break hotspots in maize. *Proc. Natl. Acad. Sci. U.S.A.* 114, 12231–12236. doi: 10.1073/pnas.1713225114

Hellsten, U., Wright, K. M., Jenkins, J., Shu, S., Yuan, Y., Wessler, S. R., et al. (2013). Fine-scale variation in meiotic recombination in *Mimulus* inferred from population shotgun sequencing. *Proc. Natl. Acad. Sci. U.S.A.* 110, 19478–19482. doi: 10.1073/pnas.1319032110

Higgins, J. D., Perry, R. M., Barakate, A., Ramsay, L., Waugh, R., Halpin, C., et al. (2012). Spatiotemporal asymmetry of the meiotic program underlies the predominantly distal distribution of meiotic crossovers in barley. *Plant Cell* 24, 4096–4109. doi: 10.1105/tpc.112.102483

Inukai, T., Sako, A., Hirano, H. Y., and Sano, Y. (2000). Analysis of intragenic recombination at *wx* in rice: correlation between the molecular and genetic maps within the locus. *Genome* 43, 589–596. doi: 10.1139/g00-015

Johns, M. A., Strommer, J. N., and Freeling, M. (1983). Exceptionally high levels of restriction site polymorphism in DNA near the maize *Adh1* gene. *Genetics* 105, 733–743.

Keeney, S., Lange, J., and Mohibullah, N. (2014). Self-organization of meiotic recombination initiation: general principles and molecular pathways. *Ann. Rev. Genet.* 48, 187–214. doi: 10.1146/annurev-genet-120213-092304

Kianian, P. M. A., Wang, M., Simons, K., Ghavami, F., He, Y., Dukowic-Schulze, S., et al. (2018). High-resolution crossover mapping reveals similarities and differences of male and female recombination in maize. *Nat. Commun.* 9:2370. doi: 10.1038/s41467-018-04562-5

Lake, C. M., and Hawley, R. S. (2016). Becoming a crossover-competent DSB. *Semin. Cell Dev. Biol.* 54, 117–125. doi: 10.1016/j.semcdb.2016.01.008

Lambing, C., Franklin, F. C. H., and Wang, C.-J. R. (2017). Understanding and manipulating meiotic recombination in plants. *Plant Physiol.* 173, 1530–1542. doi: 10.1104/pp.16.01530

Lange, J., Yamada, S., Tischfield, S. E., Pan, J., Kim, S., Zhu, X., et al. (2016). The landscape of mouse meiotic double-strand break formation, processing, and repair. *Cell* 167, 695–708.e16. doi: 10.1016/j.cell.2016.09.035

Li, X., Li, L., and Yan, J. (2015). Dissecting meiotic recombination based on tetrad analysis by single-microspore sequencing in maize. *Nat. Commun.* 6:6648. doi: 10.1038/ncomms7648

Liu, S., Schnable, J. C., Ott, A., Yeh, C. T., Springer, N. M., Yu, J., et al. (2018). Intragenic meiotic crossovers generate novel alleles with transgressive expression levels. *Mol. Biol. Evol.* doi: 10.1093/molbev/msy174 [Epub ahead of print].

Lu, P., Han, X., Qi, J., Yang, J., Wijeratne, A. J., Li, T., et al. (2012). Analysis of *Arabidopsis* genome-wide variations before and after meiosis and meiotic recombination by resequencing Landsberg *erecta* and all four products of a single meiosis. *Genome Res.* 22, 508–518. doi: 10.1101/gr.127522.111

Mancera, E., Bourgon, R., Brozzi, A., Huber, W., and Steinmetz, L. M. (2008). High-resolution mapping of meiotic crossovers and non-crossovers in yeast. *Nature* 454, 479–485. doi: 10.1038/nature07135

Marsolier-Kergoat, M.-C., Khan, M. M., Schott, J., Zhu, X., and Llorente, B. (2018). Mechanistic view and genetic control of DNA recombination during meiosis. *Mol. Cell* 70, 9–20.e6. doi: 10.1016/j.molcel.2018.02.032

Medhi, D., Goldman, A. S. H., and Lichten, M. (2016). Local chromosome context is a major determinant of crossover pathway biochemistry during budding yeast meiosis. *eLife* 5:e19669. doi: 10.7554/eLife.19669

Melamed-Bessudo, C., and Levy, A. A. (2012). Deficiency in DNA methylation increases meiotic crossover rates in euchromatic but not in heterochromatic regions in *Arabidopsis*. *Proc. Natl. Acad. Sci. U.S.A.* 109, E981–E988. doi: 10.1073/pnas.1120742109

Meyers, B. C., Tingey, S. V., and Morgante, M. (2001). Abundance, distribution, and transcriptional activity of repetitive elements in the maize genome. *Genome Res.* 11, 1660–1676. doi: 10.1101/gr.188201

Mirouze, M., Lieberman-Lazarovich, M., Aversano, R., Bucher, E., Nicolet, J., Reinders, J., et al. (2012). Loss of DNA methylation affects the recombination landscape in *Arabidopsis*. *Proc. Natl. Acad. Sci. U.S.A.* 109, 5880–5885. doi: 10.1073/pnas.1120841109

Nelson, O. E. (1957). The feasibility of investigating 'Genetic fine structure' in higher plants. *Am. Nat.* 91, 331–332. doi: 10.1086/281997

Nelson, O. E. (1959). Intracistronic recombination in the Wx/Wx region in maize. *Science* 130, 794–795. doi: 10.1126/science.130.3378.794

Nelson, O. E. (1962). The waxy locus in maize. I. Intralocus recombination frequency estimates by pollen and conventional analysis. *Genetics* 47, 737–742.

Nelson, O. E. (1968). The *WAXY* locus in maize. II. The location of the controlling element alleles. *Genetics* 60, 507–524.

Nelson, O. E. (1975). The waxy locus in maize III. Effect of structural heterozygosity on intragenic recombination and flanking marker assortment. *Genetics* 79, 31–44.

Nicolas, A., and Petes, T. D. (1994). Polarity of meiotic gene conversion in fungi: contrasting views. *Experientia* 50, 242–252. doi: 10.1007/BF01924007

Nicolas, A., Treco, D., Schultes, N. P., and Szostak, J. W. (1989). An initiation site for meiotic gene conversion in the yeast *Saccharomyces cerevisiae*. *Nature* 338, 35–39. doi: 10.1038/338035a0

Okagaki, R. J., and Weil, C. F. (1997). Analysis of recombination sites within the maize waxy locus. *Genetics* 147, 815–821.

Ott, A. (2017). *Assessment of Genetic Diversity and Recombination in Maize. Graduate Thesis and Dissertations. 16186*. Available at: https://lib.dr.iastate.edu/etd/16186

Page, S. L., and Hawley, R. W. (2003). Chromosome choreography: the meiotic ballet. *Science* 301, 785–789. doi: 10.1126/science.1086605

Pan, J., Sasaki, M., Kniewel, R., Murakami, H., Blitzblau, H. G., Tischfield, S. E., et al. (2011). A hierarchical combination of factors shapes the genome-wide topography of yeast meiotic recombination initiation. *Cell* 144, 719–731. doi: 10.1016/j.cell.2011.02.009

Pan, Q., Deng, M., and Li, L. (2017). Complexity of genetic mechanisms conferring nonuniformity of recombination in maize. *Sci. Rep.* 7:1205. doi: 10.1038/s41598-017-01240-2

Patterson, G. I., Kubo, K. M., Shroyer, T., and Chandler, V. L. (1995). Sequences required for paramutation of the maize *b* gene map to a region containing the promoter and upstream sequences. *Genetics* 140, 1389–1406.

Pawlowski, W. P., Golubovskaya, I. N., and Cande, W. Z. (2003). Altered nuclear distribution of recombination protein RAD51 in maize mutants suggests the involvement of RAD51 in meiotic homology recognition. *Plant Cell* 15, 1807–1816. doi: 10.1105/tpc.012898

Peoples-Holst, T. L., and Burgess, S. M. (2005). Multiple branches of the meiotic recombination pathway contribute independently to homolog pairing and stable juxtaposition during meiosis in budding yeast. *Genes Dev.* 19, 863–874. doi: 10.1101/gad.1293605

Petes, T. D. (2001). Meiotic recombination hot spots and cold spots. *Nat. Rev. Genet.* 2, 360–369. doi: 10.1038/35072078

Plug, A. W., Xu, J., Reddy, G., Golub, E. I., and Ashley, T. (1996). Presynaptic association of Rad51 protein with selected sites in meiotic chromatin. *Proc. Natl. Acad. Sci. U.S.A.* 93, 5920–5924. doi: 10.1073/pnas.93.12.5920

Pontecorvo, G. (1955). Gene structure and action in relation to heterosis. *Proc. R. Soc. Lond. B* 144, 171–177. doi: 10.1098/rspb.1955.0043

Porter, S. E., White, M. A., and Petes, T. D. (1993). Genetic evidence that the meiotic recombination hotspot at the *HIS4* locus of *Saccharomyces cerevisiae* does not represent a site for a symmetrically-processed double-strand break. *Genetics* 134, 5–19.

Portin, P. (1993). The concept of the gene: short history and present status. *Q. Rev. Biol.* 68, 173–223. doi: 10.1086/418039

Pradillo, M., Varas, J., Oliver, C., and Santos, J. L. (2014). On the role of AtDMC1, AtRAD51 and its paralogs during *Arabidopsis* meiosis. *Front. Plant Sci.* 5:23. doi: 10.3389/fpls.2014.00023

Rodgers-Melnick, E., Bradbury, P. J., Elshire, R. J., Glaubitz, J. C., Acharya, C. B., Mitchell, S. E., et al. (2015). Recombination in diverse maize is stable, predictable, and associated with genetic load. *Proc. Natl. Acad. Sci. U.S.A.* 112, 3823–3828. doi: 10.1073/pnas.1413864112

Sachs, M. M., Dennis, E. S., Gerlach, W. L., and Peacock, W. J. (1986). Two alleles of maize *alcohol dehydrogenase 1* have 3' structural and poly(A) addition polymorphisms. *Genetics* 113, 449–467.

Salomé, P. A., Bomblies, K., Fitz, J., Laitinen, R. A. E., Warthmann, N., Yant, L., et al. (2012). The recombination landscape in *Arabidopsis thaliana* F2 populations. *Heredity* 108, 447–455. doi: 10.1038/hdy.2011.95

Schnable, P. S., Ware, D., Fulton, R. S., Stein, J. C., Wei, F., Pasternak, S., et al. (2009). The B73 maize genome: complexity, diversity, and dynamics. *Science* 326, 1112–1115. doi: 10.1126/science.1178534

Segal, E., and Widom, J. (2009). What controls nucleosome positions? *Trends Genet. TIG* 25, 335–343. doi: 10.1016/j.tig.2009.06.002

Serrentino, M.-E., and Borde, V. (2012). The spatial regulation of meiotic recombination hotspots: are all DSB hotspots crossover hotspots? *Exp. Cell Res.* 318, 1347–1352. doi: 10.1016/j.yexcr.2012.03.025

Sidhu, G. K., Fang, C., Olson, M. A., Falque, M., Martin, O. C., and Pawlowski, W. P. (2015). Recombination patterns in maize reveal limits to crossover homeostasis. *Proc. Natl. Acad. Sci. U.S.A.* 112, 15982–15987. doi: 10.1073/pnas.1514265112

Smagulova, F., Gregoretti, I. V., Brick, K., Khil, P., Camerini-Otero, R. D., and Petukhova, G. V. (2011). Genome-wide analysis reveals novel molecular features of mouse recombination hotspots. *Nature* 472, 375–378. doi: 10.1038/nature09869

Smithies, O., and Powers, P. A. (1986). Gene conversions and their relation to homologous chromosome pairing. *Philos. Trans. R. Soc. Lond. B* 312, 291–302. doi: 10.1098/rstb.1986.0008

Stack, S. M., and Anderson, L. K. (2002). Crossing over as assessed by late recombination nodules is related to the pattern of synapsis and the distribution of early recombination nodules in maize. *Chromosome Res.* 10, 329–345. doi: 10.1023/A:1016575925934

Stadler, L. J., and Emmerling, M. H. (1956). Relation of unequal crossing over to the interdependence of Rr elements (P) and (S). *Genetics* 41, 124–137.

Stapley, J., Feulner, P. G. D., Johnston, S. E., Santure, A. W., and Smadja, C. M. (2017). Variation in recombination frequency and distribution across eukaryotes: patterns and processes. *Philos. Trans. R. Soc. B* 372:20160455. doi: 10.1098/rstb.2016.0455

Sukhapinda, K., and Peterson, P. A. (1980). Enhancement of genetic exchange in maize: intragenic recombination. *Can. J. Genet. Cytol.* 22, 213–222. doi: 10.1139/g80-026

Szostak, J. W., Orr-Weaver, T. L., Rothstein, R. J., and Stahl, F. E. (1983). The double-strand-break repair model for recombination. *Cell* 33, 25–35. doi: 10.1016/0092-8674(83)90331-8

Thuriaux, P. (1977). Is recombination confined to structural genes on the eukaryotic genome? *Nature* 268, 460–462. doi: 10.1038/268460a0

Tischfield, S. E., and Keeney, S. (2012). Scale matters. *Cell Cycle* 11, 1496–1503. doi: 10.4161/cc.19733

Varas, J., Sánchez-Morán, E., Copenhaver, G. P., Santos, J. L., and Pradillo, M. (2015). Analysis of the relationships between DNA double-strand breaks, synaptonemal complex and crossovers using the *Atfas1-4* mutant. *PLoS Genet.* 11:e1005301. doi: 10.1371/journal.pgen.1005301

Wang, G., Xu, J., Tang, Y., Zhou, L., Wang, F., Xu, Z., et al. (2011). Molecular characterization of a genomic interval with highly uneven recombination distribution on maize chromosome 10 L. *Genetica* 139, 1109–1118. doi: 10.1007/s10709-011-9613-x

Wang, Y., and Copenhaver, G. P. (2018). Meiotic recombination: mixing it up in plants. *Annu. Rev. Plant Biol.* 69, 577–609. doi: 10.1146/annurev-arplant-042817-040431

Wei, F., Zhang, J., Zhou, S., He, R., Schaeffer, M., Collura, K., et al. (2009). The physical and genetic framework of the maize B73 genome. *PLoS Genet.* 5:e1000715. doi: 10.1371/journal.pgen.1000715

Wessler, S., Tarpley, A., Purugganan, M., Spell, M., and Okagaki, R. (1990). Filler DNA is associated with spontaneous deletions in maize. *Proc. Natl. Acad. Sci. U.S.A.* 87, 8731–8735. doi: 10.1073/pnas.87.22.8731

Wijnker, E., James, G. V., Ding, J., Becker, F., Klasen, J. R., Rawat, V., et al. (2013). The genomic landscape of meiotic crossovers and gene conversions in *Arabidopsis thaliana*. *eLife* 2:e01426. doi: 10.7554/eLife.01426

Xu, X., Hsia, A. P., Zhang, L., Nikolau, B. J., and Schnable, P. S. (1995). Meiotic recombination break points resolve at high rates at the 5' end of a maize coding sequence. *Plant Cell* 7, 2151–2161. doi: 10.1105/tpc.7.12.2151

Yamada, S., Ohta, K., and Yamada, T. (2013). Acetylated Histone H3K9 is associated with meiotic recombination hotspots, and plays a role in recombination redundantly with other factors including the H3K4 methylase Set1 in fission yeast. *Nucl. Acids Res.* 41, 3504–3517. doi: 10.1093/nar/gkt049

Yandeau-Nelson, M. D., Xia, Y., Li, J., Neuffer, M. G., and Schnable, P. S. (2006). Unequal sister chromatid and homolog recombination at a tandem duplication of the *a1* locus in maize. *Genetics* 173, 2211–2226. doi: 10.1534/genetics.105.05271

Yao, H., and Schnable, P. S. (2005). Cis-effect on meiotic recombination across distinct *a1-sh2* intervals in a common Zea genetic genetic background. *Genetics* 170, 1929–1944. doi: 10.1534/genetics.104.034454

Yao, H., Zhou, Q., Li, J., Smith, H., Yandeau, M., Nikolau, B. J., et al. (2002). Molecular characterization of meiotic recombination across the 140-Kb multigenic *a1-sh2* interval of maize. *Proc. Natl. Acad. Sci. U.S.A.* 99, 6157–6162. doi: 10.1073/pnas.082562199

Yelina, N. E., Lambing, C., Hardcastle, T. J., Zhao, X., Santos, B., and Henderson, I. R. (2015). DNA methylation epigenetically silences crossover hot spots and controls chromosomal domains of meiotic recombination in *Arabidopsis*. *Genes Dev.* 29, 2183–2202. doi: 10.1101/gad.270876.115

Yu, M.-H., and Peterson, P. A. (1973). Influence of chromosomal gene position on intragenic recombination in maize. *Theor. Appl. Genet.* 43, 121–133. doi: 10.1007/BF00306561

Conflict of Interest Statement: The authors declare that the research was conducted in the absence of any commercial or financial relationships that could be construed as a potential conflict of interest.

frontiers in Plant Science

ORIGINAL RESEARCH
published: 16 July 2018
doi: 10.3389/fpls.2018.01005

ZmCom1 Is Required for Both Mitotic and Meiotic Recombination in Maize

*Yazhong Wang†, Luguang Jiang†, Ting Zhang, Juli Jing and Yan He**

MOE Key Laboratory of Crop Heterosis and Utilization, National Maize Improvement Center of China, China Agricultural University, Beijing, China

CtIP/Ctp1/Sae2/Com1, a highly conserved protein from yeast to higher eukaryotes, is required for DNA double-strand break repair through homologous recombination (HR). In this study, we identified and characterized the COM1 homolog in maize. The *ZmCom1* gene is abundantly expressed in reproductive tissues at meiosis stages. In *ZmCom1*-deficient plants, meiotic chromosomes are constantly entangled as a formation of multivalents and accompanied with chromosome fragmentation at anaphase I. In addition, the formation of telomere bouquet, homologous pairing and synapsis were disturbed. The immunostaining assay showed that the localization of ASY1 and DSY2 was normal, while ZYP1 signals were severely disrupted in *Zmcom1* meiocytes, indicating that *ZmCom1* is critically required for the proper SC assembly. Moreover, RAD51 signals were almost completely absent in *Zmcom1* meiocytes, implying that COM1 is required for RAD51 loading. Surprisingly, in contrast to the *Atcom1* and *Oscom1* mutants, *Zmcom1* mutant plants exhibited a number of vegetative phenotypes under normal growth condition, which may be partly attributed to mitotic aberrations including chromosomal fragmentation and anaphase bridges. Taken together, our results suggest that although the roles of *COM1* in HR process seem to be primarily conserved, the *COM1* dysfunction can result in the marked dissimilarity in mitotic and meiotic outcomes in maize compared to Arabidopsis and rice. We suggest that this character may be related to the discrete genome context.

Keywords: maize, meiosis, HR, DSB, COM1

OPEN ACCESS

Edited by:
Mónica Pradillo, Complutense University of Madrid, Spain

Reviewed by:
Chung-Ju Rachel Wang, Academia Sinica, Taiwan
Isabelle Colas, The James Hutton Institute, United Kingdom

****Correspondence:***
Yan He
yh352@cau.edu.cn

† These authors have contributed equally to this work.

Specialty section:
This article was submitted to Plant Cell Biology, a section of the journal Frontiers in Plant Science

Received: *28 March 2018*
Accepted: *20 June 2018*
Published: *16 July 2018*

Citation:
Wang Y, Jiang L, Zhang T, Jing J and He Y (2018) ZmCom1 Is Required for Both Mitotic and Meiotic Recombination in Maize. Front. Plant Sci. 9:1005. doi: 10.3389/fpls.2018.01005

INTRODUCTION

Meiosis is a highly conserved process producing haploid germ cells from diploid progenitors and is essential for all sexually reproductive organisms. It includes one round of DNA replication followed by two sequential rounds of cell division containing meiosis I and meiosis II (Zickler and Kleckner, 1999). During meiosis I, crossovers (COs) are formed to ensure the accurate segregation of homologous chromosomes (Mercier et al., 2015; Gray and Cohen, 2016). Homologous recombination (HR) is a prerequisite to the generation of COs. In plants, meiotic recombination is initiated by the programmed introduction of double-strand breaks (DSBs) mediated by SPO11, a conserved type II topoisomerase, and several accessory proteins (Keeney et al., 1997). The resulting DSB ends are resected by a protein complex, MRX/N (Mre11-Rad50-Xrs2/Nbs1) and Sae2/Com1/CtIP/Ctp1, to generate extended single-stranded DNA (ssDNA) overhangs, which are subsequently stabilized by replication protein A (RPA) (Borde, 2007). Next, RPA is displaced by RAD51 and DMC1 to form nucleoprotein filaments that can facilitate homologous pairing and

single-end invasion of a non-sister chromatid resulting in the formation of joint molecule (JM) intermediates (Hunter and Kleckner, 2001). Ultimately, these events give rise to either COs or non-crossovers (NCOs) (Allers and Lichten, 2001).

The evolutionarily conserved MRX/N complex functions as one of the critical guardians of genome integrity in eukaryotes and is required for DNA damage repair, cell-cycle checkpoint and telomere maintenance during both mitosis and meiosis (Daoudal-Cotterell et al., 2002; Borde, 2007; Amiard et al., 2010). The three proteins (Mre11, Rad50, and Nbs1/Xrs2) in MRX/N complex play distinct roles. Mre11 specifies 3′ to 5′ exonuclease activity on the double-stranded DNA and endonuclease activity on the single-stranded DNA as well as limited helicase activity (Puizina et al., 2004; Altun, 2008). Rad50 has two long coiled-coil domains that interact with one another to form a head-to-tail dimer to enable the binding of Mre11 and DNA (Carney et al., 1998; Hopfner et al., 2002). NBS1 is phosphorylated by ATM to link the detection of DSBs to signaling events (Waterworth et al., 2007). Null mutations in genes encoding any component of MRX/N complex result in lethality in mammals (Paull and Gellert, 1998), whereas Arabidopsis *mre11* and *rad50* mutants are viable but fully sterile (Daoudal-Cotterell et al., 2002; Puizina et al., 2004; Samanic et al., 2013). In contrast, the loss-of-function of Arabidopsis *NBS1* displays normal growth under standard conditions and shows no defects in fertility (Waterworth et al., 2007). In addition, Arabidopsis mutants defective MRX/N complex in exhibit distinct hypersensitivity to various genotoxic stresses, reflecting both common and unique features of each component of MRX/N complex acting in the different spectrum of DNA lesions and mechanism of their repair (Vannier et al., 2006; Cassani et al., 2018).

As a cofactor for MRX/N, the mammalian CtIP and its fission yeast (Ctp1), budding yeast (Sae2), and plant (Com1) orthologs play the multifunctional roles in directing DSB repair pathway choice and modulate repair activities (McKee and Kleckner, 1997; Prinz et al., 1997; Baroni et al., 2004; Chen et al., 2005; Lengsfeld et al., 2007; Limbo et al., 2007; Penkner et al., 2007; Sartori et al., 2007; Uanschou et al., 2007; Lee-Theilen et al., 2010; Ji et al., 2012). The plant homolog of *CtIP/Ctp1/Sae2/Com1* was first identified in Arabidopsis (Uanschou et al., 2007) and later in rice (Ji et al., 2012). *Atcom1* and *Oscom1* mutant plants exhibit normal vegetative growth but complete male and female sterility (Uanschou et al., 2007; Ji et al., 2012). Cytological investigations revealed that meiosis is severely inhibited, due to the defective homologous pairing and massive chromosome fragmentation (Uanschou et al., 2007; Ji et al., 2012). These studies demonstrate that the function of *Com1* homolog in controlling DSB resection is conserved in plants as in other organisms.

In contrast to Arabidopsis and rice, maize has a large genome (ca. 2.3 Gb) and fairly complex genome organization. Here, we characterize the *Com1* in maize using a reverse genetic approach. Our results demonstrate that *ZmCom1* is essential for DSB repair and HR, establishing the telomere bouquet and SC assembly in maize meiosis. We also show that *ZmCom1* is required for mitosis to occur normally in vegetative cells. These results imply that although the roles of *Com1* in DSB repair seem to be fundamentally conserved in diverse plant species, the precise behavior of *Com1* may vary in the different plant organisms.

MATERIALS AND METHODS

Plant Materials and Genotyping

Uniform*Mu* mutant lines, UF*Mu*-01240 (*Zmcom1-1*) and UF*Mu*-09026 (*Zmcom1*-2) induced by Robertsons *Mutator* transposons in the uniform W22 inbred line were obtained from Maize Stock Center and backcrossed with the W22 inbred line four times before the further analysis. All plants were grown in field or greenhouse in 2014–2017 under the normal growth condition. Genomic DNA extraction and genotyping were conducted as described previously (Li et al., 2013). To confirm a presence of the *Mutator* insertion, genomic DNA of both mutant lines was amplified with the primer pair of *Mu*TIR and COM1-L2 (**Supplementary Table S1**) and then PCR product was subject to Sanger sequencing.

Observation of Pollen Viability

Pollen viability was assessed by Alexander staining using previously described methods (Alexander, 1969; Johnson-Brousseau and McCormick, 2004). Anthers were collected from the wild type and *Zmcom1* mutants during anthesis stage. Pollen grains were dissected out of anthers in Alexander solution and analyzed under Leica EZ4 HD. The pictures of strained pollen grains were taken using the microscope (Leica DM2000 LED).

cDNA Cloning, RT-PCR and RT-qPCR Analysis

Total RNA was extracted from roots, stems, leaves, developing embryos (16 days after pollination), endosperm (16 days after pollination), meiotic ears as well as anthers of B73 plants and young ear of *Zmcom1* plants, and was then reverse-transcribed into cDNA by TaKaRa kits following manufacturer's instructions. The full-length cDNA was generated using the TransStart FastPfu Fly DNA Polymerase kit (TransGen). PCR primers used for RT-PCR and RT-qPCR are listed in **Supplementary Table S1**. The maize *UBIQUITIN* gene was used as a control standard for all tissues. RT-qPCR analysis was performed using the 7500 Fast Real-Time PCR System (Applied Biosystems).

Subcellular Localization

The coding sequence of *ZmCOM1* was amplified with the primer pair PCUN-COM1 (**Supplementary Table S1**) and sub-cloned into of the pCUN+GFP vector using the *Bam*HI and *Spe*I sites to create an ORF encoding an EGFP fusion protein driven by the 35S promoter. Mesophyll protoplasts were isolated from the second leaves of 2-week-old etiolated B73 seedlings according to the method described previously (Yoo et al., 2007) and transformed with the prepared plasmids using the polyethylene glycol (PEG) mediated transformation method as previously described (Yoo et al., 2007). The protoplasts were cultured at 25°C in the dark for 18 h and observed under a confocal laser scanning microscope (Leica sp5).

Preparation of Mitotic Chromosome Spreads

Chromosome spreads were prepared as described previously (Kato et al., 2004). Kernels were soaked for a night in sterile water before germinating at 30°C for 2–3 days. Root tips of 1–2 cm length were dissected and fixed in a 3:1 mixture of 95% ethanol: glacial acetic acid for 30 min in a vacuum environment and finally stored in 70% ethanol at −20°C until use. After washing in water on ice, the root apical meristem containing dividing cells was dissected and digested in 50 μl enzyme mix containing 1% pectolyase Y23 (ICN) and 2% cellulase Onozuka R-10 (Yakult Pharmaceutical, Tokyo) for 65 min at 37°C. After digestion, the root sections were washed in ice-cold distilled water and then briefly washed in 70% ethanol for three times. The root sections were carefully broken using a needle and vortexed at maximum speed in 75% ethanol for 30 s at room temperature to separate cells from each other. Cells were collected at the bottom of the tube by centrifugation and resuspended in 100% glacial acetic acid solution. Ten microliter of the cell suspension was dropped onto glass slides in a box lined with wet paper towels and dried slowly.

Preparation of Meiotic Chromosome Spreads

Chromosome spreads were prepared from tassels fixed in Carnoy's solution (3:1 ethanol: acetic acid, v/v). After infiltration for 30 min at room temperature, the tassels were stored in 75% ethanol at 4°C until observation. Squashes were made in a drop of 45% acetic acid. The microscope slides were frozen in liquid nitrogen and the coverslips were removed immediately. The slides were then dehydrated through an ethanol series (70% to 90% to 100%) for 5 min each and air dried. The chromosomes were stained with 4′, 6-diamidino-2-phenylindole (DAPI) in an antifade solution (Vector, H-1200, CA, United States). Images were captured using a Ci-S-FL microscope (Nikon, Tokyo) equipped with a DS-Qi2 Microscope Camera system.

FISH Analysis

The FISH procedure was performed as described previously (Li and Arumuganathan, 2001; Cheng, 2013). Plasmids carrying 5S rDNA repeats (pTa794) or the telomere-specific repeats (pAtT4) were used as FISH probes (Richards and Ausubel, 1988; Ji et al., 2012). The 5S rDNA-specific and telomere-specific probes were individually labeled with digoxigenin by nick translation (Roche, Cat.No.11745808910) and detected with a fluorescein isothiocyanate (FITC) conjugated anti-digoxigenin antibody (Vector Laboratories). The chromosomes were counterstained with DAPI in Vectashield antifade solution (Vector laboratories). Chromosome spreads were observed under a Ci-S-FL fluorescence microscope (Nikon) and captured with a DS-Qi2 Microscope Camera.

Fluorescence Immunolocalization

Young anthers at the meiotic prophase (∼1.5–2.5 mm, Zhang et al., 2014) were fixed with 4% (w/v) paraformaldehyde in 1 × Buffer A for 30 min at room temperature (25°C), washed in 1 × Buffer A at room temperature and stored in 1 × Buffer A at 4°C for several months. The procedure of immunolocalization was performed as described previously (Pawlowski et al., 2003; Cheng, 2013). All primary (ASY1, DSY2, ZYP1, and RAD51) and secondary antibodies were used at a dilution of 1:100. The images were viewed with software NIS-Elements to generate 2D projected images. Surface rendered images were colored by the ImageJ software through the Merge Channels.

RESULTS

Identification of *ZmCom1* and Isolation of Its Mutants

A BLASTP search using the rice Com1 amino acid sequence was conducted in the maize genome database (MaizeGDB) and only one candidate gene model (GRMZM2G076617) with significant similarity was identified. The cDNA sequence, which was redefined by rapid amplification of cDNA ends (RACE) PCR, contains 2,134 bp with an open reading frame of 1,668 bp. The gene has two exons and one intron (**Figure 1A**). The protein sequence consists of 555 amino acids and shows 62% of identity and 72% of similarity to OsCom1 (363/583 residues identical and 421/583 residues positive, **Supplementary Figure S1**). ZmCom1 protein harbors an N-terminal SMC-N domain and a C-terminal SAE2 superfamily domain, both of which conventionally exist in Com1 homologs of other organisms (**Supplementary Figure S1**). Phylogeny analyses revealed that Com1 homologs form two distinct clades reflecting the divergence between monocots and dicots (**Supplementary Figure S2**).

By means of quantitative RT-PCR, we examined the tissue-specific expression pattern of *ZmCom1*. We found that *ZmCom1* is expressed most highly in meiotic ears and anthers, as well as in developing embryo, less in root and endosperm, and extremely low in leaf and stem (**Figure 1B**). These results support the function of *ZmCom1* in meiosis and mitosis. To elucidate the cellular localization of *ZmCom1*, we induced expression of the ZmCom1 fused to the EGFP under the control of the CaMV35S promoter in maize protoplasts. The GFP signal was revealed in nuclei (**Figure 1C**).

Two independent *Mutator* transposon insertion lines, UF*Mu*-01240 (*Zmcom1-1*) and UF*Mu*-09026 (*Zmcom1-2*), were identified in the public maize *Mutator* line database (Harper et al., 2016). By conducting locus-specific PCR amplification followed by Sanger sequencing, we confirmed that both insertion sites are within the first exon of *ZmCom1* (**Figure 1A**). RT-PCR with primers flanking the *Mutator* insertion sites failed to detect the *ZmCom1* transcripts (**Figure 1D**), indicating that both mutants are null. The heterozygous alleles of both mutants did not exhibit any obvious defects during either the vegetative or reproductive stages in comparison to the wild type. However, we constantly observed a proportion of small kernels in the offspring of self-pollinated heterozygous plants for both mutations (**Figure 1E** and **Supplementary Figure S3A**), and the ratio of small to normal seeds was not significantly different from the expected

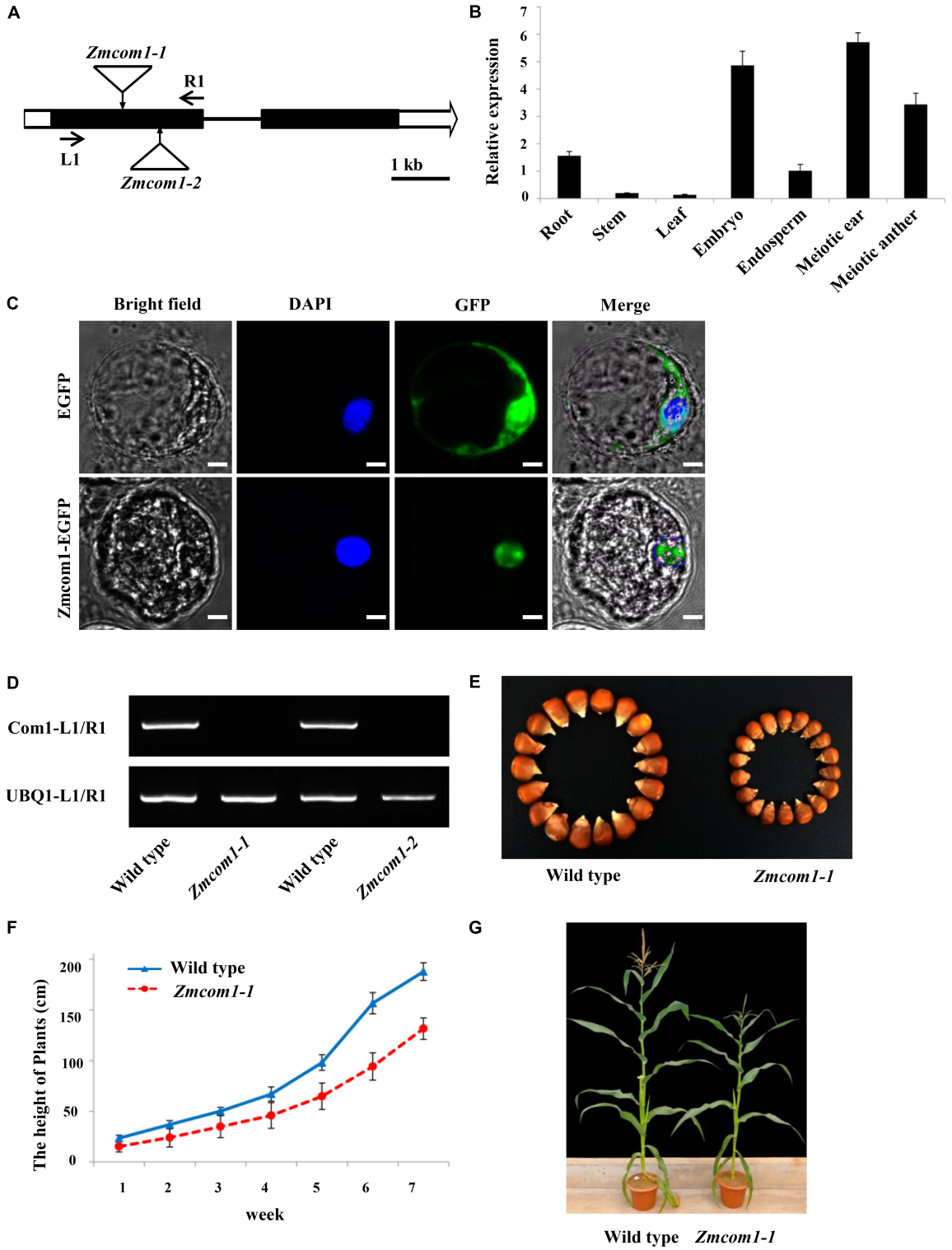

FIGURE 1 | Characterization of the *ZmCom1* gene. **(A)** Diagram of genomic structures of the *ZmCom1* genes with Mutator transposon insertion sites marked with triangles. Bars indicate exons and lines represent introns. Scale bar = 1 kb. **(B)** RT-qPCR analysis of *ZmCom1* transcription in different tissues. Expression levels relative to the expression level of the UBQ1 gene are presented with standard errors. Values are means of three independent experiments. **(C)** ZmCom1 protein is localized to nucleus in maize protoplasts. Scale bar = 5 μm. **(D)** RT-PCR analysis of *ZmCom1* transcript in different genotypes. The maize *UBQ1* gene was used as an internal control. **(E)** Morphological comparison of mature seeds between wild type and *Zmcom1-1* mutant. **(F)** Growth-curve of plant height in wild type and *zmcom1-1* mutant plants. Values are means of 10 individual plants. **(G)** Morphological comparison of mature plants between wild type and *Zmcom1-1* mutant.

1:3 ratio (Chi-square test, $P > 0.05$; **Supplementary Table S2**). More importantly, PCR analyses confirmed that these small kernels co-segregated with homozygous *Zmcom1* genotype (**Supplementary Figure S4**), indicating that the loss-of-function of *ZmCom1* has an effect on maize seed development. The overall statue of *Zmcom1* plants seemed to be comparable to wild type, but obvious dwarf phenotype started appearing from first weeks until the maturity (**Figures 1F,G** and **Supplementary Figures S3B,C**).

The *Zmcom1* plants reached the anthesis stage at the same time as wild type but were completely male sterile (**Figure 2A** and **Supplementary Figure S3D**). When pollinated with normal pollen grains from the wild type, the *Zmcom1* plants could not set any seeds (**Figure 2B** and **Supplementary Figure S3E**), suggesting that megagametogenesis was aborted. To investigate the male sterility, *Zmcom1* and wild type pollen grains were stained with the Alexander solution (**Figures 2C,D** and **Supplementary Figure S3F,G**). Pollen grains from the wild type were round (**Figure 2C** and **Supplementary Figure S3F**), while those from *Zmcom1* plants were empty and shrunken (**Figure 2D** and **Supplementary Figure S3G**), indicating that microspore development was also aborted. Taken together, these results indicate that the disruption of *ZmCom1* gene leads to defects in both vegetative and reproductive development.

Abnormal Chromosome Behavior in *Zmcom1*

To establish the cause of sterility in the *Zmcom1* mutant, we examined the meiotic chromosome behavior in pollen mother cells (PMCs) of both wild type and *Zmcom1-1* plants using 4′,6-diamidino-2-phenylindole (DAPI) staining (**Figure 3**). In the wild type, the chromosomes appeared as thin threads

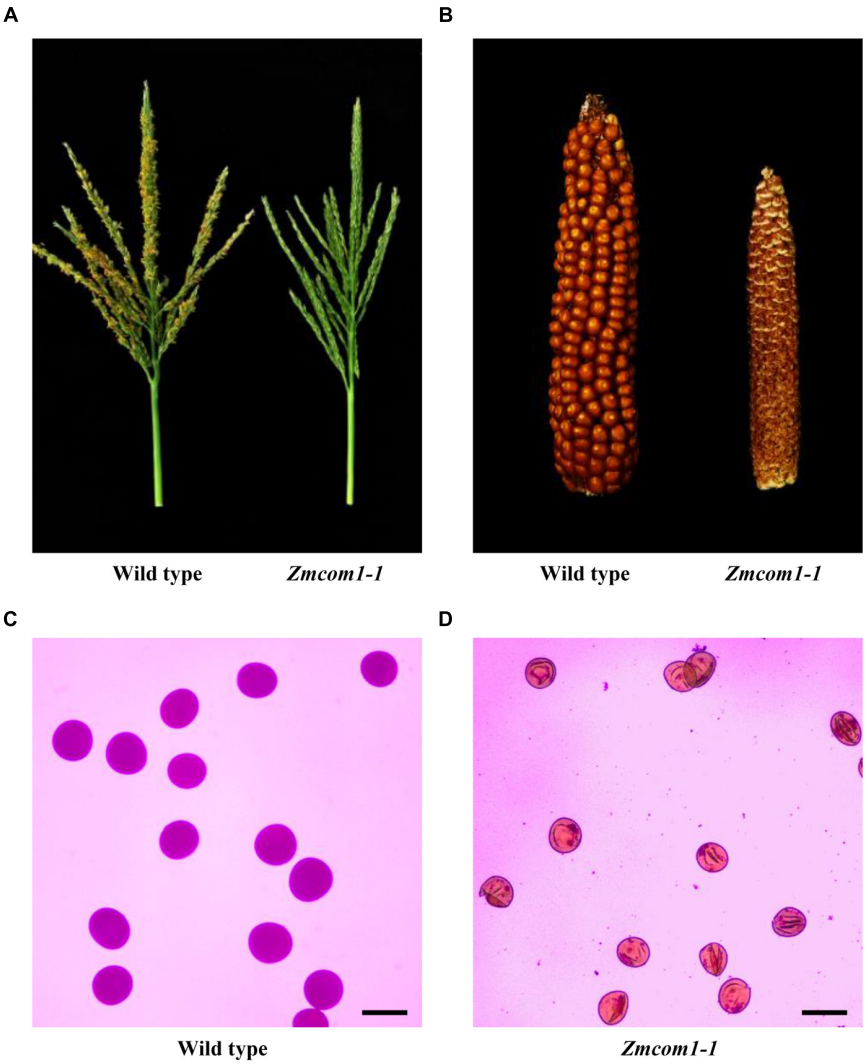

FIGURE 2 | Male and female sterility of *Zmcom-1* mutant plants. **(A)** Comparison of a wild type tassel and a *Zmcom1-1* tassel at the flowering stage. **(B)** Comparison of a wild type ear and a *Zmcom1-1* ear. **(C)** Normal pollen grains of the wild type. Scale bar = 100 μm. **(D)** Complete sterile pollen grains of the *Zmcom1-1* plant. Scale bar = 100 μm.

at leptotene (**Figure 3A**), and homologous chromosomes underwent pairing and synapsis during zygotene (**Figure 3B**). At pachytene, homologous chromosomes completed synapsis and chromosomes appeared as thick threads (**Figure 3C**). During diakinesis, chromosomes became condensed, and 10 short bivalents connected by chiasmata were observed in nuclei (**Figure 3D**). At metaphase I, all 10 bivalents aligned in an orderly manner on the equatorial plate (**Figure 3E**), and homologous chromosomes separated and migrated to opposite poles at anaphase I (**Figure 3F**). Finally, all chromosomes reached the two poles at telophase I to form regular dyads (**Figure 3G**). During meiosis II, sister chromatids separated from each other, ultimately giving rise to tetrad (**Figure 3H**).

In *Zmcom1* mutant, meiotic chromosomes behaved normally at leptotene (**Figure 3I** and **Supplementary Figure S5A**).

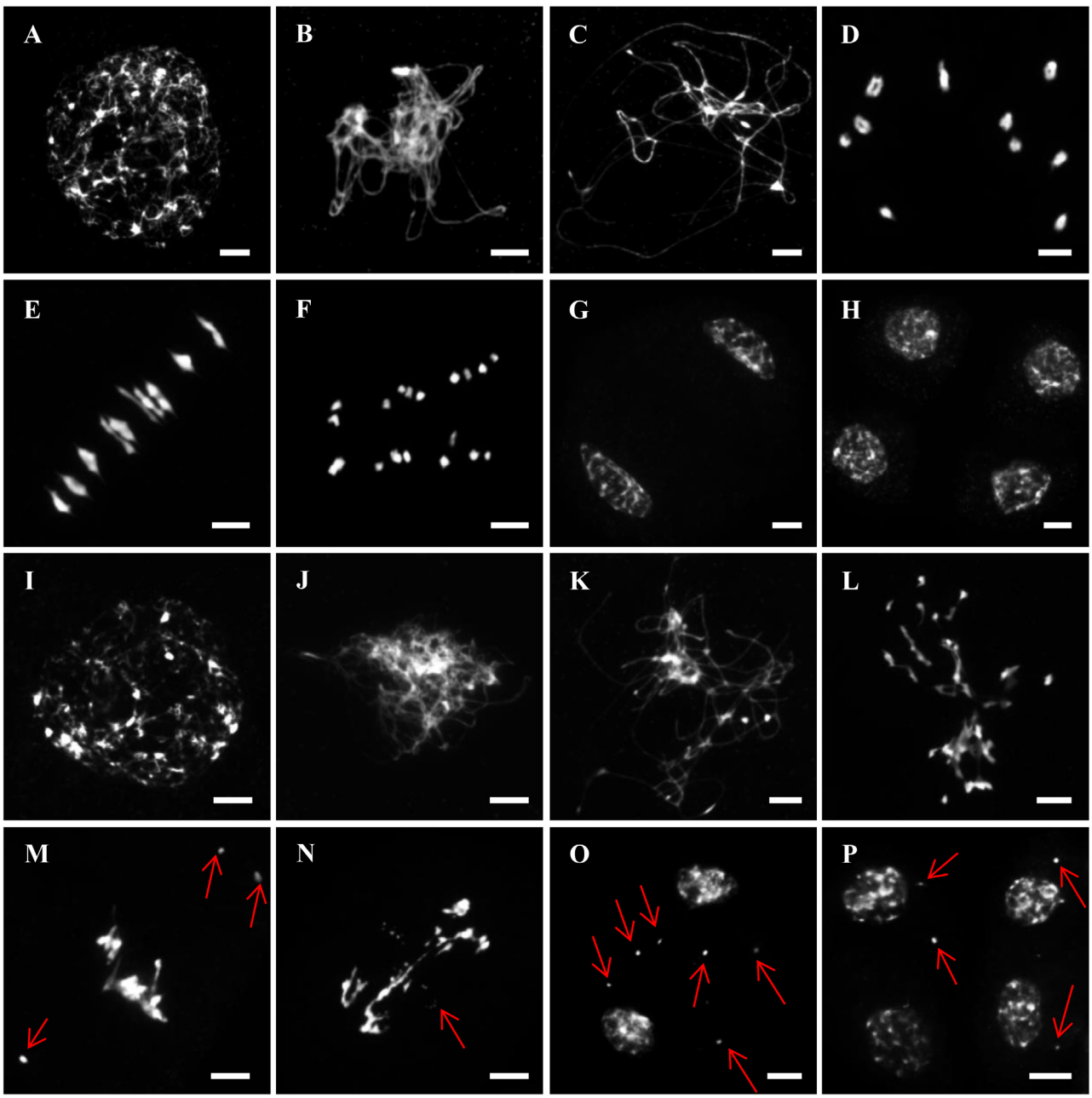

FIGURE 3 | Male meiosis in wild type and *Zmcom1-1*. **(A–H)** Meiosis in wild type. **(A)** Leptotene; **(B)** Zygotene; **(C)** Pachytene; **(D)** Diakinesis; **(E)** Metaphase I; **(F)** Anaphase I; **(G)** Dyad; **(H)** Tetrads. Scale bars = 10 μm. **(I–P)** Meiosis in *Zmcom1-1*. **(I)** Leptotene; **(J)** Zygotene; **(K)** Pachytene; **(L)** Diakinesis; **(M)** Metaphase I; **(N)** Anaphase I; **(O)** Dyad; **(P)** Tetrads. The red arrows pointed out the chromosomal fragments and abnormal bridges. Scale bars = 10 μm.

However, the chromosomes remained as single threads and did not pair with their homologs during zygotene and pachytene (**Figures 3J,K** and **Supplementary Figures S5B,C**). Irregularly shaped univalents were scattered throughout the entire nucleus during diakinesis (**Figure 3L** and **Supplementary Figure S5D**). At metaphase I, chromosomes intertwined into a block, and chromosome fragments appeared as small dots (**Figure 3M** and **Supplementary Figure S5E**). During anaphase I, these entangled chromosomes separated, resulting in unequal segregation of chromosomes to the opposite poles. Chromosome bridges were constantly observed and chromosome fragments remained at the equatorial plate (**Figure 3N** and **Supplementary Figure S5F**). Although most chromosomes had arrived in the two poles at telophase I, many lagging fragments were still randomly scatted within the nucleus (**Figure 3O** and **Supplementary Figure S5G**). After the second division, abnormal tetrads with several micronuclei were eventually generated (**Figure 3P** and **Supplementary Figure S5H**). Therefore, we concluded that the sterility of the *Zmcom1* mutant may be caused by deficiency in homologous chromosome pairing, synapsis, and profound chromosomal fragmentation.

Defective Telomere Bouquet Formation and Homologous Pairing in *Zmcom1*

Telomere bouquet clustering, a particular event in early prophase I, may facilitate the initiation of homologous pairing (Golubovskaya et al., 2002; Harper et al., 2004; Klutstein et al., 2015). To explore the pairing defects in *Zmcom1*, we conducted fluorescent *in situ* hybridization (FISH) analysis using the telomere-specific probe in wild type and *Zmcom1* meiocytes (**Figures 4A,B** and **Supplementary Figure S6A**). In wild type meiocytes ($n = 46$), 97.8% of the telomere signals attached to the nuclear envelop and were clustered at early zygotene stage, displaying a typical telomere bouquet formation (**Figure 4A**). However, in *Zmcom1* meiocytes ($n = 55$ and 41 for *Zmcom1-1* and *Zmcom1-2*, respectively), telomeres did not cluster within a certain region but scattered throughout the nucleus (**Figure 4B** and **Supplementary Figure S6A**), indicating

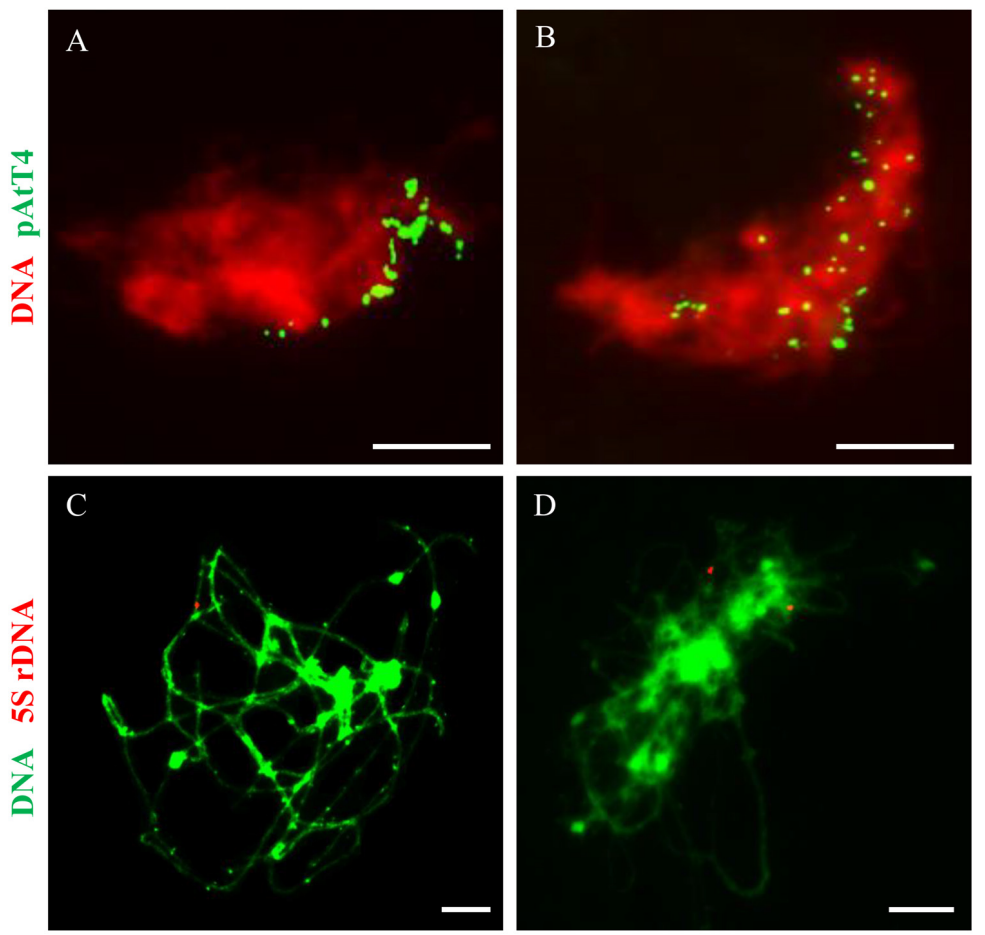

FIGURE 4 | *ZmCom1* is essential for bouquet formation and homologous pairing. **(A,B)** Bouquet formation analysis using FISH with the telomere-specific pAtT4 probe in in the wild type **(A)** and *Zmcom1-1* **(B)**. Scale bars = 10 μm. **(C,D)** Homologous pairing analysis using FISH with 5S rDNA probe in in the wild type **(C)** and *Zmcom1-1* **(D)**. Scale bars = 10 μm.

that the telomere bouquet formation was defective in the *Zmcom1* mutants.

To further determine chromosome pairing behavior in *Zmcom1* mutant, we performed FISH experiments using 5S rDNA as probes in wild type and *Zmcom1* meiocytes (**Figures 4C,D** and **Supplementary Figure S6B**). 5S rDNA is a tandemly repetitive sequence that only locates on the distal regions of the long arm of chromosome 2 (Li and Arumuganathan, 2001). In wild type meiocytes ($n = 32$), only one 5S rDNA signal was detected at pachytene stage (**Figure 4C**), indicating that two homologous chromosomes had been well paired. In contrast, two separate 5S rDNA signals were detected in *Zmcom1* meiocytes ($n = 38$ and 27 for *Zmcom1-1* and *Zmcom1-2*, respectively) (**Figure 4D** and **Supplementary Figure S6B**). These results further confirmed that homologous chromosome paring was deficient in *Zmcom1*.

Normal Axial Element Installation but Deficient Central Element Installation in *Zmcom1*

The SC consists of two parallel lateral elements (LEs – former axial elements – AEs) and one central element (CE). To investigate whether the SC was properly assembled in *Zmcom1-1*, we conducted immunostaining analysis using antibodies against the maize SC components ASY1, DSY2, and ZYP1. ASY1, a homolog of rice PAIR2, is the AE protein which plays pivotal roles in bouquet formation, homologous pairing and the SC assembly (Sanchez-Moran et al., 2008; Wang et al., 2011). We found that ASY1 distribution on chromosomes in *Zmcom1-1* meiocytes ($n = 42$) was similar to that in wild type meiocytes ($n = 53$) (**Figures 5A,D**). DSY2, a homolog of rice PAIR3 and Arabidopsis ASY3, acts as a structural protein to connect the AE/LEs to the CE for the SC assembly (Wang et al., 2011; Ferdous et al., 2012; Lee et al., 2015). In *Zmcom1-1* meiocytes ($n = 56$), DSY2 also loaded regularly onto chromosomes during zygotene, and did not show any difference from the wild type ($n = 47$) (**Figures 5B,E**). We also investigated the installation of the AE components in *Zmcom1-2*, which was similar to those of *Zmcom1-1* (**Supplementary Figures S7A,B**). Therefore, we conclude that the loss-of-function of *ZmCom1* has no significant effect on the installation of the AEs.

ZYP1, a transverse filament protein, constitutes the CE of the SC in maize (Higgins et al., 2005; Wang et al., 2010; Barakate et al., 2014). In the wild type, ZYP1 was first detected as discontinuous foci at the leptotene stage during zygotene, and it gradually formed discontinuous linear signals. At pachytene, ZYP1 signals were aligned perfectly along the entire chromosome length ($n = 35$; **Figure 5C**). In the *Zmcom1-1* meiocytes, ZYP1 signals could not elongate to form linear signals and only present as punctate signals ($n = 63$; **Figure 5F**). We also investigated the installation of the CE component in *Zmcom1-2*, which was similar to those of *Zmcom1-1* (**Supplementary Figure S7C**). Taken together, we conclude that the SC assembly is deficient in *Zmcom1*.

ZmCom1 Is Critical for DSB Repair

The chromosome fragmentation observed in *Zmcom1-1* meiocytes suggests that DSBs could still maintain due to loss-of-function of *ZmCom1*, as it was observed in *Oscom1* (Ji et al., 2012) and *Atcom1* (Uanschou et al., 2007). To ascertain whether defective homologous pairing and synapsis in *Zmcom1* were correlated with the improper DSB repair, the RAD51 immunostaining experiment was performed in wild type and *Zmcom1-1* meiocytes. Loading of RAD51 onto the ssDNA serves as a cytological marker for DSB repair via HR in different organisms (Pawlowski et al., 2003). In the wild type zygotene meiocytes, a substantial number of RAD51 foci was observed ($n = 33$, **Figure 6A**). In contrast, a parallel experiment did not detect any RAD51 foci in *Zmcom1-1* ($n = 49$, **Figure 6B**) or *Zmcom1-2* meiocytes ($n = 36$, **Supplementary Figure S8**). These results indicate that *ZmCom1* is required for the proper recruitment/loading of RAD51 onto the chromosomes and further demonstrate a serious defect in DSB repair in *Zmcom1*.

Somatic Aberrations in *Zmcom1*

Unlike *Atcom1* and *Oscom1*, *Zmcom1* exhibited vegetative aberrations under standard growth conditions. To explore whether and how the loss-of-function of *ZmCom1* influences the mitotic process, we assessed the frequency of chromosomal instability in root apical meristem for wild type and *Zmcom1* plants. At prophase, there was no obvious deviation between the wild type and *Zmcom1-1* (**Figures 7A,D**). However, we consistently observed an increased occurrence of acentric fragments at mitotic metaphase in *Zmcom1-1* (10.5%, $n = 238$; **Figure 7E** and **Table 1**) compared to that in the wild type (0.3%, $n = 323$; **Figure 7B** and **Table 1**). Later, ∼12.8% of mitotic cells had bridges or chromosome fragments in *Zmcom1-1* anaphase ($n = 258$; **Figure 7F** and **Table 1**), significantly higher than ∼0.3% of that in the wild type ($n = 351$; **Figure 7C** and **Table 1**). We also investigated the mitotic process in *Zmcom1-2*, which was similar to that of *Zmcom1-1* (**Supplementary Figure S9**). These results suggest that *Zmcom1* mutant suffers somatic chromosomal destabilization even under the normal growth condition.

DISCUSSION

Role of *ZmCom1* in Maize Meiosis

The conserved roles of CtIP/Ctp1/Sae2/Com1 in meiosis have been identified in several organisms. Consistent with this, in the present study we show that the loss-of-function of the *ZmCom1* gene leads to chromosome fragmentation and defects in homologous pairing and synapsis during meiosis, indicating that also in maize, *Com1* is an essential element in DSB repair. However, the precise effect of Com1 homolog on chromosome behavior differs from other plant organisms.

Telomere bouquet formation, a specialized arrangement of chromosomes during early prophase of meiosis in which telomeres are clustered on the nuclear envelope, has been observed in some plant species, animals and fungi (Niwa et al., 2000; Harper et al., 2004; Ding et al., 2007). Numerous maize mutants exhibit the defective bouquet including *pam1*

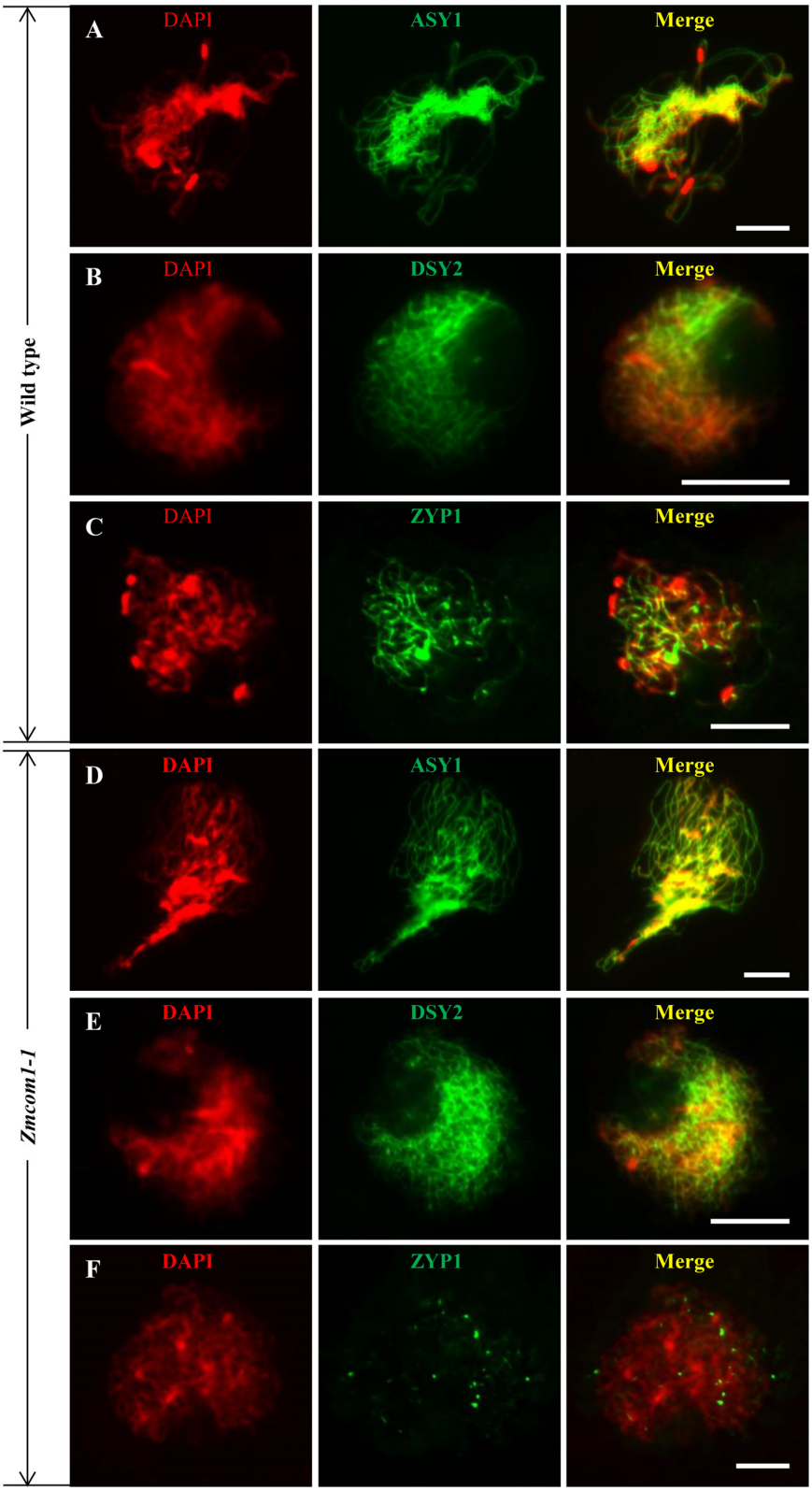

FIGURE 5 | Immunolocalization of ASY1, DSY2, and ZYP1 antibodies in the wild type and *Zmcom1-1*. **(A–C)** ASY1 **(A)**, DSY2 **(B)**, and ZYP1 **(C)** on prophase I chromosomes in the wild type. DAPI staining is used to indicate the chromosomes. Scale bars = 10 μm. **(D–F)** ASY1 **(D)**, DSY2 **(E)**, and ZYP1 **(F)** on prophase I chromosomes in *Zmcom1-1*. Scale bars = 10 μm.

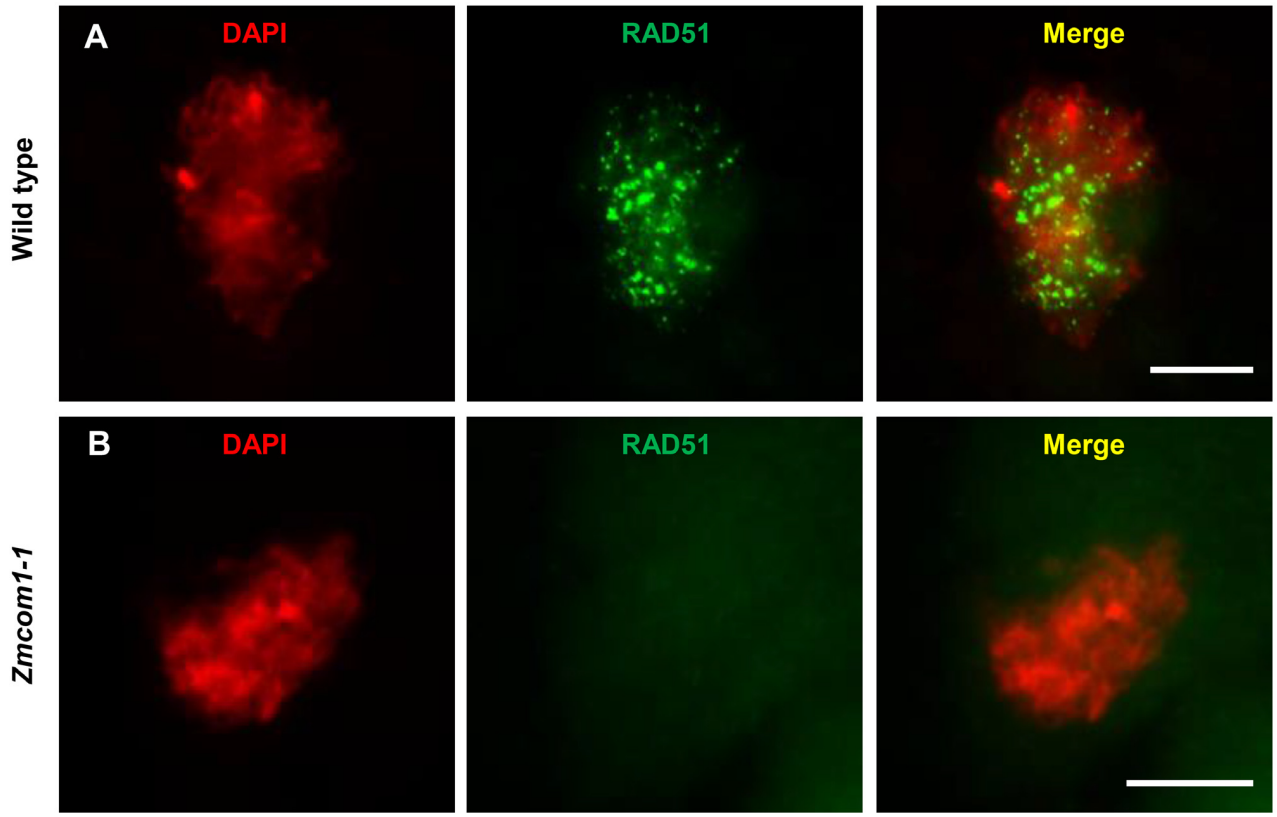

FIGURE 6 | Immunolocalization of RAD51 antibodies in the wild type and *Zmcom1-1* meioctyes at zygotene. **(A)** Wild type, **(B)** *Zmcom1-1* mutant. DAPI staining is used to indicate the chromosomes. Scale bars = 10 μm.

(Golubovskaya et al., 2002), *dy* (Murphy and Bass, 2012), *dsy1* (Bass et al., 2003), *afd1* (Golubovskaya et al., 2006), and *phs1* (Pawlowski et al., 2004), as well as the rice *pair3* (Wang et al., 2011) and *zygo1* (Zhang et al., 2017). Meanwhile, all these mutants also show the concurrent abnormality in homologous pairing, suggesting that the proper bouquet formation is a key event to facilitate homologous chromosome pairing (Zhang et al., 2017).

It is interesting that, the telomere bouquet formation is unaffected in the rice *com1* mutant and the telomere clustering is indistinguishable from that in the wild type (Ji et al., 2012), whereas in the maize *com1* mutants, a typical telomere clustering was never observed indicating that the Zm*Com1* gene is critically required for bouquet formation. Therefore, the remarkable difference between *ZmCom1* and *OsCom1* in mediating bouquet formation highlights the questions of why and how such character is conferred in different plant species. Also, the other intriguing question raised is whether the participation of *ZmCom1* in bouquet formation is restricted to its own character, or other members of MRN complex are also involved. Those questions would be of great interest in future studies.

Chromosome fragmentation and entanglements is a typical phenomenon observed in mutants deficient in DSB repair machinery. Our data showed that the *Zmcom1* mutant phenotype is similar to that of the *Oscom1* and *Atcom1* mutants, as well as other related mutants such as *Atmre11* (Samanic et al., 2013), *Atrad50* (Vannier et al., 2006), *Osxrcc3* (Zhang et al., 2015), and *Osrad51c* (Tang et al., 2014). However, chromosome segregation and the integrity of the tetrads seems to be less severe in *Zmcom1* compared to the *Oscom1* or *Atcom1* mutants. A simple explanation for this dissimilarity could be that the alternative DSB repair pathway, such as non-homologous end-joining (NHEJ) or microhomology-mediated end-joining (MMEJ) (McVey and Lee, 2008; Shrivastav et al., 2008), may be more actively stimulated in the absence of HR pathway in maize. In this scenario, *ZmCom1* act as a regulator to balance the different DSB repair pathways, a mechanism suggested in the previous studies (Ji et al., 2012). Therefore, it would be worth to investigate the meiotic consequences after combining mutation in *ZmCom11* with mutations in the genes involved in NHEJ and MMEJ pathway, which are largely unexplored yet in maize.

Role of *ZmCom1* in Maize Mitosis

Unrepaired DSBs are one of the most lethal types of DNA damage and highly threaten on chromosome stability and cell survival (Edlinger and Schlögelhofer, 2011). Beside the programmed induction during meiosis, DSBs can be triggered by both endogenous (e.g., transposition events of transposable elements (TEs), errors of oxidative metabolism, stalled, or

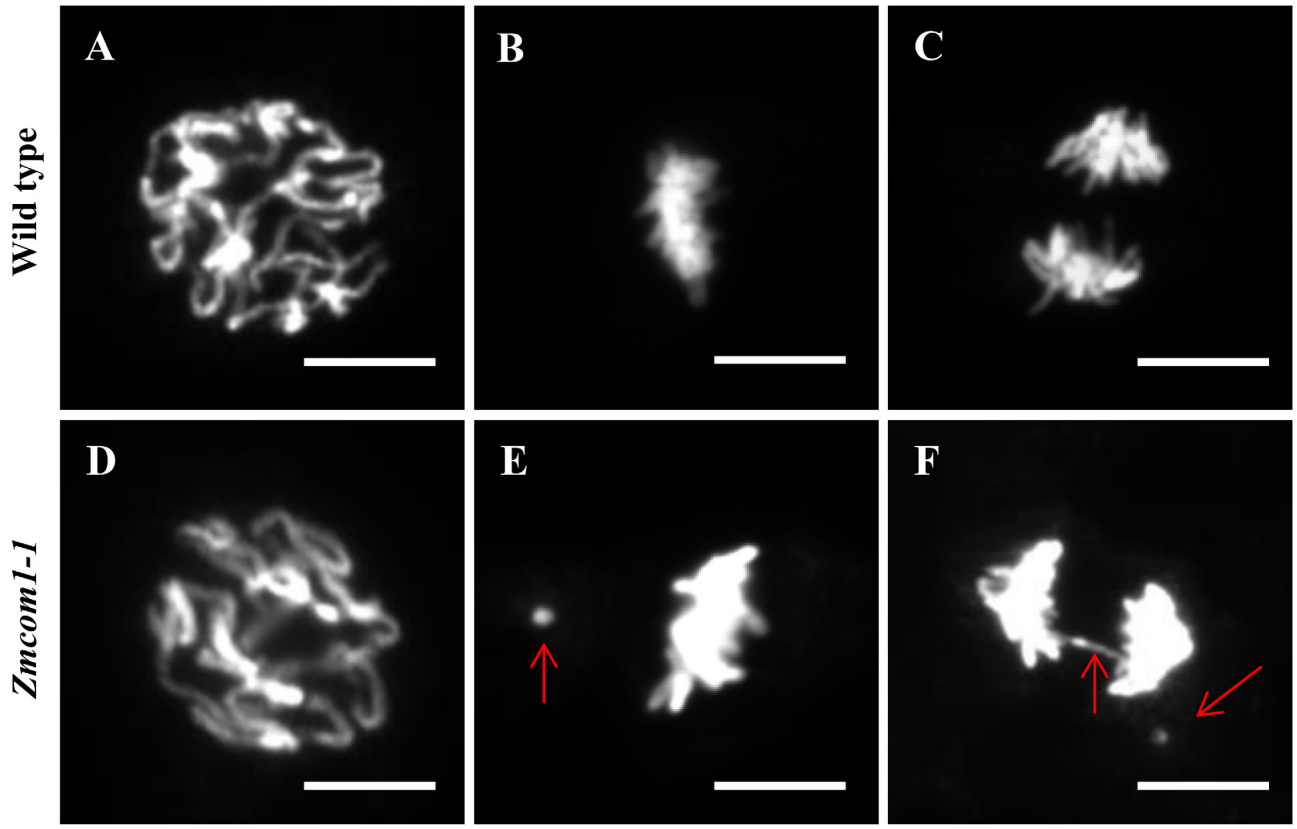

FIGURE 7 | Genome instability in mitotic cells from *Zmcom1-1* plants. **(A–C)** Wild type. **(A)** Prophase; **(B)** Metaphase; **(C)** Anaphase. Scale bars = 10 μm. **(D–F)** *Zmcom1-1*. **(D)** Prophase; **(E)** Metaphase; **(F)** Anaphase. Lagging.

TABLE 1 | Genome Instabilities in wild type and *Zmcom1* mitotic cells.

	Metaphase		Anaphase		
	No. of cell scored	**No. (percentage) of cell appearing fragment**	**No. of cell scored**	**No. (percentage) of cell appearing bridges**	**No. (percentage) of cell appearing fragments**
Wild type	323	1 (0.3%)	351	1 (0.3%)	0
Zmcom1-1	238	25 (10.5%)	258	18 (7.0%)	15 (5.8%)
Zmcom1-2	276	28 (10.1%)	231	15 (6.5%)	13 (5.6%)

collapsed replication forks) and exogenous sources (e.g., ionizing radiation or genotoxic stresses) in the vegetative growth period. Organisms have evolved two major pathways, HR and NHEJ, for repairing DSBs and maintaining genome integrity. Coordinated with MRX/N complex, CtIP/Ctp1/Sae2/Com1 plays a critical role in HR. Therefore it is not surprised to find that the mutation in those genes will result in the increased sensitivity toward various genotoxic stresses. Indeed, *Atcom1* mutants showed the retarded development of true leaves after treatment with mitomycin C (Uanschou et al., 2007). Meanwhile, without the special treatment, *Atcom1* mutant plants grew well, and did not show any vegetative phenotypes compared to the wild type. This is also the case for *Oscom1* mutant plants. Those results suggest that under the normal condition, the endogenous DSBs can be efficiently repaired in spite of lack of intact *Com1*–dependent HR in both Arabidopsis and rice. However, we observed some mitotic and vegetative abnormalities in *Zmcom1* mutants when plants were grown under standard environmental conditions. As the appearance of those vegetative phenotypes seems to be unique for *Zmcom1* mutants, we speculate that it can be attributed to the special feature of maize chromosomes. In contrast to Arabidopsis and rice, maize has a large genome with over 85% of TEs (Schnable et al., 2009; Andres and Williams, 2017). Although the mobility for the majority of TEs would be principally silenced by DNA methylation, a fraction of TEs still remains the activity for jumping around genome and driving genetic evolution (Mirouze and Vitte, 2014). In this context, maize genome may suffer from a greater frequency of transposition-derived DSBs compared to rice and Arabidopsis. Alternatively, alike mammalian cells

(Feng et al., 2016), the pervasive distribution of repetitive element on maize chromosomes may have a tendency to cause replication fork stalling and subsequent collapse of stalk fork, and can induce replication-associated DSBs (Nikolov and Taddei, 2016). In both scenarios, the Com1 activity is hypothetically required to maintain the genome integrity. Meanwhile, as both TE-transposition and the collapse of stalk fork frequently occur during the S-phase of the cell cycle, it would be also conceivable to explain how the disruption of *ZmCom*1 led to the abnormality in the seed development, a period when cells fast divide and proliferate.

AUTHOR CONTRIBUTIONS

YH conceived and supervised the project. YW, LJ, TZ, and JJ conducted the experiments. YW and YH prepared the manuscript. All authors read and approved the final manuscript.

FUNDING

This research was supported by the National Natural Science Foundation of China (31471172).

ACKNOWLEDGMENTS

We thank members of our laboratories for helpful discussion and assistance during this project. We are thankful to Chung-Ju Rachel Wang (Academia Sinica, Taiwan) for kindly providing us with ASY1, DSY2, and ZYP1 antibodies. In addition, we greatly thank Wojciech Pawlowski (Cornell University, United States) for gifting us RAD51 antibody. We thank Ljudmilla Timofejeva (Tallinn University of Technology, Estonia) for embellishing and critical reading of the article. Finally, we also greatly thank Weiwei Jin (China Agricultural University, China) for offering us the plasmids with 5S rDNA repeat and pAtT4 with telomeric repeats.

SUPPLEMENTARY MATERIALS

The Supplementary Material for this article can be found online at: https://www.frontiersin.org/articles/10.3389/fpls.2018.01005/full#supplementary-material

FIGURE S1 | Protein sequence alignment of ZmCom1 and OsCom1. The proteins were aligned with CLUSTALW and image was made by MultAlign (http://multalin.toulouse.inra.fr/multalin/). Conserved (>90% conservation) amino acid residues are red, variable (<50% conservation) are blue. Species abbreviation: Zm, *Zea mays*; Os, *Oryza sativa*. The red and green underlines indicate the conserved SMC-N and SAE2 domain, respectively.

FIGURE S2 | Neighbor-joining phylogeny reconstruction of Com1 homologs from different plant species. Numbers next to branches indicate posterior probability values. The scale indicates number of substitutions per site. Protein sequences were aligned using ClustalX (Jeanmougin et al., 1998) and phylogeny reconstruction was conducted using the online software (http://www.phylogeny.fr/, Dereeper et al., 2010). Species abbreviation: Zm, *Zea mays*; Os, *Oryza sativa*; Sb, *Sorghum bi*color; At, *Arabidopsis thaliana*; Bn, *Brassica napa*; Bd, *Brachypodium distachyon*; Hv, *Hordeum vulgare*; Ta, *Triticum aestivum*; Cs, *Camelina sativa*; Rs, *Raphanus sativus*; Es, *Eutrema salsugineum*.

FIGURE S3 | Morphological comparison between wild type and *Zmcom1-2* mutant. **(A)** Morphological comparison of mature seeds between wild type and *Zmcom1-2* mutant. **(B)** Growth-curve of plant height in wild type and *Zmcom1-2* mutant plants. Values are means of 10 individual plants. **(C)** Comparison of Morphological comparison of mature plants between wild type and *Zmcom1-2* mutant. **(D)** Comparison of a wild type tassel and a *Zmcom1-2* tassel at the flowering stage. **(E)** Comparison of a wild type ear and a *Zmcom1-2* ear. **(F)** Normal pollen grains of the wild type. Scale bar = 100 μm. **(G)** Complete sterile pollen grains of the *Zmcom1-2* plant. Scale bar = 100μm.

FIGURE S4 | PCR-based genotyping of seeds from self-propagated heterozygous *Zmcom1* plants. **(A)** F2 progeny of *Zmcom1-1*. 1–6: Seeds with normal size; 7–24: Seeds with small size. **(B)** F2 progeny of *Zmcom1-2*. 25–30: Seeds with normal size; 31–48: Seeds with small size.

FIGURE S5 | Male meiosis in *Zmcom1-2*. **(A)** Leptotene; **(B)** Zygotene; **(C)** Pachytene; **(D)** Diakinesis; **(E)** Metaphase I; **(G)** Anaphase I; **(F)** Dyad; **(H)** Tetrads. The red arrows pointed out the chromosomal fragments and abnormal bridges. Scale bars = 10 μm.

FIGURE S6 | The defective bouquet formation and homologous pairing in *Zmcom1-2*. **(A)** Bouquet formation analysis using FISH with the telomere-specific pAtT4 probe in *Zmcom1-2* ($n = 41$). Scale bars = 10 μm. **(B)** Homologous pairing analysis using FISH with 5S rDNA probe in in *Zmcom1-2* ($n = 27$). Scale bars = 10 μm.

FIGURE S7 | Immunolocalization of ASY1, DSY2, and ZYP1 antibodies in *Zmcom1-2*. ASY1 (**A**, $n = 23$), DSY2 (**B**, $n = 33$), and ZYP1 (**C**, $n = 37$) on prophase I chromosomes in *Zmcom1-2*. Scale bars = 10 μm.

FIGURE S8 | Immunolocalization of RAD51 antibodies in *Zmcom1-2* meioctyes ($n = 36$) at zygotene. DAPI staining is used to indicate the chromosomes. Scale bars = 10 μm.

FIGURE S9 | Genome instability in mitotic cells from *Zmcom1-2* plants. **(A)** Prophase; **(B)** Metaphase; **(C)** Anaphase. Lagging chromosome fragments and anaphase bridges were highlighted by red arrows. Scale bars = 10 μm.

TABLE S1 | Primers used in this study.

TABLE S2 | Segregation ratio of small seeds versus normal seeds.

REFERENCES

Alexander, M. P. (1969). Differential staining of aborted and nonaborted pollen. *Stain Technol.* 44, 117–122. doi: 10.3109/10520296909063335

Allers, T., and Lichten, M. (2001). Differential timing and control of noncrossover and crossover recombination during meiosis. *Cell* 106, 47–57. doi: 10.1016/S0092-8674(01)00416-0

Altun, C. (2008). *Maize Mre11 DNA Repair and Recombination Complex*. West Lafayette, IN: Purdue University.

Amiard, S., Charbonnel, C., Allain, E., Depeiges, A., White, C. I., and Gallego, M. E. (2010). Distinct roles of the ATR kinase and the Mre11-Rad50-Nbs1 complex in the maintenance of chromosomal stability in *Arabidopsis*. *Plant Cell* 22, 3020–3033. doi: 10.1105/tpc.110.078527

Andres, S. N., and Williams, R. S. (2017). CtIP/Ctp1/Sae2, molecular form fit for function. *DNA Repair* 56, 109–117. doi: 10.1016/j.dnarep.2017.06.013

Barakate, A., Higgins, J. D., Vivera, S., Stephens, J., Perry, R. M., Ramsay, L., et al. (2014). The synaptonemal complex protein ZYP1 is required for imposition of meiotic crossovers in barley. *Plant Cell* 26, 729–740. doi: 10.1105/tpc.113.121269

Baroni, E., Viscardi, V., Cartagena-Lirola, H., Lucchini, G., and Longhese, M. P. (2004). The functions of budding yeast SAE2 in the dna damage response require Mec1- and tel1-dependent phosphorylation. *Mol. Cell. Biol.* 24, 4151–4165. doi: 10.1128/MCB.24.10.4151-4165.2004

Bass, H. W., Bordoli, S. J., and Foss, E. M. (2003). The desynaptic (dy) and desynaptic1 (dsy1) mutations in maize (*Zea mays* L) cause distinct telomere-misplacement phenotypes during meiotic prophase. *J. Exp. Bot.* 54, 39–46. doi: 10.1093/jxb/erg032

Borde, V. (2007). The multiple roles of the Mre11 complex for meiotic recombination. *Chromosome Res.* 15, 551–563. doi: 10.1007/s10577-007-1147-9

Carney, J. P., Maser, R. S., Olivares, H., Davis, E. M., Le Beau, M., Yates, J. R., et al. (1998). The hMre11/hRad50 protein complex and Nijmegen breakage syndrome: linkage of double-strand break repair to the cellular DNA damage response. *Cell* 93, 477–486. doi: 10.1016/S0092-8674(00)81175-7

Cassani, C., Gobbini, E., Vertemara, J., Wang, W., Marsella, A., Sung, P., et al. (2018). Structurally distinct Mre11 domains mediate MRX functions in resection, end-tethering and DNA damage resistance. *Nucleic Acids Res.* 46, 2990–3008. doi: 10.1093/nar/gky086

Chen, P. L., Liu, F., Cai, S., Lin, X., Li, A., Chen, Y., et al. (2005). Inactivation of CtIP Leads to early embryonic lethality mediated by g1 restraint and to tumorigenesis by haploid insufficiency. *Mol. Cell. Biol.* 25, 3535–3542. doi: 10.1128/MCB.25.9.3535-3542.2005

Cheng, Z. (2013). Analyzing meiotic chromosomes in rice. *Methods Mol. Biol.* 990, 125–134. doi: 10.1007/978-1-62703-333-6_13

Daoudal-Cotterell, S., Gallego, M. E., and White, C. I. (2002). The plant Rad50-Mre11 protein complex. *FEBS Lett.* 516, 164–166. doi: 10.1016/S0014-5793(02)02536-X

Dereeper, A., Audic, S., Claverie, J. M., and Blanc, G. (2010). BLAST-EXPLORER helps you building datasets for phylogenetic analysis. *BMC Evol. Biol.* 10:8. doi: 10.1186/1471-2148-10-8

Ding, X., Xu, R., Yu, J., Xu, T., Zhuang, Y., and Han, M. (2007). SUN1 is required for telomere attachment to nuclear envelope and gametogenesis in mice. *Dev. Cell* 12, 863–872. doi: 10.1016/j.devcel.2007.03.018

Edlinger, B., and Schlögelhofer, P. (2011). Have a break: determinants of meiotic DNA double strand break (DSB) formation and processing in plants. *J. Exp. Bot.* 62, 1545–1563. doi: 10.1093/jxb/erq421

Feng, Y. L., Xiang, J. F., Kong, N., Cai, X. J., and Xie, A. Y. (2016). Buried territories: heterochromatic response to DNA double-strand breaks. *Acta Biochim. Biophys. Sin.* 48, 594–602. doi: 10.1093/abbs/gmw033

Ferdous, M., Higgins, J. D., Osman, K., Lambing, C., Roitinger, E., Mechtler, K., et al. (2012). Inter-homolog crossing-over and synapsis in *Arabidopsis* meiosis are dependent on the chromosome axis protein AtASY3. *PLoS Genet.* 8:e1002507. doi: 10.1371/journal.pgen.1002507

Golubovskaya, I. N., Hamant, O., Timofejeva, L., Wang, C. J., Braun, D., Meeley, R., et al. (2006). Alleles of *afd1* dissect REC8 functions during meiotic prophase I. *J. Cell Sci.* 119, 3306–3315. doi: 10.1242/jcs.03054

Golubovskaya, I. N., Harper, L. C., Pawlowski, W. P., Schichnes, D., and Cande, W. Z. (2002). The pam1 gene is required for meiotic bouquet formation and efficient homologous synapsis in maize (*Zea mays* L.). *Genetics* 162, 1979–1993.

Gray, S., and Cohen, P. E. (2016). Control of meiotic crossovers: from double-strand break formation to designation. *Annu. Rev. Genet.* 50, 175–210. doi: 10.1146/annurev-genet-120215-035111

Harper, L., Gardiner, J., Andorf, C., and Lawrence, C. J. (2016). MaizeGDB: the maize genetics and genomics database. *Methods Mol. Biol.* 1374, 187–202. doi: 10.1007/978-1-4939-3167-5_9

Harper, L., Golubovskaya, I., and Cande, W. Z. (2004). A bouquet of chromosomes. *J. Cell Sci.* 117, 4025–4032. doi: 10.1242/jcs.01363

Higgins, J. D., Sanchez-Moran, E., Armstrong, S. J., Jones, G. H., and Franklin, F. C. (2005). The *Arabidopsis* synaptonemal complex protein ZYP1 is required for chromosome synapsis and normal fidelity of crossing over. *Genes Dev.* 19, 2488–2500. doi: 10.1101/gad.354705

Hopfner, K. P., Putnam, C. D., and Tainer, J. A. (2002). DNA double-strand break repair from head to tail. *Curr. Opin. Struct. Biol.* 12, 115–122. doi: 10.1016/S0959-440X(02)00297-X

Hunter, N., and Kleckner, N. (2001). The single-end invasion: an asymmetric intermediate at the double-strand break to double-holliday junction transition of meiotic recombination. *Cell* 106, 59–70. doi: 10.1016/S0092-8674(01)00430-5

Jeanmougin, F., Thompson, J. D., Gouy, M., Higgins, D. G., and Gibson, T. J. (1998). Multiple sequence alignment with Clustal x. *Trends Biochem. Sci.* 23, 403–405. doi: 10.1016/S0968-0004(98)01285-7

Ji, J. H., Tang, D., Wang, K. J., Wang, M., Che, L. X., Li, M., et al. (2012). The role of OsCOM1 in homologous chromosome synapsis and recombination in rice meiosis. *Plant J.* 72, 18–30. doi: 10.1111/j.1365-313X.2012.05025.x

Johnson-Brousseau, S. A., and McCormick, S. (2004). A compendium of methods useful for characterizing *Arabidopsis* pollen mutants and gametophytically-expressed genes. *Plant J.* 39, 761–775. doi: 10.1111/j.1365-313X.2004.02147.x

Kato, A., Lamb, J. C., and Birchler, J. A. (2004). Chromosome painting using repetitive DNA sequences as probes for somatic chromosome identification in maize. *Proc. Natl. Acad. Sci. U.S.A.* 101, 13554–13559. doi: 10.1073/pnas.0403659101

Keeney, S., Giroux, C. N., and Kleckner, N. (1997). Meiosis-specific DNA double-strand breaks are catalyzed by Spo11, a member of a widely conserved protein family. *Cell* 88, 375–384. doi: 10.1016/S0092-8674(00)81876-0

Klutstein, M., Fennell, A., Fernandez-Alvarez, A., and Cooper, J. P. (2015). The telomere bouquet regulates meiotic centromere assembly. *Nat. Cell Biol.* 17, 458–469. doi: 10.1038/ncb3132

Lee-Theilen, M., Matthews, A. J., Kelly, D., Zheng, S., and Chaudhuri, J. (2010). CtIP promotes microhomology-mediated alternative end joining during class-switch recombination. *Nat. Struct. Mol. Biol.* 18, 75–79. doi: 10.1038/nsmb.1942

Lee, D. H., Kao, Y. H., Ku, J. C., Lin, C. Y., Meeley, R., Jan, Y. S., et al. (2015). The axial element protein desynaptic2 mediates meiotic double-strand break formation and synaptonemal complex assembly in maize. *Plant Cell* 27, 2516–2529. doi: 10.1105/tpc.15.00434

Lengsfeld, B. M., Rattray, A. J., Bhaskara, V., Ghirlando, R., and Paull, T. T. (2007). Sae2 Is an endonuclease that processes hairpin DNA cooperatively with the Mre11/Rad50/Xrs2 complex. *Mol. Cell* 28, 638–651. doi: 10.1016/j.molcel.2007.11.001

Li, H., Li, J., Cong, X. H., Duan, Y. B., Li, L., Wei, P. C., et al. (2013). A high-throughput, high-quality plant genomic DNA extraction protocol. *Genet. Mol. Res.* 12, 4526–4539. doi: 10.4238/2013.October.15.1

Li, L., and Arumuganathan, K. (2001). Physical mapping of 45S and 5S rDNA on maize metaphase and sorted chromosomes by FISH. *Hereditas* 134, 141–145. doi: 10.1111/j.1601-5223.2001.00141.x

Limbo, O., Chahwan, C., Yamada, Y., De Bruin, R. A., Wittenberg, C., and Russell, P. (2007). Ctp1 Is a cell-cycle-regulated protein that functions with Mre11 complex to control double-strand break repair by homologous recombination. *Mol. Cell.* 28, 134–146. doi: 10.1016/j.molcel.2007.09.009

McKee, A. H. Z., and Kleckner, N. (1997). A general method for identifying recessive diploid-specific mutations in *Saccharomyces cerevisiae*, its application to the isolation of mutants blocked at intermediate stages of meiotic prophase and characterization of a new gene *SAE2*. *Genetics* 146, 797–816.

McVey, M., and Lee, S. E. (2008). MMEJ repair of double-strand breaks (director's cut): deleted sequences and alternative endings. *Trends Genet.* 24, 529–538. doi: 10.1016/j.tig.2008.08.007

Mercier, R., Mezard, C., Jenczewski, E., Macaisne, N., and Grelon, M. (2015). The molecular biology of meiosis in plants. *Annu. Rev. Plant Biol.* 66, 297–327. doi: 10.1146/annurev-arplant-050213-035923

Mirouze, M., and Vitte, C. (2014). Transposable elements, a treasure trove to decipher epigenetic variation: insights from *Arabidopsis* and crop epigenomes. *J. Exp. Bot.* 65, 2801–2812. doi: 10.1093/jxb/eru120

Murphy, S. P., and Bass, H. W. (2012). The maize (*Zea mays*) desynaptic (dy) mutation defines a pathway for meiotic chromosome segregation, linking nuclear morphology, telomere distribution and synapsis. *J. Cell Sci.* 125, 3681-3690. doi: 10.1242/jcs.108290

Nikolov, I., and Taddei, A. (2016). Linking replication stress with heterochromatin formation. *Chromosoma* 125, 523–533. doi: 10.1007/s00412-015-0545-6

Niwa, O., Shimanuki, M., and Miki, F. (2000). Telomere-led bouquet formation facilitates homologous chromosome pairing and restricts ectopic interaction in fission yeast meiosis. *EMBO J.* 19, 3831–3840. doi: 10.1093/emboj/19.14.3831

Paull, T. T., and Gellert, M. (1998). The 3′ to 5′ exonuclease activity of Mre 11 facilitates repair of DNA double-strand breaks. *Mol. Cell.* 1, 969–979. doi: 10.1016/S1097-2765(00)80097-0

Pawlowski, W. P., Golubovskaya, I. N., and Cande, W. Z. (2003). Altered nuclear distribution of recombination protein RAD51 in maize mutants suggests the involvement of RAD51 in meiotic homology recognition. *Plant Cell* 15, 1807–1816. doi: 10.1105/tpc.012898

Pawlowski, W. P., Golubovskaya, I. N., Timofejeva, L., Meeley, R. B., Sheridan, W. F., and Cande, W. Z. (2004). Coordination of meiotic recombination, pairing, and synapsis by PHS1. *Science* 303, 89–92. doi: 10.1126/science.1091110

Penkner, A., Portik-Dobos, Z., Tang, L., Schnabel, R., Novatchkova, M., Jantsch, V., et al. (2007). A conserved function for a *Caenorhabditis elegans* Com1/Sae2/CtIP protein homolog in meiotic recombination. *EMBO J.* 26, 5071–5082. doi: 10.1038/sj.emboj.7601916

Prinz, S., Amon, A., and Klein, F. (1997). Isolation of *COM1*, a new gene required to complete meiotic double-strand break-induced recombination in *Saccharomyces cerevisiae*. *Genetics* 146, 781–795.

Puizina, J., Siroky, J., Mokros, P., Schweizer, D., and Riha, K. (2004). Mre11 deficiency in *Arabidopsis* is associated with chromosomal instability in somatic cells and Spo11-dependent genome fragmentation during meiosis. *Plant Cell* 16, 1968–1978. doi: 10.1105/tpc.104.022749

Richards, E. J., and Ausubel, F. M. (1988). Isolation of a higher eukaryotic telomere from *Arabidopsis thaliana*. *Cell* 53, 127–136. doi: 10.1016/0092-8674(88)90494-1

Samanic, I., Simunic, J., Riha, K., and Puizina, J. (2013). Evidence for distinct functions of MRE11 in *Arabidopsis* meiosis. *PLoS One* 8:e78760. doi: 10.1371/journal.pone.0078760

Sanchez-Moran, E., Osman, K., Higgins, J. D., Pradillo, M., Cunado, N., Jones, G. H., et al. (2008). ASY1 coordinates early events in the plant meiotic recombination pathway. *Cytogenet. Genome Res.* 120, 302–312. doi: 10.1159/000121079

Sartori, A. A., Lukas, C., Coates, J., Mistrik, J., Fu, S., Bartek, J. (2007). Human CtIP promotes DNA end resection. *Nature* 450, 509–514. doi: 10.1038/nature06337

Schnable, P. S., Ware, D., Fulton, R. S., Stein, J. C., Wei, F., Pasternak, S., et al. (2009). The B73 maize genome: complexity, diversity, and dynamics. *Science* 326, 1112–1115. doi: 10.1126/science.1178534

Shrivastav, M., De Haro, L. P., and Nickoloff, J. A. (2008). Regulation of DNA double-strand break repair pathway choice. *Cell Res.* 18, 134–147. doi: 10.1038/cr.2007.111

Tang, D., Miao, C. B., Li, Y. F., Wang, H. J., Liu, X. F., Yu, H. X., et al. (2014). OsRAD51C is essential for double-strand break repair in rice meiosis. *Front. Plant Sci.* 5:167. doi: 10.3389/fpls.2014.00167

Uanschou, C., Siwiec, T., Pedrosa-Harand, A., Kerzendorfer, C., Sanchez-Moran, E., Novatchkova, M., et al. (2007). A novel plant gene essential for meiosis is related to the human *CtIP* and the yeast *COM1/SAE2* gene. *EMBO J.* 26, 5061–5070. doi: 10.1038/sj.emboj.7601913

Vannier, J. B., Depeiges, A., White, C., and Gallego, M. E. (2006). Two roles for Rad50 in telomere maintenance. *EMBO J.* 25, 4577–4585. doi: 10.1038/sj.emboj.7601345

Wang, K., Wang, M., Tang, D., Shen, Y., Qin, B., Li, M., et al. (2011). PAIR3, an axis-associated protein, is essential for the recruitment of recombination elements onto meiotic chromosomes in rice. *Mol. Biol. Cell* 22, 12–19. doi: 10.1091/mbc.e10-08-0667

Wang, M., Wang, K., Tang, D., Wei, C., Li, M., Shen, Y., et al. (2010). The central element protein ZEP1 of the synaptonemal complex regulates the number of crossovers during meiosis in rice. *Plant Cell* 22, 417–430. doi: 10.1105/tpc.109.070789

Waterworth, W. M., Altun, C., Armstrong, S. J., Roberts, N., Dean, P. J., Young, K., et al. (2007). NBS1 is involved in DNA repair and plays a synergistic role with ATM in mediating meiotic homologous recombination in plants. *Plant J.* 52, 41–52. doi: 10.1111/j.1365-313X.2007.03220.x

Yoo, S. D., Cho, Y. H., and Sheen, J. (2007). *Arabidopsis* mesophyll protoplasts: a versatile cell system for transient gene expression analysis. *Nat. Protoc.* 2, 1565–1572. doi: 10.1038/nprot.2007.199

Zhang, B. W., Wang, M., Tang, D., Li, Y. F., Xu, M., Gu, M. H., et al. (2015). XRCC3 is essential for proper double-strand break repair and homologous recombination in rice meiosis. *J. Exp. Bot.* 66, 5713–5725. doi: 10.1093/jxb/erv253

Zhang, F., Tang, D., Shen, Y., Xue, Z., Shi, W., Ren, L., et al. (2017). The F-box protein ZYGO1 mediates bouquet formation to promote homologous pairing, synapsis, and recombination in rice meiosis. *Plant Cell* 29, 2597–2609. doi: 10.1105/tpc.17.00287

Zhang, H., Egger, R. L., Kelliher, T., Morrow, D., Fernandes, J., Nan, G. L., et al. (2014). Transcriptomes and proteomes define gene expression progression in pre-meiotic maize anthers. *G3* 4, 993–1010. doi: 10.1534/g3.113.009738

Zickler, D., and Kleckner, N. (1999). Meiotic chromosomes: integrating structure and function. *Annu. Rev. Genet.* 33, 603–754. doi: 10.1146/annurev.genet.33.1.603

Conflict of Interest Statement: The authors declare that the research was conducted in the absence of any commercial or financial relationships that could be construed as a potential conflict of interest.

frontiers in Plant Science

ORIGINAL RESEARCH
published: 29 August 2018
doi: 10.3389/fpls.2018.01236

OsRAD17 Is Required for Meiotic Double-Strand Break Repair and Plays a Redundant Role With OsZIP4 in Synaptonemal Complex Assembly

Qing Hu[1,2†], Chao Zhang[1,2†], Zhihui Xue[1†], Lijun Ma[3], Wei Liu[3], Yi Shen[1], Bojun Ma[3] and Zhukuan Cheng[1,2]**

[1] State Key Laboratory of Plant Genomics and Center for Plant Gene Research, Institute of Genetics and Developmental Biology, Chinese Academy of Sciences, Beijing, China, [2] University of Chinese Academy of Sciences, Beijing, China, [3] College of Chemistry and Life Sciences, Zhejiang Normal University, Jinhua, China

OPEN ACCESS

Edited by:
Simon Gilroy,
University of Wisconsin–Madison,
United States

Reviewed by:
Chung-Ju Rachel Wang,
Academia Sinica, Taiwan
Mónica Pradillo,
Complutense University of Madrid,
Spain
Chengwei Yang,
South China Normal University, China

***Correspondence:**
Bojun Ma
mbj@zjnu.cn
Zhukuan Cheng
zkcheng@genetics.ac.cn

† These authors have contributed equally to this work

Specialty section:
This article was submitted to Plant Cell Biology, a section of the journal Frontiers in Plant Science

Received: 30 March 2018
Accepted: 06 August 2018
Published: 29 August 2018

Citation:
Hu Q, Zhang C, Xue Z, Ma L, Liu W, Shen Y, Ma B and Cheng Z (2018) OsRAD17 Is Required for Meiotic Double-Strand Break Repair and Plays a Redundant Role With OsZIP4 in Synaptonemal Complex Assembly. Front. Plant Sci. 9:1236. doi: 10.3389/fpls.2018.01236

The repair of SPO11-dependent double-strand breaks (DSBs) by homologous recombination (HR) ensures the correct segregation of homologous chromosomes. In yeast and human, RAD17 is involved in DNA damage checkpoint control and DSB repair. However, little is known about its function in plants. In this study, we characterized the RAD17 homolog in rice. In *Osrad17* pollen mother cells (PMCs), associations between non-homologous chromosomes and chromosome fragmentation were constantly observed. These aberrant chromosome associations were dependent on the formation of programmed DSBs. OsRAD17 interacts with OsRAD1 and the meiotic phenotype of *Osrad1 Osrad17* is indistinguishable from the two single mutants which have similar phenotypes, manifesting they could act in the same pathway. OsZIP4, OsMSH5 and OsMER3 are members of ZMM proteins in rice that are required for crossover formation. We found that homologous pairing and synapsis, which was roughly unaffected in *Oszip4* and *Osrad17* single mutant, was severely disturbed in the *Oszip4 Osrad17* double mutant. Similar phenotypes were observed in the *Osmsh5 Osrad17* and *Osmer3 Osrad1* double mutants, suggesting the cooperation between the checkpoint proteins and ZMM proteins in assuring accurate HR in rice.

Keywords: OsRAD17, meiosis, homologous recombination, synaptonemal complex, rice

INTRODUCTION

Meiotic homologous recombination (HR) is initiated by the programmed formation of DNA double-strand breaks (DSBs), which was catalyzed by SPO11, a functional homolog of subunit A of an archaeal topoisomerase (TopoVIA) (Keeney et al., 1997). After resection by MRN/X complex (Mre11/Rad50/Xrs2 or Mre11/Rad50/Nbs1) and other proteins, these DSBs are processed to yield 3′ overhangs (Cao et al., 1990; Ivanov et al., 1992; Nairz and Klein, 1997). With the help of RPA (Replication Protein A), the recombinases RAD51 and DMC1 are loaded to initialize homology search and strand exchange (Bishop et al., 1992; Sung and Robberson, 1995; San Filippo et al., 2008). These early steps of HR promote homologous chromosome paring and installation of the synaptonemal complex (SC) in most organisms, including plants. The SC is a

proteinaceous structure that formed between paired homologous chromosomes. Also, synapsis could occur between non-homologous chromosomes (Nairz and Klein, 1997). HR events are eventually resolved as either crossovers (COs) or non-crossovers (NCOs) in the context of the SC (Borner et al., 2004).

The ZMM proteins (ZIP1, ZIP2, ZIP3, ZIP4, MSH4, MSH5, and MER3) are meiosis-specific proteins functionally collaborating in the formation of interference-sensitive COs, which is a majority of total COs (Lynn et al., 2007). Mutants of these genes display similar phenotypes, with significantly reduced COs and high frequency of univalent formation (Ross-Macdonald and Roeder, 1994). ZMM proteins also play important roles in the assembly of the SC central element in yeast and mouse (de Vries et al., 1999; Tsubouchi et al., 2006). In contrast, the impact of ZMM proteins on synapsis appears to be minor in plants. In Arabidopsis and rice, no apparent defects in chromosome synapsis are observed in *zmm* mutants (Chelysheva et al., 2007; Higgins et al., 2008; Shen et al., 2012; Zhang et al., 2014).

RAD17 is a replication factor C (RFC)-like protein which has been demonstrated to participate in multiple processes, such as DNA damage checkpoint signaling and DSB repair (Wang et al., 2003, 2006; Budzowska et al., 2004; Heitzeberg et al., 2004). The best known function of RAD17 is recruiting the 9-1-1 complex (RAD9/HUS1/RAD1) as part of the Rad17-RFC clamp loader in response to DNA damage (Griffith et al., 2002; Zou et al., 2002; Navadgi-Patil and Burgers, 2009). In addition, RAD17 is shown to be required for loading the MRN complex at DSB site (Wang et al., 2014). The meiotic functions of RAD17 were mainly revealed in yeast. In *Saccharomyces cerevisiae*, Rad24 (the homologue of RAD17) was proved to be required for meiotic prophase arrest induced by a *DMC1* mutation, defining a meiotic recombination checkpoint (Lydall et al., 1996). In addition, Rad24 was reported to be necessary for synapsis as well as recombination template choice (Grushcow et al., 1999; Shinohara et al., 2003, 2015).

In plants, *Atrad17* mutants show increased sensitivity to the DNA-damaging agents. The *Atrad9 Atrad17* is not more sensitive to the chemicals than the single mutants, indicating that *AtRAD17* and *AtRAD9* might be epistatic (Heitzeberg et al., 2004). Moreover, AtRAD17, as the DNA damage sensor protein, is negatively regulated by a subunit of the SMC5/6 complex, SNI1 (suppressor of *npr1-1*, inducible 1), and the direct interaction between them was detected (Yan et al., 2013). Our previous study on OsRAD1 demonstrated its roles in promoting accurate meiotic DSB repair by suppressing non-homologous end joining (NHEJ) (Hu et al., 2016). NHEJ pathway involves direct ligation of the broken ends in a Ku-dependent manner and is one of the two basic strategy for DSB repair (Deriano and Roth, 2013). However, the meiotic roles of RAD17 in plants are still elusive.

Here we report the analysis of OsRAD17, the functional homolog of the mammalian RAD17 in rice. Our study indicates that OsRAD17 is required for DSB repair during meiosis in rice. In the *Osrad17* PMCs, non-homologous chromosomes associations (associations between different homologous chromosomes at pachytene and chromosome entanglements at metaphase I) existed, while homologous pairing and SC installation is roughly normal. Unexpectedly, loss of ZMM proteins in *Osrad17* mutants results in significant defects in homologous pairing and synapsis. Taken together, our data demonstrates that OsRAD17 is essential for meiotic DSB repair, and acts cooperatively with ZMM proteins in assuring SC installation in rice.

MATERIALS AND METHODS

Plant Materials and Growth Conditions

Osrad17-1 was isolated from sterile mutants derived by tissue culture. Other *Osrad17* mutant lines were identified from the collection of mutants induced by ^{60}Co-γ -ray irradiation. The *Osspo11-1*, *Oscom1*, *Oszip4*, *Osmsh5*, *Osrad1* and *Osmer3* alleles employed in this study were previously isolated in our lab (Wang et al., 2009; Ji et al., 2012; Shen et al., 2012; Luo et al., 2013; Hu et al., 2016). Nipponbare was used as the wild type in the related experiments. All of the plants were grown in paddy fields in Beijing (China) or Sanya (Hainan Province, China) during the natural growing season.

Map-Based Cloning of *OsRAD17*

In a screen for rice meiotic mutants, we identified three mutant lines that segregated 3:1 for fertile and sterile plants, indicating that they are belonging to the single recessive mutation.

A map-based cloning approach was adopted to isolate the target gene. We crossed *Osrad17-1*, *Osrad17-2,* and *Osrad17-3* heterozygous mutant plants with the *indica* rice variety Zhongxian3037 to produce the mapping populations. Using sterile plants that segregated in F2 population (28 plants for *Osrad17-1*, 22 for *Osrad17-2*, *and* 20 for *Osrad17-3*), a linked marker to the sterile phenotype was found for all the three populations. Then we carried out fine mapping with additional sterile F2 and F3 plants to pinpoint the target gene within a 200-kilobase region. According to the MSU Rice Genome Annotation Project Database and Resource[1], we found a candidate gene (*LOC_Os03g13850*) annotated as the putative cell cycle checkpoint protein RAD17. Sequencing of this gene in the three mutant lines showed that they all had mutation sites in the coding region.

Indel (insertion–deletion) markers used for mapping were designed based on the sequence differences between *indica* variety 9311 and *japonica* variety Nipponbare according to the data published[2]. Primer sequences used were listed in **Supplementary Table S1**.

Full-Length cDNA Cloning of *OsRAD17*

Total RNA extraction from rice young panicles was conducted using the TRIzol reagent (Invitrogen). Reverse transcription was performed with primer Adaptor-T (18) using the superscript III RNaseH reverse transcriptase (Invitrogen). For RACE, 3′-Full RACE Core Set with PrimeScript^{TM} RTase (TaKaRa) and 5′-Full

[1]http://rice.plantbiology.msu.edu/

[2]http://www.ncbi.nlm.nih.gov

RACE Kit with TAP (TaKaRa) were used to identify the 3′ end and 5′ end of the cDNA, respectively. PCR using primers RO-F and RO-R was performed to amplify the open reading frame. Then the products were cloned into the PMD18-T vector (TaKaRa) and sequenced. The sequences were then spliced together to obtain the full-length cDNA sequence.

Quantitative RT-PCR Assay

Total RNA was extracted individually from roots, leaves, internodes and young panicles (5–7 cm long) of Nipponbare, and was reverse-transcribed into cDNA. Real-time RT-PCR analysis was performed using the Bio-Rad CFX96 real-time PCR instrument and EvaGreen (Biotium). All PCR experiments were conducted using 40 cycles of 95°C for 10 s, 60°C for 30 s and were performed in triplicate. Gene-specific primers (17RT-F/17RT-R) and standard control primers (Actin-F/Actin-R) were listed in **Supplementary Table S1**.

Cytology

Preparations of rice PMCs were performed as described (Shen et al., 2012). The primary antibodies used in immunofluorescence were anti-OsREC8, anti-ZEP1, anti-OsCOM1, anti-OsDMC1 and anti-γH2AX (Wang et al., 2010, 2016; Shao et al., 2011; Ji et al., 2012). FISH analysis was conducted according to Yang et al. (2016). Original images were captured under Zeiss A2 fluorescence microscope with a micro CCD camera.

Yeast Two-Hybrid (Y2H) Assay

The Y2H assays were performed using the Matchmaker Gold Yeast Two-Hybrid system (Clontech). The full length CDS of OsRAD17 and 9-1-1 proteins were cloned into pGADT7 and pGBKT7 to generate AD and BD recombinants. Quadruple dropout (QDO) selection medium with aureobasidin A and the chromogenic substrate X-a-Gal was used to verify the interaction and double dropout (DDO) selecting medium (SD -Leu -Trp) to confirm the successful transformation.

RESULTS

Characterization of *Osrad17* Mutant Alleles

In a screen for rice meiotic mutants, we obtained three mutant lines allelic for disruption in *LOC_Os03g13850* through map-based cloning (**Figure 1**). This gene was named *Oryza sativa RAD17* (*OsRAD17*), based on the homology of the protein sequence (see below) and the three mutants were *Osrad17-1* (Nipponbare), *Osrad17-2* (Yandao 8), and *Osrad17-3* (Yandao 8), respectively. *Osrad17-1* mutant exhibited normal vegetative growth but complete sterility (**Figures 1A–D**). I_2-KI staining showed that the pollen grains were completely non-viable in the mutant. Pollinating the mutant flowers with wild type pollen did not set any seeds, suggesting that the mutant is both male and female sterile.

Sequencing of the *OsRAD17* gene in the *Osrad17-1* mutant revealed a 64 bp deletion in the first exon (**Figure 1E**), which resulted in frame shift and premature stop codon formation. In *Osrad17-2* and *Osrad17-3*, a single nucleotide deletion occurred in the fifth and seventh exon, respectively, leading to frame shift and premature stop codon. We selected *Osrad17-1* for most subsequent studies.

We obtained a 2740 bp full-length cDNA of *OsRAD17* by performing rapid amplification of cDNA ends (RACE), which encoded a protein of 620 amino acids. The result of PSI-BLAST search in public databases revealed that OsRAD17 shared significant similarity with RAD17 protein of Arabidopsis (43% identity and 60% similarity), human (29% identity and 46% similarity) and fission yeast (27% identity and 38% similarity). A Reciprocal Best BLAST further confirmed that the protein that we isolated was the closest relative of RAD17 in rice. Multiple sequence alignment of OsRAD17 with its orthologs showed that the RAD17 proteins were highly conserved, especially within the AAA-ATPase domain (**Supplementary Figure S1**).

Quantitative RT-PCR showed that *OsRAD17* was expressed as early as the seedling stage. In adult-stage rice, *OsRAD17* was detectable not only in young panicles but also in leaves, roots, and internodes (**Supplementary Figure S2**).

Non-homologous Chromosome Associations and Fragmentations Shown in *Osrad17*

To determine whether pollen abortion resulted from the defects in male meiosis, we investigated chromosome behavior in PMCs by 4′,6-diamidino-2-phenylindole (DAPI) staining. By comparing *Osrad17-1* with the wild type, we found that *Osrad17-1* chromosomes behaved in a similar way to those of wild type from leptotene to zygotene (**Figures 2A,B,I,J**). However, aberrations were observed thereafter. At pachytene, *Osrad17-1* chromosomes presented as thick threads and synapsed chromosomes were visible, just like the wild type (**Figures 2C,K**). But associations between non-homologous chromosomes were found among *Osrad17-1* synapsed chromosomes (**Figure 2K**). At diakinesis and metaphase I, wild type PMCs had twelve condensed bivalents (**Figures 2D,E**), while *Osrad17-1* exhibited chromosome aggregations (**Figures 2L,M**). Homologous chromosomes separated precisely at anaphase I and chromatids separated at the second meiotic division, producing tetrads in wild type (**Figures 2F–H**). In contrast, extensive chromosome bridges and fragments were observed in *Osrad17-1*, which generated abnormal tetrads with micronuclei (**Figures 2N–P**). The chromosome behaviors of *Osrad17-2* and *Osrad17-3* showed the same meiotic defects with *Osrad17-1* (**Figure 3A**).

To explore the nature of the chromosome aggregations during metaphase I in the mutants, we performed fluorescent *in situ* hybridization (FISH) experiments using 5S rDNA and CentO probes (**Figure 3B**). The 5S rDNA was located on the centromere-proximal region of chromosome 11 and CentO is a molecular marker for all rice centromeres. In wild type PMCs, 12 bivalents were aligned in the middle of the cell. There are two CentO signals on each bivalent and two 5S rDNA signals on chromosome 11. However, on the chromosome aggregations of the mutants, more than two CentO signals were observed,

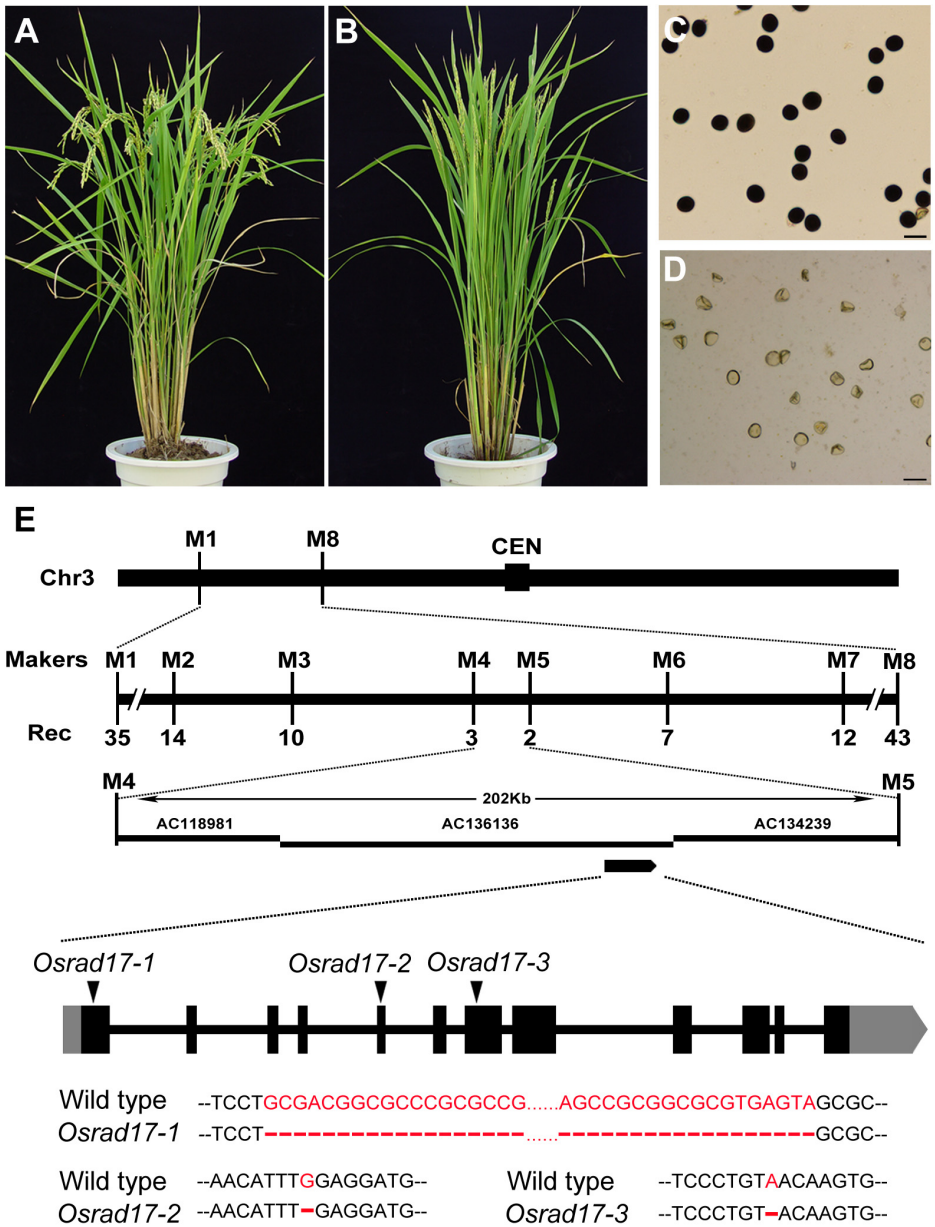

FIGURE 1 | Characterization of the *Osrad17* mutant and map-based cloning of *OsRAD17* gene. **(A)** Wild type plant. **(B)** *Osrad17* plant. **(C)** Pollen grains of wild type. Bars, 50 μm. **(D)** Pollen grains of *Osrad17* mutant. Bars, 50 μm. **(E)** Map-based cloning of *OsRAD17* gene and gene structure. CEN, centromere. Rec, the number of recombinants. Coding regions are shown as black boxes, and untranslated regions are shown as gray boxes. The triangles indicate the mutated sites and detailed mutations were listed below.

indicating that these aggregations contain more than one pair of homologous chromosomes. Thus, the chromosome aggregations were the associations among non-homologous chromosomes.

Meiotic Defects in *Osrad17* Are Dependent on Programmed DSB Formation

To determine whether the chromosomal abnormalities in *Osrad17* were acquired during meiotic DSB repair, we constructed the *Osspo11-1 Osrad17* double mutant. The *Osspo11-1* mutants display intact univalents that are randomly distributed due to the absence of meiotic DSBs (**Figures 4A–C**). Cytogenetic analysis of *Osspo11-1 Osrad17* PMCs revealed univalents in metaphase I with no evidence of chromosome aggregations or fragmentations (**Figures 4D–F**). Thus, the meiotic defects in *Osrad17* are related to the repair of the OsSPO11-dependent programmed DSBs. OsCOM1 is required for processing of meiotic DSBs. Lack of OsCOM1 leads to abolished HR (Ji et al., 2012). In the *Oscom1* mutant,

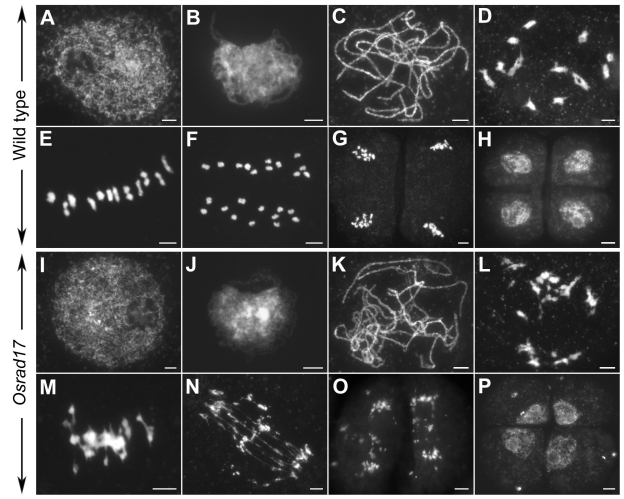

FIGURE 2 | Chromosome spreads of PMCs in wild type and *Osrad17*. Chromosomes were stained with DAPI. **(A,I)** Leptotene. **(B,J)** Zygotene. **(C,K)** Pachytene. **(D,L)** Diakinesis. **(E,M)** Metaphase I. **(F,N)** Anaphase I. **(G,O)** Anaphase II. **(H,P)** Tetrad. Bars, 5 μm.

homologous chromosomes failed in synapsis, and non-homologous associations were observed (**Figures 4G–I**). The meiotic phenotype of *Oscom1 Osrad17* double mutant mimicked that of the *Oscom1* single mutant, as synapsis in *Oscom1 Osrad17* was inhibited due to the mutation of *OsCOM1* (**Figures 4J–L**) (**Supplementary Figure S3**). This suggested that OsRAD17 may functions downstream of OsCOM1 in rice meiosis.

OsRAD17 Functions Together With OsRAD1 on Meiotic DSB Repair

The intimate relationship between RAD17 and the 9-1-1 complex has been well demonstrated by numerous researches. Our previous studies proved that the 9-1-1 complex was involved in meiotic DSB repair (Che et al., 2014; Hu et al., 2016). To determine if OsRAD17 associated with the 9-1-1 for DSB repair during rice meiosis, we conducted yeast two-hybrid assays and genetic analysis. Yeast two-hybrid assays revealed a direct interaction between OsRAD17 and OsRAD1 (**Figure 5A**). No interaction between OsRAD17 and OsRAD9 or OsHUS1 was detected. This suggests that OsRAD17 may load the 9-1-1 complex by interacting with OsRAD1 in rice meiosis.

To further verify the genetic relationship between *OsRAD17* and *OsRAD1*, we constructed the *Osrad1 Osrad17* double mutant. The double mutant exhibited similar meiotic phenotype with the single mutant, also indicating that they could act in the same meiotic DSB repair pathway (**Figure 5B**).

Homologous Chromosome Pairing and SC Assembly Are Disturbed in the *Oszip4 Osrad17* Double Mutant

To explore the relationship between ectopic chromosome interactions in *Osrad17* and interference-sensitive COs, we generated the *Oszip4 Osrad17* double mutant. Loss of OsZIP4 results in the reduction of bivalents and appearance of univalents due to reduced CO formation (Shen et al., 2012). *Oszip4 Osrad17* showed a mixture of both univalents and chromosome aggregations at metaphase I (**Figure 6A**), indicating that aberrant chromosome associations in *Osrad17* arise independently from

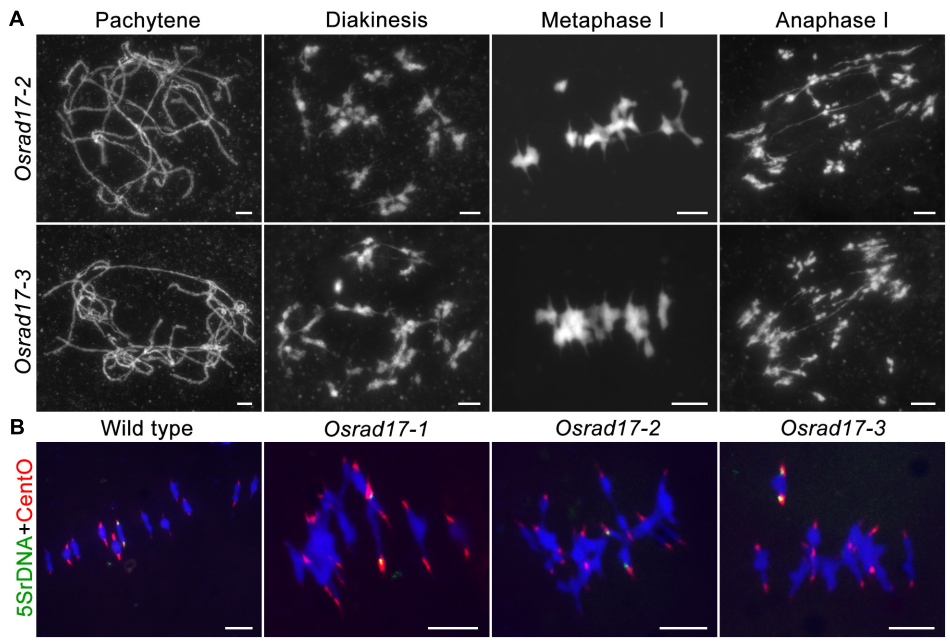

FIGURE 3 | Non-homologous associations in different *Osrad17* alleles. **(A)** Chromosome spreads of PMCs in *Osrad17-2* and *Osrad17-3* at different meiotic stages. **(B)** FISH analysis of the metaphase I chromosome interactions in wild type and three *Osrad17* mutants. Bars, 5 μm.

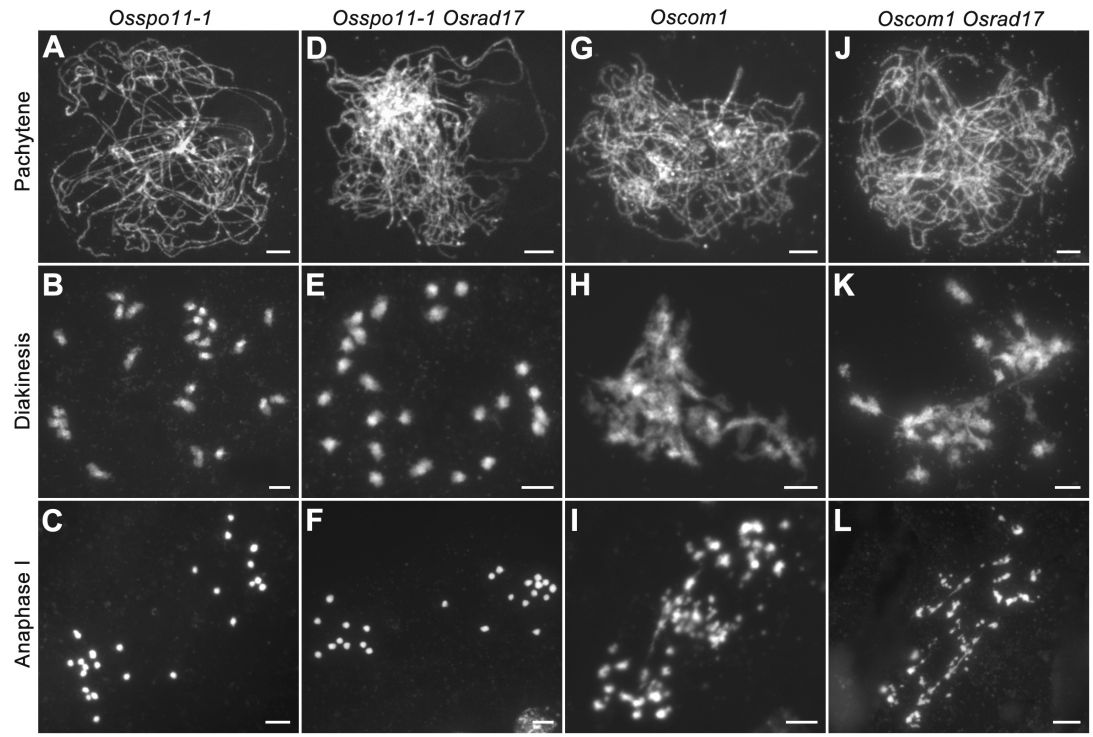

FIGURE 4 | Genetic analysis of *OsRAD17* with *OsSPO11-1* and *OsCOM1*. **(A–C)** Chromosomes behaviors in *Osspo11-1* at corresponding meiotic stages. **(D–F)** Chromosomes behaviors in *Osspo11-1 Osrad17* was similar to *Osspo11-1*. **(G–I)** Chromosomes behaviors in *Oscom1* at corresponding meiotic stages. **(J–L)** Chromosomes behaviors in *Oscom1 Osrad17* was similar to *Oscom1*. Bars, 5 μm.

the ZMM proteins-mediated pathway. We also observed a similar phenotype in the *Osmsh5 Osrad17* double mutant (**Supplementary Figure S4**).

Moreover, we found that homologous pairing seemed to be severely disturbed in the *Oszip4 Osrad17* mutant at pachytene stage (**Figure 6A**). This is quite interesting, considering that both of the single mutant displayed roughly normal pairing. We further performed chromosome-specific FISH analysis using 5S rDNA (**Figure 6B**). At early pachytene, two adjacent red signals, representing the closely paired homologous chromosomes, were observed in wild type, *Osrad17* and *Oszip4*. However, 85.7% of the *Oszip4 Osrad17* cells (n = 35) had two separated 5S rDNA signals, showing that the chromosome 11 were partially separated. This observation indicates that OsRAD17 and OsZIP4 act cooperatively to promote homologous pairing.

During meiosis, homologous pairing and synapsis are closely related. Considering abnormal homologous pairing in *Oszip4 Osrad17*, we next wanted to determine the synaptonemal complex assembly in this double mutant. We examined the localization of ZEP1 and OsREC8 in *Osrad17* as well as *Oszip4*. ZEP1 is a central element of SC and a perfect maker to indicate the extent of synapsis in rice (Wang et al., 2010). OsREC8 is the meiosis-specific cohesin, signal of which predicts the axial element of SC (Shao et al., 2011). Localization of OsREC8 and ZEP1 in *Oszip4* was indistinguishable from the wild type and ZEP1 signal in *Osrad17-1* could be detected along almost the entire chromosomes, with the exception of a few discontinuities (**Figure 7**). This suggests that SC assembly is roughly normal in these mutants. However, localization of ZEP1 was rare in *Oszip4 Osrad17* (**Figure 7** and **Supplementary Figure S5**). The percentage of synapsis in most *Oszip4 Osrad17* PMCs was less than 25% (n = 30). This proved that OsRAD17 plays a redundant role with OsZIP4 in SC assembly. We further detected immunolocalization of ZEP1 in *Osmsh5 Osrad17*, finding the similar incomplete SC formation (**Supplementary Figures S5**, **S6**). These data suggest an important role for OsRAD17 in promoting SC installation in the absence of ZMM proteins. To investigate if the 9-1-1 complex is also involved in regulating SC installation, we examined the localization of ZEP1 in *Osmer3 Osrad1* by immunofluorescence and found incomplete ZEP1 signal at pachytene (**Supplementary Figures S5**, **S6**), indicating that OsRAD1 and OsMER3 are also redundantly necessary for SC assembly. These results together manifested that there might be a mechanism for homologous pairing and synaptonemal complex assembly requiring the cooperation between the checkpoint proteins and ZMM proteins.

HR Events in *Oszip4 Osrad17* Double Mutant

To verify the cause of defects in chromosome paring and synapsis, we monitored HR in *Oszip4 Osrad17* meiosis (**Figure 8**). γH2AX is the phosphorylated form of H2AX, the DSB repair specific histone variant accumulating at the sites of DSBs (Rogakou

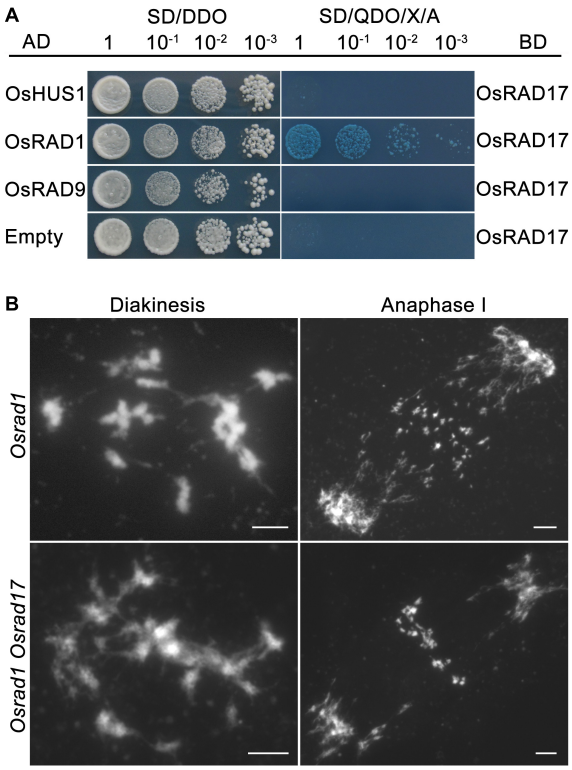

FIGURE 5 | Physical and genetic interaction between OsRAD17 and OsRAD1. **(A)** OsRAD17 interacts with OsRAD1 in yeast two-hybrid assays. **(B)** The *Osrad1 Osrad17* double mutant shows similar chromosome behaviors to those of the single mutant at corresponding meiotic stages. Bars, 5 μm.

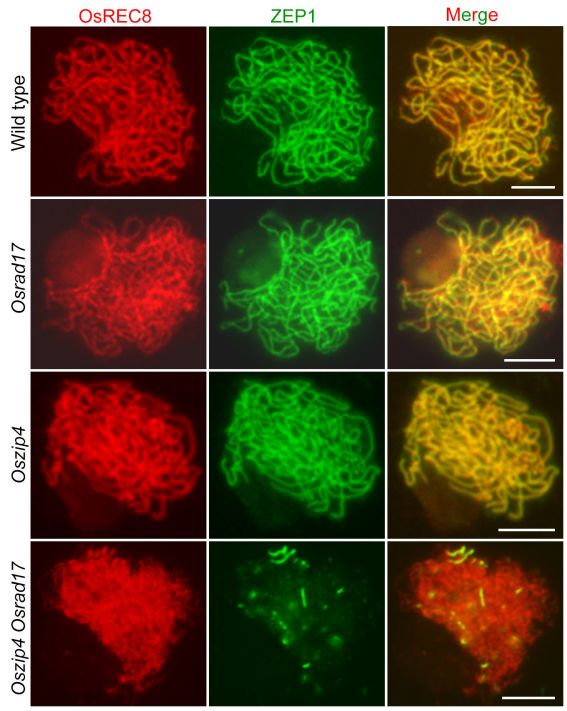

FIGURE 7 | OsRAD17 plays a redundant role with OsZIP4 in synaptonemal complex assembly. OsREC8 signals (red) were used to indicate the chromosomes. Immunostaining for ZEP1 (green) in wild type, *Osrad17*, *Oszip4* and *Oszip4 Osrad17* at pachytene are shown. Bars, 5 μm.

et al., 1999). Therefore, DSB formation is able to be inferred from the γH2AX foci. Our analysis revealed similar localization of γH2AX in wild type, *Osrad17*, *Oszip4* and *Oszip4 Osrad17* (**Figure 8A**). This suggests that DSB formation is unaffected in *Oszip4 Osrad17*.

We next investigated the localization of OsCOM1 and OsDMC1 in *Oszip4 Osrad17* mutants (**Figures 8B,C**). OsCOM1 and OsDMC1 have been proved to be essential for DSB end resection and strand-exchange, respectively (Ji et al., 2012; Wang et al., 2016). Based on our observation, there was no significantly difference in the localization of OsCOM1 as well as OsDMC1 among wild type, *Osrad17*, *Oszip4* and *Oszip4 Osrad17*. Thus,

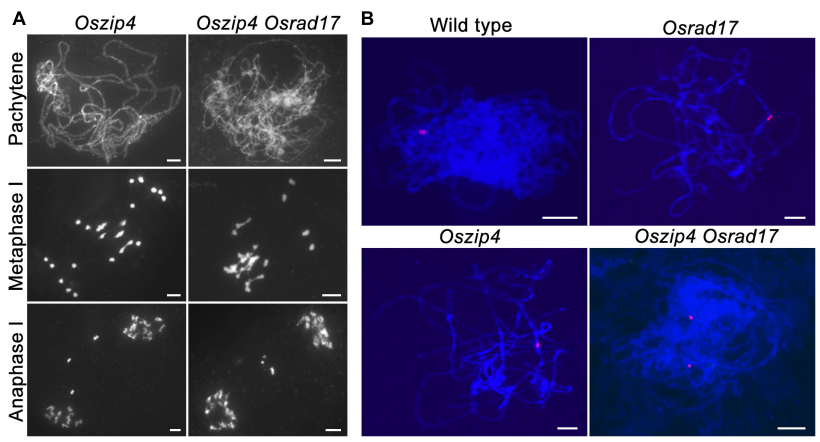

FIGURE 6 | OsRAD17 and OsZIP4 are redundantly required for homologous pairing. **(A)** Chromosomes behaviors in *Oszip4* and *Oszip4 Osrad17* at corresponding meiotic stages. **(B)** Localization of 5S rDNA signals in wild type, *Osrad17*, *Oszip4* and *Oszip4 Osrad17* PMCs during pachytene. Bars, 5 μm.

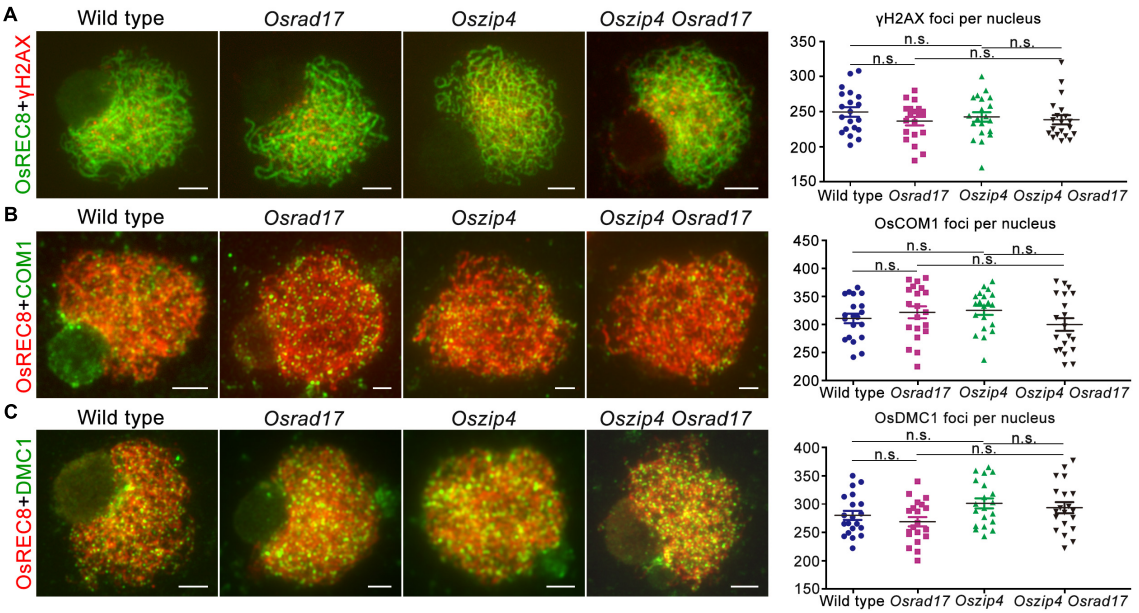

FIGURE 8 | Analysis of HR events in *Oszip4 Osrad17* double mutant. **(A)** Immunofluorescent investigation of γH2AX signals on the meiotic spreads of wild type, *Osrad17*, *Oszip4* and *Oszip4 Osrad17*. Bars, 5 μm. **(B)** Immunofluorescent investigation of OsCOM1 signals on the meiotic spreads of wild type, *Osrad17*, *Oszip4* and *Oszip4 Osrad17*. Bars, 5 μm. **(C)** Immunofluorescent investigation of OsDMC1 signals on the meiotic spreads of wild type, *Osrad17*, *Oszip4* and *Oszip4 Osrad17*. Bars, 5 μm. Scatter plot of foci per nucleus were presented (n = 20). n.s., no significant differences, $P > 0.05$ in two-tailed Student's t-tests.

despite the defective homologous pairing and synapsis, HR is normally initiated in the *Oszip4 Osrad17* double mutant.

DISCUSSION

OsRAD17 Is Required for Meiotic DSB Repair in Rice

Studies in yeast and mammals have elucidated the multiple functions of RAD17, a well-known checkpoint component (Lydall et al., 1996; Grushcow et al., 1999; Zou et al., 2002). Here, we isolated the RAD17 homolog in rice. Loss of OsRAD17 results in abnormal chromosome associations and fragmentations in PMCs. The *Osrad17* meiotic phenotype depends on programmed DSB formation, indicating the role of OsRAD17 in DSB repair. This phenotype resembles that of the 9-1-1 mutants in rice. In *Oshus1* and *Osrad1* mutant, DSB-dependent chromosome associations and fragments were also observed (Che et al., 2014; Hu et al., 2016). OsRAD17 can interact with OsRAD1 as revealed by yeast two-hybrid assays. In addition, the phenotype of *Osrad1 Osrad17* double mutant cannot be distinguished from that of each single mutant, indicating that they might function in the same pathway. Thus, we propose that OsRAD17 may participate in meiotic DSB repair by loading the 9-1-1 complex in rice.

OsRAD17 May Be Involved in DSB Repair Pathway Choice

Mitotic cells employ two basic strategies for DSB repair: HR and classical non-homologous end-joining (C-NHEJ), which involves direct ligation of the broken ends (Deriano and Roth, 2013). In *Arabidopsis*, the *Atrad17* mutant shows no significant increase in DNA damage, indicating NHEJ pathway might be sufficient to repair DNA damage (Yan et al., 2013). During meiosis, C-NHEJ competes with HR and creates de novo mutations in the gametes. Thus, this pathway should be restricted during meiotic DSB repair. Our previous study showed that C-NHEJ mediated by Ku70 accounted for most of the ectopic associations in *Osrad1*. In the *Osku70 Osrad1* PMCs, chromosome aggregations were partially suppressed compared with *Osrad1* (Hu et al., 2016). Thus, we speculated that OsRAD17 might participate in the DSB repair pathway choice during meiosis. Recent studies in yeast demonstrated the function of 9-1-1 during DNA resection, which affects DNA repair pathway choice (Blaikley et al., 2014; Ngo et al., 2014). Further studies are needed to test whether OsRAD17, together with 9-1-1 complex, functions through extensive DNA end resection in rice meiosis.

In budding yeast, the DNA damage response clamp 9-1-1 promotes ZMM proteins to take part in crossover formation and synaptonemal complex assembly (Shinohara et al., 2003, 2015). In the *rad24* mutant, Zip1 elongation is defective. In the *zip4* mutant, the synaptonemal complex protein Zip1 fails to polymerize along chromosomes (Tsubouchi et al., 2006). In mice carrying a disruption in MutS homolog Msh5, aberrant chromosome synapsis was observed (de Vries et al., 1999). These studies proved the involvement of both checkpoint proteins and ZMM proteins in SC formation. However, in plants, synapsis is almost normal in mutants related to these genes. Unexpectedly, the combination of mutations in both checkpoint proteins and ZMM proteins severely disrupted homologous pairing and

SC installation. We propose that the repair of most DSBs by HR in *Osrad17* is adequate for the homologous pairing and synapsis. However, more detailed studies are required to verify this speculation.

Functional Divergence of RAD17 in Different Plants

In Arabidopsis, AtRAD17 involves in DNA damage repair, which is negatively regulated by SMC5/6 complex (Heitzeberg et al., 2004; Yan et al., 2013). However, the mutation in *Atrad17* shows very weak effects on meiosis. The similar situations were observed for genes involved in anti-COs pathways. For example, FIGL1 and its partner FLIP in *Arabidopsis* function in limiting the number of COs. Mutants of these genes did not cause obvious defects in meiosis (Girard et al., 2015; Fernandes et al., 2018). However, disruptions of *MEICA1*, the homolog of *FLIP*, and *OsFIGNL1* led to non-homologous chromosome associations and fragmentations (Hu et al., 2017; Zhang et al., 2017). The difference in genome organization may cause the functional divergence of these proteins in meiosis (Lambing and Heckmann, 2018). Compared with *Arabidopsis*, rice has a bigger genome and contains more repetitive sequences.

AUTHOR CONTRIBUTIONS

ZC and QH conceived the original screening and research plans. YS and BM supervised the experiments. QH, CZ, and ZX performed most of the experiments. QH, LM, and WL designed the experiments and analyzed the data. QH conceived the project and wrote the article with contributions of all the authors. ZC supervised and complemented the writing.

FUNDING

This work was supported by grants from the Ministry of Sciences and Technology of China (2016YFD0100401), and the National Natural Science Foundation of China (31500255 and 31771363).

SUPPLEMENTARY MATERIAL

The Supplementary Material for this article can be found online at: https://www.frontiersin.org/articles/10.3389/fpls.2018.01236/full#supplementary-material

REFERENCES

Bishop, D. K., Park, D., Xu, L., and Kleckner, N. (1992). DMC1: a meiosis-specific yeast homolog of E. coli recA required for recombination, synaptonemal complex formation, and cell cycle progression. *Cell* 69, 439–456. doi: 10.1016/0092-8674(92)90446-J

Blaikley, E. J., Tinline-Purvis, H., Kasparek, T. R., Marguerat, S., Sarkar, S., Hulme, L., et al. (2014). The DNA damage checkpoint pathway promotes extensive resection and nucleotide synthesis to facilitate homologous recombination repair and genome stability in fission yeast. *Nucleic Acids Res.* 42, 5644-5656. doi: 10.1093/nar/gku190

Borner, G. V., Kleckner, N., and Hunter, N. (2004). Crossover/noncrossover differentiation, synaptonemal complex formation, and regulatory surveillance at the leptotene/zygotene transition of meiosis. *Cell* 117, 29–45. doi: 10.1016/S0092-8674(04)00292-2

Budzowska, M., Jaspers, I., Essers, J., de Waard, H., van Drunen, E., Hanada, K., et al. (2004). Mutation of the mouse Rad17 gene leads to embryonic lethality and reveals a role in DNA damage-dependent recombination. *EMBO J.* 23, 3548-3558. doi: 10.1038/sj.emboj.7600353

Cao, L., Alani, E., and Kleckner, N. (1990). A pathway for generation and processing of double-strand breaks during meiotic recombination in *S. cerevisiae*. *Cell* 61, 1089–1101. doi: 10.1016/0092-8674(90)90072-M

Che, L., Wang, K., Tang, D., Liu, Q., Chen, X., Li, Y., et al. (2014). OsHUS1 facilitates accurate meiotic recombination in rice. *PLoS Genet.* 10:e1004405. doi: 10.1371/journal.pgen.1004405

Chelysheva, L., Gendrot, G., Vezon, D., Doutriaux, M. P., Mercier, R., and Grelon, M. (2007). Zip4/Spo22 is required for class I CO formation but not for synapsis completion in *Arabidopsis thaliana*. *PLoS Genet.* 3:e83. doi: 10.1371/journal.pgen.0030083

de Vries, S. S., Baart, E. B., Dekker, M., Siezen, A., de Rooij, D. G., de Boer, P., et al. (1999). Mouse MutS-like protein Msh5 is required for proper chromosome synapsis in male and female meiosis. *Genes Dev.* 13, 523–531. doi: 10.1101/gad.13.5.523

Deriano, L., and Roth, D. B. (2013). Modernizing the nonhomologous end-joining repertoire: alternative and classical NHEJ share the stage. *Annu. Rev. Genet.* 47, 433-455. doi: 10.1146/annurev-genet-110711-155540

Fernandes, J. B., Duhamel, M., Seguela-Arnaud, M., Froger, N., Girard, C., Choinard, S., et al. (2018). FIGL1 and its novel partner FLIP form a conserved complex that regulates homologous recombination. *PLoS Genet.* 14:e1007317. doi: 10.1371/journal.pgen.1007317

Girard, C., Chelysheva, L., Choinard, S., Froger, N., Macaisne, N., Lemhemdi, A., et al. (2015). AAA-ATPase FIDGETIN-LIKE 1 and helicase FANCM antagonize meiotic crossovers by distinct mechanisms. *PLoS Genet.* 11:e1005369. doi: 10.1371/journal.pgen.1005369

Griffith, J. D., Lindsey-Boltz, L. A., and Sancar, A. (2002). Structures of the human Rad17-replication factor C and checkpoint Rad 9-1-1 complexes visualized by glycerol spray/low voltage microscopy. *J. Biol. Chem.* 277, 15233-15236. doi: 10.1074/jbc.C200129200

Grushcow, J. M., Holzen, T. M., Park, K. J., Weinert, T., Lichten, M., and Bishop, D. K. (1999). *Saccharomyces cerevisiae* checkpoint genes MEC1, RAD17 and RAD24 are required for normal meiotic recombination partner choice. *Genetics* 153, 607–620.

Heitzeberg, F., Chen, I. P., Hartung, F., Orel, N., Angelis, K. J., and Puchta, H. (2004). The Rad17 homologue of *Arabidopsis* is involved in the regulation of DNA damage repair and homologous recombination. *Plant J.* 38, 954-968. doi: 10.1111/j.1365-313X.2004.02097.x

Higgins, J. D., Vignard, J., Mercier, R., Pugh, A. G., Franklin, F. C., and Jones, G. H. (2008). AtMSH5 partners AtMSH4 in the class I meiotic crossover pathway in *Arabidopsis thaliana*, but is not required for synapsis. *Plant J.* 55, 28-39. doi: 10.1111/j.1365-313X.2008.03470.x

Hu, Q., Li, Y., Wang, H., Shen, Y., Zhang, C., Du, G., et al. (2017). Meiotic chromosome association 1 interacts with TOP3alpha and regulates meiotic recombination in rice. *Plant Cell* 29, 1697-1708. doi: 10.1105/tpc.17.00241

Hu, Q., Tang, D., Wang, H., Shen, Y., Chen, X., Ji, J., et al. (2016). The exonuclease homolog OsRAD1 promotes accurate meiotic double-strand break repair by suppressing nonhomologous end joining. *Plant Physiol.* 172, 1105-1116. doi: 10.1104/pp.16.00831

Ivanov, E. L., Korolev, V. G., and Fabre, F. (1992). XRS2, a DNA repair gene of *Saccharomyces cerevisiae*, is needed for meiotic recombination. *Genetics* 132, 651–664.

Ji, J., Tang, D., Wang, K., Wang, M., Che, L., Li, M., et al. (2012). The role of OsCOM1 in homologous chromosome synapsis and recombination in rice meiosis. *Plant J.* 72, 18-30. doi: 10.1111/j.1365-313X.2012.05025.x

Keeney, S., Giroux, C. N., and Kleckner, N. (1997). Meiosis-specific DNA double-strand breaks are catalyzed by Spo11, a member of a widely conserved protein family. *Cell* 88, 375–384. doi: 10.1016/S0092-8674(00)81876-0

Lambing, C., and Heckmann, S. (2018). Tackling plant meiosis: from model research to crop improvement. *Front. Plant Sci.* 9:829. doi: 10.3389/fpls.2018.00829

Luo, Q., Tang, D., Wang, M., Luo, W., Zhang, L., Qin, B., et al. (2013). The role of OsMSH5 in crossover formation during rice meiosis. *Mol. Plant* 6, 729-742. doi: 10.1093/mp/sss145

Lydall, D., Nikolsky, Y., Bishop, D. K., and Weinert, T. (1996). A meiotic recombination checkpoint controlled by mitotic checkpoint genes. *Nature* 383, 840-843. doi: 10.1038/383840a0

Lynn, A., Soucek, R., and Borner, G. V. (2007). ZMM proteins during meiosis: crossover artists at work. *Chromosome Res.* 15, 591-605. doi: 10.1007/s10577-007-1150-1151

Nairz, K., and Klein, F. (1997). mre11S–a yeast mutation that blocks double-strand-break processing and permits nonhomologous synapsis in meiosis. *Genes Dev.* 11, 2272–2290. doi: 10.1101/gad.11.17.2272

Navadgi-Patil, V. M., and Burgers, P. M. (2009). A tale of two tails: activation of DNA damage checkpoint kinase Mec1/ATR by the 9-1-1 clamp and by Dpb11/TopBP1. *DNA Repair* 8, 996-1003. doi: 10.1016/j.dnarep.2009.03.011

Ngo, G. H., Balakrishnan, L., Dubarry, M., Campbell, J. L., and Lydall, D. (2014). The 9-1-1 checkpoint clamp stimulates DNA resection by Dna2-Sgs1 and Exo1. *Nucleic Acids Res.* 42, 10516-10528. doi: 10.1093/nar/gku746

Rogakou, E. P., Boon, C., Redon, C., and Bonner, W. M. (1999). Megabase chromatin domains involved in DNA double-strand breaks in vivo. *J. Cell Biol.* 146, 905–916. doi: 10.1083/jcb.146.5.905

Ross-Macdonald, P., and Roeder, G. S. (1994). Mutation of a meiosis-specific MutS homolog decreases crossing over but not mismatch correction. *Cell* 79, 1069–1080. doi: 10.1016/0092-8674(94)90037-X

San Filippo, J., Sung, P., and Klein, H. (2008). Mechanism of eukaryotic homologous recombination. *Annu. Rev. Biochem.* 77, 229-257. doi: 10.1146/annurev.biochem.77.061306.125255

Shao, T., Tang, D., Wang, K., Wang, M., Che, L., Qin, B., et al. (2011). OsREC8 is essential for chromatid cohesion and metaphase I monopolar orientation in rice meiosis. *Plant Physiol.* 156, 1386-1396. doi: 10.1104/pp.111.177428

Shen, Y., Tang, D., Wang, K., Wang, M., Huang, J., Luo, W., et al. (2012). ZIP4 in homologous chromosome synapsis and crossover formation in rice meiosis. *J. Cell Sci.* 125(Pt 11), 2581-2591. doi: 10.1242/jcs.090993

Shinohara, M., Hayashihara, K., Grubb, J. T., Bishop, D. K., and Shinohara, A. (2015). DNA damage response clamp 9-1-1 promotes assembly of ZMM proteins for formation of crossovers and synaptonemal complex. *J. Cell Sci.* 128, 1494-1506. doi: 10.1242/jcs.161554

Shinohara, M., Sakai, K., Ogawa, T., and Shinohara, A. (2003). The mitotic DNA damage checkpoint proteins Rad17 and Rad24 are required for repair of double-strand breaks during meiosis in yeast. *Genetics* 164, 855–865.

Sung, P., and Robberson, D. L. (1995). DNA strand exchange mediated by a RAD51-ssDNA nucleoprotein filament with polarity opposite to that of RecA. *Cell* 82, 453–461. doi: 10.1016/0092-8674(95)90434-4

Tsubouchi, T., Zhao, H., and Roeder, G. S. (2006). The meiosis-specific zip4 protein regulates crossover distribution by promoting synaptonemal complex formation together with zip2. *Dev. Cell* 10, 809-819. doi: 10.1016/j.devcel.2006.04.003

Wang, H., Hu, Q., Tang, D., Liu, X., Du, G., Shen, Y., et al. (2016). OsDMC1 is not required for homologous pairing in rice meiosis. *Plant Physiol.* 171, 230-241. doi: 10.1104/pp.16.00167

Wang, K., Tang, D., Wang, M., Lu, J., Yu, H., Liu, J., et al. (2009). MER3 is required for normal meiotic crossover formation, but not for presynaptic alignment in rice. *J. Cell Sci.* 122(Pt 12), 2055-2063. doi: 10.1242/jcs.049080

Wang, M., Wang, K., Tang, D., Wei, C., Li, M., Shen, Y., et al. (2010). The central element protein ZEP1 of the synaptonemal complex regulates the number of crossovers during meiosis in rice. *Plant Cell* 22, 417-430. doi: 10.1105/tpc.109.070789

Wang, Q., Goldstein, M., Alexander, P., Wakeman, T. P., Sun, T., Feng, J., et al. (2014). Rad17 recruits the MRE11-RAD50-NBS1 complex to regulate the cellular response to DNA double-strand breaks. *EMBO J.* 33, 862-877. doi: 10.1002/embj.201386064

Wang, X., Zou, L., Lu, T., Bao, S., Hurov, K. E., Hittelman, W. N., et al. (2006). Rad17 phosphorylation is required for claspin recruitment and Chk1 activation in response to replication stress. *Mol. Cell* 23, 331-341. doi: 10.1016/j.molcel.2006.06.022

Wang, X., Zou, L., Zheng, H., Wei, Q., Elledge, S. J., and Li, L. (2003). Genomic instability and endoreduplication triggered by RAD17 deletion. *Genes Dev.* 17, 965-970. doi: 10.1101/gad.1065103

Yan, S., Wang, W., Marques, J., Mohan, R., Saleh, A., Durrant, W. E., et al. (2013). Salicylic acid activates DNA damage responses to potentiate plant immunity. *Mol. Cell* 52, 602-610. doi: 10.1016/j.molcel.2013.09.019

Yang, R., Li, Y., Su, Y., Shen, Y., Tang, D., Luo, Q., et al. (2016). A functional centromere lacking CentO sequences in a newly formed ring chromosome in rice. *J. Genet. Genomics* 43, 694-701. doi: 10.1016/j.jgg.2016.09.006

Zhang, L., Tang, D., Luo, Q., Chen, X., Wang, H., Li, Y., et al. (2014). Crossover formation during rice meiosis relies on interaction of OsMSH4 and OsMSH5. *Genetics* 198, 1447-1456. doi: 10.1534/genetics.114.168732

Zhang, P., Zhang, Y., Sun, L., Sinumporn, S., Yang, Z., Sun, B., et al. (2017). The rice AAA-ATPase OsFIGNL1 is essential for male meiosis. *Front. Plant Sci.* 8:1639. doi: 10.3389/fpls.2017.01639

Zou, L., Cortez, D., and Elledge, S. J. (2002). Regulation of ATR substrate selection by Rad17-dependent loading of Rad9 complexes onto chromatin. *Genes Dev.* 16, 198-208. doi: 10.1101/gad.950302

Conflict of Interest Statement: The authors declare that the research was conducted in the absence of any commercial or financial relationships that could be construed as a potential conflict of interest.

frontiers in Plant Science

ORIGINAL RESEARCH
published: 23 March 2018
doi: 10.3389/fpls.2018.00368

FANCM Limits Meiotic Crossovers in Brassica Crops

*Aurélien Blary[1], Adrián Gonzalo[1], Frédérique Eber[2], Aurélie Bérard[3], Hélène Bergès[4], Nadia Bessoltane[1], Delphine Charif[1], Catherine Charpentier[1], Laurence Cromer[1], Joelle Fourment[4], Camille Genevriez[1], Marie-Christine Le Paslier[3], Maryse Lodé[2], Marie-Odile Lucas[2], Nathalie Nesi[2], Andrew Lloyd[1], Anne-Marie Chèvre[2] and Eric Jenczewski[1]**

[1] Institut Jean-Pierre Bourgin, Institut National de la Recherche Agronomique, AgroParisTech, Centre National De La Recherche Scientifique, Université Paris-Saclay, Versailles, France, [2] IGEPP, Institut National de la Recherche Agronomique, Agrocampus Ouest, Université de Rennes 1, Le Rheu, France, [3] EPGV US 1279, Institut National de la Recherche Agronomique, CEA-IG-CNG, Université Paris-Saclay, Evry, France, [4] Institut National de la Recherche Agronomique UPR 1258, Centre National des Ressources Génomiques Végétales, Castanet-Tolosan, France

Meiotic crossovers (COs) are essential for proper chromosome segregation and the reshuffling of alleles during meiosis. In WT plants, the number of COs is usually small, which limits the genetic variation that can be captured by plant breeding programs. Part of this limitation is imposed by proteins like FANCM, the inactivation of which results in a 3-fold increase in COs in *Arabidopsis thaliana*. Whether the same holds true in crops needed to be established. In this study, we identified EMS induced mutations in FANCM in two species of economic relevance within the genus *Brassica*. We showed that CO frequencies were increased in *fancm* mutants in both diploid and tetraploid *Brassicas*, *Brassica rapa* and *Brassica napus* respectively. In *B. rapa*, we observed a 3-fold increase in the number of COs, equal to the increase observed previously in *Arabidopsis*. In *B. napus* we observed a lesser but consistent increase (1.3-fold) in both euploid (AACC) and allohaploid (AC) plants. Complementation tests in *A. thaliana* suggest that the smaller increase in crossover frequency observed in *B. napus* reflects residual activity of the mutant C copy of FANCM. Altogether our results indicate that the anti-CO activity of FANCM is conserved across the *Brassica,* opening new avenues to make a wider range of genetic diversity accessible to crop improvement.

Keywords: FANCM, Translational biology, *Brassica*, meiotic crossover, TILLING, plant breeding, polyploidy

OPEN ACCESS

Edited by:
Mónica Pradillo, Complutense University of Madrid, Spain

Reviewed by:
Wayne Crismani, St. Vincent's Institute of Medical Research, Australia
Hong An, University of Missouri, United States

****Correspondence:***
Eric Jenczewski
eric.jenczewski@inra.fr

Specialty section:
This article was submitted to Plant Cell Biology, a section of the journal Frontiers in Plant Science

Received: *06 December 2017*
Accepted: *06 March 2018*
Published: *23 March 2018*

Citation:
Blary A, Gonzalo A, Eber F, Bérard A, Bergès H, Bessoltane N, Charif D, Charpentier C, Cromer L, Fourment J, Genevriez C, Le Paslier M-C, Lodé M, Lucas M-O, Nesi N, Lloyd A, Chèvre A-M and Jenczewski E (2018) FANCM Limits Meiotic Crossovers in Brassica Crops. Front. Plant Sci. 9:368. doi: 10.3389/fpls.2018.00368

INTRODUCTION

Meiotic recombination is essential for proper chromosome segregation and reshuffling of genetic information through the formation of Cross-Overs (COs); i.e., reciprocal exchanges of genetic material between homologous chromosomes. Meiotic recombination plays both a direct and an indirect role in plant genome evolution because of its inherent mutagenic nature (Rattray et al., 2015) and its influence on selection (Tiley and Burleigh, 2015). It is also central to plant breeding (Wijnker and de Jong, 2008) as it produces new combinations of alleles on which selection can act. Accordingly, an increase in CO frequencies is predicted to result in a better response to selection (McClosky and Tanksley, 2013). Yet the number of COs is low in most species, rarely exceeding 2–3 per chromosome (Mercier et al., 2015).

Meiotic recombination is initiated by programmed double strand breaks (DSBs) (Keeney et al., 1997) that can be repaired as COs through two pathways. The first pathway, which forms the majority of COs (i.e., "class I" COs), is dependent on a group of proteins initially identified in *S. cerevisiae* and collectively called ZMMs (Zip1-4, Msh4/Msh5, and Mer3). In *A. thaliana, zmm* mutants, including *Atmsh4* and *Atmsh5*, show severely reduced fertility due to a decrease in CO frequency (∼15% of the WT CO level) (Higgins et al., 2004, 2008). The distribution of class I COs ensures one obligate CO per pair of homologous chromosomes and is subject to interference; this means that the presence of one CO reduces the probability of observing another CO in the vicinity. The second pathway, which is secondary in WT meiosis, depends, at least in part, on the endonuclease MUS81; the resulting class II COs are randomly distributed (i.e., not affected by CO interference) and far more difficult to mark cytologically (Anderson et al., 2014). The vast majority of DSBs however, are repaired as non-reciprocal exchanges of genetic material, termed non Cross-Overs (NCOs). Because the number of DSBs vastly outnumbers COs, negative regulators of CO frequency have been hypothesized. In *Arabidopsis thaliana,* genetic screens designed to identify these negative regulators have been carried out and have identified genes in three distinct pathways that limit class II COs (Crismani et al., 2012; Girard et al., 2014, 2015; Séguéla-Arnaud et al., 2015; Fernandes et al., in review).

The first anti-CO protein identified through these screens was FANCM (Fanconi Anemia Complementation Group M) (Crismani et al., 2012). FANCM has long been recognized as a core component of the Fanconi Anemia pathway, a network of at least 22 proteins identified in human that preserve genome stability by promoting the processing of interstrand crosslinks (Wang and Smogorzewska, 2015). In addition to a C-terminal ERCC4-like nuclease domain and a tandem helix–hairpin–helix $(HhH)_2$ domain, FANCM consists of an N-terminal bipartite SF2 helicase domain (composed of a DEXDc and a HELICc domain) (Whitby, 2010). *FANCM* orthologs have now been identified in various eukaryotes in which they do not always play the exact same role (Lorenz et al., 2012).

Studies in *A. thaliana* showed that AtFANCM regulates somatic and meiotic recombination (Knoll and Puchta, 2011; Crismani et al., 2012). During meiotic recombination, FANCM is thought to promote NCO formation through the SDSA pathway (Crismani et al., 2012). FANCM acts as a landing pad for multiple Fanconi Anemia associated proteins (Vinciguerra and D'Andrea, 2009). In Arabidopsis, only FANCM direct DNA-binding cofactors MHF1 and MHF2 were shown to contribute to the FANCM anti-CO activity (Girard et al., 2014). The SF2 helicase domain of AtFANCM appears to be critical for its anti-CO activity. Mutations in well-conserved residues of the DEXDc and a HELICc domains were indeed shown to increase MUS81-dependent CO formation in *fancm* single mutants (Crismani et al., 2012). This increase is so huge that it restores bivalent formation in *zmm* CO-defective mutants to a level indistinguishable from WT.

The boost in COs observed in *atfancm* mutants, which can be up to 3.6-fold in some intervals, could be of great interest for plant breeding. Yet, to the best of our knowledge, the effect of FANCM on CO formation has never been assessed in a crop species. The present study aimed to fill this gap using *Brassica* crops as models.

In addition to the model species *A. thaliana,* the *Brassicaceae* family includes many diploid and polyploid crops (e.g., *B. rapa*, *B. oleracea, B. napus*, *B. juncea*) that show a rich diversity of morphotypes (Cheng et al., 2014). Although many of these species can be used as vegetable, fodder, oilseed or even as ornamental crops, diploid *B. rapa* (chinese cabbage, turnip, pak choi…) and *B. oleracea* (cabbage, Brussels sprouts, broccoli, cauliflower…) are often referred to as leaf vegetables while allotetraploid *B. napus* (oilseed rape or canola) is mainly cultivated as an oilseed crop. *B. napus* (AACC; $2n = 38$) arose from multiple hybridization events between the ancestors of modern *B. oleracea* (CC; $2n = 18$) and *B. rapa* (AA; $2n = 20$). Because the progenitors of *B. napus* have experienced a whole-genome triplication (WGT) before hybridization (Lysak et al., 2005), every gene in *A. thaliana* could possibly have up to 6 homologs in *B. napus.* Such a high number of homologs is rarely observed however, as fractionation, the process by which duplicate genes are lost (Freeling, 2009; Woodhouse et al., 2010), starts right after the onset of WGD (Li Z. et al., 2016). The trend is especially strong for meiotic recombination genes that return to a single copy more rapidly than genome-wide average in angiosperms (Lloyd et al., 2014).

Intense selection in *Brassica* resulted in a notable decline in genetic diversity in modern cultivars of *B. napus*, *B. rapa,* and *B. oleracea* (Hasan et al., 2006; Qian et al., 2014; Cheng et al., 2016). Increasing meiotic crossovers in *Brassica* crops could thus be of great interest to generate novel genetic combinations and expand the range of genotypes available in these cultivated species. In this study, we explore the anti-CO activity of FANCM in two *Brassica* species, diploid *B. rapa,* and allotetraploid *B. napus,* as a proof-of-concept for all other crops in this family.

MATERIALS AND METHODS

Development of a Mutagenized Population for *Brassica napus*

Seeds from *Brassica napus* L. cv. *Tanto* (double-low spring cultivar, INRA Rennes, France) were immersed into a 0.5% EMS solution overnight under moderate shaking (200 rpm). The treated seeds were rinsed three times for 5 min in a solution of 1 M sodium thiosulfate, twice for 5 min in distilled water and then briefly dried onto a paper towel before being disposed on a water-imbibed Whatman filter paper in Petri dishes. Seeds were allowed to germinate at room temperature for two days in the dark and to elongate for two additional days under 16 h light/8 h dark.

Seedlings from treated seeds (hereafter called the M1 generation) were transferred into individual pots filled with a mixture of 20% black peat, 70% white peat and 10% perlit as substrate (Haasnoot Substraten, Zaltbommel, NL) and grown in the glasshouse (16 h light at 22°C/8 h dark at 18°C; 200 $\mu mol.m^{-2}.s^{-1}$ light intensity at the plant level). Six-leaf plants were vernalized for four weeks to ensure correct and

homogenous flowering and vernalized plants were transferred into a tunnel. At flowering, inflorescences on the primary raceme were covered with a selfing bag to avoid cross pollination while the branches were regularly cut. Pods from the main inflorescences were harvested at ∼1,000 growing degree (°C) days after flowering and the collected seeds constituted the M2 seed lots, each arising from a single mutagenized M1 plant. The whole mutagenized population (hereafter called the RAPTILL population) consists of 9,970 M2 seed lots produced by INRA Rennes and stored under controlled conditions (5% RH, 8°C).

For DNA extractions, four seeds for each of the RAPTILL M2 seed lots were sown in individual pots. Leaf material was collected on 3-to-4-week old plants as a mixture of 16 leaf discs (Ø = 5 mm) per M2 family. After sample freeze-drying and grinding, DNA extractions were performed with the DNeasy 96 Plant Kit following the manufacturer's instructions (Qiagen, Chatsworth, CA, USA) and then tested for quality and quantity.

FANCM Homologues Identification—Screening of the BAC Libraries

FANCM homologues were identified using reciprocal BLASTp and PSI-BLAST against the published *B. napus* (http://www.genoscope.cns.fr/blat-server/cgi-bin/colza/webBlat; Chalhoub et al., 2014), *B. rapa* (http://brassicadb.org/brad/blastPage.php; Wang et al., 2011) and *B. oleracea* (http://plants.ensembl.org/Multi/Tools/Blast?db=core) assemblies. Screening of the *B. napus* cv "*Darmor-bzh*" BAC library was performed by the CNRGV (INRA Toulouse) as described in (Lloyd et al., 2014).

Search for Mutations in *FANCM*—TILLING Experiment

For *Brassica rapa*, we searched for mutations in *BraA.FANCM* (and *BraA.MSH4*) in the EMS mutagenized population of *B. rapa* subsp. *trilocularis* (Yellow Sarson) developed by the John Innes Centre (Stephenson et al., 2010; work conducted by Fran Robson at RevGenUK). Above and hereafter, we used a nomenclature adapted from Ostergaard and King (2008) where "categories are listed in descending order of significance from left to right (i.e., genus—species—genome—gene name)": e.g., *Bra* stands for *B. rapa* while *Bna* stands for *B. napus*, A, and C are the two genomes where we searched for mutations in *FANCM* or *MSH4*, respectively.

In *B. napus*, two separate screens were carried out to find mutations affecting specifically *BnaA.FANCM* or *BnaC.FANCM* in a subset of 500 M2 plants from the RAPTILL population described above. These screens were based on the use of copy-specific primer pairs (Supplementary Figure S1) and implemented the PMM (Plant Mutated on its Metabolites) method (Triques et al., 2007, 2008; work conducted by Julien Schmidt at AELRED).

In both cases, TILLING targeted a region of 1Kb in the bipartite helicase domain of FANCM (Supplementary Figure S1). The list of the primers used for amplifying these regions is given in Supplementary Table S1. The primers were designed to amplify a single locus, i.e., they are copy-specific. We ensured that only one of the two homoeologous copies of FANCM was amplified in *B. napus* (Supplementary Figure S1).

Plant Material to Evaluate the Role of *FANCM* in *Brassica napus*

We initially selected three mutant alleles for *FANCM* in *B. napus* cv. *Tanto*: one nonsense mutation for the A copy (thereafter referred as to *bnaA.fancm-1*) and two missense mutations for the C copy (*bnaC.fancm-1* and *bnaC.fancm-2*). These mutations have a SIFT (Sorting Intolerant From Tolerant) score equal to zero, i.e., are predicted to be damaging to the protein (Sim et al., 2012). Two F1 hybrids combining *bnaA.fancm-1* with either *bnaC.fancm-1* or *bnaC.fancm-2* were first produced (*h1* and *h2* in Supplementary Figure S2). These F1s were then selfed to produce a full set of segregating F2 plants, among which we sought for plants homozygous for the two mutations (thereafter referred as double A/C mutants) or for the two WT alleles (thereafter referred as to WT siblings).

Two double A/C mutants (*bna.fancm_1-1*; which combined mutant alleles *bnaA.fancm-1* and *bnaC.fancm-1*) and two WT siblings (*Bna.FANCM_1-1)* were first identified in the progeny of the first F1 hybrid (*h1*; Supplementary Figure S2). These four plants, together with two single mutants homozygous for either *bnaA.fancm-1* or *bnaC.fancm-1*, were sequenced in order to identify in one go: (1) background EMS-induced mutations that can be used to develop Cleavage Amplified Polymorphism (CAPs) markers and (2) pairs of heterozygous intervals shared between mutant and WT F2s that can be used to compare crossover frequencies (Supplementary Figure S3). It turned out, however, that the *bna.fancm_1-1* mutants had no detectable effect on crossover formation (data not shown); these plants were therefore discarded for further analyses.

Two double A/C mutants (*bna.fancm_1-2*; which combined mutant alleles *bnaA.fancm-1* and *bnaC.fancm-2*) and two WT siblings (*Bna.FANCM_1-2*) were identified in the progeny of the second F1 (*h2*, Supplementary Figure S2). These plants were selfed to produce F3 progenies from which crossover frequencies were estimated genetically (Supplementary Figure S3). In the meantime, the F1 plant (*h2*), along with four other F1 hybrids combining *bnaA.fancm-1* with *bnaC.fancm-2*, were used to produce segregating populations of allohaploids following the protocol described in Jenczewski et al. (2003). For each F1 hybrid, 20–140 plants were regenerated through microspore culture; 20–40 allohaploid plants were then selected (per F1 hybrid) after validation of their ploidy level by flow cytometry. Molecular screening for *FANCM* alleles revealed the expected segregation pattern for the mutations, with 25% WT and 25% double (A/C) mutant allohaploids. For each F1 hybrid, a minimum of two double mutants and two WT siblings were selected for cytological evaluation (Supplementary Figure S2). This assay therefore encompassed two layers of replication: (1) the F1 hybrids that we used to derive allohaploids, each containing a different patchwork of background mutations inherited from the *bnaA.fancm-1* and *bnaC.fancm-2* parents and (2) the different double (A/C) *fancm* mutant and WT plants that were derived from a given F1 hybrid,

each containing different combinations of mutations present at the heterozygous stage in the F1 (Supplementary Figure S3).

The different *fancm* mutations were detected using Cleaved Amplified Polymorphic Sequences (CAPS) assay targeting the causative EMS-SNP. The list of primers and restriction enzymes in given in Supplementary Tables S1, S2.

DNA Sequencing to Identify Background Mutations

Total DNA was extracted using the NucleoSpin® Plant II Midi/Maxi (Macherey-Nagel) extraction kit. DNA sequencing was carried out by EPGV group (INRA, Evry). Whole genome libraries were prepared using the TruSeq® DNA PCR-Free LT kit (Illumina). Briefly, sample preparation was performed with the low sample protocol using a 550 bp fragment sizing; all enzymatic steps and clean-up procedures were performed according to manufacturer's instructions. The resulting indexed libraries, including the ligated adapter sequences, had a mean size of 870 bp. Clustering and pair-end sequencing (2 × 100 sequencing by synthesis (SBS) cycles) were performed in high output mode on a HiSeq® 2,000/2,500 (Illumina) according to manufacturer's instructions. The two single homozygous mutants for *bnaA.fancm-1* and *bnaC.fancm-1* were sequenced on the same single lane while the corresponding double homozygous and WT F2s were sequenced on a single lane each. Raw short-read data are available in the NCBI BioProject PRJNA432890.

Mutations were identified and annotated using the "homemade" pipeline MutDetect described in Girard et al. (2014). Briefly, sequences were aligned against the reference *B. napus* genome sequence (Chalhoub et al., 2014) allowing up to 2 mismatches and 1 indel per read. Alignments were cleaned up according to the Genome Analysis ToolKit (GATK) recommendations (McKenna et al., 2010). Raw variants were then filtered according to both quality and coverage criterions (quality> 100 and Depth>2). Homozygous variants detected on all samples were considered as natural polymorphisms between *Darmor-bzh* (reference) and *Tanto* accessions and were removed.

Genetic Assessment of Co Rate and Variation

We used the sequence data obtained with the *bna.fancm_1-1* and *Bna.FANCM_1-1* plants to develop CAPS markers. These markers were used to genotype the *bna.fancm_1-2* and *Bna.FANCM_1-2* plants and identify pairs of heterozygous intervals shared between mutant and WT F2s (Supplementary Figure S2). This approach was constrained by the fact that the F2 plants we sequenced (the first we obtained) were not the same as the ones we used for this genetic assay. Consequently, many of the CAPS markers we developed failed to identify intervals that were heterozygous in both the mutant and WT F2s.

The list of primer pairs and restriction enzymes that we eventually used for genotyping F3 progenies is given in Supplementary Table S3. Crossover frequencies were estimated using MapDisto (Lorieux, 2012). The statistical significance of the pairwise difference between WT and mutant crossover frequencies was obtained using the Welch test with a significance threshold of 5% (Bauer et al., 2013).

Cytology

Florets were fixed in Carnoy's fixative (absolute ethanol:acetic acid, 3:1, v/v). CO frequencies were inferred from male meiotic spreads after staining with either DAPI (as described by Chelysheva et al., 2013) or Acetocarmine (as described by Jenczewski et al., 2003). In *B. rapa*, in which we mainly observed bivalents (i.e., pairs of homologous chromosomes bound by COs), we used the criteria established by Moran et al. (2001) to estimate the number of chiasmata: rod bivalents were considered to be bound by one single chiasma in one arm only, whereas ring bivalents were considered to have both arms bound by one chiasma. In *B. napus* allohaploids, we rather counted the number of univalents (i.e., chromosomes that failed to form crossovers), which were a majority and easy to score. In both cases, a minimum of 20 pollen mother cells was examined in each plant.

Pyrosequencing

Pyrosequencing was performed on meiotic cDNA and on gDNA to check for amplification bias. The following primers were used for amplification and sequencing:

pFANCMR:TTTCGTTGGCTAAATCTTCTTCCT,
pFANCMF:ACGAAGCAAACAGAGAAGAAGACC,
pFANCMS:TCTTCTGCCAATTCATTA

Primer pairs have been designed with Pyromark Assay Design v2.0.1.15 and the pyrosequencing reaction has been performed with PyroMark Q24 v2.0.6 of QIAGEN®.

Directed Mutagenesis Constructs, Plant Transformation, and Plasmid Constructs

A *AtFANCM* genomic fragment from *A. thaliana* was amplified that included 618 nucleotides before the ATG and 1,029 after the stop codon. The PCR product was cloned, by Gateway (Invitrogen) into the pDONR207 (Invitrogen) to create pENTR-FANCM, on which directed mutagenesis was performed using the Stratagene Quick-change Site-Directed Mutagenesis Kit. For plant transformation, LR reaction was performed with the binary vector pGWB1 (Nakagawa et al., 2007). The resulting binary vectors were transformed using the Agrobacterium-mediated floral dip method (Clough and Bent, 1998) on double homozygous mutant plant (*fancm*$^{-/-}$/*msh5*$^{-/-}$).

RESULTS

FANCM Is Present in a Single Copy *Per Brassica* Genome

We first assessed the number of copies of *FANCM* that were retained in each Brassica genome following WGT. Querying the CDS of *At.FANCM* (JQ278026) against the available genome sequences revealed that *FANCM* has one single homologue in both *B. rapa* (*Bra034416* on chromosome A05, hereinafter referred as to *BraA.FANCM*) and *B. oleracea* (*Bo5g085100* on

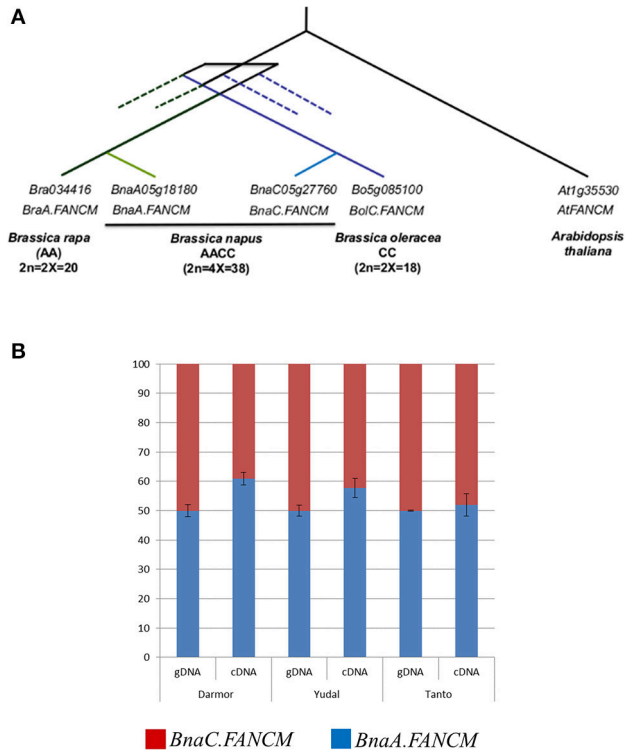

FIGURE 1 | One copy of *FANCM* per genome is present and expressed in *Brassica napus*. **(A)** Schematic representation of the relationships between FANCM homologs in *Brassica rapa*, *B. napus*, *B. oleracea,* and *Arabidopsis thaliana*. Dotted lines represent the fractionated copies; i.e., copies originating from the Brassica specific whole genome triplication (WGT) and subsequently lost. **(B)** Relative contribution of *BnaA.FANCM* and *BnaC.FANCM* to total expression of *FANCM* in *Brassica napus.* Pyrosequencing data for *BnaA.FANCM* (blue) and *BnaC.FANCM* (red) in three varieties of *B. napus*. Genomic DNA (gDNA) was used as a control for biased PCR amplification between the two copies. Error bars = 1 SD from 3 biological replicates.

chromosome C05; *BolC.FANCM*) while *B. napus* contains two copies of *FANCM* (**Figure 1A**). The presence of two *FANCM* homologues in *B. napus* (*BnaA05g18180D* / *BnaA.FANCM* on A05 and *BnaC05g27760D*/*BnaC.FANCM* on C05) was further confirmed by BAC screening and sequencing. The sequences obtained from the BACs were instrumental to complete the full-length sequences of *BnaA.FANCM* and *BnaC.FANCM* that were still pending in the published assembly. These two genes are located within syntenic regions (Supplementary Figure S4) and form a pair of homoeologues. We used mRNA-Seq data produced from *B. napus* male meiocytes (Lloyd et al., 2018) to show that *BnaA.FANCM* and *BnaC.FANCM* are almost equally transcribed during meiosis in this species; this result was subsequently confirmed by pyrosequencing (**Figure 1B**).

We also used the mRNA-Seq data to confirm the sequence of *BnaFANCM* open reading frames. *BnaA.FANCM* and *BnaC.FANCM* have almost the same intron/exon structure; they only differ by the presence of a small (70 bp) additional intron in *BnaC.FANCM* (and *BolC.FANCM*) that splits Exon 2 but does not alter the final amino acid sequence. The two predicted proteins (based on the full-length cDNA sequences derived from the mRNA-Seq data) share >97% identity across their full length. They are highly related to At.FANCM (∼81% identity and ∼84% similarity with JQ278026), in particular in the regions of the DEXDc and a HELICc helicase domains (Supplementary Figure S5).

EMS Mutagenesis Yielded Point Mutations Predicted to Alter the Function of FANCM in *Brassica*

Two EMS (Ethylmethanesulfonate) mutagenized populations (one for *B. rapa* and one for *B. napus*; ∼500 M2 plants each) were screened for mutations within ∼1 kb of the bipartite helicase domain of FANCM (Supplementary Figure S1) where many loss-of-function mutations have been found in *A. thaliana* (Crismani et al., 2012).

In total, >100 mutations were identified across the three *FANCM* genes with considerable gene-to-gene variation (Supplementary Figure S1); i.e., more than twice as many EMS mutations were found in *BnaA.FANCM* and *BnaC.FANCM* compared to *Bra.FANCM*. This reflected an average density of one mutation every 13 Kb in the *B. napus* mutagenized population compared to 1/31 Kb in the *B. rapa* population (1/60 Kb in Stephenson et al., 2010). Around 75% of these mutations (77/104) were synonymous substitutions or occurred in introns (Supplementary Figure S1) and only one non-sense mutation was identified among the three genes (in *BnaA.FANCM*). These estimates are similar to previous findings from M2 lines of the same (*B. rapa*) and other mutagenized populations (see Gilchrist et al., 2013 and ref. therein).

We retained the single non-sense mutation for *BnaA.FANCM* (hereinafter referred to as *bnaA.fancm-1)* identified in our screen; this mutation induced a premature stop codon between the DEXDc and the HELICc domain (Supplementary Figure S5). For the other two *FANCM* genes, we selected missense mutations altering amino acids conserved across representative eukaryotes species and predicted to be damaging to the protein (SIFT score = 0.00). For *BraA.FANCM*, one missense mutation (hereinafter referred as to *braA.fancm-1)* was retained, which consisted of a substitution of a proline at position 443 for a leucine (Supplementary Figure S5). For *BnaC.FANCM*, two missense mutations (hereinafter referred to as *bnaC.fancm-1* and *bnaC.fancm-2*) were selected; *bnaC.fancm-1* consisted of a leucine to phenylalanine substitution at position 330 while *bnaC.fancm-2* consisted of a glycine to arginine substitution at position 393 (Supplementary Figure S5). Interestingly, substitution of the same glycine for glutamic acid was shown to be causal for a defective FANCM protein in *A. thaliana* (Crismani et al., 2012).

FANCM Limits Co Frequencies in *Brassica rapa*

To test whether FANCM limits COs in *B. rapa*, we replicated the cytological assay that was used to first identify the anti-CO activity of this protein in *A. thaliana* (Crismani et al., 2012); i.e., we tested whether *bra.fancm-1* was able to restore bivalent formation in a class I CO-defective mutant.

For this, we first identified through TILLING a deleterious mutation in *BraA.MSH4* (hereinafter referred as to *braA.msh4-1*; Supplementary Figure S6), the single copy homologue of *AtMSH4* - an essential ZMM protein (Higgins et al., 2004) - in *B. rapa* (Lloyd et al., 2014). The mutation *braA.msh4-1* induced a substitution in the acceptor site of the 19th exon (*BraA.MSH4* has 24 exons) right after position 626; this introduced a premature STOP codon in the predicted coding sequence of the essential MutS domain of the MSH4 protein (Obmolova et al., 2000; Higgins et al., 2004; Nishant et al., 2010; Wang et al., 2016).

We first confirmed that *braA.msh4-1* resulted in a significant shortage in CO formation in *B. rapa*. Plants homozygous for *braA.msh4-1* (*braA.msh4-1*$^{-/-}$) showed a mixture of bivalents (3.7 ± 1.4 per cell; $n = 43$ cells) and univalents (6.3 ± 1.5 per cell) at metaphase I when WT plants systematically formed 10 bivalents ($n = 66$) (p-value = 6.16 E-30; **Figures 2A,B**). Coupled with this reduction in bivalent formation was a difference in the shape of the bivalents. While 50% of the bivalents in WT were rings with both arms bound by chiasmata, 88% of the bivalents in *braA.msh4-1*$^{-/-}$ were rods with only one arm bound by chiasmata (**Figures 2A,B**). Assuming that rod and ring bivalents had only one and two COs, respectively, we estimated that the mean number of COs dropped significantly from 14.8 ± 1.5 COs per cell ($n = 36$) in WT to 4.05 ± 1.82 COs per cell ($n = 40$) in *braA.msh4-1*$^{-/-}$ (p-value = 9.2 E-44). These observations are reminiscent of the meiotic behavior of *Atmsh4* single mutant (Higgins et al., 2004).

We then produced a plant containing mutations in both the *BraA.MSH4* and *BraA.FANCM* genes (*braA.msh4-1*$^{-/-}$ *braA.fancm-1*$^{-/-}$) and assessed meiotic crossover frequency in this double mutant using the same cytological approaches. We observed a large increase in bivalent formation (9.4 ± 0.7 bivalents; $n = 66$) compared to *braA.msh4-1*$^{-/-}$ (p-value =1.8 E-33; **Figures 2B,C**). However, the number of bivalents in the double mutant *braA.msh4-1*$^{-/-}$ *braA.fancm-1*$^{-/-}$ remained significantly different from that of the WT (unpaired t-test; p-value < 0.0001) due to the presence of a small number of univalents (0.57 univalent per cell in *braA.msh4-1*$^{-/-}$ *braA.fancm-1*$^{-/-}$; Supplementary Figure S7). This observation indicated a random distribution of CO consistent with the absence of obligate class I COs (Crismani et al., 2012). We also observed that ∼50% of bivalents in *braA.msh4-1*$^{-/-}$ *braA.fancm1*$^{-/-}$ were rings and estimated that the mean chiasma frequency in this plant (14.0 ± 2.9 per cell; $n = 35$) was indistinguishable from that observed in WTs. This represented an increase of at least 10 COs in *braA.msh4-1*$^{-/-}$ *braA.fancm-1*$^{-/-}$ compared to the single mutant *braA.msh4-1*$^{-/-}$. Bearing in mind that it is not possible to distinguish cytologically single from multiple COs clustered on a single arm (Supplementary Figure S7), this increase probably underestimates the extent to which FANCM shut down CO frequency in *B. rapa*. This notwithstanding, our results clearly demonstrate that BraA.FANCM, like At.FANCM, limits CO formation in *msh4* mutants.

FANCM Limits Homologous Crossovers in *Brassica napus*

Replicating the same cytological assay in *B. napus* was not feasible, due to the lack of *msh4* mutants in this species at the time of the study. We therefore developed a genetic assay to assess the effect of FANCM on crossover frequency in *B. napus*. This approach took advantage of the fact that plants defective for either *BnaA.FANCM* or *BnaC.FANCM* had to be crossed to produce a loss-of-function *fancm* double mutant in *B. napus* (Supplementary Figure S2). Given the EMS-mutation density observed within *BnaA.FANCM* and *BnaC.FANCM*, we reasoned that these (F1) hybrids contained an extensive set of EMS mutations that could be used as a source of polymorphism for subsequent genetic analyses (Supplementary Figure S3).

To identify these segregating mutations, we sequenced two *bna.fancm_1-1* mutants and two of their WT siblings (*Bna.FANCM_1-1*) (Supplementary Figure S2). Sequencing quality control process showed that around 70% of the reads were mapped (Supplementary Table S4) covering around 80 % of the genome reference with a minimum depth of 3x (Supplementary Figure S8). Using conservative criteria, we detected ∼20 763 EMS mutations in the sequenced plants (Supplementary Table S4; Supplementary dataset 1), which was consistent with

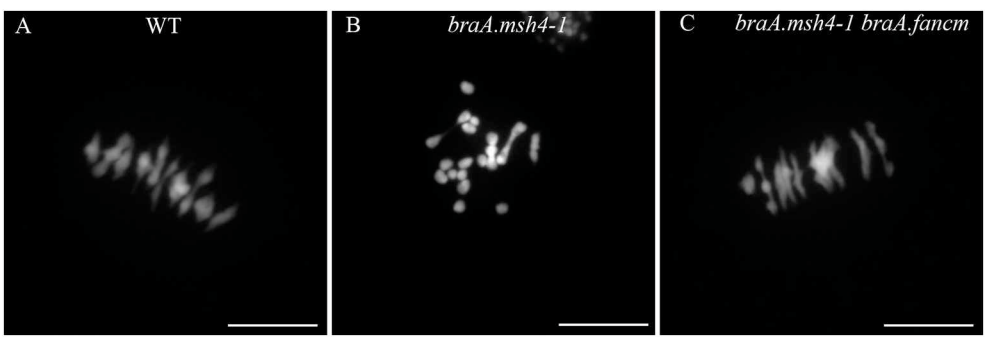

FIGURE 2 | Restoration of bivalent formation in the double mutant *braA.msh4-1*$^{-/-}$ *braA.fancm-*$^{-/-}$ **(A)** During metaphase I in WT *B. rapa*, 10 bivalents and no univalent are formed. They are all aligned on the metaphase plate. **(B)** In the single *braA.msh4-1*$^{-/-}$ mutant, only a few bivalents are formed, most of the chromosomes remain as univalents. **(C)** Metaphase I in the double mutant *braA.msh4-1*$^{-/-}$ *braA.fancm-*$^{-/-}$ is reminiscent of metaphase I in WT *B. rapa,* mostly bivalents are formed, only ∼0.5 univalent pair is found on average per cell. Scale bar = 10 μm.

mutation density within *BnaA.FANCM* and *BnaC.FANCM*. ∼23 % (4714/20763) of those mutations were found in CDS and led to non-synonymous substitutions (including splice variant and non-sense mutations) in a total of 4,438 genes (∼4% of total gene number; Supplementary dataset 2). A subset of those genes (270 genes with 298 mutations; ∼8%) constituted homoeologous pairs (as established in Chalhoub et al., 2014); in most cases (193/298, 64%), the mutations that we found in both copies of a given homoeologous pair were non synonymous or stop gained mutations (Supplementary dataset 2). None of these EMS mutations were found in the orthologs of genes that encode most other known anti-CO proteins (e.g., MHF1, MHF2, FIGL1, FLIP, RMI1, TOP3α, RECQ4a/b) in *A. thaliana* (Supplementary Table S5). Finally, overall all four sequenced plants, only 66 mutations targeting 30 homoeologous pairs were detected in the homozygous state at both loci in at least one plant. The risk of confusion between the effect of *fancm* mutations and that of another pair of homoeolog is thus very low.

We then converted a subset of the EMS induced SNPs into genetic markers and compared crossover frequencies between mutant and WT F2 plants in the corresponding F3 progeny (**Table 1**; Supplementary dataset 3). For the three intervals examined, which were all located in the most distal part of the chromosomes where CO frequencies are the highest (Lloyd et al., 2018), we observed a significant increase in crossover frequency (∼32%, Welch's *t*-test; p-value < 0.013) in the progeny of *fancm* mutants compared to the progeny of WT plants (**Table 1**). Altogether, the consistency of the increase in crossover frequency observed for three intervals suggests that FANCM limits crossover formation in *B. napus*. However, as this increase in COs was rather limited compared to what was observed in *B. rapa* mutants, our results cast doubt as to whether the *bnaC.fancm-2* mutation resulted in complete loss of FANCM anti-crossover activity (see below).

FANCM Limits Co Formation in *Brassica napus* Allohaploids

In *B. napus*, microspore culture can be used to produce allohaploid plants (AC) that contain one unique copy of each of the 19 *B. napus* chromosomes ($n = 19$) and thus no longer have homologous chromosomes. We previously reported that meiotic crossovers can readily form between homoeologous chromosomes in these plants (Grandont et al., 2014). This suggests that the recombination intermediates upon which FANCM could potentially act may also exist in *B. napus* allohaploids. We thus derived allohaploid progeny from five different plants, each combining the *bnaA.fancm-1* and *bnaC.fancm-2* mutations at the heterozygous state (Supplementary Figure S2). In each of these progenies, two to five *fancm* (A/C) double mutant and *FANCM* WT plants were recovered and used to compare CO frequencies using cytological approaches (Supplementary Figure S2).

We first observed that WT allohaploid plants showed a low number of bivalents (2.8 ± 1.3 per cell; $n = 59$ cells) and a majority of univalents (13.4 ± 2.7 per cell) at metaphase I. *Tanto* is therefore among the varieties that form little CO at the allohaploid stage (see Grandont et al., 2014) We were thus best positioned to detect a small increase in COs, if any. This is exactly what we observed: i.e., a significant and consistent increase in bivalent formation when comparing *bna.fancm_1-2* mutant allohaploid and *Bna.FANCM_1-2* WT allohaploid plants. The mean number of chromosomes that failed to form a CO decreased from 13.5 in WT (71%) to 10.5 in *fancm* (55%) (Wilcoxon signed rank test, p-value $= 0.0016$). This trend was observed for all allohaploids and all F1 hybrids, with some variation in the magnitude but no variation in the direction of the change (**Figure 3**). We believe this is unlikely to be a mere coincidence. The systematic correspondence observed between double (A/C) *fancm* mutants and increased CO frequencies across all F1s and all allohaploids rather suggests that FANCM limits CO formation between homoeologous chromosomes in *B. napus*.

BnaC.FANCM-2 Has Still Residual Anti-CO Activity

Given the small but significant increase in CO frequency repeatedly observed in *bna.fancm_1-2* mutant plants, we assessed whether the protein encoded by *bnaC.fancm-2* (thereafter BnaC.FANCM-2) has still some anti-CO activity. We reasoned that *bnaA.fancm-1*, which induced a premature stop codon between the DEXDc and the HELICc domain, is likely a

TABLE 1 | Homologous crossover frequencies in homozygous WT and mutant for *FANCM* in *Brassica napus*.

Chromosome	Interval[a]	Physical size (Mb)	Observed genetic size in WT[b]	Observed genetic size in *fancm* mutant[a]	Fold-change	p-value[c]
A01	1	1.611	19.1 cM ($n = 101$) [18.4–19.8]	24.3 ($n = 131$) [23.6–24.9]	1.3	0.011
C01	2	0.575	5.4 ($n = 96$) [5.0–5.7]	7.2 ($n = 102$) [6.8–7.5]	1.3	0.002
A05	3	1.135	11.3 ($n = 86$)[d] [10.60–11.8]	14.4 ($n = 134$) [14.0–14.8]	1.3	0.006

[a] *All these intervals are located in the most distal part of the chromosomes — see Supplementary Table S3 for detailed positions.*

[b] *The number of plants genotyped per progeny is given (in parentheses). Confidence intervals (mean ± 1.96×SE) are given [in square brackets].*

[c] *Considering a one-tailed hypothesis: i.e., crossovers in fancm mutant > crossovers in WT.*

[d] *This distance was estimated using the F3 progeny of Bna.FANCM_1-1 due to lack of polymorphim in Bna.FANCM_1-2.*

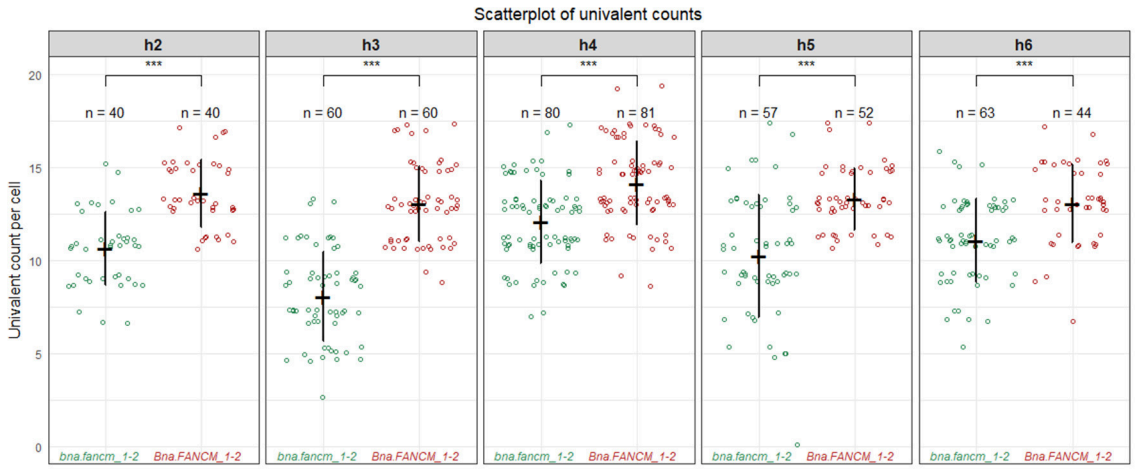

FIGURE 3 | Homoeologous crossovers in *fancm* allohaploids plants. Boxplot for the number of univalents between mutants and WT allohaploids derived from five heterozygous F1 plants combining *bnaA.fancm-1* with *bnaC.fancm-2* (h2–h6). At least 2 mutants and 2 WT allohaploids plants were derived per F1 hybrids and were used as replicates. Around 20 meiocytes have been observed per replicate and the counts per replicate were pooled together. ***$P < 0.001$, Wilcoxon Signed-Rank Test.

loss-of-function mutation and thus only questioned the effect of *bnaC.fancm-2* on CO formation.

In order to do so, we transformed an *A. thaliana msh5 fancm* double-mutant with a modified copy of *At.FANCM* that lead to the same amino acid substitution found in *BnaC.fancm-2*. The *A. thaliana msh5 fancm* double-mutant was fertile and displayed ∼5 bivalents per cell ($n = 14$) as in the WT (**Figure 4**, **Table 2**). We reasoned that the number of bivalents should remain essentially the same in the transformant if the transgene encodes a completely non-functional protein. On the contrary, the transformant should demonstrate a decay in bivalent formation if the transgene encodes a (partially) functional protein. We tested these predictions by transforming the *msh5 fancm* double-mutant with the WT allele of *At.FANCM*. As expected, the number of bivalents in the transformant dropped down to that observed in *Arabidopsis msh5* mutant (∼1.5 bivalent per cell, $n = 12$; **Figure 4**, **Table 2**). We observed essentially the same pattern with the transgene mimicking *BnaC.fancm-2*: numerous univalents, a mean number of ∼1.5 bivalents ($n = 17$) bivalents and clear evidence of unbalanced chromosome segregation after meiosis I (**Figure 4**, **Table 2**). These results indicate that BnaC.FANCM-2 retained anti-CO activity. It is worthy of note, however, that the endogenous level of BnaC.FANCM-2's residual activity in *bna.fancm_1-2* mutant plants can hardly be extrapolated from this experiment.

DISCUSSION

Identification of genes encoding anti-CO proteins in *A. thaliana* holds great promise to improve the efficiency of plant-breeding programs (Crismani et al., 2013). In this study, we combined BAC screening, TILLING, whole-genome resequencing, cytology, genotyping and complementation tests (in *Arabidopsis*) to demonstrate that FANCM limits COs in two Brassica crops. To the best of our knowledge, this is the first example of a translational biology approach to increase CO frequencies in crops (see Mieulet et al., 2016 on a related, yet different topic).

FANCM Limits Crossovers in *Brassica* Crops

Altogether our results indicate that the anti-CO activity of FANCM is conserved in two important *Brassica* crops, thus probably across the entire *Brassicaceae* family. This point is more strikingly illustrated in *B. rapa* where we observed a strong increase in COs in the *fancm/msh4* double mutant compared with the single *msh4*. This change is consistent with the 3-fold increase in COs reported in *A. thaliana* (Crismani et al., 2012); like Arabidopsis, the extra COs were sufficient to restore bivalent formation to a WT level in *B. rapa* (**Figure 2**).

A less pronounced increase in CO frequency (∼1.3-fold) was observed in *B. napus* (**Table 1**), probably because the amino acid substitution found in our *B. napus bnaC.fancm-2* mutant allele does not completely ablate FANCM's anti-CO activity (**Figure 4**). In spite of this residual anti-CO activity, we repeatedly observed a small but significant increase of: (i) crossover frequencies across three independent genetic intervals in euploids (**Table 1**) and (ii) bivalent formation across all biological replicates in allohaploids (**Figure 3**) produced from *BnaA.FANCM-1*$^{+/-}$*BnaC.FANCM-2*$^{+/-}$. These results lend support to the hypothesis that FANCM limits CO formation in *B. napus* too.

It is important to underline here that we don't know how sensitive the complementation test is. For example, it is uncertain whether expression of a transgene (in Arabidopsis) consisting in a modified version of the Arabidopsis WT allele of FANCM faithfully recapitulates the activity of the protein encoded by Brassica *BnaC.fancm-2* mutant allele expressed at its endogenous level and in *B. napus*. This approach could simply be too conservative to reveal the extent to which the substitution

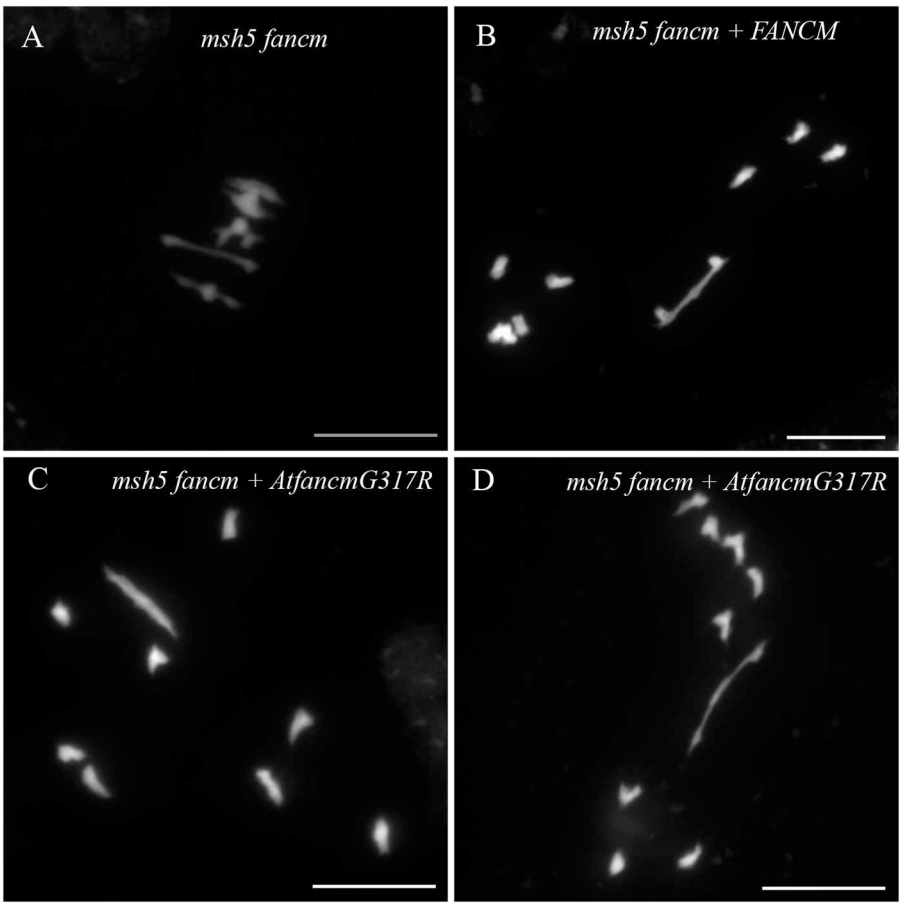

FIGURE 4 | Bivalent formation in *A. thaliana msh5 fancm* double-mutant transformed with different version of *FANCM.* During metaphase I, 5 bivalents were observed in *msh5 fancm* double-mutant meiocytes **(A)**. When complementing *msh5 fancm* with the WT allele of *At_FANCM* **(B)**, or with a modified copy of *FANCM* (*AtfancmG317R*) mimicking *BnaC.fancm-2* **(C,D)**, mainly univalents were observed. Scale bar = 10 μm.

TABLE 2 | Chromosome segregation in *A. thaliana msh5 fancm* double-mutant transformed with different version of *FANCM*.

	Number of bivalents	0	1	2	3	4	5
$msh5^{-/-}fancm^{-/-}$		0	0	0	0	1	13
$msh5^{-/-}fancm^{-/-}$	+ *AtFANCM*	0	6	4	2	0	0
$msh5^{-/-}fancm^{-/-}$	+ *Atfancm-G404R*[a]	2	9	4	1	1	0

[a]*modified version of AtFANCM mimicking bnaC.fancm-2, i.e., containing a glycine to arginine substitution at position 404.*

identified in *bnaC.fancm-2* is detrimental for FANCM anti-CO activity. Identification and/or production of loss-of-function mutations for *BnaC.FANCM* is thus required to determine how much CO frequency can be increased in *B. napus fancm* mutants.

Does FANCM Limit Crossover Formation Between Homoeologous Chromosomes?

In *A. thaliana*, increased crossover frequency in *fancm* mutants is suppressed in heterozygous regions (Girard et al., 2015; Ziolkowski et al., 2015). It is thus surprising that we detected a small but repeatable effect of *fancm* mutations on CO formation in *B. napus* allohaploids (**Figure 3**) where crossovers are necessarily formed between homoeologous chromosomes. The SNP density between homoeologous transcripts (∼3.5%; Cheung et al., 2009), which is a lower bound estimate of the overall rate of polymorphism between the A and C genomes, is indeed much higher than the allelic SNP diversity measured between *B. napus* varieties (∼0.049–0.084%; Trick et al., 2009). It is also higher than the SNP density observed between *Arabidopsis* accessions (0.5%) (Alonso-Blanco et al., 2016). Our results may therefore suggest that the extra COs observed in *B. napus fancm* mutants are either less sensitive to heterozygosity than they are in *A. thaliana* or are actually not formed between homoeologous regions in *B. napus fancm* mutant allohaploids.

In *B. napus*, genomic exchanges between homoeologous chromosomes can eliminate polymorphism in some regions i.e., some homoeologous chromosomes contain homologous segments (Chalhoub et al., 2014; He et al., 2017; Samans et al., 2017; Lloyd et al., 2018). Although homoeologous exchanges have yet to be characterized in the cultivar used in that study

(cv. *Tanto*), there is no reason to believe that this variety would be an exception. All of the *B. napus* cultivars analyzed so far contain at least one and usually 10–12 homoeologous exchanges (Chalhoub et al., 2014; He et al., 2017; Samans et al., 2017). It is therefore tempting to hypothesize that the increase in bivalent formation observed in allohaploid *fancm* mutants results from increased CO formation within shared homologous regions on otherwise homoeologous chromosomes. This would represent a similar situation to that described by Ziolkowski et al. (2015), where juxtaposed heterozygous and homozygous regions biased the distribution of extra CO in *Arabidopsis fancm* mutants toward the homozygous intervals. Our hypothesis is also supported by the fact that bivalent formation between chromosomes 5D of wheat and 5M of *Aegilops geniculta* is promoted by pre-existing homoeologous exchanges; Koo et al. (2016) observed that >60% of the crossovers formed between 5D and 5M occurred in the terminal homologous part that is shared between the two chromosomes, even though this region only represents 5% of the physical length of those chromosomes.

Thus, the difference observed between *fancm* mutant and WT allohaploids could reflect a difference of homologous rather than homoeologous recombination. Testing this hypothesis would require assessing whether (i) the increase in CO frequencies occurs in very specific and usually small (Samans et al., 2017) chromosomal regions and (ii) these regions experienced homoeologous exchanges beforehand. This approach, which can theoretically be envisaged in *B. napus* (Howell et al., 2008), will first require homoeologous exchanges to be identified in cv. *Tanto*.

Translational Biology to Increase Crossover Frequencies in Crops

As reviewed by Wijnker and de Jong (2008), "meiotic recombination has a pivotal role in successful plant breeding." Increasing crossover frequencies could notably generate new allelic combinations and a broader range of genotypes, decrease and slow down the loss of genetic variance during selection process, reduce linkage drag, facilitate a more efficient purging of mutation load… These opportunities are now within reach (Fernandes et al., 2017), provided that basic research on meiotic recombination is translated into crops. Our results show that this is possible, paving the way for further studies in other crops and/or with other antiCO proteins.

Translating the knowledge gained in *A. thaliana* into cultivated species, e.g., producing hyper-recombinant crop plants, supposes first to knock-out the homologs for genes encoding antiCO proteins in crops. For many species, the most common approach remains TILLING. In our study, we successfully applied TILLING to find mutations across three *FANCM* genes in *Brassica*. Our results clearly demonstrate that the effect of missense mutations on protein function is difficult to predict, even if these mutations target highly conserved amino acids located in essential domains. This observation, which is not specific to our study (Kumar et al., 2009), is well illustrated by the mutation *BnaC.fancm*-2. As described above, this missense mutation did not completely abolish BnaC.FANCM anti-CO activity (**Figure 4**) while it altered the same glycine that was shown to be essential for FANCM anti-CO activity in *A. thaliana* (Crismani et al., 2012). Looking to the future, new methodologies that increase the chance of finding nonsense mutations should be favored. This may involve the use of next-generation sequencing to "enable a deep search for mutations in targeted loci" (Tsai et al., 2011; see also Gilchrist et al., 2013) or the development of sequenced mutant populations (Krasileva et al., 2017; see also http://revgenuk.jic.ac.uk/search-databases/ for *B. rapa*). As a matter of fact, screening the RAPTILL population for mutations along the entire coding sequence of *BnaC.FANCM* would have reduced the chances of detecting no nonsense mutations from ∼42 to ∼3.5%.

However efficient the new TILLING approaches may be, it remains that the use of highly mutagenized populations raises concern about the risk of mistaking the consequences of a background EMS mutation for a mutation in the targeted gene. While it is necessary to control that risk, attempts to purge the mutation load off through backcrossing would be both inefficient and ineffective. In *B. napus*, given the density of EMS mutations we disclosed in this study, we estimated that >1,000 EMS mutations would still be segregating after 3 backcrosses to the WT (i.e., ∼2 years). In the context of translational biology, verifying how strong is the correlation between the presence of the mutation in the target and the phenotype of biological replicates (siblings mutant plants harboring different combinations of EMS background mutations) constitutes a more reasonable approach. When possible, the use of series of allelic mutations can also be used to demonstrate the causal relationship between these mutations and the phenotype (Stephenson et al., 2010).

It is however important to note that we searched for a very specific and uncommon phenotype (increase of CO frequencies) to which only a few genes have been shown to contribute. Thus, the risk of confounding the effect of background mutations with the targeted mutant alleles should not be overestimated. In this regards, we verified that the plants we sequenced were free of mutations in the orthologs of *MHF1*, *MHF2*, *FIGL1*, *FLIP, RMI1, TOP3α,* or *RECQ4ab* (Girard et al., 2014, 2015; Séguéla-Arnaud et al., 2015; Fernandes et al., in review) (Supplementary Table S5). The possibility remains, however, that new anti-CO factors could have been targeted, which have yet to be identified in Arabidopsis or in another model plant (Hu et al., 2017).

In addition, we showed here that the chance that a *fancm* mutant plant also contains deleterious mutations affecting another pair of homoeologous genes (each at the homozygous stage) is very low. As expected, this probability peaks in the vicinity of *Bna.FANCM* genes (on chromosome A05 and C05), due to linkage drag (Supplementary Figure S9). Because each of the F2 plants contains a different patchwork of background EMS mutations due to independent segregation, the chance of finding such events shared between two F2 mutants or a F2 mutant and a WT sibling is even lower. We found only 4 such events in our assay, 2 mutations in common between two F2 mutants and 2 mutations in common between the 2 wild type siblings.

The rapid development of the CRISPR-CAS9 technology offers new opportunities to target mutagenesis and circumvent the off-target mutations issue in many crops (Brooks et al., 2014; Wang et al., 2014; Li J. et al., 2016), including *B. napus* (Braatz et al., 2017; Yang et al., 2017). The ability of

CRISPR-CAS9 to simultaneously generate stable and heritable mutations in the different homoeologous copies of a gene, opens new avenues for future translational research. For example, it makes it possible to test whether, like in *A. thaliana,* meiotic crossover is unleashed in plants defective for multiple antiCO proteins (Séguéla-Arnaud et al., 2015; Fernandes et al., 2017). The challenge of producing and characterizing hyper-recombinant plants should not however overshadow the need for strategies aimed at maximizing the benefits of increasing CO frequencies in crops. In order to be adopted, the use of hyper-recombinant plants must fit into the framework of the current breeding schemes. In that regard, the fact that all causal mutations conferring increased CO frequency are recessive constitutes a limitation. Both methodological (e.g., breeding strategies) and biotechnological (e.g., dominant systems) developments will therefore be needed before "engineered meiotic recombination" becomes part of plant breeders' arsenal.

AUTHOR CONTRIBUTIONS

EJ, AL, and A-MC designed the research. ABlary, AG, FE, ABérard, HB, NB, DC, CC, LC, JF, CG, M-CLP, ML, M-OL, NN, and AL performed the research. ABlary, AG, A-MC, and EJ analyzed the data. ABlary, AG, and EJ wrote the paper.

ACKNOWLEDGMENTS

We would like to thank Mathilde Grelon, Raphael Mercier, Fabien Nogue, Christine Mézard and three reviewers for critical reading and discussion of the manuscript. We would also like to thank Marie Gilet for plant care, and Aurélie Chauveau and Elodie Marquand from EPGV group for producing the DNA libraries and processing the raw data, respectively. This work was funded through the ANR project ANR-14-CE19-0004 – CROC and with the support of INRA BAP division (Appel à Manifestation d'intérêt 2012; HyperRec). The IJPB benefits from the support of the LabEx Saclay Plant Sciences-SPS (ANR-10-LABX-0040-SPS). We want to acknowledge CEA-IG/CNG for supporting the INRA-EPGV group for QC of DNA and Illumina high throughput sequencing, especially Anne Boland, Marie-Thérèse Bihoreau and their staff. We also want to acknowledge Julien Schmidt at AELRED and Fran Robson at RevGenUK for performing the TILLING experiment in *B. napus* and *B. rapa,* respectively and the plant genetic resources center BrACySol for providing seeds for *B. napus* cv Tanto. RevGenUK (https://www.jic.ac.uk/technologies/genomic-services/revgenuk-tilling-reverse-genetics/) was supported by the Biotechnology and Biological Sciences Research Council, UK (BB/F010591/1 and BB/I025891/1). ABlary was funded by a Young Scientist Contracts (CJS) from INRA. AG is funded by the Marie-Curie COMREC network FP7 ITN-606956. AL was funded by the International Outgoing Fellowships PIOF-GA-2013-628128 POLYMEIO.

SUPPLEMENTARY MATERIAL

The Supplementary Material for this article can be found online at: https://www.frontiersin.org/articles/10.3389/fpls.2018.00368/full#supplementary-material

REFERENCES

Alonso-Blanco, C., Andrade, J., Becker, C., Bemm, F., Bergelson, J., Borgwardt, K. M., et al. (2016). 1,135 genomes reveal the global pattern of polymorphism in *Arabidopsis thaliana*. *Cell* 166, 481–491. doi: 10.1016/j.cell.2016.05.063

Anderson, L. K., Lohmiller, L. D., Tang, X., Hammond, D. B., Javernick, L., Shearer, L., et al. (2014). Combined fluorescent and electron microscopic imaging unveils the specific properties of two classes of meiotic crossovers. *Proc. Natl. Acad. Sci. U.S.A.* 111, 13415–13420. doi: 10.1073/pnas.1406846111

Bauer, E., Falque, M., Walter, H., Bauland, C., Camisan, C., Campo, L., et al. (2013). Intraspecific variation of recombination rate in maize. *Genome Biol.* 14:R103. doi: 10.1186/gb-2013-14-9-r103

Braatz, J., Harloff, H.-J., Mascher, M., Stein, N., Himmelbach, A., and Jung, C. (2017). CRISPR-Cas9 targeted mutagenesis leads to simultaneous modification of different homoeologous gene copies in polyploid oilseed rape (*Brassica napus*). *Plant Physiol.* 174, 935–942. doi: 10.1104/pp.17.00426

Brooks, C., Nekrasov, V., Lippman, Z. B., and Van Eck, J. (2014). Efficient gene editing in tomato in the first generation using the clustered regularly interspaced short palindromic repeats/CRISPR-associated9 system. *Plant Physiol.* 166, 1292–1297. doi: 10.1104/pp.114.247577

Chalhoub, B., Denoeud, F., Liu, S., Parkin, I. A. P.,Tang, H., Wang, X., et al. (2014). Early allopolyploid evolution in the post-neolithic *Brassica napus* oilseed genome. *Science* 345, 950–953. doi: 10.1126/science.1253435

Chelysheva, L. A., Grandont, L., and Grelon, M. (2013). Immunolocalization of meiotic proteins in *Brassicaceae*: method 1. *Methods Mol. Biol.* 990, 93–101. doi: 10.1007/978-1-62703-333-6_9

Cheng, F., Wu, J., and Wang, X. (2014). Genome triplication drove the diversification of Brassica plants. *Hortic. Res.* 1:14024. doi: 10.1038/hortres.2014.24

Cheng, F., Sun, R., Hou, X., Zheng, H., Zhang, F., Zhang, Y., et al. (2016). Subgenome parallel selection is associated with morphotype diversification and convergent crop domestication in *Brassica rapa* and *Brassica oleracea*. *Nat. Genet.* 48, 1218–1224. doi: 10.1038/ng.3634

Cheung, F., Trick, M., Drou, N., Lim, Y. P., Park, J.-Y., Kwon, S.-J., et al. (2009). Comparative analysis between homoeologous genome segments of *Brassica napus* and its progenitor species reveals extensive sequence-level divergence. *Plant Cell* 21, 1912–1928. doi: 10.1105/tpc.108.060376

Clough, S. J., and Bent, A. F. (1998). Floral dip: a simplified method for Agrobacterium-mediated transformation of *Arabidopsis thaliana*. *Plant J.* 16, 735–743. doi: 10.1046/j.1365-313x.1998.00343.x

Crismani, W., Girard, C., Froger, N., Pradillo, M., Santos, J. L., Chelysheva, L., et al. (2012). FANCM limits meiotic crossovers. *Science* 336, 1588–1590. doi: 10.1126/science.1220381

Crismani, W., Girard, C., and Mercier, R. (2013). Tinkering with meiosis. *J. Exp. Bot.* 64, 55–65. doi: 10.1093/jxb/ers314

Fernandes, J. B., Seguéla-Arnaud, M., Larchevêque, C., Lloyd, A. H., and Mercier, R. (2017). Unleashing meiotic crossovers in hybrid plants. *Proc. Natl. Acad. Sci. U.S.A.* 115, 2431–2436. doi: 10.1073/pnas.1713078114

Freeling, M. (2009). Bias in plant gene content following different sorts of duplication: tandem, whole-genome, segmental, or by transposition. *Annu. Rev. Plant Biol.* 60, 433–453. doi: 10.1146/annurev.arplant.043008.092122

Gilchrist, E. J., Sidebottom, C. H. D., Koh, C. S., MacInnes, T., Sharpe, A. G., and Haughn, G. W. (2013). A mutant *Brassica napus* (Canola) population for

the identification of new genetic diversity via TILLING and next generation sequencing. *PLoS ONE* 8:e84303. doi: 10.1371/journal.pone.0084303

Girard, C., Crismani, W., Froger, N., Mazel, J., Lemhemdi, A., Horlow, C., et al. (2014). FANCM-associated proteins MHF1 and MHF2, but not the other Fanconi anemia factors, limit meiotic crossovers. *Nucleic Acids Res*. 42, 9087–9095. doi: 10.1093/nar/gku614

Girard, C., Chelysheva, L., Choinard, S., Froger, N., Macaisne, N., Lehmemdi, A., et al. (2015). AAA-ATPase FIDGETIN-LIKE 1 and Helicase FANCM antagonize meiotic crossovers by distinct mechanisms. *PLoS Genet*. 11:e1005369. doi: 10.1371/journal.pgen.1005369

Grandont, L., Cu-ado, N., Coriton, O., Huteau, V., Eber, F., Chèvre, A. M., et al. (2014). Homoeologous chromosome sorting and progression of meiotic recombination in *Brassica napus*: ploidy does matter!. *Plant Cell* 26, 1448–1463. doi: 10.1105/tpc.114.122788

Hasan, M., Seyis, F., Badani, A. G., Pons-Kühnemann, J., Friedt, W., Lühs, W., et al. (2006). Analysis of genetic diversity in the *Brassica napus* L. gene pool using SSR markers. *Genet. Resour. Crop Evol*. 53, 793–802. doi: 10.1007/s10722-004-5541-2

He, Z., Wang, L., Harper, A. L., Havlickova, L., Pradhan, A. K., Parkin, I. A. P., et al. (2017). Extensive homoeologous genome exchanges in allopolyploid crops revealed by mRNAseq-based visualization. *Plant Biotechnol. J*. 15, 594–604. doi: 10.1111/pbi.12657

Higgins, J. D., Armstrong, S. J., Franklin, F. C. H., and Jones, G. H. (2004). The Arabidopsis MutS homolog AtMSH4 functions at an early step in recombination: Evidence for two classes of recombination in Arabidopsis. *Genes Dev*. 18, 2557–2570. doi: 10.1101/gad.317504

Higgins, J. D., Vignard, J., Mercier, R., Pugh, A. G., Franklin, F. C. H., and Jones, G. H. (2008). AtMSH5 partners AtMSH4 in the class I meiotic crossover pathway in *Arabidopsis thaliana*, but is not required for synapsis. *Plant J*. 55, 28–39. doi: 10.1111/j.1365-313X.2008.03470.x

Howell, E. C., Kearsey, M. J., Jones, G. H., King, G. J., and Armstrong, S. J. (2008). A and C genome distinction and chromosome identification in *Brassica napus* by sequential fluorescence *in situ* hybridization and genomic *in situ* hybridization. *Genetics* 180, 1849–1857. doi: 10.1534/genetics.108.095893

Hu, Q., Li, Y., Wang, H., Shen, Y., Zhang, C., Du, G., et al. (2017). MEICA 1 (meiotic chromosome association 1) interacts with TOP3α and regulates meiotic recombination in rice. *Plant Cell* 29, 1697–1708. doi: 10.1105/tpc.17.00241

Jenczewski, E., Eber, F., Grimaud, A., Huet, S., Lucas, M. O., Monod, H., et al. (2003). PrBn, a major gene controlling homeologous pairing in oilseed rape (*Brassica napus*) haploids. *Genetics* 164, 645–653.

Keeney, S., Giroux, C. N., and Kleckner, N. (1997). Meiosis-specific DNA double-strand breaks are catalyzed by Spo11, a member of a widely conserved protein family. *Cell* 88, 375–384. doi: 10.1016/S0092-8674(00)81876-0

Knoll, A., and Puchta, H. (2011). The role of DNA helicases and their interaction partners in genome stability and meiotic recombination in plants. *J. Exp. Bot*. 62, 1565–1579. doi: 10.1093/jxb/erq357

Koo, D.-H., Liu, W., Friebe, B., and Gill, B. S. (2016). Homoeologous recombination in the presence of Ph1 gene in wheat. *Chromosoma* 126, 531–540. doi: 10.1007/s00412-016-0622-5

Krasileva, K. V., Vasquez-Gross, H. A., Howell, T., Bailey, P., Paraiso, F., Clissold, L., et al. (2017). Uncovering hidden variation in polyploid wheat. *Proc. Natl. Acad. Sci. U.S.A*. 114, E913–E921. doi: 10.1073/pnas.1619268114

Kumar, P., Henikoff, S., and Ng, P. C. (2009). Predicting the effects of coding non-synonymous variants on protein function using the SIFT algorithm. *Nat. Protoc*. 4, 1073–1081. doi: 10.1038/nprot.2009.86

Li, J., Meng, X., Zong, Y., Chen, K., Zhang, H., Liu, J., et al. (2016). Gene replacements and insertions in rice by intron targeting using CRISPR-Cas9. *Nat. Plants* 2:16139. doi: 10.1038/nplants.2016.139

Li, Z., Defoort, J., Tasdighian, S., Maere, S., Van de Peer, Y., and De Smet, R. (2016). Gene duplicability of core genes is highly consistent across all angiosperms. *Plant Cell* 28, 326–344. doi: 10.1105/tpc.15.00877

Lloyd, A. H., Ranoux, M., Vautrin, S., Glover, N., Fourment, J., Charif, D., et al. (2014). Meiotic gene evolution: can you teach a new dog new tricks? *Mol. Biol. Evol*. 31:172. doi: 10.1093/molbev/msu119

Lloyd, A., Blary, A., Charif, D., Charpentier, C., Tran, J., Balzergue, S., et al. (2018). Homoeologous exchanges cause extensive dosage-dependent gene expression changes in an allopolyploid crop. *New Phytol*. 217, 367–377. doi: 10.1111/nph.14836

Lorenz, A., Osman, F., Sun, W., Nandi, S., Steinacher, R., and Whitby, M. C. (2012). The fission yeast FANCM ortholog directs non-crossover recombination during meiosis. *Science* 336, 1585–1588. doi: 10.1126/science.1220111

Lorieux, M. (2012). MapDisto: fast and efficient computation of genetic linkage maps. *Mol. Breed*. 30, 1231–1235. doi: 10.1007/s11032-012-9706-y

Lysak, M. A., Koch, M. A., Pecinka, A., and Schubert, I. (2005). Chromosome triplication found across the tribe Brassiceae. *Genome Res*. 15, 516–525. doi: 10.1101/gr.3531105

McClosky, B., and Tanksley, S. D. (2013). The impact of recombination on short-term selection gain in plant breeding experiments. *Theor. Appl. Genet*. 126, 2299–2312. doi: 10.1007/s00122-013-2136-3

McKenna, A., Hanna, M., Banks, E., Sivachenko, A., Cibulskis, K., Kernytsky, A., et al. (2010). The genome analysis toolkit: A MapReduce framework for analyzing next-generation DNA sequencing data. *Genome Res*. 20, 1297–1303. doi: 10.1101/gr.107524.110

Mercier, R., Mézard, C., Jenczewski, E., Macaisne, N., and Grelon, M. (2015). The molecular biology of meiosis in plants. *Annu. Rev. Plant Biol*. 66, 297–327. doi: 10.1146/annurev-arplant-050213-035923

Mieulet, D., Jolivet, S., Rivard, M., Cromer, L., Vernet, A., Mayonove, P., et al. (2016). Turning rice meiosis into mitosis. *Cell Res*. 26, 1242–1254. doi: 10.1038/cr.2016.117

Moran, E. S., Armstrong, S. J., Santos, J. L., Franklin, F. C. H., and Jones, G. H. (2001). Chiasma formation in *Arabidopsis thaliana* accession Wassileskija and in two meiotic mutants. *Chromosom. Res*. 9, 121–128. doi: 10.1023/A:1009278902994

Nakagawa, T., Kurose, T., Hino, T., Tanaka, K., Kawamukai, M., Niwa, Y., et al. (2007). Development of series of gateway binary vectors, pGWBs, for realizing efficient construction of fusion genes for plant transformation. *J. Biosci. Bioeng*. 104, 34–41. doi: 10.1263/jbb.104.34

Nishant, K. T., Chen, C., Shinohara, M., Shinohara, A., and Alani, E. (2010). Genetic analysis of baker's yeast msh4-msh5 reveals a threshold crossover level for meiotic viability. *PLoS Genet*. 6:e1001083. doi: 10.1371/journal.pgen.1001083

Obmolova, G., Ban, C., Hsieh, P., and Yang, W. (2000). Crystal structures of mismatch repair protein MutS and its complex with a substrate DNA. *Nature* 407, 703–710. doi: 10.1038/35037509

Ostergaard, L., and King, G. J. (2008). Standardized gene nomenclature for the Brassica genus. *Plant Methods* 4:10. doi: 10.1186/1746-4811-4-10

Qian, L., Qian, W., and Snowdon, R. J. (2014). Sub-genomic selection patterns as a signature of breeding in the allopolyploid *Brassica napus* genome. *BMC Genomics* 15, 1–17. doi: 10.1186/1471-2164-15-1170

Rattray, A., Santoyo, G., Shafer, B., and Strathern, J. N. (2015). Elevated mutation rate during meiosis in *Saccharomyces cerevisiae*. *PLoS Genet*. 11:e1004910. doi: 10.1371/journal.pgen.1004910

Samans, B., Chalhoub, B., and Snowdon, R. J. (2017). Surviving a genome collision: genomic signatures of allopolyploidization in the recent crop species. *Plant Genome* 10. doi: 10.3835/plantgenome2017.02.0013

Séguéla-Arnaud, M., Crismani, W., Larchevêque, C., Mazel, J., Froger, N., Choinard, S., et al. (2015). Multiple mechanisms limit meiotic crossovers: TOP3α and two BLM homologs antagonize crossovers in parallel to FANCM. *Proc. Natl. Acad. Sci. U.S.A*. 112, 4713–4718. doi: 10.1073/pnas.1423107112

Sim, N.-L., Kumar, P., Hu, J., Henikoff, S., Schneider, G., and Ng, P. C. (2012). SIFT web server: predicting effects of amino acid substitutions on proteins. *Nucleic Acids Res*. 40, W452–W457. doi: 10.1093/nar/gks539

Stephenson, P., Baker, D., Girin, T., Perez, A., Amoah, S., King, G. J., et al. (2010). A rich TILLING resource for studying gene function in *Brassica rapa*. *BMC Plant Biol*. 10:62. doi: 10.1186/1471-2229-10-62

Tiley, G. P., and Burleigh, J. G. (2015). The relationship of recombination rate, genome structure, and patterns of molecular evolution across angiosperms. *BMC Evol. Biol*. 15, 194. doi: 10.1186/s12862-015-0473-3

Trick, M., Long, Y., Meng, J., and Bancroft, I. (2009). Single nucleotide polymorphism (SNP) discovery in the polyploid *Brassica napus* using Solexa transcriptome sequencing. *Plant Biotechnol. J.* 7, 334–346. doi: 10.1111/j.1467-7652.2008.00396.x

Triques, K., Sturbois, B., Gallais, S., Dalmais, M., Chauvin, S., Clepet, C., et al. (2007). Characterization of *Arabidopsis thaliana* mismatch specific endonucleases: Application to mutation discovery by TILLING in pea. *Plant J.* 51, 1116–1125. doi: 10.1111/j.1365-313X.2007.03201.x

Triques, K., Piednoir, E., Dalmais, M., Schmidt, J., Le Signor, C., Sharkey, M., et al. (2008). Mutation detection using ENDO1: application to disease diagnostics in humans and TILLING and Eco-TILLING in plants. *BMC Mol. Biol.* 9:42. doi: 10.1186/1471-2199-9-42

Tsai, H., Howell, T., Nitcher, R., Missirian, V., Watson, B., Ngo, K. J., et al. (2011). Discovery of rare mutations in populations: TILLING by sequencing. *Plant Physiol.* 156, 1257–1268. doi: 10.1104/pp.110.169748

Vinciguerra, P., and D'Andrea, A. D. (2009). FANCM: a landing pad for the Fanconi anemia and bloom's syndrome complexes. *Mol. Cell* 36, 916–917. doi: 10.1016/j.molcel.2009.12.007

Wang, A. T., and Smogorzewska, A. (2015). SnapShot: Fanconi anemia and associated proteins. *Cell* 160, 354–354.e1. doi: 10.1016/j.cell.2014.12.031

Wang, X., Wang, H., Wang, J., Sun, R., Wu, J., Liu, S., et al. (2011). The genome of the mesopolyploid crop species *Brassica rapa*. *Nat. Genet.* 43, 1035–1039. doi: 10.1038/ng.919

Wang, Y., Cheng, X., Shan, Q., Zhang, Y., Liu, J., Gao, C., et al. (2014). Simultaneous editing of three homoeoalleles in hexaploid bread wheat confers heritable resistance to powdery mildew. *Nat. Biotechnol.* 32, 947–951. doi: 10.1038/nbt.2969

Wang, C., Wang, Y., Cheng, Z., Zhao, Z., Chen, J., Sheng, P., et al. (2016). The role of OsMSH4 in male and female gamete development in rice meiosis. *J. Exp. Bot.* 67, 1447–1459. doi: 10.1093/jxb/erv540

Whitby, M. C. (2010). The FANCM family of DNA helicases/translocases. *DNA Repair.* 9, 224–236. doi: 10.1016/j.dnarep.2009.12.012

Wijnker, E., and de Jong, H. (2008). Managing meiotic recombination in plant breeding. *Trends Plant Sci.* 13, 640–646. doi: 10.1016/j.tplants.2008.09.004

Woodhouse, M. R., Schnable, J. C., Pedersen, B. S., Lyons, E., Lisch, D., Subramaniam, S., et al. (2010). Following tetraploidy in maize, a short deletion mechanism removed genes preferentially from one of the two homologs. *PLoS Biol.* 8:e1000409. doi: 10.1371/journal.pbio.1000409

Yang, H., Wu, J. J., Tang, T., Liu, K. D., and Dai, C. (2017). CRISPR/Cas9-mediated genome editing efficiently creates specific mutations at multiple loci using one sgRNA in *Brassica napus*. *Sci. Rep.* 7, 1–13. doi: 10.1038/s41598-017-07871-9

Ziolkowski, P. A., Berchowitz, L. E., Lambing, C., Yelina, N. E., Zhao, X., Kelly, K. A., et al. (2015). Juxtaposition of heterozygosity and homozygosity during meiosis causes reciprocal crossover remodeling via interference. *Elife* 4, 1–29. doi: 10.7554/eLife.03708

Conflict of Interest Statement: The authors declare that the research was conducted in the absence of any commercial or financial relationships that could be construed as a potential conflict of interest.

frontiers in Plant Science

ORIGINAL RESEARCH
published: 20 June 2019
doi: 10.3389/fpls.2019.00774

Arabidopsis NSE4 Proteins Act in Somatic Nuclei and Meiosis to Ensure Plant Viability and Fertility

*Mateusz Zelkowski[1], Katarzyna Zelkowska[1], Udo Conrad[1], Susann Hesse[1], Inna Lermontova[1,2], Marek Marzec[1,3], Armin Meister[1], Andreas Houben[1] and Veit Schubert[1]**

[1] Leibniz Institute of Plant Genetics and Crop Plant Research, Gatersleben, Germany, [2] Plant Cytogenomics Research Group, Central European Institute of Technology, Masaryk University, Brno, Czechia, [3] Department of Genetics, Faculty of Biology and Environmental Protection, University of Silesia, Katowice, Poland

The SMC 5/6 complex together with cohesin and condensin is a member of the structural maintenance of chromosome (SMC) protein family. In non-plant organisms SMC5/6 is engaged in DNA repair, meiotic synapsis, genome organization and stability. In plants, the function of SMC5/6 is still enigmatic. Therefore, we analyzed the crucial δ-kleisin component NSE4 of the SMC5/6 complex in the model plant *Arabidopsis thaliana*. Two functional conserved *Nse4* paralogs (*Nse4A* and *Nse4B*) are present in *A. thaliana*, which may have evolved via gene subfunctionalization. Due to its high expression level, *Nse4A* seems to be the more essential gene, whereas *Nse4B* appears to be involved mainly in seed development. The morphological characterization of *A. thaliana* T-DNA mutants suggests that the NSE4 proteins are essential for plant growth and fertility. Detailed investigations in wild-type and the mutants based on live cell imaging of transgenic GFP lines, fluorescence *in situ* hybridization (FISH), immunolabeling and super-resolution microscopy suggest that NSE4A acts in several processes during plant development, such as mitosis, meiosis and chromatin organization of differentiated nuclei, and that NSE4A operates in a cell cycle-dependent manner. Differential response of NSE4A and NSE4B mutants after induced DNA double strand breaks (DSBs) suggests their involvement in DNA repair processes.

Keywords: ***Arabidopsis thaliana*, meiosis, mitosis, NSE4 δ-kleisin, nucleus, phylogeny, SMC5/6 complex, super-resolution microscopy**

OPEN ACCESS

Edited by:
Mónica Pradillo, Complutense University of Madrid, Spain

Reviewed by:
Jan J. Palecek, Masaryk University, Czechia
Pablo Bolaños-Villegas, University of Costa Rica, Costa Rica

****Correspondence:***
Veit Schubert
schubertv@ipk-gatersleben.de

Specialty section:
This article was submitted to Plant Cell Biology, a section of the journal Frontiers in Plant Science

Received: *22 February 2019*
Accepted: *28 May 2019*
Published: *20 June 2019*

Citation:
Zelkowski M, Zelkowska K, Conrad U, Hesse S, Lermontova I, Marzec M, Meister A, Houben A and Schubert V (2019) Arabidopsis NSE4 Proteins Act in Somatic Nuclei and Meiosis to Ensure Plant Viability and Fertility. Front. Plant Sci. 10:774. doi: 10.3389/fpls.2019.00774

INTRODUCTION

The evolutionarily conserved structural maintenance of chromosome (SMC) protein complexes are ubiquitous across different organisms from bacteria to humans, and act in basic biological processes such as sister chromatid cohesion, chromosome condensation, transcription, replication, DNA repair and recombination. The SMC proteins realize these many different functions via ATP-stimulated DNA-bridging to perform intra- and intermolecular linking. Together

Abbreviations: aa, amino acids; ANOVA, analysis of variance; dsDNA, double strand DNA; DSB, double strand break; FISH, fluorescence *in situ* hybridization; GFP, green fluorescent protein; PCR, polymerase chain reaction; PMC, pollen mother cell; PPT, phosphinothricin; SIM, structured illumination microscopy.

with non-SMC proteins, including kleisin subunits, SMC proteins form ring-shaped multi-protein complexes, such as cohesins, condensins and SMC5/6 complexes (Nasmyth and Haering, 2005; Hirano, 2006; Jeppsson et al., 2014b; Haering and Gruber, 2016a,b).

It has been proposed that a bacterial or archaea SMC is the forerunner of all eukaryotic SMC complexes. Due to its interactions with the conserved kite (kleisin-interacting tandem winged-helix elements) proteins the SMC5/6 complex is regarded to represent the closest eukaryotic relative to the common SMC ancestor compared to cohesin and condensin (Palecek and Gruber, 2015).

SMC5/6 complexes are formed through the interaction of the hinge domains of the SMC5 and SMC6 proteins resulting in a heterodimer connected by the δ-kleisin NSE4 (NON-SMC ELEMENT 4) at the head domains of SMC5 and SMC6. In human and yeasts six (NSE1–6) different non-SMC elements were identified (Fousteri and Lehmann, 2000; Hazbun et al., 2003; Palecek et al., 2006; Taylor et al., 2008; Räschle et al., 2015).

Originally, the SMC5/6 complex has mainly been investigated for its function in DNA repair (Lehmann, 2005) by regulating homologous recombination at DNA breaks, stalled replication forks and rDNA (Torres-Rosell et al., 2005, 2007a,b; De Piccoli et al., 2006; Lindroos et al., 2006; Irmisch et al., 2009). In yeast, together with cohesin, SMC5/6 is involved in DSB repair to manage proper sister chromatid segregation (Uhlmann and Nasmyth, 1998; Sjögren and Nasmyth, 2001; Ünal et al., 2004; Torres-Rosell et al., 2005; De Piccoli et al., 2006). Similarly, in human cells, SMC5/6 is also involved in the recruitment of cohesin to DSB sites (Potts et al., 2006).

Furthermore, SMC5/6 facilitates the resolution of sister chromatid intertwinings and replication-induced DNA supercoiling to allow correct chromosome segregation (Bermúdez-López et al., 2010; Kegel et al., 2011; Gallego-Paez et al., 2014; Jeppsson et al., 2014a). The complex is required for telomere maintenance (Zhao and Blobel, 2005; Potts and Yu, 2007), and it has been found that SMC5/6 regulates chromosome stability and dynamics via ATP-regulated intermolecular DNA linking (Kanno et al., 2015).

The involvement of SMC5/6 components in DNA repair pathways and in activities known from cohesin, condensin indicates that SMC5/6 has a key role in maintaining chromosome stability (De Piccoli et al., 2009). The participation of SMC5/6 in cohesin- and condensin-like functions indicates that these functions seem to be realized via the DNA-bridging activity of SMC5/6, and/or through direct or indirect control of the other two complexes (Jeppsson et al., 2014b).

In addition to functions of SMC5/6 in somatic tissues, different essential roles during meiosis were proven in model organisms as yeasts, worm, mouse and human. The data indicate the involvement of SMC5/6 components in such meiotic processes as response to DSBs, meiotic recombination, heterochromatin maintenance, centromere cohesion, homologous chromosome synapsis and meiotic sex chromosome inactivation (Verver et al., 2016).

Similar as in other organisms, SMC complexes are also present in plants to perform different essential functions together with interacting factors (Schubert, 2009; Diaz and Pecinka, 2018). Due to the presence of two alternative SMC6 (SMC6A and SMC6B) and δ-kleisin NSE4 (NSE4A and NSE4B) subunits in *Arabidopsis thaliana*, different SMC5/6 complexes may be formed (**Figure 1A**). While NSE1-4 are highly conserved in eukaryotes, NSE5 and NSE6 are not conserved at the DNA sequence level. Nevertheless, based on protein complex purification and interaction data the proteins ASAP1 and SNI1 were suggested to be the functional *A. thaliana* counterparts of NSE5 and NSE6 found in other multicellular organisms (Yan et al., 2013).

SMC5, SMC6A, and SMC6B are required together with SYN1 (the α-kleisin of *A. thaliana* cohesin) to align sister chromatids after DNA breakage, apparently to facilitate repair via homologous recombination in somatic cells (Mengiste et al., 1999; Hanin et al., 2000; Watanabe et al., 2009). The *A. thaliana* SUMO E3 ligase AtMMS21 (a homolog of NSE2) regulates cell proliferation in roots via cell-cycle regulation and cytokinin signaling (Huang et al., 2009), and is involved in root stem cell niche maintenance and DNA damage responses (Xu et al., 2013). NSE1 and NSE3 of *A. thaliana* have a role in DNA damage repair and are required for early embryo and seedling development (Li et al., 2017). Transcripts of *Nse4A* but not of *Nse4B* were detected in seedlings, rosette leaves, and immature flower buds, suggesting that *Nse4A* is a functional gene in *A. thaliana* cells (Watanabe et al., 2009).

However, the biological function of the two *A. thaliana* NSE4 homologs has not yet been determined in detail. Here we show that both genes are essential for plant growth and fertility. Via applying live cell imaging, FISH, immunolabeling and super-resolution microscopy, we found that especially NSE4A proteins act in transcriptionally active somatic interphase chromatin and that they are essential for proper mitosis and meiosis.

MATERIALS AND METHODS

Plant Material and Genotyping

The *A. thaliana* (L.) Heynh. SALK and SAIL T-DNA insertion lines in ecotype Columbia (Col-0) were obtained from the Salk Institute, Genomic Analysis Laboratory[1] (Alonso et al., 2003) and from the Syngenta collection of T-DNA insertion mutants (Sessions et al., 2002), respectively. The GABI T-DNA mutants (GK in Col-0) were generated in the context of the GABI-Kat program (MPI for Plant Breeding Research, Cologne, Germany[2]; Rosso et al., 2003). All lines were provided by the Nottingham Arabidopsis Stock Centre[3].

Seeds were germinated in soil followed by cultivation under short day conditions (8 h light/16 h dark) at 18°C. After 1 month the plants were transferred to long day conditions (16 h light, 22°C/8 h dark, 21°C). Genomic DNA was isolated from rosette leaves and used for PCR-based genotyping to identify heterozygous and homozygous T-DNA insertion mutants. The PCR primers used for genotyping are listed

[1]http://signal.salk.edu/cgi-bin/tdnaexpress

[2]http://www.gabi-kat.de/

[3]http://nasc.nott.ac.uk

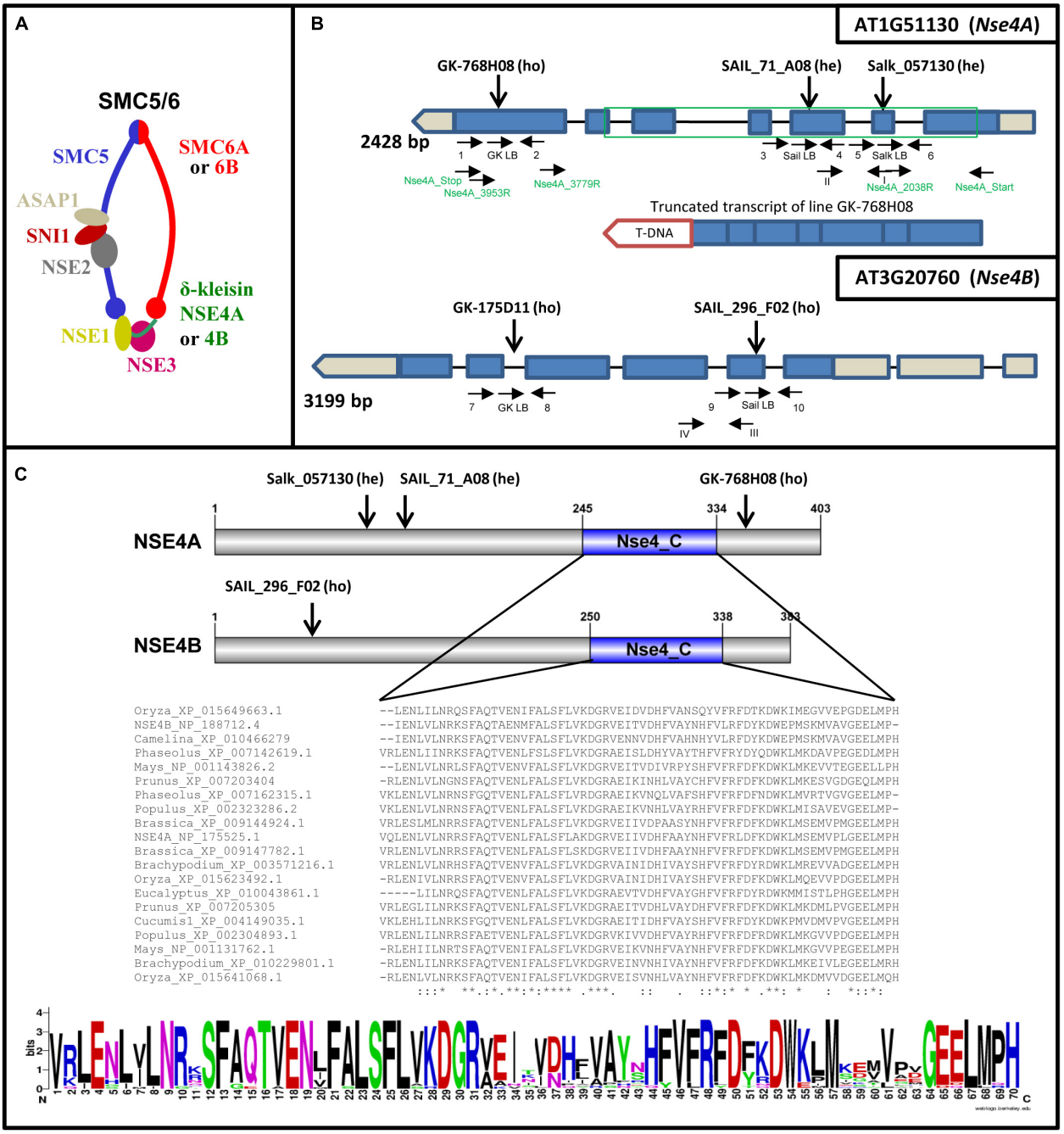

FIGURE 1 | *A. thaliana* SMC5/6 complexes and their δ-kleisin subunits NSA4A and NSE4B. **(A)** Subunit composition of SMC5/6 complexes based on a model according to Nasmyth and Haering (2005) and Schubert (2009). The SMC5/6 complexes presumably have one SMC5 subunit, two alternative SMC6 subunits, the NSE1, NSE2, NSE3, NSE5-like (SNI1), NSE6-like (ASAP1) subunits, and in addition, the two different δ-kleisins NSA4A and NSE4B. The sub-complexes NSE2-SNI1-ASAP1, NSE1-NSE3-NSE4, and SNI1-ASAP1 may act as specialized functional modules (Sergeant et al., 2005; Palecek et al., 2006; Duan et al., 2009). **(B)** Schematic view of the *Nse4A* and *Nse4B* gene structures (mips.helmholtz-muenchen.de, Version 10; ncbi.nlm.nih.gov; pfam.sanger.ac.uk) and the expressed truncated transcript of the T-DNA line GK-768H08. Exons are shown as blue boxes. UTRs are visible in gray. The green frame indicates the region used for recombinant protein expression and the production of antibodies. The T-DNA insertions (*A. thaliana* SALK, SAIL, and GK lines) and gene-specific primers used for genotyping are indicated by arrows. Arabic numbers indicate gene-specific primers used for genotyping. Roman numbers denote primers applied for RT and real-time PCR. The primers used to confirm the truncated transcript of line GK-768H08 (T-DNA insertion visualized as red box) are indicated in green (see also **Supplementary Figure S9**). **(C)** Top: schematic view of the NSE4A and NSE4B protein structures. The conserved NSE4_C motif and the T-DNA insertion positions are indicated. Middle: Alignment of the NSE4_C motifs present in putative NSE4 orthologs of higher plants. The alignment was performed by the Clustal Omega 2.1 software. *, Identical amino acids; :, similar amino acids; –, missing amino acids. Bottom: the same alignment as above presented in the sequence logo format (WebLogo; http://weblogo.berkeley.edu/logo.cgi) to compare similarities and differences in all selected sequences of the NSE4_C motif more easily.

in **Supplementary Table S1**, and their positions are shown in **Figure 1B**. The following PCR program was used: initial denaturation for 5 min at 95°C, then 40 cycles with 15 s denaturation at 95°C, 30 s annealing at 55°C, and 60 s final elongation at 72°C.

Polymerase chain reaction using the gene-specific primer sets yielded DNA fragments of ∼1 kb representing the wild-type alleles. The PCR fragments specific for the disrupted allele yielded PCR products of ∼0.5 kb. The positions of T-DNA insertion were confirmed by sequencing the PCR-amplified T-DNA junction fragments (**Supplementary Table S2**).

To obtain double T-DNA insertion mutants cross-fertilization was performed.

Brassica rapa L. plants were grown under long day conditions (16 h light, 22°C/8 h dark, 18°C) to obtain meiocytes for immunolocalization of NSE4A via specific antibodies.

In silico Analysis of Gene and Protein Structures and the Phylogenetic Tree Construction

Gene structures of NSE4A and NSE4B were predicted at mips.helmholtz-muenchen.de (Version 10[4,5]). The conserved functional domains of known putative NSE4 orthologs of higher plants (full-length sequences are available at www.ncbi.nlm.nih.gov/) were identified using the Conserved Domain Database[6]. The same sequences were used to generate a phylogenetic tree by Bayesian phylogenetic inference in MrBayes 3.2.6[7]. All alignments were performed by the Clustal Omega 2.1 software[8].

Gene Expression Analysis

Total RNA was isolated from seedlings, three and 6 weeks old leaves, flower buds, and root tissues using the Trizol (Thermo Fisher Scientific) method according to manufacturer's instructions. Then, the samples were DNase-treated applying the TURBO DNA-free™ Kit (Thermo Fisher Scientific). Reverse transcription (RT) was performed using the random hexamer RevertAid Reverse Transcriptase Kit (Thermo Fisher Scientific). After 5 min initial denaturation at 95°C, followed by 60 min cDNA synthesis at 42°C, the reaction was terminated at 70°C for 5 min.

Quantitative real-time PCR with SYBR Green was performed using a QuantStudio 5 flex machine and the QuantStudio™ Real-Time PCR Software (v1.1). One microliter of cDNA was applied for each reaction with three replicates and three independent biological repetitions for each tissue or developmental stage. The following PCR program was used: initial denaturation for 5 min at 95°C, then 40 cycles with 15 s denaturation at 95°C, 30 s annealing at 60°C, and 20 s final elongation at 72°C. *PP2A* (AT1G13320) and *RHIP1* (AT4G26410) served as standards (Czechowski et al., 2005). Calculations were based on the delta CT values of the reference genes (Livak and Schmittgen, 2001). The quantitative real-time RT-PCR primers used to amplify transcripts are shown in **Figure 1B** and **Supplementary Table S3**.

Cloning and Transformation

PCR-based amplification of cDNA (for 35S::*Nse4A*::EYFP) and genomic DNA (for promoterNse4A::gNse4A::GFP) as templates were performed using the KOD Xtreme™ Hot Start DNA Polymerase (Merck). The PCR products were cloned into the pJET 1.2 vector using the CloneJET PCR Cloning Kit (Thermo Fisher Scientific). Sequence-confirmed inserts were cloned into the Gateway® pENTR™ 1A Dual Selection Vector (Thermo Fisher Scientific). Next, the inserts were re-cloned into the pGWG (complementation vector without promoter and tag), pGWB642 (35S promoter with EYFP tag on N-term) and pGWB604 (no promoter, GFP-tag on C-terminus) vectors (Neyagawa vectors, doi.org/10.1271/bbb.100184; Nakamura et al., 2010) using the BP Clonase II kit (Gateway® Technology, Thermo Fisher Scientific). The binary vectors were transferred into *Agrobacterium tumefaciens*, and then used to transform *A. thaliana* Col-0 wild-type plants via the floral dip method (Clough and Bent, 1998). Seeds from these plants were propagated on PPT medium (16 μg/ml). Positively selected seedlings were transferred into soil and genotyped for the presence of the construct. Homozygous F2 plants were used in further studies. Primers used for the cloning are listed in **Supplementary Table S4**.

Recombinant Protein and Antibody Production

For antibody production the partial NSE4A peptide (from 49 to 289 aa) (**Supplementary Figure S1**) was expressed in the *E. coli* BL21 pLysS strain using the pET23a (Novagen) vector. Primers used for the recombinant protein production are listed in **Supplementary Table S4**. The recombinant proteins containing 6xHis-tags were purified using Dynabeads His-Tag (Thermo Fisher Scientific) according to manufacturer's instructions. Five hundred microliters cleared extract was mixed with 500 μl binding buffer (50 mM NaP, pH 8.0, 300 mM NaCl, 0.01% Tween-20), and 50 μl washed Dynabeads were added. After 10 min incubation on a roller, the beads were washed 7 × with binding buffer, and 7 × with binding buffer, 5 mM imidazole. The elution was done with binding buffer, 150 mM imidazole, and the protein concentration (90 ng/μl) was determined using a Bradford kit (Bio-Rad Laboratories GmbH, Munich) (Bradford, 1976).

The separation on SDS gels and the protein size determination by Western analysis was done as described (Conrad et al., 1997; **Supplementary Figure S2A**).

Two rabbits were immunized with 1 mg NSE4A protein and complete Freund's adjuvants. Four and five weeks later, booster immunizations were performed with 0.5 mg NSE4A protein and incomplete Freund's adjuvants, respectively. Ten days later blood was taken, serum isolated, precipitated in 40% saturated ammonium sulfate, dialysed against 1 × PBS and affinity purified.

[4] ncbi.nlm.nih.gov

[5] pfam.sanger.ac.uk

[6] https://www.ncbi.nlm.nih.gov/Structure/cdd/wrpsb.cgi

[7] mrbayes.sourceforge.net/

[8] www.ebi.ac.uk/Tools/msa/clustalo/

The specific binding behavior of the rabbit anti-NSE4 antibodies was investigated by competitive ELISA according to Conrad et al. (2011). The wells were coated with 46 ng/100 µl recombinant affinity-purified NSE4A in 1 × PBS and incubated overnight at room temperature. After blocking with 3% w/v BSA in 1 × PBS-0.05% w/v Tween 20 (1 × PBS-T) for 2 h, the known amounts of affinity-purified anti-NSE4A antibodies were mixed with various concentrations of NSE4A in 1% w/v BSA in 1 × PBS-T, incubated for 30 min in a master plate, added to the antigen-coated wells and incubated for 1 h at 25°C. Antibodies bound to the plate were visualized with anti-rabbit-IgG alkaline phosphatase diluted in 1 × PBS-T/1% BSA. The enzymatic substrate was pNP phosphate, and the absorbance (405 nm) was measured after 30 min incubation at 37°C (**Supplementary Figure S2B**).

To further prove the NSE4A antibody specificity in immuno-histological experiments antigen competition experiments were performed. NSE4A was added to the antibodies at a concentration of 800 nM, and applied to flow-sorted 8C *A. thaliana* interphase nuclei. The signal reduction compared to the control nuclei without addition of antigen clearly confirmed the specificity (**Supplementary Figure S2C**).

Complementation Assay

To confirm that the phenotypes of the of *Nse4A* mutant GK-768H08 are indeed caused by this mutation we complemented the mutant by the genomic wild-type *Nse4A* gene. The genomic intron-exon containing *Nse4A* gene with a 1.7 kbp-long upstream promoter region was amplified by PCR using the KOD Xtreme™ Hot Start DNA Polymerase (Merck), and then sequenced. Next, it was cloned into the pBWG vector (Nakamura et al., 2010), and transformed into *A. tumefaciens*. Plant transformation was performed by the bacteria-mediated vector transfer via the floral dipping method (Clough and Bent, 1998), and afterward propagated under long-day conditions. The harvested seeds were grown on selective PPT medium (16 µg/ml), and positively selected seedlings were transferred to soil and genotyped for the presence of the construct. Homozygous F2 plants were used in further studies.

Fertility Evaluation and Alexander Staining

Mature dry siliques were collected to evaluate silique length and seed setting. The seeds were classified into normal and shriveled (**Figure 2**). For clearing, fully developed green siliques were treated in an ethanol:acetic acid (9:1) solution overnight at room temperature, then washed in 70 and 90% ethanol for 5 min each, followed by storage in a chloral hydrate:glycerol:water (8:1:3) solution at 4°C.

To evaluate anther shape and pollen viability, Alexander staining (Alexander, 1969) was performed. Undamaged anthers were used for total pollen (per anther) counting. Afterward, the anthers were squashed and the released pollen grains were evaluated into two classes: normal (viable, pink round grains), and aborted (gray/green abnormal shape).

Images from siliques, seeds and anthers were acquired using a Nikon SMZ1500 binocular and the NIS-Elements AR 3.0 software.

Bleomycin Treatment

To induce DNA DSBs via bleomycin application *A. thaliana* wild-type and NSE4A mutant seeds were sterilized 10 min in 70% ethanol, then 15 min in 4% Na-hypochlorite + 1 drop Tween-20, followed by washing 3 × 5 min in sterile water. The seeds were germinated on wet filter paper for 5 days, and then placed in liquid germination medium (Murashige and Skoog, Duchefa, prod. no. M0231.0025; 10 g/l sucrose, 500 mg/l MES, pH 5.7) without and with bleomycin (bleomycin sulfate from *Streptomyces verticillus*, Sigma, cat. no. 15361) of increasing concentration. Accordingly, in a second experiment the sterilized seeds were grown on agar plates (germination medium + 2% agar-agar; Roth, cat. no. 2266.2) without and with bleomycin. Both experiments were repeated twice and contained two repetitions.

Immunostaining and FISH

Flower bud fixation, chromosome slide preparation, and FISH followed by chiasma counting were performed according to Sánchez-Morán et al. (2001). To identify individual chromosomes, 5S and 45S rDNA FISH was performed.

Fluorescence *in situ* hybridization with telomere- and centromere-specific probes was applied to identify chromosomes at metaphase I. The 180-bp centromeric repeat probe (pAL) (Martinez-Zapater et al., 1986) was generated by PCR as previously described (Kawabe and Nasuda, 2005). The telomere-specific probe was generated by PCR in the absence of template DNA using the primers $(TAAACCC)_7$ and $(GGGTTTA)_7$ (Ijdo et al., 1991).

Immunostaining of *A. thaliana* and *B. rapa* PMCs followed the protocol of Armstrong and Osman (2013). The following primary antibodies were applied: rabbit anti-NSE4A (1:250) and rat anti-ZYP1 (1:1000; kindly provided by Chris Franklin). ZYP1 is the *A. thaliana* transverse filament protein of the synaptonemal complex (Higgins et al., 2005). The primary antibodies were detected by donkey anti-rabbit-Alexa488 (Dianova, no. 711545152) and goat anti-rat-DyLight594 (Abcam, no. ab98383), respectively, as secondary antibodies.

8C leaf interphase nuclei were flow sorted according to Weisshart et al. (2016), and also immuno-labeled against NSE4A as described above.

Microscopy

To image fixed and live cell preparations an Olympus BX61 microscope (Olympus) and a confocal laser scanning microscope LSM 780 (Carl Zeiss GmbH), respectively, were used.

To analyze the ultrastructure of immunosignals and chromatin beyond the classical Abbe/Raleigh limit at a lateral resolution of ∼120 nm (super-resolution, achieved with a 488 nm laser) spatial structured illumination microscopy (3D-SIM) was applied using a 63 × 1.4NA Oil Plan-Apochromat objective of an Elyra PS.1 microscope system and the software ZEN (Carl Zeiss GmbH). Images were captured separately for each fluorochrome

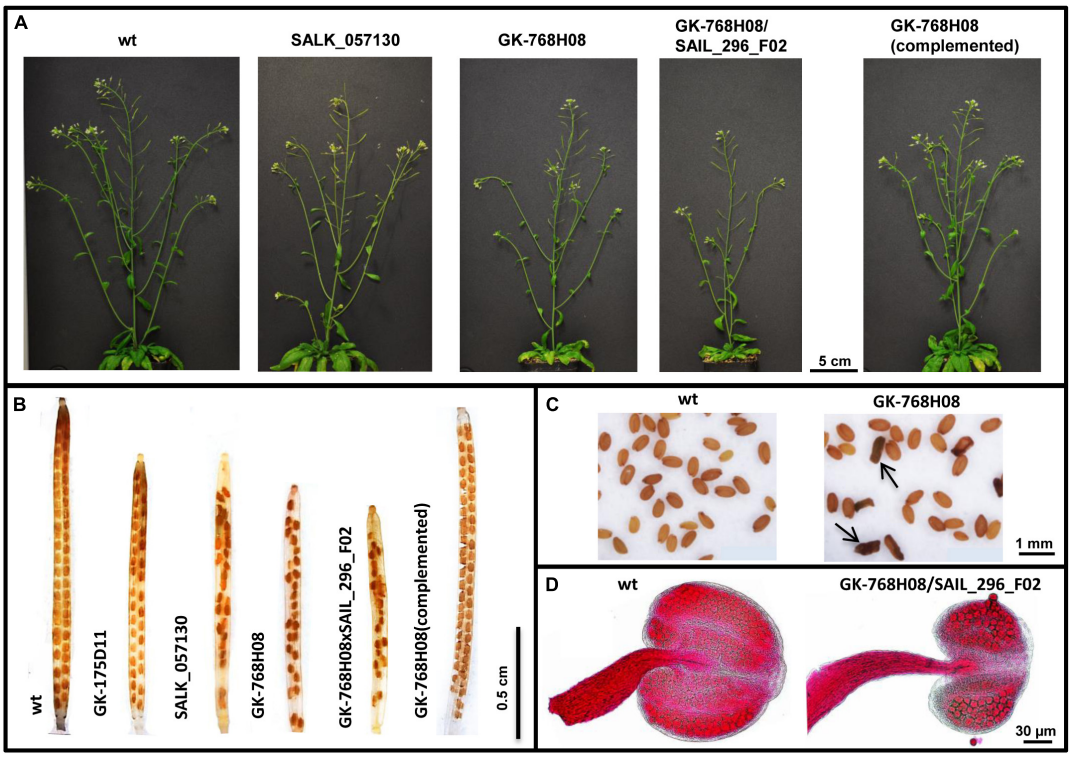

FIGURE 2 | Impaired growth and fertility of *nse4* mutants compared to wild-type (wt). **(A)** Reduced plant size of the mutants GK-768H08 and the double mutant GK-768H08/SAIL_296_F02. Mutant SALK_057130 and the complemented GK-768H08 mutant show a wild-type habit. **(B)** Reduced seed set per silique in the nse4A and nse4B mutants. **(C)** Shriveled seeds (arrows) of the GK-768H08 mutant. **(D)** Reduced pollen grain number and aborted pollen grains in an anther of the double mutant GK-768H08/SAIL_296_F02.

using the 561, 488, and 405 nm laser lines for excitation and appropriate emission filters (Weisshart et al., 2016).

RESULTS

Two Conserved *Nse4* Genes Are Present and Expressed in *A. thaliana*

According to previous SMC5/6 subunit prediction studies (Schubert, 2009) *A. thaliana* encodes two *Nse4* homologs: *Nse4A* (AT1G51130) and *Nse4B* (AT3G20760) (**Figures 1A,B**). Both NSE4 proteins show similar lengths (NSE4A: 403 aa; NSE4B: 383 aa), and a high amino acid sequence identity (67.7%) (**Supplementary Figure S1**). Both *A. thaliana* NSE4 proteins show similar lengths as those of budding yeast (402 aa), mouse (381 aa for NSE4A; 375 aa for NSE4B), and human NSE4A (385 aa), but are longer than the fission yeast NSE4 (300 aa) and the human NSE4B (333 aa) proteins (NSE4A[9]; NSE4B[10]).

NSE4A shows a relatively high amino acid similarity compared to both *B. rapa* putative NSE4 proteins (**Supplementary Figure S3**), and other plant species (**Supplementary Figure S4A**). Non-plant organisms such as fission yeast, *Entamoeba*, *Dictyostelium*, mouse and human display a lower similarity (**Supplementary Table S5**).

The phylogenetic analysis of the full-length protein sequences of eudicot and monocot species suggests also a relatively high conservation of both *A. thaliana Nse4* genes (**Supplementary Figure S4B**).

According to Uniprot databases[11], both *A. thaliana* NSE4 proteins possess conserved C-terminal domains typical for other plant NSE4 proteins (**Figure 1C** and **Supplementary Figures S1**, **S3**). The C-terminal domain binds to SMC5 in the similar way as the other kleisin molecules interact with their kappa-SMC partners (Palecek et al., 2006; Hassler et al., 2018). This interaction is crucial for the function of SMC5/6. The NSE4 N-terminal domain is also conserved and binds to SMC6 (Palecek et al., 2006). In NSE4 of fungi and vertebrates, a NSE3/MAGE binding domain was identified next to the N-terminal kleisin motif (Guerineau et al., 2012). Based on the Motif Scan analysis[12] the SMC6-binding domain can also be predicted in the NSE4 proteins of *A. thaliana* (**Supplementary Figure S1**). However, to define this identified region as the SMC6-binding motif clearly, protein–protein interaction, domain dissection and mutagenesis experiments have to be performed. Additionally, putative

[9]https://www.uniprot.org/uniprot/Q9NXX6
[10]https://www.uniprot.org/uniprot/Q8N140
[11]https://www.ebi.ac.uk/interpro/entry/IPR014854
[12]https://myhits.isb-sib.ch/cgi-bin/motif_scan

degradation regions and SUMOlisation sites were identified using Eukaryotic Linear Motif[13] resources (**Supplementary Figure S1**), suggesting that the cellular amount of NSE4 proteins during the cell cycle might be regulated via their proteolytic degradation.

In silico analysis shows a similar expression behavior (with peaks at the young rosette and flowering stages) during plant development of the *Nse4A* gene and other SMC5/6 subunit candidate genes, supporting a synchronized activity (**Supplementary Figure S5**). However, it is not clear whether they act separately or as multi-subunit complexes in various subunit combinations. *In silico* analysis indicated also a high co-expression of *Nse4A*, among others, with meiosis- and chromatin-related genes (**Supplementary Table S6**).

The *in silico* analysis of the relative expression level of *Nse4A* and *Nse4B* in ten anatomical parts of *A. thaliana* seedlings displayed that the expression of *Nse4B* is limited to generative tissues and seeds. A relatively high expression is evident only in seeds (embryo and especially endosperm) (**Supplementary Figure S6**).

By quantitative real-time PCR we found that *Nse4A* is highly expressed in flower buds and roots, but transcripts are also present in seedlings, young and old leaves (**Supplementary Figure S7**). In agreement with previous studies (Watanabe et al., 2009), the expression of *Nse4B* in these tissues is not detectable. Obviously, most *Nse4B* transcripts are present in already well developed seeds, as also indicated by *in silico* analysis (**Supplementary Figure S6**).

To figure out whether the NSE4 proteins interact with the other components of the SMC5/6 complex (**Figure 1**) a protein-protein interactions analysis was performed *in silico* using the STRING program[14]. Interestingly, all SMC5/6 subunits accessible via the STRING program were identified as interacting partners of the NSE proteins at a very high score >0.95, suggesting that both NSE4A and NSE4B act also within the SMC5/6 complex. In addition, cohesin and condensin subunits were detected as parts of the same protein-protein interaction network at the high score of >0.70 (**Supplementary Figure S8**). An interaction with cell cycle factors could not be identified at a medium score >0.5.

The results indicate that both *A. thaliana Nse4* genes are highly conserved, and that the corresponding proteins may act in combination with other SMC5/6 complex components, as well as cohesin and condensin. Based on the level of expression, *Nse4A* seems to be the more essential gene, although Nse4B appears to be specialized to act during seed development.

Selection and Molecular Characterization of *A. thaliana nse4* Mutations and Their Effect on Plant Viability, Fertility, and DNA Damage Repair

From the *A. thaliana* SALK, Syngenta SAIL and GABI-Kat collections, homo- and heterozygous T-DNA insertion mutants were selected for both genes (**Figure 1B** and **Table 1**). The presence and positions of corresponding T-DNA insertions were confirmed by PCR using gene-specific and T-DNA specific primers and by sequencing the PCR products (**Supplementary Table S2**). With exception of line GK-175D11 (intron-insertion in *Nse4B*), all the other T-DNA insertions were found in exons.

For the *Nse4A* lines Salk_057130 and SAIL_71_A08 only heterozygous mutants could be selected and the progeny segregated into heterozygous and wild-type plants. This indicates the requirement of *Nse4A* for plant viability. The confirmed truncated transcripts downstream outside of the conserved region of the homozygous line GK-768H08 (**Figure 1** and **Supplementary Figure S9**) obviously are able to code at least partially functional proteins. For *Nse4B* two homozygous lines, SAIL_296_F02 and GK-175D11, containing the T-DNA insertion in the second exon and fourth intron, respectively, were identified.

The selected mutants showed a wild-type growth habit, with only a slightly reduced plant size (especially line GK-768H08) compared to wild-type (**Figure 2A** and **Table 1**). To combine the mutation effects of *nse4A* and *nse4B*, lines GK-768H08 and SAIL_296_F02 were crossed. The resulting homozygous double mutants showed a further decreased growth. The complementation of the mutation in line GK-768H08 by the genomic wild-type *Nse4A* construct recovered the plant viability.

Thus, the essential character of *Nse4A* becomes confirmed. Although knocking out of *Nse4B* does not induce obvious growth effects, this second *Nse4* homolog is likely not completely free of function.

The selected T-DNA insertion lines were further analyzed more in detail to investigate the influence of the NSE4 proteins on meiosis and fertility. In addition to the reduced plant size, reduced pollen grain number, silique size and seed set together with shriveled seeds were observed in the mutants (**Table 1**, **Figures 2B–D**, and **Supplementary Figure S10**). The aborted seeds might represent the segregating homozygous progeny. The complementation of the mutation in line GK-768H08 by the genomic Nse4A construct recovered pollen fertility and seed setting.

To investigate the DNA damage response of the nse4 mutants compared to wild-type we applied bleomycin at different concentrations in liquid medium to induce DSBs. The treatment clearly impaired the seedling growth of both, the wild-type (Col-0) and the *nse4A* and *nse4B* mutants with increasing bleomycin concentration (**Supplementary Figure S11A**). To figure out whether the nse4 mutations influence the repair capacity of the plantlets, we performed a similar experiment on solid agar medium plates, and measured the seedling root lengths within 18 days growth (**Supplementary Figure S11B**). According to a two-way ANOVA a highly significant difference between wild-type and all mutants has been proven regarding the root development without bleomycin treatment. In addition, significantly decreased root growth rates of all three mutants were present after bleomycin application at all concentrations (0.25; 0.5; and 1.0 μg/ml) (**Supplementary Figure S11C**). These results suggest the involvement of NSE4A and NSE4B in the repair of induced DSBs, and that their

[13] http://elm.eu.org/

[14] http://string-db.org/

TABLE 1 | Characterization of the T-DNA insertion mutants of the *A. thaliana Nse4* genes.

Gene symbol	T-DNA mutant	Zygosity	Habit	Pollen fertility (%)	Silique length (mm)	Seeds per silique	Shriveled seeds per silique	% mitotic cells with bridges/ fragments	% meiocytes with bridges/fragments		
									Metaphase I	Anaphase I	Anaphase II
Col-wt	–	–	wt	100 (10790)	12.8 (28)	44.5 (1468)	0.7	1.5 (417)	0 (60)	1.2 (67)	0 (23)
Nse4A	Salk_057130	He	Smaller	98.2 (3808)	11.3** (24)	30.3** (726)	2.7**	11.9** (242)	8.4* (59)	4.2 (47)	10.0 (21)
	SAIL_71_A08	He									
	GK-768H08	Ho	Smaller	50.2** (6396)	10.0** (25)	21.0** (525)	7.8**	25.7** (175)	25.2** (115)	40.4** (114)	47.4** (19)
	GK-768H08 (complemented)	Ho	wt-like	102 (6270)	12.3* (25)	31.8** (795)	3.4**	2.6 (373)	5.0** (121)	19.1** (131)	15.0* (20)
Nse4B	SAIL_296_F02	Ho	wt-like	97.2 (3770)	10.8** (30)	30.5** (916)	1.6	2.1 (278)	0 (59)	5.9 (85)	8.3 (12)
	GK-175D11	Ho	wt-like	64.3** (3206)	11.3** (30)	34.8** (1080)	2.9**	1.7 (178)	6.2** (113)	17.8** (106)	0 (18)
Nse4A/ Nse4B	GK-768H08/SAIL_294_F02	Ho/ho	Smaller	34.8** (4529)	10.2** (30)	17.9** (536)	5.6**	28.6** (619)	30.6** (72)	65.0** (172)	50.0** (34)

*The numbers of pollen, siliques, seeds, somatic and meiotic cells analyzed are indicated in parentheses. **$p < 0.01$; *$p < 0.05$.*

mutations may reduce the repair efficiency compared to the wild-type proteins.

NSE4 Is Essential for Correct Meiosis

The reduced number of pollen grains of the *nse4* mutants suggests meiotic disturbances. Therefore, we stained meiocytes by DAPI. During prophase I no apparent alterations were found in the *nse4A* mutant GK-768H08 compared to wild-type. However, anaphase bridges, chromosome fragments and micronuclei appear in later meiotic stages and in tetrad cells, respectively (**Figure 3A** and **Supplementary Figure S12**). Micronuclei are a possible product of chromosome fragmentation. In addition to line GK-768H08, all investigated *nse4* mutants showed an increase in meiotic defects, with a clearly increased level in the homozygous GK-768H08/SAIL_294_F02 double mutants. The complementation of the mutation in line GK-768H08 by the genomic *Nse4A* construct abolished mainly the accumulation of meiotic abnormalities (**Table 1** and **Supplementary Figure S13**).

To study the meiotic abnormalities more in detail, FISH experiments using 5S and 45S rDNA probes for chromosome identification were performed (**Supplementary Figure S14**). The analysis of the *nse4A* mutant GK-768H08 suggests that the occurrence of stretched bivalents, possibly causing chromosome fragments, is not related to specific chromosomes. This indicates that the defects may be induced by disturbing a general meiotic process.

Telomere- and centromere-specific FISH probes were applied to evaluate the proportion of pericentromeric, interstitial and subtelomeric fragments during anaphase I. Most fragments were found to be of subtelomeric origin, followed by interstitial fragments (**Figures 3B,C**). Obviously, the fragments are the result of a disturbed degree of chromatin condensation along rod bivalents. The increased number of rod bivalents in the mutants seems to be the consequence of a reduced recombination leading to less chiasmata. To test this hypothesis, the chiasma frequency of the *nse4A* mutant GK-768H08 (n = 43) was evaluated, and was found to be nearly identical with ∼10.0 chiasmata per diakinesis/metaphase I cell to that of wild-type (Higgins et al., 2004). Thus, the truncation of NSE4A seems not to influence the number of chiasmata.

The occurrence of disturbed meiosis suggests the involvement NSE4 in meiotic processes. Indeed, transgenic *A. thaliana* meiocytes expressing the gNse4A::GFP construct under control of the endogenous promoter showed line-like signals at pachytene, typical for the synaptonemal complex (**Figure 4A**). In addition, by applying anti-GFP antibodies NSE4A was proven to be present in G2, leptotene, zygotene, and pachytene cells. After mainly disappearing from meta- and anaphase I chromosomes NSE4A recovered in prophase II, tetrads and young pollen (**Figure 4B**). To confirm the presence of NSE4A in a related species, immunolabeling of *B. rapa* meiocytes with NSE4A-specific antibodies and with ZYP1, the *A. thaliana* transverse filament protein of the synaptonemal complex at pachytene, was performed. The co-localization of both proteins indicated the presence of NSE4A at the synaptonemal complex during pachytene (**Figure 4C**). The immunolabeling of ZYP1 in pachytene meiocytes of the *nse4A* mutant GK-768H08 indicated

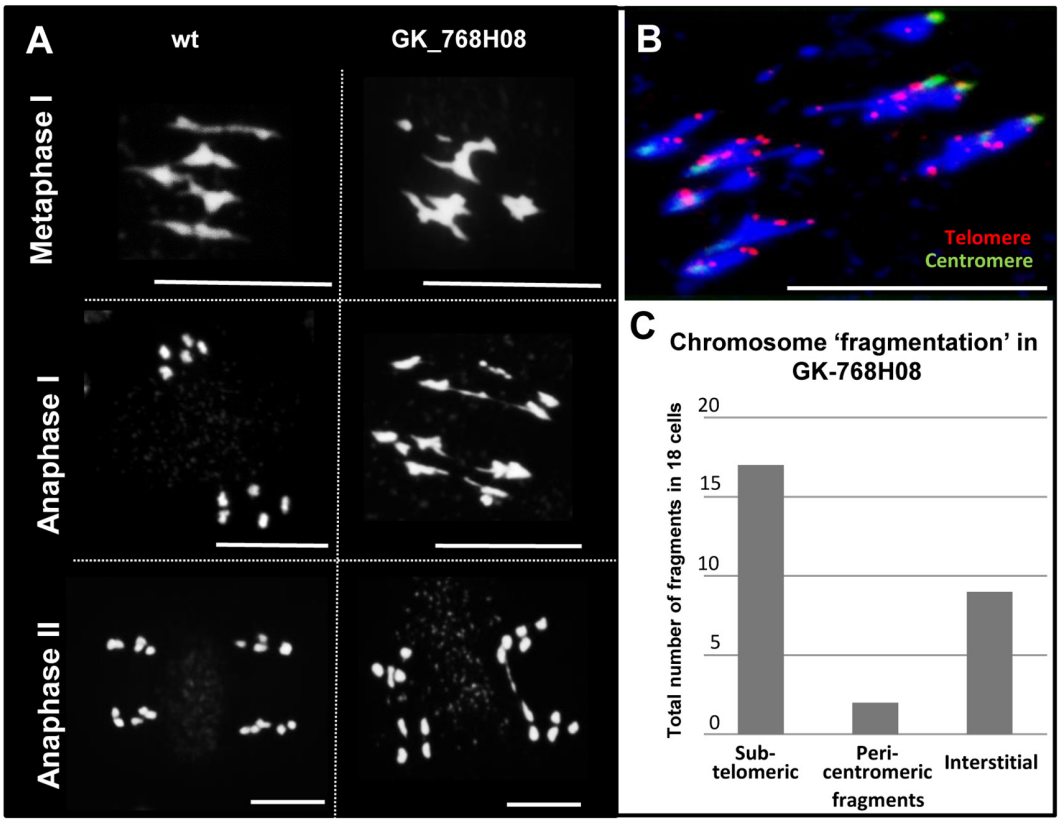

FIGURE 3 | Meiotic defects in the *nse4* mutant GK-768H08. **(A)** Disturbed meiosis (anaphase bridges, fragments) in the *A. thaliana* mutant GK-768H08 compared to wild-type (wt). **(B)** Chromosome fragmentation in GK-768H08 during anaphase I. Telomeres and centromeres were labeled by FISH using centromere- and telomere-specific probes. **(C)** Total number of subtelomeric, pericentromeric, and interstitial chromosome fragments in 18 meiotic cells of the GK-768H08 mutant. Bars = 10 μm.

that this mutation does not alter the synaptonemal complex structure (**Supplementary Figure S15**).

We conclude that both NSE4 proteins, but NSE4A again more substantially than NSE4B, are involved in meiotic processes to achieve normal fertility. However, both proteins seem not to influence the frequency of chiasmata, although NSE4A was proven to be present at the synaptonemal complex during prophase I.

NSE4 Is Present in Interphase Nuclei of Meristem and Differentiated Cells

Similar as during meiosis, abnormalities occur during mitosis in somatic flower bud nuclei of the *A. thaliana nse4* mutants. These mitotic defects occur predominantly in the *nse4A* mutants, and less prominent in the *Nse4B* knock-out mutants (**Figure 5**).

For live imaging gNSE4A::GFP signals were detected by confocal microscopy in root meristem cells. NSE4A was present in interphase nuclei, disappeared mainly during mitosis from the chromosomes and recovered at telophase at chromatin. Only a slight cytoplasm labeling remained during meta- and anaphase (**Figure 6A**). To analyze the distribution of NSE4A at the ultrastructural level, fixed interphase nuclei were stained with anti-GFP, and super-resolution microscopy (3D-SIM) has been performed. Thereby, it became obvious that NSE4A is distributed within euchromatin, but absent from nucleoli and chromocenters. During meta- and anaphase only few NSE4A signals were present within cytoplasm, confirming the live cell investigations (**Figure 6B**).

3D-SIM has also been applied to demonstrate the distribution of NSE4A in differentiated nuclei. Similar as in meristematic tissue, somatic flower bud and 8C leaf interphase nuclei display NSE4A exclusively within euchromatin (**Figure 7**).

We conclude that, in addition to their meiotic function, NSE4 proteins play also a role in somatic tissue, due to its exclusive presence within the euchromatin of cycling and differentiated interphase nuclei. NSE4A is more prominent than NSE4B also in somatic tissue.

DISCUSSION

Until now, only few investigations were performed to elucidate the functions of the plant SMC5/6 complexes, their components and interacting factors. We found that *A. thaliana* NSE4 is conserved and multifunctional in distinct chromatin-associated processes during mitosis, meiosis and in differentiated tissue.

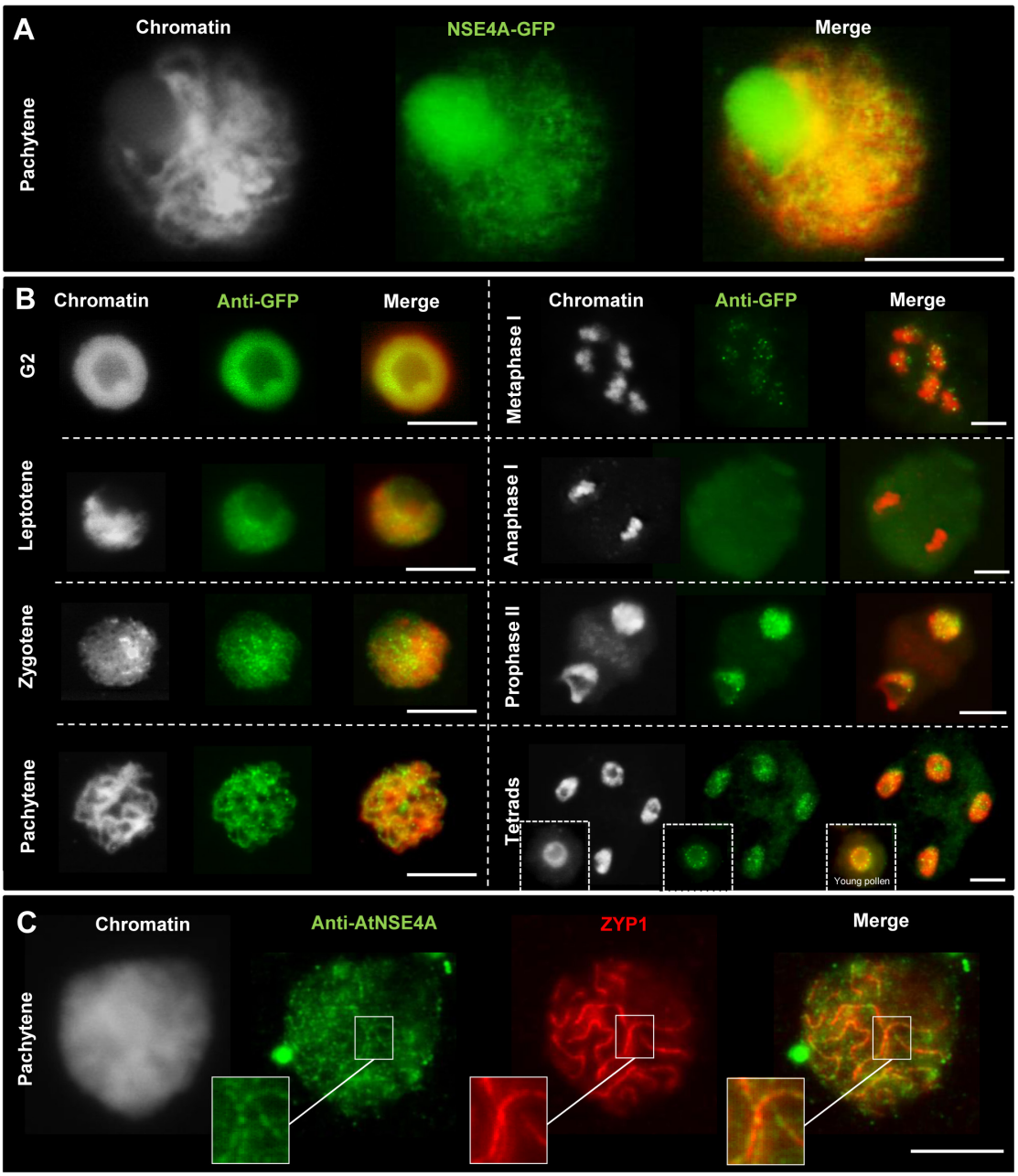

FIGURE 4 | Localization of NSE4A during the meiosis of *A. thaliana* **(A,B)** and the closely related species *B. rapa* **(C)**. **(A)** Line-like NSE4A-GFP signals are detectable in an unfixed meiocyte at pachytene of a transgenic pnse4A::gNse4A::GFP *A. thaliana* plant. **(B)** Dynamics and localization of NSE4A-GFP signals during meiosis of pnse4A::gNse4A::GFP transgenic *A. thaliana* plants, detected by anti-GFP. The NSE4A-GFP signals are detectable in G2, leptotene, zygotene, and pachytene cells. The signals are weak or not visible in condensed metaphase I and anaphase I chromosomes, respectively, but are recovered in prophase II, tetrads and young pollen. **(C)** Anti-AtNSE4A labels the synaptonemal complex of *B. rapa* and colocalizes to ZYP1 during pachytene. Gray color indicates chromatin counterstained with DAPI. Bars = 10 μm.

A. thaliana Encodes Two Functional and Specialized *Nse4* Variants

Gene duplication has been regarded as a major force in the genome evolution of plants leading to the establishment of new biological functions, such as the production of floral structures, the development of disease resistance, and the adaptation to stress. Duplicated genes can be generated by unequal crossing over, retroposition, chromosomal, and genome duplication (Hurles, 2004; Magadum et al., 2013; Wang and Adams, 2015; Panchy et al., 2016). Compared to other organisms, angiosperms tend to frequent chromosomal duplications and subsequent gene loss (Bowers et al., 2003; Coghlan et al., 2005). In addition,

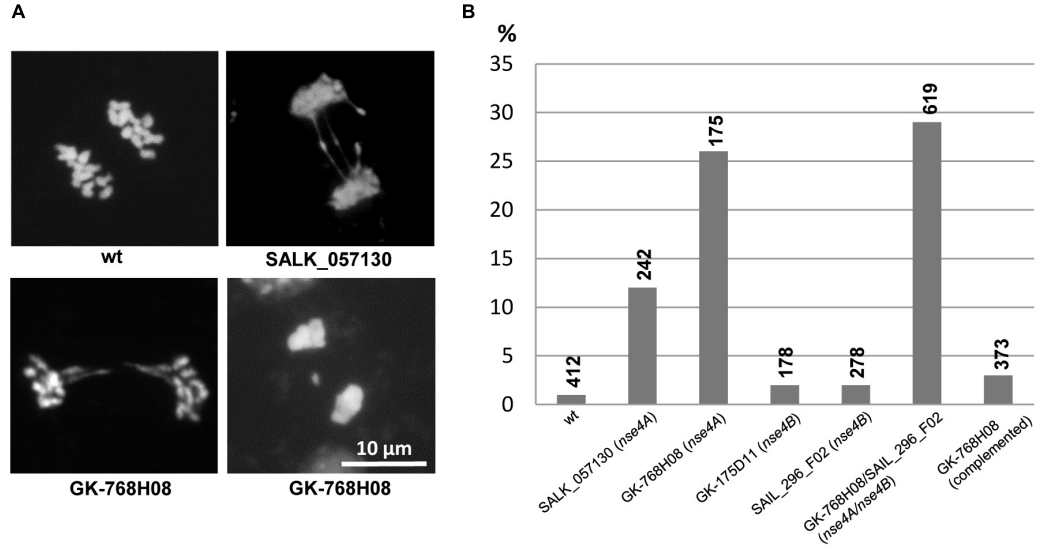

FIGURE 5 | Mitotic defects (anaphase bridges, laggards) in somatic flower bud nuclei of the *A. thaliana nse4* mutants **(A)**. The diagram **(B)** indicates the frequency (%) of abnormalities in the mutants compared to wild-type. The percentage of abnormalities is clearly increased in the *nse4A* mutants SALK_057130 and GK-768H08, as well as in the homozygous double mutant GK-768H08/SAIL_296_F02 representing both *nse4A* and *nse4B* mutations, respectively. The complementation of the mutation in GK-768H08 clearly decreases the number of abnormalities indicating that they are induced by the dysfunction of the Nse4A gene. The numbers of cells analyzed are indicated above the diagram bars.

genome duplication in some angiosperms, in particular such with small genomes, seems to be recurrent (Schubert and Vu, 2016). This mediates increased fitness that, however, erodes over time, thus favoring new polyploidization events (Chapman et al., 2006; Innan and Kondrashov, 2010).

The *A. thaliana* genome is a product of a large segment or an entire genome duplication event, which occurred during the early evolution of this species. A comparative sequence analysis against tomato suggests that a first duplication occurred ∼112 million years ago to form a tetraploid (Ku et al., 2000). Altogether, three different duplication events seem to have occurred (Blanc et al., 2003; Bowers et al., 2003). The estimated gene duplication frequency in *A. thaliana* varies from 47% (Blanc and Wolfe, 2004) to 63% (Ambrosino et al., 2016) depending on the methods and parameters used for evaluation.

We confirmed that *A. thaliana* encodes two NSE4 δ-kleisin variants homologous to known NSE4 proteins in other organisms. Both variants show a high and moderate amino acid sequence similarity to plant and non-plant organisms, respectively, and contain a conserved C-terminal domain and a less conserved SMC6 binding motif at its N-terminus (**Supplementary Figure S1**). Our screening of *Nse4* homologs in other plant species revealed different *Nse4* gene copy numbers, which varied from one in *Eucalyptus grandis* and *Cucumis sativus* up to three copies in *Oryza sativa*. The most other species contain two copies.

Generally, it is not advantageous for species to carry identical functional duplicated genes. Functional and expression divergence are regarded as important mechanisms for the retention of duplicated genes (Semon and Wolfe, 2007). This divergence by mutations results in either pseudogenization (no function anymore), subfunctionalization (partial change of the original function, e.g., tissue specificity) or neofunctionalization (adoption of a new function) (Innan and Kondrashov, 2010; Magadum et al., 2013). The major forces to produce pseudogenes free of function are mutations and deletions, if the gene is not under any selection (Lynch and Conery, 2000). Subfunctionalization appears when the duplicated daughter genes differentiate in some aspects of their functions and adopt a part of the functions of their parental gene (Force et al., 1999). Neofunctionalization leads to evolutionary novel gene functions based on a chance event (mutation) in one of the duplicated genes (Rastogi and Liberles, 2005).

We assume that the two *A. thaliana Nse4* genes are the products of a gene duplication and a subsequently subfunctionalization event (Force et al., 1999). They display a similar sequence and gene structure, but different expression profiles based on our quantitative real-time PCR and *in silico* analyses. While *Nse4A* is expressed in different tissues and developmental stages, *Nse4B* is, in agreement with the findings of Watanabe et al. (2009) almost undetectable in seedlings, rosette leaves, and immature floral buds. Its expression is limited to inflorescence, embryo and endosperm tissues indicating an altered function of NSE4B during seed development, which apparently can be substituted, at least in part, by other cellular components in *nse4B* mutants.

The results suggest that *Nse4A* and *Nse4B* became specialized during evolution, possibly based on a process named duplication-degeneration-complementation. This process comprises complementary degenerative mutations in different regulatory

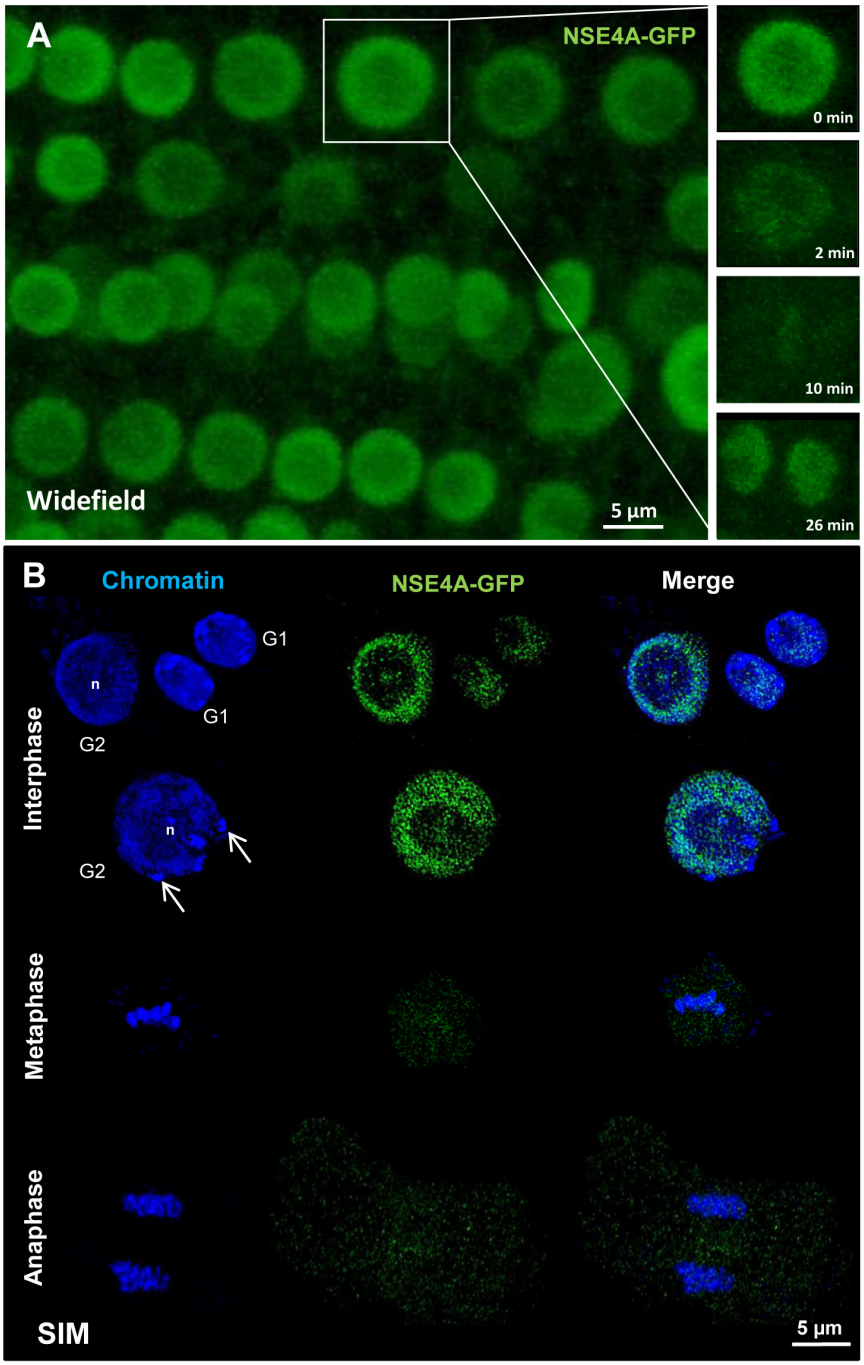

FIGURE 6 | The localization of NSE4A in root meristem cells. **(A)** Global view of a living *A. thaliana* root meristem expressing a genomic *NseA*::GFP construct under the control of the endogenous *Nse4A* promoter. The cell undergoing mitosis (in the rectangle) shows that the nuclear NSE4A-GFP signals are present in interphase (0 min), disappear from the chromosomes during metaphase (2–10 min) and are recovered in telophase at chromatin (26 min). During metaphase a slight cytoplasm labeling is visible. **(B)** The ultrastructural analysis by super-resolution microscopy (SIM) confirms the presence of NSE4A within euchromatin, and indicates its absence from the nucleolus (n) and heterochromatin (chromocenters, arrows) in root meristem G1 and G2 nuclei. During meta- and anaphase NSE4A mainly disappears from the chromosomes, but stays slightly present within the cytoplasm. In young daughter nuclei (G1 phase) NSA4A becomes recovered. The localization of NSE4A-GFP expressed by pnse4A::gNse4A::GFP transgenic *A. thaliana* plants was detected by anti-GFP antibodies in fixed roots.

elements of duplicated genes which can facilitate the preservation of both duplicates. Thus, the process provokes that degenerative mutations in regulatory elements can increase the probability of duplicate gene preservation, and that the ancestral gene function is rather portioned out to the daughter genes, instead of developing new functions (Force et al., 1999, 2005; Feder,

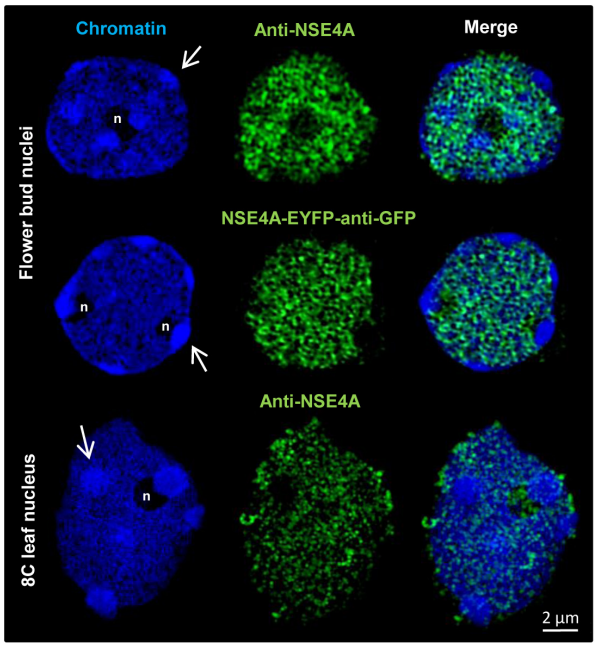

FIGURE 7 | The distribution of NSE4A in differentiated somatic flower bud and 8C leaf interphase nuclei analyzed by 3D-SIM. In agreement, both NSE4A antibodies (anti-NSE4A) and NSE4A-EYFP signals detected by anti-GFP antibodies indicate that NSE4A is distributed within euchromatin, but absent from heterochromatin (DAPI-intense chromocenters, arrows). The NSE4A labeling visible in the merged image of the 8C nucleolus (maximum intensity projection) originates from optical sections outside of the nucleolus.

2007). Based on such a process *Nse4A* may have maintained its multiple functions in the various tissues like the ancestral gene before duplication. Instead, *Nse4B* achieved specialized functions during seed development as a paralog of *Nse4A*.

Interestingly, in other plant and non-plant organisms, the expression patterns differ also between the two *Nse4* variants suggesting a gene subfunctionalization process. In *Z. mays*, two *Nse4* homologs exist. One of them is highly expressed across different tissues, whereas its paralog is expressed in seed tissues and only weakly or not at all in other tissues[15].

The finding that NSE4A and NSE4B contain specific degradation motifs, and SUMOylation sites in addition to the common ones suggests, that the amount of both proteins in different tissues of *A. thaliana* might be differentially regulated not only at the level of transcription, but also at the protein level. The presence of some specific SUMOylation sites in both proteins might suggest their different regulation during the cell cycle and development, since SUMOylation plays an important role in these processes (Park et al., 2011).

The human genome encodes also two *Nse4* gene variants which are ∼50% identical depending on the isoform analyzed[16]. Also in human one *Nse4* gene is expressed in different somatic tissues, whereas the second one is expressed exclusively in generative tissues (Båvner et al., 2005; Taylor et al., 2008). NSE1, NSE3, and NSE4 can form a sub-complex associated to the SMC5–SMC6 head domain binding sites in yeast (Sergeant et al., 2005; Pebernard et al., 2008; Hudson et al., 2011; Kozakova et al., 2015). Thus, the finding of Li et al. (2017) that NSE1 and NSE3 of *A. thaliana* are required for early embryo and seedling development, confirms our observation that also NSE4 is expressed in these tissues.

We conclude that *A. thaliana* comprises two conserved *Nse4* genes, which may have undergone subfunctionalization and can be regarded as functional paralogs.

NSE4 Acts in Meristematic and Differentiated Interphase Nuclei

In interphase nuclei, SMC complexes organize chromatin into a higher order and are responsible for the dynamics of chromatin. They regulate replication, segregation, repair, and transcription (Carter and Sjögren, 2012). The composition of the *A. thaliana* SMC5/6 complex (**Figure 1**) was predicted based on data available for yeast and animals. Our *in silico* generated protein-protein interaction network (**Supplementary Figure S8**) confirmed this prediction. In a recent publication of Diaz et al. (2019) interactions of both NSE4A and NSE4B with NSE3 and SMC5 were confirmed experimentally. However, the interactions of NSE4A and NSE4B with SMC6A, SMC6B, and NSE1 could not be detected. The similar composition and structure of the SMC5/6 complex compared to cohesin and condensin and the ability to bind to DNA (Alt et al., 2017) suggests that all SMC complexes may share a similar topological distribution in interphase chromatin. This idea is supported by the observation that SMC5/6 binds to DNA also via the kleisin-kite subcomplex NSE1-NSE3-NSE4 (Zabrady et al., 2016), similar as the condensin binding to DNA via the kleisin-hawk subcomplex (Kschonsak et al., 2017). Using the protein-protein interaction database STRING, we can also predict interactions of the SMC5/6 complex components with cohesin and condensin proteins (**Supplementary Figure S8**).

Interestingly, in *Drosophila* SMC5/6 is enriched in heterochromatin and required to prevent abnormal homologous recombination repair (Chiolo et al., 2011). Instead, we found *A. thaliana* NSE4 distributed exclusively within the euchromatin of differentiated and meristematic interphase nuclei, similar as described for components of the *A. thaliana* cohesin and condensin complex (Schubert et al., 2013). This suggests a similar role of these proteins in interphase. Interestingly, also transiently expressed *A. thaliana* NSE1 and NSE3 (components of the NSE1-NSE3-NSE4 sub-complex) proteins were shown to be present in tobacco leave nuclei (Li et al., 2017).

Our finding that NSE4 localized in relaxed "open" euchromatin known to be transcriptionally active (Li et al., 2007) and not in "closed" highly condensed heterochromatin suggest a role of these proteins in transcriptional regulation. This idea is supported by the observations that human NSE4 is present in interphase chromatin but absent from nucleoli (Taylor et al., 2001), and that it is acting as a transcriptional suppressor (Båvner et al., 2005). Based on Hi-C investigations

[15]https://www.maizegdb.org/gene_center/gene/GRMZM2G026802
[16]https://www.uniprot.org/uniprot

Lieberman-Aiden et al. (2009) suggested the organization of human interphase chromatin in open and closed regions. SMC complexes may be involved in the control of the extrusion or drawing back of transcriptional loops.

RNA polymerase II molecules, similar as SMC proteins, are exclusively distributed within the euchromatin of interphase nuclei. SMCs may contribute to transfer chromatin into a transcriptional active form ("open" euchromatin), to be accessible for RNA polymerase II performing transcription (Schubert, 2014; Schubert and Weisshart, 2015).

While *A. thaliana* NSE4 was present in interphase nuclei, it mainly disappeared from the chromosomes during mitosis. In non-plant organisms, the localization of SMC5/6 is contradictory. Similar as *A. thaliana* NSE4, human SMC5 and SMC6 are present in interphase nuclei, dissociate from chromosomes at mitosis and then, co-localizes again with chromatin at the G1 phase. In addition, a cytoplasm staining was detectable (Taylor et al., 2001; Gallego-Paez et al., 2014; Verver et al., 2014). In contrast, mouse SMC6 co-localized with centromeric heterochromatin during interphase as well as in mitosis, and with the chromatid axes of somatic metaphase chromosomes (Gomez et al., 2013). In budding yeast SMC6, NSE1, SMC5, and NSE4 all interact with the centromeric regions in G2/M phase-arrested cells (Lindroos et al., 2006). In fission yeast SMC5/6 complexes combine recombination repair with kinetochore protein regulation (Yong-Gonzales et al., 2012), and NSE4 is required for the metaphase to anaphase transition (Hu et al., 2005). These observations indicate a role of SMC5/6 in the maintenance of centromere and higher order metaphase chromosome structure in these organisms.

Similar as described for *A. thaliana nse1* and *nse3* (Li et al., 2017) we found mitotic defects (anaphase bridges, chromosome fragmentation, micronuclei formation) in our *nse4* mutants. Somatic anaphase bridges and micronuclei were also documented in human and yeast SMC5/6 subunit depleted cells (Pebernard et al., 2004; Bermúdez-López et al., 2010; Gallego-Paez et al., 2014). Importantly, micronuclei and chromatin phenotypes are associated with *nse3* mutations in human LICS syndrome cells, exhibiting a reduced level of SMC5/6 complexes (van der Crabben et al., 2016). SMC5/6 is essential in DNA replication by preventing the formation of supercoiled DNA and/or sister chromatid intertwining (Jeppsson et al., 2014a; Verver et al., 2016; Diaz and Pecinka, 2018) which may cause anaphase bridges and chromosome missegregation. These mitotic defects may originate from disturbed SMC5/6 complex functions in G2 and prophase. Although we document the absence of NSE4A from mitotic chromosomes, it seems that the *A. thaliana* SMC5/6 complex is involved in the topological organization of chromatin during mitotic chromosome condensation and decondensation. The mitotic defects in our *nse4A* mutants might be explained by an incorrect SMC5/6 ring formation which is essential for its proper function. Thus, the lack or truncation of NSE4 may result in an impaired catalytic and/or topological SMC5/6 complex function.

The catalytic activity of SMC5/6 is provided by the E3 SUMO-protein ligase NSE2 (Fernandez-Capetillo, 2016), and is essential to globally facilitate the resolution of intermediates during homologous sister chromatid recombination (Bermúdez-López et al., 2010; Chavez et al., 2010), which unresolved may also cause anaphase bridges (Chan et al., 2018).

Mitotic defects may also be induced by an impaired topological function of SMC5/6. Similar as the other SMC complexes, SMC5/6 is an ATP-dependent intermolecular DNA linker (Kanno et al., 2015). Hence, it is not astonishing that the inhibition of SMC5/6 has also been linked to sister chromatid cohesion defects in *Arabidopsis*, chicken and human cells (Watanabe et al., 2009; Stephan et al., 2011; Gallego-Paez et al., 2014).

The idea that SMC5/6 is involved in organizing chromatin topology is also supported by the finding that human SMC5/6 is required for regulating topoisomerase IIα and condensin localization on replicated chromatids in cells during mitosis, thus ensuring correct chromosome morphology and segregation (Gallego-Paez et al., 2014). By introducing DSBs topoisomerase II resolves DNA topological constraints and decatenates dsDNA to reduce supercoiling (Nitiss, 2009).

We found a slight *A. thaliana* NSE4A labeling within the cytoplasm during meta- and anaphase. Mitotically released SMC5/6 complexes might be engaged in a NSE2 mediated signaling pathway in the cytoplasm to regulate the mitotic cell cycle in plant and non-plant organisms (Huang et al., 2009; Ishida et al., 2009; Park et al., 2011; Mukhopadhyay and Dasso, 2017). It has also been reported that yeast SMC5 can bind and stabilize microtubules to realize proper spindle structures and mitotic chromosome segregation (Laflamme et al., 2014).

We applied bleomycin to induce DNA DSBs and found that both *nse4A* and *nse4B* mutations cause a reduced DNA repair efficiency compared to wild-type. In contrast, although Diaz et al. (2019) report an effect of NSE4A on somatic DNA damage repair, they did not prove an influence of bleomycin treatment, possibly due to the significantly lower concentration applied. We conclude, that the presence of *A. thaliana* NSE4A in euchromatin and the disturbance of mitotic divisions by NSE4 mutations indicate an involvement of this SMC5/6 complex component in interphase chromatin organization of differentiated and cycling somatic nuclei. Thus, NSE4 seems to be important for transcriptional regulation, as well as for correct DNA repair and replication by preventing chromatin supercoiling and resolving sister chromatid intertwining to realize correct mitosis.

NSE4 Acts During Meiosis

The mutants of both *Nse4A* and *Nse4B* display reduced silique length, pollen and seed number. This fertility reduction seems to be related to the observed meiotic abnormalities, such as anaphase bridges, lagging chromosomes, chromosome fragmentation and micronuclei formation. Previously, a decreased seed set has also been observed in other *A. thaliana* SMC5/6 subunit mutants, such as *smc6B* (Watanabe et al., 2009), *nse1*, *nse3* (Li et al., 2017), and *nse2* (Ishida et al., 2012).

Similar abnormalities in meiosis as found in mitosis may be based on similar disturbed molecular mechanisms. Somatic anaphase bridges may originate from unresolved sister chromatid intertwining, whereas bridges between bivalents can also be caused by aberrant recombination intermediates between

homologous chromosomes. as found in yeast (Copsey et al., 2013; Xaver et al., 2013). DSBs induce the activation of the SMC5/6 complex by auto-SUMOylation, thus activating the yeast SGS1-TOP3-RMI (STR) complex. STR is engaged in a proper DSB repair and crossover pathway during homologous recombination in somatic cells (Bermudez-Lopez et al., 2016; Bermúdez-López and Aragon, 2017). A critical role for STR was also demonstrated in meiosis of yeast (Jessop et al., 2006; Oh et al., 2007). In *A. thaliana*, a similar mechanism might exist, as suggested by the presence of the yeast STR complex ortholog AtRTR (RECQ4A-TOP3α-RMI). The RTR complex is responsible for genome stability and the dissolution of recombination intermediates in meiosis (Knoll et al., 2014). The involvement of SMC5/6 in preventing aberrant meiotic recombination intermediates was also found in non-plant organisms such as yeast (Farmer et al., 2011) and worm (Hong et al., 2016).

We describe that *A. thaliana* NSE4A does not influence the number of chiasmata. Also data from yeast (Farmer et al., 2011; Lilienthal et al., 2013) and worm (Bickel et al., 2010) indicate that SMC5/6 functions during joint-molecule resolution without influencing crossover formation, suggesting that SMC5/6 is primarily involved in resolving the intermediates of sister chromatid recombination rather than of inter-homolog recombination. On the other hand, a linkage between SMC5/6 and crossover formation cannot be excluded, because in rye the colocalization of human enhancer of invasion-10 (HEI10) and *A. thaliana* NSE4A homologs has been proven (Hesse et al., 2019). HEI10 is a member of the ZMM (ZIP1/ZIP2/ZIP3/ZIP4, MSH4/MSH5, and MER3) protein family essential for meiotic recombination in different eukaryotes (Toby et al., 2003; Whitby, 2005; Osman et al., 2011; Chelysheva et al., 2012; Wang et al., 2012).

The observed meiotic anaphase bridges and the formation of chromosome fragments may be caused not only by a disturbed recombination intermediate resolution. As observed in our *nse4A* mutant, rod bivalents may be extensively stretched. Such a chromatin elongation may also be due to impaired chromatin condensation. Condensin I and II are essential factors involved in correct chromatin condensation and chromosome segregation during mitosis and meiosis. They localize at the metaphase chromatid axes and thus, form a dynamic chromosome scaffold (Maeshima and Laemmli, 2003; Chan et al., 2004; Cuylen and Haering, 2011; Houlard et al., 2015; Kinoshita and Hirano, 2017; Kakui and Uhlmann, 2018; Paul et al., 2018).

Several publications indicate that there is a functional relationship between condensin and SMC5/6. In worms inter-homolog bridges were described in *smc5* mutants inducing an irregular condensin distribution along bivalents, as well as chromosome condensation defects (Hong et al., 2016). Also in mouse oocytes SMC5/6 was shown to assist condensin functions during meiosis I (Houlard et al., 2015; Hwang et al., 2017) and in embryonic stem cells during mitosis (Pryzhkova and Jordan, 2016). Furthermore, in human RPE-1 cells the RNAi-mediated depletion of SMC5 and SMC6 resulted in defective axial localization of condensin in mitosis (Gallego-Paez et al., 2014).

In non-plant organisms, such as worm, mouse and human (Taylor et al., 2001; Bickel et al., 2010; Gomez et al., 2013; Verver et al., 2013, 2014) SMC5/6 subunits were observed at the synaptonemal complex. We found a chromatin-specific localization of *A. thaliana* NSE4A in premeiotic G2, in prophase I, II and in tetrad cells. At prophase I of rye (Hesse et al., 2019), *A. thaliana* and *B. rapa*, NSE4A creates line-like structures colocalizing to ZYP1, a central element of the synaptonemal complex. This suggests that NSE4 might also be involved in the synaptonemal complex formation of plants. Thus, impaired NSE4 in the *nse4* mutants could be another reason for the observed meiotic defects and reduced fertility.

Our data indicate a role of plant NSE4A in proper meiotic chromosome segregation via realizing correct chromatin condensation, recombination intermediate resolution and synapsis.

DATA AVAILABILITY

Publicly available datasets were analyzed in this study. This data can be found here: https://myhits.isb-sib.ch/cgi-bin/motif_scan.

AUTHOR CONTRIBUTIONS

VS, MZ, UC, and AH conceived the study and designed the experiments. AH and VS contributed equally to supervise the project. MZ, KZ, UC, SH, IL, MM, and VS performed the experiments. AM performed the statistics. VS and MZ wrote the manuscript. All authors read and approved the final manuscript.

FUNDING

This study has been funded by the European Union project Marie-Curie "COMREC" network FP7 ITN-606956.

ACKNOWLEDGMENTS

We thank Jörg Fuchs for flow sorting of nuclei, Katrin Kumke, Oda Weiss, Sylvia Swetik, and Karla Meier for excellent technical assistance, Juan L. Santos (Complutense University of Madrid) for help to evaluate *A. thaliana* bivalent configurations, and Chris Franklin (University of Birmingham) for delivering ZYP1 and ASY1 antibodies. We are grateful to Mariana Diaz and Ales Pecinka (Institute of Experimental Botany, Olomouc) for sending us the *A. thaliana* double mutant, Ingo Schubert and Stefan Heckmann (both IPK Gatersleben) for critical reading of the manuscript.

SUPPLEMENTARY MATERIAL

The Supplementary Material for this article can be found online at: https://www.frontiersin.org/articles/10.3389/fpls.2019.00774/full#supplementary-material

FIGURE S1 | Amino acids sequence alignment between full-length NSE4A and NSE4B. The alignment was performed by the Clustal Omega 2.1 software (https://www.ebi.ac.uk/Tools/msa/clustalo/). *, Identical amino acids; :, similar amino acids; –, missing amino acids. The conserved functional protein domains were predicted using the Motif Scan (https://myhits.isb-sib.ch/cgi-bin/motif_scan) and Eukaryotic Linear Motif (http://elm.eu.org/) resources. The putative SMC6-binding domain and the conserved C-terminal NSE4_C domain are highlighted in turquoise and yellow, respectively. The amino acids of putative degradation regions and SUMOlisation sites are labeled in red and in green, respectively. The amino acids "VKPE" marked in blue are a SUMOlisation site overlapping with the amino acids "KPGAGVKPE" of a putative degradation site. The region used to produce recombinant anti-NSE4A antibodies is underlined. NSE4A and NSE4B share 67.7% sequence identity.

FIGURE S2 | Proof of the NSE4A antibody specificity. **(A)** Western blots showing the correct size (~28 kDa) of the expressed recombinant NSE4A protein. The purified NSE4A proteins (1: 1.4 μg, 2: 1.4 μg, 3: 0.7 μg) were separated on a 10% SDS-PAA gel, stained with Coomassie Blue (1) or electro-transferred and visualized after Western Blot by anti His-Tag antibodies (2), or anti T7 antibodies via anti mouse-POD conjugate by ECL detection (3) (Conrad et al., 1997). **(B)** Competitive ELISA showing the specific NSE4A antibody binding behavior. The binding of antibodies to the solid phase adsorbed antigens was specifically inhibited in a concentration-dependent manner by competition with different concentrations of soluble NSE4A to detect at which concentrations of soluble antigens a strong competition can be achieved. A nearly complete inhibition was observed at 200 nmol. **(C)** The incubation of the anti-NSE4A antibodies with recombinant NSE4A proteins prior immunostaining resulted in the signal reduction in *A. thaliana* 8C leaf interphase nuclei.

FIGURE S3 | Amino acids sequence alignment between NSE4A of *A. thaliana* and two putative NSE4A proteins (XP_009144924 and XP_009147782) of *B. rapa*. The alignment was performed by the Clustal Omega 2.1 software (https://www.ebi.ac.uk/Tools/msa/clustalo/). *, Identical amino acids; :, similar amino acids; –, missing amino acids. The conserved C-terminal NSE4 domain is highlighted in yellow. NSE4A shows 77.7 and 80.1% identity to XP_009144924 and XP_009147782, respectively.

FIGURE S4 | Phylogenetic relationships of the *A. thaliana* NSE4A and NSE4B proteins. **(A)** Percentage of plant protein identities compared to *A. thaliana* NSE4A. **(B)** The phylogenic NSE4 tree was reconstructed based on full-length protein sequences of known putative NSE4 orthologs of plants available at NCBI https://www.ncbi.nlm.nih.gov/. *Physcomitrella* was defined as outgroup. Eudicot-derived sequences are given in blue, monocots in red. Numbers at nodes provide Bayesian posterior probabilities indicating clade support. The scale bar represents the average number of amino acid substitutions per site.

FIGURE S5 | *In silico* analysis of the relative *in silico* expression level of the *Nse4A* and *Nse4B* genes during plant development compared to other SMC5/6 subunit genes (genevestigator.com). Stages 1–3 indicate young seedlings and rosettes; 4–6 developed rosettes, bolting and young flowers; 7–9 mature flowers, siliques, and seed stages.

FIGURE S6 | *In silico* analysis of the relative expression level of *Nse4A* (blue) and *Nse4B* (red) in ten anatomical parts from 431 individual sequencing samples of *A. thaliana* (Col-0; AT_mRNASeq_ARABI_GL-0 databases https://genevestigator.com/). Standard deviation is indicated.

FIGURE S7 | Relative expression of *Nse4A* in different *A. thaliana* tissues compared to the reference genes *Pp2A* **(A)** and *Rhip1* **(B)**. The experiments were performed by quantitative real-time PCR. Three technical and biological replicates were realized. Standard deviation is indicated.

FIGURE S8 | Both *A. thaliana* NSE4 proteins interact potentially with other SMC5/6 components **(A)**, as well as with cohesin and condensin complex subunits **(B)**. The protein-protein interaction network was generated based on a STRING program (http://string-db.org/) analysis at scores >0.95 and >0.70, respectively. The black lines in between the proteins indicate the supporting evidence from experimental data available from different species. Interactions confirmed experimentally for *A. thaliana* by Diaz et al. (2019) are indicated by red lines.

FIGURE S9 | RT-PCR-based confirmation of the NSE4A truncation in the T-DNA mutant line GK-768H08. **(A)** Schemata of the *nse4A* gene structure and length of PCR products in wt and the mutant. **(B)** Electrophoresis indicates the absence of the full-length Nse4A transcript in line GK-768H08 compared to wt.

FIGURE S10 | *nse4* mutations result in reduced fertility (% pollen per anther). Only the SALK_057130 and SAIL_296_F02 T-DNA insertion lines do not show a significantly decreased fertility compared to wild-type (wt). In the complemented line GK-768H08 the complete wild-type fertility is recovered. The numbers of evaluated pollen grains are indicated above the diagram bars. Standard deviation is indicated.

FIGURE S11 | DNA damage response of the *nse4* mutants compared to wild-type (Col-0) after bleomycin application at different concentrations (μg/ml) to induce DSBs. **(A)** The increasing bleomycin concentration clearly impairs the plantlet growth in liquid medium. **(B)** The bleomycin treatment (here shown, e.g., 0.5 μg/ml; right) also reduces the root growth of the plantlets on agar plates in comparison to the untreated control (left), as indicated here on 14-day-old plantlets. **(C)** Diagrams C_1–C_4 show the root development on agar plates of Col-0 compared to the mutants at different bleomycin concentrations. All mutants show a significantly decreased root length growth relative to Col-0 according to a two-way ANOVA. Diagram C_5 demonstrates the negative influence of the increasing bleomycin concentration on the root development. Diagram C_6 demonstrates that compared to Col-0 all mutants are significantly stronger negatively influenced at all bleomycin concentrations (ANOVA: $P < 0.05$). Standard errors of mean are indicated in diagrams C_1–C_5.

FIGURE S12 | No abnormalities during prophase I **(A)**, but micronuclei appear in prophase II and tetrads **(B)** of the *nse4A* mutant GK-768H08 compared to wt. The micronuclei (arrows) may originate from chromatin bridges and fragment formation during metaphase I, anaphase I and II (see **Figure 3**). Chromatin was stained with DAPI.

FIGURE S13 | Meiotic abnormalities (% fragments, anaphase bridges) in *nse4* mutants during different meiotic stages compared to wt. The complementation in line GK-768H08 partially recovers the normal meiotic wt behavior. The numbers of evaluated meiocytes are indicated above the diagram bars.

FIGURE S14 | Chromosomal abnormalities during metaphase I in the *nse4A* mutant GK-768H08 compared to wt. **(A)** Karyotype of *A. thaliana* indicating the chromosomal positions of 5S rDNA (red) and 45S rDNA (green). **(B)** The chromosomal distribution of the 5S and 45S rDNA repeats allows the identification of the different *A. thaliana* bivalents. Due to stretched rod bivalents, chromatin fragments (arrows) occur at chromosomes 4 **(C)** and 2 **(D)**.

FIGURE S15 | The *nse4A* mutant GK-768H08 shows a wt-like localization of the central synaptonmal complex protein ZYP1 at pachytene. Chromatin was counterstained with DAPI (blue).

TABLE S1 | Primers used to identify the T-DNA insertion alleles.

TABLE S2 | Sequences of the left border junctions of the T-DNA insertion lines. The red letters represent the sequence derived from the T-DNA, and their position in each of the sequences reflects the orientation of the inserted T-DNA.

TABLE S3 | Quantitative real-time RT-PCR primers used to amplify transcripts.

TABLE S4 | Primers used to clone the *Nse4A* genes, to produce clones for recombinant protein expression, and for the transcript analyses of the mutants and transgenic lines.

TABLE S5 | *Arabidopsis thaliana* NSE4 protein sequence identities (%) compared to orthologs of non-plant organisms. The matrix was generated by the Clustal Omega 2.1 software.

TABLE S6 | Genes showing high co-expression with Nse4A predicted from 18 different anatomical tissues. The data were obtained from the AT_mRNASeq_ARABI_GL-0 database of https://genevestigator.com. Scores indicate the level of correlation of expression in different anatomical samples. Bold gene names indicate meiosis- or chromatin-related genes.

REFERENCES

Alexander, M. P. (1969). Differential staining of aborted and nonaborted pollen. *Stain Technol.* 44, 117–122. doi: 10.3109/10520296909063335

Alonso, J. M., Stepanova, A. N., Leisse, T. J., Kim, C. J., Chen, H., Shinn, P., et al. (2003). Genome-wide insertional mutagenesis of *Arabidopsis thaliana*. *Science* 301, 653–657. doi: 10.1126/science.1086391

Alt, A., Dang, H. Q., Wells, O. S., Polo, L. M., Smith, M. A., McGregor, G. A., et al. (2017). Specialized interfaces of Smc5/6 control hinge stability and DNA association. *Nat. Commun.* 8:14011. doi: 10.1038/ncomms14011

Ambrosino, L., Bostan, H., di Salle, P., Sangiovanni, M., Vigilante, A., and Chiusano, M. L. (2016). pATsi: Paralogs and Singleton Genes from *Arabidopsis thaliana*. *Evol. Bioinform. Online* 12, 1–7. doi: 10.4137/EBO.S32536

Armstrong, S., and Osman, K. (2013). Immunolocalization of meiotic proteins in *Arabidopsis thaliana*: method 2. *Methods Mol. Biol.* 990, 103–107. doi: 10.1007/978-1-62703-333-6_10

Båvner, A., Matthews, J., Sanyal, S., Gustafsson, J. A., and Treuter, E. (2005). EID3 is a novel EID family member and an inhibitor of CBP-dependent co-activation. *Nucleic Acids Res.* 33, 3561–3569. doi: 10.1093/nar/gki667

Bermúdez-López, M., and Aragon, L. (2017). Smc5/6 complex regulates Sgs1 recombination functions. *Curr. Genet.* 63, 381–388. doi: 10.1007/s00294-016-0648-5

Bermúdez-López, M., Ceschia, A., de Piccoli, G., Colomina, N., Pasero, P., Aragon, L., et al. (2010). The Smc5/6 complex is required for dissolution of DNA-mediated sister chromatid linkages. *Nucleic Acids Res.* 38, 6502–6512. doi: 10.1093/nar/gkq546

Bermudez-Lopez, M., Villoria, M. T., Esteras, M., Jarmuz, A., Torres-Rosell, J., Clemente-Blanco, A., et al. (2016). Sgs1's roles in DNA end resection, HJ dissolution, and crossover suppression require a two-step SUMO regulation dependent on Smc5/6. *Genes Dev.* 30, 1339–1356. doi: 10.1101/gad.278275.116

Bickel, J. S., Chen, L., Hayward, J., Yeap, S. L., Alkers, A. E., and Chan, R. C. (2010). Structural maintenance of chromosomes (SMC) proteins promote homolog-independent recombination repair in meiosis crucial for germ cell genomic stability. *PLoS Genet.* 6:e1001028. doi: 10.1371/journal.pgen.1001028

Blanc, G., Hokamp, K., and Wolfe, K. H. (2003). A recent polyploidy superimposed on older large-scale duplications in the *Arabidopsis* genome. *Genome Res.* 13, 137–144. doi: 10.1101/gr.751803

Blanc, G., and Wolfe, K. H. (2004). Widespread paleopolyploidy in model plant species inferred from age distributions of duplicate genes. *Plant Cell* 16, 1667–1678. doi: 10.1105/tpc.021345

Bowers, J. E., Chapman, B. A., Rong, J., and Paterson, A. H. (2003). Unravelling angiosperm genome evolution by phylogenetic analysis of chromosomal duplication events. *Nature* 422, 433–438. doi: 10.1038/nature01521

Bradford, M. M. (1976). A rapid and sensitive method for the quantitation of microgram quantities of protein utilizing the principle of protein-dye binding. *Anal. Biochem.* 72, 248–254. doi: 10.1006/abio.1976.9999

Carter, S. D., and Sjögren, C. (2012). The SMC complexes, DNA and chromosome topology: right or knot? *Crit. Rev. Biochem. Mol. Biol.* 47, 1–16. doi: 10.3109/10409238.2011.614593

Chan, R. C., Severson, A. F., and Meyer, B. J. (2004). Condensin restructures chromosomes in preparation for meiotic divisions. *J. Cell Biol.* 167, 613–625. doi: 10.1083/jcb.200408061

Chan, Y. W., Fugger, K., and West, S. C. (2018). Unresolved recombination intermediates lead to ultra-fine anaphase bridges, chromosome breaks and aberrations. *Nat. Cell Biol.* 20, 92–103. doi: 10.1038/s41556-017-0011-1

Chapman, B. A., Bowers, J. E., Feltus, F. A., and Paterson, A. H. (2006). Buffering of crucial functions by paleologous duplicated genes may contribute cyclicality to angiosperm genome duplication. *Proc. Natl. Acad. Sci. U.S.A.* 103, 2730–2735. doi: 10.1073/pnas.0507782103

Chavez, A., George, V., Agrawal, V., and Johnson, F. B. (2010). Sumoylation and the structural maintenance of chromosomes (Smc) 5/6 complex slow senescence through recombination intermediate resolution. *J. Biol. Chem.* 285, 11922–11930. doi: 10.1074/jbc.M109.041277

Chelysheva, L., Vezon, D., Chambon, A., Gendrot, G., Pereira, L., Lemhemdi, A., et al. (2012). The *Arabidopsis* HEI10 is a new ZMM protein related to Zip3. *PLoS Genet.* 8:e1002799. doi: 10.1371/journal.pgen.1002799

Chiolo, I., Minoda, A., Colmenares, S. U., Polyzos, A., Costes, S. V., and Karpen, G. H. (2011). Double-strand breaks in heterochromatin move outside of a dynamic HP1a domain to complete recombinational repair. *Cell* 144, 732–744. doi: 10.1016/j.cell.2011.02.012

Clough, S. J., and Bent, A. F. (1998). Floral dip: a simplified method for *Agrobacterium*-mediated transformation of *Arabidopsis thaliana*. *Plant J.* 16, 735–743. doi: 10.1046/j.1365-313x.1998.00343.x

Coghlan, A., Eichler, E. E., Oliver, S. G., Paterson, A. H., and Stein, L. (2005). Chromosome evolution in eukaryotes: a multi-kingdom perspective. *Trends Genet.* 21, 673–682. doi: 10.1016/j.tig.2005.09.009

Conrad, U., Fiedler, U., Artsaenko, O., and Phillips, J. (1997). "Recombinmant proteins from plantas: production and isolation of clinically useful compounds"," in *Methods in Biotechnology*, eds C. Cunningham and S. Porter (Totowa, NJ: Humana Press), 103–127. doi: 10.1111/j.1467-7652.2010.00523.x

Conrad, U., Plagmann, I., Malchow, S., Sack, M., Floss, D. M., Kruglov, A. A., et al. (2011). ELPylated anti-human TNF therapeutic single-domain antibodies for prevention of lethal septic shock. *Plant Biotechnol. J.* 9, 22–31. doi: 10.1111/j.1467-7652.2010.00523.x

Copsey, A., Tang, S., Jordan, P. W., Blitzblau, H. G., Newcombe, S., Chan, A. C., et al. (2013). Smc5/6 coordinates formation and resolution of joint molecules with chromosome morphology to ensure meiotic divisions. *PLoS Genet.* 9:e1004071. doi: 10.1371/journal.pgen.1004071

Cuylen, S., and Haering, C. H. (2011). Deciphering condensin action during chromosome segregation. *Trends Cell Biol.* 21, 552–559. doi: 10.1016/j.tcb.2011.06.003

Czechowski, T., Stitt, M., Altmann, T., Udvardi, M. K., and Scheible, W. R. (2005). Genome-wide identification and testing of superior reference genes for transcript normalization in *Arabidopsis*. *Plant Physiol.* 139, 5–17. doi: 10.1104/pp.105.063743

De Piccoli, G., Cortes-Ledesma, F., Ira, G., Torres-Rosell, J., Uhle, S., Farmer, S., et al. (2006). Smc5-Smc6 mediate DNA double-strand-break repair by promoting sister-chromatid recombination. *Nat. Cell Biol.* 8, 1032–1034. doi: 10.1038/ncb1466

De Piccoli, G., Torres-Rosell, J., and Aragon, L. (2009). The unnamed complex: what do we know about Smc5-Smc6? *Chromosome Res.* 17, 251–263. doi: 10.1007/s10577-008-9016-8

Diaz, M., and Pecinka, A. (2018). Scaffolding for repair: understanding molecular functions of the SMC5/6 complex. *Genes* 9:E36. doi: 10.3390/genes9010036

Diaz, M., Pecinkova, P., Nowicka, A., Baroux, C., Sakamoto, T., Gandha, P. Y., et al. (2019). SMC5/6 complex subunit NSE4A is involved in DNA damage repair and seed development in *Arabidopsis*. *Plant Cell.* doi: 10.1105/tpc.18.00043 [Epub ahead of print].

Duan, X., Yang, Y., Chen, Y. H., Arenz, J., Rangi, G. K., Zhao, X., et al. (2009). Architecture of the Smc5/6 Complex of *Saccharomyces cerevisiae* reveals a unique interaction between the Nse5-6 subcomplex and the hinge regions of Smc5 and Smc6. *J. Biol. Chem.* 284, 8507–8515. doi: 10.1074/jbc.M809139200

Farmer, S., San-Segundo, P. A., and Aragon, L. (2011). The Smc5-Smc6 complex is required to remove chromosome junctions in meiosis. *PLoS One* 6:e20948. doi: 10.1371/journal.pone.0020948

Feder, M. E. (2007). Evolvability of physiological and biochemical traits: evolutionary mechanisms including and beyond single-nucleotide mutation. *J. Exp. Biol.* 210, 1653–1660. doi: 10.1242/jeb.02725

Fernandez-Capetillo, O. (2016). The (elusive) role of the SMC5/6 complex. *Cell Cycle* 15, 775–776. doi: 10.1080/15384101.2015.1137713

Force, A., Cresko, W. A., Pickett, F. B., Proulx, S. R., Amemiya, C., and Lynch, M. (2005). The origin of subfunctions and modular gene regulation. *Genetics* 170, 433–446. doi: 10.1534/genetics.104.027607

Force, A., Lynch, M., Pickett, F. B., Amores, A., Yan, Y. L., and Postlethwait, J. (1999). Preservation of duplicate genes by complementary, degenerative mutations. *Genetics* 151, 1531–1545.

Fousteri, M. I., and Lehmann, A. R. (2000). A novel SMC protein complex in *Schizosaccharomyces pombe* contains the Rad18 DNA repair protein. *EMBO J.* 19, 1691–1702. doi: 10.1093/emboj/19.7.1691

Gallego-Paez, L. M., Tanaka, H., Bando, M., Takahashi, M., Nozaki, N., Nakato, R., et al. (2014). Smc5/6-mediated regulation of replication progression contributes to chromosome assembly during mitosis in human cells. *Mol. Biol. Cell* 25, 302–317. doi: 10.1091/mbc.E13-01-0020

Gomez, R., Jordan, P. W., Viera, A., Alsheimer, M., Fukuda, T., Jessberger, R., et al. (2013). Dynamic localization of SMC5/6 complex proteins during mammalian

meiosis and mitosis suggests functions in distinct chromosome processes. *J. Cell Sci.* 126, 4239–4252. doi: 10.1242/jcs.130195

Guerineau, M., Kriz, Z., Kozakova, L., Bednarova, K., Janos, P., and Palecek, J. (2012). Analysis of the Nse3/MAGE-binding domain of the Nse4/EID family proteins. *PLoS One* 7:e35813. doi: 10.1371/journal.pone.0035813

Haering, C. H., and Gruber, S. (2016a). SnapShot: SMC Protein Complexes Part I. *Cell* 164, 326–326.e1. doi: 10.1016/j.cell.2015.12.026

Haering, C. H., and Gruber, S. (2016b). SnapShot: SMC Protein Complexes Part II. *Cell* 164:818.e1. doi: 10.1016/j.cell.2016.01.052

Hanin, M., Mengiste, T., Bogucki, A., and Paszkowski, J. (2000). Elevated levels of intrachromosomal homologous recombination in *Arabidopsis* overexpressing the MIM gene. *Plant J.* 24, 183–189. doi: 10.1046/j.1365-313x.2000.00867.x

Hassler, M., Shaltiel, I. A., and Haering, C. H. (2018). Towards a unified model of SMC complex function. *Curr. Biol.* 28, R1266–R1281. doi: 10.1016/j.cub.2018.08.034

Hazbun, T. R., Malmstrom, L., Anderson, S., Graczyk, B. J., Fox, B., Riffle, M., et al. (2003). Assigning function to yeast proteins by integration of technologies. *Mol. Cell* 12, 1353–1365. doi: 10.1016/s1097-2765(03)00476-3

Hesse, S., Zelkowski, M., Mikhailova, E., Keijzer, K., Houben, A., and Schubert, V. (2019). Ultrastructure, and dynamics of synaptonemal complex components during meiotic pairing and synapsis of standard (A) and accessory (B) rye chromosomes. *Front. Plant Sci.* doi: 10.3389/fpls.2019.00773

Higgins, J. D., Armstrong, S. J., Franklin, F. C., and Jones, G. H. (2004). The *Arabidopsis* MutS homolog AtMSH4 functions at an early step in recombination: evidence for two classes of recombination in *Arabidopsis*. *Genes Dev.* 18, 2557–2570. doi: 10.1101/gad.317504

Higgins, J. D., Sanchez-Moran, E., Armstrong, S. J., Jones, G. H., and Franklin, F. C. (2005). The Arabidopsis synaptonemal complex protein ZYP1 is required for chromosome synapsis and normal fidelity of crossing over. *Genes Dev.* 19, 2488–2500. doi: 10.1101/gad.354705

Hirano, T. (2006). At the heart of the chromosome: SMC proteins in action. *Nat. Rev. Mol. Cell Biol.* 7, 311–322. doi: 10.1038/nrm1909

Hong, Y., Sonneville, R., Agostinho, A., Meier, B., Wang, B., Blow, J. J., et al. (2016). The SMC-5/6 complex and the HIM-6 (BLM) helicase synergistically promote meiotic recombination intermediate processing and chromosome maturation during *Caenorhabditis elegans* meiosis. *PLoS Genet.* 12:e1005872. doi: 10.1371/journal.pgen.1005872

Houlard, M., Godwin, J., Metson, J., Lee, J., Hirano, T., and Nasmyth, K. (2015). Condensin confers the longitudinal rigidity of chromosomes. *Nat. Cell Biol.* 17, 771–781. doi: 10.1038/ncb3167

Hu, B., Liao, C., Millson, S. H., Mollapour, M., Prodromou, C., Pearl, L. H., et al. (2005). Qri2/Nse4, a component of the essential Smc5/6 DNA repair complex. *Mol. Microbiol.* 55, 1735–1750. doi: 10.1111/j.1365-2958.2005.04531.x

Huang, L., Yang, S., Zhang, S., Liu, M., Lai, J., Qi, Y., et al. (2009). The *Arabidopsis* SUMO E3 ligase AtMMS21, a homologue of NSE2/MMS21, regulates cell proliferation in the root. *Plant J.* 60, 666–678. doi: 10.1111/j.1365-313X.2009.03992.x

Hudson, J. J. R., Bednarova, K., Kozakova, L., Liao, C. Y., Guerineau, M., Colnaghi, R., et al. (2011). Interactions between the Nse3 and Nse4 components of the SMC5-6 Complex identify evolutionarily conserved interactions between MAGE and EID families. *PLoS One* 6:e17270. doi: 10.1371/journal.pone.0017270

Hurles, M. (2004). Gene duplication: the genomic trade in spare parts. *PLoS Biol.* 2:E206. doi: 10.1371/journal.pbio.0020206

Hwang, G., Sun, F., O'Brien, M., Eppig, J. J., Handel, M. A., and Jordan, P. W. (2017). SMC5/6 is required for the formation of segregation-competent bivalent chromosomes during meiosis I in mouse oocytes. *Development* 144, 1648–1660. doi: 10.1242/dev.145607

Ijdo, J. W., Wells, R. A., Baldini, A., and Reeders, S. T. (1991). Improved telomere detection using a telomere repeat probe (TTAGGG)n generated by PCR. *Nucleic Acids Res.* 19, 4780–4780. doi: 10.1093/nar/19.17.4780

Innan, H., and Kondrashov, F. (2010). The evolution of gene duplications: classifying and distinguishing between models. *Nat. Rev. Genet.* 11, 97–108. doi: 10.1038/nrg2689

Irmisch, A., Ampatzidou, E., Mizuno, K., O'Connell, M. J., and Murray, J. M. (2009). Smc5/6 maintains stalled replication forks in a recombination-competent conformation. *EMBO J.* 28, 144–155. doi: 10.1038/emboj.2008.273

Ishida, T., Fujiwara, S., Miura, K., Stacey, N., Yoshimura, M., Schneider, K., et al. (2009). SUMO E3 ligase HIGH PLOIDY2 regulates endocycle onset and meristem maintenance in *Arabidopsis*. *Plant Cell* 21, 2284–2297. doi: 10.1105/tpc.109.068072

Ishida, T., Yoshimura, M., Miura, K., and Sugimoto, K. (2012). MMS21/HPY2 and SIZ1, two *Arabidopsis* SUMO E3 ligases, have distinct functions in development. *PLoS One* 7:e46897. doi: 10.1371/journal.pone.0046897

Jeppsson, K., Carlborg, K. K., Nakato, R., Berta, D. G., Lilienthal, I., Kanno, T., et al. (2014a). The chromosomal association of the Smc5/6 complex depends on cohesion and predicts the level of sister chromatid entanglement. *PLoS Genet.* 10:e1004680. doi: 10.1371/journal.pgen.1004680

Jeppsson, K., Kanno, T., Shirahige, K., and Sjogren, C. (2014b). The maintenance of chromosome structure: positioning and functioning of SMC complexes. *Nat. Rev. Mol. Cell Biol.* 15, 601–614. doi: 10.1038/nrm3857

Jessop, L., Rockmill, B., Roeder, G. S., and Lichten, M. (2006). Meiotic chromosome synapsis-promoting proteins antagonize the anti-crossover activity of sgs1. *PLoS Genet.* 2:e155. doi: 10.1371/journal.pgen.0020155

Kakui, Y., and Uhlmann, F. (2018). SMC complexes orchestrate the mitotic chromatin interaction landscape. *Curr. Genet.* 64, 335–339. doi: 10.1007/s00294-017-0755-y

Kanno, T., Berta, D. G., and Sjogren, C. (2015). The Smc5/6 Complex Is an ATP-dependent intermolecular DNA linker. *Cell Rep.* 12, 1471–1482. doi: 10.1016/j.celrep.2015.07.048

Kawabe, A., and Nasuda, S. (2005). Structure and genomic organization of centromeric repeats in *Arabidopsis* species. *Mol. Genet. Genomics* 272, 593–602. doi: 10.1007/s00438-004-1081-x

Kegel, A., Betts-Lindroos, H., Kanno, T., Jeppsson, K., Strom, L., Katou, Y., et al. (2011). Chromosome length influences replication-induced topological stress. *Nature* 471, 392–396. doi: 10.1038/nature09791

Kinoshita, K., and Hirano, T. (2017). Dynamic organization of mitotic chromosomes. *Curr. Opin. Cell Biol.* 46, 46–53. doi: 10.1016/j.ceb.2017.01.006

Knoll, A., Schröpfer, S., and Puchta, H. (2014). The RTR complex as caretaker of genome stability and its unique meiotic function in plants. *Front. Plant Sci.* 5:33. doi: 10.3389/fpls.2014.00033

Kozakova, L., Vondrova, L., Stejskal, K., Charalabous, P., Kolesar, P., Lehmann, A. R., et al. (2015). The melanoma-associated antigen 1 (MAGEA1) protein stimulates the E3 ubiquitin-ligase activity of TRIM31 within a TRIM31-MAGEA1-NSE4 complex. *Cell Cycle* 14, 920–930. doi: 10.1080/15384101.2014.1000112

Kschonsak, M., Merkel, F., Bisht, S., Metz, J., Rybin, V., Hassler, M., et al. (2017). Structural basis for a safety-belt mechanism that anchors condensin to chromosomes. *Cell* 171, 588–600.e24. doi: 10.1016/j.cell.2017.09.008

Ku, H. M., Vision, T., Liu, J., and Tanksley, S. D. (2000). Comparing sequenced segments of the tomato and *Arabidopsis* genomes: large-scale duplication followed by selective gene loss creates a network of synteny. *Proc. Natl. Acad. Sci. U.S.A.* 97, 9121–9126. doi: 10.1073/pnas.160271297

Laflamme, G., Tremblay-Boudreault, T., Roy, M. A., Andersen, P., Bonneil, E., Atchia, K., et al. (2014). Structural maintenance of chromosome (SMC) proteins link microtubule stability to genome integrity. *J. Biol. Chem.* 289, 27418–27431. doi: 10.1074/jbc.M114.569608

Lehmann, A. R. (2005). The role of SMC proteins in the responses to DNA damage. *DNA Repair* 4, 309–314. doi: 10.1016/j.dnarep.2004.07.009

Li, B., Carey, M., and Workman, J. L. (2007). The role of chromatin during transcription. *Cell* 128, 707–719. doi: 10.1016/j.cell.2007.01.015

Li, G., Zou, W., Jian, L., Qian, J., Deng, Y., and Zhao, J. (2017). Non-SMC elements 1 and 3 are required for early embryo and seedling development in *Arabidopsis*. *J. Exp. Bot.* 68, 1039–1054. doi: 10.1093/jxb/erx016

Lieberman-Aiden, E., van Berkum, N. L., Williams, L., Imakaev, M., Ragoczy, T., Telling, A., et al. (2009). Comprehensive mapping of long-range interactions reveals folding principles of the human genome. *Science* 326, 289–293. doi: 10.1126/science.1181369

Lilienthal, I., Kanno, T., and Sjögren, C. (2013). Inhibition of the Smc5/6 complex during meiosis perturbs joint molecule formation and resolution without significantly changing crossover or non-crossover levels. *PLoS Genet.* 9:e1003898. doi: 10.1371/journal.pgen.1003898

Lindroos, H. B., Ström, L., Itoh, T., Katou, Y., Shirahige, K., and Sjögren, C. (2006). Chromosomal association of the Smc5/6 complex reveals that it functions in

differently regulated pathways. *Mol. Cell* 22, 755–767. doi: 10.1016/j.molcel.2006.05.014

Livak, K. J., and Schmittgen, T. D. (2001). Analysis of relative gene expression data using real-time quantitative PCR and the 2DDCT method. *Methods* 25, 402–408. doi: 10.1006/meth.2001.1262

Lynch, M., and Conery, J. S. (2000). The evolutionary fate and consequences of duplicate genes. *Science* 290, 1151–1155. doi: 10.1126/science.290.5494.1151

Maeshima, K., and Laemmli, U. K. (2003). A two-step scaffolding model for mitotic chromosome assembly. *Dev. Cell* 4, 467–480. doi: 10.1016/S1534-5807(03)00092-3

Magadum, S., Banerjee, U., Murugan, P., Gangapur, D., and Ravikesavan, R. (2013). Gene duplication as a major force in evolution. *J. Genet.* 92, 155–161. doi: 10.1007/s12041-013-0212-8

Martinez-Zapater, J. M., Estelle, M. A., and Somerville, C. R. (1986). A highly repeated DNA sequence in *Arabidopsis thaliana*. *Mol. Gen. Genet.* 204, 417–423. doi: 10.1007/bf00331018

Mengiste, T., Revenkova, E., Bechtold, N., and Paszkowski, J. (1999). An SMC-like protein is required for efficient homologous recombination in *Arabidopsis*. *EMBO J.* 18, 4505–4512. doi: 10.1093/emboj/18.16.4505

Mukhopadhyay, D., and Dasso, M. (2017). The SUMO pathway in mitosis. *Adv. Exp. Med. Biol.* 963, 171–184. doi: 10.1007/978-3-319-50044-7_10

Nakamura, S., Mano, S., Tanaka, Y., Ohnishi, M., Nakamori, C., Araki, M., et al. (2010). Gateway binary vectors with the bialaphos resistance gene, bar, as a selection marker for plant transformation. *Biosci. Biotechnol. Biochem.* 74, 1315–1319. doi: 10.1271/bbb.100184

Nasmyth, K., and Haering, C. H. (2005). The structure and function of SMC and kleisin complexes. *Annu. Rev. Biochem.* 74, 595–648. doi: 10.1146/annurev.biochem.74.082803.133219

Nitiss, J. L. (2009). DNA topoisomerase II and its growing repertoire of biological functions. *Nat. Rev. Cancer* 9, 327–337. doi: 10.1038/nrc2608

Oh, S. D., Lao, J. P., Hwang, P. Y., Taylor, A. F., Smith, G. R., and Hunter, N. (2007). BLM ortholog, Sgs1, prevents aberrant crossing-over by suppressing formation of multichromatid joint molecules. *Cell* 130, 259–272. doi: 10.1016/j.cell.2007.05.035

Osman, K., Higgins, J. D., Sanchez-Moran, E., Armstrong, S. J., and Franklin, F. C. (2011). Pathways to meiotic recombination in *Arabidopsis thaliana*. *New Phytol.* 190, 523–544. doi: 10.1111/j.1469-8137.2011.03665.x

Palecek, J., Vidot, S., Feng, M., Doherty, A. J., and Lehmann, A. R. (2006). The Smc5-Smc6 DNA repair complex. bridging of the Smc5-Smc6 heads by the kleisin, Nse4, and non-kleisin subunits. *J. Biol. Chem.* 281, 36952–36959. doi: 10.1074/jbc.M608004200

Palecek, J. J., and Gruber, S. (2015). Kite proteins: a superfamily of SMC/kleisin partners conserved across bacteria, archaea, and eukaryotes. *Structure* 23, 2183–2190. doi: 10.1016/j.str.2015.10.004

Panchy, N., Lehti-Shiu, M., and Shiu, S. H. (2016). Evolution of Gene Duplication in Plants. *Plant Physiol.* 171, 2294–2316. doi: 10.1104/pp.16.00523

Park, H. J., Kim, W. Y., Park, H. C., Lee, S. Y., Bohnert, H. J., and Yun, D. J. (2011). SUMO and SUMOylation in plants. *Mol. Cells* 32, 305–316. doi: 10.1007/s10059-011-0122-7

Paul, M. R., Hochwagen, A., and Ercan, S. (2018). Condensin action and compaction. *Curr. Genet.* 65, 407–415. doi: 10.1007/s00294-018-0899-4

Pebernard, S., McDonald, W. H., Pavlova, Y., Yates, J. R. III, and Boddy, M. N. (2004). Nse1, Nse2, and a novel subunit of the Smc5-Smc6 complex, Nse3, play a crucial role in meiosis. *Mol. Biol. Cell* 15, 4866–4876. doi: 10.1091/mbc.e04-05-0436

Pebernard, S., Perry, J. J., Tainer, J. A., and Boddy, M. N. (2008). Nse1 RING-like domain supports functions of the Smc5-Smc6 holocomplex in genome stability. *Mol. Biol. Cell* 19, 4099–4109. doi: 10.1091/mbc.E08-02-0226

Potts, P. R., Porteus, M. H., and Yu, H. T. (2006). Human SMC5/6 complex promotes sister chromatid homologous recombination by recruiting the SMC1/3 cohesin complex to double-strand breaks. *EMBO J.* 25, 3377–3388. doi: 10.1038/sj.emboj.7601218

Potts, P. R., and Yu, H. (2007). The SMC5/6 complex maintains telomere length in ALT cancer cells through SUMOylation of telomere-binding proteins. *Nat. Struct. Mol. Biol.* 14, 581–590. doi: 10.1038/nsmb1259

Pryzhkova, M. V., and Jordan, P. W. (2016). Conditional mutation of Smc5 in mouse embryonic stem cells perturbs condensin localization and mitotic progression. *J. Cell Sci.* 129, 1619–1634. doi: 10.1242/jcs.179036

Räschle, M., Smeenk, G., Hansen, R. K., Temu, T., Oka, Y., Hein, M. Y., et al. (2015). Proteomics reveals dynamic assembly of repair complexes during bypass of DNA cross-links. *Science* 348:1253671. doi: 10.1126/science.1253671

Rastogi, S., and Liberles, D. A. (2005). Subfunctionalization of duplicated genes as a transition state to neofunctionalization. *BMC Evol. Biol.* 5:28. doi: 10.1186/1471-2148-5-28

Rosso, M. G., Li, Y., Strizhov, N., Reiss, B., Dekker, K., and Weisshaar, B. (2003). An *Arabidopsis thaliana* T-DNA mutagenized population (GABI-Kat) for flanking sequence tag-based reverse genetics. *Plant Mol. Biol.* 53, 247–259. doi: 10.1023/B:PLAN.0000009297.37235.4a

Sánchez-Morán, E., Armstrong, S. J., Santos, J. L., Franklin, F. C., and Jones, G. H. (2001). Chiasma formation in *Arabidopsis thaliana* accession Wassileskija and in two meiotic mutants. *Chromosome Res.* 9, 121–128.

Schubert, I., and Vu, G. T. H. (2016). Genome stability and evolution: attempting a holistic view. *Trends Plant Sci.* 21, 749–757. doi: 10.1016/j.tplants.2016.06.003

Schubert, V. (2009). SMC proteins and their multiple functions in higher plants. *Cytogenet. Genome Res.* 124, 202–214. doi: 10.1159/000218126

Schubert, V. (2014). RNA polymerase II forms transcription networks in rye and *Arabidopsis* nuclei and its amount increases with endopolyploidy. *Cytogenet. Genome Res.* 143, 69–77. doi: 10.1159/000365233

Schubert, V., Lermontova, I., and Schubert, I. (2013). The *Arabidopsis* CAP-D proteins are required for correct chromatin organisation, growth and fertility. *Chromosoma* 122, 517–533. doi: 10.1007/s00412-013-0424-y

Schubert, V., and Weisshart, K. (2015). Abundance and distribution of RNA polymerase II in *Arabidopsis* interphase nuclei. *J. Exp. Bot.* 66, 1687–1698. doi: 10.1093/jxb/erv091

Semon, M., and Wolfe, K. H. (2007). Consequences of genome duplication. *Curr. Opin. Genet. Dev.* 17, 505–512. doi: 10.1016/j.gde.2007.09.007

Sergeant, J., Taylor, E., Palecek, J., Fousteri, M., Andrews, E. A., Sweeney, S., et al. (2005). Composition and architecture of the *Schizosaccharomyces pombe* Rad18 (Smc5-6) complex. *Mol. Cell. Biol.* 25, 172–184. doi: 10.1128/MCB.25.1.172-184.2005

Sessions, A., Burke, E., Presting, G., Aux, G., McElver, J., Patton, D., et al. (2002). A high-throughput *Arabidopsis* reverse genetics system. *Plant Cell* 14, 2985–2994. doi: 10.1105/tpc.004630

Sjögren, C., and Nasmyth, K. (2001). Sister chromatid cohesion is required for postreplicative double-strand break repair in *Saccharomyces cerevisiae*. *Curr. Biol.* 11, 991–995. doi: 10.1016/S0960-9822(01)00271-8

Stephan, A. K., Kliszczak, M., Dodson, H., Cooley, C., and Morrison, C. G. (2011). Roles of vertebrate Smc5 in sister chromatid cohesion and homologous recombinational repair. *Mol. Cell. Biol.* 31, 1369–1381. doi: 10.1128/MCB.00786-10

Taylor, E. M., Copsey, A. C., Hudson, J. J. R., Vidot, S., and Lehmann, A. R. (2008). Identification of the proteins, including MAGEG1, that make up the human SMC5-6 protein complex. *Mol. Cell. Biol.* 28, 1197–1206. doi: 10.1128/mcb.00767-07

Taylor, E. M., Moghraby, J. S., Lees, J. H., Smit, B., Moens, P. B., and Lehmann, A. R. (2001). Characterization of a novel human SMC heterodimer homologous to the *Schizosaccharomyces pombe* Rad18/Spr18 complex. *Mol. Biol. Cell* 12, 1583–1594. doi: 10.1091/mbc.12.6.1583

Toby, G. G., Gherraby, W., Coleman, T. R., and Golemis, E. A. (2003). A novel RING finger protein, human enhancer of invasion 10, alters mitotic progression through regulation of cyclin B levels. *Mol. Cell. Biol.* 23, 2109–2122. doi: 10.1128/MCB.23.6.2109-2122.2003

Torres-Rosell, J., De Piccoli, G., Cordon-Preciado, V., Farmer, S., Jarmuz, A., Machin, F., et al. (2007a). Anaphase onset before complete DNA replication with intact checkpoint responses. *Science* 315, 1411–1415. doi: 10.1126/science.1134025

Torres-Rosell, J., Sunjevaric, I., De Piccoli, G., Sacher, M., Eckert-Boulet, N., Reid, R., et al. (2007b). The Smc5-Smc6 complex and SUMO modification of Rad52 regulates recombinational repair at the ribosomal gene locus. *Nat. Cell Biol.* 9, 923–931. doi: 10.1038/ncb1619

Torres-Rosell, J., Machin, F., and Aragon, L. (2005). Smc5-Smc6 complex preserves nucleolar integrity in *S. cerevisiae*. *Cell Cycle* 4, 868–872. doi: 10.4161/cc.4.7.1825

Uhlmann, F., and Nasmyth, K. (1998). Cohesion between sister chromatids must be established during DNA replication. *Curr. Biol.* 8, 1095–1101. doi: 10.1016/S0960-9822(98)70463-4

Ünal, E., Arbel-Eden, A., Sattler, U., Shroff, R., Lichten, M., Haber, J. E., et al. (2004). DNA damage response pathway uses histone modification to assemble a double-strand break-specific cohesin domain. *Mol. Cell* 16, 991–1002. doi: 10.1016/j.molcel.2004.11.027

van der Crabben, S. N., Hennus, M. P., McGregor, G. A., Ritter, D. I., Nagamani, S. C., Wells, O. S., et al. (2016). Destabilized SMC5/6 complex leads to chromosome breakage syndrome with severe lung disease. *J. Clin. Invest.* 126, 2881–2892. doi: 10.1172/JCI82890

Verver, D. E., Hwang, G. H., Jordan, P. W., and Hamer, G. (2016). Resolving complex chromosome structures during meiosis: versatile deployment of Smc5/6. *Chromosoma* 125, 15–27. doi: 10.1007/s00412-015-0518-9

Verver, D. E., Langedijk, N. S., Jordan, P. W., Repping, S., and Hamer, G. (2014). The SMC5/6 complex is involved in crucial processes during human spermatogenesis. *Biol. Reprod.* 91:22. doi: 10.1095/biolreprod.114.118596

Verver, D. E., van Pelt, A. M., Repping, S., and Hamer, G. (2013). Role for rodent Smc6 in pericentromeric heterochromatin domains during spermatogonial differentiation and meiosis. *Cell Death Dis.* 4:e749. doi: 10.1038/cddis.2013.269

Wang, K., Wang, M., Tang, D., Shen, Y., Miao, C., Hu, Q., et al. (2012). The role of rice HEI10 in the formation of meiotic crossovers. *PLoS Genet.* 8:e1002809. doi: 10.1371/journal.pgen.1002809

Wang, S., and Adams, K. L. (2015). Duplicate gene divergence by changes in microRNA binding sites in *Arabidopsis* and *Brassica*. *Genome Biol. Evol.* 7, 646–655. doi: 10.1093/gbe/evv023

Watanabe, K., Pacher, M., Dukowic, S., Schubert, V., Puchta, H., and Schubert, I. (2009). The STRUCTURAL MAINTENANCE OF CHROMOSOMES 5/6 complex promotes sister chromatid alignment and homologous recombination after DNA damage in *Arabidopsis thaliana*. *Plant Cell* 21, 2688–2699. doi: 10.1105/tpc.108.060525

Weisshart, K., Fuchs, J., and Schubert, V. (2016). Structured Illumination Microscopy (SIM) and Photoactivated Localization Microscopy (PALM) to analyze the abundance and distribution of RNA polymerase II molecules in flow-sorted *Arabidopsis* nuclei. *Bioprotocol* 6:e1725. doi: 10.21769/BioProtoc.1725

Whitby, M. C. (2005). Making crossovers during meiosis. *Biochem. Soc. Trans.* 33, 1451–1455. doi: 10.1042/BST20051451

Xaver, M., Huang, L., Chen, D., and Klein, F. (2013). Smc5/6-Mms21 prevents and eliminates inappropriate recombination intermediates in meiosis. *PLoS Genet.* 9:e1004067. doi: 10.1371/journal.pgen.1004067

Xu, P., Yuan, D., Liu, M., Li, C., Liu, Y., Zhang, S., et al. (2013). AtMMS21, an SMC5/6 complex subunit, is involved in stem cell niche maintenance and DNA damage responses in *Arabidopsis* roots. *Plant Physiol.* 161, 1755–1768. doi: 10.1104/pp.112.208942

Yan, S., Wang, W., Marques, J., Mohan, R., Saleh, A., Durrant, W. E., et al. (2013). Salicylic acid activates DNA damage responses to potentiate plant immunity. *Mol. Cell* 52, 602–610. doi: 10.1016/j.molcel.2013.09.019

Yong-Gonzales, V., Hang, L. E., Castellucci, F., Branzei, D., and Zhao, X. (2012). The Smc5-Smc6 complex regulates recombination at centromeric regions and affects kinetochore protein sumoylation during normal growth. *PLoS One* 7:e51540. doi: 10.1371/journal.pone.0051540

Zabrady, K., Adamus, M., Vondrova, L., Liao, C., Skoupilova, H., Novakova, M., et al. (2016). Chromatin association of the SMC5/6 complex is dependent on binding of its NSE3 subunit to DNA. *Nucleic Acids Res.* 44, 1064–1079. doi: 10.1093/nar/gkv1021

Zhao, X., and Blobel, G. (2005). A SUMO ligase is part of a nuclear multiprotein complex that affects DNA repair and chromosomal organization. *Proc. Natl. Acad. Sci. U.S.A.* 102, 4777–4782. doi: 10.1073/pnas.0500537102

Conflict of Interest Statement: The authors declare that the research was conducted in the absence of any commercial or financial relationships that could be construed as a potential conflict of interest.

frontiers in Plant Science

ORIGINAL RESEARCH
published: 09 January 2019
doi: 10.3389/fpls.2018.01924

Competition for Chiasma Formation Between Identical and Homologous (But Not Identical) Chromosomes in Synthetic Autotetraploids of *Arabidopsis thaliana*

Pablo Parra-Nunez, Mónica Pradillo and Juan Luis Santos*

Department of Genetics, Physiology and Microbiology, Faculty of Biology, Complutense University of Madrid, Madrid, Spain

Polyploid organisms provide additional opportunities to study meiosis in a more complex context since more than two potential homologous chromosomes are available. When the chromosome complement of a diploid individual is duplicated, each chromosome is accompanied by one identical and two homologous chromosomes within the same nucleus. In this situation, a competition in pairing/synapsis/chiasma formation between identical and homologous (but not necessarily identical) chromosomes can occur. Several studies have been conducted in different species to address whether there are preferences in crossover formation between identical rather than homologous chromosomes. In this study, multivalent and chiasma frequencies were cytologically analyzed in synthetic autotetraploids of *Arabidopsis thaliana* including the accessions Col, L*er,* and the Col/L*er* hybrid. Fluorescence *in situ* hybridization was conducted to identify each chromosome at metaphase I. The new Col and L*er* tetraploids showed high multivalent frequencies, exceeding the theoretical 66.66% expected on a simple random end-pairing model, thus indicating that there are more than two autonomous synaptic sites per chromosome despite their small size. However, a significant excess of bivalent pairs was found in the Col/L*er* hybrid, mainly due to the contribution of chromosomes 2 and 3. The mean chiasma frequencies of the three artificial autotetraploids were about twofold the corresponding mean cell chiasma frequencies of their diploid counterparts. The relative contribution of each chromosome to the total chiasma frequency was similar in the three genotypes, with the exception of a lower contribution of chromosome 3 in the hybrid. Preferences for chiasma formation between identical and homologous chromosomes were analyzed in Col/L*er* 4x, taking advantage of the cytological differences between the accessions: variations in the size of the 45S rDNA region on the short arm of chromosome 2 and changes in the size and localization of the 5S rDNA region in chromosome 3. We observed a different behavior of chromosomes 2 and 3, i.e., random chiasma formation between identical and homologous chromosomes 2, and preferences for chiasma formation between homologous chromosomes 3. Hence, our results reveal the existence of chromosome-specific mechanisms responsible for these preferences.

Keywords: ***Arabidopsis thaliana,*** **autotetraploids, chiasma, homologous chromosomes, meiosis**

OPEN ACCESS

Edited by:
Simon Gilroy,
University of Wisconsin–Madison,
United States

Reviewed by:
Paul Fransz,
University of Amsterdam, Netherlands
James D. Higgins,
University of Leicester,
United Kingdom

****Correspondence:***
Mónica Pradillo
pradillo@bio.ucm.es

Specialty section:
This article was submitted to Plant Cell Biology, a section of the journal Frontiers in Plant Science

Received: *29 June 2018*
Accepted: *11 December 2018*
Published: *09 January 2019*

Citation:
Parra-Nunez P, Pradillo M and Santos JL (2019) Competition for Chiasma Formation Between Identical and Homologous (But Not Identical) Chromosomes in Synthetic Autotetraploids of Arabidopsis thaliana. Front. Plant Sci. 9:1924. doi: 10.3389/fpls.2018.01924

INTRODUCTION

Meiosis is a specialized eukaryotic cell division which reduces the number of chromosomes in a parent diploid cell by half to produce haploid gametes. During meiosis, the correct segregation of homologous chromosomes at anaphase I is ensured by the combined action of sister chromatid cohesion and chiasma formation. In many species, chiasmata (the physical attachments between homologous chromosomes) are formed after the recognition of homologous chromosomes (pairing), the close association of paired chromosomes by the synaptonemal complex (SC), and the reciprocal exchange of sequences by the homologous recombination (HR) process.

Polyploids provide additional opportunities to study meiosis in a more complex context since more than two potential partners for these exchanges are available. Depending on their origin, they can show different meiotic behaviors (Sybenga, 1996). Polyploids resulting from the merging of two chromosomal sets from different species (allopolyploids) are expected to show disomic inheritance, with pairs of related chromosomes from the same parental forming preferentially bivalents (Le Comber et al., 2010; Lloyd and Bomblies, 2016). On the other hand, polyploids resulting from within-species duplication events (autopolyploids) generally show tetrasomic inheritance (random synapsis, recombination and segregation of all homologous chromosomes) as a consequence of an extensive multivalent formation (Soltis and Rieseberg, 1986; Wolf et al., 1989; Muthoni et al., 2015; Lloyd and Bomblies, 2016). In this landscape, synapsis and recombination preferences among the members of a tetrasome (set of four homologous chromosomes) can be responsible for cases that present an intermediate behavior between a disomic and a tetrasomic inheritance, and even for the diploidization process (Jannoo et al., 2004; Stift et al., 2008; Meirmans and Van Tienderen, 2013).

The degree of relationship of two chromosomes may be greater than mere homology. For example, when the chromosome complement of a diploid individual is duplicated, each tetrasome is formed by two pairs of completely identical chromosomes; i.e., each chromosome is accompanied by one identical and two homologous chromosomes within the same nucleus. In this landscape, a competition in pairing, synapsis, and recombination between identical and homologous (but not necessarily identical) chromosomes can occur. Attempts to address this issue have been performed mainly in plants since it is very easy to obtain autotetraploids by a colchicine treatment, with only a few examples in animals. Possible preferences between chromosomes of a tetrasome were inferred from analyses to determine the segregation of genetic and/or chromosomal markers (Giraldez and Santos, 1981; Santos et al., 1983; Benavente and Orellana, 1991; Curole and Hedgecock, 2005). The most exhaustive cytological studies were conducted on rye, taking advantage of the existence of C-bands polymorphisms, especially in the nucleolar organizing region (NOR)-bearing chromosome 1R (Orellana and Santos, 1985; Benavente and Orellana, 1989, 1991; Benavente and Sybenga, 2004). In general, in this species there is a trend to identical over homologous preferential associations at metaphase I. This tendency is greater in hybrids with higher chromosomal divergence between the parental diploid plants. This fact indicates chromosome differentiation may play a relevant role in the establishment of such preferences (Benavente and Orellana, 1991; Jenkins and Chatterjee, 1994). These preferences could contribute to the diploidization process of autopolyploids.

In this study, we have analyzed chromosome configurations at metaphase I in autotetraploid meiocytes from the plant model species *Arabidopsis thaliana*. Tetraploid plants were obtained by applying a colchicine treatment to hybrid diploid plants from the cross between Col-0 and L*er*-1 accessions (Col and L*er* onward). We have used the 45S and 5S rDNA sequences as cytological markers. These sequences show quantitative and qualitative variations in chromosomes 2 and 3 of these accessions (Sanchez-Moran et al., 2002). In *Arabidopsis*, the initiation and progression of meiotic recombination is required to establish the SC-mediated pairwise association between homologous chromosomes (Grelon et al., 2001). Therefore, we consider more appropriate the use of the term "chiasma formation preferences" instead of "pairing preferences" throughout this paper. This clarification is necessary because in the mid-20th century and first decade of the current century, in most of the traditional literature on plant cytogenetics, the term chromosome pairing was used as the equivalent of chromosome associations mediated by chiasmata at metaphase I.

MATERIALS AND METHODS

Plant Materials and Growth Condition

Diploid plants of Columbia (Col-0) and Landsberg *erecta* (L*er*-1) accessions ($2n = 2x = 10$), and also Col-0/L*er*-1 hybrid plants were treated with colchicine in order to obtain the corresponding autotetraploids ($2n = 4x = 20$) (Santos et al., 2003). This treatment consists in applying a 10 μL drop of colchicine at a 0.25% w/v concentration on the center of the plant rosette prior to the first flowering. Seeds from these plants were sown on a mixture of 3 parts of soil and 1 part of vermiculite and grown under constant conditions of 16h day-length, 70% relative humidity and 19°C.

Cytological Analyses

Fixation of flower buds, slide preparations of pollen mother cells (PMCs), and fluorescence *in situ* hybridization (FISH) were conducted according to Sanchez-Moran et al. (2001), with minor modifications due to the polyploid samples. The DNA probes used comprise ribosomal DNA 45S and 5S loci (Gerlach and Bedbrook, 1979; Campell et al., 1992). The existence of changes in the localization of the 5S rDNA locus belonging to chromosome 3 (Fransz et al., 1998; Sanchez-Moran et al., 2002), and variations in the size of the 45S rDNA locus located at chromosome 2 (this work) made possible the differentiation of the parental origin of these chromosomes in the diploid and tetraploid hybrid plants analyzed (**Figure 1**). Images were captured using an Olympus BX-60 microscope with an Olympus DP71 camera and processed with Adobe Photoshop CS5 software.

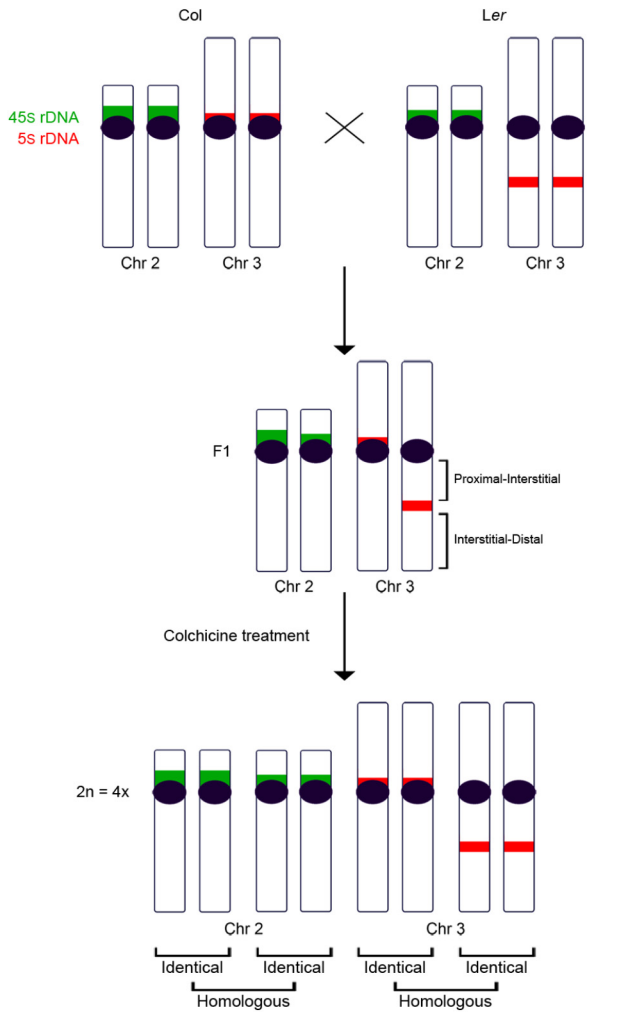

FIGURE 1 | Ideogram of chromosomes 2 and 3 in Col, *Ler* and in the hybrid progeny obtained from the cross between both accessions before and after the chromosome duplication. Col and *Ler* chromosomes 2 and 3 can be distinguished after applying FISH with 5S (red) and 45S (green) rDNA probes. These differences allow the identification of the parental origin of each chromosome in the hybrid, before and after the colchicine treatment. In the tetraploid hybrid, each chromosome is accompanied by one identical chromosome and two homologous chromosomes.

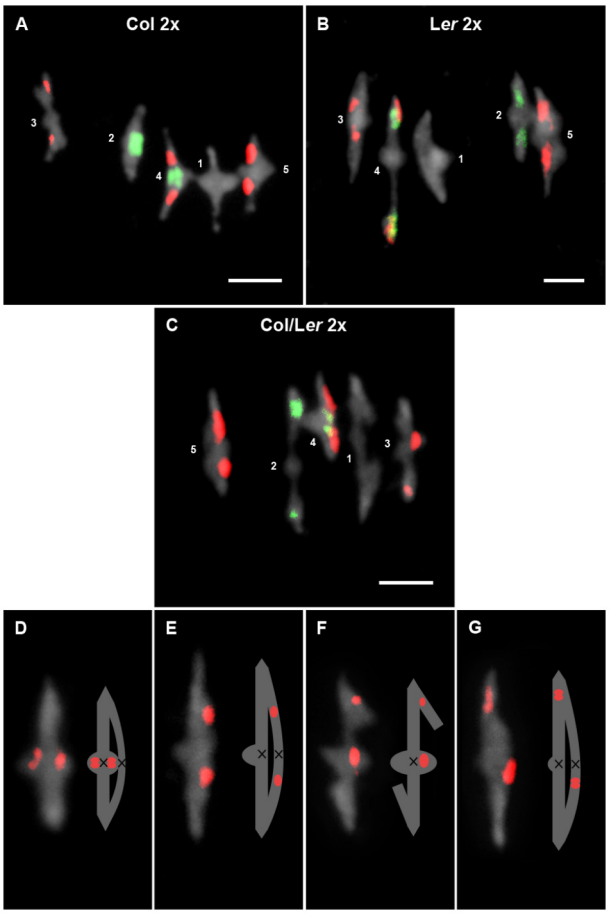

FIGURE 2 | Cytological analysis of diploid cells at metaphase I. Representative examples of metaphases I from Col 2x **(A)**, *Ler* 2x **(B)**, and Col/*Ler* 2x **(C)**. Chromosomes are identified by FISH with 5S (red) and 45S rDNA (green) probes. Images and representations of bivalents formed by chromosomes 3 in which the chiasma (black cross) has been formed before (**D,F**) or after (**E,G**) the position of the 5S rDNA in a *Ler* (**D,E**) and in a Col/*Ler* (**F,G**) background. Bars represent 5 μm.

RESULTS

Chiasma Analyses in Diploid Plants of Col, *Ler* and Col/*Ler* Hybrids

Chromosome morphology together with 45S (NOR) and 5S rDNA FISH probes allow the identification of the whole complement set of *Arabidopsis* in some accessions (Fransz et al., 1998; Sanchez-Moran et al., 2002). Chromosomes 1, 3 and 5 are submetacentric/metacentric, while chromosomes 2 and 4 are acrocentric. Chromosomes 1 do not possess any rRNA genes. Chromosomes 2 are characterized by the presence of 45S rDNA sequences distally on their short arms. Chromosomes 3 and 5 bear 5S rRNA genes and chromosomes 4 have both 45S and 5S rDNA sequences also located on the short arm. Col and *Ler* are distinguished because 5S rRNA genes are located on a different arm at chromosome 3 (short arm in Col and long arm in *Ler*). In this study, we have also detected another difference between both accessions. The NOR region belonging to chromosome 2 is bigger in Col than in *Ler* (**Figures 1**, **2A–C**).

Chiasma scoring was conducted in PMCs at metaphase I. Three plants were analyzed in each accession and also in the hybrid progeny obtained from the cross between both accessions. Since there were no significant differences in the mean chiasma frequencies per cell among them, individual plant data were grouped. In all of the cells assessed in this study, the five chromosome pairs invariably formed five bivalents that could be classified into two categories: rod and ring. A rod (open) bivalent has a single chiasma, whereas in a ring (close) bivalent both chromosome arms are bound by chiasmata.

TABLE 1 | Chiasma frequencies observed for the different chromosomes (1–5) in PMCs from Col, L*er,* and Col/L*er* diploid plants.

	Chromosomes						
	1	2	3	4	5	$\bar{X}$	*N*
Col 2x	2.55 (25.0)	1.73 (17.0)	2.16 (21.2)	1.50 (14.7)	2.28 (22.4)	10.20	70
L*er* 2x	2.09 (22.9)	1.74 (19.1)	1.79 (19.6)	1.61 (17.6)	1.90 (20.8)	9.13	158
Col/L*er* 2x	2.14 (22.6)	1.76 (18.6)	1.85 (19.5)	1.70 (17.9)	2.04 (21.5)	9.48	120

Values showed in parentheses represent the contribution in percentage of each chromosome to the total mean chiasma frequency ($\bar{X}$). Number of cells analyzed (N).

TABLE 2 | Multivalents (M), bivalent pairs (II) and chiasma frequency (Xta) observed for the different chromosomes (1–5) in PMCs from Col, L*er,* and Col/L*er* autotetraploid plants.

		Chromosomes							
		1	2	3	4	5	Total	$\bar{X}$	*N*
Col 4x	M	153 (82.3)	129 (69.4)	150 (80.6)	122 (65.9)	151 (81.2)	705 (75.9)	3.79	186
	II	33 (17.7)	57 (30.6)	36 (19.4)	63 (34.1)	35 (18.8)	224 (24.1)	1.20	
	Xta	4.19 (21.0)	4.02 (20.1)	3.91 (19.6)	3.82 (19.1)	4.05 (20.2)		19.99	
L*er* 4x	M	40 (80)	31 (64.6)	36 (73.5)	33 (70.2)	39 (73.6)	179 (72.5)	3.58	53
	II	10 (20)	17 (35.4)	13 (26.5)	14 (29.8)	14 (26.4)	68 (27.5)	1.36	
	Xta	4.00 (21.6)	3.60 (19.5)	3.64 (19.7)	3.54 (19.1)	3.72 (20.1)		18.50	
Col/L*er* 4x	M	97 (69.8)	70 (51.5)	70 (50.7)	89 (64)	99 (71.2)	425 (61.5)	3.06	139
	II	42 (30.2)	66 (48.5)	68 (49.3)	50 (36)	40 (28.8)	266 (38.5)	1.91	
	Xta	4.07 (21.4)	3.78 (19.9)	3.60 (18.9)	3.59 (18.9)	3.99 (20.9)		19.03	

Values showed in parentheses represent the percentage of multivalents and pairs of bivalents to the total cells (N), and the contribution of each chromosome to the total mean chiasma frequency ($\bar{X}$). Number of cells analyzed (N).

The mean chiasma frequencies per bivalent and per cell are summarized in **Table 1**. Col showed a significantly higher mean chiasma frequency per cell (10.20 ± 0.14) than L*er* (9.13 ± 0.10; $t = 6.2$, $p < 0.001$). The value for the Col/L*er* hybrid was intermediate to the previous ones (9.48 ± 0.11; $n = 120$), and it was statistically significant respect to both Col ($t = 4.14$, $p < 0.001$) and L*er* ($t = 2.39$, $p < 0.05$). In all the backgrounds analyzed, individual bivalent chiasma frequencies changed according to the chromosome size (the chromosome 1 had the highest mean chiasma frequency while the short acrocentric chromosomes, 2 and 4, presented the lowest frequencies).

In L*er*, the interstitial 5S rDNA region on chromosome 3 divides the long arm of this chromosome in two regions: a proximal region between the centromere and the 5S rRNA genes, and a distal region from these genes to the telomere. This feature has allowed a more accurate analysis of chiasma distribution on this arm not only in this accession but also in the Col/L*er* hybrid (**Figures 2D–G**). In both backgrounds, about 50% of chiasmata were located in each region (L*er*: $\chi^2_1 = 1.58$, $p > 0.05$; Col/L*er*: $\chi^2_1 = 1.09$, $p > 0.05$). Therefore, chiasma localization on this chromosome arm do not change in the hybrid.

Multivalent and Chiasma Analyses in Autotetraploid Plants of Col, L*er* and Col/L*er* Hybrids

Frequencies for the different configurations observed at metaphase I were recorded for each chromosome in three plants of each genotype (**Table 2**). Data from plants sharing the same background were grouped since there were no significant differences in multivalent and chiasma frequencies among them. Chromosomes were predominantly associated as bivalents, quadrivalents, and trivalent + univalent (**Figures 3A–C**). Since the frequency of the latter was very low (16/186 = 9% in Col 4x; 8/50 = 16% in L*er*; 11/139 = 8% in Col/L*er* 4x), no distinction was made between quadrivalents and trivalents and they were simply grouped as multivalents (**Table 2**).

Synaptic configurations in autotetraploids with metacentric chromosomes have usually been estimated under the following premises (for review see Sybenga, 1975): (i) the presence of two independent synapsis initiation points per chromosome, one at each end; (ii) the absence of synapsis preferences; (iii) the existence of same probabilities for chiasma formation in all meiotic configurations; and (iv) the possibility of free partner switches between the two synapsis initiation points at each chromosome. In this context, there are nine possible configurations to be formed among each group of homologous chromosomes (tetrasome), of which six are quadrivalents (2/3) and the remaining three are pairs of bivalents (1/3), i.e., the ratio of multivalents to bivalent pairs at prophase I would be 2:1.

The observed ratios of multivalents to bivalent pairs were tested for the agreement with the theoretical 2:1 ratio for each chromosome in the three autotetraploid genotypes analyzed (**Tables 2**, **3**). The level of multivalent formation over the five chromosomes (705 multivalents: 224 bivalent pairs) displayed by Col 4x significantly excess the 2:1 ratio (66.66% multivalents) [$\chi^2_{(1)} = 35.55$; $p < 0.001$]. In this accession, at the chromosomal level, only the three largest chromosomes of the complement (1, 3 and 5) showed multivalent frequencies consistently in excess of the 66.66%. L*er* 4x also presented an excess of multivalents (72.5%), but with a value that is at the limit of the significance level [$\chi^2_{(1)} = 3.74$; $p = 0.053$]. In this case, only chromosome 1 showed a significant excess of multivalents, while the other four chromosomes fitted to the random theoretical expectations. Conversely, there was a significant excess of bivalent pairs in the Col/L*er* 4x hybrid (38.5%) [$\chi^2_{(1)} = 8.28$; $p < 0.01$], mainly due to the behavior of chromosomes 2 and 3 (**Table 3**).

Col 4x showed the highest mean cell chiasma frequency (19.99 ± 0.11) followed by the hybrid Col/L*er* 4x (19.03 ± 0.15). L*er* 4x presented the lowest frequency (18.5 ± 0.27) (**Table 2**). These means are about twofold the corresponding mean cell

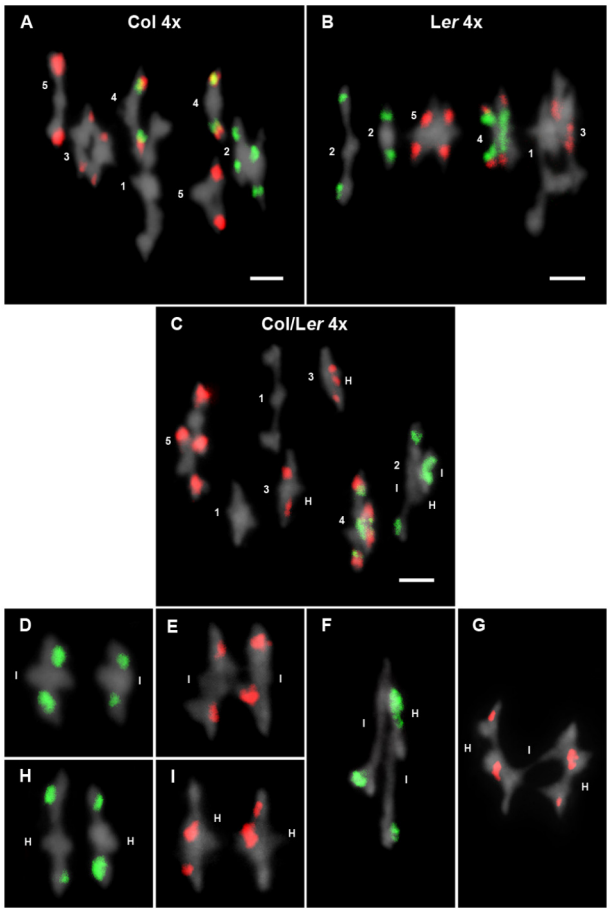

FIGURE 3 | Cytological analysis of autotetraploid cells at metaphase I. Representative examples of metaphases I from Col 4x **(A)**, L*er* 4x **(B)**, and Col/L*er* 4x **(C)**. Chromosomes are identified by FISH with 5S (red) and 45S rDNA (green) probes. In Col 4x, tetrasomes 1, 2, and 3 appear as quadrivalents, whereas two bivalents are formed in tetrasomes of chromosomes 4 and 5. In L*er* 4x, only the tetrasome of chromosomes 2 appears as two bivalents. In the hybrid, two bivalents are formed in tetrasomes of chromosomes 1 and 3, whereas the remaining tetrasomes appear as quadrivalents. The figure also includes examples of associations between identical chromosomes in bivalents formed by chromosomes 2 **(D)** and chromosomes 3 **(E)**. Examples of associations between homologous chromosomes in bivalents formed by chromosomes 2 **(H)** and chromosomes 3 **(I)**. Examples of quadrivalents formed by chromosomes 2 **(F)** and 3 **(G)**. Capital letters I and H represent identical and homologous association, respectively. Bars represent 5 μm.

chiasma frequencies of the diploid counterparts. There were significant differences between the means of Col 4x and L*er* 4x ($t = 5.19$, $p < 0.001$), and also between Col 4x and the hybrid 4x ($t = 3.24$, $p < 0.001$), but not between L*er* 4x and the hybrid 4x ($t = 1.19$, $p = 0.08$). The relative contribution of each chromosome to the total mean cell chiasma frequency was similar in these three backgrounds, with the exception of a slightly lower contribution of chromosome 3 in the hybrid (**Table 2**). In addition, chiasma localization was analyzed in the long arm of chromosome 3 in L*er* 4x and also in the hybrid 4x, but only in cells in which chromosomes 3 did not form a multivalent. As well as in diploid cells, about 50% of chiasmata were located in the proximal region (centromere – 5S rDNA) and the remaining 50% in the distal region (5S rDNA – telomere).

Competition for Chiasma Formation Between Identical and Homologous Chromosomes in the Hybrid Col/L*er* 4x

One of the main objectives of this study was to analyze whether chromosome intraspecific differences in autotetraploid plants are enough to determine preferences in terms of chiasma formation. Taking into account the cytological differences between Col and L*er* accessions, namely: variations in the size of the NOR region located on the short arm of chromosome 2 and changes in the localization of the 5S rDNA at chromosome 3, Col/L*er* diploid hybrids were treated with colchicine to obtain autotetraploid plants. In these hybrids, there is one pair of identical chromosomes from Col and another identical pair from L*er*. These two pairs of identical chromosomes are homologous, but non-identical with each other (**Figure 1**). Then, two types of two-by-two metaphase I associations are possible for any chromosome arm: between identical chromosomes or between homologous chromosomes (**Figures 3D–I**). Assuming that chiasma formation takes place randomly among the four members of each tetrasome, homologous associations will be twice as common as identical ones.

Following the criteria established by Benavente and Orellana (1991), in this analysis we have included cells with at least one chiasma between identical or homologous chromosomes (regardless of the chromosome configuration adopted by the corresponding tetrasome) to test randomness (**Figures 3D–I** and **Table 4**). When data from multivalents and bivalent pairs were grouped, we detected a different behavior of chromosomes 2 and 3. We observed random chiasma formation between identical and homologous arms of chromosome 2, and homologous preferences for chiasma formation in both arms of chromosome 3. This tendency was also maintained when only data from bivalent pairs were considered, although in this case the excess of chiasmata between homologous short arms of chromosome 3 was at the limit of the significance level.

DISCUSSION

Multivalent and Chiasma Frequencies at Metaphase I

The frequencies of multivalents observed in Col 4x plants significantly exceed the 2:1 ratio (66.66% multivalents) expected on the random-end pairing model (**Table 3**), which means that, despite their small size, at least in this accession chromosomes have more than two autonomous synaptic initiation sites (López et al., 2008), and more than one synaptic partner switch per tetrasome. In addition, there was a significant excess of bivalent pairs in the autotetraploid Col/L*er* hybrid (**Table 2**; $\chi^2_1 = 8.30$, $p < 0.01$). It might be produced, at least partially, as a consequence of the heterozygosity.

TABLE 3 | Chi-square test values (χ_1^2) testing goodness of fit to 2:1 ratio of multivalents: bivalent pairs for the different chromosomes (1–5) in PMCs from Col, L*er* and Col/L*er* autotetraploid plants.

	Chromosomes					
	1	**2**	**3**	**4**	**5**	**Total**
Col 4x	> 20.35***	= 0.60^{NS}	> 16.35***	= 0.04^{NS}	> 17.64***	> 35.55***
L*er* 4x	> 4.00*	= 0.09^{NS}	= 1.02^{NS}	= 0.64^{NS}	= 0.64^{NS}	= 3.74^{NS}
Col/L*er* 4x	= 0.61^{NS}	< 14.13***	< 15.78***	= 0.44^{NS}	= 1.30^{NS}	< 8.28**

*Less than and greater than symbols indicate direction of deviation: < (< 2:1), > (> 2:1). *p ≤ 0.05; **p ≤ 0.01; ***p ≤ 0.001; NS, not significant.*

TABLE 4 | Number of Col/L*er* 4x chromosome configurations with at least one chiasma between identical (I) or homologous (H) chromosomes in bivalent pairs (II) and multivalents + bivalent pairs (M+II) and the goodness of fit to the expected ratio 1I:2H.

	Chromosome 2						Chromosome 3					
	Short arm			Long arm			Short arm			Long arm		
	I	**H**	χ_1^2	**I**	**H**	χ_1^2	**I**	**H**	χ_1^2	**I**	**H**	χ_1^2
M+II	36	63	0.41	34	67	0.01	21	78 ↑	6.58*	20	85 ↑	9.64*
II	24	42	0.27	22	44	0.00	15	51	3.34	14	54 ↑	4.97*

*Chi-square test values obtained (χ_1^2). Values that exceed the 1:2 (I:H) ratio expected at random (↑). Chi-square test values statistically significant, *p ≤ 0.05.*

Col and L*er* diverged ∼200,000 years ago (Koch et al., 2000). Around 16,000 single feature polymorphisms between Col and *Ler* accessions were detected in ∼8,000 of the ∼26,000 genes represented in a 44,000 feature exon-specific oligonucleotide array (Singer et al., 2006). Furthermore, more than 6,000 insertions or deletions distinguish both accessions, which differ in 564 transpositions and 47 inversions that comprise around 3.6 Mb (Ziolkowski et al., 2009; Zapata et al., 2016). Increases in bivalent frequency are strongly chromosome dependent and are generally ascribed to overall decreases in chiasma frequency and/or changes in chiasma distribution, with a more rapid response of the shortest chromosomes to these alterations. The behavior of chromosome 3 in L*er* can shed some light to this issue since it carries a 170 kb inversion on the short arm (Zapata et al., 2016). Hence, Col/L*er* hybrid is heterozygous for such inversion, and it is well known that the heterozygosity for inversions suppresses meiotic recombination.

The mean cell chiasma frequencies of chromosome 3 in L*er* 4x and Col/L*er* 4x are similar (3.64 vs. 3.60; $t = 0.31$, $p = 0.76$), but there are significant differences between the means of bivalent pairs (0.26 vs. 0.49; $t = 3.03$, $p < 0.001$) (**Table 2**). Hence, other factors in addition to chromosome rearrangements, such as genotypic, epigenetic or cryptic structural differences along chromosomes, may be involved in the increase of bivalent frequency observed not only in this hybrid but also, for instance, in established autotetraploid lines of *Arabidopsis* (Santos et al., 2003). On these grounds, Zhang et al. (2015) reported that, after 49 self-pollinated generations, autotetraploid rice showed a significant increase in the methylation of class II transposons in relation to its diploid donor that may affect gene expression. Also, Dar et al. (2017) observed differences between the frequency of both quadrivalents and bivalents from C_0 to C_2 synthetic autotetraploids of *Phlox drummondii,* associated with changes in both repetitive and non-repetitive regions.

Polyploidy is a major process in plant speciation. The potential evolutionary success of polyploids has been linked, among other hypotheses, to the buffering of mutations and sub- and neo-functionalization of duplicated genes (see for reviews, Otto, 2007; Soltis and Soltis, 2009; Parisod et al., 2010; Zielinski and Mittelsten Scheid, 2012). It has been reported that polyploids of *Gossypium* and *Arabidopsis* enhance meiotic recombination compared with diploids (Desai et al., 2006; Pecinka et al., 2011). Increases in chiasma frequency could help to the establishment of new polyploid species by rapid creation of genetic diversity when population sizes are small. The data reported in the present work unfit to this proposal since the autotetraploids showed chiasma frequencies about twofold in comparison with their diploid counterparts (**Tables 1**, **2**). However, the possibility to obtain an increase in recombination in certain chromosome regions cannot be ruled out. It would be interesting to test this hypothesis by examining chiasma frequencies not only in other *Arabidopsis* accessions but also in other non-related species.

Competition for Chiasma Formation Among Identical and Homologous Chromosomes

Benavente and Orellana (1991) analyzed preferences for chiasma formation in synthetic autotetraploids of *Secale cereale* obtained from heterozygous hybrids for telomeric C-bands at chromosome 1R. They found a clear tendency for preferences between identical partners in inter-subspecific hybrids. This tendency increased in inter-specific hybrids with a higher chromosomal divergence between homologous chromosomes. These results reflect the potential effect of chromosomal differentiation on chiasma preferences in polyploids (see also Jenkins and Chatterjee, 1994). However, the hybrids resulting from crosses between inbred lines showed a wide range of

preferential associations. Therefore, chiasmata between identical partners are not always favored.

In this study, we have observed that although chromosomes 2 and 3 exhibited similar frequencies of bivalent pairs (0.47 and 0.49, respectively) and chiasmata (3.78 and 3.60, respectively) (**Table 2**), they presented different preferences in chiasma formation in the hybrid Col/L*er* 4x. Chiasmata were randomly formed between identical and homologous chromosomes 2, but preferentially established between homologous chromosomes 3 (**Table 4**). These results indicate that although chromosome differentiation between related genomes may be the main cause of the excess of bivalents in the hybrid, bivalent formation between identical chromosomes is not necessarily favored (Sybenga, 1992, 1994; Bourke et al., 2015). In this regard, random chiasma formation among identical and homologous chromosomes 2 could be related to their close spatial nuclear location as a consequence of bearing the NOR region on the short arm, since differences in the number of 45S tandem repeats (Rabanal et al., 2017) do not seem to have an influence. On the other hand, preferences for chiasma formation between homologous chromosomes 3 could be more related to specific features of particular chromosome regions. Actually, in L*er* the 5S rDNA region on the long arm of this chromosome is close (∼6 Mb) to the 170 kb inversion mentioned before (Simon et al., 2018). This means that the genomes of the two accessions are different in a large region, which would have important consequences for meiotic recombination. However, recent meiotic recombination analysis suggests that high levels of sequence divergence are not necessarily inhibitors of meiotic recombination (Barth et al., 2001; Singer et al., 2006; Salomé et al., 2012). This idea is in agreement with a positive correlation of ancestral recombination frequencies and regions with high sequence divergence (Kim et al., 2007). In addition, heterozygous regions increase chiasma formation when are juxtaposed with homozygous regions, which reciprocally decrease (Ziolkowski et al., 2015). In relation to chromosome 3, Barth et al. (2001) found a strong negative correlation between genetic similarities of ecotypes and recombination frequencies for two adjacent markers located on the long arm of this chromosome, but not for other genomic regions. In general, there are difficulties in mapping and sequencing this chromosome, consequently this fact suggests the existence of unusual chromatin-related features respect to the other chromosomes of the complement (Schmidt, 2018).

Taking into account the information compiled in this work, it is evident that when the chromosome complement of a diploid individual is duplicated, the degree of relationship between two chromosomes within each tetrasome may be greater than mere homology. In this situation, there is a competition for chiasma formation between identical and homologous chromosomes that can be resolved through different ways depending on the chromosome. Accordingly, identical and homologous chromosome regions will persist in each tetrasome in a differential pattern throughout generations. This chromosomal genetic variation has not be considered in current models about tetrasomic and disomic inheritance and it could produce a relevant impact on haplotypes.

AUTHOR CONTRIBUTIONS

PP-N completed the experiments and performed the data analyses. All authors conceived and designed the experiments, wrote and reviewed the manuscript.

FUNDING

This work was funded through the Spanish National Project AGL2015-67349-P. PP-N was funded by the Marie-Curie COMREC network FP7 ITN-606956.

ACKNOWLEDGMENTS

We would like to thank Bianca Martín, M. Carmen Moreno, and José Barrios for technical assistance.

REFERENCES

Barth, S., Melchinger, A. E., Devezi-Savula, B., and Lübberstedt, T. (2001). Influence of genetic background and heterozygosity on meiotic recombination in *Arabidopsis thaliana*. *Genome* 44, 971–978. doi: 10.1139/g01-094

Benavente, E., and Orellana, J. (1989). Pairing competition between metacentric and telocentric chromosomes in autotetraploid rye. *Heredity* 62, 327–334. doi: 10.1038/hdy.1989.47

Benavente, E., and Orellana, J. (1991). Chromosome differentiation and pairing behavior of polyploids: an assessment on preferential metaphase I associations in colchicine-induced autotetraploid hybrids within the genus *Secale*. *Genetics* 128, 433–442.

Benavente, E., and Sybenga, J. (2004). The relation between pairing preference and chiasma frequency in tetrasomics of rye. *Genome* 47, 122–133. doi: 10.1139/g03-134

Bourke, P. M., Voorrips, R. E., Visser, R. G. F., and Maliepaard, C. (2015). The double-reduction landscape in tetraploid potato as revealed by a high-density linkage map. *Genetics* 201, 853–863. doi: 10.1534/genetics.115.181008

Campell, B. R., Song, Y., Posch, T. E., Cullis, C. A., and Town, C. D. (1992). Sequence and organization of 5S ribosomal RNA-encoding genes of *Arabidopsis thaliana*. *Gene* 112, 225–228. doi: 10.1016/0378-1119(92)90380-8

Curole, J. P., and Hedgecock, D. (2005). Estimation of preferential pairing rates in second-generation autotetraploid pacific oysters (*Crassostrea gigas*). *Genetics* 171, 855–859. doi: 10.1534/genetics.105.043042

Dar, T. H., Raina, S. N., and Goel, S. (2017). Cytogenetic and molecular evidences revealing genomic changes after autopolyploidization: a case study of synthetic autotetraploid *Phlox drummondii* hook. *Physiol. Mol. Biol. Plants* 23, 641–650. doi: 10.1007/s12298-017-0445-8

Desai, A., Chee, P. W., Rong, J., May, O. L., and Paterson, A. H. (2006). Chromosome structural changes in diploid and tetraploid a genomes of *Gossypium*. *Genome* 49, 336–345. doi: 10.1139/g05-116

Fransz, P., Armstrong, S., Alonso-Blanco, C., Fischer, T. C., Torres-Ruiz, R. A., and Jones, G. (1998). Cytogenetics for the model system *Arabidopsis thaliana*. *Plant J.* 13, 867–876. doi: 10.1046/j.1365-313X.1998.00086.x

Gerlach, W. L., and Bedbrook, J. R. (1979). Cloning and characterization of ribosomal RNA genes from wheat and barley. *Nucleic Acids Res.* 7, 1869–1885. doi: 10.1093/nar/7.7.1869

Giraldez, R., and Santos, J. L. (1981). Cytological evidence for preferences of identical over homologous but not-identical meiotic pairing. *Chromosoma* 82, 447–451. doi: 10.1007/BF00285769

Grelon, M., Vezon, D., Gendrot, G., and Pelletier, G. (2001). AtSPO11-1 is necessary for efficient meiotic recombination in plants. *EMBO J.* 20, 589–600. doi: 10.1093/emboj/20.3.589

Jannoo, N., Grivet, L., David, J., D'Hont, A., and Glaszmann, J. C. (2004). Differential chromosome pairing affinities at meiosis in polyploid sugarcane revealed by molecular markers. *Heredity* 93, 460–467. doi: 10.1038/sj.hdy.6800524

Jenkins, G., and Chatterjee, R. (1994). Chromosome structure and pairing preferences in autotetraploid rye (*Secale cereale*). *Genome* 37, 784–793. doi: 10.1139/g94-112

Kim, S., Plagnol, V., Hu, T. T., Toomajian, C., Clark, R. M., Ossowski, S., et al. (2007). Recombination and linkage disequilibrium in *Arabidopsis thaliana*. *Nat. Genet.* 39, 1151–1155. doi: 10.1038/ng2115

Koch, M. A., Haubold, B., and Mitchell-Olds, T. (2000). Comparative evolutionary analysis of chalcone synthase and alcohol dehydrogenase loci in *Arabidopsis, Arabis*, and related genera (Brassicaceae). *Mol. Biol. Evol.* 17, 1483–1498. doi: 10.1093/oxfordjournals.molbev.a026248

Le Comber, S. C., Ainouche, M. L., Kovarik, A., and Leitch, A. R. (2010). Making a functional diploid: from polysomic to disomic inheritance. *New Phytol.* 186, 113–122. doi: 10.1111/j.1469-8137.2009.03117.x

Lloyd, A., and Bomblies, K. (2016). Meiosis in autopolyploid and allopolyploid *Arabidopsis*. *Curr. Opin. Plant Biol.* 30, 116–122. doi: 10.1016/j.pbi.2016.02.004

López, E., Pradillo, M., Romero, C., Santos, J. L., and Cuñado, N. (2008). Pairing and synapsis in wild type *Arabidopsis thaliana*. *Chromosome Res.* 16, 701–708. doi: 10.1007/s10577-008-1220-z

Meirmans, P. G., and Van Tienderen, P. H. (2013). The effects of inheritance in tetraploids on genetic diversity and population divergence. *Heredity* 110, 131–137. doi: 10.1038/hdy.2012.80

Muthoni, J., Kabira, J., Shimelis, H., and Melis, R. (2015). Tetrasomic inheritance in cultivated potato and implications in conventional breeding. *Aust. J. Crop Sci.* 9, 185–190.

Orellana, J., and Santos, J. L. (1985). Pairing competition between identical and homologous chromosomes in autotetraploid rye. I. Submetacentric chromosomes. *Genetics* 111, 933–944.

Otto, S. P. (2007). The evolutionary consequences of polyploidy. *Cell* 131, 452–462. doi: 10.1016/j.cell.2007.10.022

Parisod, C., Holderegger, R., and Brochmann, C. (2010). Evolutionary consequences of autopolyploidy. *New Phytol.* 186, 5–17. doi: 10.1111/j.1469-8137.2009.03142.x

Pecinka, A., Fang, W., Rehmsmeier, M., Levy, A. A., and Mittelsten Scheid, O. (2011). Polyploidization increases meiotic recombination frequency in *Arabidopsis*. *BMC Biol.* 9:24. doi: 10.1186/1741-7007-9-24

Rabanal, F. A., Nizhynska, V., Mandáková, T., Novikova, P. Y., Lysak, M. A., Mott, R., et al. (2017). Unstable inheritance of 45S rRNA genes in *Arabidopsis thaliana*. *G3* 7, 1201–1209. doi: 10.1534/g3.117.040204

Salomé, P. A., Bomblies, K., Fitz, J., Laitinen, R. A. E., Warthmann, N., Yant, L., et al. (2012). The recombination landscape in *Arabidopsis thaliana* F2 populations. *Heredity* 108, 447–455. doi: 10.1038/hdy.2011.95

Sanchez-Moran, E., Armstrong, S. J., Santos, J. L., Franklin, F. C., and Jones, G. H. (2001). Chiasma formation in *Arabidopsis thaliana* accession wassileskija and in two meiotic mutants. *Chromosome Res.* 9, 121–128. doi: 10.1023/A:1009278902994

Sanchez-Moran, E., Armstrong, S. J., Santos, J. L., Franklin, F. C. H., and Jones, G. H. (2002). Variation in chiasma frequency among eight accessions of *Arabidopsis thaliana*. *Genetics* 162, 1415–1422.

Santos, J. L., Alfaro, D., Sanchez-Moran, E., Armstrong, S. J., Franklin, F. C. H., and Jones, G. H. (2003). Partial diploidization of meiosis in autotetraploid *Arabidopsis thaliana*. *Genetics* 165, 1533–1540.

Santos, J. L., Orellana, J., and Giraldez, R. (1983). Pairing competition between identical and homologous chromosomes in rye and grasshoppers. *Genetics* 104, 677–684.

Schmidt, R. (2018). "The *Arabidopsis thaliana* genome: towards a complete physical map," in *Annual Plant Reviews Online*, ed. J. A. Roberts (Chichester: John Wiley & Sons), 1–32. doi: 10.1002/9781119312994.apr0001

Simon, L., Rabanal, F. A., Dubos, T., Oliver, C., Lauber, D., Poulet, A., et al. (2018). Genetic and epigenetic variation in 5S ribosomal RNA genes reveals genome dynamics in *Arabidopsis thaliana*. *Nucleic Acids Res.* 46, 3019–3033. doi: 10.1093/nar/gky163

Singer, T., Fan, Y., Chang, H. S., Zhu, T., Hazen, S. P., and Briggs, S. P. (2006). A high-resolution map of *Arabidopsis* recombinant inbred lines by whole-genome exon array hybridization. *PLoS Genet.* 2:e144. doi: 10.1371/journal.pgen.0020144

Soltis, D. E., and Rieseberg, L. H. (1986). Autopolyploidy in *Tolmiea menziesii* (Saxifragaceae): genetic insights from enzyme electrophoresis. *Am. J. Bot.* 73, 310–318. doi: 10.1002/j.1537-2197.1986.tb08534.x

Soltis, P. S., and Soltis, D. E. (2009). The role of hybridization in plant speciation. *Annu. Rev. Plant Biol.* 60, 561–588. doi: 10.1146/annurev.arplant.043008.092039

Stift, M., Berenos, C., Kuperus, P., and van Tienderen, P. H. (2008). Segregation Models for disomic, tetrasomic and intermediate inheritance in tetraploids: a general procedure applied to rorippa (Yellow Cress) microsatellite data. *Genetics* 179, 2113–2123. doi: 10.1534/genetics.107.085027

Sybenga, J. (1975). *Meiotic Configurations*. Berlin: Springer, doi: 10.1007/978-3-642-80960-6

Sybenga, J. (1992). "Manipulation of genome composition. B. gene dose: duplication, polyploidy and gametic chromosome number," in *Cytogenetics in Plant Breeding*, ed. J. Sybenga (Berlin: Springer-Verlag), 327–371. doi: 10.1007/978-3-642-84083-8_11

Sybenga, J. (1994). Preferential pairing estimates from multivalent frequencies in tetraploids. *Genome* 37, 1045–1055. doi: 10.1139/g94-149

Sybenga, J. (1996). Chromosome pairing affinity and quadrivalent formation in polyploids: do segmental allopolyploids exist? *Genome* 39, 1176–1184. doi: 10.1139/g96-148

Wolf, P. G., Soltis, P. S., and Soltis, D. E. (1989). Tetrasomic inheritance and chromosome pairing behaviour in the naturally occurring autotetraploid *Heuchera grossulariifolia* (Saxifragaceae). *Genome* 32, 655–659. doi: 10.1139/g89-494

Zapata, L., Ding, J., Willing, E. M., Hartwig, B., Bezdan, D., Jiao, W. B., et al. (2016). Chromosome-level assembly of *Arabidopsis thaliana* Ler reveals the extent of translocation and inversion polymorphisms. *Proc. Natl. Acad. Sci. U.S.A.* 113, E4052–E4060. doi: 10.1073/pnas.1607532113

Zhang, J., Liu, Y., Xia, E. H., Yao, Q. Y., Liu, X. D., and Gao, L. Z. (2015). Autotetraploid rice methylome analysis reveals methylation variation of transposable elements and their effects on gene expression. *Proc. Natl. Acad. Sci. U.S.A.* 112, E7022–E7029. doi: 10.1073/pnas.1515170112

Zielinski, M. L., and Mittelsten Scheid, O. (2012). "Meiosis in polyploid plants," in *Polyploidy and Genome Evolution*, eds P. S. Soltis and D. E. Soltis (Berlin: Springer), 33–55. doi: 10.1007/978-3-642-31442-1_3

Ziolkowski, P. A., Berchowitz, L. E., Lambing, C., Yelina, N. E., Zhao, X., Kelly, K. A., et al. (2015). Juxtaposition of heterozygous and homozygous regions causes reciprocal crossover remodelling via interference during *Arabidopsis* meiosis. *eLife* 4:e03708. doi: 10.7554/eLife.03708

Ziolkowski, P. A., Koczyk, G., Galganski, L., and Sadowski, J. (2009). Genome sequence comparison of Col and Ler lines reveals the dynamic nature of *Arabidopsis* chromosomes. *Nucleic Acids Res.* 37, 3189–3201. doi: 10.1093/nar/gkp183

Conflict of Interest Statement: The authors declare that the research was conducted in the absence of any commercial or financial relationships that could be construed as a potential conflict of interest.

frontiers in Plant Science

ORIGINAL RESEARCH
published: 20 April 2018
doi: 10.3389/fpls.2018.00509

Magnesium Increases Homoeologous Crossover Frequency During Meiosis in *ZIP4* (*Ph1* Gene) Mutant Wheat-Wild Relative Hybrids

María-Dolores Rey[1]*, *Azahara C. Martín*[1], *Mark Smedley*[1], *Sadiye Hayta*[1], *Wendy Harwood*[1], *Peter Shaw*[2] and *Graham Moore*[1]

[1] Department of Crop Genetics, John Innes Centre, Norwich Research Park, Norwich, United Kingdom, [2] Department of Cell and Developmental Biology, John Innes Centre, Norwich Research Park, Norwich, United Kingdom

OPEN ACCESS

Edited by:
Tomás Naranjo, Complutense University of Madrid, Spain

Reviewed by:
Andreas Houben, Leibniz-Institut für Pflanzengenetik und Kulturpflanzenforschung (IPK), Germany
Fangpu Han, Institute of Genetics and Developmental Biology (CAS), China

***Correspondence:**
María-Dolores Rey
mdoloresrey@ias.csic.es

Specialty section:
This article was submitted to Plant Cell Biology, a section of the journal Frontiers in Plant Science

Received: *08 March 2018*
Accepted: *03 April 2018*
Published: *20 April 2018*

Citation:
Rey M-D, Martín AC, Smedley M, Hayta S, Harwood W, Shaw P and Moore G (2018) Magnesium Increases Homoeologous Crossover Frequency During Meiosis in ZIP4 (Ph1 Gene) Mutant Wheat-Wild Relative Hybrids. Front. Plant Sci. 9:509. doi: 10.3389/fpls.2018.00509

Wild relatives provide an important source of useful traits in wheat breeding. Wheat and wild relative hybrids have been widely used in breeding programs to introduce such traits into wheat. However, successful introgression is limited by the low frequency of homoeologous crossover (CO) between wheat and wild relative chromosomes. Hybrids between wheat carrying a 70 Mb deletion on chromosome 5B (*ph1b*) and wild relatives, have been exploited to increase the level of homoeologous CO, allowing chromosome exchange between their chromosomes. In *ph1b*-rye hybrids, CO number increases from a mean of 1 CO to 7 COs per cell. CO number can be further increased up to a mean of 12 COs per cell in these *ph1b* hybrids by treating the plants with Hoagland solution. More recently, it was shown that the major meiotic crossover gene *ZIP4* on chromosome 5B (*TaZIP4-B2*) within the 70 Mb deletion, was responsible for the restriction of homoeologous COs in wheat-wild relative hybrids, confirming the *ph1b* phenotype as a complete *Tazip4-B2* deletion mutant (*Tazip4-B2 ph1b)*. In this study, we have identified the particular Hoagland solution constituent responsible for the increased chiasma frequency in *Tazip4-B2 ph1b* mutant-rye hybrids and extended the analysis to *Tazip4-B2* TILLING and CRISPR mutant-*Ae variabilis* hybrids. Chiasma frequency at meiotic metaphase I, in the absence of each Hoagland solution macronutrient ($NH_4H_2PO_4$, KNO_3, Ca $(NO_3)2{\cdot}4H_2O$ or Mg $SO_4{\cdot}7H_2O$) was analyzed. A significant decrease in homoeologous CO frequency was observed when the Mg^{2+} ion was absent. A significant increase of homoeologous CO frequency was observed in all analyzed hybrids, when plants were irrigated with a 1 mM Mg^{2+} solution. These observations suggest a role for magnesium supplementation in improving the success of genetic material introgression from wild relatives into wheat.

Keywords: wheat, wild relatives, magnesium, *Ph1* locus, *TaZIP4-B2*, homoeologous crossover, CRISPR/Cas9 system

INTRODUCTION

Despite possessing related ancestral genomes (genome AABBDD), bread wheat behaves as a diploid during meiosis. Deletion of chromosome 5B in tetraploid and hexaploid wheat results in a level of incorrect chromosome pairing and exchange, visualized as a low level of multivalents at metaphase I, and homoeologous crossovers (COs) between related chromosomes in wheat-wild relative hybrids (Riley and Chapman, 1958; Sears and Okamoto, 1958). From these observations, it was proposed that chromosome 5B carries a locus termed *Pairing homoeologous 1* (*Ph1*), which evolved on wheat's polyploidisation and restricted chromosome pairing and COs to true homologs (Riley and Chapman, 1958). A hexaploid wheat cv. Chinese Spring (CS) line carrying a 70 Mb deletion on the long arm of chromosome 5B (*ph1b*) has been exploited over the last 40 years to allow exchange between wild relative and wheat chromosomes. Recently, it was shown that on wheat's polyploidisation, a segment of 3B carrying the major crossover gene *ZIP4* and a block of heterochromatin, duplicated and inserted between two *CDK2*-like genes within a cluster of *CDK2-like* and methyl-transferase genes (Griffiths et al., 2006; Al-Kaff et al., 2008; Martín et al., 2014, 2017). Using exploitation of TILLING mutants, it was shown that the duplicated *ZIP4* gene (*TaZIP4-B2*) within this cluster, both promotes homologous CO and restricts homoeologous CO (Rey et al., 2017). Therefore, *TaZIP4-B2* within the 70 Mb *ph1b* deletion region is responsible for the effect on homoeologous CO in wheat-wild relative hybrids, and as such the *ph1b* line can be described as a complete-deletion (or complete loss-of-function) mutant of *Tazip4-B2 (Tazip4-B2 ph1b* mutant). In terms of the effect on chromosome synapsis/pairing, cell biological studies reveal that the *ph1b* deletion in wheat has little effect, with most synapsis occurring during clustering of the telomeres as a bouquet. Furthermore, in wheat-wild relative hybrids, which only possess homoeologues, the *ph1b* deletion also has little effect on the level of synapsis, except that most pairing occurs after dispersal of the telomere bouquet. In wheat itself, a few chromosomes also undergo delayed pairing until after dispersal of the bouquet, with the subsequent incorrect pairing leading to the low level of multivalents observed at metaphase I (Martín et al., 2014, 2017).

For the last 40 years, the wheat CS *ph1b* deletion line has been exploited in crosses with wild relatives to allow exchange between chromosomes at meiosis. As indicated previously, in these hybrids, the extent of chromosome synapsis is similar whether the line carries the *ph1b* deletion or not. Moreover, on the synapsed chromosomes, similar numbers of MLH1 sites (normally a marker for CO), are observed (Martín et al., 2014). However significant site CO frequency is only observed in those hybrids carrying the *ph1b* deletion. However even in this case, the frequency of resulting COs still does not reflect the number of available MLH1 sites (Martín et al., 2014). This implies that there is potential for increased processing of MLH1 sites into COs. Fortuitously, it has been observed that a nutrient solution (Hoagland's solution) added to the soil when *Tazip4-B2 ph1b* mutant-rye hybrids are growing resulted in increased CO frequency, although it was not known which nutrient component was responsible for the effect (Martín et al., 2017).

Mineral elements are essential nutrients for plants to complete their life cycle. They are classified into macro and micronutrients, which are required in relatively large and small amounts, respectively (Hoagland and Arnon, 1950). The importance of each of these macronutrients has been reported in numerous physiological processes, such as plant growth, cell division, and metabolism (Huber, 1980; Maathuis, 2009). However, limited studies have been performed as to their effect on meiosis. Early studies have previously reported that alterations of external factors, such as temperature, or nutrient composition, can produce profound effects on chiasma frequency (Grant, 1952; Wilson, 1959; Law, 1963; Bennett and Rees, 1970; Fedak, 1973).

The main objective of the present study was to determine whether a specific macronutrient present in the Hoagland solution was responsible for the observed increased homoeologous CO frequency in *Tazip4-B2 ph1b* mutant-rye hybrids described in Martín et al. (2017). We also analyzed whether this macronutrient increased homoeologous CO frequency in each of the *Tazip4-B2 ph1b* (complete deletion), TILLING (point mutation) and CRISPR (partial deletion) mutant-*Ae. variabilis* hybrids.

MATERIALS AND METHODS

Plant Material

Plant material used in this study included: *Triticum aestivum* (2n = 6x = 42; AABBDD) cv. Chinese Spring *Tazip4-B2-ph1b* mutant line (Sears, 1977); *Triticum aestivum* cv. Chinese Spring-rye hybrids—crosses between the *Tazip4-B2-ph1b* mutant line hexaploid wheat and rye [*Secale cereal* cv. Petkus (2n = 2x = 14; RR)]; *Triticum aestivum* cv. Chinese Spring-*Aegilops variabilis* hybrids—crosses between *Tazip4-B2-ph1b* mutant and *Ae. variabilis* Eig. (2n = 4x = 28; UUS^vS^v); *Triticum aestivum* cv. Cadenza-*Ae. variabilis* hybrids—crosses between Cad1691 and Cad0348, *Tazip4-B2* TILLING mutants and *Ae. variabilis* (Krasileva et al., 2017; Rey et al., 2017); and *Triticum aestivum* cv. Fielder-*Ae. variabilis* hybrids—crosses between *Tazip4-B2* CRISPR mutant and *Ae. variabilis* (see Production of *TaZIP4-B2* knock-out using RNA-guided Cas9, section Materials and Methods).

Nutrient Solution Treatments

The total number of plants used in this work is described in **Table S1**. All seedlings were vernalized for 3 weeks at 7°C under a photoperiod of 16 h light/8 h dark, and then transferred to a controlled environmental room until meiosis (approximately 2 months later for all genotypes used in this study). The growth conditions were 16 h/8 h, light/dark photoperiod at 20°C day and 15°C night, with 70% humidity. At least 2 weeks before meiosis, irrigation of plants with a Hoagland solution (100 mL per plant) was commenced following the method previously described in Martín et al. (2017). Briefly, plants were irrigated once a week with a Hoagland solution (100 mL) from the stem elongation stage of the vegetative stage (stage 7–8, Feeke's scale).

The composition of the Hoagland solution was: (*macronutrients*) KNO_3 (12 mM), Ca $(NO_3)2{\cdot}4H_2O$ (4 mM), NH_4 H_2PO_4 (2 mM), Mg $SO_4{\cdot}7H_2O$ (1 mM); and (*micronutrients*) NaFe-EDTA (60 mM), KCl (50 μM), H_3BO_3 (25 μM), Mn $SO_4{\cdot}H_2O$ (2 μM), Zn SO_4 (4 μM), Cu $SO_4{\cdot}5H_2O$ (0.5 μM), H_2MoO_4 (0.5 μM). Four treatments were carried out to analyze the effect of the absence of NH_4 H_2PO_4, KNO_3, Ca $(NO_3)2{\cdot}4H_2O$ or Mg $SO_4{\cdot}7H_2O$ from the Hoagland solution on homoeologous CO frequency in *Tazip4-B2-ph1b* mutant-rye hybrids. For each treatment, a different Hoagland solution was prepared in the absence of each macronutrient (NH_4 H_2PO_4, KNO_3, Ca $(NO_3)2{\cdot}4H_2O$ or Mg $SO_4{\cdot}7H_2O$). Moreover, the effect of the presence of only Mg $SO_4{\cdot}7H_2O$ (Mg $SO_4{\cdot}7H_2O$ is designed as Mg^{2+} in the manuscript) in only water rather than in Hoagland solution on CO frequency was also analyzed in *Tazip4-B2-ph1b* mutant-rye hybrids in comparison to the effects of Hoagland solution. Also, two different concentrations of Mg^{2+} (1 and 2 mM of Mg^{2+} in water) were used to assess the homoeologous CO frequency in *Tazip4-B2-ph1b* mutant-rye hybrids. The treatment with either Mg^{2+} in water alone or Hoagland solution in *Tazip4-B2 ph1b* mutant-*Ae. variabilis,* and *Tazip4-B2* TILLING and CRISPR mutant-*Ae. variabilis* hybrids was also assessed.

Assessment of the addition of Mg^{2+} in water alone on homoeologous CO frequency was also made on non-irrigated plants, by injecting into *Tazip4-B2 ph1b* mutant-rye hybrids tillers a solution containing 1 mM Mg^{2+} in water (0.5 mL per spike) just above every spike at the stage 9 on the Feekes's scale (three spikes with water alone and three spikes with Mg^{2+} in water). All spikes were analyzed 24–48 h after the injection.

Feulgen-Stained Analysis

After either irrigating with Hoagland or Mg^{2+} solution, or injecting the Mg^{2+} solution, tillers were harvested when the flag leaf was completely emerged, and only anthers at meiotic metaphase I were collected and fixed in 100% ethanol/acetic acid 3:1 (v/v). The anthers used in this study were taken from spikelets in the lower half of the spike. From each spikelet, the 2 largest florets (on opposing sides of the floret) were used. From each dissected floret, one of the three synchronized anthers was squashed in 45% acetic acid/distilled water (v/v) and the meiocytes assessed for being at meiotic metaphase I by observation under a phase contrast microscope [LEICA DM2000 microscope (LeicaMicrosystems, http://www.leica-microsystems.com/)]. The two remaining anthers were left then fixed in 100% ethanol/acetic acid 3:1 (v/v) for cytological analysis of meiocytes. The anthers were incubated in ethanol/acetic acid at 4°C for at least 24 h. Cytological analysis of meiocytes at metaphase I was performed using Feulgen reagent as previously described in Sharma and Sharma (2014). Metaphase I meiocytes were observed under a phase contrast microscope equipped with a Leica DFC450 camera and controlled by LAS v4.4 system software (Leica Biosystems, Wetzlar, Germany). The digital images were used to determine the meiotic configurations of the meiocytes by counting the number of univalents, rod (1 chiasma) and ring (2 chiasmata) bivalents and multivalents (trivalents (1–2 chiasmata), tetravalents (3 chiasmata) and pentavalents (4 chiasmata)). Two different methods depending on the number of chiasma (single or double chiasmata) were used to calculate chiasma frequency per meiocyte (see **Figure S1** for examples of the scored structures). Images were processed using Adobe Photoshop CS5 (Adobe Systems Incorporated, US) extended version 12.0 × 64.

Production of *TaZIP4-B2* CRISPR Mutants Using RNA-Guided Cas9

Three single guide RNAs (sgRNA) were designed manually to specifically target *TaZIP4-B2*. These guides were in the limited regions where there was sufficient variation between *ZIP4* on 5BL and homoeologous group 3 chromosomes (**Figure 3**). The specific guides were: Guide 4: 5′GATGAG CGACGCATCCTGCT3′, Guide 11: 5′GATGCGTCGCTC ATCCTCCG3′ and Guide 12: 5′GAAGAAGGATGCGGCC TTGA3′ (**Figure 3**). Two constructs were assembled using standard Golden Gate assembly (Werner et al., 2012) with each construct containing the Hygromycin resistance gene under the control of a rice Actin1 promoter, Cas9 under the control of the rice ubiquitin promoter and two of the sgRNAs each under the control of a wheat U6 promoter (**Figure 3**). Construct 1 contained guides 4 and 12 and construct 2 contained guides 11 and 12. To produce each gRNA, a PCR reaction was performed using Phusion High-Fidelity Polymerase (Thermo Scientific M0530S) with a forward primer containing the gRNA sequence, and a standard reverse primer 5′TGTGGT CTCAAGCGTAATGCCAACTTTGTAC3′ using the plasmid pICSL70001::U6p::gRNA (Addgene plasmid 46966) as template. Each gRNA was cloned individually into the level 1 vectors pICH47751 (gRNA4 & 11) and pICH47761 (gRNA12). Level 1 construct pICH47802-RActpro::Hpt::NosT (selection maker), pICH47742-ZmUbipro::Cas9::NosT and the gRNAs were then assembled in the binary Level 2 vector pGoldenGreenGate (pGGG) a Golden Gate compatible vector based on pGreen (Hellens et al., 2000) (**Figure 3**).

The two constructs were introduced to *T. aestivum* cv. Fielder by Agrobacterium-mediated inoculation of immature embryos. 450 immature embryos were inoculated with Agrobacterium strain AGL1 containing each construct. Briefly, after 3 days co-cultivation with Agrobacterium, immature embryos were selected on 15 mg/l hygromycin during callus induction for 2 weeks and 30 mg/l hygromycin for 3 weeks in the dark at 24°C on Murashige and Skoog medium (MS; Murashige and Skoog, 1962) 30 g/l Maltose, 1.0 g/l Casein hydrolysate, 350 mg/l Myo-inositol, 690 mg/l Proline, 1.0 mg/lThiamine HCl (Harwood et al., 2009) supplemented with 2 mg/l Picloram, 0.5 mg/l 2,4-Dichlorophenoxyacetic acid (2,4-D). Regeneration was under low light (140 μmol.m-2.s-1) conditions on MS medium with 0.5 mg/l Zeatin and 2.5 mg/l CuSO45H2O.

Primary transgenic plants (T0) were analyzed by PCR across the region of interest. The sequences for the forward and reverse primers used for the screening in T0 were 5′GCCGCCAT GACGATCTCCGAG3′ and 5′GGACGCGAGGGACGCGAG3′, respectively (Rey et al., 2017), followed by direct sequencing. The PCR was performed using RedTaq ReadyMix PCR Reaction

Mix (Sigma, St. Louis, MO, USA; R2523) according to the manufacturer's instructions. PCR conditions were: 3 min 95C, 35 cycles of 15 s at 95C, 15 s at 58C and 30 s at 72C. T0 plants with edits in *TaZIP4-B2* were progressed to the T1 generation and 24 T1 seedlings from each original T0 plant were analyzed in the same way for the presence of edits.

Statistical Analyses

Statistical analyses were performed using STATISTIX 10.0 software (Analytical Software, Tallahassee, FL, USA). Analysis of variance (ANOVA) in *Tazip4-B2 ph1b* mutant-rye hybrids, *Tazip4-B2* TILLING mutant-*Ae. variabilis* hybrids and *Tazip4-B2* CRISPR mutant-*Ae. variabilis* hybrids was based on a completely randomized design. Several transformations were carried out: tangent (ring bivalents), arcsine (trivalents), and logarithm (double CO) transformations in the analysis of the effect of absence of each macronutrients in homoeologous CO frequency in *Tazip4-B2 ph1b* mutant-rye hybrids; exponential (ring bivalents) transformation in *Tazip4-B2 ph1b* mutant-*Ae. variabilis* hybrids; exponential (rod bivalents, rings bivalents and trivalents) transformation in *Tazip4-B2* TILLING mutant (Cad1691)-*Ae. variabilis* hybrids; and square root (ring bivalents) and exponential (trivalents) transformations in *Tazip4-B2* TILLING mutant (Cad0348)-*Ae. variabilis* hybrids. Means were separated using the Least Significant Difference (LSD) test with a probability level of 0.05. Both *Tazip4-B2* CRISPR mutant lines and *Tazip4-B2* CRISPR mutant-*Ae. variabilis* hybrids were analyzed by the Kruskal–Wallis test (non-parametric one-way analysis of variance). Means were separated using the Dunn's test with a probability level of 0.05.

RESULTS

Magnesium Increases Homoeologous COs in *Tazip4-B2 ph1b* Mutant-Rye Hybrids

The *Tazip4-B2 ph1b* mutant-rye hybrids were obtained by crosses between the hexaploid wheat cv. Chinese Spring *Tazip4-B2 ph1b* mutant and rye. These hybrids were used to analyse which macronutrient (NH_4 H_2PO_4, KNO_3, Ca $(NO_3)2{\cdot}4H_2O$ or Mg $SO_4{\cdot}7H_2O$) present within in the Hoagland solution detailed in Martín et al. (2017) could be responsible for the increased CO number observed in the *Tazip4-B2 ph1b* mutant-rye hybrids. To assess the effect of the absence of each macronutrient in homoeologous CO frequency in meiotic metaphase I, we irrigated several *Tazip4-B2 ph1b* mutant-rye hybrids with: (1) Hoagland solution; (2) water alone; (3) Hoagland solution minus KNO_3; (4) Hoagland solution minus Ca $(NO_3)_2{\cdot}4H_2O$; (5) Hoagland solution minus NH_4 H_2PO_4; (6) Hoagland solution minus $MgSO_4{\cdot}7H_2O$ ($MgSO_4{\cdot}7H_2O$ is designed as Mg^{2+} in the manuscript) (**Table 1**). The absence of each Hoagland solution macronutrient caused a slight increase in homoeologous CO frequency, except for the treatment lacking Mg^{2+}, where a significant decrease in homoeologous CO frequency per meiocyte was observed at meiotic metaphase I in these hybrids (**Table 1**). No significant differences in CO frequency at metaphase I were observed between hybrids treated with water alone and those

TABLE 1 | Effect of the absence of each macronutrient in the Hoagland solution on the homoeologous CO frequency of *T. aestivum* cv. Chinese Spring *Tazip4-B2 ph1b* mutant-rye hybrids.

	No. of cell examined	Univalents	Rod bivalents	Ring bivalents	Trivalents	Chiasma frequency	
		Mean ± SE (Range)	Mean ± SE (Range)	Mean ± SE (Range)	Mean ± SE (Range)	Mean ± SE (Range)	Mean ± SE (Range)
						Single chiasma	Double chiasmata
Hoagland solution	109	12.36 ± 0.21^{c} (7–18)	4.39 ± 0.14^{a} (2–8)	2.57 ± 0.10^{abc} (0–5)	0.58 ± 0.07^{a} (0–3)	10.74 ± 0.16^{a} (7–14)	12.03 ± 0.22^{a} (7–18)
Water alone	108	15.93 ± 0.16^{a} (12–20)	4.03 ± 0.13^{ab} (1–7)	1.68 ± 0.09^{bc} (0–4)	0.22 ± 0.04^{bc} (0–1)	7.91 ± 0.13^{d} (5–10)	8.15 ± 0.15^{d} (5–12)
Hoagland solution - NH_4 H_2PO_4	92	13.61 ± 0.22^{b} (8–17)	3.83 ± 0.14^{b} (2–8)	2.78 ± 0.13^{a} (0–6)	0.39 ± 0.06^{ab} (0–2)	10.25 ± 0.18^{b} (7–14)	11.03 ± 0.23^{b} (7–17)
Hoagland solution - KNO_3	93	13.86 ± 0.22^{b} (6–18)	4.34 ± 0.16^{a} (2–8)	2.35 ± 0.12^{abc} (0–5)	0.25 ± 0.05^{c} (0–2)	9.57 ± 0.18^{c} (7–16)	9.96 ± 0.19^{c} (7–16)
Hoagland solution - $Ca(NO_3)2{\cdot}4H_2O$	102	13.84 ± 0.20^{b} (9–18)	4.14 ± 0.13^{ab} (1–7)	2.50 ± 0.09^{c} (0–4)	0.29 ± 0.05^{bc} (0–2)	9.79 ± 0.15^{c} (7–14)	10.12 ± 0.17^{c} (7–15)
Hoagland solution - Mg $SO_4{\cdot}7H_2O$	90	15.63 ± 0.24^{a} (10–20)	4.12 ± 0.16^{ab} (1–8)	1.68 ± 0.13^{ab} (0–4)	0.26 ± 0.06^{bc} (0–2)	8.09 ± 0.20^{d} (5–12)	8.62 ± 0.22^{d} (5–13)
P-value		0.0000	0.0538	0.0592	0.0516	0.0000	0.0000

Frequencies of univalents, bivalents, trivalents and chiasma frequency (single and double chiasmata) were scored at meiotic metaphase I in Tazip4-B2 ph1b mutant-rye hybrids. Values in parenthesis indicate range of variation between cells. P < 0.05 indicates significant differences according to LSD test. Different letters indicate significant differences between treatments.

treated with the Hoagland solution minus Mg^{2+} [a mean of 7.91 chiasmata for hybrids treated with water alone and 8.09 chiasmata for hybrids treated with Hoagland solution minus Mg^{2+} (**Table 1**)].

Additionally, we scored all meiocytes for the occurrence of double chiasmata in the metaphase I chromosomal configurations (examples highlighted by arrows in **Figure S1**). When double chiasmata were considered in the chiasma frequency, a mean of 8.15 chiasmata and 8.62 chiasmata was observed respectively in *Tazip4-B2 ph1b* mutant-rye hybrids treated with water alone, and those treated with the Hoagland solution minus Mg^{2+} (**Table 1**). As expected, no significant differences were observed between the two treatments when double chiasmata were considered in these *Tazip4-B2 ph1b* hybrids.

Once the absence of Mg^{2+} was demonstrated to decrease homoeologous CO frequency in *Tazip4-B2 ph1b* mutant-rye hybrids, the effect of irrigating with only Mg^{2+} present at a final concentration of 1 mM in water rather than in the Hoagland solution, was also analyzed on homoeologous COs in *Tazip4-B2 ph1b* mutant-rye hybrids (**Figure 1**). Treatment with a solution containing only Mg^{2+} also increased homoeologous COs at metaphase I per meiocyte in these hybrids, showing no significant difference in comparison to the Hoagland solution treatment. A mean of 11.09 chiasmata was observed after treatment with 1 mM Mg^{2+} in water, and 10.74 chiasmata after treatment with the Hoagland solution (**Figure 1**), when a single chiasma was considered. A similar situation was seen when double chiasmata were considered: no significant differences were observed in homoeologous COs per meiocyte in *Tazip4-B2 ph1b* mutant-rye hybrids after treatment with either 1 mM Mg^{2+} or Hoagland solutions (**Figure 1**).

The concentration of Mg^{2+} was subsequently increased to a final concentration of 2 mM to assess whether the number of homoeologous COs could be increased further (**Figure 1**). Surprisingly, numbers of COs were reduced under these conditions (mean 11.09 for 1 mM Mg^{2+} and 8.84 for 2 mM Mg^{2+} treatments respectively, when single chiasma were considered, and 12.11 and 9.90, respectively, when double chiasmata were considered).

In addition to irrigating the plants with either Hoagland or Mg^{2+} solutions, we analyzed the effect of treatment with 1 mM Mg^{2+} in water following injection into the tillers of *Tazip4-B2 ph1b* mutant-rye hybrids. Injections were made just above each spike. Once again, homoeologous CO frequency was significantly increased in hybrids treated with 1 mM Mg^{2+} when the solution was injected into the tiller (**Table 2**). A mean of 8.98 chiasmata in hybrids treated with water alone and 10.60 chiasmata in hybrids treated with 1 mM Mg^{2+} was observed in the hybrids considering a single chiasma (**Table 2**) and a mean of 9.67 chiasmata and 11.30 chiasmata considering double chiasmata (**Table 2**).

Magnesium Increases Homoeologous COs in *Tazip4-B2 ph1b* Mutant-*Ae. variabilis* Hybrids

The addition of Mg^{2+} is thus identified as responsible for the increase in homoeologous CO at meiotic metaphase I in *Tazip4-B2 ph1b* mutant-rye hybrids. We then assessed the effect of 1 mM Mg^{2+} on *T. aestivum* cv. Chinese spring *Tazip4-B2 ph1b* mutant-*Ae. variabilis* hybrids. Firstly, we scored the number of univalents, bivalents and multivalents, and total chiasma frequency in this hybrid, to compare the level of chiasma

A

	No. of cell examined	Univalents	Rod bivalents	Ring bivalents	Trivalents	Chiasma frequency	
		Mean ± SE (Range)	Mean ± SE (Range)	Mean ± SE (Range)	Mean ± SE (Range)	Mean ± SE (Range)	Mean ± SE (Range)
						Single Chiasma	Double Chiasmata
With Hoagland solution	109	12.36 ± 0.21^{b} (7-18)	4.39 ± 0.14^{a} (2-8)	2.57 ± 0.10^{a} (0-5)	0.58 ± 0.07^{b} (0-3)	10.74 ± 0.16^{a} (7-14)	12.03 ± 0.22^{a} (7-18)
With 1mM Mg^{2+}	117	12.26 ± 0.25^{b} (4-17)	3.88 ± 0.13^{b} (1-7)	2.81 ± 0.10^{a} (0-5)	0.79 ± 0.07^{a} (0-3)	11.09 ± 0.19^{a} (7-18)	12.11 ± 0.23^{a} (7-19)
With 2mM Mg^{2+}	107	14.62 ± 0.24^{a} (7-20)	4.09 ± 0.14^{ab} (1-7)	1.89 ± 0.12^{b} (0-5)	0.46 ± 0.06^{b} (0-2)	8.84 ± 0.18^{b} (6-14)	9.90 ± 0.21^{b} (6-15)
P-value		*0.0000*	*0.0316*	*0.0000*	*0.0022*	*0.0000*	*0.0000*

B

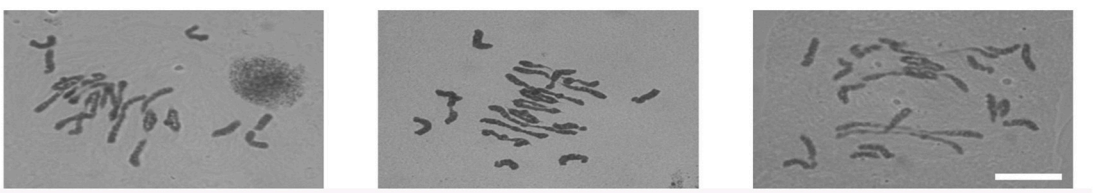

FIGURE 1 | Effect of either 1 mM or 2 mM Mg^{2+} on homoeologous CO frequency of *T. aestivum* cv. Chinese Spring *Tazip4-B2 ph1b* mutant-rye hybrids. **(A)** Frequencies of univalents, bivalents, trivalents, and chiasma frequency (single and double chiasmata) were scored at meiotic metaphase I in *Tazip4-B2 ph1b* mutant-rye hybrids treated with either Hoagland solution, 1 mM Mg^{2+} or 2 mM Mg^{2+}solution. Values in parenthesis indicate range of variation between cells. $P < 0.05$ indicates significant differences according to LSD test. Different letters indicate significant differences between treatments. **(B)** Representative meiotic configurations of *Tazip4-B2 ph1b* mutant-rye hybrids. From left to right: treatment with Hoagland solution, 1 mM Mg^{2+}or 2 mM Mg^{2+} solution. Bar: 20 μm.

TABLE 2 | Effect of injecting 1 mM Mg^{2+} solution into the tillers of *Tazip4-B2 ph1b* mutant-rye hybrids.

	No. of cell examined	Univalents	Rod bivalents	Ring bivalents	Trivalents	Chiasma frequency	
		Mean ± SE (Range)	Mean ± SE (Range)	Mean ± SE (Range)	Mean ± SE (Range)	Mean ± SE (Range)	Mean ± SE (Range)
						Single chiasma	Double chiasmata
Water alone	87	15.02 ± 0.26^{a} (3–20)	3.43 ± 0.16^{b} (0–7)	2.12 ± 0.10 (0–4)	0.63 ± 0.08 (0–3)	8.98 ± 0.18^{b} (6–16)	9.67 ± 0.21^{b} (6–17)
With 1 mM Mg^{2+}	79	12.32 ± 0.26^{b} (5–18)	4.32 ± 0.17^{a} (1–8)	2.37 ± 0.12 (0–5)	0.77 ± 0.08 (0–3)	10.60 ± 0.19^{a} (7–16)	11.30 ± 0.22^{a} (8–18)
P-value		0.0000	0.0001	0.1079	0.2312	0.0000	0.0000

Frequencies of univalents, bivalents, trivalents, and chiasma frequency (single and double chiasmata) were scored at meiotic metaphase I in Tazip4-B2 ph1b mutant-rye hybrids treated with water alone and with 1 mM Mg^{2+} solution. Values in parenthesis indicate range of variation between cells. $P < 0.05$ indicates significant differences according to LSD test. Different letters indicate significant differences between treatments.

frequency to that previously reported by Kousaka and Endo (2012) in *T. aestivum* cv. Chinese spring-*Ae. variabilis* hybrids in the absence of chromosome 5B. We observed a similar chiasma frequency in our hybrid (mean 14.15 chiasmata per meiocyte), to that previously reported in *T. aestivum* cv. Chinese spring-*Ae. variabilis* hybrids in the absence of chromosome 5B (mean of 14.09 chiasmata per meiocyte), confirming a similar level of meiotic metaphase I configuration in these hybrids.

We then analyzed the effect of treatment with water alone and with either 1 mM Mg^{2+} solution or complete Hoagland solution on the *Tazip4-B2 ph1b* mutant-*Ae. variabilis* hybrids. The total number of COs was significantly higher after treatment with 1 mM Mg^{2+} than after treatment with water alone (without Mg^{2+} control), both in the case of single chiasma and double chiasmata, showing a mean of 15.31 and 14.15 chiasmata in the case of single chiasma, and a mean of 16.54 and 15.10 chiasmata in the case of double chiasmata, respectively (**Figure 2**). The number of univalents was significantly decreased and the number of trivalents was significantly increased when the plants were treated with 1 mM Mg^{2+} solution in comparison to when Mg^{2+} was absent (a mean of 11.14 and 1.99, respectively, after treatment with 1 mM Mg^{2+} and a mean of 12.49 and 1.60, respectively, after treatment with water alone were observed in **Figure 2**). With regard to the Hoagland solution treatment, significant differences were observed between hybrids treated with water alone and hybrids treated with Hoagland solution (**Figure 2**). Hoagland solution treatment showed the highest chiasma frequency, followed by 1 mM Mg^{2+} and water alone [means of 16.53, 15.31, and 14.15 chiasmata were observed, respectively, when a single chiasma was considered, and means of 18.05, 16.54, and 15.10 chiasmata were observed, respectively, when double chiasmata were considered (**Figure 2**)].

Magnesium Increases Homoeologous COs in Wheat *Tazip4-B2* TILLING Mutant-*Ae. variabilis* Mutant Hybrids

Recently we reported that *Tazip4-B2* TILLING mutants crossed with *Ae. variabilis* exhibited homoeologous COs at meiotic metaphase I (Rey et al., 2017). We therefore decided to analyse whether the level of homoeologous COs induced by *Tazip4-B2* TILLING mutants was also affected by treatment with 1 mM Mg^{2+} solution. To assess the effect of 1 mM Mg^{2+} on homoeologous CO frequency at metaphase I, we added 100 mL per plant of a solution of either 1 mM Mg^{2+} in water or Hoagland solution once a week to the soil in which these hybrids were growing. In this experiment, we analyzed both *Tazip4-B2* TILLING mutant lines (Cad1691 and Cad0348) (Rey et al., 2017), crossed with *Ae. variabilis*. Both TILLING mutant hybrids showed a significant increase in chiasma frequency after treatment with 1 mM Mg^{2+}, compared to chiasma frequency obtained in both the hybrids treated with water alone. The *Tazip4-B2* TILLING mutant (Cad1691)-*Ae. variabilis* and the *Tazip4-B2* TILLING mutant (Cad0348)-*Ae. variabilis* hybrids showed means of 13.41 and 13.66 single chiasma frequency,

A

	No. of cell examined	Univalents	Rod bivalents	Ring bivalents	Trivalents	Tetravalents	Pentavalents	Chiasma frequency	
		Mean ± SE (Range)	Mean ± SE (Range)	Mean ± SE (Range)	Mean ± SE (Range)	Mean ± SE (Range)	Mean ± SE (Range)	Mean ± SE (Range)	Mean ± SE (Range)
								Single Chiasma	Double Chiasmata
Without 1mM Mg^{2+}	136	12.49 ± 0.59^{a} (4-22)	6.54 ± 0.33^{a} (2-10)	1.84 ± 0.20^{c} (0-5)	1.60 ± 0.21^{b} (0-4)	0.18 ± 0.08 (0-2)	0.05 ± 0.04 (0-1)	14.15 ± 0.42^{c} (8-19)	15.10 ± 0.53^{c} (8-23)
With 1mM Mg^{2+}	175	11.14 ± 0.22^{b} (1-17)	6.32 ± 0.13^{a} (2-11)	2.11 ± 0.10^{b} (0-6)	1.99 ± 0.08^{a} (0-4)	0.15 ± 0.03 (0-2)	0.08 ± 0.02 (0-1)	15.31 ± 0.16^{b} (11-23)	16.54 ± 0.18^{b} (11-23)
With Hoagland solution	104	10.44 ± 0.27^{b} (1-17)	5.74 ± 0.16^{b} (2-11)	2.86 ± 0.13^{a} (0-5)	2.01 ± 0.09^{a} (0-4)	0.20 ± 0.04 (0-2)	0.11 ± 0.03 (0-1)	16.53 ± 0.21^{a} (12-23)	18.05 ± 0.26^{a} (12-24)
P-value		*0.0000*	*0.0012*	*0.0000*	*0.0008*	*0.6642*	*0.2913*	*0.0000*	*0.0000*

B

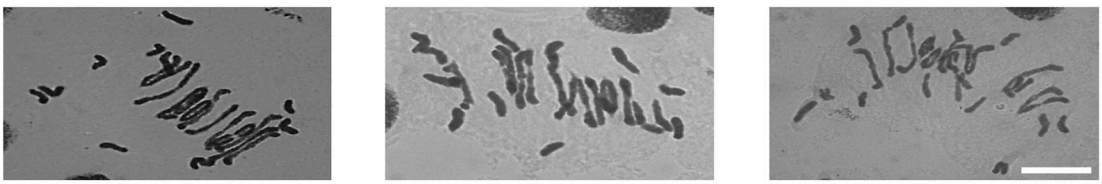

FIGURE 2 | Effect of either 1 mM Mg^{2+} or Hoagland solution on homoeologous CO frequency of *T. aestivum* cv. Chinese Spring *Tazip4-B2 ph1b* mutant-*Ae. variabilis* hybrids. **(A)** Frequencies of univalents, bivalents, trivalents, tetravalents, pentavalents and chiasma frequency (single and double chiasmata) were scored at meiotic metaphase I in *Tazip4-B2 ph1b* mutant-*Ae. variabilis* hybrids treated with either 1 mM Mg^{2+} or Hoagland solution. Values in parenthesis indicate range of variation between cells. $P < 0.05$ indicates significant differences according to LSD test. Different letters indicate significant differences between treatments. **(B)** Representative meiotic configurations of *Tazip4-B2 ph1b* mutant-*Ae. variabilis* hybrids. From left to right: water alone, 1 mM Mg^{2+} treatment and Hoagland solution treatment. Bar: 20 μm.

respectively, after treatment with 1 mM Mg^{2+} and means of 12.21 and 12.23 single chiasma frequency, respectively, in water alone (**Table 3**; **Figure S2**). Significant differences were also observed when double chiasmata were scored in both mutant lines (**Table 3**; **Figure S2**). Numbers of univalents and trivalents were also affected by treatment with 1 mM Mg^{2+} in both mutant lines as in the *Tazip4-B2 ph1b* mutant-*Ae. variabilis* hybrids described in the previous section. Numbers of univalents were significantly decreased both in *Tazip4-B2* TILLING mutant (Cad1691)-*Ae. variabilis* and *Tazip4-B2* TILLING mutant (Cad0348)-*Ae. variabilis* hybrids treated with 1 mM Mg^{2+} [means of 12.74 and 12.11 univalents respectively with Mg^{2+} and means of 14.74 and 14.63 univalents respectively with water alone (**Table 3**)]. Numbers of trivalents were significantly increased both in wheat (Cad1691)-*Ae. variabilis* and wheat (Cad0348)-*Ae. variabilis* hybrids, after treatment with 1 mM Mg^{2+} [means of 1.63 and 1.93 trivalents respectively with Mg^{2+}, and means of 1.05 and 1.27 trivalents respectively with water alone (**Table 3**)].

Finally, we assessed the effect of treating with Hoagland solution and with water alone, finding significant differences in homoeologous COs between the two treatments, both in *Tazip4-B2* TILLING mutant (Cad1691)-*Ae. variabilis* and *Tazip4-B2* TILLING mutant (Cad0348)-*Ae. variabilis* hybrids. Numbers of univalents and trivalents were also affected to the same extent (**Table 3**). In the *Tazip4-B2* TILLING mutant (Cad1691)-*Ae. variabilis* hybrid, means of 14.74 univalents and 1.05 trivalents were observed in hybrids treated with water alone, and means of 11.94 univalents and 1.50 trivalents observed in hybrids treated with Hoagland solution (**Table 3**). In the *Tazip4-B2* TILLING mutant (Cad0348)-*Ae. variabilis* hybrid, means of 14.63 univalents and 1.27 trivalents were observed in hybrids with water alone and means of 12.48 univalents and 1.76 trivalents in hybrids treated with Hoagland solution (**Table 3**).

Phenotypic Analysis of *Tazip4-B2* Mutants Generated by CRISPR/Cas9 System

Firstly, eighty-one primary transgenic plants (T0) were analyzed by PCR followed by direct sequencing. Four plants were identified with edits in the target region. One plant had a perfect 115 bp deletion between guides G11 and G12. Twenty-four T1 plants from this line were screened and 5 homozygous edited plants with the 115 bp deletion were recovered. These plants were used to score the number of univalents, bivalents, and multivalents, and total chiasma frequency in the *Tazip4-B2* mutant CRISPR lines (**Figure 3**). Wild-type Fielder lines were used as control plants (**Figure 3**). The *Tazip4-B2* CRISPR mutant lines exhibited a significant reduction in ring bivalents, from a mean of 18.33 to 14.84 in the wild-type Fielder and CRISPR mutant lines respectively (**Figure 3**). A significant increase in the number of univalents and rod bivalents was also observed, from means of 0.51 univalents and 2.38 rod bivalents in the wild-type Fielder line, to means of 1.16 univalents and 4.93 rod bivalents in the CRISPR mutant lines (**Figure 3**). This indicates a significant reduction in homologous COs in these *Tazip4-B2* mutant lines (**Figure 3**). Chiasma frequency decreased from a mean of 39.07 single chiasma and 40.50 double chiasmata in the wild-type Fielder line, to a mean of 35.55 single chiasma and 37.11 double chiasmata in the *Tazip4-B2* CRISPR mutant (**Figure 3**).

TABLE 3 | Effect of either 1 mM Mg^{2+} or Hoagland solution on the homoeologous CO frequency of *T. aestivum* cv. Cadenza (Cad1691-*Tazip4-B2*)-*Ae. variabilis* and *T. aestivum* cv. Cadenza (Cad0348-*Tazip4-B2*)-*Ae. variabilis* hybrids.

		No. of cell examined	Univalents	Rod bivalents	Ring bivalents	Trivalents	Tetravalents	Pentavalents	Chiasma frequency	
			Mean ± SE (Range)	Mean ± SE (Range)	Mean ± SE (Range)	Mean ± SE (Range)	Mean ± SE (Range)	Mean ± SE (Range)	Mean ± SE (Range) Single chiasma	Mean ± SE (Range) Double chiasmata
Wateralone*	Cad1691 × *Ae. variabilis* hybrids	106	14.74 ± 0.29^{a} (7–26)	6.75 ± 0.17 (3–11)	1.26 ± 0.08 (0–4)	1.05 ± 0.08^{b} (0–4)	0.22 ± 0.04 (0–2)	0.03 ± 0.02 (0–1)	12.21 ± 0.19^{b} (8–18)	12.74 ± 0.21^{b} (8–20)
	Cad0348 × *Ae. variabilis* hybrids	102	14.63 ± 0.28^{a} (6–21)	6.64 ± 0.18 (3–10)	1.12 ± 0.10 (0–4)	1.27 ± 0.11^{b} (0–4)	0.21 ± 0.04 (0–1)	0.05 ± 0.02 (0–1)	12.23 ± 0.20^{b} (7–19)	12.68 ± 0.23^{b} (7–21)
With 1 mM Mg^{2+}	Cad1691 × *Ae. variabilis* hybrids	95	12.74 ± 0.33^{b} (5–19)	7.06 ± 0.20 (2–11)	1.18 ± 0.11 (0–3)	1.63 ± 0.13^{a} (0–5)	0.17 ± 0.30 (0–1)	0.04 ± 0.02 (0–1)	13.41 ± 0.22^{a} (8–18)	13.75 ± 0.23^{a} (8–19)
	Cad0348 × *Ae. variabilis* hybrids	110	12.11 ± 0.32^{b} (3–20)	6.93 ± 0.18 (1–12)	1.51 ± 0.11 (0–4)	1.93 ± 0.11^{a} (0–5)	0.24 ± 0.04 (0–2)	0.07 ± 0.02 (0–1)	14.21 ± 0.23^{a} (9–21)	14.90 ± 0.25^{a} (10–22)
With Hoagland solution	Cad1691 × *Ae. variabilis* hybrids	118	11.94 ± 0.33^{b} (2–20)	6.76 ± 0.23 (0–12)	1.17 ± 0.10 (0–4)	1.50 ± 0.11^{a} (0–5)	0.26 ± 0.05 (0–2)	0.04 ± 0.02 (0–1)	13.66 ± 0.21^{a} (9–20)	14.14 ± 0.22^{a} (9–21)
	Cad0348 × *Ae. variabilis* hybrids	142	12.48 ± 0.25^{b} (2–20)	6.70 ± 0.17 (1–12)	1.37 ± 0.09 (0–4)	1.76 ± 0.10^{a} (0–5)	0.23 ± 0.04 (0–2)	0.04 ± 0.02 (0–1)	13.84 ± 0.19^{a} (9–21)	14.30 ± 0.21^{a} (9–22)
P-value	Cad1691 × *Ae. variabilis* hybrids		0.0000	0.1930	0.6630	0.0026	0.3278	0.9376	0.0000	0.0000
	Cad0348 × *Ae. variabilis* hybrids		0.0000	0.3220	0.5967	0.0003	0.9720	0.3650	0.0000	0.0000

*Frequencies of univalents, bivalents, trivalents, tetravalents, pentavalents, and chiasma frequency (single and double chiasmata) were scored at meiotic metaphase I in Tazip4-B2 TILLING mutant-Ae. variabilis hybrids treated with either 1 mM Mg^{2+} or Hoagland solution. Values in parenthesis indicate range of variation between cells. $P < 0.05$ indicates significant differences according to LSD test. *This data published in Rey et al. (2017). Different letters indicate significant differences between treatments.*

Magnesium Also Increases Homoeologous COs in Wheat *Tazip4-B2* CRISPR Mutant-*Ae. variabilis* Mutant Hybrids

For this study, a wild-type Fielder and a *Tazip4-B2* CRISPR Fielder mutant line were crossed with *Ae. variabilis* to assess the level of homoeologous COs in the resulting hybrids (**Table S2**). Frequency of univalents, bivalents and multivalents, and total chiasma frequency were scored at meiotic metaphase I (**Table S2**). *Tazip4-B2* CRISPR mutant hybrids exhibited a significant increase in single chiasma frequency, from a mean of 3.15 in the wild-type Fielder-*Ae. variabilis* hybrid to 16.66 in the *Tazip4-B2* CRISPR-*Ae. variabilis* hybrid (**Table S2**). Double chiasma frequency was also increased in the *Tazip4-B2* CRISPR mutant hybrids (**Table S2**). There was also a similar increase in the chiasma frequency to that reported previously in *Tazip4-B2* TILLING-*Ae. variabilis* hybrids (Rey et al., 2017).

Having observed the effect of treatment with Mg^{2+} on homoeologous CO frequency in the *Tazip4-B2* TILLING mutant hybrids, we also analyzed the effect of this ion on *Tazip4-B2* CRISPR mutants-*Ae. variabilis* hybrids. We added 100 mL of a solution of 1 mM Mg^{2+} in water or Hoagland solution once a week to the soil in which the hybrids were growing. As expected, the addition of nutrients to these mutant hybrids caused a significant increase in chiasma frequency (**Table 4**; **Figure S2**). *Tazip4-B2* CRISPR-*Ae. variabilis* hybrids treated with water alone exhibited means of 16.66 single chiasma frequency and 18.10 double chiasma frequency. Addition of 1 mM Mg^{2+} caused a significant increase in chiasma frequency of these mutant hybrids (means of 17.67 and 18.75 single and double chiasma frequency respectively) (**Table 4**). Also, the addition of Hoagland solution increased the homoeologous COs in these *Tazip4-B2* CRISPR hybrids. Means of 18.34 and 19.82 single and double chiasma frequency respectively, were observed in those plants treated with Hoagland solution (**Table 4**).

DISCUSSION

Introgression of genetic material from relative species into bread wheat has been used in plant breeding for over 50 years, although classical plant breeding methods to introgress wild relative segments into wheat are both inefficient and time consuming (Ko et al., 2002). Recent availability of SNP based arrays, combined with classical cytogenetic approaches, significantly enhanced our ability to exploit wild relatives (King et al., 2017a,b), using lines carrying a deletion of either the whole of chromosome 5B, or a smaller 70 Mb segment (*ph1b*) (Riley and Chapman, 1958; Sears and Okamoto, 1958; Sears, 1977), to increase the level of homoeologous crossovers between wild relatives and wheat chromosomes. Recombination between wild relative chromosomes and wheat chromosomes is, however, still limited. Thus, there is a need to find abiotic or biotic treatments such as temperature, nutritional availability, DNA-damaging agents, among others (Lambing et al., 2017) to enhance recombination. Martín et al. (2017) recently reported an alternative tool to increase CO number in *Tazip4-B2 ph1b* mutant-rye hybrids, using the addition of a Hoagland solution

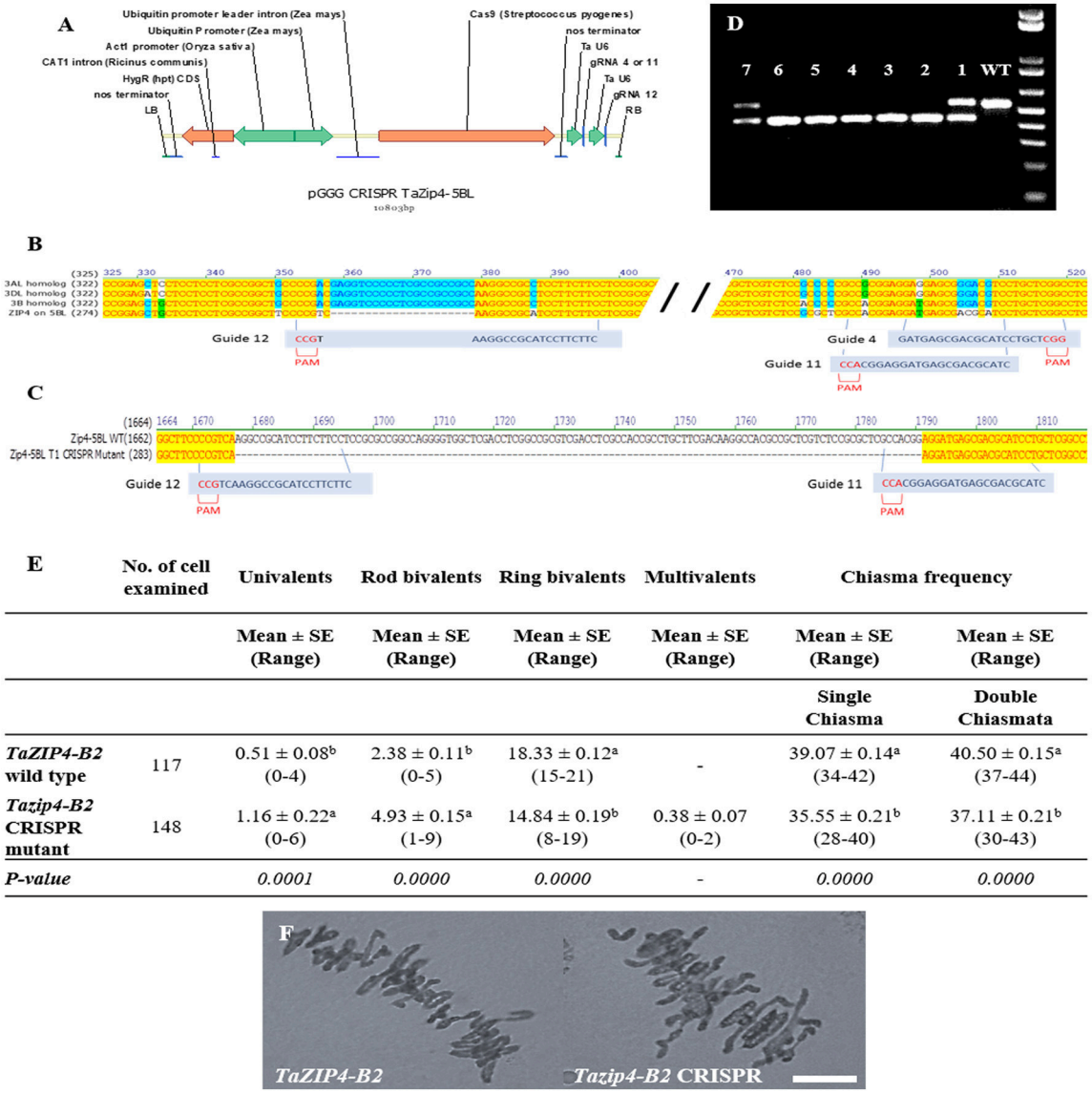

E

	No. of cell examined	Univalents	Rod bivalents	Ring bivalents	Multivalents	Chiasma frequency	
		Mean ± SE (Range)	Mean ± SE (Range)	Mean ± SE (Range)	Mean ± SE (Range)	Mean ± SE (Range)	Mean ± SE (Range)
						Single Chiasma	Double Chiasmata
***TaZIP4-B2* wild type**	117	0.51 ± 0.08^{b} (0-4)	2.38 ± 0.11^{b} (0-5)	18.33 ± 0.12^{a} (15-21)	-	39.07 ± 0.14^{a} (34-42)	40.50 ± 0.15^{a} (37-44)
***Tazip4-B2* CRISPR mutant**	148	1.16 ± 0.22^{a} (0-6)	4.93 ± 0.15^{a} (1-9)	14.84 ± 0.19^{b} (8-19)	0.38 ± 0.07 (0-2)	35.55 ± 0.21^{b} (28-40)	37.11 ± 0.21^{b} (30-43)
P-value		*0.0001*	*0.0000*	*0.0000*	-	*0.0000*	*0.0000*

FIGURE 3 | Development and phenotypic analysis of *Tazip4-B2* CRISPR mutants generated using RNA-guided Cas9. **(A)** Schematic of the structure of the pGGG CRISPR *TaZip4-B2* vector used in this study. **(B)** Alignment of all copies of the *ZIP4* gene in wheat showing sequences and positions of the three sgRNAs designed to specifically target *TaZIP4-B2* with their corresponding protospacer-adjacent motif (PAM). **(C)** Alignment of *TaZIP4-B2* wild type and *Tazip4-B2 CRISPR* mutant sequences sowing the localization of the large deletion (115 bp) in *TaZIP4-B2*. **(D)** Genotypic assays for the identification of homozygous edited lines (lines: #2, #3, #4, #5, and #6) and heterozygous lines (lines: #1 and #7). Wild-type Fielder (WT) was used as a control line. **(E)** Frequencies of univalents, bivalents and multivalents, and total chiasma frequency (single and double chiasmata) were scored at meiotic metaphase I in wild-type Fielder and *Tazip4-B2* CRISPR mutant. Values in parenthesis indicate range of variation between cells. $P < 0.05$ indicates significant differences according to Dunn's test. Different letters indicate significant differences between treatments. **(F)** Representative meiotic metaphase I configurations of wild-type Fielder and *Tazip4-B2* CRISPR Fielder mutants. Left: wheat cv. Fielder and right: *Tazip4-B2* CRISPR mutant. Bar: 20 μm.

to the soil in which the plants are grown. Martín et al. (2017) also showed that the presence of the Hoagland solution did not affect the homoeologous CO number in wild-type wheat-rye hybrids.

Here, we report the successful identification of the particular Hoagland solution constituent responsible for the observed increase in homoeologous CO frequency. After analyzing *Tazip4-B2 ph1b* mutant-rye hybrids in the absence of each separate Hoagland solution macronutrient, we observed a significant reduction in homoeologous CO frequency when the Mg^{2+} ion was absent. This suggests that the Mg^{2+} ion is mainly responsible for the effect of Hoagland solution on homoeologous COs described previously by Martín et al. (2017). These observations were obtained after cytogenetic analysis of meiotic configurations at meiotic metaphase I. The analysis involved scoring single and double chiasmata in the chromosomal structures (**Figure S1**). Single chiasma counting has commonly been used in many

TABLE 4 | Effect of either 1 mM Mg^{2+} or Hoagland solution on the homoeologous CO frequency of wheat *Tazip4-B2* CRISPR-*Ae. variabilis* mutant hybrids.

	No. of cell examined	Univalents	Rod bivalents	Ring bivalents	Trivalents	Tetravalents	Pentavalents	Hexavalents	Chiasma frequency	
		Mean ± SE (Range)	Mean ± SE (Range)	Mean ± SE (Range)	Mean ± SE (Range)	Mean ± SE (Range)	Mean ± SE (Range)	Mean ± SE (Range)	Mean ± SE (Range) Single chiasma	Mean ± SE (Range) Double chiasmata
Water alone	124	9.64 ± 0.27^{a} (3–17)	5.64 ± 0.17^{b} (2–10)	1.94 ± 0.11^{b} (0–6)	2.37 ± 0.11 (0–6)	0.52 ± 0.06 (0–3)	0.20 ± 0.04^{a} (0–2)	0.00 ± 0.00 (0–0)	16.66 ± 0.21^{c} (11–22)	18.10 ± 0.23^{c} (12–24)
With 1 mM Mg^{2+}	135	7.92 ± 0.25^{b} (0–14)	6.19 ± 0.15^{a} (3–11)	2.02 ± 0.09^{b} (0–6)	2.68 ± 0.09 (0–3)	0.50 ± 0.06 (0–2)	0.10 ± 0.01^{b} (0–1)	0.01 ± 0.01 (0–1)	17.67 ± 0.17^{b} (14–23)	18.75 ± 0.20^{b} (14–24)
With Hoagland solution	125	7.90 ± 0.28^{b} (0–15)	5.56 ± 0.17^{b} (1–11)	2.82 ± 0.11^{a} (0–6)	2.53 ± 0.11 (0–5)	0.59 ± 0.07 (0–3)	0.08 ± 0.03^{b} (0–2)	0.00 ± 0.00 (0–0)	18.34 ± 0.21^{a} (14–24)	19.82 ± 0.23^{a} (15–25)
P-value		0.0000	0.0121	0.0000	0.1021	0.5929	0.0259	0.1575	0.0000	0.0000

Frequencies of univalents, bivalents, trivalents, tetravalents, pentavalents, and chiasma frequency (single and double chiasmata) were scored at meiotic metaphase I in Tazip4-B2 CRISPR mutant-Ae. variabilis hybrids treated with either 1 mM Mg^{2+} or Hoagland solution. Values in parenthesis indicate range of variation between cells. $P < 0.05$ indicates significant differences according to LSD test. Different letters indicate significant differences between treatments.

studies to measure chiasma frequency in wheat (Dhaliwal et al., 1977; Sears, 1977; Roberts et al., 1999). However, other studies have suggested that double chiasmata may occur in these chromosomal configurations (Gennaro et al., 2012; Dreissig et al., 2017). Double chiasmata were considered in the present study, as a high number of MLH1 sites were previously reported in *Tazip4-B2 ph1b* mutant-rye hybrids in Martín et al. (2014). In our studies, up to 19 chiasmata were scored in *Tazip4-B2 ph1b* mutant-rye hybrids, which is similar to the number of MLH1 sites observed previously (Martín et al., 2014).

The effect of treatment with a solution of 1mM Mg^{2+} in water, was analyzed to confirm whether that the Mg^{2+} ion was responsible for the increase in homoeologous COs observed in these hybrids. The effect of treatment with this solution was assessed either by irrigation of, or injection into *Tazip4-B2 ph1b* mutant-rye hybrids. Surprisingly, both methods of application increased homoeologous CO frequency in the *Tazip4-B2 ph1b* mutant-rye hybrids. Thus, the results from the injection method of application suggested that the 1 mM Mg^{2+} concentration was directly responsible for the increased homoeologous CO effect seen in the *Tazip4-B2 ph1b* mutant-rye hybrids, rather than through indirect effects on the plant growth or development. However, homoeologous CO frequency was decreased when the Mg^{2+} concentration was increased further (**Figure 1**). This reduction in COs was associated with a significant increase in the number of univalents, and decrease in the number of ring bivalents and trivalents.

A recent study revealed that *TaZIP4-B2* within the 5B region defined by the 70 Mb *ph1b* deletion, was responsible for the suppression of homoeologous COs in hybrids (Rey et al., 2017). *Tazip4-B2* TILLING mutants (one with a missense mutation and another with a nonsense mutation), when crossed with *Ae. variabilis,* exhibit similar levels of homoeologous CO that observed in *ph1b-Ae. variabilis* hybrids (Rey et al., 2017). It was therefore important to assess the effect of 1 mM Mg^{2+} solution on these *Tazip4-B2* TILLING mutant-*Ae. variabilis* hybrids to confirm that the effect was associated with *Tazip4-B2*, and that the Mg^{2+} effect could also be observed in a different hybrid. Moreover, we also applied the CRISPR/Cas9 genome editing system in hexaploid wheat cv. Fielder to the mutant *TaZIP4-B2* to compare its mutant phenotype with those observed in TILLING mutant lines, and their *Ae. variabilis* hybrids. *Tazip4-B2* CRISPR mutants showed a significant decrease in homologous COs compared to control plants (*TaZIP4-B2* wild type wheat), similar to that already reported for *Tazip4-B2* TILLING mutants (Rey et al., 2017). Also, as expected, a significant increase was observed in *Tazip4-B2* CRISPR mutant-*Ae. variabilis* hybrids, similar to that observed in both *ph1b-Ae. variabilis* and *Tazip4-B2* TILLING mutant-*Ae. variabilis* hybrids. Furthermore, the addition of 1 mM Mg^{2+} to all these hybrids increased the frequency of homoeologous CO. This confirms that the Mg^{2+} effect is associated with *Tazip4-B2*, and occurs in different hybrids. The only difference observed with the *Tazip4-B2* CRISPR and TILLING mutants was the occurrence of multivalents in the CRISPR mutants compared to the TILLING mutants (**Figure 3** and Rey et al., 2017). This suggests that

TaZIP4-B2 not only promotes homologous COs and restricts homoeologous COs, but also contributes to the efficiency of homologous pairing. We hypothesize that the CRISPR deletion disrupts more of the *TaZIP4-B2* function than the TILLING mutants. Interestingly, in rice, *ZIP4* mutants have previously been reported to show a delay in completing homologous synapsis (Shen et al., 2012), however, in that diploid species, this does not lead to homoeologous COs because only homologs are present. However, in the *ph1b* mutant, delayed pairing of some homologs is observed until after the telomere bouquet, allowing some subsequent homoeologous pairing to take place. This delayed pairing of homologs in the *ph1b* mutant is consistent with a *ZIP4* mutant phenotype.

Magnesium is one of the most important nutrients, mainly involved in the general promotion of plant growth and development. In terms of CO function, Mg^{2+} may affect multiple proteins in the class I interference crossover pathway either in a positive or negative manner. For example, recent studies have suggested that $Mg^{2+}$is required for the endonuclease activity of the MLH1-MLH3 heterodimer (Rogacheva et al., 2014). The MLH1-MLH3 heterodimer shows a strong preference for HJs in the absence of Mg^{2+} (Ranjha et al., 2014). Whatever the target, our present study reveals that homoeologous COs can be increased by the 1 mM Mg^{2+} treatment of *Tazip4-B2* (*ph1b*, TILLING or CRISPR derived) mutant-wild relative hybrids. Thus, this treatment can be used as a tool to enhance the introgression of wild relative traits into wheat.

AUTHOR CONTRIBUTIONS

M-DR, AM, PS, and GM: conceived and designed the study; MS, SH, and WH: participated in the development of the *Tazip4-B2* mutant in bread wheat cv. Fielder by CRISPR/Cas9 system; M-DR: analyzed the research results and wrote the first draft; PS and GM: modified the paper. All authors have read and approved the final version of the manuscript.

ACKNOWLEDGMENTS

The authors thank Ali Pendle (John Innes Centre, UK) for her valuable comments in the writing of the manuscript. This work was supported by the UK Biotechnology and Biological Research Council (BBSRC), through a grant part of the Designing Future Wheat (DFW) Institute Strategic Programme (BB/P016855/1), three grants (Grant BB/J004588/1; Grant BB/M009599/1; Grant BB/J007188/1); and by a Marie Curie Fellowship Grant (H2020-MSCA-IF-2015-703117).

SUPPLEMENTARY MATERIAL

The Supplementary Material for this article can be found online at: https://www.frontiersin.org/articles/10.3389/fpls.2018.00509/full#supplementary-material

Figure S1 | Chromosomal configurations with single chiasma or double chiasmata highlighted with arrows. These structures marked by an arrow were counted as either single or double chiasmata in all analyzed meiocytes. Both datasets are shown in all analyzed genotypes. Bar: 20 μm.

Figure S2 | Representative meiotic configurations of *Triticum aestivum* cv. Cadenza (Cad1691-*Tazip4-B2* mutant)-*Ae. variabilis* **(A)** and *Triticum aestivum* cv. Cadenza (Cad0348-*Tazip4-B2* mutant)-*Ae. variabilis* **(B)** and wheat *Tazip4-B2* CRISPR mutant-*Ae. variabilis* mutant **(C)** hybrids. From left to right: water alone, treated with either 1 mM Mg^{2+} or Hoagland solution. Bar: 20 μm.

Table S1 | Genotypes and number of plants used for analyzing the effect of a nutrient solution in homoeologous CO frequency in wheat and its relative species.

Table S2 | Frequencies of univalents, bivalents, multivalents and chiasma frequency (single and double chiasmata) were scored at meiotic metaphase I in wheat Tazip4-B2 CRISPR mutant-Ae. variabilis hybrids. Values in parenthesis indicate range of variation between cells. $P < 0.05$ indicates significant differences according to Dunn's test. Different letters indicate significant differences between treatments.

REFERENCES

Al-Kaff, N., Knight, E., Bertin, I., Foote, T., Hart, N., Griffiths, S., et al. (2008). Detailed dissection of the chromosomal region containing the Ph1 locus in wheat *Triticum aestivum*: with deletion mutants and expression profiling. *Ann. Bot.* 101, 863–872. doi: 10.1093/aob/mcm252

Bennett, M. D., and Rees, H. (1970). Induced variation in chiasma frequency in rye in response to phosphate treatments. *Genet. Res.* 16, 325–331. doi: 10.1017/S0016672300002585

Dhaliwal, H. S., Gill, B. S., and Waines, J. G. (1977). Analysis of induced homoeologous pairing in a ph mutant wheat x rye hybrid. *J. Hered.* 68, 207–209. doi: 10.1093/oxfordjournals.jhered.a108815

Dreissig, S., Fuchs, J., Himmelbach, A., Mascher, M., and Houben, A. (2017). Sequencing of single pollen nuclei reveals meiotic recombination events at megabase resolution and circumvents segregation distortion caused by postmeiotic processes. *Front. Plant Sci.* 8:1620. doi: 10.3389/fpls.2017.01620

Fedak, G. (1973). Increased chiasma frequency in desynaptic barley in response to phosphate treatments. *Can. J. Genet. Cytol.* 15, 647–649. doi: 10.1139/g73-076

Gennaro, A., Forte, P., Panichi, D., Lafiandra, D., Pagnotta, M. A., D'Egidio, M. G., et al. (2012). Stacking small segments of the 1D chromosome of bread wheat containing major gluten quality genes into durum wheat: transfer strategy and breeding prospects. *Mol. Breed.* 30, 149–167. doi: 10.1007/s11032-011-9606-6

Grant, V. (1952). Cytogenetics of the hybrid *Gilia millefoliata* x achilleaefolia. 1. Variations in meiosis and polyploidy rate as affected by nutritional and genetics conditions. *Chromosoma* 5, 372–390. doi: 10.1007/BF01271494

Griffiths, S., Sharp, R., Foote, T. N., Bertin, I., Wanous, M., Reader, S., et al. (2006). Molecular characterization of Ph1 as a major chromosome pairing locus in polyploid wheat. *Nature* 439, 749–752. doi: 10.1038/nature04434

Harwood, W. A., Bartlett, J. G., Alves, S. C., Perry, M. A., Smedley, M., Leyland, N., et al. (2009). "Barley transformation using Agrobacterium-mediated techniques," in *Methods in Molecular Biology, Transgenic Wheat, Barley and Oats, Vol. 478*, eds H. D. Jones and P. R. Shewry (Human press), 137–147.

Hellens, R. P., Edwards, E. A., Leyland, N. R., Bean, S., and Mullineaux, P. M. (2000). pGreen: a versatile and flexible binary Ti vector for Agrobacterium-mediated plant transformation. *Plant Mol. Biol.* 42, 819–832. doi: 10.1023/A:1006496308160

Hoagland, D. R., and Arnon, D. I. (1950). The water-culture method of growing plants without soil. *Calif. Agr. Expt. Sta. Circ.* 347, 1–39.

Huber, D. M. (1980). The role of mineral nutrition in defense. *Plant Disease* 5, 381–405.

King, J., Grewal, S., Yang, C. Y., Hubbart Edwards, S., Scholefield, D., Ashling, S., et al. (2017a). Introgression of *Aegilops speltoides* segments in *Triticum*

aestivum and the effect of the gametocidal genes. *Ann. Bot.* 121, 229–240. doi: 10.1093/aob/mcx149

King, J., Grewal, S., Yang, C. Y., Hubbart, S., Scholefield, D., Ashling, S., et al. (2017b). A step change in the transfer of interspecific variation into wheat from *Amblyopyrum muticum*. *Plant Biotechnol. J.* 15, 217–226. doi: 10.1111/pbi.12606

Ko, J. M., Seo, B. B., Suh, D. Y., Do, G. S., Park, D. S., and Kwack, Y. H. (2002). Production of a new wheat line possessing the 1BL.1RS wheat-rye translocation derived from Korean rye cultivar Paldanghomil. *Theor. Appl. Genet.* 104, 171–176. doi: 10.1007/s00122-001-0783-2

Kousaka, R., and Endo, T. R. (2012). Effect of a rye B chromosome and its segments on homoeologous pairing in hybrids between common wheat and *Aegilops variabilis*. *Genes Genet. Syst.* 87, 1–7. doi: 10.1266/ggs.87.1

Krasileva, K. V., Vasquez-Gross, H. A., Howell, T., Bailey, P., Paraiso, F., Clissold, L., et al. (2017). Uncovering hidden variation in polyploid wheat. *Proc. Natl. Acad. Sci. U.S.A.* 114, E913–E921. doi: 10.1073/pnas.1619268114

Lambing, C., Franklin, F. C. H., and Wang, C. J. R. (2017). Understanding and manipulating meiotic recombination in plants. *Plant Physiol.* 173, 1530–1542. doi: 10.1104/pp.16.01530

Law, C. N. (1963). An effect of potassium on chiasma frequency and recombination. *Genetica* 33, 313–329. doi: 10.1007/BF01725768

Maathuis, F. J. (2009). Physiological functions of mineral macronutrients. *Curr. Opin. Plant Biol.* 12, 250–258. doi: 10.1016/j.pbi.2009.04.003

Martín, A. C., Rey, M. D., Shaw, P., and Moore, G. (2017). Dual effect of the wheat Ph1 locus on chromosome synapsis and crossover. *Chromosoma* 126, 669–680. doi: 10.1007/s00412-017-0630-0

Martín, A. C., Shaw, P., Phillips, D., Reader, S., and Moore, G. (2014). Licensing MLH1 sites for crossover during meiosis. *Nat. Commun.* 5, 1–5. doi: 10.1038/ncomms5580

Murashige, T., and Skoog, F. (1962). A revised medium for rapid growth and bio assays with tobacco tissue cultures. *Physiol. Plant.* 15, 473–497. doi: 10.1111/j.1399-3054.1962.tb08052.x

Ranjha, L., Anand, R., and Cejka, P. (2014). The *Saccharomyces cerevisiae* Mlh1-Mlh3 heterodimer is an endonuclease that preferentially binds to Holliday junctions. *J. Biol. Chem.* 289, 5674–5686. doi: 10.1074/jbc.M113.533810

Rey, M. D., Martín, A. C., Higgins, J., Swarbreck, D., Uauy, C., Shaw, P., et al. (2017). Exploiting the ZIP4 homologue within the wheat Ph1locus has identified two lines exhibiting homoeologous crossover in wheat-wild relative hybrids. *Mol. Breed.* 37:95. doi: 10.1007/s11032-017-0700-2

Riley, R., and Chapman, V. (1958). Genetic control of the cytological diploid behaviour of hexaploid wheat. *Nature* 182, 713–715. doi: 10.1038/182713a0

Roberts, M. A., Reader, S. M., Dalgliesh, C., Miller, T. E., Foote, T. N., Fish, L. J., et al. (1999). Induction and characterisation of the Ph1 wheat mutants. *Genetics* 153, 1909–1918.

Rogacheva, M. V., Manhart, C. M., Chen, C., Guarne, A., Surtees, J., and Alani, E. (2014). Mlh1-Mlh3, a meiotic crossover and DNA mismatch repair factor, is a Msh2-Msh3-stimulated endonuclease. *J. Biol. Chem.* 289, 5664–5673. doi: 10.1074/jbc.M113.534644

Sears, E. R. (1977). Induced mutant with homoeologous pairing in common wheat. *Can. J. Genet. Cytol.* 19, 585–593. doi: 10.1139/g77-063

Sears, E. R., and Okamoto, M. (1958). Intergenomic chromosome relationships in hexaploid wheat. *Proc Xth Internat Congr Genet, Montreal*, 2, 258–259.

Sharma, A. K., and Sharma, A. (2014). *Chromosome Techniques: Theory and Practice*. Michigan, IN: Butterworth-Heinemann.

Shen, Y., Tang, D., Wang, K., Wang, M., Huang, J., Luo, W., et al. (2012). ZIP4 in homologous chromosome synapsis and crossover formation in rice meiosis. *J. Cell Biol.* 125, 2581–2591. doi: 10.1242/jcs.090993

Werner, S., Engler, C., Weber, E., Gruetzner, R., and Marillonnet, S. (2012). Fast track assembly of multigene constructs using golden gate cloning and the MoClo system. *Bioeng. Bugs* 3, 38–43. doi: 10.4161/bbug.3.1.18223

Wilson, J. Y. (1959). Chiasma frequency in relation to temperature. *Genetica* 29, 290–303. doi: 10.1007/BF01535715

Conflict of Interest Statement: The authors declare that the research was conducted in the absence of any commercial or financial relationships that could be construed as a potential conflict of interest.

frontiers in Plant Science

ORIGINAL RESEARCH
published: 02 July 2018
doi: 10.3389/fpls.2018.00880

Variable Patterning of Chromatin Remodeling, Telomere Positioning, Synapsis, and Chiasma Formation of Individual Rye Chromosomes in Meiosis of Wheat-Rye Additions

*Tomás Naranjo**

Departamento de Genética, Fisiología y Microbiología, Facultad de Biología, Universidad Complutense de Madrid, Madrid, Spain

Meiosis, the type of cell division that halves the chromosome number, shows a considerable degree of diversity among species. Unraveling molecular mechanisms of the meiotic machinery has been mainly based on meiotic mutants, where the effects of a change were assessed on chromosomes of the particular species. An alternative approach is to study the meiotic behavior of the chromosomes introgressed into different genetic backgrounds. As an allohexaploid, common wheat tolerates introgression of chromosomes from related species, such as rye. The behavior of individual pairs of rye homologues added to wheat has been monitored in meiotic prophase I and metaphase I. Chromosome 4R increased its length in early prophase I much more than other chromosomes studied, implying chromosome specific patterns of chromatin organization. Chromosome conformation affected clustering of telomeres but not their dispersion. Telomeres of the short arm of submetacentric chromosomes 4R, 5R, and 6R failed more often to be included in the telomere cluster either than the telomeres of the long arms or telomeres of metacentrics such as 2R, 3R, and 7R. The disturbed migration of the telomeres of 5RS and 6RS was associated with failure of synapsis and chiasma formation. However, despite the failed convergence of its telomere, the 4RS arm developed normal synapsis, perhaps because the strong increase of its length in early prophase I facilitated homologous encounters in intercalary regions. Surprisingly, chiasma frequencies in both arms of 4R were reduced. Similarly, the short arm of metacentric chromosome 2R often failed to form chiasmata despite normal synapsis. Chromosomes 1R, 3R, and 7R showed a regular meiotic behavior. These observations are discussed in the context of the behavior that these chromosomes show in rye itself.

Keywords: chromatin remodeling, telomere dynamics, synapsis, chiasmata, rye, wheat, FISH

OPEN ACCESS

Edited by:
Simon Gilroy,
University of Wisconsin-Madison,
United States

Reviewed by:
Adam Lukaszewski,
University of California, Riverside,
United States
Fangpu Han,
Institute of Genetics
and Developmental Biology (CAS),
China

***Correspondence:**
Tomás Naranjo
toranjo@bio.ucm.es

Specialty section:
This article was submitted to Plant Cell Biology, a section of the journal Frontiers in Plant Science

Received: *15 March 2018*
Accepted: *06 June 2018*
Published: *02 July 2018*

Citation:
Naranjo T (2018) Variable Patterning of Chromatin Remodeling, Telomere Positioning, Synapsis, and Chiasma Formation of Individual Rye Chromosomes in Meiosis of Wheat-Rye Additions. Front. Plant Sci. 9:880. doi: 10.3389/fpls.2018.00880

INTRODUCTION

Bivalents formed during meiotic prophase I are essential to halve the chromosome number. Bivalent formation requires that homologous chromosomes, mainly located in separate nuclear territories in premeiotic interphase nuclei (Bass et al., 2000; Maestra et al., 2002), move to find one another. In many species, concomitant with a chromatin remodeling process that causes a

considerable chromosome elongation during leptotene, telomeres undergo an oriented migration and converge in a tight cluster in a small area of the nuclear envelop. This suprachromosomal meiotic configuration, the so-called bouquet, facilitates chromosome interactions that culminate in the identification of the homologous partner (Bass et al., 1997, 2000; Niwa et al., 2000; Trelles-Sticken et al., 2000; Cowan et al., 2001; Scherthan, 2001). The bouquet is disorganized once homologues undergo synapsis.

A programed production of double-strand DNA breaks (DSBs) catalyzed by Spo11 in conjunction with other proteins triggers the initiation of chromosome interactions (Keeney et al., 1997; Neale and Keeney, 2006). DSBs are resected to generate 3′ single-strand DNA overhangs that bind recombinases RAD51 and DMC1. These nucleoprotein filaments invade a double-strand DNA stretch of the homologous chromosome to find its complementary strand (Hunter and Kleckner, 2001). During leptotene, chromosomes form the axial element, a protein-rich backbone that will keep the sister chromatids together until the second division. The search of a repair template in the homologous chromosome is instigated by proteins of the axis such as Hop1-Red1 in budding yeast, ASY1-ASY3 in *Arabidopsis* and PAIR2-PAIR3 in rice (Hollingsworth and Byers, 1989; Thompson and Roeder, 1989; Caryl et al., 2000; Nonomura et al., 2006; Wang et al., 2011; Ferdous et al., 2012). The identification of the homologous partner in the invaded chromatid is necessary for chromosome pairing and synapsis in many organisms (Roeder, 1997; Baudat et al., 2000; Romanienko and Camerini-Otero, 2000). Then, homologues become aligned, form the tripartite synaptonemal complex (SC) during zygotene, and are fully synapsed at pachytene (Page and Hawley, 2004). The SC maintains homologues in close juxtaposition along their length and serves as a scaffold for factors of the recombinational repairing machinery (Zickler and Kleckner, 2015). The genetic control of the repairing machinery ensures a minimum of one crossover (CO) per homologous pair. However, repair of the majority (95%) of DSBs produced in plants and animals culminates in a non-crossover (NCO) (Higgins et al., 2014). The SC disassembles at diplotene, once COs formation is completed, and chromatin undergoes a progressive condensation. Meanwhile, homologues remain physically connected by chiasmata, the cytological expression of COs, until their disjunction in anaphase I.

Deviations from this meiotic prophase I program have been reported in several organisms (reviewed in Zickler and Kleckner, 2016). In fission yeast, homologous pairing is recombination-independent and COs are formed in the absence of SC (Ding et al., 2004). In *Drosophila melanogaster* females and in *Caenorhabditis elegans*, pairing and synapsis can occur independently of recombination (Lake and Hawley, 2012; Rog and Dernburg, 2013). However, in both cases, DSBs are produced after SC formation. The *D. melanogaster* males and the silk worm (*Bombyx mori*) females both with achiasmate meiosis, show well-aligned bivalents at metaphase I. The presence of the SC until anaphase I provides the physical connection between homologues in *B. mori* females (Rasmussen, 1977). *B. mori* males form chiasmate bivalents. In *D. melanogaster* males, which do not form SC, pairing initiates at a specific site in sex chromosomes, and probably in chromosome 4, but no pairing center has been found in the other two autosomes (Tsai and McKee, 2011). Sex differences in the meiotic process have been observed in other organisms such as, planarian worms (Pastor and Callan, 1952; Oakley and Jones, 1982; Oakley, 1982), *Lilium* and *Fritillaria* (Fogwill, 1958), grasshoppers (Perry and Jones, 1974), *Arabidopsis thaliana* (Drouaud et al., 2007), mice (Petkov et al., 2007), or humans (Hou et al., 2013).

Studies aimed at unraveling the molecular mechanisms underlying the chromosome dynamics in meiotic prophase I are based on the use of meiotic mutants and often focus on the full chromosome complement, neglecting the behavior of individual chromosomes. However, individual chromosomes may respond in different way to the general program of the meiotic cell. An apparent example of this differential behavior is the case of the sex chromosomes in the heterogametic sex of species with XX/XY, XX/X0, or ZZ/ZW. Non-homologous regions of sex chromosomes appear usually unmatched and with apparent changes in the chromatin organization during prophase I, which, in the case of mammals, is accompanied by silencing of unsynapsed chromatin (Page et al., 2006; Turner, 2013). It is also remarkable the variable chromosome behavior in spermatocytes of the planarian worm *Mesostoma ehrenbergii ehrenbergii*. Chiasma formation is extremely restricted: three homologous pairs form one distal chiasmata and appear as bivalents at metaphase I, while the other two pairs do not form chiasmata and appear as univalents (Croft and Jones, 1989). Chromosomes of common wheat *Triticum aestivum* show differences in the chiasma distribution and in their ability to form chiasmata after deletion of terminal regions (Naranjo, 2015).

An alternative approach to the use of meiotic mutants in a given species is the study of the meiotic behavior of its chromosomes when they are introgressed in the genetic background of a different species. Common wheat (genome formula, AABBDD, 2n = 6x = 42) as an allohexaploid, tolerates the addition of chromosomes from related species such as rye, *Secale cereale* (RR, 2n = 14). A handful of complete sets of wheat-rye additions are available (Lukaszewski, 2015). These lines can be used in the study of the behavior of individual rye chromosomes both in somatic and meiotic cells, in the assignation of genetic markers to chromosomes, or in the study of genetic interactions between wheat and rye chromosomes. In addition they represent an excellent start point for the introgression of useful genes of rye into wheat.

Painting of the rye chromosomes present in each disomic addition allows to monitor their pairing and synapsis and to estimate the number of chiasmata formed (Maestra et al., 2002; Corredor and Naranjo, 2007; Naranjo and Corredor, 2008; Naranjo et al., 2010; Valenzuela et al., 2012; Naranjo, 2014, 2015). Rye chromosomes bear apparent subtelomeric heterochromatin blocks (Darvey and Gustafson, 1975), which can be visualized by fluorescence *in situ* hybridization (FISH) making possible to identify the position of the adjacent telomere in the meiotic bouquet (Naranjo et al., 2010; Naranjo, 2014). The position of the telomere of the short arm of chromosome 5R (5RS) at the bouquet depends of the length of the other arm of

this submetacentric chromosome. The 5RS arm of the standard chromosome 5R is much shorter than the long arm (5RL), but in a truncated chromosome 5R (del5R) lacking the last 70% distal of 5RL (del5RL) both arms have a similar length. Although the 5RS arm is the same in chromosomes 5R and del5R, its telomere fails more often in its incorporation to the telomere cluster in the standard chromosome than in the truncated one. Disturbed telomere migration has a negative effect on the development of synapsis and chiasma formation (Naranjo et al., 2010). Chromosomes 1R and 6R carry subtelomeric heterochromatin chromomeres in both ends. This allowed to verify that the end of their long arms, 1RL and 6RL, were included in the telomere cluster in almost all cells (>99%) while one or both telomeres of 1RS, or 6RS, were separated of the telomere cluster in 27 and 40% of meiocytes, respectively. Thus, incomplete telomere migration occurs more often in the short arm of the submetacentric chromosome 6R than in the short arm of the almost metacentric chromosome 1R. Failure of synapsis and chiasma formation is also relatively frequent in the 6RS arm (Naranjo, 2014). This result is consistent with the behavior of 5RS in chromosomes 5R and del5R.

The meiotic behavior of chromosomes 1R, 5R, and 6R in a wheat background suggests that the genetic and structural chromosome identity is manifested in the appearance of chromosome specific features in the development of the meiotic program. Verification of this idea implies the analysis of all individual chromosomes. In the case of rye, it remains to be studied the meiotic behavior of metacentric chromosomes 2R, 3R, and 7R and submetacentric chromosome, 4R. On the other hand, from the effect of chromosome structure on telomere clustering the question arises whether telomere dynamics during bouquet dissolution is also chromosome conformation-dependent or not. The aim of this paper is to carry out a comparative study of the dynamics of individual rye chromosomes in a wheat background during prophase I. Three different aspects of the meiotic process are concerned: (i) chromatin remodeling (ii) the telomere movement leading to the formation of the bouquet and its resolution; (iii) the effect of telomere positioning at the bouquet on synapsis and chiasma formation.

MATERIALS AND METHODS

Plant Material

Seven wheat-rye introgression lines, each carrying one of the seven chromosome pairs of rye (*S. cereale,* 2n = 14) introgressed in hexaploid wheat *T. aestivum*, were used. The wheat-2R, wheat-3R, wheat-4R, wheat-5R, wheat-6R, and wheat-7R lines are disomic additions of the Imperial rye chromosome in a Chinese Spring wheat background (Driscoll and Sears, 1971). The wheat-1R line is a disomic substitution for chromosome 1A generated in hexaploid wheat Pavon 76 (Lukaszewski, 2008), and used for other purpose (Valenzuela et al., 2012). All wheat-rye introgression lines used were provided by A. J. Lukaszeski. The chromosome constitution of the plants studied was verified by FISH analysis of root tips in squashed preparations as described for meiosis. Seeds were germinated in November and grew in a greenhouse under natural light. Spikes at meiosis were cut and checked to establish the meiotic stage of each flower, One anther per flower was examined. When this anther was at prophase I or metaphase I the other 2 were fixed in 3:1 ethanol: acetic acid and stored at 4°C.

Fluorescence *in Situ* Hybridization

Preparations of fixed anthers were carried out as described (Maestra et al., 2002). Telomeres of wheat and rye chromosomes were labeled with the pAtT4 DNA probe, from *Arabidopsis* (Richards and Ausubel, 1988). The arrangement of telomere was used to identify the leptotene, zygotene, and pachytene stages as described (Corredor et al., 2007; Naranjo et al., 2010). Subtelomeric chromomeres of rye were visualized using clone pSc74, which contains a rye-specific 480-bp tandem repeat (Bedbrook et al., 1980; Cuadrado and Schwarzacher, 1998). The subtelomeric pSc74 signal identified the position of the adjacent rye telomere. Rye centromeres labeled with the rye-specific clone pAWRC.1 (Franki, 2001) were positioned at the bouquet and in the bivalents at pachytene and metaphase I. A fourth DNA probe, pUCM600, containing a rye-specific repeat (Gonzalez-Garcia et al., 2011) was added to paint each rye bivalent and quantify its level of synapsis in Pollen Mother Cells (PMCs) at pachytene. The probes, pUCM600, pAWRC.1, and pSc74, were used for the identification of each rye bivalent and the arms associated at metaphase I. Concentrations of DNA probes in the hybridization mixes were as described (Naranjo et al., 2010) In the analysis of the position of rye telomeres at the bouquet, probes pAtT4 and pAWRC.1 were labeled with biotin-16-dUTP and probe pSc74 with digoxigenin-11-dUTP. For painting of the rye bivalent at pachytene and metaphase I, the rye-specific DNA probes pAWRC.1 and pUCM600 were labeled with biotin-11-dUTP, while either digoxigenin-11-dUTP or biotin-16-dUTP were used in the case of probe pSc74. In nuclei at pachytene, the telomeres of wheat and rye chromosomes were visualized with the pAtT4 DNA probe labeled with digoxigenin-11-dUTP. Labeled probes were detected as described (Naranjo et al., 2010).

Fluorescence Microscopy and Image Processing

Cells at mitotic metaphases and PMCs at pachytene and metaphase I were viewed under an Olympus BX60 fluorescence microscope equipped with an Olympus DP70 CCD camera. Cells at the bouquet stage were studied under an Olympus BX61 fluorescence microscope and processed as described (Naranjo, 2014)

Chromosome Length and Telomere Arrangement

The length of rye chromosomes in both mitotic metaphases and meiocytes at pachytene, as well as different distances in nuclei at the bouquet stage and pachytene, were measured using the Adobe Photoshop CS4 software. In each wheat-rye addition line, the lengths of 10 mitotic chromosomes and 10 completely synapsed pachytene bivalents were scored. Separation between

the rye chromosome ends, and the major axis of each nucleus were measured in 2D projections of cells at the bouquet stage and pachytene. The distance of the ends of each rye chromosome to the center of the telomere cluster was also measured in cells at the bouquet. An average number of 100 cells per meiotic stage and line were scored.

RESULTS

Rye Chromatin Remodeling During Leptotene Shows a Distinctive Pattern in the Wheat-4R Addition

Concomitant with the bouquet organization, chromatin undergoes a remodeling process that reduces its packaging level and causes a large elongation of chromosomes. At the bouquet, decondensation of rye chromatin was apparent but a considerable folding degree was still observed (**Figure 1**). This remnant folding of chromatin made it difficult to trace and measure the complete chromosome length. The assessment of chromatin reorganization in each rye chromosome was based on the variation of its length in completely synapsed bivalents at pachytene relative to that in mitotic metaphase. **Figure 2** compares the karyotype of rye chromosomes in both types of cells. In addition to the chromosome length, karyotypes show the position of the centromere and heterochromatin chromomeres. The two arms of all rye chromosomes show a distinctive pattern of heterochromatin markers. Chromosomes 4R and 5R bear a subtelomeric chromomere only in the short arm, the 4RL arm shows no marker and the subdistal chromomere of 5RL is smaller than that of 5RS. The subtelomeric chromomeres of the short and long arms of chromosomes 1R, 2R, 3R, 6R, and 7R differ in the heterochromatin contain. In addition to the subtelomeric marker, the arms 1RL, 2RS, 2RL, 6RL, and 7RL carry one or two intercalary chromomeres. Values of chromosome length and centromere index (100 × short arm length/chromosome length) are given in **Table 1**. The length of mitotic chromosomes ranges between 12.9 and 16.4 μm with an average of 15.1 μm. Bivalents at pachytene of chromosomes 1R, 2R, 3R, 5R, 6R, and 7R reached a length that ranges between six and seven times the size of the mitotic chromosome. Surprisingly, chromosome 4R is 11.2 times longer in pachytene than in mitotic metaphase. This result supports a different reorganization pattern of rye chromatin in leptotene in the wheat-4R addition relative to the others.

Clustering, but Not Dispersion, of Telomeres Is Chromosome Conformation-Dependent

The position of the telomere of the short arm of all rye chromosomes and of the long arms 1RL, 2RL, 3RL, 6RL, and 7RL in PMCs at early prophase I was identified by its close proximity to the adjacent subtelomeric heterochromatin marker. FISH analysis combining the telomeric and the rye-specific heterochromatin DNA probes in nuclei at the bouquet stage revealed whether rye telomeres were included in the telomere cluster or not. **Figure 3** shows nuclei with the two ends of

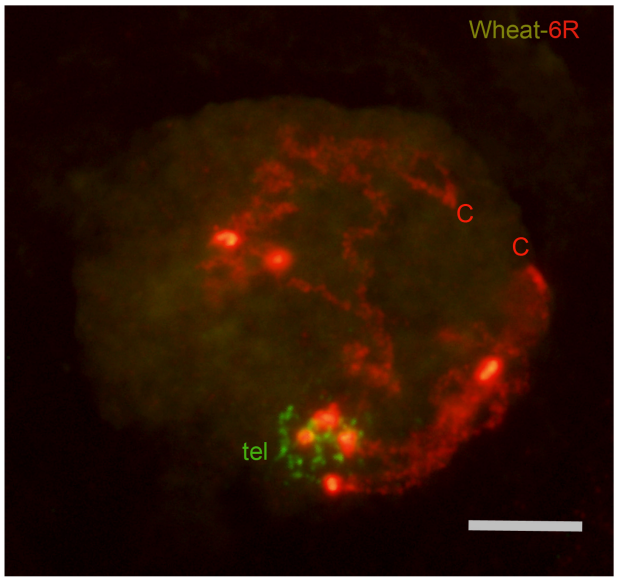

FIGURE 1 | Nucleus of the wheat-6R addition at the bouquet stage. Chromatin folding makes it difficult to trace the chromosomal axis along its entire length. Centromeres (C) and telomeres (tel) are indicated. Bar represents 10 μm.

chromosomes 2R and 3R, and the end of chromosome arm 4RS at the telomere cluster (**Figures 3A,B,D**, respectively). In all of these cases the homologous chromosome ends are intimately associated denoting the initiation of synapsis. The telomere of one chromosome arm 3RS, one chromosome arm 6RS and the two arms 4RS are not included in the telomere cluster in nuclei of **Figures 3C,E,F**, respectively. From the number of cells with zero, one or two homologous ends included in the telomere pole it was possible to estimate the probability of incorporation to the telomere cluster of the telomere of the seven short chromosome arms and the long arms 1RL, 2RL, 3RL, 6RL, and 7RL. This probability appears diagrammed in **Figure 4**. The telomere of both arms of metacentric chromosomes 2R, 3R, and 7R as well as the telomere of 1RL and 6RL migrated to the telomere pole in almost all cells. However, the telomere of the short arm of submetacentric chromosomes 4R, 5R, and 6R failed in its incorporation to the telomere pole in more than 25% of the meiocytes. On average, such telomeres were separated 10 μm from the telomere cluster. Accordingly, the probability of incorporation of the telomere of the short arm of the seven rye chromosomes and the centromere index were positively correlated ($r = 0.828$, $t = 13.16$, d.f. = 5, and $p < 0.01$). This result supports an effect of chromosome conformation in the positioning of telomeres during the organization of the bouquet. Although the centromere index of 1R identifies this chromosome as submetacentric, the location of the nucleolar organizing region on 1RS probably represents an additional factor conditioning its arrangement in leptotene. Consistent with the disturbed positioning of the telomeres of 4RS, 5RS, and 6RS is the reduction in the frequency of association of their subtelomeric markers in cells with the two homologous ends included in the telomere

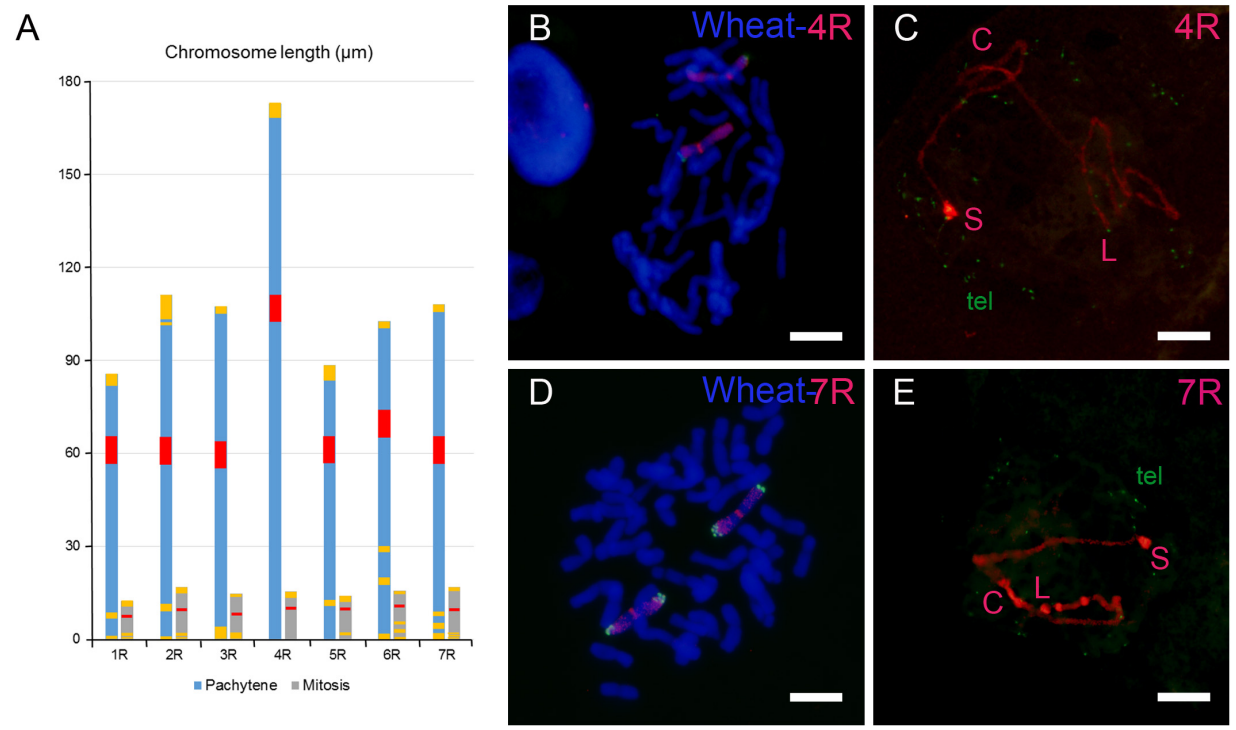

FIGURE 2 | Chromosomes of rye in mitosis and pachytene in wheat-rye additions. **(A)** Karyotypes showing the different size of mitotic and meiotic chromosomes. The position of the centromere (red) and heterochromatic chromomeres (yellow) is indicated. **(B)** Mitotic metaphase of the wheat-4R addition. **(C)** Bivalent 4R at pachytene. Green signals correspond to telomeres (tel). **(D)** Mitotic metaphase of the wheat-7R addition. **(E)** Bivalent 7R at pachytene. Bars represent 10 μm.

TABLE 1 | Length (μm) of rye chromosomes in mitotic metaphase (M) and pachytene (P), P/M ratio and centromere index (100 × short arm length/chromosome length) in wheat-rye additions.

Chromosome	M	P	P/M ratio	Centromere index
1R	14.2 ± 2.1	85.6 ± 5.3	6.0	37
2R	16.4 ± 3.4	111.1 ± 5.7	6.8	46
3R	15.3 ± 1.2	107.3 ± 12.0	7.0	46
4R	15.4 ± 0.6	172.8 ± 23.2	11.2	39
5R	12.9 ± 1.3	88.5 ± 15.2	6.9	33
6R	15.8 ± 2.5	102.6 ± 7.7	6.5	33
7R	15.7 ± 1.7	108.2 ± 9.4	7.0	45

cluster. While the subtelomeric chromomeres of 4RS, 5RS, and 6RS were intimately associated on average in 46% of the cells studied, the homologous ends of metacentric chromosomes were in 86%.

The fact that telomere clustering was chromosome conformation dependent led to verify whether the dispersive telomere movement responsible of the bouquet disorganization was also affected by chromosome conformation or not. When both ends of rye chromosome pairs 1R, 2R, 3R, 6R, or 7R were included in the telomere cluster, they were situated at an average distance of 2 mμ. Such a distance is expected to increase because of telomere dispersion during zygotene. Thus, the spatial separation between the ends of each bivalent in nuclei at pachytene, in which the bouquet is completely disorganized, should provide an assessment of the effect of the dispersive telomere movement. The distance between the chromosome ends was scored in completely synapsed bivalents. A great between cells variation was found. **Figure 5** shows nuclei with the chromosomal ends of the rye bivalent relatively close or occupying diametrically opposed positions, respectively. The mean distance between the ends of each chromosome, as well as the size of the nuclear diameter, appear indicated in **Table 2**. The ends of metacentric chromosome 3R and submetacentric chromosomes 4R and 5R, show very similar separation and the same happens in the group formed by metacentric chromosomes 2R and 7R and submetacentric chromosome 6R. There is no significant correlation between the inter-chromosome ends distance and the centromeric index ($r = 0.471$, $t = 1.194$, d.f = 5, and $p > 0.05$). Thus, chromosome conformation does not affect the telomere movement during the bouquet dissolution. Between chromosomes variation in the degree of separation of the two ends was correlated to the size of the nuclear diameter ($r = 0.858$, $t = 3.73$, d.f. = 5, $p < 0.05$). Such a variation should at least in part be a result of manipulation during the realization of preparations. In fact, with the exception of chromosome 3R, the between ends distance/nuclear diameter ratio was similar in all remaining chromosomes. The telomere dispersion produced in zygotene separated the chromosomal ends to nuclear positions distant on average 43% of the nuclear diameter.

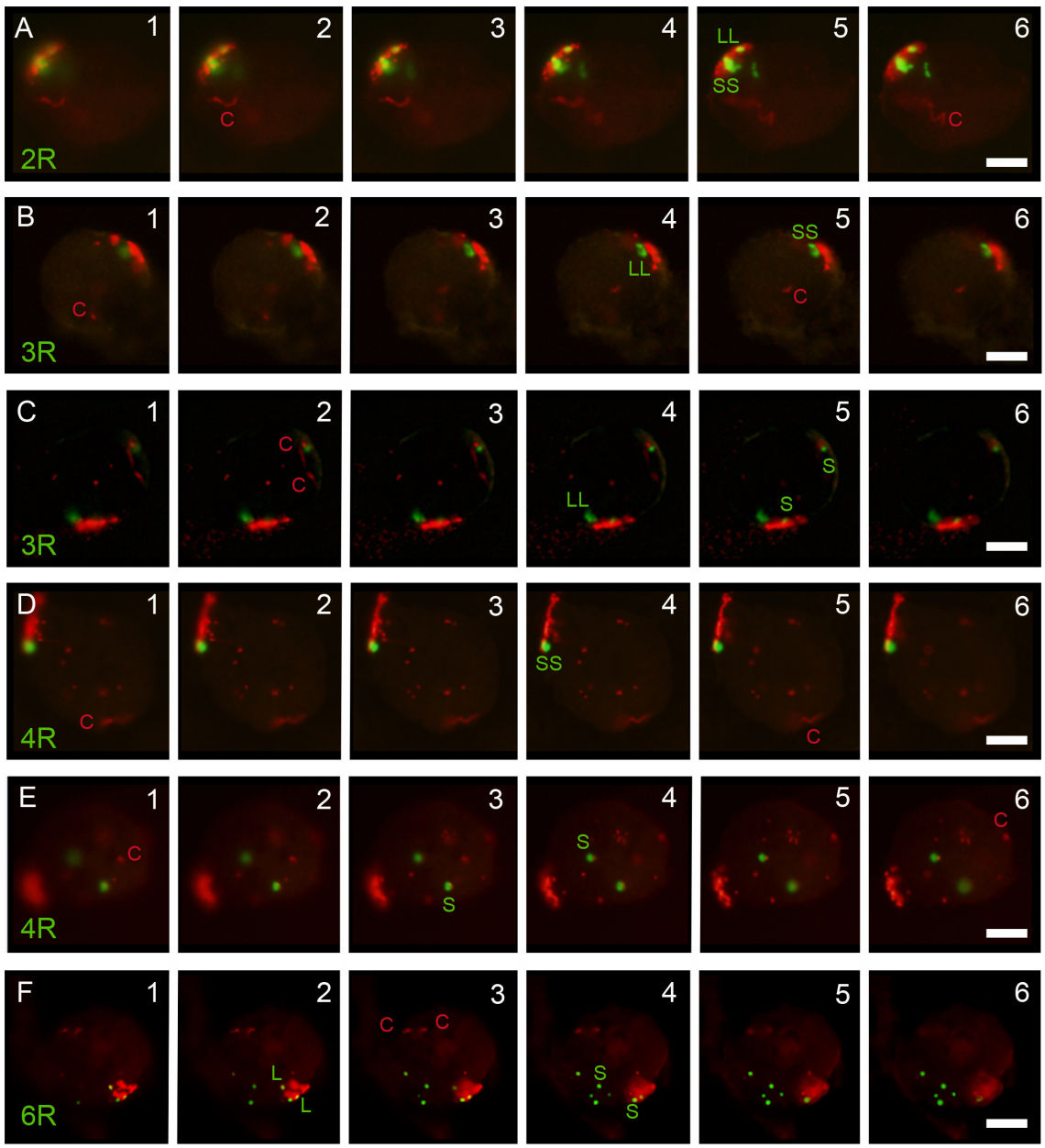

FIGURE 3 | 3D analysis of the arrangement of the subtelomeric chromomeres (green) of the short (S) and long (L) arm or rye chromosomes at the bouquet in wheat-rye additions. The telomere cluster (red) and the rye centromeres (c) are indicated. **(A)** Nucleus with the two ends of 2R at the telomere cluster. Homologous chromomeres of both arms are associated. **(B)** The subtelomeric chromomeres of 3RS and 3RL are associated and incorporated to the telomere cluster. **(C)** The subtelomeric chromomeres of 3RL are associated and incorporated to the telomere cluster. Only one 3RS telomere is in the telomere cluster. **(D)** The ends of 4RS are associated and locate at the telomere cluster. **(E)** The 4RS telomeres are separated and locate out of the telomere cluster. **(F)** Both ends of the chromosome pair 6R are separated, the two 6RL telomeres and one telomere of 6RS are included in the telomere cluster. Bars represent 10 μm.

Rye Chromosome Arms Differ in the Level of Synapsis of Their Distal Half

In many plant species crossovers are non-random distributed along the chromosomes. In wheat, barley and rye, they are confined to the distal half of each chromosome arm (Lukaszewski and Curtis, 1993; Akhunov et al., 2003; Lukaszewski, 2008; Valenzuela et al., 2012; Higgins et al., 2014). Such regions should undergo synapsis in order to facilitate the occurrence of crossovers. Most rye pachytene bivalents showed synapsed the distal half of both chromosome arms (**Figures 2C,E**, **5A,B**), however, unmatched chromosome arms were also observed (**Figures 6A,B**). Failure of synapsis in the distal half varied between chromosomes arms (**Figure 6C** and **Table 3**). Chromosome arms 5RS and

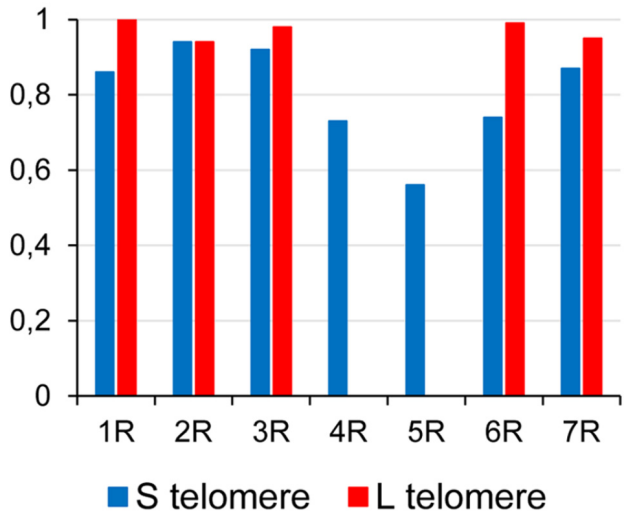

FIGURE 4 | Probability of inclusion in the telomere cluster of the telomeres of rye chromosome arms carrying subtelomeric chromomeres in wheat-rye additions.

6RS, with disturbed telomere migration during leptotene, showed the lowest level of synapsis. Chromosome arm 4RS, despite restricted telomere migration, completed synapsis in most PMCs. Because synapsis progresses from the end to the center of the chromosomes (Corredor et al., 2007), unsynapsed stretches were more often observed in proximal regions, especially in chromosomes 6R and 7R (**Table 3**).

TABLE 2 | Mean separation between the two ends of each completely synapsed rye bivalent (S-L distance), average nuclear diameter (ND) and S-L distance/ND rate in PMCs at pachytene of wheat-rye additions.

Chromosome	S-L distance (μm)	ND (μm)	S-L distance/ND	PMCs
1R	21.6 ± 1.9	48.4 ± 1.6	0.45	143
2R	25.8 ± 2.7	61.8 ± 2.7	0.42	101
3R	19.4 ± 2.2	52.4 ± 2.3	0.37	107
4R	21.6 ± 2.3	50.9 ± 2.1	0.42	115
5R	18.8 ± 3.1	41.0 ± 2.9	0.46	43
6R	22.7 ± 2.3	48.4 ± 2.2	0.47	94
7R	26.0 ± 2.7	61.2 ± 2.4	0.42	126

Chiasma Formation Is Affected in Arms That Fail to Synapse and in Arms With a High Level of Synapsis

Chiasmata formed by rye chromosomes were inferred from the occurrence of association between each homologous arm pair in PMCs at metaphase I (**Figure 7**). Two homologous arms bound at metaphase I had formed at least one chiasmata, but it is difficult to establish whether additional chiasmata were present or not. Thus, the frequency of homologous arms association at metaphase I represents an underestimation of the number of chiasmata per chromosome arm. **Table 4** shows the frequency of association for the different rye chromosome arms as well as the total number of associations per cell. Both arms of chromosomes 1R, 3R, and 7R, and the long arm of chromosome 2R formed chiasmata with frequencies higher than 90%. The remaining arms showed lower frequencies, especially the arms 2RS, 4RS, 4RL, 5RS, and 6RS, whose frequencies ranged between 25 and 70%. The total number of associations varied between lines. A maximum number of 42 arm associations can be formed in the wheat-1R line and 44 in the

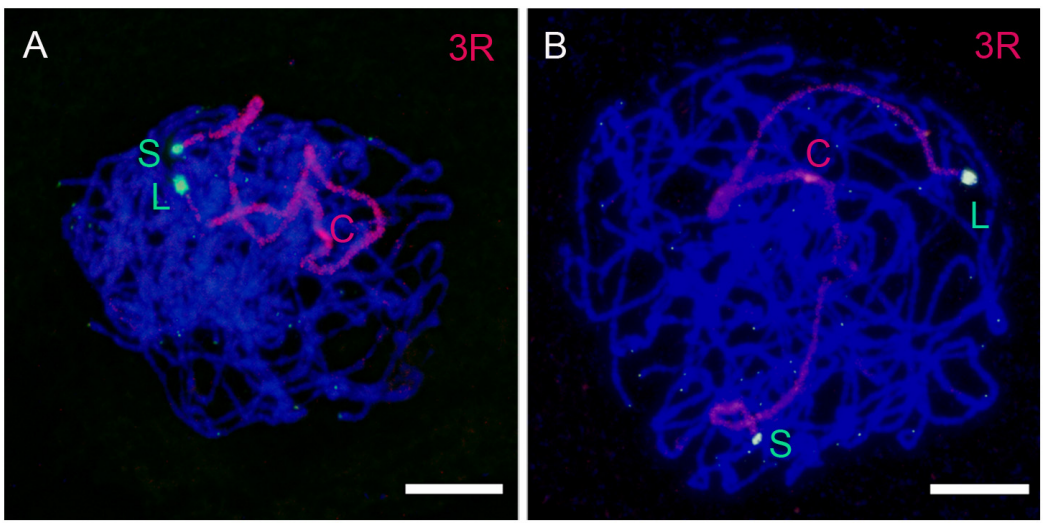

FIGURE 5 | Variable separation of the ends of the rye bivalent in pachytene nuclei of the wheat-3R addition. **(A)** Chromosome ends closely located. **(B)** Very distant chromosome ends. Bars represent 10 μm.

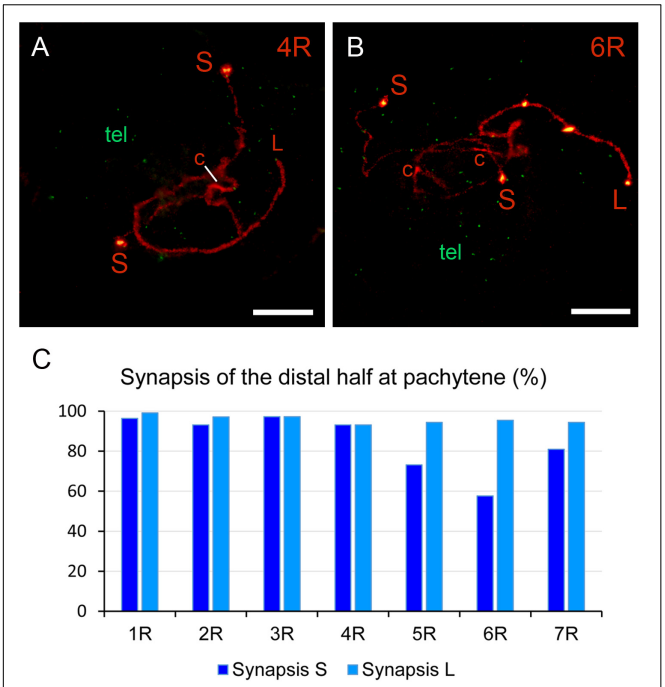

FIGURE 6 | Synapsis of rye chromosomes in nuclei at pachytene in wheat-rye additions. **(A,B)** Nuclei showing partial synapsis of chromosomes 4R **(A)** and 6R **(B)**. The ends of the short (S) and long (L) arms, the rye centromeres (c) and all telomeres (green) are shown. **(C)** Level of synapsis in the distal half of both arms of the seven rye chromosomes. Bars represent 10 μm.

other six lines. Thus, chiasma formation failed not only between rye chromosome arms but also between wheat chromosomes, especially in the addition lines wheat-4R and wheat-5R.

DISCUSSION

The majority of rye chromosomes of the addition lines studied undergo a meiotic behavior that it is different from that observed in rye itself. This is apparent, if attention is paid to the number of chiasmata formed. In rye, a total of 13.4 (1.9/chromosome) chiasmate bonds are formed at metaphase I (Naranjo and Lacadena, 1980). This figure represents an association frequency of 95.7% per chromosome arm. In the wheat-rye additions, the arms 2RS, 4RS, 4RL, 5RS, and 6RS show much lower frequencies of association (<71%, **Table 4**). But let us analyze separately the different steps of prophase I that precedes chiasma formation.

Chromatin Remodeling

Remodeling of chromatin produced in leptotene leads to a more relaxed chromosome organization, which most likely facilitates the search of the homologous partner. During the SC assembly, the axial elements (chromosomes) become shortened. This shortening has been quantified in electron microscopic studies of spread nuclei of both rye (Gillies, 1985) and wheat (Martínez et al., 2001). The length of SCs at pachytene is approximately 80% of the length in zygotene. One can assume that rye chromosomes suffered a similar shortening in the course of zygotene in wheat-rye addition lines. According to the length of pachytene bivalents in the wheat-rye additions studied, rye chromosomes fall into two categories, one corresponds to chromosome 4R, with a length of 172.8 μm, and the other contains the six remaining chromosomes, with an average length of 100.6 μm. Such a divergence does not exist in rye itself. The length of SC bivalents at pachytene in two different stocks of rye, ranged between 72.2–61.8 μm and 64.0–54.1 μm, respectively (Gillies, 1985). Thus, the appearance of two different chromatin reorganization patterns between the chromosomes of rye suggests chromosome-specific responses to the new genetic background in which they have been introgressed.

One could assume that differences in length between chromosomes in pachytene might be a result of differences in their DNA content, given the large size, 8.1 Gb, of the rye genome (Doležel et al., 1998). Chromosome 4R consists of a DNA sequence of 1435 Mb, which represents 17.4% of the rye genome. This sequence is higher than those of the other six chromosomes, which range between 1023 Mb (1R) and 1253 Mb (2R) with an average size of 1136 Mb/chromosome (Martis et al., 2013). Taken into account the chromosomal length, the group of six chromosomes shows a mean packaging level of 11.3 Mb per μm in the pachytene bivalents while the ratio decreases to 8.3 Mb per μm in the case of 4R. The packaging level of chromosome 4R represents 73% of that observed in the other chromosomes. Thus, differences between chromosomes in their length at pachytene are the result, not only of differences in the DNA content, but also of distinct patterns of chromatin reorganization during early prophase I.

TABLE 3 | Frequency (%) of PMCs with synapsis involving the distal half or the proximal half of individual rye chromosome arms at pachytene in disomic wheat-rye additions.

Chromosome	Distal half of the S arm	Proximal half of the S arm	Distal half of the L arm	Proximal half of the L arm	PMCs
1R	96.4	88.1	99.1	96.4	194
2R	93.1	82.2	97.1	86.1	101
3R	97.2	95.3	97.2	95.3	107
4R	93.1	87.0	93.1	84.7	131
5R	73.2	66.2	94.4	87.3	71
6R	57.7	57.7	95.4	78.5	130
7R	81.0	61.9	94.4	57.9	126

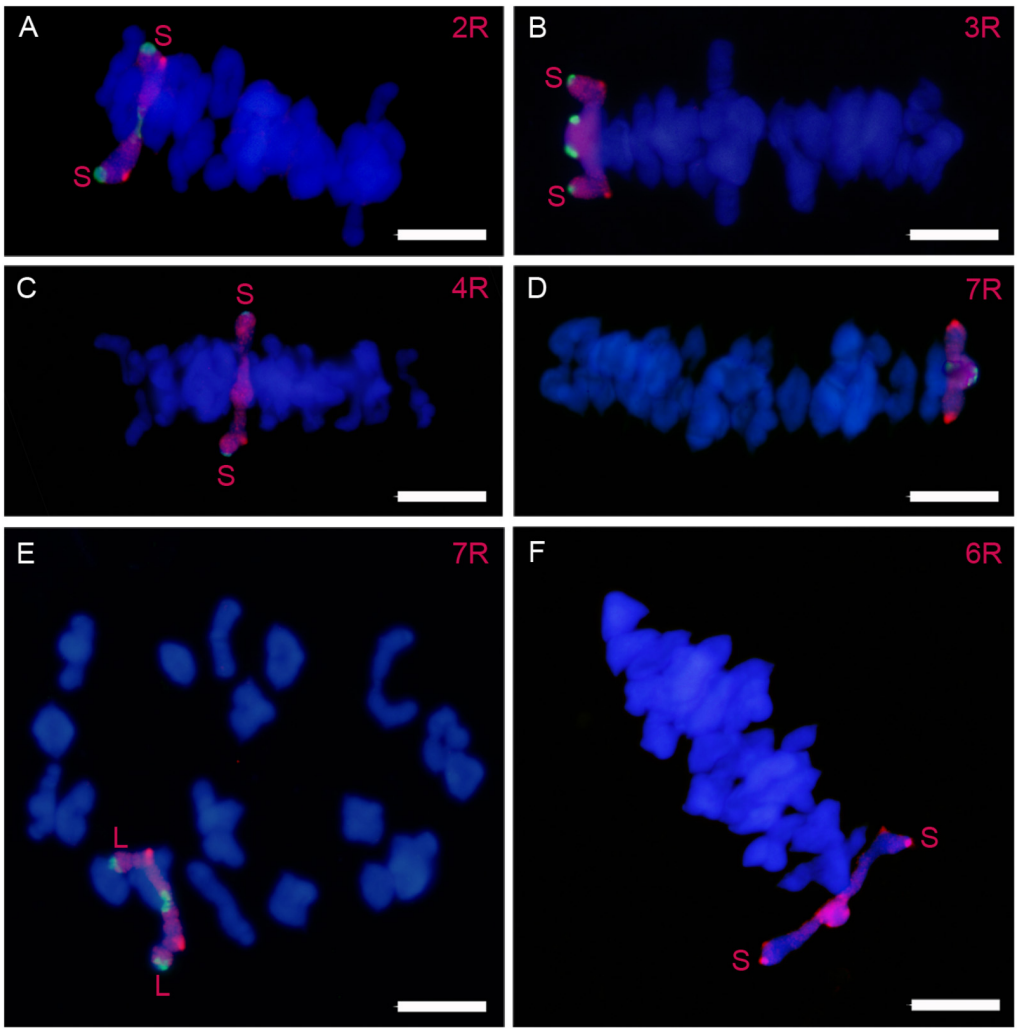

FIGURE 7 | Rye bivalents in cells at metaphase I in wheat-rye additions. An open bivalent with the long arm bound is formed by chromosomes 2R **(A)**, 3R **(B)**, 4R **(C)**, and 6R **(F)** The long arm is bound in the open bivalent formed by chromosome 7R **(E)**. Chromosome pair 3R **(D)** forms a ring bivalent. Bars represent 10 μm.

It is also noteworthy that the mean length of rye chromosomes at pachytene is much higher in the addition lines, 110.9 μm, than in rye itself, 62.5 μm (Gillies, 1985). The mean length of 110.9 μm found in the wheat-rye additions fits the average length of 90.2 μm of wheat chromosomes (Martínez et al., 2001). This variation of the mean chromosome length supports that the pattern of chromatin remodeling of a given chromosome at leptotene is controlled by the genetic background in which such a chromosome is present. In pachytene bivalents, the two homologues are closely juxtaposed along their entire length by the installation of the SC. Each chromatid of the bivalent consists of a linear arrangement of loops whose bases are anchored to the SC lateral element. Axes of sister chromatids are closely juxtaposed and their loops project out of the SC (Zickler and Kleckner, 2015). The density of loops along the pachytene axis is quite conserved in different organisms (∼20 loops per micron) (Kleckner, 2006). The evolutionarily conserved loop spacing implies that variation in the chromosome axis length should be accompanied by inversely correlated differences in the loops size. This is manifested in mice mutants that have altered the meiotic-specific cohesin Smc1β and the SC lateral component Sycp3; relatively long chromosome axes project short loops while shorter chromosome axes are coupled with longer loops (Revenkova and Jessberger, 2006; Novak et al., 2008). Thus, the increase of the length of rye pachytene bivalents in wheat-rye addition lines relative to plants of rye, as well as differences between lines, should be the result of modifications in the number and size of the loops.

Little is known about the impact of molecular interactions underlying the introgression of rye chromatin in a wheat background. A comparison of the transcriptomes of wheat, barley and a wheat-barley ditelosomic 7HL addition revealed reprograming of the transcriptomes of wheat and 7HL in the addition line (Rey et al., 2018). Only 3% of wheat genes underwent a different transcription rate in the addition line relative to wheat, while 42% of genes of 7HL were up- or

TABLE 4 | Frequency (%) of association of individual rye chromosomes arms and total number of bounds in cells at metaphase I of disomic wheat-rye additions.

Chromosome	S arm	L arm	Total bounds	PMCs
1R	91.1[a]	98.9[a]	41.7 ± 0.1	90
2R	67	96	41.3 ± 0.2	100
3R	95	96	43.3 ± 0.2	100
4R	46	70	37.9 ± 0.2	100
5R	36.4[a]	83.2[a]	39.7 ± 0.1	173
6R	25[a]	86[a]	40.9 ± 0.1	200
7R	92	98	42.4 ± 0.4	100

[a]*After Naranjo (2014).*

down-regulated in the addition line relative to barley. These results evidence the existence of interactions between genes of both species, which may change with the introgressed chromosome. Thus, chromosome-specific molecular interactions affecting genetic functions related to the reorganization of chromatin during prophase I could cause differences between lines. Whether comparable genetic interactions exist or not in other sets of wheat-rye additions is unknown. This point may be addressed in future research works.

Clustering and Dispersion of Telomeres

Telomeres of the long arms 1RL, 2RL, 3RL, 6RL, and 7RL as well as telomeres of the short arm of metacentric chromosomes 2R, 3R, and 7R, were included in the telomere cluster in almost all PMCs. By contrast, the telomere of the short arm of submetacentric chromosomes 4R, 5R, and 6R showed a lower probability of inclusion in the telomere cluster. This result reinforces previous studies supporting a chromosome conformation dependence in the ability of telomeres to converge in the telomere pole (Naranjo et al., 2010; Naranjo, 2014). Chromosome 1R with a centromeric index lower than that of 4R shows, however, a behavior more similar to that of metacentric chromosomes. It is possible that the presence in its short arm of the nucleolar organizing region, where chromatin is more relaxed, could affect the arrangement of this chromosome during leptotene.

The organization of the bouquet is the result of three interdependent events: the attachment of telomeres to the cytoskeleton through a nuclear envelope protein bridge, the oriented telomere cytoskeleton-mediated movement, and the clustering of telomeres in a small region of the nuclear membrane. Some of these steps were affected in the telomeres of the arms 4RS, 5RS, and 6RS. The link between the cytoskeleton and the chromosome ends during meiosis is provided by a complex of proteins among which are the transmembrane SUN (sad1/UNC-84) domain protein that interact with the chromosome ends (Starr, 2009) and the KASH (Klarsicht/Anc/Syne homology) domain protein that in turn interact with elements of the cytoskeleton (Starr and Fridolfsson, 2010). The function that the SUN and KASH proteins develop in fungi and animals is conserved in the plant kingdom from the most ancestral plant species to advanced angiosperms (Poulet et al., 2017). In maize and *Arabidobsis*, SUN protein foci spread through the nuclear envelop during leptotene, cluster in the periphery of one hemisphere at the bouquet, and back to spread through all the nuclear envelop during and beyond pachytene (Murphy et al., 2014; Varas et al., 2015). This SUN proteins distribution suggests that any chromosome end, regardless its location, has the possibility of finding its attachment to the nuclear envelope prior to migration. Thus, failure of the attachment of telomeres of 4RS, 5RS, and 6RS to the nuclear envelope does not seem the reason of their disturbed positioning.

Another explanation of the behavior of telomeres of 4RS, 5RS, and 6RS is that they have to cover longer distances than other telomeres to reach the telomere pole during the bouquet organization. This explanation is based under the assumption that the site of the telomere pole is most likely installed in the region of the telomeric hemisphere with the highest density of telomeres, that is, in the region where telomeres of long arms are located. In such a situation, telomeres of metacentric chromosomes can be equidistant relative to the telomere pole, while telomeres of the short arms of submetacentric chromosomes lay farther away of this pole. In support of this assumption are two facts: (i) telomeres of the long arms are included in the telomere cluster in almost all cells, (ii) the centromeric end of telocentric chromosomes fails also in its incorporation to the telomere pole (Corredor and Naranjo, 2007). The telomere of the centromeric end of the 5RL telocentric locates at the centromere pole at early leptotene. In the course of leptotene this chromosome end abandons the centromere pole to cluster with the other telomeres in the opposite pole. However, only 51% of the centromeric ends incorporate into the telomere cluster at the consolidated bouquet stage.

The effect of chromosome conformation on telomere clustering is not extended to the movement produced during zygotene, which disperses telomeres through all the nuclear periphery. Telomeres of any chromosome pair are very close at the bouquet and their separation seems to be at random, i.e., without any programed itinerary. Within lines variation of the distance between the ends of the rye bivalent at pachytene agrees with a random dispersion of telomeres. Most likely, the overall arrangement of bivalents in the nucleus and the simultaneous movement of all chromosomes should condition severely the distance covered by each telomere.

Synapsis and Chiasma Formation

Restriction of chiasma formation to the distal half of chromosome arms in species such as wheat, rye or barley (Lukaszewski and Curtis, 1993; Akhunov et al., 2003; Lukaszewski, 2008; Valenzuela et al., 2012; Higgins et al., 2014) implies that such chromosome regions should develop synapse regularly. This was so for most rye chromosome arms. All of the arms with normal telomere migration during the bouquet organization showed normal synapsis. Failure of synapsis affected mainly the short arm of submetacentric chromosomes 5R and 6R. Synapsis failure in these arms was preceded of disturbed migration of their telomere during the bouquet formation, which most likely impeded the occurrence of physical interactions and synapsis initiation between their subtelomeric homologous. The behavior of 5RS and 6RS is in

contrast with that of 4RS, which completed synapsis despite its telomere failed also to be included in the telomere cluster. What makes chromosome arm 4RS different? This arm reaches a much higher length at pachytene than 5RS and 6RS. Unfolding of chromatin produced in leptotene obliges chromosomes to move and span the entire nucleus because their length exceeds largely the nuclear diameter. The intensity of the movement is expected to increase with the length reached by each chromosome. Such a chromosome dynamics might promote the occurrence of chance encounters between intercalary homologous regions regardless their respective telomeres were separated. Under this assumption, the probability of intercalary interactions between homologues is expected to be higher in chromosome arm 4RS than in 5RS and 6RS. Synapsis initiated intercalarily in 4RS could extend later to its distal region, although the telomeres were not initially associated. This situation is comparable to that found in an inversion heterozygote for the long arm of chromosome 1R. In this heterozygote, the crossover-rich region is positioned distally in the standard chromosome and proximally in the inverted chromosome at the initiation of meiosis, i.e., they are located in opposite poles of the nucleus. However, during zygotene, a non-telomere led chromosome movement, the movement generated by chromosome elongation, makes it possible that these homologous regions find one another and that the entire arm complete synapsis (Lukaszewski, 2008; Valenzuela et al., 2012; Naranjo, 2014). Thus, the high level of synapsis of chromosome 4R can be the result of homologous interactions facilitated either by the bouquet organization or, in cells with disturbed migration of the 4RS telomere, by the chromosome movement derived of chromatin unfolding. The distal half of the short arm of metacentric chromosome 7R showed a level of synapsis of 81%, which is higher than that of 5RS (73%) or 6RS (57%) but lower than the level of the remaining arms (**Table 2**). However, the frequency 92% of association of chromosome arm 7RS at metaphase I suggests an almost normal level of synapsis in the anther where metaphase I was studied.

Chiasma distribution in rye chromosomes of wheat-rye addition lines was earlier studied (Drögenmüller and Lelley, 1984). However, the number of chiasmate bonds per bivalent instead the association frequency of each chromosome arm was reported. Nevertheless, chromosomes 5R and 6R formed a more reduced number of chiasmata than the remaining rye chromosomes. Reduction of the number of chiasmata in chromosomes 5R and 6R affects mainly their short arm (**Table 4**) and is the consequence of the synapsis failure that such arms showed at pachytene. However, other arms with normal synapsis suffered a considerable reduction of the chiasma frequency. This was the case of the arms 2RS, 4RS, and 4RL. The wheat-4R addition line showed the lowest number of chiasmate bonds, 37.9, which is far from 44, the expected maximum number. Environmental variation could explain minor differences between lines, but the low chiasma frequency observed in the wheat-4R addition suggests a negative effect of the genetic background of this line on chiasma formation, which affects both wheat and rye chromosomes. Addition of individual chromosomes of rye to wheat produce changes in traits such as spike and spikelet morphology (Driscoll and Sears, 1971). Addition of chromosome 4R increases also the length of the anthers and the number of pollen grains, while the addition of 1R or 2R reduce fertility (Nguyen et al., 2015). It is possible that chromosome 4R carries some genetic information that interferes on chiasma formation. The wheat-2R addition forms, however, a high number of chiasmata, 41.3. The reduction observed in chromosome arm 2RS seems to be chromosome-specific and derived from the genetic constitution or chromatin organization of this arm. In fact, chromosome arm 2RS carries a large subtelomeric heterochromatin chromomere and such a heterochromatin has been shown to reduce the number of chiasmata of rye chromosomes in wheat-rye derivatives (Naranjo and Lacadena, 1980).

AUTHOR CONTRIBUTIONS

TN designed and conducted the research and wrote the work.

FUNDING

This work was supported by grant AGL2015-67349-P from Dirección General de Investigación Científica y Técnica, Ministerio de Economía y Competitividad of Spain.

ACKNOWLEDGMENTS

I would like to thank A. Lukaszewski for kindly supplying the wheat-rye introgression lines.

REFERENCES

Akhunov, E. D., Goodyear, A. W., Geng, S., Qi, L. L., Echalier, B., Gill, B. S., et al. (2003). The organization and rate of evolution of wheat genomes are correlated with recombination rates along chromosome arms. *Genome Res.* 13, 753–763. doi: 10.1101/gr.808603

Bass, H. W., Marshall, W. F., Sedat, J. W., Agard, D. A., and Cande, W. Z. (1997). Telomeres cluster de novo before the initiation of synapsis: a three-dimensional spatial analysis of telomere positions before and during meiotic prophase. *J. Cell Biol.* 137, 5–18. doi: 10.1083/jcb.137.1.5

Bass, H. W., Riera-Lizarazu, O., Ananiev, E. V., Bordoli, S. J., Rines, H. W., Phillips, R. L., et al. (2000). Evidence for the coincident initiation of homolog pairing and synapsis during the telomere-clustering (bouquet) stage of meiotic prophase. *J. Cell Sci.* 113, 1033–1042.

Baudat, F., Manova, K., Yuen, J. P., Jasin, M., and Keeney, S. (2000). Chromosome synapsis defects and sexually dimorphic meiotic progression in mice lacking Spo11. *Mol. Cell* 6, 989–998. doi: 10.1016/S1097-2765(00)00098-8

Bedbrook, J. R., Jones, J., O'Dell, M., Thompson, R. D., and Flavell, R. B. (1980). A molecular description of telomeric heterochromatin in *Secale* species. *Cell* 19, 545–560. doi: 10.1016/0092-8674(80)90529-2

Caryl, A. P., Armstrong, S. J., Jones, G. H., and Franklin, F. C. H. (2000). A homologue of the yeast *HOP1* gene is inactivated in the *Arabidopsis* meiotic mutant asy1. *Chromosoma* 109, 62–71. doi: 10.1007/s004120050413

Corredor, E., Lukaszewski, A. J., Pachón, P., Allen, D. C., and Naranjo, T. (2007). Terminal regions of wheat chromosomes select their pairing partner in meiosis. *Genetics* 177, 699–706. doi: 10.1534/genetics.107.078121

Corredor, E., and Naranjo, T. (2007). Effect of colchicine and telocentric chromosome conformation on centromere and telomere dynamics at meiotic prophase I in wheat-rye additions. *Chromosome Res.* 15, 231–245. doi: 10.1007/s10577-006-1117-7

Cowan, C. R., Carlton, P. M., and Cande, W. Z. (2001). The polar arrangement of telomeres in interphase and meiosis. Rabl organization and the bouquet. *Plant Physiol.* 125, 532–538. doi: 10.1104/pp.125.2.532

Croft, J. A., and Jones, G. H. (1989). Meiosis in *Mesostoma ehrenbergii ehrenbergii.* IV. Recombination nodules in spermatocytes and a test of the correspondence of late recombination nodules and chiasmata. *Genetics* 121, 255–262.

Cuadrado, A., and Schwarzacher, T. (1998). The chromosomal organization of simple sequence repeats in wheat and rye genomes. *Chromosoma* 107, 587–594. doi: 10.1007/s004120050345

Darvey, N. L., and Gustafson, J. P. (1975). Identification of rye chromosomes in wheat-rye addition lines and triticale by heterochromatin bands. *Crop Sci.* 15, 239–243. doi: 10.2135/cropsci1975.0011183X001500020029x

Ding, D. Q., Yamamoto, A., Haraguchi, T., and Hiraoka, Y. (2004). Dynamics of homologous chromosome pairing during meiotic prophase in fission yeast. *Dev. Cell* 6, 329–341. doi: 10.1016/S1534-5807(04)00059-0

Doležel, J., Greilhuber, J., Lucretti, S., Meister, A., Lysák, M. A., Nardi, L., et al. (1998). Plant genome size estimation by flow cytometry: inter-laboratory comparison. *Ann. Bot.* 82, 17–26. doi: 10.1093/oxfordjournals.aob.a010312

Driscoll, C. J., and Sears, E. R. (1971). Individual addition of the chromosomes of "imperial" rye to wheat. *Agron. Abst.* 6.

Drögenmüller, E. M., and Lelley, T. (1984). Chiasma distribution in rye chromosomes of diploid rye and in wheat/rye addition lines in relation to C-heterochromatin. *Theor. Appl. Genet.* 67, 457–461. doi: 10.1007/BF00263412

Drouaud, J., Mercier, R., Chelysheva, L., Bérard, A., Falque, M., Martin, O., et al. (2007). Sex-specific crossover distributions and variations in interference level along *Arabidopsis thaliana* chromosome 4. *PLoS Genet.* 3:e106. doi: 10.1371/journal.pgen.0030106

Ferdous, M., Higgins, J. D., Osman, K., Lambing, C., Roitinger, E., Mechtler, K., et al. (2012). Inter-homolog crossing-over and synapsis in *Arabidopsis* meiosis are dependent on the chromosome axis protein AtASY3. *PLoS Genet.* 8:e1002507. doi: 10.1371/journal.pgen.1002507

Fogwill, M. (1958). Differences in crossing-over and chromosome size in the sex cells of Lilium and Fritillaria. *Chromosoma* 9, 493–504. doi: 10.1007/BF02568089

Franki, M. G. (2001). Identification of Bilby, a diverged centromeric Ty1-copia retrotransposon family from cereal rye (*Secale cereale* L.). *Genome* 44, 266–274. doi: 10.1139/g00-112

Gillies, C. B. (1985). An electron microscopic study of synaptonemal complex formation at zygotene in rye. *Chromosoma* 92, 165–175. doi: 10.1007/BF00348690

Gonzalez-Garcia, M., Cuacos, M., Gonzalez-Sanchez, M., Puertas, M. J., and Vega, J. M. (2011). Painting the rye genome with genome-specific sequences. *Genome* 54, 555–564. doi: 10.1139/G11-003

Higgins, J. D., Osman, K., Jones, G. H., and Franklin, F. C. H. (2014). Factors underlying restricted crossover localization in barley meiosis. *Annu. Rev. Genet.* 48, 29–47. doi: 10.1146/annurev-genet-120213-092509

Hollingsworth, N. M., and Byers, B. (1989). *Hop1*: a yeast meiotic pairing gene. *Genetics* 121, 445–462.

Hou, Y., Fan, W., Yan, L., Li, R., Lian, Y., Huang, J., et al. (2013). Genome analyses of single human oocytes. *Cell* 155, 1492–1506. doi: 10.1016/j.cell.2013.11.040

Hunter, N., and Kleckner, N. (2001). The single-end invasion: an asymmetric intermediate at the double-strand break to double-holliday junction transition of meiotic recombination. *Cell* 106, 59–70. doi: 10.1016/S0092-8674(01)00430-5

Keeney, S., Giroux, C. N., and Kleckner, N. (1997). Meiosis-specific DNA double-strand breaks are catalyzed by Spo11, a member of a widely conserved protein family. *Cell* 88, 375–384. doi: 10.1016/S0092-8674(00)81876-0

Kleckner, N. (2006). Chiasma formation: chromatin/axis interplay and the role(s) of the synaptonemal complex. *Chromosoma* 115, 175–194. doi: 10.1007/s00412-006-0055-7

Lake, C. M., and Hawley, R. S. (2012). The molecular control of meiotic chromosomal behavior: events in early meiotic prophase in Drosophila oocytes. *Annu. Rev. Physiol.* 74, 425–451. doi: 10.1146/annurev-physiol-020911-153342

Lukaszewski, A. J. (2008). Unexpected behavior of an inverted rye chromosome arm in wheat. *Chromosoma* 117, 569–578. doi: 10.1007/s00412-008-0174-4

Lukaszewski, A. J. (2015). "Introgressions between wheat and rye," in *Alien Introgression in Wheat*, eds M. Molnár-Láng, C. Ceoloni, and J. Doležel (Cham: Springer), 163–189. doi: 10.1007/978-3-319-23494-6_7

Lukaszewski, A. J., and Curtis, C. A. (1993). Physical distribution of recombination in B-genome chromosomes of tetraploid wheat. *Theor. Appl. Genet.* 86, 121–127. doi: 10.1007/BF00223816

Maestra, B., De Jong, J. H., Shepherd, K., and Naranjo, T. (2002). Chromosome arrangement and behavior of two rye telosomes at the onset of meiosis in disomic wheat-5RL addition lines with and without the *Ph1* locus. *Chromosome Res.* 10, 655–667. doi: 10.1023/A:1021564327226

Martínez, M., Cuñado, N., Carcelén, M., and Romero, C. (2001). The Ph1 and Ph2 loci play different roles in the synaptic behavior of hexaploid wheat *Triticum aestivum*. *Theor. Appl. Genet.* 103, 398–405. doi: 10.1007/s00122-001-0543-3

Martis, M. M., Zhou, R., Haseneyer, G., Schmutzer, T., Vrána, J., Kubaláková, M., et al. (2013). Reticulate evolution of the rye genome. *Plant Cell* 25, 3685–3698. doi: 10.1105/tpc.113.114553

Murphy, S., Gumber, H. K., Mao, Y., and Bass, H. (2014). A dynamic meiotic SUN belt includes the zygotene-stage telomere bouquet and is disrupted in chromosome segregation mutants of maize (*Zea mays* L.). *Front. Plant Sci.* 5:314. doi: 10.3389/fpls.2014.00314

Naranjo, T. (2014). Dynamics of rye telomeres in a wheat background during early meiosis. *Cytogenet. Genome Res.* 143, 60–68. doi: 10.1159/000363524

Naranjo, T. (2015). Forcing the shift of the crossover site to proximal regions in wheat chromosomes. *Theor. Appl. Genet.* 128, 1855–1863. doi: 10.1007/s00122-015-2552-7

Naranjo, T., and Corredor, E. (2008). Nuclear architecture and chromosome dynamics in the search of the pairing partner in meiosis in plants. *Cytogenet. Genome Res.* 120, 320–330. doi: 10.1159/000121081

Naranjo, T., and Lacadena, J. R. (1980). Interaction between wheat chromosomes and rye telomeric heterochromatin on meiotic pairing of chromosome pair 1R of rye in wheat-rye derivatives. *Chromosoma* 81, 249–261. doi: 10.1007/BF00285951

Naranjo, T., Valenzuela, N., and Perera, E. (2010). Chiasma frequency is region-specific and chromosome conformation-dependent in a rye chromosome added to wheat. *Cytogenet. Genome Res.* 129, 133–142. doi: 10.1159/000314029

Neale, M. J., and Keeney, S. (2006). Clarifying the mechanics of DNA strand exchange in meiotic recombination. *Nature* 442, 153–158. doi: 10.1038/nature04885

Nguyen, V., Fleury, D., Timmins, A., Laga, H., Hayden, M., Mather, D., et al. (2015). Addition of rye chromosome 4R to wheat increases anther length and pollen grain number. *Theor. Appl. Genet.* 128, 953–964. doi: 10.1007/s00122-015-2482-4

Niwa, O., Simanuki, M., and Miki, F. (2000). Telomere-led bouquet formation facilitates homologous chromosome pairing and restricts ectopics interactions in fission yeast meiosis. *EMBO J.* 19, 3831–3840. doi: 10.1093/emboj/19.14.3831

Nonomura, K. I., Nakano, M., Eiguchi, M., Suzuki, T., and Kurata, N. (2006). PAIR2 is essential for homologous chromosome synapsis in rice meiosis I. *J. Cell Sci.* 119, 217–225. doi: 10.1242/jcs.02736

Novak, I., Wang, H., Revenkova, E., Jessberger, R., Scherthan, H., and Höög, C. (2008). Cohesin Smc1b determines meiotic chromatin axis loop organization. *J. Cell Biol.* 180, 83–90. doi: 10.1083/jcb.200706136

Oakley, H. A. (1982). Meiosis in *Mesostoma ehrenbergii ehrenbergii* (Turbellaria, Rhabdocoela). 11. Synaptonemal complexes, chromosome pairing and disjunction in achiasmate oogenesis. *Chromosoma* 87, 133–147. doi: 10.1007/BF00338485

Oakley, H. A., and Jones, G. H. (1982). Meiosis in *Mesostoma ehrenbergii ehrenbergii* (Turbellaria, Rhabdocoela)- I. Chromosome pairing, synaptonemal complexes and chiasma localisation in spermatocytes. *Chromosoma* 85, 311–322. doi: 10.1007/BF00330355

Page, J., de la Fuente, R., Gómez, R., Calvente, A., Viera, A., and Parra, M. T. (2006). Sex chromosomes, synapsis, and cohesins: a complex affair. *Chromosoma* 115, 250–259. doi: 10.1007/s00412-006-0059-3

Page, S. L., and Hawley, R. S. (2004). The genetics and molecular biology of the synaptonemal complex. *Annu. Rev. Cell Dev. Biol.* 20, 525–558. doi: 10.1146/annurev.cellbio.19.111301.155141

Pastor, J. B., and Callan, H. G. (1952). Chiasma formation in spermatocytes and oocytes of the turbellarian *Dendrocoelum lacteum*. *J. Genet.* 50, 449–454. doi: 10.1007/BF02986840

Perry, P. E., and Jones, G. H. (1974). Male and female meiosis in grasshoppers. *Chromosoma* 47, 227–236. doi: 10.1007/BF00328858

Petkov, P. M., Broman, K. W., Szatkiewicz, J. P., and Paigen, K. (2007). Crossover interference underlies sex differences in recombination rates. *Trends Genet.* 23, 539–542. doi: 10.1016/j.tig.2007.08.015

Poulet, A., Probst, A. V., Graumann, K., Tatout, C., and Evans, D. (2017). Exploring the evolution of the proteins of the plant nuclear envelope. *Nucleus* 8, 46–59. doi: 10.1080/19491034.2016.1236166

Rasmussen, S. W. (1977). Meiosis in *Bombyx mori* females. *Philos. Trans. R. Soc. Lond. B Biol. Sci.* 277, 343–350. doi: 10.1098/rstb.1977.0022

Revenkova, E., and Jessberger, R. (2006). Shaping meiotic prophase chromosomes: cohesins and synaptonemal complex proteins. *Chromosoma* 115, 235–240. doi: 10.1007/s00412-006-0060-x

Rey, E., Abrouk, M., Keeble-Gagnère, G., Karafiátová, M., Vrána, J., Balzergue, S., et al. (2018). Transcriptome reprogramming due to the introduction of a barley telosome into bread wheat affects more barley genes than wheat. *Plant Biotechnol. J.* doi: 10.1111/pbi.12913 [Epub ahead of print].

Richards, E. J., and Ausubel, S. M. (1988). Isolation of a higher eukaryotic telomere sequence from *Arabidopsis thaliana*. *Cell* 53, 127–136. doi: 10.1016/0092-8674(88)90494-1

Roeder, G. S. (1997). Meiotic chromosomes: it takes two to tango. *Genes Dev.* 11, 2600–2621. doi: 10.1101/gad.11.20.2600

Rog, O., and Dernburg, A. F. (2013). Chromosome pairing and synapsis during *Caenorhabditis elegans* meiosis. *Curr. Opin. Cell Biol.* 25, 349–356. doi: 10.1016/j.ceb.2013.03.003

Romanienko, P. J., and Camerini-Otero, R. D. (2000). The mouse *Spo11* gene is required for meiotic chromosome synapsis. *Mol. Cell* 6, 975–987. doi: 10.1016/S1097-2765(00)00097-6

Scherthan, H. (2001). A bouquet makes ends meet. *Nat. Rev. Mol. Cell* 2, 621–627. doi: 10.1038/35085086

Starr, D. A. (2009). A nuclear-envelope bridge positions nuclei and moves chromosomes. *J. Cell Sci.* 122, 577–586. doi: 10.1242/jcs.037622

Starr, D. A., and Fridolfsson, H. N. (2010). Interactions between nuclei and the cytoskeleton are mediated by SUN-KASH nuclear-envelope bridges. *Ann. Rev. Cell Dev. Biol.* 26, 421–444. doi: 10.1146/annurev-cellbio-100109-104037

Thompson, E. A., and Roeder, G. S. (1989). Expression and DNA sequence of *RED1*, a gene required for meiosis I chromosome segregation in yeast. *Mol. Gen. Genet.* 218, 293–301. doi: 10.1007/BF00331281

Trelles-Sticken, E., Dresser, M. E., and Scherthan, H. (2000). Meiotic telomere protein Ndj1p is required for meiosis-specific telomere distribution, bouquet formation and efficient homologue pairing. *J. Cell Biol.* 151, 95–106. doi: 10.1083/jcb.151.1.95

Tsai, J. H., and McKee, B. D. (2011). Homologous pairing and the role of pairing centers in meiosis. *J. Cell Sci* 124, 1955–1963. doi: 10.1242/jcs.006387

Turner, J. M. A. (2013). Meiotic silencing in mammals. *Annu. Rev. Genet.* 49, 395–412. doi: 10.1146/annurev-genet-112414-055145

Valenzuela, N. T., Perera, E., and Naranjo, T. (2012). Dynamics of rye chromosome 1R regions with high and low crossover frequency in homology search and synapsis development. *PLoS One* 7:e36385. doi: 10.1371/journal.pone.0036385

Varas, J., Graumann, K., Osman, K., Pradillo, M., Evans, D. E., Santos, J. L., et al. (2015). Absence of SUN1 and SUN2 proteins in *Arabidopsis thaliana* leads to a delay in meiotic progression and defects in synapsis and recombination. *Plant J.* 81, 329–346. doi: 10.1111/tpj.12730

Wang, K. J., Wang, M., Tang, D., Shen, Y., Qin, B. X., Li, M., et al. (2011). PAIR3, an axis-associated protein, is essential for the recruitment of recombination elements onto meiotic chromosomes in rice. *Mol. Biol. Cell* 22, 12–19. doi: 10.1091/mbc.E10-08-0667

Zickler, D., and Kleckner, N. (2015). Recombination, pairing, and synapsis of homologs during meiosis. *Cold Spring Harb. Perspect. Biol.* 7:a016626. doi: 10.1101/cshperspect.a016626

Zickler, D., and Kleckner, N. (2016). A few of our favorite things: pairing, the bouquet, crossover interference and evolution of meiosis. *Sem. Cell Dev. Biol.* 54, 135–148. doi: 10.1016/j.semcdb.2016.02.024

Conflict of Interest Statement: The author declares that the research was conducted in the absence of any commercial or financial relationships that could be construed as a potential conflict of interest.

frontiers in Plant Science

ORIGINAL RESEARCH
published: 01 May 2018
doi: 10.3389/fpls.2018.00585

Homoeologous Chromosomes From Two *Hordeum* Species Can Recognize and Associate During Meiosis in Wheat in the Presence of the *Ph1* Locus

María C. Calderón[1], *María-Dolores Rey*[2], *Antonio Martín*[1] *and Pilar Prieto*[1]*

[1] *Plant Breeding Department, Institute for Sustainable Agriculture, Agencia Estatal Consejo Superior de Investigaciones Científicas (CSIC), Córdoba, Spain,* [2] *John Innes Centre, Norwich Research Park, Norwich, United Kingdom*

Understanding the system of a basic eukaryotic cellular mechanism like meiosis is of fundamental importance in plant biology. Moreover, it is also of great strategic interest in plant breeding since unzipping the mechanism of chromosome specificity/pairing during meiosis will allow its manipulation to introduce genetic variability from related species into a crop. The success of meiosis in a polyploid like wheat strongly depends on regular pairing of homologous (identical) chromosomes and recombination, processes mainly controlled by the *Ph1* locus. This means that pairing and recombination of related chromosomes rarely occur in the presence of this locus, making difficult wheat breeding trough the incorporation of genetic variability from related species. In this work, we show that wild and cultivated barley chromosomes associate in the wheat background even in the presence of the *Ph1* locus. We have developed double monosomic wheat lines carrying two chromosomes from two barley species for the same and different homoeology chromosome group, respectively. Genetic *in situ* hybridization revealed that homoeologous *Hordeum* chromosomes recognize each other and pair during early meiosis in wheat. However, crossing over does not occur at any time and they remained always as univalents during meiosis metaphase I. Our results suggest that the *Ph1* locus does not prevent chromosome recognition and pairing but crossing over between homoeologous. The role of subtelomeres in chromosome recognition is also discussed.

Keywords: wheat, barley, homoeologous pairing, introgressions, meiosis, chromosome recognition

OPEN ACCESS

Edited by:
Mónica Pradillo, Complutense University of Madrid, Spain

Reviewed by:
Eric Jenczewski, INRA Centre Versailles-Grignon, France
Pierre Sourdille, INRA Centre Auvergne Rhône Alpes, France

***Correspondence:**
Pilar Prieto
pilar.prieto@ias.csic.es

Specialty section:
This article was submitted to Plant Cell Biology, a section of the journal Frontiers in Plant Science

Received: *13 February 2018*
Accepted: *13 April 2018*
Published: *01 May 2018*

Citation:
Calderón MC, Rey M-D, Martín A and Prieto P (2018) Homoeologous Chromosomes From Two Hordeum Species Can Recognize and Associate During Meiosis in Wheat in the Presence of the Ph1 Locus. Front. Plant Sci. 9:585. doi: 10.3389/fpls.2018.00585

INTRODUCTION

More than two-thirds of global cropland features annual grain crops, which represent roughly 70% of humanity's food energy needs and typically grown in monoculture. Annual grain production, at its current scale, is fundamentally unsustainable. Thus, the growing human population demands greater crops, more productive and better adapted to specific agro-climatic conditions (Godfray et al., 2010). Plant breeders are playing a major role in worldwide efforts to understand gene functions and interactions with the aim of increasing quality and productivity of major crops. Wide-crossing in plant breeding is an important tool and sometimes the results are the starting point for new crops (Omara, 1953). For example, wide-crossing has been carried out in the Triticeae

tribe, which includes wheat, to develop new plant species such as ×*Triticosecale*, obtained after crossing wheat and rye, or ×*Tritordeum*, an amphyploid between the wild barley *Hordeum chilense* Roem. et Schult. and wheat (Omara, 1953; Martín and Sanchez-Monge Laguna, 1982). Breeders have also used related species as genetic donors for widening the genetic basis of wheat to get for example wheat cultivars better adapted to specific agro-climatic conditions, improving the quality or carrying resistance to diseases (Lukaszewski, 2000; Liu et al., 2005; Calderón et al., 2012; Rey et al., 2015a). In fact, there are many wild species carrying interesting traits that would be useful to be exploited in wheat breeding programmes, but unfortunately, hybridization between wheat and a wild related species produces only a low level of chromosome pairing and recombination. So understanding wheat genetics and genome organization is essential for plant breeding purposes.

Bread wheat is an hexaploid, which possesses three sets of related chromosomes because of doubling of chromosomes following sexual hybridization between closely related species. However, chromosomes associate regularly in pairs in wheat during meiosis, the cellular process to produce gametes in sexually reproducing organisms. Thus, at meiosis each chromosome only recognize and associate with its homologous and not with the related (homoeologous) chromosomes, which have a similar gene content and order but differ in repetitive DNA sequences. Several pairing homologous (*Ph*) genes control chromosome associations in wheat, although the major effect is due to the *Ph1* locus (Sears, 1976). The efficiency of chromosome associations during meiosis have a big influence on the fertility of wheat plants, being crucial for success in breeding, but has a negative effect preventing pairing and recombination between wheat chromosomes and those from related species. Therefore, it seems reasonable to go deeper into the knowledge of the biology of chromosome associations during meiosis in wheat, which will be valuable for wheat breeding.

Chromosome dynamics during meiosis have been extensively studied in a polyploidy such as hexaploid wheat (Moore, 2002; Corredor et al., 2007; Colas et al., 2008; Naranjo and Corredor, 2008). It is now well established that both interactions during recombination at the DNA level and assembly of a meiosis-specific proteinaceous structure known as the synaptonemal complex (SC) play roles in stabilizing associations between homologous chromosomes. However, how homologs became colocalized and how initial recognition is accomplished to establish chromosome associations remains poorly understood. When a chromosome recognizes its homolog (and not another chromosome) in wheat, a localized conformational change in adjacent chromatin is triggered in both partners. This process facilitates recognition and association of homologous versus homoeologous chromosomes and is affected by the *Ph1* locus (Prieto et al., 2005; Greer et al., 2012). Thus, *Ph1* stabilizes wheat during meiosis by both, promoting homolog synapsis during early meiosis and preventing homoeologous recombination later in meiosis (Martín et al., 2014, 2017). The effect on synapsis occurs during the telomere bouquet *Ph1* stage, when promotes more efficient homologous synapsis, thereby reducing the chance of homoeologous synapsis (Martín et al., 2017). The effect on CO formation occurs later in meiosis, when *Ph1* prevents MLH1 sites (Double Holliday Junctions marked to become COs) on synapsed homoeologues from becoming COs. In addition, it has been also described that the level of a ZIP4 paralog included within the *Ph1* locus alters the number of CO between homoeologous chromosomes (Rey et al., 2017).

Efforts focused on centromeres and telomeres behavior during meiosis have been also made (Martinez-Perez et al., 2000, 2001, 2003; Naranjo et al., 2005). Telomeres, which are highly conserved structures among plants, including wheat (Simpson et al., 1990; Ganal et al., 1991; Schwarzacher and Heslop-Harrison, 1991), play an important role on initial chromosome associations at the onset of meiosis. In this stage, the association of telomeres in a bouquet facilitates the search and recognition of homologous chromosomes by bringing chromosomes closer (Corredor and Naranjo, 2007; Koszul et al., 2008; Moore and Shaw, 2009) and its formation is affected by the *Ph1* locus (Richards et al., 2012). Subtelomeres, which are the telomere associated sequences (TAS), are highly polymorphic and extraordinarily dynamic sequences (Eichler and Sankoff, 2003). The complex and variable nature of subtelomeres has made difficult to assess the possible functions(s) of these regions so far, but studies on *Arabidopsis* and *Hordeum* subtelomeres might suggest a possible role on chromosome specificity between homolog chromosomes at the onset of meiosis (Kotani et al., 1999; Heacock et al., 2004; Calderón et al., 2014). In fact, subtelomeres in *Hordeum* showed high variability not only from different chromosomes but also among chromosome arms within the same chromosome (Schubert et al., 1998; Prieto et al., 2004b). Thus, the copy number of the subtelomeric HvT01 sequence was variable among chromosomes in both *H. chilense* and *H. vulgare*. Since chromosome associations are initiated at the distal regions of the chromosomes and homologous chromosomes are zipping up from those to the centromeres (Prieto et al., 2004a; Corredor et al., 2007), it seems reasonable to go deeper into the role of the subtelomeric regions on homolog chromosome associations, rather than focusing on features that are common to all chromosomes like telomeres.

The addition of a pair of "alien" chromosomes to the full genome complement of a crop species is commonly used as a first step for accessing genetic variation from the secondary gene pool, but addition lines are also relevant for understanding meiotic pairing behavior and chromosome structure (Friebe et al., 2005; Lukaszewski, 2010). Sets of both cultivated (*Hordeum vulgare*) and wild (*H. chilense*) barley addition lines in a hexaploid wheat background were developed (Islam et al., 1978, 1981; Miller et al., 1982) and have potential in plant meiosis studies. Certainly, it allows tracking one specific pair of chromosomes or chromosome segments within the wheat background using genomic *in situ* hybridization (GISH) and study chromosome rearrangements and associations exclusively in a pair of homologs (Naranjo et al., 2010; Rey et al., 2015b).

In this study, we have developed double monosomic addition lines of wild and cultivated barley in wheat for the same and for different homoeology group to go deeper into the knowledge of chromosome associations during meiosis. These double

monosomic addition lines enabled to distinguish chromosomes from two different barley species in the wheat background, observe conformational changes during meiosis and analyze whether subtelomeres might play a role on chromosome recognition/pairing at early meiosis in the absence of homologs. Results showed that homoeologous chromosomes can recognize each other to associate correctly in pairs, even in the presence of the *Ph1* locus, although crossing over does not occur as they remained as univalents during metaphase I.

MATERIALS AND METHODS

Plant Material

Crosses between *H. chilense* and *H. vulgare* addition lines in bread wheat (*Triticum aestivum* cv. Chinese Spring; AABBDD + pair of $H^{ch}H^{ch}$ and AABBDD + pair of $H^{v}H^{v}$, respectively) for the same and for different homoeology group were made to obtain double monosomic wheat lines carrying one *H. chilense* and one *H. vulgare* chromosome for the same and for different homoeology group. *H. chilense* and *H. vulgare* addition lines were kindly provided by Steve Reader, JIC, Norwich, UK. The presence of each *Hordeum* sp. chromosome in parental and F1 wheat lines used in this work was confirmed by both PCR assays previously described (Liu et al., 1996; Hagras et al., 2005) and *in situ* hybridization.

Seeds obtained from genetic crosses were germinated on wet filter paper in the dark for 5 days at 4°C, followed by a period of 24h at 25°C. Plants were then growth in the greenhouse at 26°C during the day and 18°C during the night (16 h photoperiod).

Fluorescence *in Situ* Hybridization

Fluorescence genomic *in situ* hybridization (GISH) was used to study chromosome associations between *H. chilense* and *H. vulgare* chromosomes in the wheat background as described previously (Prieto et al., 2004b). Root tips were collected from germinating seeds and were pre-treated for 4 h in a 0.05% colchicine solution at 25°C and fixed in 100% ethanol-acetic acid, 3:1 (v/v), for at least a week at room temperature. Spikes in meiosis were collected from mature plants and preserved in 100% ethanol-acetic acid, 3:1 (v/v) until were used to characterize chromosome associations. Chromosome spreads were prepared from both root tips cells and pollen mother cells (PMCs) at meiosis. Root tips and anthers were macerated in a drop of 45% glacial acetic acid on ethanol-cleaned slides, squashed under a cover slip and dipped in liquid nitrogen in order to fix the plant material on the slide. The cover slip was removed and the slides were air-dried and stored at 4°C until used.

Both total genomic *H. vulgare* and *H. chilense* DNA were labeled by nick translation with biotin-11-(Boehringer Mannheim Biochemicals, Germany) and digoxigenin-11-dUTP (Roche Applied Science, Indianapolis, IN, USA), respectively, and used as probes. Both probes were mixed to a final concentration of 5 ng/μl in the hybridization mixture. The hybridization mixture consisted of 50% formamide, 2 × SCC, 5 ng of biotin-labeled or digoxigenin-labeled probe, 10% dextran sulfate, 0.14 μg of yeast tRNA, 0.1 μg of sonicated salmon sperm DNA and 0.005 μg of glycogen. Biotin-labeled *H. vulgare* DNA and digoxigenin-labeled *H. chilense* DNA were detected with a streptavidin- Cy3 conjugate (Sigma, St. Louis, MO, USA) and antidigoxigenin-FITC (Roche Diagnostics, Meylan, France), respectively. Chromosomes were counterstained with DAPI (4′, 6-diamidino-2-phenylindole) and mounted in Vectashield (Vector Laboratories, Burlingame, CA, USA).

Chromosome spreads from somatic cells and anthers of the F1 wheat lines were reprobed with the barley subtelomeric tandem repeat HvT01, which was obtained by amplification by the polymerase chain reaction (PCR) from genomic DNA from the barley cv. Betzes using primers made according to the published sequence (Belostotsky and Ananiev, 1990). PCR conditions were previously described by Prieto et al. (2004b). The PCR product corresponding to this barley satellite HvT01 probe was labeled with digoxigenin-11-dUTP, (Roche Applied Science, Indianapolis, IN, USA) by nick translation and detected with antidigoxigenin-FITC (Roche Diagnostics, Meylan, France). Meiosis metaphase samples were also reprobed to label centromeres using the RT sequence included in the barley centromeric BAC7 (Hudakova et al., 2001), amplified by PCR following the same conditions as the amplification of the CCS1 centromeric repeat (Aragón-Alcaide et al., 1996), labeled with biotin-11-(Boehringer Mannheim Biochemicals, Germany) and detected with the streptavidin- Cy3 conjugate (Sigma, St. Louis, MO, USA).

Fluorescence Microscopy and Image Processing

Hybridization signals were visualized using a Nikon Eclipse 80i epifluorescence microscope. Images were captured with a Nikon CCD camera using the Nikon 3.0 software (Nikon Instruments Europe BV, Amstelveen, The Netherlands) and processed with Photoshop 11.0.2 software (Adobe Systems Inc., San Jose, California, USA).

Statistical Analysis

Statistical analyses were performed using STATISTIX 10.0 software (Analytical Software, Tallahassee, FL, USA). Anaphase I combinations were evaluated by an analysis of variance (ANOVA) as a completely randomized design. This analysis included a tangent transformation in the anaphase I combination where only one pole of the meiocytes showed *H. chilense* and *H. vulgare* signals. Tetrad combinations were analyzed by the Kruskal–Wallis test (nonparametric one-way analysis of variance).

RESULTS

Development of Double Monosomic *H. vulgare-H*. Chilense Addition Lines in Wheat

Crosses between disomic *H. chilense* and *H. vulgare* addition lines in bread wheat carrying chromosomes $7H^{ch}$ and $7H^{v}$, respectively, were made to obtain double monosomic barley additions in wheat carrying homoeologous *H. chilense* and *H. vulgare* chromosome 7. Similarly, genetic crosses between

disomic *H. chilense* and *H. vulgare* addition lines in bread wheat for chromosomes $7H^{ch}$ and $5H^{v}$, respectively, were made to obtain double monosomic wheat lines carrying non-homoeologous chromosomes $7H^{ch}$ and $5H^{v}$. Finally, to corroborate observations on chromosome associations in a different homoeology group, we also developed genetic crosses between disomic *H. chilense* and *H. vulgare* addition lines in bread wheat for chromosomes $5H^{ch}$ and $5H^{v}$, respectively, to obtain double monosomic barley additions in wheat lines carrying homoeologous *H. chilense* and *H. vulgare* chromosomes for group 5. The F_1 hybrid progeny from each genetic cross was analyzed by GISH to ensure that they retained the expected both *H. chilense* and *H. vulgare* chromosomes (**Figure 1**). All the plants from all the genetic crosses carried both barley chromosomes. In addition, fluorescence *in situ* hybridization (FISH) was also performed in these wheat lines using the barley subtelomeric HvT01 repeat as a probe to label polymorphisms between the subtelomeric regions from the *H. chilense* and *H. vulgare* chromosomes added to the wheat background (**Figure 1**). Chromosome $7H^{v}$ had two strong signals for the barley subtelomeric HvT01 sequence on both chromosome arms meanwhile there was only a weaker signal on the short arm of chromosome $7H^{ch}$. Both $5H^{ch}$ and $5H^{v}$ chromosomes had a signal on the short arm for the HvT01 probe, which was stronger in the case of $5H^{v}$ chromosome, and only a weak signal on the subtelomeric region of the long arm of chromosome $5H^{v}$ was detected, which sometimes cannot be clearly seen and depended on the FISH experiment (**Figure 1**). No HvT01 subtelomeric signals were detected on the wheat chromosomes. The F1 progeny from each genetic cross was also growth until meiosis with the aim of studying the meiotic behavior of both *Hordeum* chromosomes by *in situ* hybridization in PMCs in the wheat background.

Homoeologous Wild and Cultivated Barley Chromosomes Can Fully Associate in Pairs in Wheat in the Presence of the Ph1 Locus

Chromosome pairing was analyzed during early meiosis by GISH in F_1 plants carrying one copy of *H. chilense* and one copy of *H. vulgare* homoeologous chromosomes ($7H^{ch}$ and $7H^{v}$) and it was compared to those carrying non-homoeologous

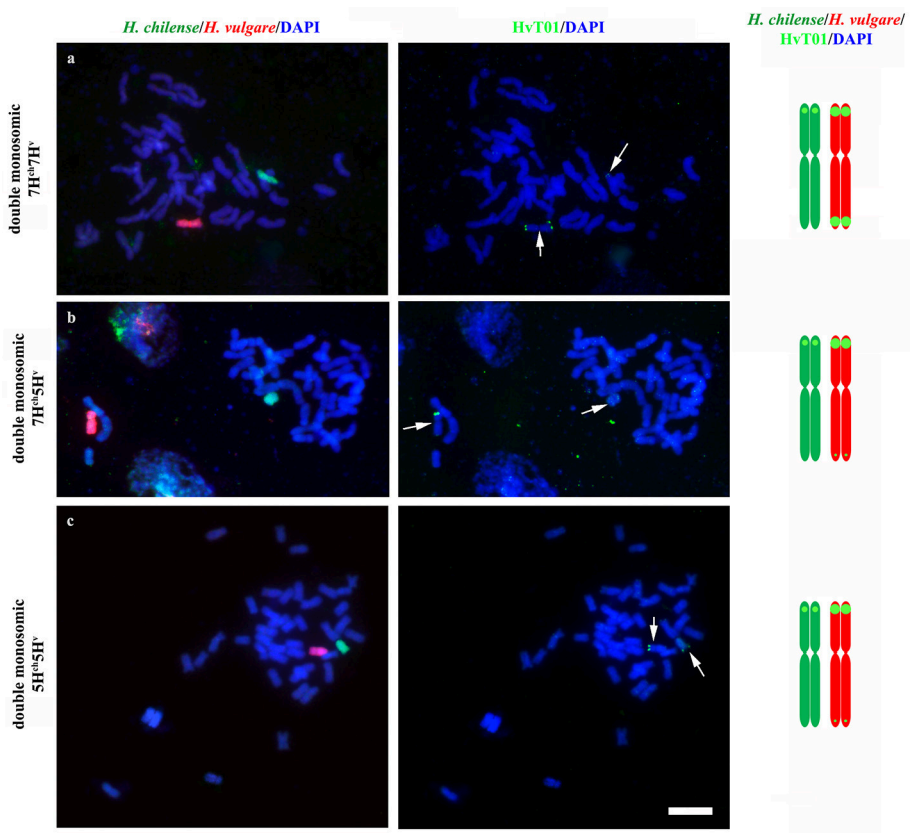

FIGURE 1 | *Hordeum chilense* and *H. vulgare* double monosomic addition lines in wheat and physical location of the HvT01 subtelomeric repeat on barley chromosomes. *Hordeum chilense* (green) and *H. vulgare* (red) chromosomes were detected in GISH experiments in somatic chromosome spreads. In addition, the HvT01 subtelomeric sequence from barley was also detected (green). Total genomic DNA was counterstained with DAPI (blue). **(a)** Double monosomic $7H^{ch}7H^{v}$ addition line, including a diagram showing the HvT01subtelomeric signals in all barley chromosome arms, except in $7H^{ch}$L arm. **(b)** Double monosomic $7H^{ch}5H^{v}$ addition line, including a diagram showing the subtelomeric barley sequence in all barley chromosome arms except in $7H^{ch}$L arm. **(c)** Double monosomic $5H^{ch}5H^{v}$ addition line, including a diagram showing the subtelomeric barley sequence in all barley chromosome arms, except in $5H^{ch}$L arm. Bar represents 10 μm.

H. chilense and *H. vulgare* chromosomes ($7H^{ch}$ and $5H^{v}$, respectively). Experiments were developed in around a 100 cells of each genomic combination in prophase I of meiosis. Both wild and cultivated barley chromosomes were visualized simultaneously in the wheat background (**Figure 2**). In both cases, *H. chilense* and *H. vulgare* chromosomes were in proximity in the nucleus in early prophase (**Figures 2a,c**). As meiosis progressed, GISH experiments showed homoeologous *H. chilense* and *H. vulgare* chromosomes always fully-associated in pairs along the whole chromosome (**Figure 2b**). In contrast, non-homoeologous *Hordeum* chromosomes $7H^{ch}$ and $5H^{v}$ were not observed associated at this meiotic stage at any time, remaining always un-associated (**Figure 2d**).

GISH experiments were also carried out in cells in prophase I of meiosis in F_1 plants carrying homoeologous chromosomes from *H. chilense* and *H. vulgare* for another homoeology group (group 5), with the aim of confirming the observations on chromosome associations between homoeologous chromosomes $7H^{ch}$ and $7H^{v}$ in the wheat background. Results showed that homoeologous *Hordeum* chromosomes $5H^{ch}$ and $5H^{v}$ did also associate in pairs during early meiosis in the wheat background, even in the presence of the *Ph1* locus (**Figures 2e,f**), suggesting that chromosome pairing between homoeologous chromosomes from two different *Hordeum* species is not hampered by the *Ph1* locus. In addition, results suggested that homoeologous barley chromosomes shared enough similar DNA sequences to

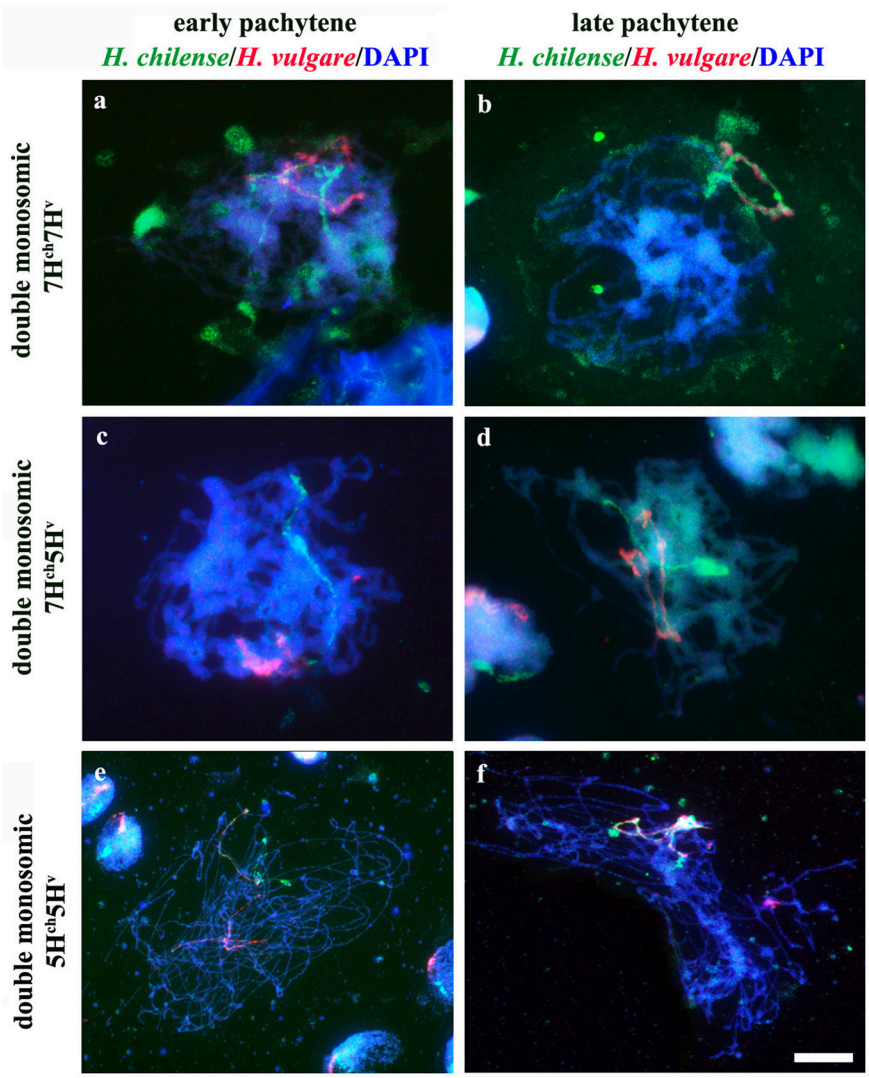

FIGURE 2 | Behavior of homoeologous and non-homoeologous barley chromosomes during early meiosis in wheat. *Hordeum chilense* chromosomes are visualized in green and *H. vulgare chromosomes* are visualized in red. **(a)** Double monosomic $7H^{ch}7H^{v}$ addition line showing both barley chromosomes un-associated at early pachytene. **(b)** Homoeologous barley chromosomes are fully associated at late pachytene in the double monosomic $7H^{ch}7H^{v}$ addition line. **(c)** Double monosomic $7H^{ch}5H^{v}$ addition line showing both barley chromosomes un-associated at early pachytene. **(d)** Non-homoeologous $7H^{ch}$ and $5H^{v}$ chromosomes remained un-associated at late pachytene. **(e)** Double monosomic $5H^{ch}5H^{v}$ addition line showing homoeologous wild and cultivated barley chromosomes half-paired at early pachytene. **(f)** Double monosomic $5H^{ch}5H^{v}$ addition line showing both homoeologous *Hordeum* chromosomes fully associated. Bar represents 10 μm.

recognize each other, a conformational chromatin change is observed in both homoeologues and chromosomes are finally associated completely in pairs.

Subtelomeres Might Hamper Chromosome Associations Between Non-homologous Hordeum Chromosomes in the Wheat Background

We have described that in the absence of homologous chromosomes, wild and cultivated barley homoeologous chromosomes can still recognize each other and associate completely in pairs during early meiosis. In addition, we have observed that, in these cases, initial chromosome recognition occurred by the chromosome ends where none or little copy number of the subtelomeric HvT01 repeat were detected, i.e., the long arm of homoeologous chromosomes $5H^{ch}$ and $5H^{v}$ (**Figure 3**). Thus, homoeologous *Hordeum* chromosomes did recognize and associate in pairs by these chromosome ends, which made chromosome recognition less restrictive and allowed homoeologous to recognize and associate in pairs. These observations were similar in the cells detected at the same stage from the double monosomic $7H^{ch}7H^{v}$ addition line in wheat (data not shown). Moreover, the observations were consistent in all the cells detected at the initiation of pairing (26 and 18 cells from the double monosomic $5H^{ch}5H^{v}$ and $7H^{ch}7H^{v}$ addition lines in wheat, respectively). Once homoeologous chromosomes had associated by these chromosome ends, a conformational change was observed along both homoeologous *Hordeum* chromosomes and pairing progressed along both chromosomes allowing a complete chromosome association between them (**Figure 3**).

Crossing Over Does Not Occur Between Wild and Cultivated Barley Chromosomes in Wheat Although They Previously Associated in Early Meiosis

Once we observed full chromosome associations between homoeologous *Hordeum* chromosomes during early meiosis in the wheat background, we also analyzed chromosome behavior of both wild and cultivated barley chromosomes during metaphase I of meiosis in PMCs from double monosomic *H. chilense* and *H. vulgare* additions in wheat lines, both for the same and different homoeologous chromosomes. Meiosis metaphase I was also checked in the disomic *H. chilense* and *H. vulgare* addition lines in wheat used as parental lines for the genetic crosses developed in this work, to obtain the double *H. chilense* and *H. vulgare* double monosomic addition lines. Chromosome stability of the parental lines was confirmed as the homologous barley chromosomes carried in the *H. chilense* and *H. vulgare* disomic addition lines were always observed associated in pairs, indicating that crossing over occurred between homologous barley chromosomes (**Figure 4**). Similarly, wheat chromosomes associated correctly in bivalents at meiosis metaphase I and orientated by centromeres properly in double monosomic *H. chilense* and *H. vulgare* additions in wheat lines, both for the same and different homoeologous chromosomes (**Figure 5**). In contrast, *H. chilense* and *H. vulgare* chromosomes remained always un-associated in all the cells analyzed for the three different genetic combinations analyzed (**Figure 5**), despite the fact that homoeologous *H. chilense* and *H. vulgare* chromosomes ($7H^{ch}7H^{v}$ and $5H^{ch}5H^{v}$, respectively) did completely associate in pairs in early meiosis. These observations suggested that, although wild and cultivated barley homoeologous chromosomes can fully associate during pachytene, crossing over did not occur later between these chromosomes. Consequently, *Hordeum* homoeologous chromosomes were never observed associated by chiasmata during metaphase I and always remained as univalent (**Figure 5**), suggesting other requirements for crossing over rather than full previous chromosome associations or similarities in the DNA sequence.

Chromosome Segregation Does Not Depend on Previous Chromosome Associations During Early Meiosis

Each PMC analyzed at the MI stage was characterized by the presence of two barley univalents in double monosomic *H. chilense-H. vulgare* addition lines. Around 300 cells were observed in meiosis anaphase I. GISH analysis showed that both wild and cultivated barley univalents segregated simultaneously

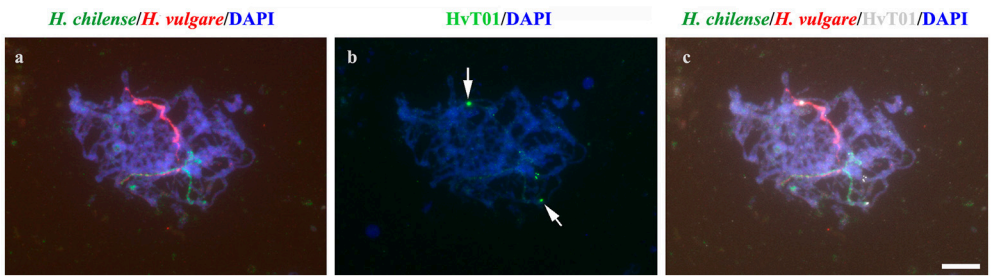

FIGURE 3 | Detection of the subtelomeric HvT01 sequence in the wild and cultivated barley chromosomes in the $5H^{ch}5H^{v}$ double monosomic addition line. DNA was counterstained with DAPI (blue). **(a)** GISH of both *H. chilense* (green) and *H. vulgare* (red) homoeologous chromosomes initiating pairing during early pachytene. **(b)** Detection of the subtelomeric HvT01 probe (green) on the same cell. **(c)** Merge image showing the subtelomeric HvT01 signal (overlay in white) on the terminal region of the unpaired homoeologous wild and cultivated barley chromosome arms (arrowed). Bar represents 10 μm.

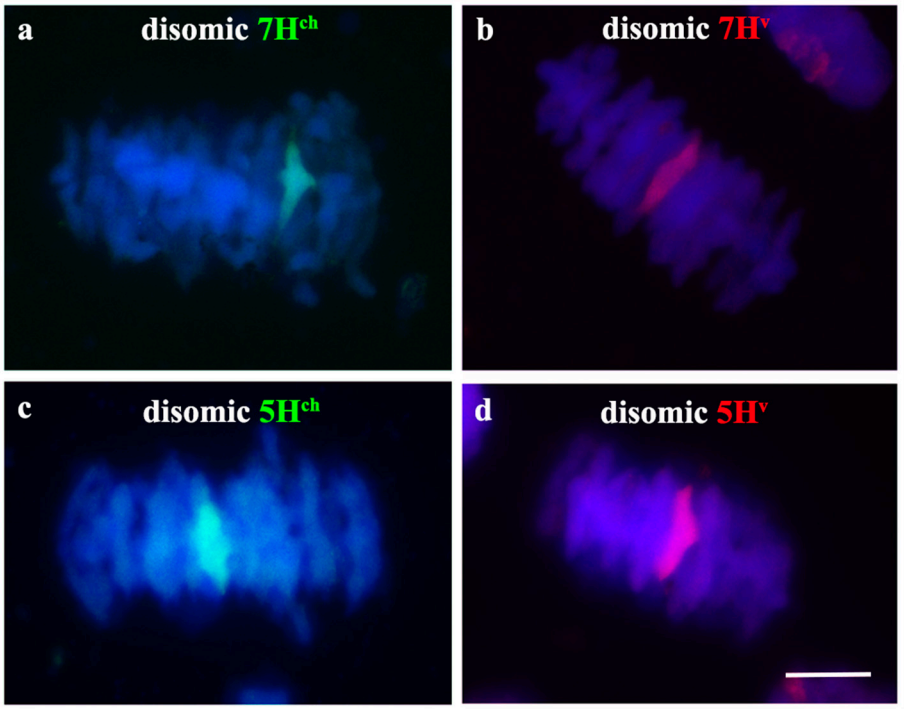

FIGURE 4 | *Hordeum chilense* and *H. vulgare* chromosome behavior during metaphase I in parental *H. chilense* and *H. vulgare* disosomic addition lines in wheat. *Hordeum chilense* (green) and *H. vulgare* (red) chromosomes were observed always associated in pairs in all the cells in metaphase I in each *H. chilense* and *H. vulgare* disomic addition line. DNA was counterstained with DAPI (blue). **(a)** *H. chilense* chromosome $7H^{ch}$ disomic addition line. **(b)** *H. vulgare* chromosome $7H^{v}$ disomic addition line. **(c)** *H. chilense* chromosome $5H^{ch}$ disomic addition line. **(d)** *H. vulgare* chromosome $5H^{v}$ disomic addition line. Bar represents 10 μm.

with wheat bivalents at stage anaphase I (**Figure 6**). All the different possible situations for chromosome segregation of the unpaired *H. chilense* and *H. vulgare* chromosomes were identified (**Figures 6a–e**, **Table 1**): (i) both barley chromosome were detected in both nuclei; (ii) only *H. vulgare* chromosome was detected in both nuclei; (iii) only *H. chilense* chromosome was detected in both nuclei; (iv) each barley chromosome was detected in each daughter nucleus; and (v) both barley chromosomes were detected in the same anaphase/telophase pole. These different situations for chromosome segregation of both barley chromosomes were found in all the genetic combinations ($7H^{ch}7H^{v}$, $5H^{ch}5H^{v}$, and $7H^{ch}5H^{v}$ double monosomic addition lines) in the wheat background, although the ratio between them varied depending on the genetic stock (**Table 1**). Nevertheless, no significant differences were found for *H. chilense* and *H. vulgare* chromosome segregation between the different genetic combinations (**Table 1**), despite the fact that the most frequent observation for the segregation of the wild and cultivated barley chromosomes was different in $7H^{ch}7H^{v}$ addition line compared to $5H^{ch}5H^{v}$, and $7H^{ch}5H^{v}$ addition lines (**Table 1**). Moreover, no significant differences were found on the behavior of the *Hordeum* chromosomes within the same F1 line. These results suggest that chromosome segregation in double *H. chilense* and *H. vulgare* monosomic addition lines in wheat occurred randomly, regardless the barley chromosomes added to the wheat background and whether or not chromosome associations took place previously in early meiosis.

Chromosomes delay was usually observed in double monosomic *H. chilense* and *H. vulgare* addition lines in late anaphase I/telophase I (**Figures 6f,g**), and the presence of chromatin across the equator during phragmoplast formation either from *H. chilense*, *H. vulgare* or both species was also observed (**Figures 6h–j**). Missegregation or chromosome breaks that occurred in anaphase I in the double monosomic *H. chilense* and *H. vulgare* addition lines cannot be distinguished from sister chromatids segregation unless using, among others, the HvT01 subtelomeric probe (**Figures 6k,l**).

Depending on chromosome segregation of both wild and cultivated barley univalents during meiosis I, the number of different genetic combinations in the PMC increased during MII, resulting in a wide range of meiotic phenotypes observed (nineteen different cases; **Table 2**). The most frequent *H. chilense* and *H. vulgare* chromosome combination observed for each genetic combination during telophase II was different depending on whether *H. chilense* and *H. vulgare* chromosomes were included in the same or in different homoeology group (**Figure 7**; **Table 2**), but no significant differences were found. Results suggested that both sister chromatids separation and misdivision did occur randomly independently of the barley chromosome combination.

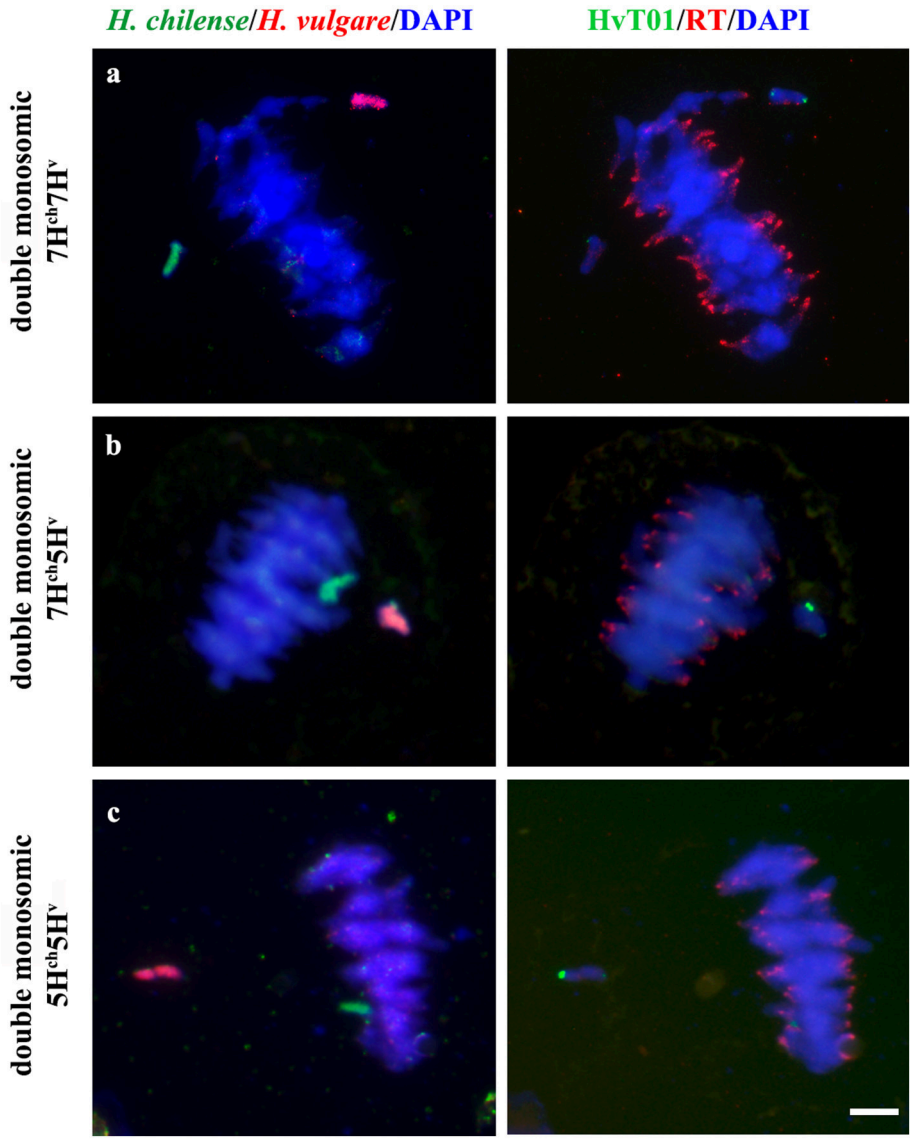

FIGURE 5 | *Hordeum chilense* and *H. vulgare* chromosome behavior in double monosomic barley addition lines in wheat during metaphase I. *Hordeum chilense* (green) and *H. vulgare* (red) chromosomes remained unassociated in all the cases. DNA was counterstained with DAPI (blue). Centromeres (red) were labeled with RT sequence to show the correct orientation of wheat chromosomes during metaphase I. Subtelomeres on barley chromosomes were labeled in green. **(a)** Double monosomic $7H^{ch}7H^{v}$ addition line. **(b)** Double monosomic $7H^{ch}5H^{v}$ addition line. **(c)** Double monosomic $5H^{ch}5H^{v}$ addition line. Bar represents 10 μm.

DISCUSSION

Little is known about how chromosomes recognize each other to correctly associate in pairs at early meiosis and recombine. This is a key question for plant breeders to transfer genetic variability from related species into a crop like wheat. The lack of recombination between cultivated wheat and alien chromosomes limits the transfer of novel traits from relatives to wheat because *Ph1* suppresses homoeologous recombination between wheat and related species (Riley and Chapman, 1958; Sears, 1976). Different meiosis studies on chromosome pairing have been developed using wheat lines carrying an addition of one pair of homologous chromosomes or chromosome segments from one related species into wheat (Mikhailova et al., 1998; Maestra et al., 2002; Prieto et al., 2004a) or hybrids between wheat and relatives (Molnár-Láng et al., 2014; Rey et al., 2017). In this work, we have developed wheat lines carrying double monosomic chromosome additions for wild and cultivated barley for the same and for different homoeology group, respectively, which allowed us to track simultaneously by GISH a couple of extra homoeologous and non-homoeologous chromosomes from two different *Hordeum* species during early meiosis. These double monosomic addition lines can contribute to go deeper into the knowledge of how chromosomes recognize and associate in pairs

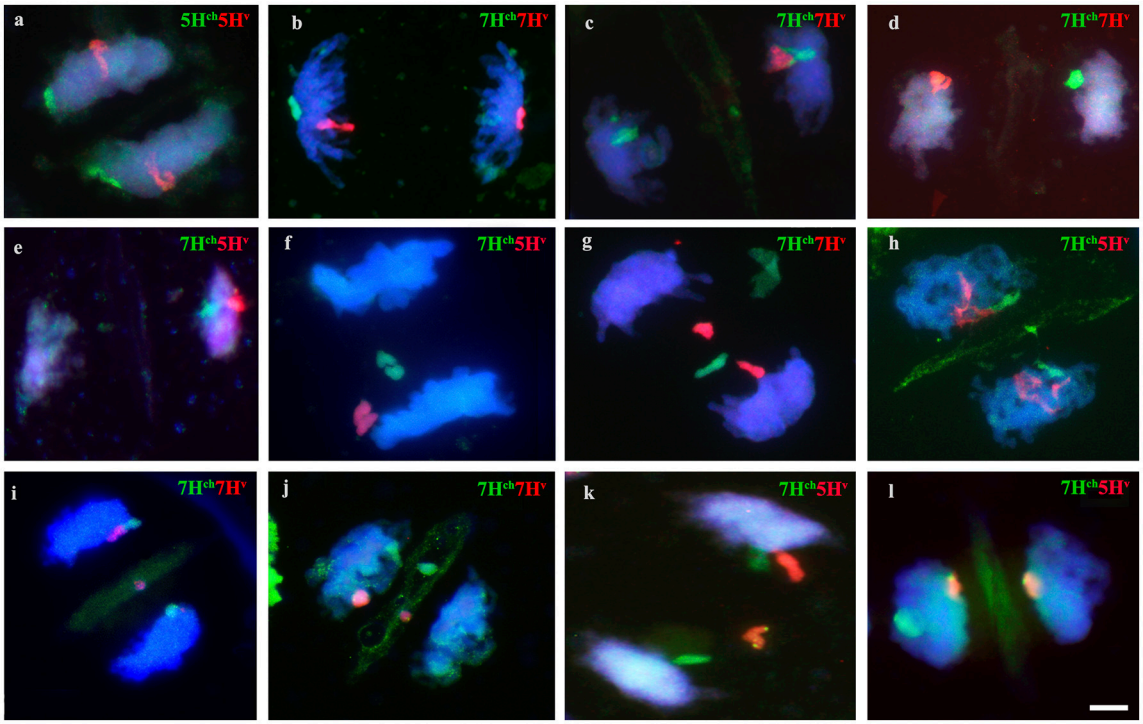

FIGURE 6 | Behavior of *Hordeum chilense* and *H. vulgare* chromosomes in double monosomic barley addition lines in wheat during anaphase I of meiosis. Examples of barley chromosome segregation after metaphase I. *Hordeum chilense* and *H. vulgare* were visualized in green and red, respectively. DNA was counterstained with DAPI (blue). **(a)** Double monosomic $5H^{ch}5H^{v}$ addition line, **(b)** Double monosomic $7H^{ch}7H^{v}$ addition line, **(c)** Double monosomic $7H^{ch}7H^{v}$ addition line; **(d)** Double monosomic $7H^{ch}7H^{v}$ addition line. **(e)** Double monosomic $7H^{ch}5H^{v}$ addition line. **(f)** Both $7H^{ch}5H^{v}$ barley chromosomes remained delayed. **(g)** Both $7H^{ch}7H^{v}$ barley chromosomes remained delayed and a misdivision of chromosome $7H^{v}$ was also observed. One or both barley micronuclei were positioned in the equatorial region on telophase I in **(h)** Double monosomic $7H^{ch}5H^{v}$ addition line, **(i)** Double monosomic $7H^{ch}7H^{v}$ addition line, and **(j)** Double monosomic $7H^{ch}7H^{v}$ addition line. The subtelomeric HvT01 probe was used in GISH experiments performed in cells in telophase I from the double monosomic $7H^{ch}5H^{v}$ addition line to visualize **(k)** $5H^{v}$ chromosome misdivision or **(l)** $5H^{v}$ chromosome segregation. Bar represents 10 μm.

in the wheat background in the presence of the *Ph1* locus. In addition, most of the works carrying alien chromosomes in the wheat background are focused in meiosis metaphase I or later stages (Molnár-Láng et al., 2000; Silkova et al., 2014). The analysis of chromosome pairing focused only in metaphase I can result in an underestimation of homoeologous associations that might occur earlier in meiosis, as chromosomes might remain mostly as univalents due to the lack of homoeologous recombination. Few works analyzed the behavior of an extra pair of chromosomes at early stages of meiosis (Aragón-Alcaide et al., 1997; Prieto et al., 2004a; Valenzuela et al., 2012, 2013; Koo et al., 2016). Homologous barley chromosomes have been previously observed associated during early meiosis and metaphase I in disomic addition lines in wheat (Aragón-Alcaide et al., 1997; Calderón et al., 2014). In this study we have reported by GISH analysis that homoeologous wild and cultivated barley chromosomes can also fully associate in pairs in the wheat background during early meiosis and that such chromosome pairing occurred even in the presence of the *Ph1* locus, although homoeologous barley chromosomes did not cross over and were always observed as univalent in metaphase I. The role of the *Ph1* locus was recently narrowed down preventing recombination between related chromosomes in interspecific hybrids (Moore, 2014; Martín et al., 2017). Our results clearly showed that the *Ph1* locus does not hamper homoeologous chromosome associations but crossing over. Nevertheless, homoeologous recombination between related *Aegilops geniculata* and *Ae. searsii* has been detected in the wheat background in the presence of the *Ph1* locus due to the presence of chromosome 5 Mg of *Ae. geniculata*, which harbors a homoeologous recombination promoter factor (Koo et al., 2016). Recombination frequencies between *H. vulgare* and *H. bulbosum* homoeologues have been previously detected but are lower than association frequencies (Zhang et al., 1999), probably because of non-chiasmate associations (Orellana, 1985). Homologous pairing has been also described in the absence of synapsis and meiotic recombination in *Caenorhabditis elegans* (Dernburg et al., 1998). Our results showed that homoeologous *H. chilense* and *H. vulgare* chromosomes associated in pairs in wheat in the absence of crossing over and that the *Ph1* locus does not prevent such chromosome recognition and association between homoeologues. It is also worthy to mention that, although *H. chilense* and *H. vulgare* are phylogenetically quite distant, even included in two different sections among the *Hordeum* genus (Blattner, 2009), both species share a high degree

TABLE 1 | (A) Total number of PMCs scored at anaphase I showing the different combinations observed for both *Hordeum* chromosomes added to the wheat background. The most frequent observation per line and the total number of meiocytes examined are shown in bold. **(B)** Quantification of meiocytes (%) for each observation.

(A)

Wheat lines	Number of PMCs scored in Anaphase I					
	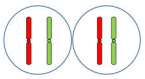	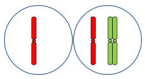	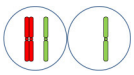	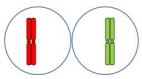	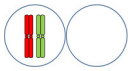	**Total**
$7H^{ch}$ $7H^{v}$ addition	23	**49**	9	35	12	128
$7H^{ch}5H^{v}$ addition	**24**	19	12	6	16	77
$5H^{ch}5H^{v}$ addition	**35**	22	5	14	10	86
Total	82	90	26	55	38	**291**

(B)

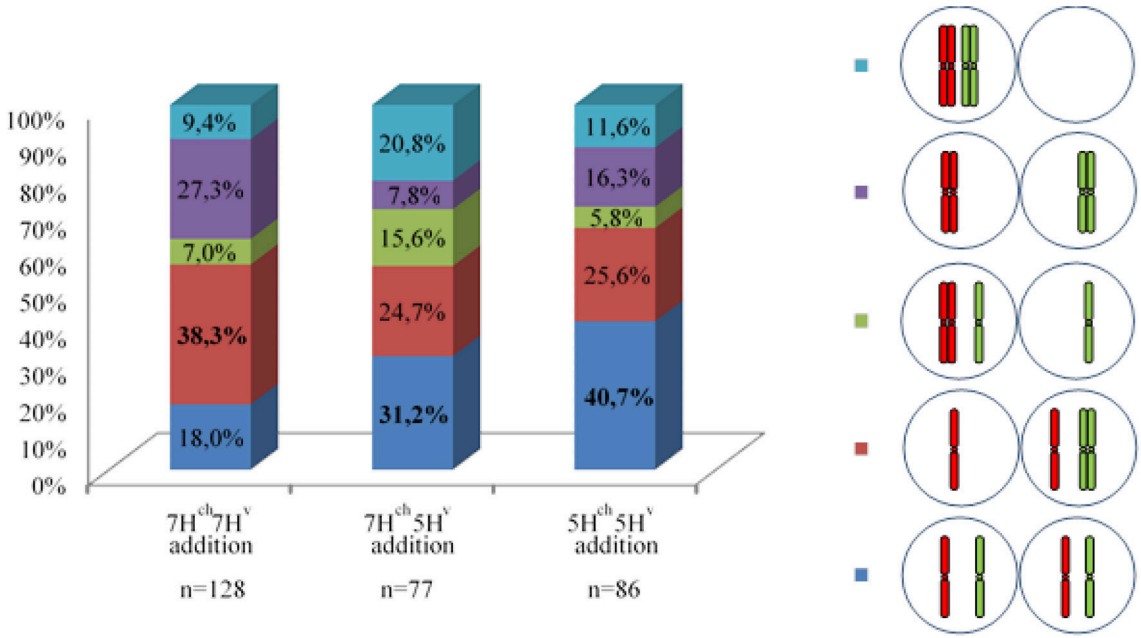

of similarities at the chromosomal level, as it has been reported between them and other species within this genus (Hernández et al., 2001; Aliyeva-Schnorr et al., 2016). Thus, other elements such as cohesins or the DNA sequence itself might play a major role on chromosome recognition and pairing at the onset of meiosis in a polyploidy like wheat.

So far, it is unclear whether initial recognition is mediated through protein-protein interactions, DNA base-pairing, or other chromosomal features. For example, a noncoding RNA (meiRNA-L) is responsible for the recombination-independent pairing of homologous loci in *Schizosaccharomyces pombe* (Ding et al., 2012). Other chromosomal features different from DNA/DNA recombinational interactions or RNA-mediated pairing have been proposed to be involved in the homologous recognition such as the pattern of cohesins distribution in the axial elements of unmatched meiotic chromosomes in mice and *S. pombe* (Ishiguro et al., 2011; Ding et al., 2016). Subtelomeres have been also reported as crucial to promote chromosome recognition and pairing between homologous chromosomes (González-García et al., 2006; Calderón et al., 2014). In our study, variability for the HvT01 subtelomeric sequence was found between *H. chilense* and *H. vulgare* chromosomes 5 and 7, particularly for the long arm of both chromosomes. We observed that although homoeologous chromosomes can potentially associate by the telomeres, subtelomeric DNA blocks might hamper homoeologous chromosome to correctly associate in pairs and thus, in the absence of homologs, chromosome recognition and association between homoeologues can occurred by the chromosome end where the subtelomeric repeats are shorter or absent. However, as meiosis progressed, the pairing signal initiated at these chromosome ends can be propagated along the whole chromosome, so that the homoeologues became fully associated by late pachytene. Thus, our results might suggest

TABLE 2 | (A) Number of meiocytes showing the different combinations for both *Hordeum* chromosomes added to the wheat background. The most frequent observation per line and the total number of PMCs examined are shown in bold. **(B)** Quatification of meiocytes (%) for each observation.

(A)

Wheat lines	**Number of PMCs scored in tetrads**																			
																				**Total**
$7H^{ch}7H^{v}$ addition	2	**6**	5	1	0	1	3	0	0	0	0	1	1	1	1	2	1	1	0	26
$7H^{ch}5H^{v}$ addition	1	1	0	2	2	**5**	0	0	0	3	1	1	0	0	0	0	3	0	3	22
$5H^{ch}5H^{v}$ addition	4	**10**	2	**10**	7	2	0	1	0	3	3	0	0	0	0	1	0	0	0	43
Total	7	17	7	13	9	8	3	1	0	6	4	2	1	1	1	3	4	1	3	**91**

(B)

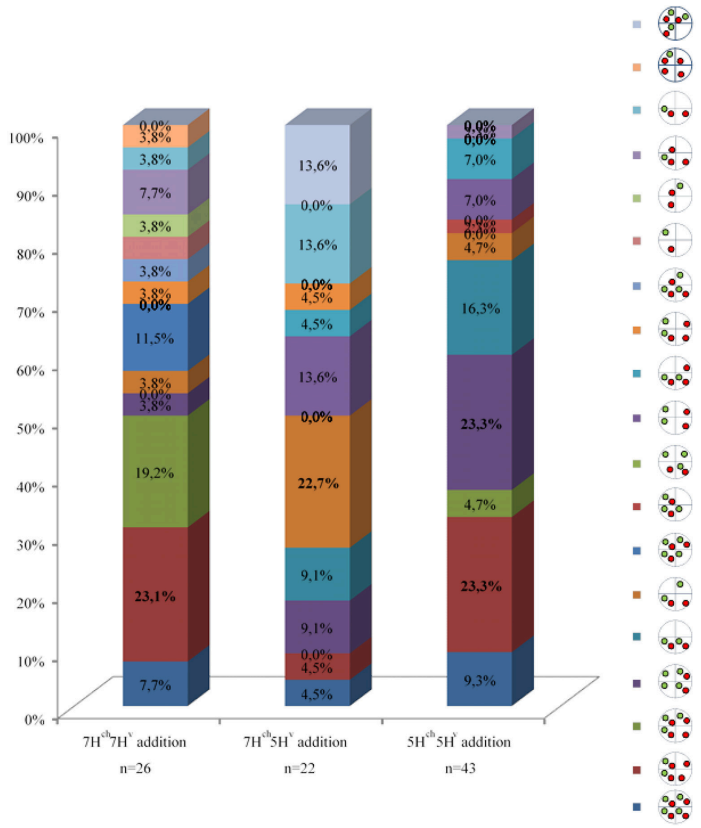

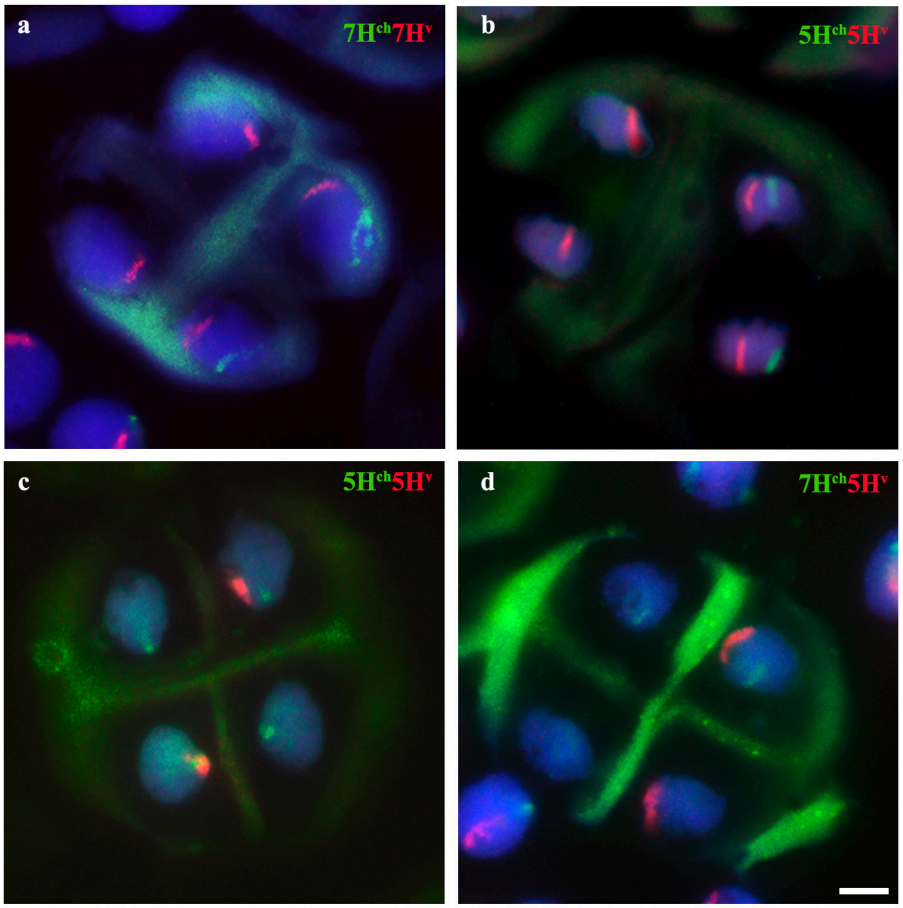

FIGURE 7 | Behavior of *H. chilense* and *H. vulgare* chromosomes in double monosomic *Hordeum* addition lines in wheat after the second meiosis division. Examples of the most frequent observations for both *H. chilense* (green) and *H. vulgare* (red) chromosomes are shown. DNA was counterstained with DAPI (blue). **(a)** *Hordeum vulgare* and *H. chilense* chromatin detected in four and two PMCs, respectively, in the double monosomic $7H^{ch}7H^{v}$ wheat line. **(b)** *Hordeum vulgare* and *H. chilense* chromatin detected in four and in two PMCs, respectively, in the double monosomic $5H^{ch}5H^{v}$ wheat line. **(c)** Four *H. chilense* signals and two *H. vulgare* signals were observed in the double monosomic $5H^{ch}5H^{v}$ wheat line at the same frequency as reported in **b**. **(d)** Wild and cultivated barley signals are present in the same nucleus and only one each in another two different nucleus. Bar represents 10 μm.

that subtelomeres can play a key role in the specificity of chromosome recognition, restricting chromosome recognition to true homologs and therefore hampering homoeologous chromosomes to recognize each other and associate. The implication was that DNA sequence(s) within the subtelomeric region must be important for the process of initial homolog recognition and pairing, although further studies are required to reveal how subtelomeres take part in such important meiosis processes.

The peculiarities of univalent behavior in meiosis have been extensively studied in wheat aneuploids, particularly for the relation between the means of a chromosome segregation and its inclusion into a microspore (Sears, 1952; Marais and Marais, 1994; Friebe et al., 2005; Lukaszewski, 2010). The knowledge about univalent behavior in meiosis is necessary for the directed development of wheat lines carrying alien introgressions since univalent are subjected of incorrect division and segregation. Thus, abnormities in meiosis result in various modifications and/or in the loss of a transferred chromosome (Silkova et al., 2014). Univalents in meiosis have a tendency to misdivide (break) across their centromeres producing telocentric. This process has been deeply described in wheat (Sears, 1952; Steinitz-Sears, 1966; Friebe et al., 2005), and used to generate different cytogenetic stocks (Sears and Sears, 1978; Lukaszewski, 1993, 1997). The most common alien introgression in wheat, chromosome translocations, is the result of centric misdivision and fusion of misdivision products. Translocations between *H. chilense* and *H. vulgare* have been detected previously when the genomes of these species are in the same background (Prieto et al., 2001). Our results overview the univalent behavior of two homoeologous and non-homoeologous barley chromosomes in the wheat background. We observed that chromosome misdivisions and sister chromatids segregated randomly at anaphase I similarly to previous works (Friebe et al., 2005), and independently of whether or not related chromosomes associate in pairs in early meiosis.

In summary, homoeologous wild and cultivated barley chromosomes were observed fully associated in pairs in early meiosis in the presence of the *Ph1* although crossing over did not occur at any time, as both chromosomes were always visualized as univalents during metaphase I. Whether or not homoeologous *Hordeum* chromosomes can crossover in the absence of the *Ph1* locus remains to be elucidated. In addition, the role of the terminal chromosome regions in chromosome recognition and paring and the proteins interacting with these chromosomes ends will be key questions to shed light in future works.

HUMAN AND ANIMAL RIGHTS AND INFORMED CONSENT

This article does not contain any studies with human participants or animals.

AUTHORS CONTRIBUTIONS

All authors contributed to this manuscript. MC and PP designed the research and performed the experiments. MC, MR, AM, and PP analyzed, discussed the results. PP and MC wrote the manuscript. All authors read and approved the manuscript.

ACKNOWLEDGMENTS

This research was supported by grants AGL2015-64833R from Spanish Ministerio de Economía y Competitividad (MINECO) and ERC-StG- 243118 from the FP7 and The European Regional Development Fund (FEDER) from the European Union. Authors deeply appreciate the comments from the independent reviewers during the revision of the manuscript.

REFERENCES

Aliyeva-Schnorr, L., Stein, N., and Houben, A. (2016). Collinearity of homoeologous group 3 chromosomes in the genus *Hordeum* and *Secale cereale* as revealed by 3H-derived FISH analysis. *Chromosome Res.* 24, 231–242. doi: 10.1007/s10577-016-9518-8

Aragón-Alcaide, L., Miller, T., Schwarzacher, T., Reader, S., and Moore, G. (1996). A cereal centromeric sequence. *Chromosoma* 105, 261–268. doi: 10.1007/BF02524643

Aragón-Alcaide, L., Reader, S., Beven, A., Shaw, P., Miller, T., and Moore, G. (1997). Association of homologous chromosomes during floral development. *Curr. Biol.* 7, 905–908.

Belostotsky, D. A., and Ananiev, E. V. (1990). Characterization of relic DNA from barley genome. *Theor. Appl. Genet.* 80, 374–380. doi: 10.1007/BF00210075

Blattner, F. R. (2009). Progress in phylogenetic analysis and a new infrageneric classification of the barley genus *Hordeum* (Poaceae: Triticeae). *Breed. Sci.* 59, 471–480. doi: 10.1270/jsbbs.59.471

Calderón, M. C., Ramírez, M. C., Martín, A., and Prieto, P. (2012). Development of *Hordeum chilense* introgression lines in durum wheat: a tool for breeders and complex trait analysis. *Plant Breed.* 131, 733–738. doi: 10.1111/j.1439-0523.2012.02010.x

Calderón, M. C., Rey, M.-D., Cabrera, A., and Prieto, P. (2014). The subtelomeric region is important for chromosome recognition and pairing during meiosis. *Sci. Rep.* 4:6488. doi: 10.1038/srep06488

Colas, I., Shaw, P., Prieto, P., Wanous, M., Spielmeyer, W., Mago, R., et al. (2008). Effective chromosome pairing requires chromatin remodeling at the onset of meiosis. *Proc. Natl. Acad. Sci. U.S.A.* 105, 6075–6080. doi: 10.1073/pnas.0801521105

Corredor, E., Lukaszewski, A. J., Pachon, P., Allen, D. C., and Naranjo, T. (2007). Terminal regions of wheat chromosomes select their pairing partners in meiosis. *Genetics* 177, 699–706. doi: 10.1534/genetics.107.078121

Corredor, E., and Naranjo, T. (2007). Effect of colchicine and telocentric chromosome conformation on centromere and telomere dynamics at meiotic prophase I in wheat-rye additions. *Chromosome Res.* 15, 231–245. doi: 10.1007/s10577-006-1117-7

Dernburg, A. F., McDonald, K., Moulder, G., Barstead, R., Dresser, M., and Villeneuve, A. M. (1998). Meiotic recombination in *C. elegans* initiates by a conserved mechanism and is dispensable for homologous chromosome synapsis. *Cell* 94, 387–398. doi: 10.1016/S0092-8674(00)81481-6

Ding, D. Q., Matsuda, A., Okamasa, K., Nagahama, Y., Haraguchi, T., and Hiraoka, Y. (2016). Meiotic cohesin-based chromosome structure is essential for homologous chromosome pairing in *Schizosaccharomyces pombe*. *Chromosoma* 125, 205–214. doi: 10.1007/s00412-015-0551-8

Ding, D. Q., Okamasa, K., Yamane, M., Tsutsumi, C., Haraguchi, T., Yamamoto, M., et al. (2012). Meiosis-specific noncoding RNA mediates robust pairing of homologous chromosomes in meiosis. *Science* 336, 732–736. doi: 10.1126/science.1219518

Eichler, E. E., and Sankoff, D. (2003). Structural dynamics of eukaryotic chromosome evolution. *Science* 301, 793–797. doi: 10.1126/science.1086132

Friebe, B., Zhang, P., Linc, G., and Gill, B. S. (2005). Robertsonian translocations in wheat arise by centric misdivision of univalents at anaphase I and rejoining of broken centromeres during interkinesis of meiosis II. *Cytogenet. Genome Res.* 109, 293–297. doi: 10.1159/000082412

Ganal, M. W., Lapitan, N. L., and Tanksley, S. D. (1991). Macrostructure of the tomato telomeres. *Plant Cell* 3, 87–94. doi: 10.1105/tpc.3.1.87

Godfray, H. C., Crute, I. R., Haddad, L., Lawrence, D., Muir, J. F., Nisbett, N., et al. (2010). The future of the global food system. *Phil. Trans. R. Soc. B.* 365, 2769–2777. doi: 10.1098/rstb.2010.0180

González-García, M., González-Sánchez, M., and Puertas, M. J. (2006). The high variability of subtelomeric heterochromatin and connections between nonhomologous chromosomes, suggest frequent ectopic recombination in rye meiocytes. *Cytogenet. Genome Res.* 115, 179–185. doi: 10.1159/000095240

Greer, E., Martin, A. C., Pendle, A., Colas, I., Jones, A. M. E., Moore, G., et al. (2012). The Ph1 locus suppresses Cdk2-type activity during premeiosis and meiosis in wheat. *Plant Cell* 24, 152–162. doi: 10.1105/tpc.111.094771

Hagras, A. A. A., Masahiro, K., Tanaka, K., Sato, K., and Tsujimoto, H. (2005). Genomic differentiation of *Hordeum chilense* from *H. vulgare* as revealed by repetitive and EST sequences. *Genes Genet. Syst.* 80, 147–159. doi: 10.1266/ggs.80.147

Heacock, M., Spangler, E., Riha, K., Puizina, J., and Shippen, D. E. (2004). Molecular analysis of telomere fusions in *Arabidopsis*: multiple pathways for chromosome end-joining. *EMBO J.* 23, 2304–2313. doi: 10.1038/sj.emboj.7600236

Hernández, P., Dorado, G., Prieto, P., Giménez, M. J., Ramírez, M. C., Laurie, D. A., et al. (2001). A core genetic map of *Hordeum chilense* and comparisons with maps of barley (*Hordeum vulgare*) and wheat (*Triticum aestivum*). *Theor. Appl. Genet.* 102, 1259–1264. doi: 10.1007/s001220000514

Hudakova, S., Michalek, W., Presting, G. G., ten Hoopen, R., dos Santos, K., Jasencakova, Z., et al. (2001). Sequence organization of barley centromeres. *Nucleid Acids Res.* 29, 5029–5035. doi: 10.1093/nar/29.24.5029

Ishiguro, K., Kim, J., Fujiyama-Nakamura, S., Kato, S., and Watanabe, Y. (2011). A new meiosis-specific cohesin complex implicated in the cohesin code for homologous pairing. *EMBO Rep.* 12, 267–275. doi: 10.1038/embor.2011.2

Islam, A. K. M. R., Shepherd, K. W., and Sparrow, D. H. B. (1978). "Production and characterization of wheat-barley addition lines," in *Proceedings 5th International Wheat Genetics Symposium* (New Delhi), 365–371.

Islam, A. K. M. R., Shepherd, K. W., and Sparrow, D. H. B. (1981). Isolation and characterization of euplasmic wheat-barley chromosome addition lines. *Heredity* 46, 161–174. doi: 10.1038/hdy.1981.24

Koo, D. H., Liu, W. X., Friebe, B., and Gill, B. S. (2016). Homoeologous recombination in the presence of Ph1 gene in wheat. *Chromosoma* 126, 531–540. doi: 10.1007/s00412-016-0622-5

Koszul, R., Kim, K. P., Prentiss, M., Kleckner, N., and Kameoka, S. (2008). Meiotic chromosomes move by linkage to dynamic actin cables with transduction of force through the nuclear envelope. *Cell* 133, 1188–1201. doi: 10.1016/j.cell.2008.04.050

Kotani, H., Hosouchi, T., and Tsuruoka, H. (1999). Structural Analysis and Complete Physical Map of *Arabidopsis thaliana* Chromosome 5 Including Centromeric and Telomeric Regions. *DNA Res.* 6, 381–386. doi: 10.1093/dnares/6.6.381

Liu, S. B., Wang, H. G., Zhang, X. Y., Li, X. F., Li, D. Y., Duan, X. Y., et al. (2005). Molecular cytogenetic identification of a wheat-*Thinopyron intermedium* (Host) Barkworth & DR Dewey partial amphiploid resistant to powdery mildew. *J. Integr. Plant. Biol.* 47, 726–733. doi: 10.1111/j.1744-7909.2005.00051.x

Liu, Z. W., Biyashev, R. M., and Saghai Maroof, M. A. (1996). Development of simple sequence repeat DNA markers and their integration into a barley linkage map. *Theor. Appl. Genet.* 93, 869–876. doi: 10.1007/BF00224088

Lukaszewski, A. J. (1993). Reconstruction in wheat of complete chromosome-1B and chromosome-1R from the 1RS.1BL translocation of Kavkaz origin. *Genome* 36, 821–824. doi: 10.1139/g93-109

Lukaszewski, A. J. (1997). Further manipulation by centric misdivision of the 1RS.1BL translocation in wheat. *Euphytica* 94, 257–261. doi: 10.1023/A:1002916323085

Lukaszewski, A. J. (2000). Manipulation of the 1RS.1BL translocation in wheat by induced homoeologous recombination. *Crop Sci.* 40, 216–225. doi: 10.2135/cropsci2000.401216x

Lukaszewski, A. J. (2010). Behavior of centromeres in univalents and centric misdivision in wheat. *Cytogenet. Genome Res.* 129, 97–109. doi: 10.1159/000314108

Maestra, B., de Jong, J. H., Shepherd, K., and Naranjo, T. (2002). Chromosome arrangement and behaviour of two rye homologous telosomes at the onset of meiosis in disomic wheat-5RL addition lines with and without the Ph1 locus. *Chromosome Res.* 10, 655–667. doi: 10.1023/A:1021564327226

Marais, G. F., and Marais, A. S. (1994). The derivation of compensating translocations involving homoeologous group-3 chromosomes of wheat and rye. *Euphytica* 79, 75–80. doi: 10.1007/BF00023578

Martín, A. C., Rey, M. D., Shaw, P., and Moore, G. (2017). Dual effect of the wheat *Ph1* locus on chromosome synapsis and crossover. *Chromosoma* 126, 669–680. doi: 10.1007/s00412-017-0630-0

Martín, A. C., Shaw, P., Phillips, D., Reader, S., and Moore, G. (2014). Licensing MLH1 sites for crossover during meiosis. *Nat. Commun.* 5:4580. doi: 10.1038/ncomms5580

Martín, A., and Sanchez-Monge Laguna, E. (1982). Cytology and morphology of the amphiploid *Hordeum chilense* x *Triticum turgidum* conv. durum. *Euphytica* 31, 261–267. doi: 10.1007/BF00028329

Martinez-Perez, E., Shaw, P., Aragon-Alcaide, L., and Moore, G. (2003). Chromosomes form into seven groups in hexaploid and tetraploid wheat as a prelude to meiosis. *Plant J.* 36, 21–29. doi: 10.1046/j.1365-313X.2003.01853.x

Martinez-Perez, E., Shaw, P., and Moore, G. (2000). Polyploidy induces centromere association. *J. Cell Biol.* 148, 233–238. doi: 10.1083/jcb.148.2.233

Martinez-Perez, E., Shaw, P., and Moore, G. (2001). The *Ph1* locus is needed to ensure specific somatic and meiotic centromere association. *Nature* 411, 204–207. doi: 10.1038/35075597

Mikhailova, E. I., Naranjo, T., Shepherd, K., Eden, J. W., Heyting, C., and de Jong, J. H. (1998). The effect of the wheat Ph1 locus on chromatin organization and meiotic chromosome pairing analysed by genome painting. *Chromosoma* 107, 339–350. doi: 10.1007/s004120050316

Miller, T. E., Reader, S. M., and Chapman, V. (1982). "The addition of Hordeum chilense chromosomes to wheat," in *Paper Presented at the Proceedings of the International Symposium Eucarpia on Induced Variability in Plant Breeding*. (Pudoc, Wageningen), 79–81.

Molnár-Láng, M., Linc, G., Logojan, A., and Sutka, J. (2000). Production and meiotic pairing behaviour of new hybrids of winter wheat (*Triticum aestivum*) x winter barley(*Hordeum vulgare). Genome* 43, 1045–1054. doi: 10.1139/g00-079

Molnár-Láng, M., Linc, G., and Szakács, E. (2014). Wheat–barley hybridization: the last 40 years. *Euphytica* 195, 315–329. doi: 10.1007/s10681-013-1009-9

Moore, G. (2002). Meiosis in allopolyploids - the importance of 'Teflon' chromosomes. *Trends Genet.* 18, 456–463. doi: 10.1016/S0168-9525(02)02730-0

Moore, G. (2014). "The control of recombination in wheat by Ph1 and its use in breeding," in *Methods in Molecular Biology*, ed N. J. Clifton (New York, NY: Humana Press), 143–153.

Moore, G., and Shaw, P. J. (2009). Improving the chances of finding the right partner. *Curr. Opin. Genet. Dev.* 19, 99–104. doi: 10.1016/j.gde.2009.02.006

Naranjo, T., and Corredor, E. (2008). Nuclear architecture and chromosome dynamics in the search of the pairing partner in meiosis in plants. *Cytogenet. Genome Res.* 120, 320–330. doi: 10.1159/000121081

Naranjo, T., Maestra, B., and Corredor, E. (2005). The search of the homologous partner at early meiosis in wheat. *Chromosome Res.* 13:9.

Naranjo, T., Valenzuela, N. T., and Perera, E. (2010). Chiasma frequency is region specific and chromosome conformation dependent in a rye chromosome added to wheat. *Cytogenet. Genome Res.* 129, 133–142. doi: 10.1159/000314029

Omara, J. G. (1953). The cytogenetics of Triticale. *Bot. Rev.* 19, 587–605. doi: 10.1007/BF02861827

Orellana, J. (1985). Most of the homoeologous pairing at metaphase-i in wheat-rye hybrids is not chiasmatic. *Genetics* 111, 917–931.

Prieto, P., Martin, A., and Cabrera, A. (2004b). Chromosomal distribution of telomeric and telomeric-associated sequences in *Hordeum chilense* by *in situ* hybridization. *Hereditas* 141, 122–127. doi: 10.1111/j.1601-5223.2004.01825.x

Prieto, P., Moore, G., and Reader, S. (2005). Control of conformation changes associated with homologue recognition during meiosis. *Theor. Appl. Genet.* 111, 505–510. doi: 10.1007/s00122-005-2040-6

Prieto, P., Ramirez, M. C., Ballesteros, J., and Cabrera, A. (2001). Identification of intergenomic translocations involving Wheat, *Hordeum vulgare* and *Hordeum chilense* chromosomes by FISH. *Hereditas* 135, 171–174. doi: 10.1111/j.1601-5223.2001.t01-1-00171.x

Prieto, P., Shaw, P., and Moore, G. (2004a). Homologue recognition during meiosis is associated with a change in chromatin conformation. *Nature Cell Biol.* 6, 906–908. doi: 10.1038/ncb1168

Rey, M. D., Calderón, M. C., and Prieto, P. (2015b). The use of the *ph1b* mutant to induce recombination between the chromosomes of wheat and barley. *Front. Plant Sci.* 6:160. doi: 10.3389/fpls.2015.00160

Rey, M. D., Calderón, M. C., Rodrigo, M. J., Zacarías, L., Alós, E., and Prieto, P. (2015a). Novel bread wheat lines enriched in carotenoids carrying *Hordeum chilense* chromosome arms in the ph1b background. *PLoS ONE* 10:e0134598. doi: 10.1371/journal.pone.0134598

Rey, M. D., Martin, A. C., Higgins, J., Swarbreck, D., Uauy, C., Shaw, P., et al. (2017). Exploiting the ZIP4 homologue within the wheat *Ph1* locus has identified two lines exhibiting homoeologous crossover in wheat-wild relative hybrids. *Mol. Breed.* 37:95. doi: 10.1007/s11032-017-0700-2

Richards, D. M., Greer, E., Martin, A. C., Moore, G., Shaw, P. J., et al. (2012). Quantitative dynamics of telomere bouquet formation. *PLoS Comput. Biol.* 8:e1002812. doi: 10.1371/journal.pcbi.1002812

Riley, R., and Chapman, V. (1958).Genetic control of the cytologically diploid behaviour of hexaploid wheat. *Nature* 182, 713–715. doi: 10.1038/18 2713a0

Schubert, I., Shi, F., Fuchs, J., and Endo, T. R. (1998). An efficient screening for terminal deletions and translocations of barley chromosomes added to common wheat. *Plant J.* 14, 489–495. doi: 10.1046/j.1365-313X.1998.00125.x

Schwarzacher, T., and Heslop-Harrison, J. S. (1991). *In situ* hybridization to plant telomeres using synthetic oligomers. *Genome* 34, 317–323. doi: 10.1139/g91-052

Sears, E. R. (1952). Misdivision of univalents in common wheat. *Chromosoma* 4, 535–550.

Sears, E. R. (1976). Genetic control of chromosome pairing in wheat. *Ann. Rev. Genet.* 10, 31–51. doi: 10.1146/annurev.ge.10.120176.000335

Sears, E. R., and Sears, L. M. S. (1978). "The telocentric chromosomes of common wheat," *Proceedings of 5th International Wheat Genetics Symposium* (New Delhi), 389–407.

Silkova, O. G., Kabanenko, Y. N., and Loginova, D. V. (2014). The effect of wheat-rye substitution on chromosome elimination: an analysis of univalents' behavior in wheat meiosis with dimonosomy and tetramonosomy. *Russ. J. Genet.* 50, 245–252. doi: 10.1134/S102279541402015X

Simpson, P. R., Newman, M. A., Davies, D. R., Noel Ellis, T. H., Matthews, P. M., and Lee, D. (1990). Identification of translocations in pea by *in situ* hybridization with chromosome-specific probes. *Genome* 33, 745–749. doi: 10.1139/g90-112

Steinitz-Sears, L. M. (1966). Somatic instability of telocentric chromosomes in wheat and the nature of the centromere. *Genetics* 54, 241–248.

Valenzuela, N. T., Perera, E., and Naranjo, T. (2012). Identifying crossover-rich regions and their effect on meiotic homologous interactions by partitioning chromosome arms of wheat and rye. *Chromosome Res.* 21, 433–445. doi: 10.1007/s10577-013-9372-x

Valenzuela, N. T., Perera, E., and Naranjo, T. (2013). Dynamics of rye chromosome 1R regions with high and low crossover frequency in homology search and synapsis development. *PLoS ONE* 7:e36385. doi: 10.1371/journal.pone.0036385

Zhang, L. T., Pickering, R., and Murray, B. (1999). Direct measurement of recombination frequency in interspecific hybrids between *Hordeum vulgare* and *H. bulbosum* using genomic *in situ* hybridization. *Heredity* 83, 304–309. doi: 10.1038/sj.hdy.6885710

Conflict of Interest Statement: The authors declare that the research was conducted in the absence of any commercial or financial relationships that could be construed as a potential conflict of interest.

frontiers in Plant Science

ORIGINAL RESEARCH
published: 19 December 2017
doi: 10.3389/fpls.2017.02161

Chromosome Pairing in Hybrid Progeny between *Triticum aestivum* and *Elytrigia elongata*

Fang He[1], Piyi Xing[2], Yinguang Bao[2], Mingjian Ren[1], Shubing Liu[2], Yuhai Wang[3], Xingfeng Li[2] and Honggang Wang[2]**

[1] Guizhou Subcenter of National Wheat Improvement Center, College of Agronomy, Guizhou University, Guiyang, China, [2] State Key Laboratory of Crop Biology, Shandong Key Laboratory of Crop Biology, College of Agronomy, Shandong Agricultural University, Taian, China, [3] College of Life Science, Zaozhuang University, Zaozhuang, China

In this study, the intergeneric hybrids F_1, F_2, BC_1F_1, BC_1F_2, and BC_2F_1 from *Elytrigia elongata* and *Triticum aestivum* crosses were produced to study their chromosome pairing behavior. The average *E. elongata* chromosome configuration of the two F_1 hybrids agreed with the theoretical chromosome configuration of 21I+7II, indicating that the genomic constitution of this F_1 hybrid was $ABDStStE^eE^bE^x$. Compared with the BC_1F_1 generation, the BC_2F_1 generation showed a rapid decrease in the number of *E. elongata* chromosomes and the BC_1F_2 generation showed a more extensive distribution of *E. elongata* chromosomes. In addition, pairing between wheat and *E. elongata* chromosomes was detected in each of the wheat-*E. elongata* hybrid progenies, albeit rarely. Our results demonstrated that genomic *in situ* hybridization (GISH) using an *E. elongata* genomic DNA probe offers a reliable approach for characterizing chromosome pairing in wheat and *E. elongata* hybrid progenies.

Keywords: *E. elongata*, *T. aestivum*, chromosome pairing, hybrid progenies, genomic *in situ* hybridization

OPEN ACCESS

Edited by:
Mónica Pradillo, Complutense University of Madrid, Spain

Reviewed by:
Pilar Prieto, Consejo Superior de Investigaciones Científicas (CSIC), Spain
Isabelle Colas, James Hutton Institute, United Kingdom

****Correspondence:***
Xingfeng Li
lixf@sdau.edu.cn
Honggang Wang
hgwang@sdau.edu.cn

Specialty section:
This article was submitted to Plant Genetics and Genomics, a section of the journal Frontiers in Plant Science

Received: *24 July 2017*
Accepted: *07 December 2017*
Published: *19 December 2017*

Citation:
He F, Xing P, Bao Y, Ren M, Liu S, Wang Y, Li X and Wang H (2017) Chromosome Pairing in Hybrid Progeny between Triticum aestivum and Elytrigia elongata. Front. Plant Sci. 8:2161. doi: 10.3389/fpls.2017.02161

INTRODUCTION

Modern cultivation strategies have diminished the genetic base of common wheat (*Triticum aestivum*). A number of wild relatives and related species were popularly used to increase the genetic diversity available to wheat breeders. *Elytrigia elongata* (Host) Nevisk. [Syn. *Thinopyrum ponticum* (Podp.) Barkworth] ($2n = 10x = 70$) was initially hybridized with wheat approximately 70 years ago because of its resistance to several wheat diseases, as well as its stress tolerance and high crossing ability with various *Triticum* species (Sepsi, 2010; Hu et al., 2011; Fu et al., 2012; Ayala-Navarrete et al., 2013; He et al., 2013; Zheng et al., 2014; Li et al., 2016). Many desirable genes, such as Sr25, Sr43, Lr19, Cmc2, and Pm51, have been characterized and transferred from this wild grass species into wheat. These translocations have supported the development of several wheat germplasms that are used in wheat improvement programs throughout the world (Li and Wang, 2009; Niu et al., 2014; Zhan et al., 2014). The genomic composition of the decaploid species *E. elongata* has been a subject of interest for quite some time and is designated $JJJJJJJ^sJ^sJ^sJ^s$ (Chen et al., 1998) or $StStStStE^eE^eE^bE^bE^xE^x$ (Zhang et al., 1996). There is some evidence that the St chromosomes in *E. elongata* are closely related to those of *Pseudoroegneria strigosa* and that the J/E^b and J^s/E^e genomes are closely related to the *Thinopyrum bessarabicum* and/or *Thinopyrum elongatum* genomes (Chen et al., 2001). However, the genomic composition of *E. elongata* has not yet been clarified.

Chromosome engineering is the procedure of altering ploidy, chromosome structure, and/or chromosome number of an organism intended for genetic improvement. This technology has been used to incorporate favorable genes from wild species into the wheat genome for germplasm and variety development. These favorable genes can be introduced into wheat from wild species through chromosome addition, substitution, and translocation. Alien chromosome addition and substitution, which introduce one or more entire foreign chromosomes into the wheat genome, usually include desirable genes, as well as undesirable genes. There is a general demand to quickly utilize those lines in wheat breeding. Chromosome translocation, which integrates alien chromosome segments containing the gene of interest into the wheat genome, has been the most effective approach for alien gene introgression (Guo et al., 2015; Li et al., 2016). The translocations generally result from meiotic recombination between wheat chromosomes and their homoeologous complements from wild species (Bagherikia et al., 2014; Song et al., 2016).

The corresponding chromosomes of the A, B, and D genomes are genetically closely related. However, the pairing propinquity between genetically analogous chromosomes of these genomes is suppressed, largely by the activity of the *Ph1* gene in the long arm of chromosome 5B (Sears, 1976). *Ph1* represses homoeologous pairing so that only homologous partners can pair. So far, allelic variation inducing different levels of homoeologous pairing in wheat or in wheat hybrids has not been found in *Ph1*. Such variation can best be discovered in intergeneric hybrids where homologs are not present and homoeologous pairing is normally very low so that any change in the level of pairing can be demonstrably detected. While in several intergeneric hybrids, the action of *Ph1* is counterbalanced by pairing promoters of the alien species, and in most intergeneric wheat hybrids there is either little or no effect of the alien genome on homoeologous pairing (Qi et al., 2007).

Metaphase I (MI) pairing reflects cross-formation that might be associated with recombination. Metamorphic chromosomal pairing from meiosis between interspecific or intraspecific hybrids is an efficient method for estimating interphase gene transfer and revealing phylogenetic relationships among these species (Bao et al., 2014; Su et al., 2016). Cytogenetic studies on intergeneric hybrids between *Elytrigia* species have shown close relationships between J/E^b, J^s/E^e, and St chromosomes (Chen et al., 2001; Liu et al., 2007). Although some information on chromosome pairing in *Elytrigia* and wheat hybrids is available (Roundy, 1985; Cai and Jones, 1997), little is known about the pairing frequency between *E. elongata* and wheat chromosomes because of the complexity of wheat-*E. elongata* chromosome pairings and the difficulty of distinguishing chromosomes in hybrids using conventional chromosome techniques.

In this study, hybrid progeny involving F_1, F_2, BC_1F_1, BC_1F_2, and BC_2F_1 were created by hybridizing *T. aestivum* with *E. elongata* to transfer desirable traits from *E. elongata* into wheat. The objective of this work was to characterize the meiotic behavior and genomic composition of the progeny from wheat-*E. elongata* hybrids using cytogenetic analysis and genomic *in situ* hybridization (GISH) technology.

MATERIALS AND METHODS

Plant Material

E. elongata was provided by Prof. Zhensheng Li, formerly of the Northwest Institute of Botany, Chinese Academy of Sciences, Yangling, China. The *E. elongata* × *T. aestivum* (cv. Yannong15) and *E. elongata* × *T. aestivum* (cv. Lumai5hao) were obtained from Prof. Honggang Wang (College of Agronomy, Shandong Agricultural University, Taian, China). All plant materials were maintained through selfing at the Tai'an Subcenter of the National Wheat Improvement Center, Shandong, China. The crosses and results of offspring production are described in **Figure 1**.

Meiotic Preparations

When the plants reached the flag leaf stage, spikes were sampled, stages of meiosis were determined in acetocarmine squashes of 1 of 3 anthers per flower. If appropriate stages were present, the remaining 2 anthers were fixed in ethanol-acetic acid (3:1) for 24 h and stored at 4°C in 70% alcohol until use. Preparations were made from pollen mother cells (PMCs) by squashing pieces of anthers in 45% acetic acid. Slide preparations were examined

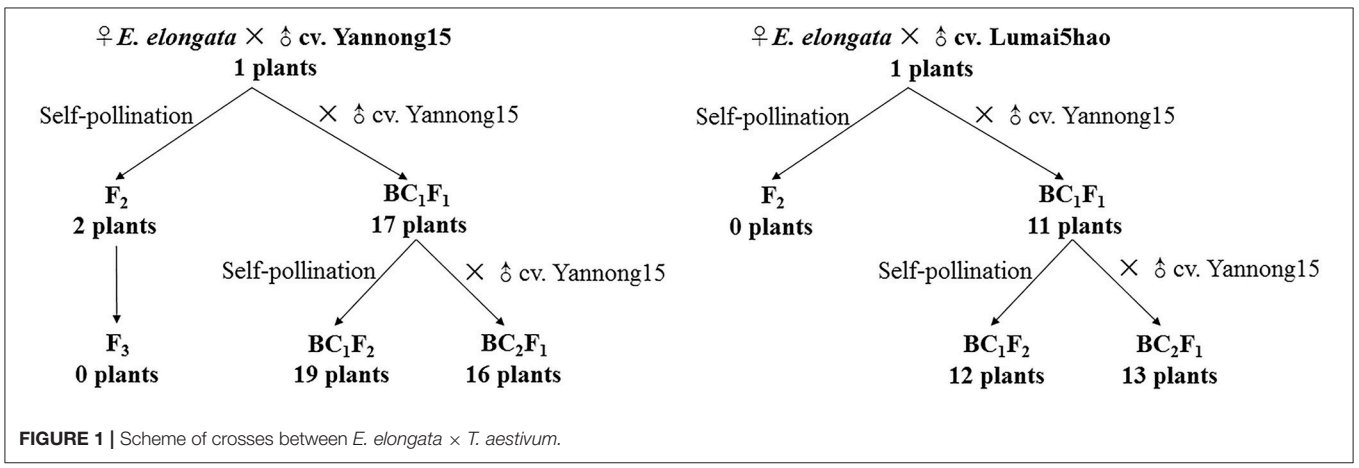

FIGURE 1 | Scheme of crosses between *E. elongata* × *T. aestivum*.

using phase-contrast microscopy and then placed on dry ice to remove the cover glass. The images were captured with an Olympus BX-60.

Gish Techniques

Elytrigia elongata DNA was labeled with fluorescein-12-dUTP by nick translation to be used as a probe. Sheared genomic DNA from Yannong15 (AABBDD, $2n = 42$) was used as blocking DNA. Detailed procedures of the hybridization mixture were performed as previously described (Kato et al., 2004). The slides were counterstained with propidium iodide (PI, 0.25 mg/mL) in Vectashield mounting medium (Vector Laboratories, USA).

Statistical Analyses

The data concerning the number of univalents, bivalents, trivalents, quadrivalents, pentavalents, and hexavalents for all PMCs of BC_1F_1, BC_1F_2, and BC_2F_1 hybrids studied were considered binomial responses, with the appropriate totals, obtained in a one-way classification. They were analyzed by the generalized linear model with logit link function to estimate mean values for plants and to test the significance of differences between plants. The calculation of mean values, standard deviations and coefficient of variation were analyzed by Excel 2013 with the statistics function. ANOVA analysis was carried out using Excel 2013, and the statistical significance (P) is shown in the Tables S1–S3.

RESULTS

Chromosome Pairing in F_1 Hybrids

The F_1 hybrids from the *E. elongata* × *T. aestivum* cross exhibited a low setting percentage and were morphologically different from the 2 parents, except for a similar perennial of *E. elongata*. All plants had 56 somatic chromosomes with 35 chromosomes from *E. elongata*. Meiotic association was determined in 29 PMCs at the MI stage from *E. elongata* × *T. aestivum* cv. Yannong15 (F_1-1) and 37 PMCs at the MI stage from *E. elongata* × *T. aestivum* cv. Lumai5hao (F_1-2) (**Table 1**), and the average chromosome configurations were 14.96I+17.8II+0.69III+0.63IV+0.17V (F_1-1, **Figure 2A**) and 18.02I+16.61II+0.61III+0.57IV+0.13V (F_1-2, **Figure 2B**), respectively. Chromosome pairing configurations in the hybrid PMCs were very complex, and a high frequency of univalent and a variety of trivalent and tetravalent configurations were observed.

GISH was performed to detect *E. elongata* chromosomes in F_1-1 and F_1-2 (**Figure 2C**) using total genomic DNA from *E. elongata* as a probe and ABD-genomic DNA from Yannong15 wheat as a blocker. The mean *E. elongata* chromosome configurations determined after GISH analysis were 11.03I+9.81II+0.37III+0.61IV+0.16V and 14.45I+8.4II+0.33III+0.54IV+0.12V, respectively (**Table 1**). The chromosome configurations of wheat-*E. elongata* in the hybrid included bivalents, one type of trivalent (W/W/E), one chain quadrivalent (W/W/E/E), and one chain pentavalent (W/W/W/E/E) (**Table 1**).

TABLE 1 | Chromosome configuration of PMC MI in wheat-*E. elongata* F_1 hybrids.

Lines	Cells No. of cytogenetic analysis	Chromosome No.	Average chromosome configurations					Average Chromosome configurations of *E. elongata*					Average Chromosome configurations of wheat-*E. elongata*					*E. elongata* chromosome No.	Cells No. of GISH	Seed setting rate
			I	II	III	IV	V	I	II	III	VI	V	II	III	VI	V				
F_1-1	29	56	14.96 (6–19)	17.8 (15–23)	0.69 (0–5)	0.63 (0–2)	0.17 (0–2)	11.03 (3–13)	9.81 (7–17)	0.37 (0–3)	0.61 (0–1)	0.16 (0–1)	0.41 (0–2)	0.09 (0–1)[a]	0.03 (0–1)[b]	0.02 (0–1)[c]		35	31	0.17%
F_1-2	37	56	18.02 (7–21)	16.61 (14–22)	0.61 (0–4)	0.57 (0–2)	0.13 (0–2)	14.45 (5–16)	8.4 (6–16)	0.33 (0–2)	0.54 (0–1)	0.14 (0–1)	0.38 (0–2)	0.08 (0–1)[a]	0.02 (0–1)[b]			35	24	0
mean value			16.49	17.21	0.65	0.60	0.15	12.74	9.11	0.35	0.58	0.15	0.40	0.09	0.025	0.01				

[a] *W/W/E.*
[b] *W/W/E/E.*
[c] *W/W/W/E/E.*

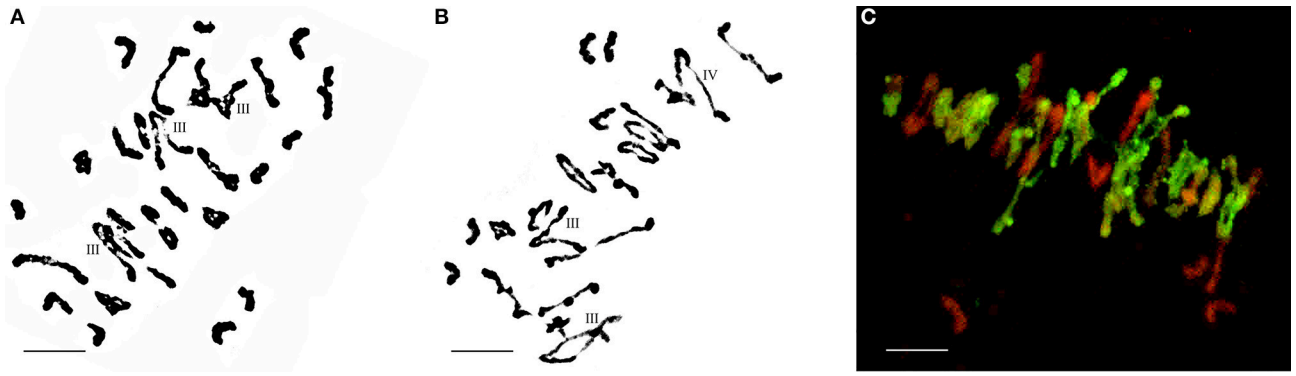

FIGURE 2 | Chromosome configuration of PMC MI in wheat-*E. elongata* F_1 hybrids. **(A)** Chromosome configurations of F_1-1: $2n = 7I+20II+3III$; **(B)** Chromosome configurations of F_1-2: $2n = 6I+20II+2III+1IV$; **(C)** *E. elongata* chromosome configurations of F_1-1: $2n = 3I+16II$. Wheat chromosomes were detected in red and *E. elongata* chromosomes or chromosome segments were visualized in green. Bar = 10 μm

Chromosome Pairing in F_2 Progeny

Although five of the F_1-1 selfed F_2 seeds were obtained, wherein two survived, the F_1-2 and these two F_2 plants were self-sterile. These F_2 plants (F_2-1 and F_2-2) were identified by cytogenetic analysis and GISH (**Table 2**). The F_2-1 plant had 49 chromosomes, 18 of which were from *E. elongata*, and the F_2-2 plant had 52 chromosomes, 20 of which were from *E. elongata*. The average chromosome configurations were 11.22I+15.32II+0.93III+0.41IV+0.29V+0.21VI (F_2-1, **Figure 3A**) and 11.92I+16.5II+0.79III+0.37IV+0.37V+0.23VI (F_2-2, **Figure 3B**), respectively. GISH analysis showed that the average *E. elongata* chromosome configurations were 5.39I+5.68II+0.27III+0.11IV (F_2-1, **Figure 3C**) and 8.87I+5.337II+0.152III (F_2-2, **Figure 3D**), respectively. The chromosome configurations of wheat-*E. elongata* in the hybrid included bivalents, one kind of trivalent (W/W/E), and one chain quadrivalent (W/W/W/E) (**Table 1**). In addition, a translocation or interspecific chromosome pairing between wheat and *E. elongata* chromosomes was also detected in some of these plants (**Figure 3D**, arrows).

Chromosome Pairing and Separation Trend in Hybrid Derivatives

Seventeen plants were produced from F_1-1 hybrids with *T. aestivum* cv. Yannong15, and 11 plants were produced from F_1-2 hybrids with *T. aestivum* cv. Yannong15. The PMCs from these 28 BC_1F_1 hybrid plants were analyzed with cytogenetic and GISH techniques (Table S1). The mean chromosome number of the BC_1F_1 progeny was $2n = 48.25$. Most lines (18 plants) had $2n = 47–49$; the distribution range was 44–52 (**Table 3**). The combinations of average chromosome configurations included 6.17–11.92 univalents, 15.07–18.6 bivalents, 0.31–1.52 trivalents, 0.1–0.79 tetravalents, 0–0.41 pentavalents and 0–0.23 hexavalents (Table S1, **Figures 4A–F**). GISH analysis revealed that 10–20 *E. elongata* chromosomes were detected in BC_1F_1 progeny (**Table 3**); the distribution range of average *E. elongata* chromosome configurations was 1.96–8.87 univalents, 2.62–6.41 bivalents, 0.12–1.04 trivalents, and 0.12–1.04 tetravalents (Table S1, **Figures 5A,B**). The average pairing configuration for wheat-*E. elongata* chromosomes included 0.15–0.32 bivalents, 0.02–0.06 trivalents, 0–0.03 tetravalents, and 0–0.04 pentavalents (Table S1).

Thirty-one BC_1F_2 plants were randomly selected from BC_1F_1 self-fertilization progeny for further cytogenetic analysis. The mean chromosome number of the progenies was $2n = 50.13$; the distribution range was 42–55 (**Table 3**). The distribution range of average chromosome configuration at meiotic metaphase I in BC_1F_2 PMCs included 2.51–16.01 univalents, 11.01–24.25 bivalents, 0.17–2.67 trivalents, 0–1.37 quadrivalents, 0–1.17 pentavalents and 0–0.83 hexavalents (Table S2, **Figures 4G–J**). GISH analysis during meiosis revealed 7-21 chromosomes with hybridization signals in these 31 plants (**Table 3**). The average pairing configuration of *E. elongata* chromosomes included 0.34–6.69 univalents, 0.5–7.94 bivalents, 0–1.14 trivalents and 0–0.54 tetravalents (Table S2, **Figures 5C–G**). The distribution range of average wheat-*E. elongata* chromosome configurations was 0.15–0.3 bivalents, 0.02–0.07 trivalents, 0–0.04 tetravalents, and 0–0.05 pentavalents (Table S2).

Twenty-nine BC_2F_1 plants produced from BC_1F_1 hybrids with *T. aestivum* cv. Yannong15 were analyzed by cytogenetic techniques and GISH. Overall, 42–50 total chromosomes and 6–11 *E. elongata* chromosomes were detected in these plants (**Table 3**). The distribution range of average chromosome configurations included 8.21–11.77 univalents, 12.68–17.34 bivalents, 0–1.77 trivalents, 0–1.38 tetravalents, 0–0.31 pentavalents and 0–0.1 hexavalents (Table S3, **Figures 4K,L**). GISH analysis revealed that the average pairing configuration for *E. elongata* chromosomes included 0.33–0.67 univalents, 4.21–9.64 bivalents, and 0.15–2.39 trivalents (Table S3, **Figure 5H,I**). The average pairing configuration of wheat-*E. elongata* chromosomes included 0.17–0.39 bivalents, 0.03–0.14 trivalents, 0–0.04 tetravalents, and 0–0.04 pentavalents (Table S3).

The separation trend is the chromosome variation amplitude of total chromosome number and *E. elongata* chromosome number of BC_1F_2 and BC_2F_1 compared with BC_1F_1. Obviously, the number of bivalents, trivalents and tetravalents among

TABLE 2 | Chromosome configuration of PMC MI in wheat-*E. elongata* F_2 hybrids.

Lines	Cells No. of cytogenetic analysis	Chromosome No.	Average chromosome configurations						Average Chromosome configurations of *E. elongata*				Average Chromosome configurations of wheat-*E. elongata*				*E. elongata* chromosome No.	Cells No. of GISH
			I	II	III	IV	V	VI	I	II	III	IV	II	III	IV			
F_2-1	47	49	11.22 (7–13)	15.32 (11–17)	0.93 (0–4)	0.41 (0–2)	0.29 (0–2)	0.21 (0–1)	5.39 (3–8)	5.68 (3–7)	0.27 (0–2)	0.11 (0–1)	0.21 (0–2)	0.03 (0–1)[a]	0.03 (0–1)[b]	18	33	
F_2-2	52	52	11.92 (6–14)	16.5 (14–21)	0.79 (0–4)	0.37 (0–3)	0.37 (0–2)	0.23 (0–1)	8.87 (6–11)	5.337 (3–8)	0.152 (0–2)		0.13 (0–2)	0.03 (0–1)[a]	0.03 (0–1)[b]	20	36	
mean value			11.57	15.91	0.86	0.39	0.33	0.22	7.13	5.509	0.211	0.11	0.17	0.03	0.03			

[a]*W/W/E.*
[b]*W/W/W/E.*

BC_1F_1, BC_1F_2, and BC_2F_1 plants were different. The numbers of chromosomes increased after selfing according to the result, and the pairing chromosome number also increased after selfing and backcrossing. Additionally, exogenous chromosomes decreased after backcrossing. These results were consistent with the theoretical hypothesis.

DISCUSSION

E. elongata is an influential perennial *Triticeae* species with a considerable number of traits with the potential to improve wheat. Several studies have reported wide hybridization between *E. elongata* and other species of Triticeae (Fu et al., 2012; Ayala-Navarrete et al., 2013; Guo et al., 2015). A higher seed set was usually obtained when *T. aestivum* was used as the female parent, whereas hybrid seed development was usually less successful. In wide hybridization between wheat and *E. elongata*, a 15.9% (0–76.9%) average seed setting rate in the dozens of combinations showed a very low crossability (Group of Eemote and Northwestern Institute, 1977). It is difficult to obtain offspring from the wheat and *E. elongata* hybrid; over the years, we have only obtained two perennial F_1 plants. Early studies in our laboratory found that, in distant hybridization, when *T. aestivum* cv. Yannong15 was a parent, the seed setting rate and seed survival rate of the offspring were the highest. Therefore, in order to obtain more seeds, we use *T. aestivum* cv. Yannong15 as a backcross parent. In this study, we harvested only five seeds from *E. elongata* × *T. aestivum* cv. Yannong15 offspring, and only two survived. This may be due to the genome ploidy gap between wheat and *E. elongata*, although the genetic relationship between them is very close, and may also be caused by the difference between common wheat varieties.

In recent decades, several wheat-*E. elongata* amphiploid, addition, substitution, and translocation lines have been developed in various laboratories throughout the world and are promising sources of multiple disease resistance (Fu et al., 2012; Zheng et al., 2014; Li et al., 2016). However, few studies have focused on the transmission characteristics of *E. elongata* chromosomes in the *T. aestivum* background. GISH has proved to be a useful technique to genetically differentiate closely related genomes, to distinguish alien chromosomes from wheat chromosomes, and to identify wheat-alien translocated chromosomes in a wheat background (Jiang and Gill, 2006; Scoles et al., 2010; Guo et al., 2015). In this study, GISH using *E. elongata* DNA as a probe was a powerful tool to differentiate chromosomes from *T. aestivum* and *E. elongata* hybrid progeny in PMCs at the MI stage. This differentiation allowed the precise analysis of the chromosome composition and the relationships between *E. elongata* and wheat chromosomes in a wheat genetic background. Using this approach, the genomic composition of the wheat-*E. elongata* BC_1F_1, BC_1F_2, and BC_2F_1 hybrid progenies was clearly identified in the MI stage and was shown to contain 10–20, 7–21, and 6–11 *E. elongata* chromosomes, respectively. In the backcross generation, the number of *E. elongata* chromosomes decreased rapidly; the distribution of *E. elongata* chromosomes was more extensive in

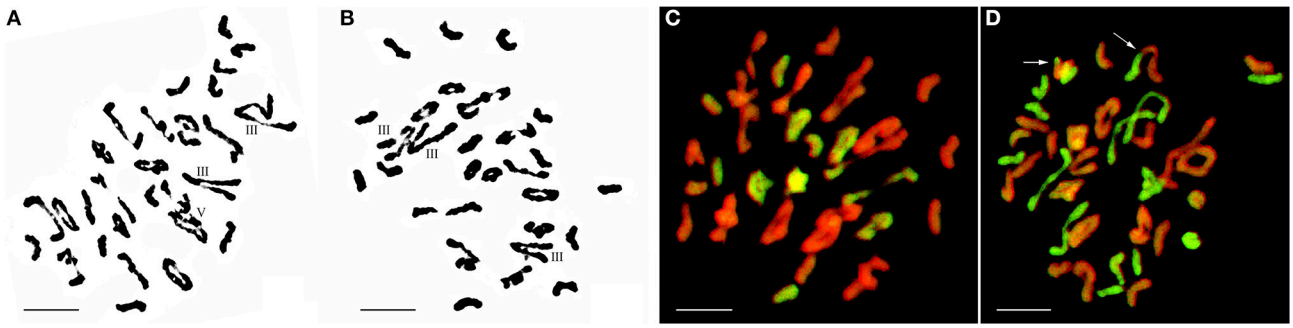

FIGURE 3 | Chromosome configuration in PMC MI for wheat-*E. elongata* F_2 hybrids. **(A)** Chromosome configuration of F_2-1: $2n = 10I+14II+2III+1V$; **(B)** Chromosome configuration of F_2-2: $2n = 7I+18II+3III$; **(C)** *E. elongata* chromosome configuration of F_2-1: $2n = 5I+6II$; **(D)** *E. elongata* chromosome configuration of F_2-2: $2n = 10I+5II$. Wheat chromosomes were detected in red and *E. elongata* chromosomes or chromosome segments were visualized in green. The arrows indicate pairing between wheat and *E. elongata* chromosomes. Bar = 10 μm.

TABLE 3 | Chromosome segregation trends in wheat-*E. elongata* BC_1F_1, BC_1F_2, and BC_2F_1 hybrids.

Lines	Chromosome No.														Plants No.	*E. elongata* chromosome No.											
	42	43	44	45	46	47	48	49	50	51	52	53	54	55		6	7	8	9	10	11	13	14	15	16	17	18	20	21
BC_1F_1	–	–	1	–	3	5	9	4	3	–	3	–	–	–	28	–	–	–	–	1	1	2	3	7	9	2	2	1	–
BC_1F_2	1	1	1	1	1	2	2	2	2	5	4	4	4	1	31	–	1	–	1	–	–	1	9	4	7	4	3	–	1
BC_2F_1	5	3	5	5	3	3	2	2	–	–	–	–	–	–	29	3	5	9	7	3	2	–	–	–	–	–	–	–	–

self-progeny. This observation indicated that backcrossing will promote cytological stability and that inbreeding will increase variability.

The genomic composition of *E. elongata* has been reported to be decaploid, with the genomic designation $JJJJJJJ^sJ^sJ^sJ^s$ (Chen et al., 1998) or $StStStStE^eE^eE^bE^bE^xE^x$ (Zhang et al., 1996). The F_1 hybrids were expected to have the genomic constitution of $ABDJJJJ^sJ^s$ or $ABDStStE^eE^bE^x$ ($2n = 56$ chromosomes), and the theoretical *E. elongata* chromosome configuration of these F_1 should be 7II+7III ($JJJJ^sJ^s$) or 21I+7II ($StStE^eE^bE^x$). In this study, the average *E. elongata* chromosome configurations of F_1 hybrids after GISH analysis were 11.03I+9.81II+0.37III+0.61IV+0.16V and 14.45I+8.4II+0.33III+0.54IV+0.12V. The earlier conclusion that the St and J/E^b (including J/E^b and J^s/E^e) genomes are very closely related was drawn from molecular and cytogenetic studies (Liu et al., 2007; Mahelka et al., 2013; Kantarski et al., 2017; Linc et al., 2017). In meiotic metaphase I, these closely related chromosomes may be associated with allosyndetic pairing, thereby reducing the number of univalents and increasing the number of bivalents and multivalents. Thus, in the actual statistical chromosome configuration, the univalents will be less than the theoretical value, while the bivalents and multivalents will be greater than the theoretical value. The average *E. elongata* chromosome configuration of these two F_1 lines accorded with the theoretical chromosome configuration of 21I+7II. Therefore, the genomic composition of *E. elongata* should be $StStStStE^eE^eE^bE^bE^xE^x$.

The strict pairing of homologous chromosomes in hexaploid wheat reflects a delicate balance between genes that inhibit homologous pairing, such as *Ph1* and *Ph2*, and genes that promote pairing, such as those located on homologous groups 2, 3, and 5 (Naranjo and Benavente, 2015). A similar theory was suggested for *Elytrigia* species. Dvorák (1987) proposed that the chromosome arms 3ES, 3EL, 4ES, and 5Ep and chromosome 6E of *T. elongatum* had genes that induce homoeologous chromosome pairing. Charpentier et al. (1988) further demonstrated that the role of 5E in the wheat and *Agropyron elongatum* hybrid was similar to the deletion of the *Ph1* gene. Later, Zhang et al. (1995) implied that two basic chromosomes in *E. elongata* encode genes that promote homoeologous chromosome pairing and might have additive effects. Although more recent studies observed similar inferences, there is no direct evidence to confirm these hypotheses. In the present study, pairing between wheat and *E. elongata* was detected in each of the wheat-*E. elongata* hybrid progenies, albeit rarely. This result suggests a close genetic relationship between wheat and *E. elongata* chromosomes. Similar results were detected on meiotic chromosomes at MI in trigeneric hybrids produced from a heterozygous Langdon *Ph* mutant (*Ph1ph1b*) or Langdon 5D (5B) disomic substitution line (without *Ph1*) hybridization with the JJEE amphidiploids using multicolor fluorescent GISH by Jauhar et al. (2004) and (Jauhar and Peterson (2006)). The pairing between wheat and *E. elongata* chromosomes can be used as direct evidence that genes promoting homoeologous chromosome pairing or *Ph* suppressor genes exist in *E. elongata*. Although it is worthwhile for *E. elongata* chromosomes to promote homoeologous pairing or inhibit *Ph* gene effects, the use of these genotypes might promote the homoeologous pairing of *E. elongata* and wheat

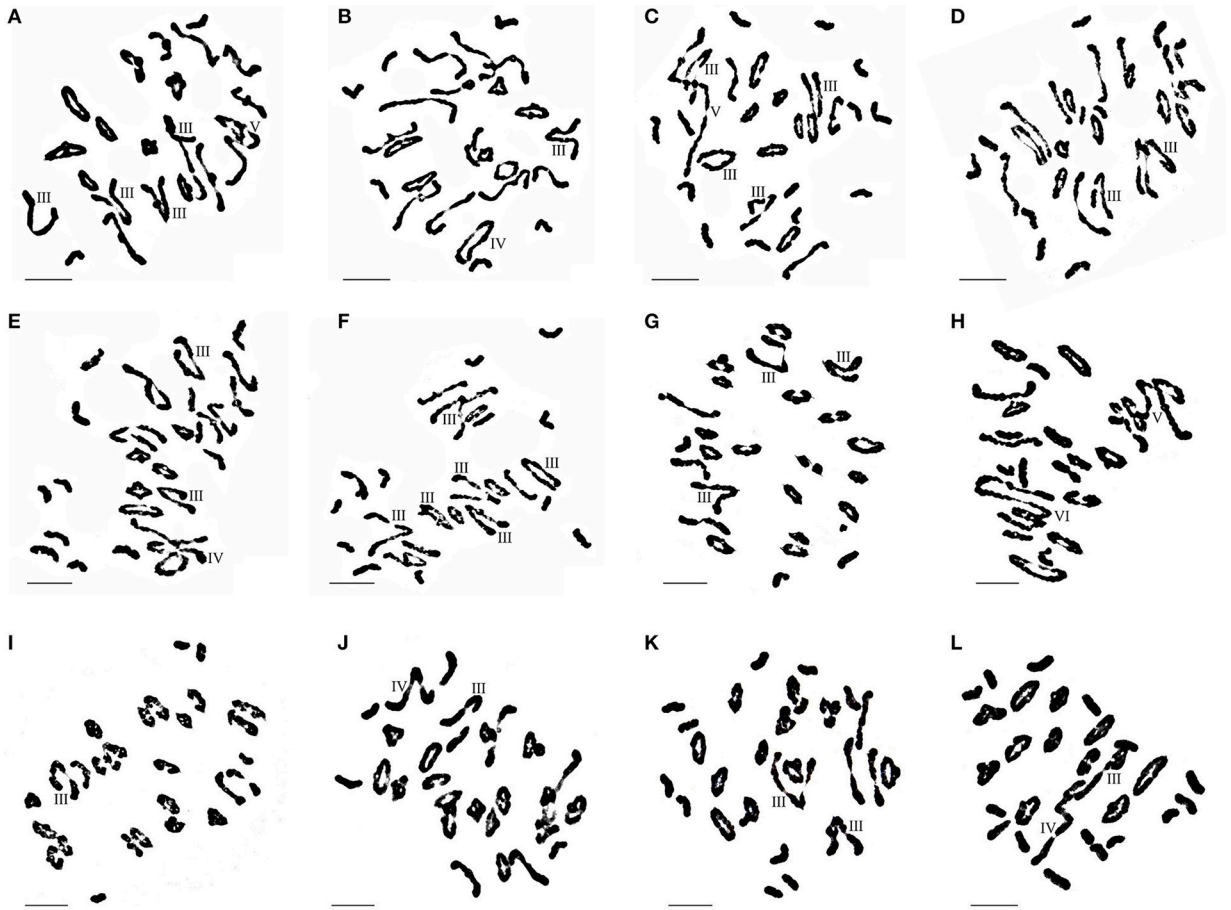

FIGURE 4 | Chromosome configuration of wheat- *E. elongata* BC_1F_1, BC_1F_2 and BC_2F_1 hybrids. **(A–F)** Chromosome configurations in BC_1F_1 **(A)** $2n$ = 3I+15II+4III+1IV; **(B)** $2n$ = 6I+17II+1III+1IV; **(C)** $2n$ = 12I+10II+4III+1V; **(D)** $2n$ = 8I+16II+2III; **(E)** $2n$ = 11I+12II+2III+1IV; **(F)** 2n=10I+9II+6III; **(G–J)** Chromosome configurations in BC_1F_2 **(G)** $2n$ = 3I+19II+3III; **(H)** $2n$ = 5I+14II+1V+1VI; **(I)** $2n$ = 7I+21II+1III; **(J)** $2n$ = 3I+20II+1III+1IV; **(K–L)** Chromosome configurations in BC_2F_1 **(K)** $2n$ = 10I+13II+2III; **(L)** $2n$ = 15I+11II+1III+1IV. Bar = 10 μm.

chromosomes and facilitate alien gene transfer into the wheat genome.

Common wheat is a major, global cereal crop that accounts for approximately 20% of the calories consumed by humans (Brenchley et al., 2012). However, effective wheat breeding has been hindered by a narrow genetic base (Friebe et al., 1996). Genes from wild relatives have been exploited to confer desirable agronomic traits to wheat, as illustrated by the application of many wheat-alien translocation lines (Lukaszewski, 2001). For example, *Lr26*/*Sr31*/*Yr9*/*Pm8* have endowed the translocation line T1RS·1BL with improved environmental adaption and enhanced kernel numbers (Friebe et al., 1996). Both *T. aestivum-Thinopyrum bessarabicum* T2JS-2BS·2BL and *T. aestivum-Dasypyrum villosum* T2VS·2DL translocation lines have been reported with elevated grain numbers per spike (Qi et al., 2010; Zhang et al., 2015). However, the formation of these translocation lines is rarely reported. GISH patterns of meiotic chromosomes at MI in these hybrids of wheat with *E. elongata* indicated that chromosome pairing in these hybrids mainly occurred among wheat chromosomes and among *E. elongata* chromosomes and that allosyndetic pairing between wheat and *E. elongata* chromosomes was very rare (**Table 1**). The much higher frequencies of autosyndetic pairing than allosyndetic pairing in these hybrids of wheat with *E. elongata* demonstrated that the relationships among *T. aestivum* genomes and among *E. elongata* genomes are much closer than the relationship between *T. aestivum* and *E. elongata* genomes. Meanwhile, these allosyndetic pairings promote the recombination between homologous chromosomes, enrich the genetic diversity of distant hybrid progeny, and improve the frequency of the offspring to obtain a translocation line, which will benefit from the selection of excellent genetic resources, and thus applied to wheat breeding. Our results demonstrate that GISH using *E. elongata* genomic DNA as a probe provided a reliable approach to discriminate the identity of chromosomes involved in pairing. This observation might significantly improve our understanding of the genomic relationships within *Triticeae*. Knowledge of the relationships between wheat and grass genomes also improves our understanding of characteristic inheritance to generate efficient strategies for transferring target gene(s) from *E. elongata*

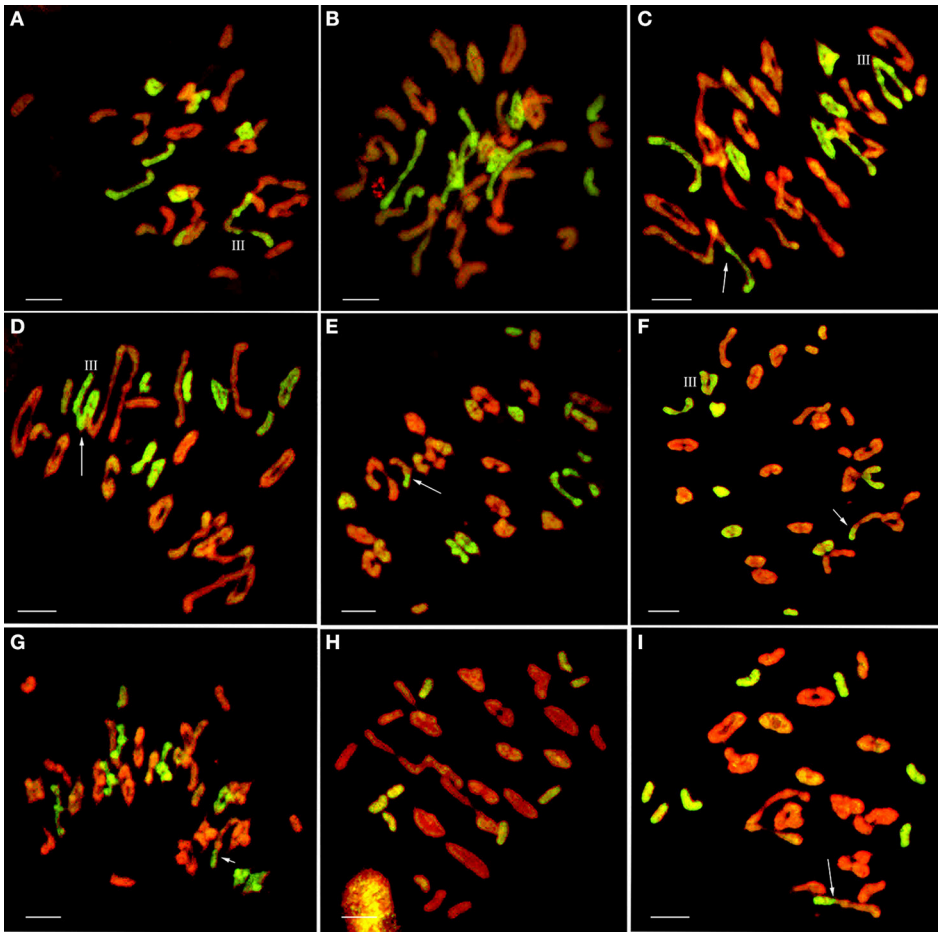

FIGURE 5 | GISH patterns of PMC MI in wheat-*E. elongata* BC_1F_1, BC_1F_2, and BC_2F_1 hybrids**. (A,B)** *E. elongata* chromosome configurations in BC_1F_1 **(A)** $2n = 1I+6II+1III$; **(B)** $2n = 3I+7II$; **(C–G)** *E. elongata* chromosome configurations in BC_1F_2 **(C)** $2n = 1I+6II+1III$; **(D)** $2n = 3I+4II+1III$; **(E)** $2n = 5I+6II$; **(F)** $2n = 2I+6II+1III$; **(G)** $2n = 3I+7II$; **(H–I)** *E. elongata* chromosome configurations in BC_2F_1 **(H)** $2n = 8I$; **(I)** $2n = 8I$. Wheat chromosomes were detected in red and *E. elongata* chromosomes or chromosome segments were visualized in green. The arrows indicate pairing between wheat and *E. elongata* chromosomes. Bar = 10 μm.

to wheat. With the advancement and development of technology, multicolor GISH (mcGISH) has been widely used in academic research to simultaneously visualize two or more genomes in a polyploid species (Zheng et al., 2014; Guo et al., 2015). Although there are few reports analyzing chromosome pairing behavior using mcGISH, our future research will focus on these types of analyses. This approach might extend the analysis of chromosomes, genomes and phylogenies, especially for the analysis of complex polyploids and their hybrids in wheat.

AUTHOR CONTRIBUTIONS

FH, PX, and YB performed the experiments, analyzed the data and wrote the manuscript. MR, SL, YW, XL, and HW designed the study and discussed the manuscript.

ACKNOWLEDGMENTS

This work was funded by the National Key Research and Development Plan of China (2016YFD0102004), the National Natural Science Foundation of China (Grant No. 31501298, No. 31671675 and No. 31660390), the National Key Research and Program of China (2017YFD0100900) and the Provincial Science and Technology Plan for Colleges in Shandong Province (Grant No. J17KA151).

SUPPLEMENTARY MATERIAL

The Supplementary Material for this article can be found online at: https://www.frontiersin.org/articles/10.3389/fpls.2017.02161/full#supplementary-material

REFERENCES

Ayala-Navarrete, L. I., Mechanicos, A. A., Gibson, J. M., Singh, D., Bariana, H. S., Fletcher, J., et al. (2013). The Pontin series of recombinant alien translocations in bread wheat: single translocations integrating combinations of Bdv2, Lr19 and Sr25 disease-resistance genes from Thinopyrum intermedium and *Th. ponticum*. *Theor. Appl. Genet.* 126, 2467–2475. doi: 10.1007/s00122-013-2147-0

Bagherikia, S., Karimzadeh, G., and Naghavi, M. R. (2014). Distribution of 1AL.1RS and 1BL.1RS wheat-rye translocations in *Triticum aestivum* using specific PCR. *Biochem. Syst. Ecol.* 55, 20–26. doi: 10.1016/j.bse.2014.02.001

Bao, Y., Wu, X., Zhang, C., Li, X., He, F., Qi, X., et al. (2014). Chromosomal constitutions and reactions to powdery mildew and stripe rust of four novel wheat-Thinopyrum intermedium partial amphiploids. *J. Genet. Genomics* 41, 663–666. doi: 10.1016/j.jgg.2014.11.003

Brenchley, R., Spannagl, M., Pfeifer, M., Barker, G. L. A., D'Amore, R., Allen, A. M., et al. (2012). Analysis of the bread wheat genome using whole-genome shotgun sequencing. *Nature* 491, 705–710. doi: 10.1038/nature11650

Cai, X., and Jones, S. (1997). Direct evidence for high level of autosyndetic pairing in hybrids of *Thinopyrum intermedium* and *Th. ponticum* with *Triticum aestivum*. *Theor. Appl. Genet.* 95, 568–572. doi: 10.1007/s001220050597

Charpentier, A., Cauderon, Y., and Feldman, M. (1988). "Control of chromosome pairing in Agropyron elongatum", in *Proceedings of the Seventh International Wheat Genetics Symposium,* eds T. E. Miller and R. M. D. Koebner (Cambridge: Published by the Institute of Plant Science Research, Cambridge Laboratory).

Chen, Q., Conner, R., Laroche, A., and Ahmad, F. (2001). Molecular cytogenetic evidence for a high level of chromosome pairing among different genomes in *Triticum aestivum-Thinopyrum intermedium* hybrids. *Theor. Appl. Genet.* 102, 847–852. doi: 10.1007/s001220000496

Chen, Q., Conner, R., Laroche, A., and Thomas, J. (1998). Genome analysis of *Thinopyrum intermedium* and *Thinopyrum ponticum* using genomic *in situ* hybridization. *Genome* 41, 580–586. doi: 10.1139/g98-055

Dvorák, J. (1987). Chromosomal distribution of genes in diploid *Elytrigia elongata* that promote or suppress pairing of wheat homoeologous chromosomes. *Genome* 29, 34–40. doi: 10.1139/g87-006

Friebe, B., Jiang, J., Raupp, W. J., McIntosh, R. A., and Gill, B. S. (1996). Characterization of wheat-alien translocations conferring resistance to diseases and pests: current status. *Euphytica* 91, 59–87. doi: 10.1007/BF00035277

Fu, S., Lv, Z., Qi, B., Guo, X., Li, J., Liu, B., et al. (2012). Molecular cytogenetic characterization of wheat-*Thinopyrum elongatum* addition, substitution and translocation lines with a novel source of resistance to wheat Fusarium Head Blight. *J. Genet. Genomics* 39, 103–110. doi: 10.1016/j.jgg.2011.11.008

Group of Eemote and Northwestern Institute (1977). The cross breeding and its genetic analysis between *Triticum aestivum* and Agropyron elongatum. *J. Genet. Genomics* (04), 283–293.

Guo, X., Shi, Q., Wang, J., Hou, Y., Wang, Y., and Han, F. (2015). Characterization and genome changes of new amphiploids from wheat wide hybridization. *J. Genet. Genomics* 42, 459–461. doi: 10.1016/j.jgg.2015.06.006

He, F., Xu, J., Qi, X., Bao, Y., Li, X., Zhao, F., et al. (2013). Molecular cytogenetic characterization of two partial wheat-*Elytrigia elongata* amphiploids resistant to powdery mildew. *Plant Breed.* 132, 553–557. doi: 10.1111/pbr.12104

Hu, L. J., Li, G. R., Zeng, Z. X., Chang, Z. J., Liu, C., and Yang, Z. J. (2011). Molecular characterization of a wheat-*Thinopyrum ponticum* partial amphiploid and its derived substitution line for resistance to stripe rust. *J. Appl. Genet.* 52, 279–285. doi: 10.1007/s13353-011-0038-0

Jauhar, P. P., Dogramaci, M., and Peterson, T. (2004). Synthesis and cytological characterization of trigeneric hybrids of durum wheat with and without Ph1. *Genome* 47, 1173–1181. doi: 10.1139/g04-082

Jauhar, P., and Peterson, T. (2006). Cytological analyses of hybrids and derivatives of hybrids between durum wheat and *Thinopyrum bessarabicum,* using multicolour fluorescent GISH. *Plant Breed.* 125, 19–26. doi: 10.1111/j.1439-0523.2006.01176.x

Jiang, J., and Gill, B. S. (2006). Current status and the future of fluorescence *in situ* hybridization (FISH) in plant genome research. *Genome* 49, 1057–1068. doi: 10.1139/g06-076

Kantarski, T., Larson, S., Zhang, X., DeHaan, L., Borevitz, J., Anderson, J., et al. (2017). Development of the first consensus genetic map of intermediate wheatgrass (*Thinopyrum intermedium*) using genotyping-by-sequencing. *Theor. Appl. Genet.* 130, 137–150. doi: 10.1007/s00122-016-2799-7

Kato, A., Lamb, J. C., and Birchler, J. A. (2004). Chromosome painting using repetitive DNA sequences as probes for somatic chromosome identification in maize. *Proc. Natl. Acad. Sci. U.S.A.* 101, 13554–13559. doi: 10.1073/pnas.0403659101

Li, H., and Wang, X. (2009). *Thinopyrum ponticum* and *Th. intermedium*: the promising source of resistance to fungal and viral diseases of wheat. *J. Genet. Genomics* 36, 557–565. doi: 10.1016/S1673-8527(08)60147-2

Li, H., Zheng, Q., Pretorius, Z. A., Li, B., Tang, D., and Li, Z. (2016). Establishment and characterization of new wheat-*Thinopyrum ponticum* addition and translocation lines with resistance to Ug99 races. *J. Genet. Genomics* 43, 573–575. doi: 10.1016/j.jgg.2016.07.004

Linc, G., Gaal, E., Molnar, I., Icso, D., Badaeva, E., and Molnar-Lang, M. (2017). Molecular cytogenetic (FISH) and genome analysis of diploid wheatgrasses and their phylogenetic relationship. *PLoS ONE* 12:e0173623. doi: 10.1371/journal.pone.0173623

Liu, Z., Li, D., and Zhang, X. (2007). Genetic relationships among Five Basic Genomes St, E., A, B and D in Triticeae Revealed by Genomic Southern and *in situ* hybridization. *J. Integr. Plant Biol.* 49, 1080–1086. doi: 10.1111/j.1672-9072.2007.00462.x

Lukaszewski, A. J. (2001). Breeding behavior of the cytogenetically engineered wheat-rye translocation chromosomes 1RS.1BL. *Crop Sci.* 41, 1062–1065. doi: 10.2135/cropsci2001.4141062x

Mahelka, V., Kopecky, D., and Baum, B. R. (2013). Contrasting patterns of evolution of 45S and 5S rDNA families uncover new aspects in the genome constitution of the agronomically important grass *Thinopyrum intermedium* (Triticeae). *Mol. Biol. Evol.* 30, 2065–2086. doi: 10.1093/molbev/mst106

Naranjo, T., and Benavente, E. (2015). "The mode and regulation of chromosome pairing in wheat–alien hybrids (*Ph* Genes, an Updated View)," in *Alien Introgression in Wheat*, eds M. Molnar, C. Ceoloni, and J. DoleŽel (Cham: Springer), 133–162. doi: 10.1007/978-3-319-23494-6_6

Niu, Z., Klindworth, D. L., Yu, G., T, L.F., Chao, S., Jin, Y., et al. (2014). Development and characterization of wheat lines carrying stem rust resistance gene Sr43 derived from *Thinopyrum ponticum*. *Theor. Appl. Genet.* 127, 969–980. doi: 10.1007/s00122-014-2272-4

Qi, L., Friebe, B., Zhang, P., and Gill, B. S. (2007). Homoeologous recombination, chromosome engineering and crop improvement. *Chromosome Res.* 15, 3–19. doi: 10.1007/s10577-006-1108-8

Qi, Z., Du, P., Qian, B., Zhuang, L., Chen, H., Chen, T., et al. (2010). Characterization of a wheat–*Thinopyrum bessarabicum* (T2JS-2BS•2BL) translocation line. *Theor. Appl. Genet.* 121, 589–597. doi: 10.1007/s00122-010-1332-7

Roundy, B. A. (1985). Emergence and establishment of basin wildrye and tall wheatgrass in relation to moisture and salinity. *J. Range Manag.* 38, 126–131. doi: 10.2307/3899254

Scoles, G., Wang, Q., Xiang, J., Gao, A., Yang, X., Liu, W., et al. (2010). Analysis of chromosomal structural polymorphisms in the St, P., and Y genomes of Triticeae (Poaceae). *Genome* 53, 241–249. doi: 10.1139/G09-098

Sears, E. R. (1976). Genetic control of chromosome pairing in wheat. *Annu. Rev. Genet.* 10, 31–51. doi: 10.1146/annurev.ge.10.120176.000335

Sepsi, A. I. (2010). *Molecular Cytogenetic Characterisation of a Leaf-Rust Resistant Wheat-Thinopyrum pontificum Partial Amphiploid*. Doctoral Dissert, Eotvos Lorand Univesity of Science, Budapest.

Song, L., Lu, Y., Zhang, J., Pan, C., Yang, X., Li, X., et al. (2016). Cytological and molecular analysis of wheat - *Agropyron cristatum* translocation lines with 6P chromosome fragments conferring superior agronomic traits in common wheat. *Genome* 59, 840–850. doi: 10.1139/gen-2016-0065

Su, Y., Zhang, D., Li, Y., and Li, S. (2016). Nonhomologous chromosome pairing in aegilops-secale hybrids. *Cytogenet. Genome Res.* 147, 268–273. doi: 10.1159/000444435

Zhan, H., Li, G., Zhang, X., Li, X., Guo, H., Gong, W., et al. (2014). Chromosomal location and comparative genomics analysis of powdery mildew resistance gene Pm51 in a putative wheat-*Thinopyrum ponticum* introgression line. *PLoS ONE* 9:e113455. doi: 10.1371/journal.pone.0113455

Zhang, R., Hou, F., Feng, Y., Zhang, W., Zhang, M., and Chen, P. (2015). Characterization of a *Triticum aestivum–Dasypyrum villosum* T2VS●2DL translocation line expressing a longer spike and more kernels traits. *Theor. Appl. Genet.* 128, 2415–2425. doi: 10.1007/s00122-015-2596-8

Zhang, X., Dong, Y., and Wang, R. R.-C. (1996). Characterization of genomes and chromosomes in partial amphiploids of the hybrid *Triticum aestivum*× *Thinopyrum ponticum* by *in situ* hybridization, isozyme analysis, and RAPD. *Genome* 39, 1062–1071. doi: 10.1139/g96-133

Zhang, X., Dong, Y., and Yang, X. (1995). Cytogenitic research on hybrids of Triticum with both Thinopyrum ponticum and Th. Intermedium as well as their derivatives- III. Primary detection of genrtic base for introgression of useful genes from the two alien species to wheat. *J. Genet. Genomics* 22, 217–222

Zheng, Q., Lv, Z., Niu, Z., Li, B., Li, H., Xu, S. S., et al. (2014). Molecular cytogenetic characterization and stem rust resistance of five wheat–*Thinopyrum ponticum* partial amphiploids. *J. Genet. Genomics* 41, 591–595. doi: 10.1016/j.jgg.2014.06.003

Conflict of Interest Statement: The authors declare that the research was conducted in the absence of any commercial or financial relationships that could be construed as a potential conflict of interest.

frontiers in Plant Science

ORIGINAL RESEARCH
published: 01 November 2018
doi: 10.3389/fpls.2018.01501

3D Molecular Cytology of Hop (*Humulus lupulus*) Meiotic Chromosomes Reveals Non-disomic Pairing and Segregation, Aneuploidy, and Genomic Structural Variation

Katherine A. Easterling[1,2], *Nicholi J. Pitra*[2], *Rachel J. Jones*[2], *Lauren G. Lopes*[1], *Jenna R. Aquino*[1], *Dong Zhang*[2], *Paul D. Matthews*[2] *and Hank W. Bass*[1]*

[1] Department of Biological Science, Florida State University, Tallahassee, FL, United States, [2] Hopsteiner, S.S. Steiner, Inc., New York, NY, United States

Hop (*Humulus lupulus* L.) is an important crop worldwide, known as the main flavoring ingredient in beer. The diversifying brewing industry demands variation in flavors, superior process properties, and sustainable agronomics, which are the focus of advanced molecular breeding efforts in hops. Hop breeders have been limited in their ability to create strains with desirable traits, however, because of the unusual and unpredictable inheritance patterns and associated non-Mendelian genetic marker segregation. Cytogenetic analysis of meiotic chromosome behavior has also revealed conspicuous and prevalent occurrences of multiple, atypical, non-disomic chromosome complexes, including those involving autosomes in late prophase. To explore the role of meiosis in segregation distortion, we undertook 3D cytogenetic analysis of hop pollen mother cells stained with DAPI and FISH. We used telomere FISH to demonstrate that hop exhibits a normal telomere clustering bouquet. We also identified and characterized a new sub-terminal 180 bp satellite DNA tandem repeat family called HSR0, located proximal to telomeres. Highly variable 5S rDNA FISH patterns within and between plants, together with the detection of anaphase chromosome bridges, reflect extensive departures from normal disomic signal composition and distribution. Subsequent FACS analysis revealed variable DNA content in a cultivated pedigree. Together, these findings implicate multiple phenomena, including aneuploidy, segmental aneuploidy, or chromosome rearrangements, as contributing factors to segregation distortion in hop.

Keywords: cytogenetics, FISH, non-Mendelian inheritance, segregation distortion, telomere bouquet

OPEN ACCESS

Edited by:
Tomás Naranjo, Complutense University of Madrid, Spain

Reviewed by:
André Luís Laforga Vanzela, Universidade Estadual de Londrina, Brazil
Andrew Lloyd, Aberystwyth University, United Kingdom

***Correspondence:**
Hank W. Bass
bass@bio.fsu.edu

Specialty section:
This article was submitted to Plant Cell Biology, a section of the journal Frontiers in Plant Science

Received: *28 June 2018*
Accepted: *25 September 2018*
Published: *01 November 2018*

Citation:
Easterling KA, Pitra NJ, Jones RJ, Lopes LG, Aquino JR, Zhang D, Matthews PD and Bass HW (2018) 3D Molecular Cytology of Hop (Humulus lupulus) Meiotic Chromosomes Reveals Non-disomic Pairing and Segregation, Aneuploidy, and Genomic Structural Variation. Front. Plant Sci. 9:1501. doi: 10.3389/fpls.2018.01501

INTRODUCTION

Humulus lupulus (hop), a member of the Cannabaceae family of flowering plants, is a dioecious, high-climbing, herbaceous bine that is best known as a flavoring agent in beer. Hop cultivation for this purpose has been traced back to Germany, 736 AD (Neve, 1991). For hop, despite its long successful history of domestication, modern breeding practices are associated with a number of challenges. For instance, although hop is generally cultivated vegetatively by rhizomes, sexual crosses are necessary in order to breed for new disease-resistant and chemically

desirable varieties. The long history of cultivation includes colchicine-induced polyploidization (Roborgh, 1969) and the introgression of genetically distinct wild populations (Small, 1980; Reeves and Richards, 2011). Recent genetic, genomic, and quantitative trait analyses have demonstrated that the genome of hop is complex and structurally diverse (Zhang et al., 2017). Irregularities in hop transmission genetics are reflected in non-Mendelian segregation distortion and sex ratio bias (Seefelder et al., 2000; Jakse et al., 2008, 2011; McAdam et al., 2013, 2014).

Meiotic chromosome behavior is implicated as a cause for the unusual transmission genetics that are found in hop (Zhang et al., 2017). In sexually reproducing organisms, meiosis reduces the genomes from diploid to haploid (John, 1990) and homologous chromosomes from each parental genome undergo pairing, synapsis, recombination (John, 1990). These events ensure proper segregation of chromosomes into balanced gametes for subsequent fertilization and transmission to the progeny of the next generation (Stebbins, 1935; John, 1990; Murphy and Bass, 2012). Deviations from such normal disomic pairing and disjunction can lead to a variety of genetic inheritance problems including gene dosage imbalance, aneuploidy, and chromosomal rearrangements.

Among the hallmarks of meiosis that are cytologically evident are (1) the presence of a telomere bouquet in early prophase that guides homology search and subsequent synapsis, (2) the presence of bivalents at diakinesis during late prophase, (3) complete and equal separation of homologs at meiosis I, and (4) the production of 4 haploid nuclei with 1:1:1:1 segregation, as evidenced from tetrad analysis. For hop, non-disomic and heteromorphic sex chromosome figures have been noted and speculated to impact segregation patterns (Sinotô, 1929; Jacobsen, 1957; Neve, 1958; Haunold, 1991; Shephard et al., 2000; Zhang et al., 2017). However, neither the early prophase telomere bouquet nor the post-meiotic segregation has been characterized cytogenetically.

Here we set out to further examine the cytogenetics of male hop meiosis. To date, several somatic karyotypes for hop have been produced (Sinotô, 1929; Winge, 1929; Shephard et al., 2000). The more recent hop karyotypes include FISH-mapped loci for the *Humulus lupulus*-specific subtelomeric repeat-1 (HSR1), the Humulus japonicus-specific subtelomeric repeat (HSJR), the nucleolus organizer region (NOR), and 5S rDNA (Karlov et al., 2003; Divashuk et al., 2011; Alexandrov et al., 2012). Telomere FISH has also been used in hop, but not to test for the presence of the telomere bouquet at early prophase. In this study, we employed 3D acrylamide FISH (Howe et al., 2013) to show that hop has a classical zygotene telomere bouquet, but non-uniform segregation of 5S rDNA loci. Detection of anaphase bridges and variable DNA content further implicate genome structure variability in the unusual inheritance patterns of hop.

METHODS

Plant Materials and Fixation

Plants were collected and fixed according to previously described methods (Zhang et al., 2017), with exceptions on timing and paraformaldehyde concentration during the meiocyte buffer A (MBA) steps. Briefly, hop panicles were field collected and immediately fixed in Farmer's fluid (3:1 ethanol:acetic acid) overnight, replaced with Farmer's fluid for a second overnight period, and exchanged into 70% ethanol for storage at −20C. Hopsteiner varieties were collected on site in the company's male yard, and were grown under standard agronomic conditions at the Golden Gate Ranches, S.S. Steiner, Inc, Yakima, WA. The *H. lupulus* var. *neomexicanus*, plant SH2, was collected in the Coronado National Forest in Arizona.

Bioinformatic Identification of Tandem Repeat Family, *H. lupulus* Subterminal Repeat 0, HSR0

DNA from Apollo was used to make a library of large DNA fragments using the RSII technology. PacBio Single Molecule, Real-Time (SMRT) DNA sequences were manually and randomly screened for tandem repeats using the dot plot function of GenomeMatcher (Ohtsubo et al., 2008). Tandem repeats in the clones were detected as parallel stripes exhibiting a striping pattern evenly spaced and parallel to the main diagonal of identity. This striping pattern is diagnostic for DNA containing tandemly repeated sequences, easily detected by dot plot inspection, and was used to find new candidate loci for FISH probe development. Potential hits were further analyzed by dot-plotting against other hits to detect "allelism" among the repeats found within individual clones. Computational tandem repeat searching was done using "ksift" (https://github.com/dvera/ksift) Jellyfish-2 (https://github.com/zippav/Jellyfish-2) and YASS dot-plotter (https://github.com/laurentnoe/yass).

The two most frequent tandem repeat families found in this way were the ∼385 bp tandemly repeated sequence previously defined as the *Humulus*-specific subtelomeric repeat-1, HSR1, GenBank Accession GU831574, (Divashuk et al., 2014), and a new ∼180 bp tandemly-repeated sequence designated here as *H. lupulus* Subterminal Repeat 0, HSR0. The names of five HSR0-containing Apollo genomic DNA sequences from PacBio SMRT and their length and GenBank Accession numbers are HuluTR180-120 (6,005 bp, Acc. MH188533), HuluTR180-69 (11,761 bp, Acc. MH188534), HuluTR180TEL-954 (10,443 bp, Acc. MH188536), HuluTR180TEL-316 (5,717 bp, Acc. MH188537), and HuluTR180-270 (10,794 bp, Acc. MH188538). Two of these, HuluTR180TEL-316 and HuluTR180TEL-316, contain both HSR0 and telomeric repeats. For comparison, a clone with telomeric DNA repeats but lacking HSR0 has also been deposited as HuluTEL-347 (5,551 bp, Acc. MH188535).

Fluorescence *in-situ* Hybridization, FISH

For 3D FISH, whole Farmer's-fixed buds attached to peduncles were equilibrated in meiocyte Buffer A (Bass et al., 1997) for 30 min at RT, repeated twice, followed by fixation in 1% formaldehyde in MBA for 1 h at RT. After fixation, the tissue was washed three times in MBA for 15-min each at RT and stored in MBA at 4C. Meiotic cells were micro-dissected from buds of various sizes spanning meiosis (from ∼1.5 to 2.5 mm in length) and embedded in acrylamide as described for the 3D acrylamide FISH technique (Howe et al., 2013).

FISH probes used in this study were synthetic oligonucleotides co-synthetically coupled to fluorescent dyes and designed to detect telomeres ("MTLF-29," 5′-[FITC]-$(CCCTAAA)_4$-3′ or "MTLY-28-16" 5′-[ATTO647N]-$(CCCTAAA)_4$-3′), HSR0 tandem repeats ("ZERO-Y," 5′-[ATTO647N]-AGAAATATG AGTGAATTACGAAATCGC-3′), HSR1 tandem repeats ("HSR1a_22," 5′-Alexa488-GGTACCCCTCTGGTGAAT TGGA-3′), or 5S rDNA (pool of three oligos: "5SBOB1F," 5′-[Alexa488]-GCACCGGATCCCATCAGAACTCC-3′]; "5SBOB2F," 5′-[Alexa488]-AGTTAAGCGTGCTTGGGCGAG AG-3′; and "5SBOB3F," 5′-[Alexa488]-GTGACCTCCTGGGAA GTCCTCGTG-3′). The three 5S rDNA probes were selected on the basis of their 100% identity, according to the 5S rRNA Database (Szymanski et al., 2002), for *Cannabis sativa* (5sRNAdb Record ID E00464), *Gossypium hirsutum* (5sRNAdb Record ID E00193), and *Zea mays* (5sRNAdb Record ID E00011). Prehybridization, hybridization, post-hybridization washes, DAPI counterstaining, and slide mounting were done as described (Howe et al., 2013) using denaturation temperatures ranging from 88 to 92°C.

Collection, Analysis, and Display of 3D Deconvolution Microscopy Images

Three-dimensional images were collected on a DeltaVision deconvolution microscope, using a 60X lens and 0.2 micron Z-step optical sections as described (Zhang et al., 2017) for DAPI imaging, but also including FITC, TRITC, or CY5 imaging for FISH probes that fluoresce green, red, or far-red, respectively. Distance measurements between the 5S rDNA FISH signals were obtained as point-to-point Euclidean distances using the *Measure Distances* program, manually selecting the brightest voxel centered in the X, Y, and Z dimensions for any given FISH signal.

FACS Analysis of DNA Content

A two-step protocol (Pellicer and Leitch, 2014) was followed to isolate hop nuclei from 20 mg of fresh leaf tissue chopped and stained in LB01 buffer. The homogenate was filtered through a 30–42 um nylon mesh filter, centrifuged, and resuspended in LB01 buffer. Samples were vortexed before being analyzed at the Iowa State University (Ames, IA) Flow Cytometry Facility using an unmodified BD Biosciences FACSCanto (San Jose, CA) flow cytometer.

RESULTS

Telomere FISH Reveals Bouquet Formation in Hop

Given the pervasive irregularities noted in Zhang et al. (2017) for meiotic chromosome behavior together with SD, we first wanted to ask which, if any, of the cytological hallmarks of normal meiotic prophase are found in hop using molecular cytology. The unusual chromosome interactions and genetic segregation defects previously observed in hop could result from missing or faulty bouquet, given the importance of that structure in efficient pairing and recombination. For comparison, a normal bouquet involves the clustering of telomeres on the nuclear envelope in early meiotic prophase. Specifically, the bouquet stage actually spans from late leptotene, through all of zygotene, and into early pachytene (Bass et al., 1997; Bass, 2003; Scherthan, 2007). Using 3D telomere FISH, we document the presence of a telomere bouquet, as summarized in **Figure 1**. Of the hop nuclei exhibiting a telomere FISH bouquet ($n = 59$ from plants 255C, 243C, 243D, Male 15), 36 nuclei showed tightly clustered signals and 23 nuclei showed less tightly clustered FISH signals at the nuclear periphery. For two representative hop nuclei at early meiotic prophase, the telomere FISH signals are clustered in one area of the nuclear periphery, forming a normal-looking bouquet (**Figures 1B,E**, labeled "BQ") (Bass et al., 1997). The first nucleus (**Figures 1A–C**) shows a common pattern in which the nuclear volume (**Figure 1A**, circle traces at the nucleus-cytoplasm boundary) is larger than that occupied by the chromatin mass. This clumping of chromatin is a zygotene stage-specific, coagulative-fix-dependent artifact, producing the so-called the synizetic knot, as described for *Oenothera* and other plant species (Golczyk et al., 2008). A second nucleus (**Figures 1D–F**) shows that the bouquet is clearly present in a nucleus that appears to be a later stage than the first nucleus, but still in early prophase, as evidenced by the presence of discrete chromosome fibers. These experiments showed that the telomere bouquet does indeed occur in hop male meiocytes, and was observed in both modern cultivars (**Figure 1**) and wild-collected plants (not shown). From these analyses, we find no compelling evidence to implicate a faulty or missing bouquet as causal for segregation distortion in hop. These analyses thereby establish that the bouquet appears normal in both structure and timing.

HSR0 Is an Abundant Subtelomeric 180 bp Satellite DNA Tandem Repeat

In order to further characterize the behavior of hop meiotic chromosomes, we set out develop new FISH probes for cytological tracking of multiple and specific regions of chromosomes. New probes would help solve the problem that hop chromosomes are very similar in centromere location and size but linkage groups remain largely unassigned to chromosomes. We focused on tandem repeats as a class of sequences that make for ideal FISH probes suitable for karyotype development (Albert et al., 2010; Divashuk et al., 2011) They yield bright, discrete signals that can be seen to pair and segregate as reporter loci in meiosis (Bass et al., 2000, 2003).

We used dot plot and kmer analysis of long-read PacBio genomic sequence data to find tandem repeat candidates for new FISH probes. The two most frequent tandem repeat families found were the ∼385 bp tandemly repeated sequence previously defined as the *Humulus*-specific subtelomeric repeat-1, HSR1 (Divashuk et al., 2014), and a new ∼180 bp tandemly-repeated satellite DNA sequence designated HSR0 (*H. lupulus* Subterminal Repeat 0). As shown in **Figure 2**, the HSR0 repeat sequence arrays can span an entire sequence (**Figure 2A**), part of a PacBio sequence (**Figure 2B**), or arranged as blocks of inverted polarity within a single sequence (**Figure 2F**). The HSR0 repeats also showed an intriguing pattern, occasionally appearing adjacent

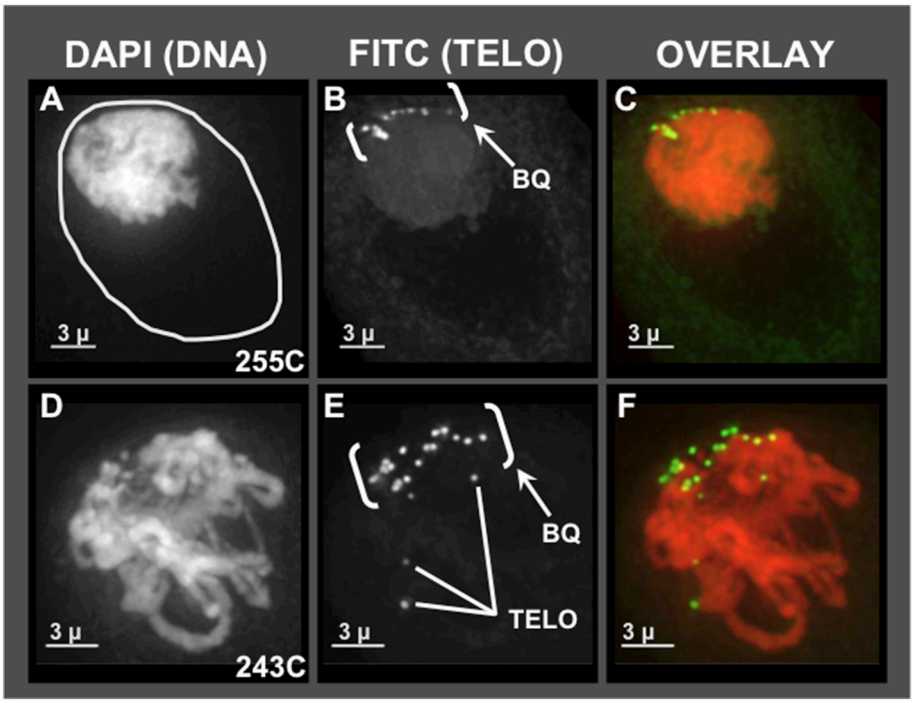

FIGURE 1 | Telomere bouquet in pollen mother cells of hop. Male flower buds were harvested and fixed in Farmer's Fluid, then exchanged into Buffer A and formaldehyde fixed before microdissecting pollen mother cells from anthers for 3D acrylamide FISH. Through-focus projections of nuclei, one nucleus per row, are shown as through-focus maximum-intensity projections in gray-scale for individual wavelengths or in color for overlay images, as labeled across the top. **(A–C)** Hop nucleus from plant 255C at early prophase showing the nuclear periphery (**A**- white circle) and the telomere cluster region (bracketed, BQ). **(D–F)** Hop nucleus from plant 243C at early-middle prophase showing the bouquet (BQ), with three examples of single telomere FISH signals (Tel, **E**) indicated.

to telomere repeat DNA (**Figure 2D**) or even interspersed with telomere repeats (**Figure 2E**). These observations suggest that HSR0 should make a good FISH probe that is predicted to be near telomeres. The HSR0 sequence is different than HSR1, and none of the HSR0 pac-bio clones examined included HSR1 repeats.

Given that HSR0 and telomere repeats occur together in clones, we predicted that HSR0 satellite DNA may be subtelomeric, and if so should stain bouquet and co-localize with HSR1. To test this, we carried out FISH using HSR0 together with either telomere ($n = 21$) or HSR1 ($n = 13$). Most of the HSR0 FISH signals did indeed colocalize with telomere FISH signals (**Figures 3A–H**). Most, but not all, of the HSR0 FISH signals also clearly co-localized with HSR1 FISH signals (**Figures 3I–L**). Despite the tendency for HSR0 and HSR1 to co-localize, we did find a few cases where only one was detected (arrowheads in **Figures 2J,K**). These solo signals from combined FISH probes could be useful for distinguishing otherwise similar chromosomes. Together, the molecular and cytogenetic analyses indicate that the 180 bp satellite repeat family HSR0 comprises a newly characterized and abundant subtelomeric tandem repeat sequence family. The HRS0 oligo FISH probe, ZERO-Y, represents a valuable new reagent for karyotyping and analysis of meiosis.

Meiotic Chromosome Abnormalities Are Evident at Mid-prophase, Meiosis I, and II

Having shown that hop has a normal bouquet (**Figure 1**), we wanted to examine in more detail the middle prophase/pachytene stage, when long thick fibers should appear and telomere distributions typically transition from clustered in early pachytene to dispersed in middle and late pachytene (Bass et al., 1997). We observed evidence of meiotic irregularities in pachytene, as shown in **Figure 4**. Specifically, all of the meiotic nuclei imaged at mid-prophase ($n = 72$ total from 7 different plants) showed conspicuous lack of uniformity of fiber appearance, a pattern resembling that of some meiotic mutants with disruption or loss of synchronous progression (Bass et al., 2003). For instance, in the example shown in **Figure 4A**, plant 243D and wild collected var. *neomexicanus* plant SH2, thick fiber (Tk) cross sections were measured and averaged 670–850 nm whereas thin (Tn) fibers averaged 320–460 nm. The fact that the telomeres are dispersed in this nucleus (**Figure 4A**) indicates that the cell has progressed beyond the bouquet stage which ends in early pachytene, at which point there should be no unpaired or unsynapsed chromosomes in a normal diploid cell. This bimodal fiber thickness is a conspicuous and invariant recurring phenotype in hop that appears to persist through all of pachytene. In addition to this conspicuous non-uniformity in fiber morphology, nuclei at this stage also showed heteropycnotic

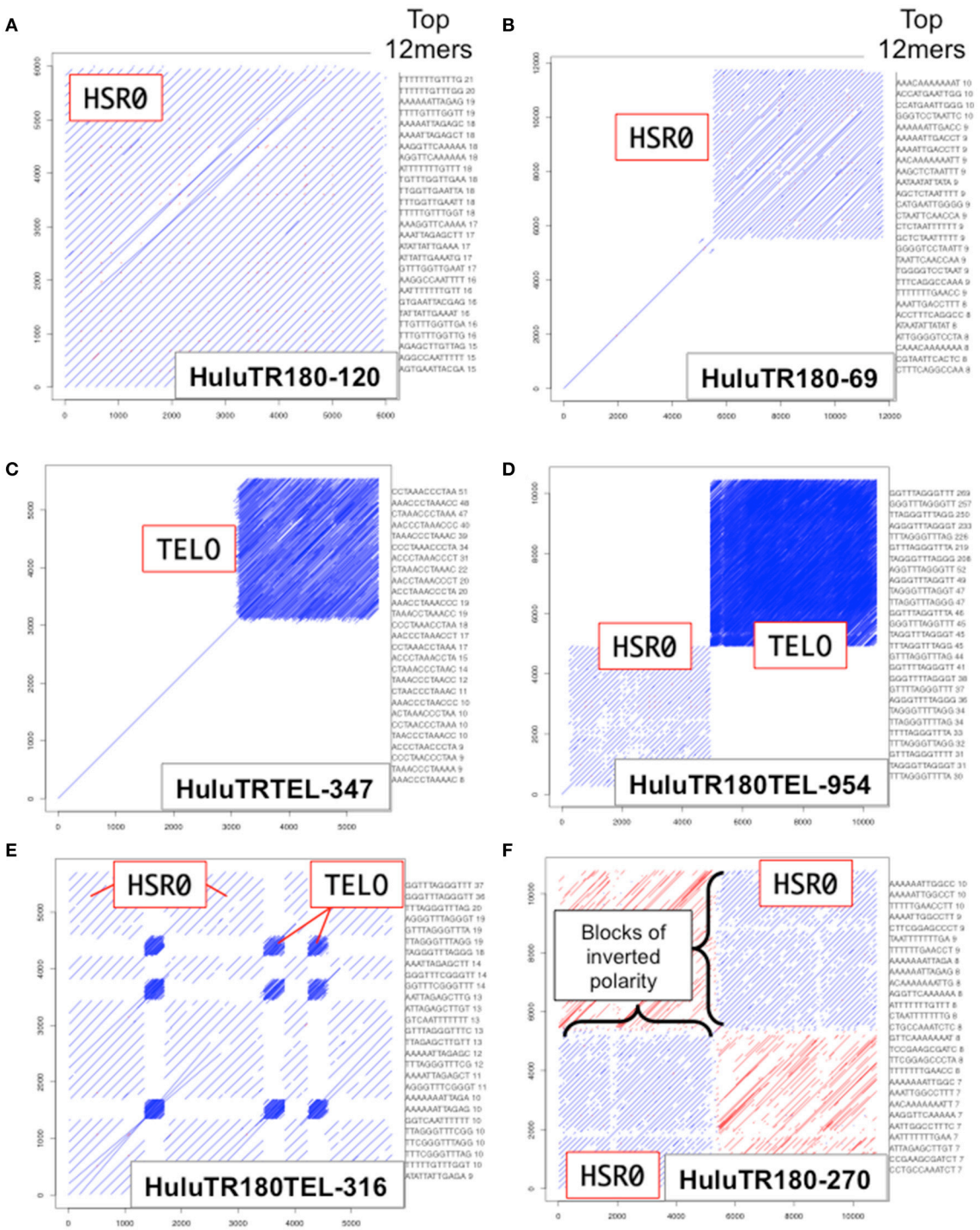

FIGURE 2 | HSR0 dot plot outputs of tandemly repetitive genomic regions. PacBio Single Molecule, Real-Time (SMRT) DNA sequences were screened for tandem repeats (Ohtsubo et al., 2008). For each clone, a self dot-plot is shown along with the top 20 12mers for that clone using kmer analysis. The stripes represent internal tandem repeats of HSR0 (blue stripes) or telomere repeats (tightly packed blue stripe blocks). **(A)** The HuluTR180-120 clone showing HSR0 repeat occupies the entire 6 Kbp clone. **(B)** The HuluTR180-69 clone showing HSR0 repeat occupies around one half of the 6 Kbp clone, whereas the single diagonal represents sequences that are not repeated within the clone. **(C)** The HuluTRTEL-347 clone showing with unique sequences in the first 3 kbp followed by telomere repeat DNA ($(CCCTAAA)_n$) in the last ~3 kbp. **(D)** The HuluTR180TEL-954 clone showing a large block of HSR0 repeats immediately followed by more than 5 Kbp of telomere repeat DNA ($(TTTAGGG)_n$). **(E)** The HuluTR180TEL-316 clone showing interspersed blocks of HSR0 and telomere repeat DNA ($(TTTAGGG)_n$). **(F)** The HuluTR180–270 clone showing a block of HSR0 repeats in one direction (blue) followed by blocks of inverted repeat polarity (red) in another.

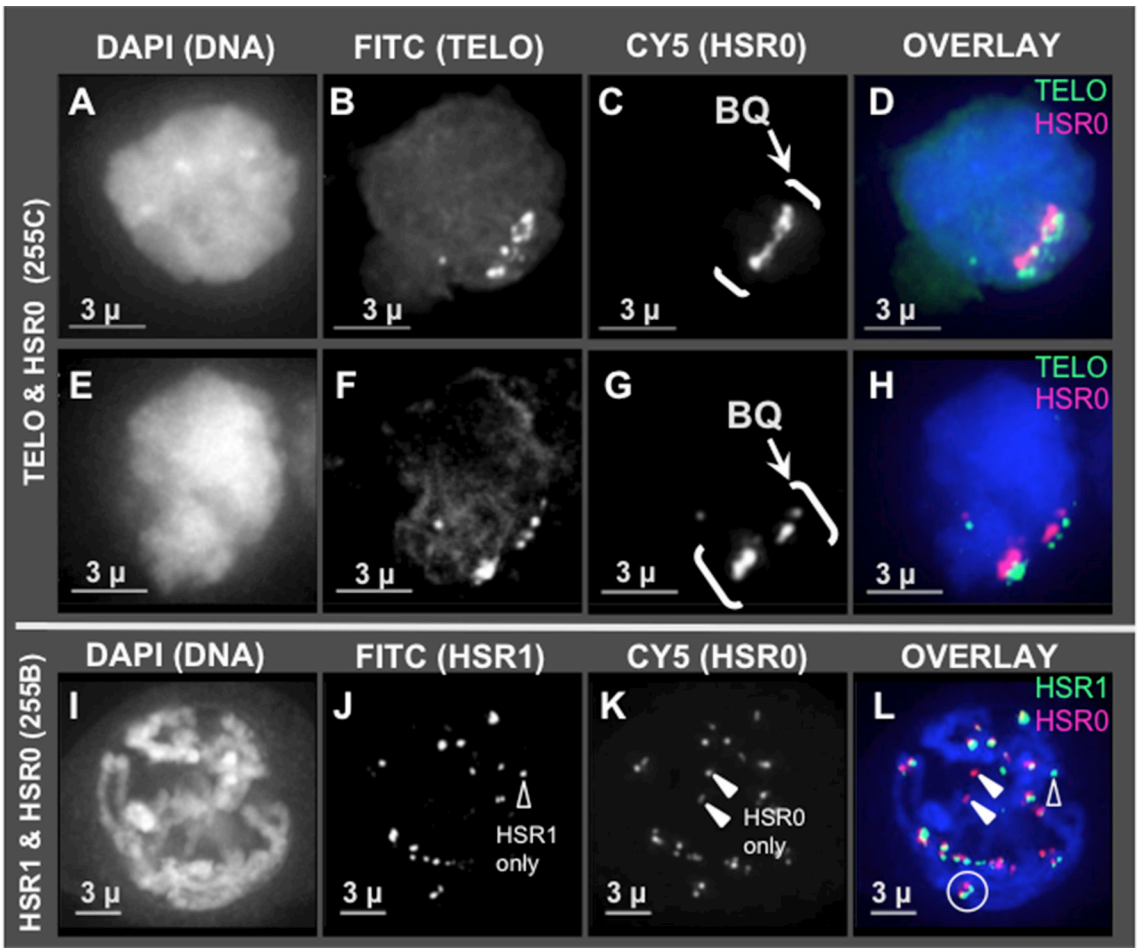

FIGURE 3 | HSR0 co-localization with telomere and HSR1. Projections of 3D FISH datasets were produced as described in **Figure 1** with an additional probe, HSR0. **(A–D,E–H)** Two hop nuclei from plant 255C at early prophase showing telomeres and HSR0 FISH signals clustered in one area on the nuclear periphery, the bouquet (bracketed, BQ). **(I–L)** One hop nucleus from plant 255B at middle-late prophase, homologous chromosomes paired in diplotene showing HSR0 and HSR1 co-localizing at the ends of chromosomes. **(J)** Showing HSR1 signal not co-localized (open arrowhead) and **(K)** showing two HSR0 signals not co-localized (closed arrowheads). **(L)** Circle denotes clear example of co-localization and polarity of the two FISH signals at the ends of chromosomes. Open and closed arrowheads show HSR1 and HSR0 signals, respectively, not co-localized. The length of the scale bars (3 microns) is indicated.

regions (hp, **Figure 4A**), possible entanglements, and presumed synapsis branch points (bp, **Figure 4C**).

Having observed unusual chromosome morphology in mid prophase (**Figure 4**), and non-disomic pairing in late prophase (Zhang et al., 2017), we next examined the stages immediately following meiotic prophase, the divisions of meiosis I and II. Some genera, such as *Oenothera* and *Clarkia,* can have translocation heterozygosity and meiotic chromosome complexes with surprisingly low segregation defects (Golczyk et al., 2014). It was therefore unclear if hop would deviate from the expectation of complete and balanced chromosome separation. To explore this question, we examined the first and second meiotic divisions for anomalies. We found that hop does exhibit anaphase bridges in both meiosis I and II as summarized in **Figure 5**. Bridges implicate dicentric chromosomes, which are indicative of inversions or pairing of rearranged chromosomes, and were observed in both Cascade (cross 243) and Apollo (cross 255) families (BR in **Figures 5A,D,G,J**). These bridges included interstitial FISH signals for telomeres (TELO, plant 243B, **Figures 5B,E**) or HSR0 (HSR0, plant 255B, **Figures 5H,K**). Hop appears to initially deviate from normal meiosis at some point in mid meiotic prophase, after the bouquet stage but prior to diakinesis just after homologous pairing and recombination typically occur (Zhang et al., 2017).

Tetrad Analysis With 5S rDNA FISH Reveals Both Premeiotic Aneuploidy and Unbalanced Segregation

We next set out to characterize the transmission of the 5S rDNA loci, which are discrete, euchromatic genic loci. The 5S rDNA FISH analyses also allowed us to survey segregation distortion in several contexts: within single plants, between progeny from a single cross, between different crosses, and between varieties

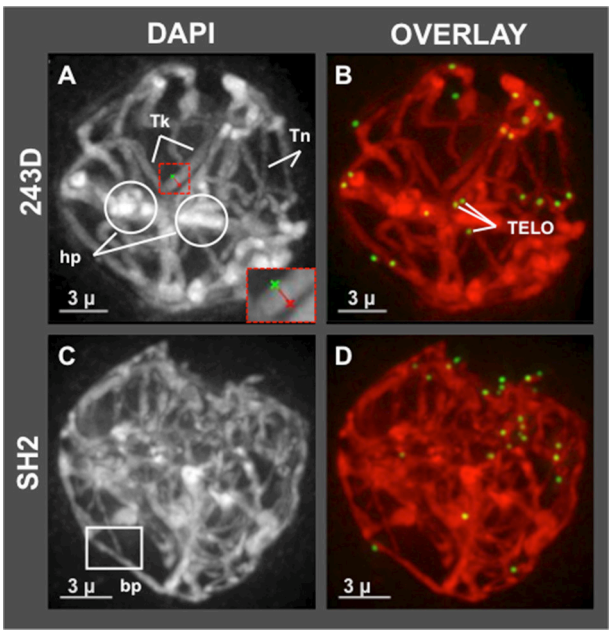

FIGURE 4 | Hop pachytene nuclei with differential chromosome fiber thickness. Hop nuclei at pachytene showing distinct areas of non-uniform chromosome fibers. Fiber widths were measured at four locations per fiber and averaged, distinguishing thick (Tk) from thin (Tn) fibers. **(A,B)** Pachytene (middle prophase, post-bouquet) nucleus from plant 243D also shows heteropycnotic (circled, hp) regions. Red dashed box indicates an example of measurement tool for distance across fibers. **(C,D)** Middle prophase nucleus (early pachytene, post-bouquet) from wild-collected var. *neomexicanus*, plant SH2, shows a structure resembling a synapsis branch point (bp, white box). The length of the scale bars (3 microns) is indicated.

of hop. For these experiments, the tetrad stage was selected because it is ideal for observing transmission genetics in a single generation, as the products of normal meiosis are expected to result in four daughter cells with equal segregation in a ratio of 1:1:1:1 per locus. Previously reported hop karyotyping (Karlov et al., 2003; Divashuk et al., 2011) showed that 5S rDNA loci reside on two chromosomes, one near the centromere of chromosome two and one in the telomeric region of chromosome five. In a somatic diploid nucleus stained by 5S rDNA FISH, signals therefore would appear as four distinct dots. During a normal Mendelian meiosis, signals would assort into the four daughter nuclei equally in a ratio of 2:2:2:2.

We examined seven different plants (n = 10–14 tetrads per plant) at the tetrad stage by 3D 5S rDNA FISH as summarized in **Figure 6**. The 5S rDNA FISH signals were also counted from multiple nuclei (n = 45–95 nuclei/plant) at different stages of meiosis in order to confirm the 5S rDNA constitution of plants and their progeny. We observed highly variable and extreme segregation defects as illustrated by tetrads from male progeny of cross 243 (**Figure 6**, top two rows). From images collected from a single plant (tetrads in **Figures 6A–C**), we found multiple types of non-Mendelian ratios including 1:1:0:0 and 1:1:0. These cells also sometimes included micronuclei or three nuclei, indicative of asynchronous division or whole nuclei non-disjunction (**Figure 6B**). Additional progeny of cross 243 showed even more segregation anomalies, including 5S rDNA tetrad ratios of 2:2:2:3 (**Figure 6D**) and 1:1:2:2 (**Figure 6F**) and chromosome micronuclei and laggards (MN in **Figure 5C**, LG in **Figure 6D**). Nuclei from two progeny of a separate cross, 255 in the Apollo family, confirmed that siblings from a single cross can show unbalanced 5S rDNA in tetrads (**Figures 5H,I**). Despite the frequency of abnormal 5S rDNA segregation patterns, we occasionally observed the normal, expected ratio of 2:2:2:2 in two cases, one from cross 243 (**Figure 6E**) and one from a wild-collected var. *neomexicanus* (**Figure 6G**). These observations show that the 5S rDNA ratios at the tetrad stage can vary between and within plants.

The progeny from Hopsteiner breeding cross 255 is of particular interest because it shows signs of meiotic problems from multiple lines of evidence, including diakinesis multivalent complexes (Zhang et al., 2017), chromosome bridges (**Figures 5A–F**), and unbalanced 5S rDNA loci after meiosis II (**Figures 6H,I**), We were particularly interested in plant 255A because it showed a recurring and obvious pattern of 2:2:3:3 segregation in meiotic daughter cells (**Figure 6I**), which is distinct from both normally expected ratios and from those of its sibling 255B (**Figure 6H**). Previously reported European karyotypes (Karlov et al., 2003; Divashuk et al., 2014) have two unlinked 5S rDNA loci. As summarized in **Figure 7**, we frequently observed three bright and two dim 5S rDNA FISH loci per nucleus during meiotic prophase (**Figure 7A**) in cells (n = 61) from 255A. This 5-locus pattern is also seen at metaphase I (**Figure 7B**), where one of the three bright dots appears to be alone, and unpaired (labeled "L" in **Figure 7B**). After meiotic prophase, the FISH signals for each locus often appear as double dots likely reflecting slight spatial separation of sister chromatid signals. The late anaphase I nucleus (**Figure 7C**) shows a chromosome bridge and an unbalanced distribution of 5S rDNA signals (**Figure 7C**). At telophase I, metaphase II, and anaphase II we find additional evidence for the 5-locus pattern (**Figures 7D–F**).

Regarding the nature of the three bright 5S rDNA loci, which reflect some type of aneuploidy, segmental or chromosomal, we wanted to distinguish between two explanatory scenarios—trisomy with 3 homologous loci or disomy plus a single 5S rDNA locus surrounded by non-homologous segments. If trisomic, the three bright loci should co-localize during pairing, but if disomic plus monosomic then the monosomic locus should show no preferential co-localization with the other bright dots. We measured pairwise distances in 3D space for the five 5S rDNA signals in late meiotic prophase nuclei (**Figure 7G**). The lone bright signal was found to be no closer to the other bright signals than to the dim signals, a pattern consistent with one disomic pair and one monosomic, unlinked locus. The chromosome bearing the lone 5S rDNA signal in nuclei from plant 255A has nonetheless been observed to pair with one or more other chromosomes (**Figure S1**, and spinning projection movie **File S1**), suggesting that the chromosome bearing the "lone" signal may share homology with other chromosomes. Notably, this plant illustrates but one of several types of deviation from the expected 5S rDNA pattern of 2:2:2:2. Other plants have

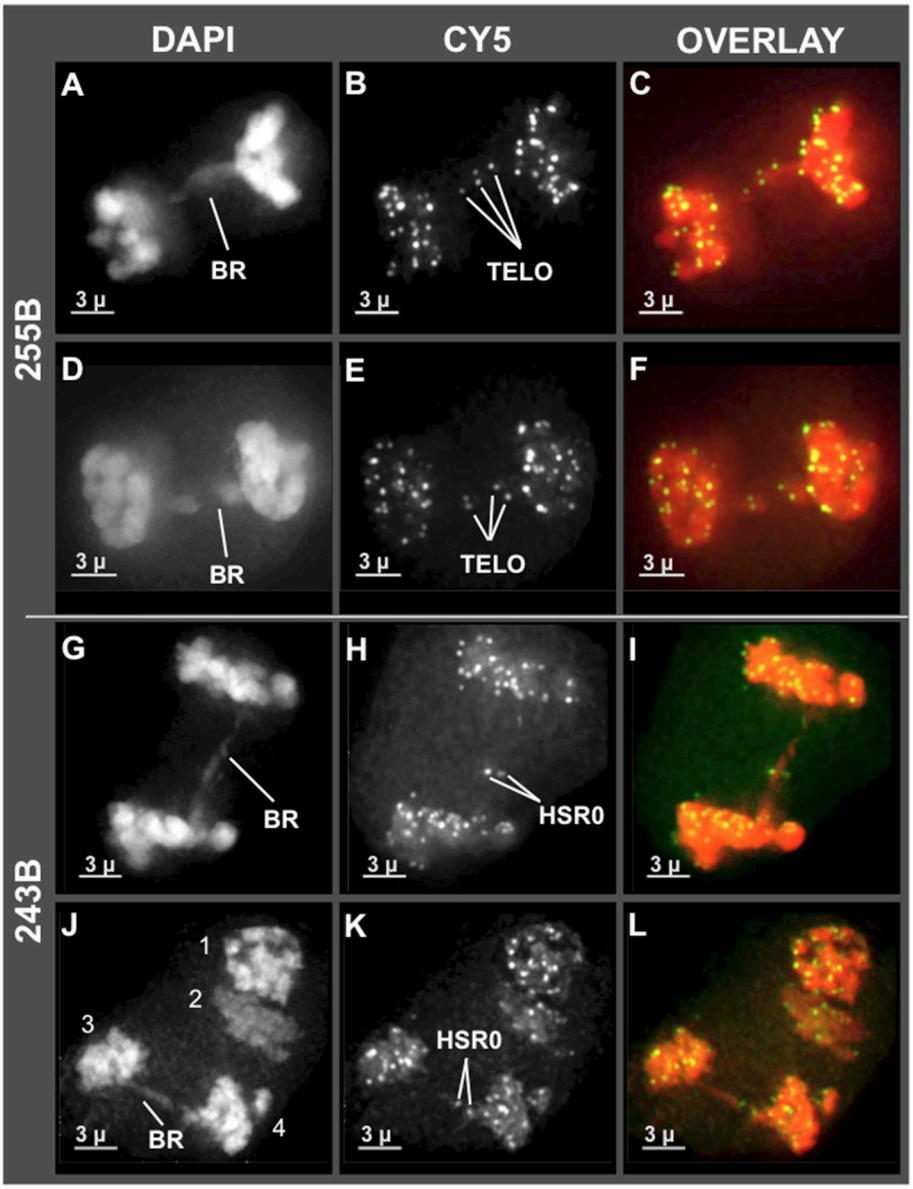

FIGURE 5 | Chromosome bridges with interstitial telomere and HSR0 signals at meiosis I and II. Projections of 3D FISH datasets were produced as described in **Figure 1**. **(A–F)** Through-focus projections showing hop nuclei at anaphase I in plant 255B. The wavelength is indicated at top and the chromosome bridges (BR) and telomere FISH signals are (TELO) are indicated. **(G–L)** Through-focus projections of a hop nuclei at anaphase I **(G–I)** or anaphase II **(J–L)** from plant 243B. The chromosome bridges (BR) and HSR0 FISH signals (HSR0) are indicated. Telomere and HSR0 FISH signals can be observed on the bridges. The length of the scale bars (3 microns) is indicated.

their own characteristic 5S rDNA aneuploidy, as illustrated by the 3 tetrads from plant 243B (**Figures 6A–C**).

Pedigree and FACS Data Show Alternating DNA Content Over Multiple Generations

In order to investigate the nature of segregation distortion of hop in a broader context, we examined the hop family tree in relation to cross 255 as summarized in **Figure 8**. In this pedigree, plant 255A is the proband and it has a DNA content designated 2C, similar to that of a reference diploid, Apollo (**Figure 8**, FACS inset). We noted an unexpected and intriguing DNA content pattern whereby the first two generations (I and II) have plants with 2C genome content but the third (III) has two female progeny of Apollo with 3C genome content (_07270 and Eureka!), followed by a fourth generation (IV) with 2C genome content (255A). Notably, two female progeny of Apollo, with two different male parents, both have 3C genome content. The 3C content of _07270 provides a possible explanation for why some of its progeny appear aneuploid (e.g., **Figure 7**, for 255A).

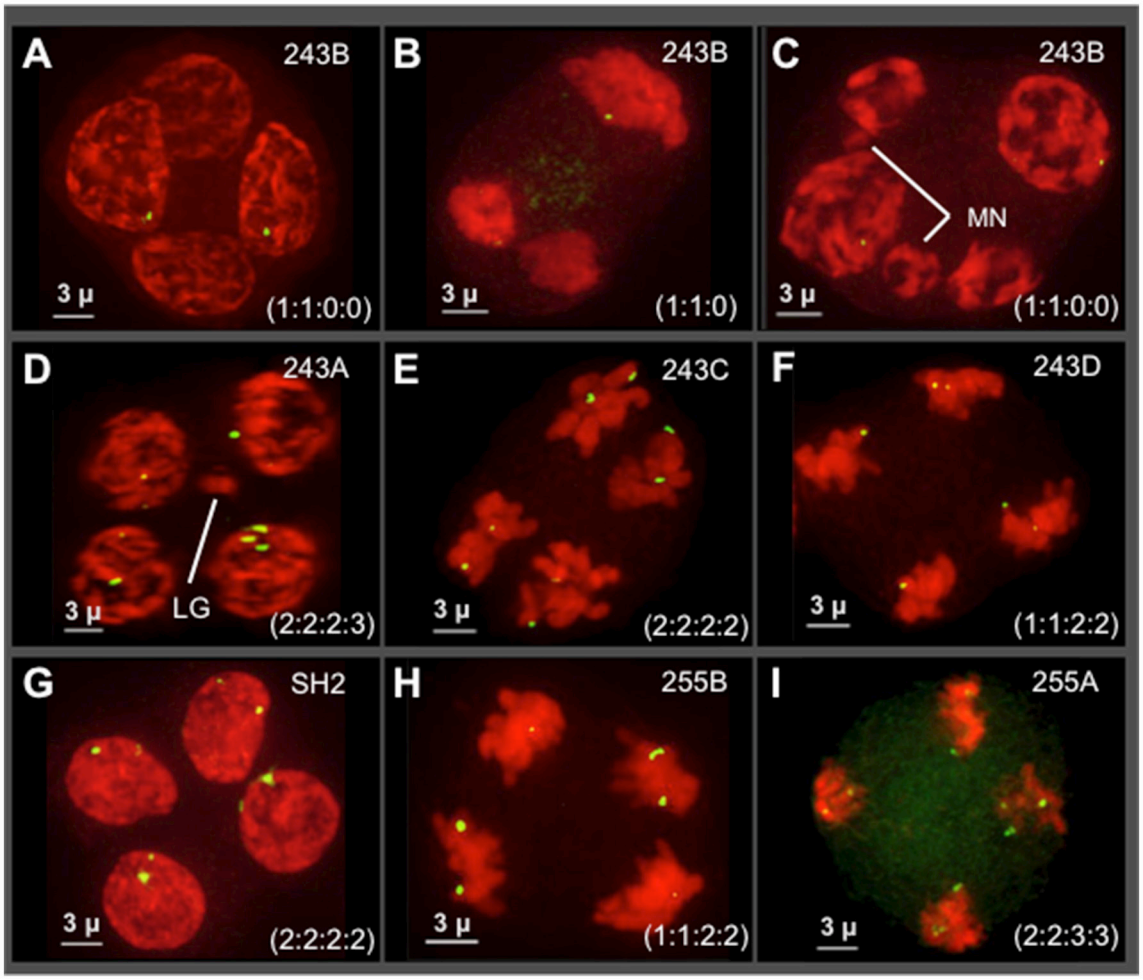

FIGURE 6 | Survey of 5S rDNA FISH in tetrads (meiosis II) of seven different plants. Projections of 3D FISH datasets were produced as described in **Figure 1** but with DAPI shown in red and 5S rDNA FISH, green. Hop tetrads are highly variable. **(A–F)** Four progeny of cross 243, in the Cascade family. **(A–C)** A single progeny of cross 243 from the plant designated 243B. **(D)** Plant 243A. **(E)** Plant 243C. **(F)** Plant 243D. **(G)** Plant SH2, a wild collected var. *neomexicanus* hop. **(H–I)** Two progeny of cross 255 from the Apollo family. **(H)** Plant 255B. **(I)** Plant 255A. The 5S rDNA ratios for each tetrad are listed in each panel. The occurrence of micronuclei (MN) and chromosome laggards (LG) are indicated in some of the panels. The length of the scale bars (3 microns) is indicated.

Histograms for genome content of all other notated plants in the pedigree are shown in **Figure S2**.

DISCUSSION

The hop breeding industry has long grappled with segregation distortion and non-Mendelian inheritance, but the causal mechanisms of these problems remain largely unexplained. Here, we used 3D molecular cytology to ask at what point does hop first appear to deviate from the normal processes of meiosis. We found that early meiotic prophase appears normal, with a diagnostic telomere bouquet signifying proper commencement of the homology search process. The first clear signs of meiotic chromosome irregularities in hops appear in middle prophase, when the effects of aneuploidy should become apparent and readily detectable via 3D imaging. Specifically, we found a mixture of thick and thin pachytene fibers, interpreted as paired and unpaired, respectively, similar to those seen with the meiosis-specific maize mutant *desynaptic1* (Golubovskaya et al., 1997; Bass et al., 2003). We have considered several possible explanations for such non-uniform fiber appearance at mid-prophase, including differential progression of chromatin condensation or axial contraction or, more likely, the persistence of non-synapsed chromosome regions.

Non-disomic pairing in hop has been reported for chromosome complexes that include the XY sex bivalents (Sinotô, 1929) and those involving only autosomes (Zhang et al., 2017). Polyploidy, aneuploidy, paracentric inversions, and translocation heterozygosity can all lead to chromosomes with extra or missing centromeres, resulting in anaphase bridges or chromosome laggards. Although we do not know the extent to which each of these occur in hop, we found that nearly half of the cells examined in this study displayed bridges at anaphase I and II. These bridges should be prone to breakage, which could

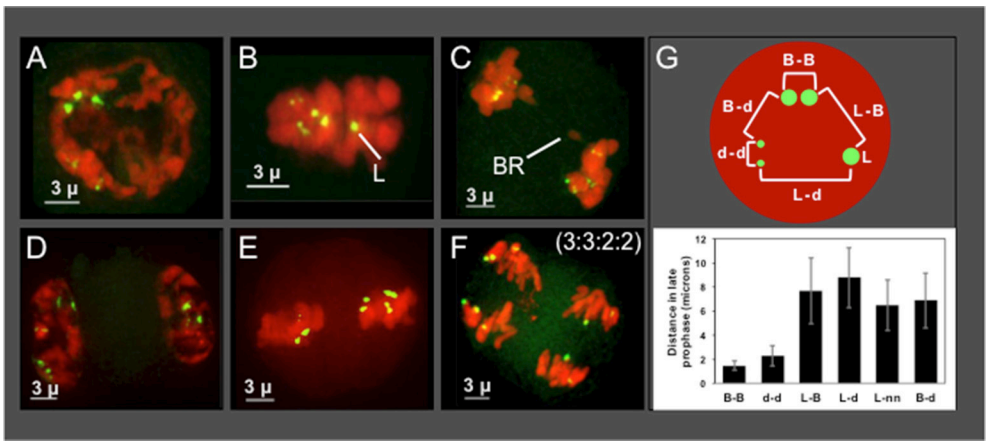

FIGURE 7 | Plant 255A 5S rDNA FISH signal images through meiosis and distance mapping in late prophase. Projections of 3D FISH datasets were produced as described in **Figure 1** but with DAPI shown in red and 5S rDNA FISH, green. **(A)** Early diplotene showing three bright 5S rDNA dots and two smaller and dimmer signals, referred to as the 5-locus pattern. **(B)** Metaphase I showing two dim double dots, representing homologous pairs of sister chromatids, and three bright dots, one of which is alone and designated the lone (L) signal. **(C)** Anaphase I showing a bridge (BR) and 5S rDNA FISH signals as 2 pairs (upper left) and 3 pairs (lower right). 5S rDNA FISH signals at **(D,E)** Telophase I **(D)** metaphase II **(E)**, and anaphase II **(F)** indicating the 5S rDNA FISH signal ratios (3:3:2:2) in the daughter nuclei. **(G)** Top: Schematic of pairwise distance measurements within a nucleus with FISH signals indicated (B, bright; d, dim; L, lone). Each distance mapped is represented by a bracket. Bottom: Graph of distance averages in microns. The length of the scale bars (3 microns) is indicated.

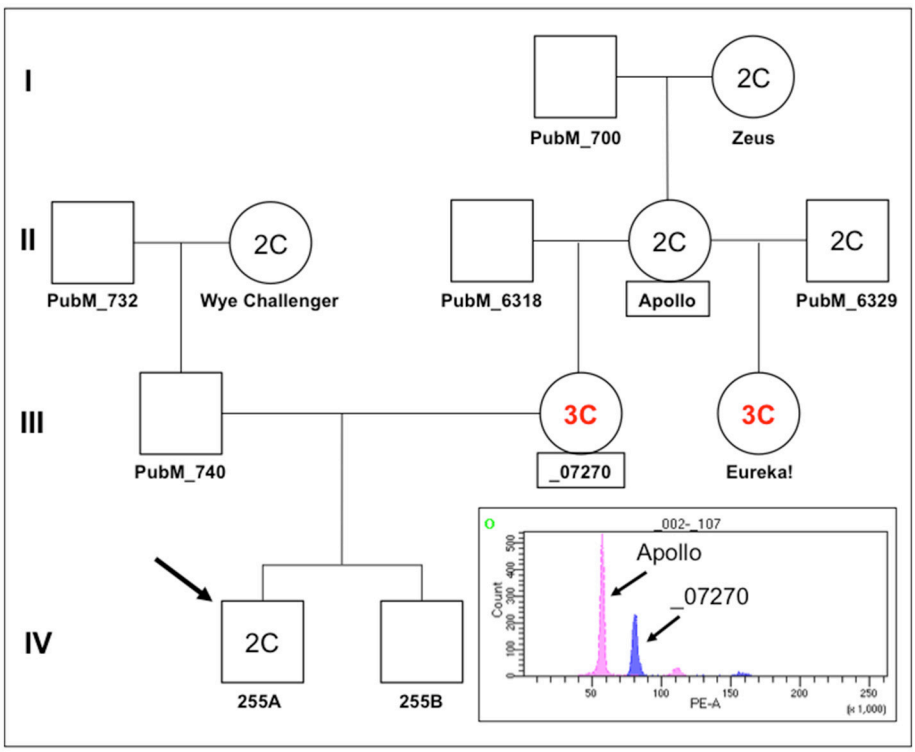

FIGURE 8 | Pedigree of Apollo family and FACS. A partial pedigree of hops relevant to this study was constructed and annotated. Fluorescence-activated cell sorting was carried out for several plants in the Apollo family in relation to plant 255A (IV,1, the proband/arrow). Where determined by FACS, the DNA content is indicated as either 2C or 3C. The histogram showing fluorescence intensity peaks for nuclei from Apollo around 56 PE-A (2C) and for nuclei from _07270 around 80 PE-A (3C). Smaller fluorescence peaks at about double each main peak can also be observed at ∼110 and ∼160, indicative of nuclei that have likely undergone one round of endoreduplication.

lead to the breakage-fusion-bridge (BFB) cycle as described by Barbara McClintock in maize (McClintock, 1939, 1941). She observed that radiation-induced chromosome breakage could initiate a BFB cycle in which broken ends can fuse and recreate more bridge-producing break-inducing dicentric chromosomes. BFB-generated acentric fragments can also become laggards and micronuclei which are not transmitted to progeny, and thus contribute to loss of genetic material and partial aneuploidy. We observed all the hallmarks of the BFB, including bridges, laggards, and micronuclei. Consequently, the BFB cycle can create a cascade of downstream chromosome structural variants, which in turn creates new problems for the next generation (Zheng et al., 1999; Han et al., 2006, 2009; Liu et al., 2015). We propose that the persistence of unpaired regions well into pachytene and the generation of anaphase bridges are the natural consequence of structural heterozygosity or aneuploidy, and through a BFB process could generate even more genomic structural diversity.

To untangle some of the complexities of hop meiosis, we FISH-stained the highly conserved 5S rDNA sequences which conveniently mark discrete, euchromatic genic loci. This study clearly shows that the number of 5S rDNA loci can be different in individual plants, even among siblings with the same parents. This premeiotic 5S rDNA aneuploidy has not been shown before, but is consistent with the emerging picture of structural genomic diversity. From a practical point of view, the 5S rDNA oligo FISH probes provide one efficient method to cytotype somatic seedling tissue in progeny to ascertain the severity of aneuploidy (an odd number of FISH signals) from a given cross.

Among the discoveries reported in this study is the identification and characterization of a new subtelomeric satellite DNA designated here as HSR0. HSR0 has a high %A+T content (63% for clone HuluTR180-120, GenBank MH188533) and is similar to the previously reported sub-terminal tandem repeat family HSR1 (Divashuk et al., 2011). However, unlike HSR1, we found several cases where the HSR0 repeats were in the same PacBio clone as telomere repeat sequences from Apollo DNA. This suggests that HSR0 may be the most distal non-telomeric repeat sequence. The interdigitation of telomere repeats with HSR0 is a curious feature that may implicate HSR0 in telomeric recombination, although multiple dispersed repeat clusters are not normally recombinagenic. Tandem repeats will be useful as a FISH probes for karyotyping different varieties of hop, for facilitating genome assemblies, and for identifying areas of aneuploidy and monitoring homologous pairing and segregation during meiosis.

Polyploidization and variable cytotypes are common in plants (Kolár et al., 2017) and can be advantageous due to gene redundancy and optimization of heterozygosity (Comai, 2005). Hop has been shown to tolerate variable ploidy, including triploidy, which can produce desirable traits such as seedlessness (Haunold, 1970, 1971, 1974; Beatson and Brewer, 1994; Beatson et al., 2003). In a study of crosses between triploid and diploid plants, a series of aneuploid plants with chromosome numbers between 20 and 55 were observed (Haunold, 1970). In a more recent study, triploid plants, which are generally expected to be sterile, were open pollinated with other triploid plants, and FACS analysis of progeny revealed a range of polyploidy ranging from haploid to tetraploid (Beatson et al., 2003). These results were similar to Haunold's, noting that FACS was unable to resolve minor aneuploidies such as monosomy (2n−1) or trisomy (2n+1). Here, we report that plants in the Apollo family can have variable DNA content, which predicts meiotic anomalies. In considering how two parents with 2C DNA content can produce 3C progeny (**Figure 8**, Eureka from Apollo x PubM_6329), we occasionally observed cases where meiosis II whole genome non-disjunction seems to have occurred in a male (e.g., **Figure 6B**). If such a non-reduced nucleus with two sets of chromosomes fertilized a normal haploid egg nucleus, a triploid zygote could result, providing one possible mechanism for a shift in DNA content. It will be interesting to explore whether or not there might be a natural genetic contribution to these DNA content switches.

In this study, we have used 3D imaging to investigate meiotic chromosome behavior at stages that are difficult to study using conventional squash or spread techniques. We found that hop has a canonical bouquet, a structure that occurs in zygotene and early pachytene. In contrast, following the bouquet stage, hop chromosomes begin to show conspicuous and dramatic deviation from the normal progression of chromosome morphology and behavior. From these data we conclude that pairing and synapsis irregularities commence in mid-prophase and later manifest in chromosome bridges, breaks, and non-disomic assortment with varied degrees of complexity. In addition, the occurrence of 3C DNA content plants in the hop lineages may further contribute to genomic instability. Taken together, these findings reveal that there may be multiple and complex mixtures of contributing factors to the segregation distortion of hop, with the possibility that the majority of transmission anomalies are associated with domestication and breeding. However, very few native North American wild accessions have been cytologically analyzed. It will therefore be important to systematically investigate meiosis in multiple truly wild and native North American populations. Developing a more comprehensive understanding of transmission genetics in both wild and cultivated hop species will facilitate and accelerate efforts to meet the growing demands for new hop varieties in all of its associated industries.

AUTHOR CONTRIBUTIONS

KE, HB, RJ, and PM, collected and processed samples for microscopy. NP and DZ collected and analyzed genomic data. KE collected and analyzed 3D image data. KE, HB, LL, and JA characterized and tested tandem repeat FISH probes. RJ and PM obtained FACS data and NP helped develop the pedigree analysis. KE and HB produced the figures, analyzed the cytogenetics and were primary in the design and interpretation of the results.

ACKNOWLEDGMENTS

We thank Taylan Morcol (The Graduate Center, City University of New York, Biology Ph.D. program) for help with wild hop collection, Shawn Rigby for help with FACS, Ruth Didier for

help with FACS plotting, and Daniel Vera for help with the tandem repeat analysis. This work was supported by a Hopsteiner Doctoral Research Fellowship to KE (FSU OMNI Award ID: 0000030675), a Hopsteiner Research Scientist fellowship to DZ and an FSU Planning Grant to HB (FSU OMNI Award ID: 0000032134).

SUPPLEMENTARY MATERIAL

The Supplementary Material for this article can be found online at: https://www.frontiersin.org/articles/10.3389/fpls.2018.01501/full#supplementary-material

Figure S1 | Plant 255A highlighting the lone 5S rDNA-bearing chromosome at diakinesis. Projections of 3D FISH datasets were produced as described in **Figure 1**. Two nuclei from plant 255A at diplotene-diakinesis **(A,D)** show pairs (BB, dd) of 5S rDNA signals (green) and the lone, unpaired signal (L) in a whole-nucleus through-focus projection. Chromosomes (DAPI, red) bearing the lone signals were cropped out of the nucleus and shown from two angles **(B,C,E,F)**. The nucleus in panel D is also shown as spinning projections movie (**File S1**).

Figure S2 | FACS data for DNA content of selected hops. PE-A fluorescence intensity histograms for leaf-tissue nuclei are shown for plants from the pedigree shown in **Figure 8**. Plants called with 2C DNA content (peaks around 58 PE-A, **(A,B,C,E)** or with 3C DNA content (peak around 80 PE-A, **(D)** are shown along with the names of the individual plants.

File S1 | Spinning projection movie of 5S rDNA signals at late prophase from plant 255A. Quicktime movie showing maximum intensity projections of 3D dataset from plant 255A (KAE_CC5a_D3D_CAC_VOL_XY). A single diakinesis nucleus DAPI (red) and 5S rDNA FISH signals (green) are shown. This nucleus is the same as that shown in **Figure S1D**.

REFERENCES

Albert, P. S., Gao, Z., Danilova, T. V., and Birchler, J. A. (2010). Diversity of chromosomal karyotypes in maize and its relatives. *Cytogenet. Genome Res.* 129, 6–16. doi: 10.1159/000314342

Alexandrov, O. S., Divashuk, M. G., Yakovin, N. A., and Karlov, G. I. (2012). Sex chromosome differentiation in *Humulus japonicus* Siebold & Zuccarini, 1846 (Cannabaceae) revealed by fluorescence *in situ* hybridization of subtelomeric repeat. *Comp. Cytogenet.* 6, 239–247. doi: 10.3897/compcytogen.v6i3.3261

Bass, H. W. (2003). Telomere dynamics unique to meiotic prophase: formation and significance of the bouquet. *Cell. Mol. Life Sci.* 60, 2319–2324. doi: 10.1007/s00018-003-3312-4

Bass, H. W., Bordoli, S. J., and Foss, E. M. (2003). The desynaptic (dy) and desynaptic1 (dsy1) mutations in maize (*Zea mays* L.) cause distinct telomere-misplacement phenotypes during meiotic prophase. *J. Exp. Bot.* 54, 39–46. doi: 10.1093/jxb/erg032

Bass, H. W., Marshall, W. F., Sedat, J. W., Agard, D. A., and Cande, W. Z. (1997). Telomeres cluster *de novo* before the initiation of synapsis: a three-dimensional spatial analysis of telomere positions before and during meiotic prophase. *J. Cell Biol.* 137, 5–18. doi: 10.1083/jcb.137.1.5

Bass, H. W., Riera-Lizarazu, O., Ananiev, E. V., Bordoli, S. J., Rines, H. W., Phillips, R. L., et al. (2000). Evidence for the coincident initiation of homolog pairing and synapsis during the telomere-clustering (bouquet) stage of meiotic prophase. *J. Cell Sci.* 113 (Pt 6), 1033–1042.

Beatson, R. A., and Brewer, V. R. (1994). Regional trial evaluation and cultivar selection of triploid hop hybrids. *N. Z. J. Crop Hortic. Sci.* 22, 1–6. doi: 10.1080/01140671.1994.9513799

Beatson, R. A., Ferguson, A. R., Weir, I. E., Graham, L. T., Ansell, K. A., and Ding, H. (2003). Flow cytometric identification of sexually derived polyploids in hop (*Humulus lupulus* L.) and their use in hop breeding. *Euphytica* 134, 189–194. doi: 10.1023/B:EUPH.0000003882.23615.c5

Comai, L. (2005). The advantages and disadvantages of being polyploid. *Nat. Rev. Genet.* 6, 836–846. doi: 10.1038/nrg1711

Divashuk, M. G., Alexandrov, O. S., Kroupin, P. Y., and Karlov, G. I. (2011). Molecular cytogenetic mapping of *Humulus lupulus* sex chromosomes. *Cytogenet. Genome Res.* 134, 213–219. doi: 10.1159/000328831

Divashuk, M. G., Alexandrov, O. S., Razumova, O. V., Kirov, I. V., and Karlov, G. I. (2014). Molecular cytogenetic characterization of the dioecious Cannabis sativa with an XY chromosome sex determination system. *PLoS ONE* 9:e85118. doi: 10.1371/journal.pone.0085118

Golczyk, H., Massouh, A., and Greiner, S. (2014). Translocations of chromosome end-segments and facultative heterochromatin promote meiotic ring formation in evening primroses. *Plant Cell* 26, 1280–1293. doi: 10.1105/tpc.114.122655

Golczyk, H., Musiał, K., Rauwolf, U., Meurer, J., Herrmann, R. G., and Greiner, S. (2008). Meiotic events in Oenothera - a non-standard pattern of chromosome behaviour. *Genome* 51, 952–958. doi: 10.1139/G08-081

Golubovskaya, I. N., Grebennikova, Z. K., Auger, D. L., and Sheridan, W. F. (1997). The maize *desynaptic1* mutation disrupts meiotic chromosome synapsis. *Dev. Genet.* 21, 146–159. doi: 10.1002/(SICI)1520-6408(1997)21:2<146::AID-DVG4>3.0.CO;2-7

Han, F., Gao, Z., and Birchler, J. A. (2009). Reactivation of an inactive centromere reveals epigenetic and structural components for centromere specification in maize. *Plant Cell* 21, 1929–1939. doi: 10.1105/tpc.109.066662

Han, F., Lamb, J. C., and Birchler, J. A. (2006). High frequency of centromere inactivation resulting in stable dicentric chromosomes of maize. *Proc. Natl. Acad. Sci. U.S.A.* 103, 3238–3243. doi: 10.1073/pnas.0509650103

Haunold, A. (1970). Fertility studies and cytological analysis of the progeny of a triploid × diploid cross in hop, *Humulus lupulus* L. *Can. J. Genet. Cytol.* 12, 582–588. doi: 10.1139/g70-077

Haunold, A. (1971). Cytology, sex expression, and growth of a tetraploid × diploid cross in hop (*Humulus lupulus* L.). *Crop Sci.* 11, 868–871. doi: 10.2135/cropsci1971.0011183X001100060031x

Haunold, A. (1974). Meiotic chromosome behavior and pollen fertility of a triploid hop 1. *Crop Sci.* 14, 849–852. doi: 10.2135/cropsci1974.0011183X001400060022x

Haunold, A. (1991). "Cytology and cytogenetics of hops," in *Chromosome Engineering in Plants: Genetics, Breeding, Evolution*, eds P. K. Gupta and T. Tsuchiya (Amsterdam), 551–563.

Howe, E. S., Murphy, S. P., and Bass, H. W. (2013). Three-dimensional acrylamide fluorescence *in situ* hybridization for plant cells. *Methods Mol. Biol.* 990, 53–66. doi: 10.1007/978-1-62703-333-6_6

Jacobsen, P. (1957). The sex chromosomes in *Humulus*. *Hereditas* 43, 357–370. doi: 10.1111/j.1601-5223.1957.tb03444.x

Jakse, J., Stajner, N., Kozjak, P., Cerenak, A., and Javornik, B. (2008). Trinucleotide microsatellite repeat is tightly linked to male sex in hop (*Humulus lupulus* L.). *Mol. Breed.* 21, 139–148. doi: 10.1007/s11032-007-9114-x

Jakse, J., Stajner, N., Luthar, Z., Jeltsch, J.-M., and Javornik, B. (2011). Development of transcript-associated microsatellite markers for diversity and linkage mapping studies in hop (*Humulus lupulus* L.). *Mol. Breed.* 28, 227–239. doi: 10.1007/s11032-010-9476-3

John, B. (1990). *Meiosis*. Cambridge, UK: Cambridge University Press.

Karlov, G. I., Danilova, T. V., Horlemann, C., and Weber, G. (2003). Molecular cytogenetics in hop (*Humulus lupulus* L.) and identification of sex chromosomes by DAPI-banding. *Euphytica* 132, 185–190. doi: 10.1023/A:1024646818324

Kolár, F., Certner, M., Suda, J., Schönswetter, P., and Husband, B. C. (2017). Mixed-ploidy species: progress and opportunities in polyploid research. *Trends Plant Sci.* 22, 1041–1055. doi: 10.1016/j.tplants.2017.09.011

Liu, Y., Su, H., Pang, J., Gao, Z., Wang, X. J., Birchler, J. A., et al. (2015). Sequential *de novo* centromere formation and inactivation on a chromosomal fragment in maize. *Proc. Natl. Acad. Sci. U.S.A.* 112, E1263–E1271. doi: 10.1073/pnas.1418248112

McAdam, E. L., Freeman, J. S., Whittock, S. P., Buck, E. J., Jakse, J., Cerenak, A., et al. (2013). Quantitative trait loci in hop (*Humulus lupulus* L.) reveal complex

genetic architecture underlying variation in sex, yield and cone chemistry. *BMC Genomics* 14:360. doi: 10.1186/1471-2164-14-360

McAdam, E. L., Vaillancourt, R. E., Koutoulis, A., and Whittock, S. P. (2014). Quantitative genetic parameters for yield, plant growth and cone chemical traits in hop (*Humulus lupulus* L.). *BMC Genet.* 15:22. doi: 10.1186/1471-2156-15-22

McClintock, B. (1939). The behavior in successive nuclear divisions of a chromosome broken at meiosis. *Proc. Natl. Acad. Sci. U.S.A.* 25, 405–416. doi: 10.1073/pnas.25.8.405

McClintock, B. (1941). The stability of broken ends of chromosomes in zea mays. *Genetics* 26, 234–282.

Murphy, S. P., and Bass, H. W. (2012). "Genetics and cytology of meiotic chromosome behavior in plants," in *Plant Cytogenetics: Genome Structure and Chromosome Function*, eds H. W. Bass, and J. A. Birchler (New York, NY: Springer New York), 193–229.

Neve, R. A. (1958). Sex chromosomes in the hop *Humulus lupulus*. *Nature* 181, 1084–1085. doi: 10.1038/1811084b0

Neve, R. A. (ed.). (1991). *Hops*. London, UK: Chapman and Hall.

Ohtsubo, Y., Ikeda-Ohtsubo, W., Nagata, Y., and Tsuda, M. (2008). GenomeMatcher: a graphical user interface for DNA sequence comparison. *BMC Bioinformatics* 9:376. doi: 10.1186/1471-2105-9-376

Pellicer, J., and Leitch, I. J. (2014). The application of flow cytometry for estimating genome size and ploidy level in plants. *Methods Mol. Biol.* 1115, 279–307. doi: 10.1007/978-1-62703-767-9_14

Reeves, P. A., and Richards, C. M. (2011). Species delimitation under the general lineage concept: an empirical example using wild North American hops (Cannabaceae: *Humulus lupulus*). *Syst. Biol.* 60, 45–59. doi: 10.1093/sysbio/syq056

Roborgh, R. H. J. (1969). The production of seedless varieties of hop (*Humulus lupulus*) with colchicine. *N. Z. J. Agri. Res.* 12, 256–259. doi: 10.1080/00288233.1969.10427094

Scherthan, H. (2007). Telomere attachment and clustering during meiosis. *Cell. Mol. Life Sci.* 64, 117–124. doi: 10.1007/s00018-006-6463-2

Seefelder, S., Ehrmaier, H., Schweizer, G., and Seigner, E. (2000). Male and female genetic linkage map of hops, *Humulus lupulus*. *Plant Breed.* 119, 249–255. doi: 10.1046/j.1439-0523.2000.00469.x

Shephard, H. L., Parker, J. S., and Darby, P. (2000). Sexual development and sex chromosomes in hop. *New Phytol.* 148, 397–411. doi: 10.1046/j.1469-8137.2000.00771.x/full

Sinotô, Y. (1929). On the tetrapartite chromosome in *Humulus lupulus*. *Proc. Imp. Acad.* 5, 46–47. doi: 10.2183/pjab1912.5.46

Small, E. (1980). The relationships of hop cultivars and wild variants of *Humulus lupulus*. *Can. J. Bot.* 58, 676–686. doi: 10.1139/b80-086

Stebbins, G. L. (1935). Chromosome structure and the mechanism of meiosis in plants. *Am. Nat.* 69:81.

Szymanski, M., Barciszewska, M. Z., Erdmann, V. A., and Barciszewski, J. (2002). 5S Ribosomal RNA database. *Nucleic Acids Res.* 30, 176–178. doi: 10.1093/nar/30.1.176

Winge, Ö. (1929). On the nature of the sex chromosomes in *Humulus*. *Hereditas* 12, 53–63. doi: 10.1111/j.1601-5223.1929.tb02497.x

Zhang, D., Easterling, K. A., Pitra, N. J., Coles, M. C., Buckler, E. S., Bass, H. W., et al. (2017). Non-mendelian single-nucleotide polymorphism inheritance and atypical meiotic configurations are prevalent in hop. *Plant Genome* 10:14. doi: 10.3835/plantgenome2017.04.0032

Zheng, Y. Z., Roseman, R. R., and Carlson, W. R. (1999). Time course study of the chromosome-type breakage-fusion-bridge cycle in maize. *Genetics* 153, 1435–1444.

Conflict of Interest Statement: The authors declare that the research was conducted in the absence of any commercial or financial relationships that could be construed as a potential conflict of interest.

frontiers in Plant Science

ORIGINAL RESEARCH
published: 13 June 2018
doi: 10.3389/fpls.2018.00785

Meiotic Studies on Combinations of Chromosomes With Different Sized Centromeres in Maize

*Fangpu Han[1,2†], Jonathan C. Lamb[1†], Morgan E. McCaw[1], Zhi Gao[1], Bing Zhang[2], Nathan C. Swyers[1] and James A. Birchler[1]**

[1] Division of Biological Sciences, University of Missouri, Columbia, MO, United States, [2] State Key Laboratory of Plant Cell and Chromosome Engineering, Institute of Genetics and Developmental Biology, Chinese Academy of Sciences, Beijing, China

Multiple centromere misdivision derivatives of a translocation between the supernumerary B chromosome and the short arm of chromosome 9 (TB-9Sb) permit investigation of how centromeres of different sizes behave in meiosis in opposition or in competition with each other. In the first analysis, heterozygotes were produced between the normal TB-9Sb and derivatives of it that resulted from centromere misdivision that reduced the amounts of centromeric DNA. These heterozygotes could test whether these drastic differences would result in meiotic drive of the larger chromosome in female meiosis. Cytological determinations of the segregation of large and small centromeres among thousands of progeny of four combinations were made. The recovery of the larger centromere was at a few percent higher frequency in two of four combinations. However, examination of phosphorylated histone H2A-Thr133, a characteristic of active centromeres, showed a lack of correlation with the size of the centromeric DNA, suggesting an expansion of the basal protein features of the kinetochore in two of the three cases despite the reduction in the size of the underlying DNA. In the second analysis, plants containing different sizes of the B chromosome centromere were crossed to plants with TB-9Sb with a foldback duplication of 9S (TB-9Sb-Dp9). In the progeny, plants containing large and small versions of the B chromosome centromere were selected by FISH. A meiotic "tug of war" occurred in hybrid combinations by recombination between the normal 9S and the foldback duplication in those cases in which pairing occurred. Such pairing and recombination produce anaphase I bridges but in some cases the large and small centromeres progressed to the same pole. In one combination, new dicentric chromosomes were found in the progeny. Collectively, the results indicate that the size of the underlying DNA of a centromere does not dramatically affect its segregation properties or its ability to progress to the poles in meiosis potentially because the biochemical features of centromeres adjust to the cellular conditions.

Keywords: centromere misdivision, centromere competition, sister chromatids, recombination, B chromosome, meiotic drive

OPEN ACCESS

Edited by:
Changbin Chen,
University of Minnesota Twin Cities, United States

Reviewed by:
Yingxiang Wang,
Fudan University, China
Lorinda Anderson,
Colorado State University, United States

***Correspondence:**
James A. Birchler
BirchlerJ@missouri.edu

† Co-first authors

Specialty section:
This article was submitted to Plant Cell Biology, a section of the journal Frontiers in Plant Science

Received: *09 March 2018*
Accepted: *23 May 2018*
Published: *13 June 2018*

Citation:
Han F, Lamb JC, McCaw ME, Gao Z, Zhang B, Swyers NC and Birchler JA (2018) Meiotic Studies on Combinations of Chromosomes With Different Sized Centromeres in Maize. Front. Plant Sci. 9:785. doi: 10.3389/fpls.2018.00785

INTRODUCTION

The centromere is the part of the chromosome that organizes the kinetochore for movement functions. In any one species, there is typically characteristic DNA repeats at the primary constriction but it is not clear to what extent this DNA functions in determining the position of the kinetochore. For example, in maize, there are two typical repetitive DNA elements at centromeres, namely the 156 base pair unit satellite, CentC, and an active retrotransposon, Centromere Retrotransposon Maize, CRM (Ananiev et al., 1998; Zhong et al., 2002; Nagaki et al., 2003; Schneider et al., 2016). Nevertheless, inactive centromeres have been described in maize that still contain these sequences (Han et al., 2006; Gao et al., 2011) and in addition the occurrence of *de novo* centromere formation over unique sequences on maize chromosomal fragments has been shown to occur in several examples (Topp et al., 2009; Fu et al., 2013; Zhang et al., 2013; Liu et al., 2015). Thus, the DNA does not appear to be necessary or sufficient to establish the site of the kinetochore. The consistent biochemical feature of active centromeres in maize is the presence of a Histone 3 variant called CENH3 (Zhong et al., 2002) and other associated proteins. They are missing in the inactive centromeres and present at the *de novo* sites (Han et al., 2006; Gao et al., 2011; Fu et al., 2013; Liu et al., 2015).

The centromere sequences evolve quickly and are exchanged across the genome rapidly in evolutionary time. In contrast, the biochemical machinery of the kinetochore is highly conserved. This difference has been referred to as the centromere paradox (Henikoff et al., 2001). One possible scenario to explain this paradox is that the histone associated with the centromeric DNA, CENH3, is in an evolutionary conflict with the associated DNA. Expansion or contraction of the DNA cluster might cause a greater recovery of the larger DNA array through female meiosis via its progression to the basal megaspore, which is the only product of meiosis in the female gametophyte that is passed to the next generation. Since this hypothesis was formulated, there has been accumulating evidence for an epigenetic aspect to centromere specification as evidenced by numerous cases of inactive centromeres as well as *de novo* centromere formation over unique DNA, as noted above. Such events have been documented in various inbred lines of maize with the homogenization of centromeres being accomplished by preferential insertion of the common elements into centromeric chromatin (Schneider et al., 2016). Nevertheless, the availability of a collection of chromosomes that are all derived from a common progenitor but having drastically reduced amounts of centromeric DNA would allow a test of whether centromere size affects the frequency of segregation between the two sizes of centromeres.

In previous studies in our laboratory, a collection of reduced sized centromeres was produced via misdivision of a particular centromere (Kaszas and Birchler, 1996, 1998). Centromere misdivision results when there is attachment of a single kinetochore to both poles that sever the chromosome at the primary constriction but for which both products are capable of function (Carlson, 1970; Carlson and Chou, 1981). The particular centromere involved is that of the supernumerary B chromosome that is present in a translocation between a B chromosome and the short arm of chromosome 9 (TB-9Sb). This chromosome arm has been used extensively in maize genetics because it contains several useful phenotypic markers. The B chromosome is a non-vital one that survives in maize lines by an accumulation mechanism consisting of non-disjunction at the second pollen mitosis (Roman, 1947) with the sperm containing the two B chromosomes preferentially fertilizing the egg in the process of double fertilization (Roman, 1948). The centromere of TB-9Sb was shown to undergo misdivision by Carlson (1970). Subsequently a large collection of misdivision derivatives was recovered and studies of their molecular features demonstrated a progressive reduction in underlying DNA sequences (Kaszas and Birchler, 1996, 1998) that were fractured at the centromeric core (Jin et al., 2005). The B chromosome centromere has an advantage for centromere studies because it contains a specific repeat sequence in and around its centromere (Alfenito and Birchler, 1993; Jin et al., 2005). This collection of different sized centromeres on the same chromosome placed in heterozygotes with the progenitor chromosome with a normal sized centromere was examined in the present study for any evidence of differential segregation or meiotic drive of the divergently sized centromeres.

In addition to segregation properties of large and small centromeres, the collection allowed a determination of segregation strength against the progenitor centromere by using a modified form of TB-9Sb that contains a reverse duplication. Barbara McClintock generated a chromosome that has a duplication of most of 9S but in reverse order (McClintock, 1939, 1941). She used this chromosome to study the breakage-fusion-bridge (B-F-B) cycle because recombination within its limits would generate a dicentric chromosome that would break and initiate the cycle. This duplication was recombined onto TB-9Sb by Zheng and colleagues (Zheng et al., 1999) to produce TB-9Sb-Dp9 to study the chromosome type of B-F-B cycle. By producing heterozygotes of this chromosome with selected misdivision derivatives with reduced sized centromeres, recombination can occur between the derivative and the reversely oriented portion of TB-9Sb-Dp9 to form a dicentric with large and small centromeres. A previous study with one such derivative found dicentric chromosomes in the progeny in which the large centromere was active but the small centromere was inactive (Han et al., 2009). Here we report the results with other misdivision derivatives with regard to the ability to recombine and to the strength of the segregation of the opposed large and small centromeres.

The collection of centromere misdivision derivatives of the same chromosome together with its normal progenitor provide a unique opportunity to examine whether changing the amount of centromeric DNA has an impact on the segregation property or on the strength of its segregation. Interestingly, an examination of a biochemical feature of active centromeres, phosphorylation of histone H2A, revealed that the size of its signal was not always correlated with the relative amount of underlying DNA suggesting an adjustment of the functional size of the centromere similarly to what occurs when maize chromosomes are placed into oat (Wang et al., 2014). The results reveal that the amount of underlying DNA is not a reflection of the size of the biochemical

foundation of kinetochores and there is little discernible effect of the size of the DNA array on segregation fidelity or strength.

MATERIALS AND METHODS

Plant Materials

Homozygous stocks were produced of TB-9Sb and its misdivision derivatives Telocentric 3-5(+), Telo 2-2, Telo 4-5 and Telo 4-11 (**Table 1**) and confirmed cytologically. Crosses were performed to produce heterozygous combinations of the normal TB-9Sb and each of the misdivision chromosomes. Heterozygotes containing two copies of the 9-B chromosome and the normal and derivative B-9 chromosomes were grown to maturity for crosses made with pollen from a *c1 sh1 wx1* tester, which possesses three recessive mutations in 9S. In the progeny of such crosses, classifications of the segregation frequency were determined by FISH with the B chromosome specific sequence to identify the presence of the large or small centromere chromosome.

The chromosome, TB-9Sb-Dp9, was produced by Zheng et al. (1999) by recombining onto TB-9Sb a reverse duplication involving the short arm of chromosome 9 (McClintock, 1939, 1941). Telocentrics 2-2, 3-5(+), 4-4, 4-5, 4-11, and 6-9 (**Table 1**) have been described (Kaszas and Birchler, 1998). Seedlings of TB-9Sb-Dp9 heterozygous with telocentric chromosomes were identified by FISH of root tip cells. Male inflorescences in meiosis were collected from the heterozygotes and were fixed in ethanol: acetic-acid (3:1, v/v) on ice for 2 h, and transferred to 70% ethanol and stored at −20°C.

DNA Probe Preparation

For classification of chromosomes in meiosis, the B-specific sequence (Alfenito and Birchler, 1993) was labeled with Texas-red-5-dUTP and knob heterochromatin sequence (Peacock et al., 1981) with fluorescein-12-dUTP, as described (Kato et al., 2004). In some cases, a labeled oligonucleotide probe of the telomere sequence was used to detect the B centromere due to cross hybridization with the B specific sequence (Alfenito and Birchler, 1993).

TABLE 1 | Comparative size estimates of misdivision derivatives and the progenitor, TB-9Sb.

Chromosome	Estimated size of the B specific array (kb)
TB-9Sb	9000
Telo 4-11	2360
Telo 4-5	2180
Telo 2-2	2150
Telo 3-5(+)	1665
Telo 6-9	1160
Telo 4-4	490

Sizes are based on restriction digests separated on CHEF gels and probed with the B chromosome specific centromeric repeat, which is present in and around the B chromosome centromere (Jin et al., 2005). Size estimates are derived from Kaszas and Birchler (1996, 1998).

Immunolocalization of H2AphThr133

Antibodies to H2AphThr133 were produced against peptides with a single phosphorylated Thr at position 133 (LPKK(pT)AEKA) of H2A as described (Su et al., 2017). Immunolocalization was performed as described (Han et al., 2009). Briefly, the samples were fixed in 4% paraformaldehyde for 2 h on ice. Then, the samples were treated with 1% Triton X-100 (1X PBS and 1 mM EDTA). The primary antibody was incubated overnight at 4 degrees followed by secondary antibody incubation at 37 degrees and DAPI staining. The primary and secondary antibodies were diluted in 3% BSA. For the immuno-FISH procedure, FISH was performed after immunolabeling. The concentrations of anti-H2Aph, anti-rabbit IgG and DAPI were 0.93 mg/ml, 0.015 mg/ml and 0.5 μg/ml, respectively.

Meiotic Analysis

Meiotic images at various stages were collected from heterozygotes as described (Gao et al., 1999; Han et al., 2009).

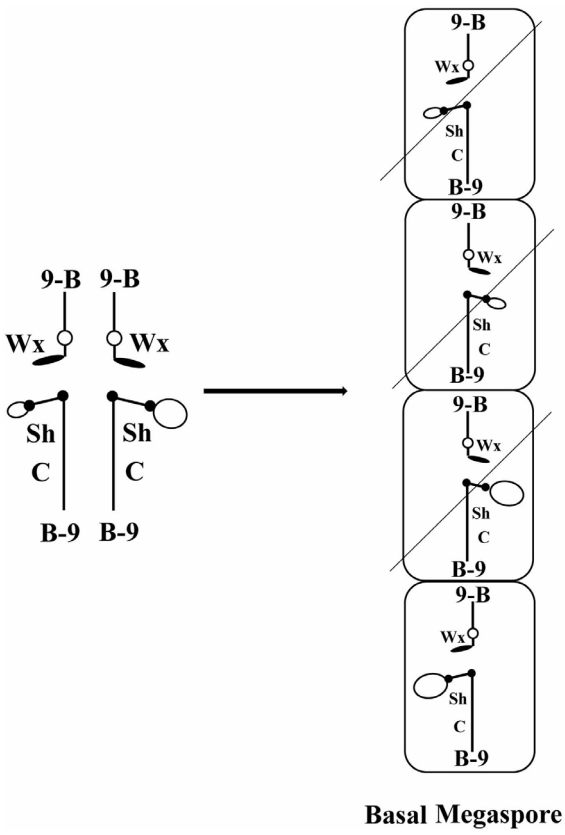

FIGURE 1 | Diagram of how meiotic drive would operate in a heterozygote of two centromeres. At the left is diagrammed the configuration of a heterozygote of TB-9Sb/misdivision derivatives of the same. Large and small open ovals represent the normal and misdivision centromere, respectively. At the right is diagrammed the megaspores resulting from meiosis. Only the basal megaspore proceeds to form the female gametophyte, which produces the egg. If larger centromeres were directed to the basal megaspore, they would be present in the progeny at a frequency greater than Mendelian predictions.

RESULTS

A Test of Meiotic Drive Between Large and Small Centromeres

The rationale to examine the issue of meiotic drive of different sized centromeres was to produce heterozygotes of TB-9Sb for which one copy is a misdivision derivative with a reduced size centromere and the other is the normal B chromosome centromere. The heterozygotes were then crossed as a female by a tester and the progeny were screened for the presence of the large and small centromeres, which are readily cytologically distinguishable. A skewed segregation ratio in the progeny would be indicative of meiotic drive.

Toward this end, selected misdivision derivatives of TB-9Sb were self-pollinated in a pedigree until they were homozygous for the 9-B and B-9Sb chromosomes (with the understanding that the copy number of the B-9S chromosome can be variable in this stock because it undergoes non-disjunction at the second pollen mitosis). Then, four derivatives (Telo 3-5(+), Telo 2-2, Telo 4-5 and Telo 4-11) were crossed to homozygous TB-9Sb. Plants were selected that were homozygous for the 9-B chromosome, which is identical in all stocks, but heterozygous for the B-9Sb chromosomes (**Figure 1**). These plants were crossed as female by a tester stock for 9S, *c1 sh1 wx1*. The progeny of these crosses were germinated and individuals were examined in root tip cells for the presence of the large centromere (progenitor B-9Sb) or the small centromere (misdivision derivative of B-9Sb) based on the visible distinction of the FISH signal for the B chromosome centromere specific repeat, ZmBs (**Figure 2**). When both the large and small centromeres were found in a single individual in the progeny, these cases were recorded as female non-disjunction. The results are presented in **Table 2**.

All of the four comparisons showed a higher numerical recovery of the larger centromere. Two of the four comparisons were significantly different in Chi Square tests (**Table 2**). Interestingly, the two that are significantly different also have the highest rates of non-disjunction in which both centromeres were recovered in a single individual. If the difference in segregation of the chromosomes with normal and reduced sized centromeres and the frequency of non-disjunction are related phenomena, it is worthy of note that the numbers for non-disjunction generally could account for the disparity of the large and small frequencies if they are added to the small class. Of course, the difference of segregation and the rate of non-disjunction are possibly unrelated.

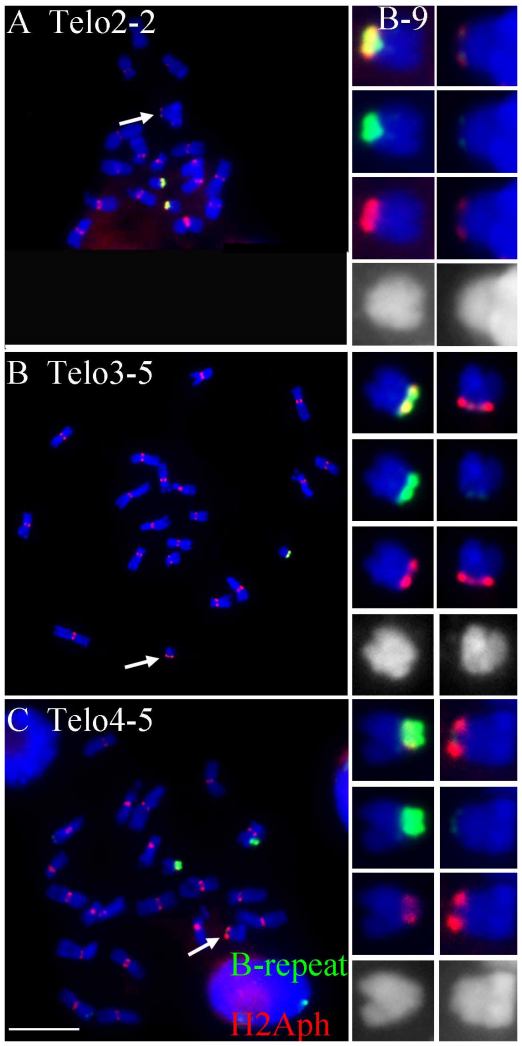

FIGURE 2 | Comparisons of B specific repeat and H2Aph signals in heterozygotes of Telo 2-2 **(A)**, Telo 3-5 **(B)** and Telo 4-5 **(C)** with TB-9Sb, the progenitor chromosome. The B specific repeat is labeled in green and the label for H2Aph is red. In **A–C**, one misdivision chromosome is present, respectively (designated by arrows); **(A,C)** have two copies of the TB-9Sb, which contains the normal B centromere (green). Insets compare TB-9Sb normal (B-9) with the respective misdivision derivative. In the insets, the TB-9Sb chromosome is on the left and the respective misdivision chromosome is on the right; shown in descending order for each combination are composite, B specific (green), H2Aph (red) and gray scale for DAPI. Bar = 10 μm.

Estimation of the Size of the Biochemical Feature H2ApThr133 of Selected Misdivision Derivatives

To test whether the differences in transmission of the large and small centromeres correlated with the biochemical features of

TABLE 2 | Determination of segregation ratio of large and small centromeres.

Derivative/TB-9Sb	Large	Small	NDJ	X^2	*p*
Telo 3-5(+)	3054	2822	65	9.14	< 0.005
Telo 2-2	718	680	10	1.03	< 0.50
Telo 4-5	249	207	31	3.87	< 0.05
Telo 4-11	68	62	12	0.28	< 0.9

The respective misdivision derivative paired with TB-9Sb are shown in the first column. The normal B centromere in TB-9Sb is designated "Large" and the misdivision centromere as "Small". The number of seedlings in the segregating progeny of each type is shown. The number of seedlings in which both centromeres were recovered indicate non-disjunction (NDJ). Chi square and p-values are given for the null hypothesis of equal segregation.

active centromeres, immunolocalization of a marker of active centromeres was performed on the three heterozygotes for which the greatest progeny sizes were assayed, Telo 3-5(+), Telo 2-2 and Telo 4-5. The phosphorylated form at Thr133 of Histone H2A has been shown to be a mark of active centromeres (Su et al., 2017). Heterozygotes were probed for H2Aph and with the B centromere specific repeat. **Figure 2** shows the results. In all three misdivision derivatives the amount of B specific repeat is barely detectable confirming the presence of the derivative. Telo 2-2 has a reduced H2Aph signal compared to TB-9Sb in the spreads illustrating that there is a correspondence between the amounts of centromeric DNA and biochemical features in this case. However, Telo 3-5(+) has an H2Aph signal that is comparable in size to TB-9Sb. Lastly, the H2Aph signal size for Telo 4-5 actually exceeds that of TB-9Sb. It is possible that the biochemical foundation of the kinetochore in these latter two cases expands similarly to how maize centromeres behave when introduced into oat (Wang et al., 2014). In the respective species, oat kinetochores are larger than maize, but when a maize chromosome is introduced into oat, the domain size expands (Wang et al., 2014). In the present study, there is a range of H2Aph quantities associated with the various active centromeres despite the small amount of centromeric DNA present in the three derivatives, which might indicate that in some cases the domain size of the centromere can expand if the centromere size is reduced.

Segregation Strength Between the Normal B Centromere and Smaller Derivatives

Meiotic Analysis of TB-9Sb-Dp9 With Telo 2-2 in a Tug of War

From the collection of B chromosome centromere misdivision derivatives that have been described (Kaszas and Birchler, 1996, 1998), selected examples were used to cross with the plants containing the TB-9Sb-Dp9 chromosome. Plants containing TB-9Sb-Dp9 and Telo 2-2 were classified via FISH on root tip metaphase chromosomes using the B chromosome specific repeat (ZmBs) and knob heterochromatin (Peacock et al., 1981) probes. The TB-9Sb-Dp9 chromosome contains a large centromere and Telo 2-2 has a small one, which in comparison are distinct in cytological preparations (**Figure 3A**). Recombination in the 9S region between the foldback chromosome and the misdivision derivative occurs and forms a bridge as illustrated by a large and small centromere tied together in anaphase I (**Figure 3**).

The association in meiotic prophase between TB-9Sb-Dp9 and Telo 2-2 (+) is 60.43% (**Table 3**). There were 54.79% bridges formed in meiotic anaphase I (**Table 3**). The behavior of the two centromeres at various meiotic stages is shown in **Figure 3**. In the progeny of the heterozygotes of TB-9Sb-Dp9 and Telo 2-2, we did not find new dicentric chromosomes as occurred in the progeny of TB-9Sb-Dp9 with Telo 3-5(+) (Han et al., 2009).

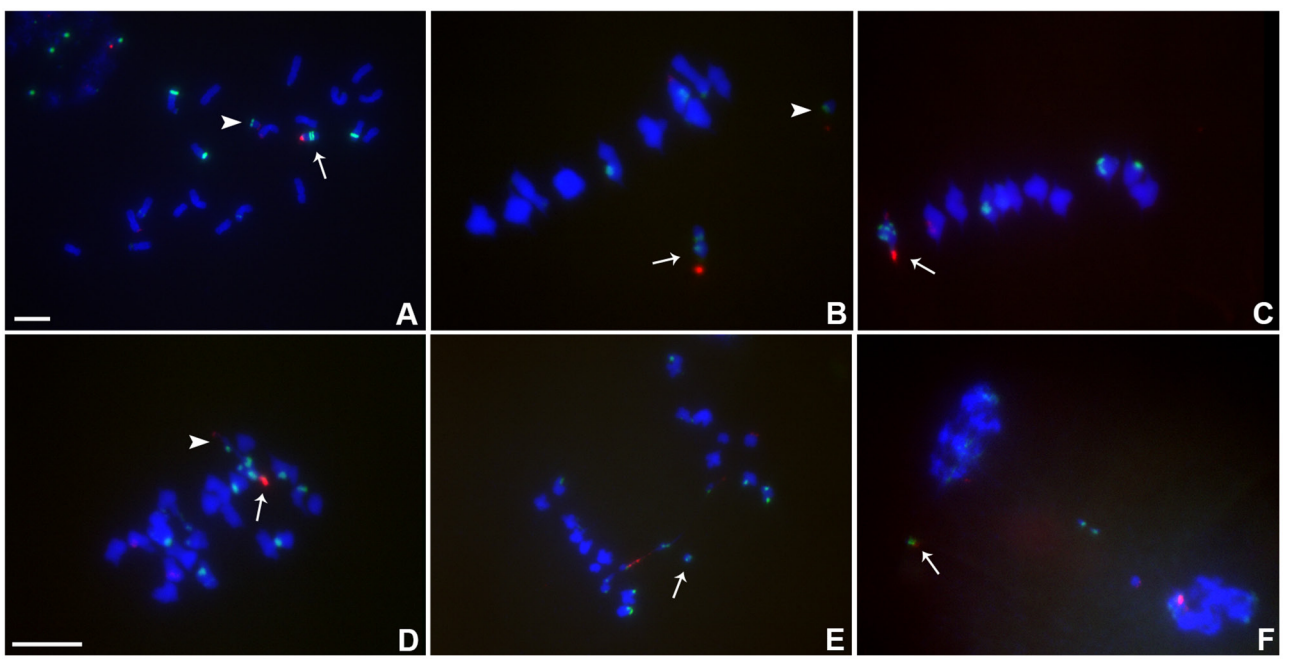

FIGURE 3 | Cytological analysis of plants containing TB-9Sb-Dp9 and Telo 2-2. ZmBs, which is a B chromosome specific sequence in and around the centromere, is labeled in red. Knob heterochromatin is labeled in green. Chromosomes were counterstained with DAPI in blue. **(A)** Somatic cell, arrow indicates TB-9Sb-Dp9 chromosome and arrowhead denotes the Telo 2-2 chromosome. **(B)** Metaphase I, TB-9Sb-Dp9 does not pair with Telo 2-2 (arrow indicates TB-9Sb-Dp9; arrowhead indicates Telo 2-2). **(C)** Metaphase I. TB-9Sb-Dp9 paired with Telo 2-2 forming a bivalent (arrow). The large and small B centromeres (red) are directed to opposite poles. **(D)** Early anaphase I. An example of the large (arrow) and small (arrowhead) centromeres proceeding to different poles is shown (arrow). **(E)**. Anaphase I. A bridge was formed and an acentric fragment was released (arrow). **(F)**. Early telophase I. A bridge was formed and an acentric fragment was released (arrow). Bar = 10 μm.

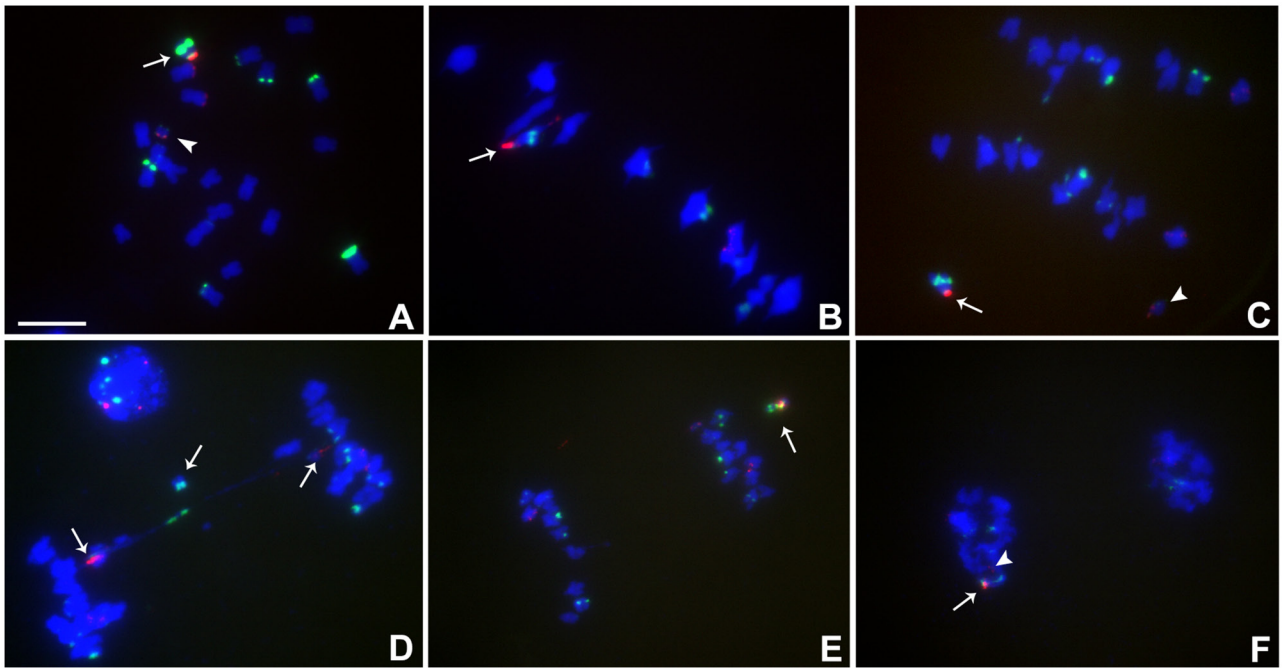

FIGURE 4 | Cytological analysis of plants containing TB-9Sb-Dp9 and Telo 6-9. ZmBs is red; knob is labeled in green and chromosomes counterstained with DAPI. **(A)** Somatic cell, arrow indicates the TB-9Sb-Dp9 chromosome and the arrowhead indicates the Telo 6-9 chromosome. **(B)** Metaphase I. TB-9Sb-Dp9 pairs with Telo 6-9 (arrow). The two centromeres progress toward opposite poles. **(C)** Anaphase I. TB-9Sb-Dp9 (arrow) and Telo 6-9 (arrowhead) moved to the same pole and formed no bridge. **(D)** Anaphase I. An example of the large and small centromeres (arrows to red signals) proceeding to different poles is shown. A bridge was formed and an acentric fragment was released (arrow). **(E)** Anaphase I. TB-9Sb-Dp9 and Telo 6-9 moved to the same pole. Arrow indicates the TB-9Sb-Dp9 chromosome. **(F)** Telophase I. One telophase cell contained both red signals (arrow and arrowhead). Bar = 10 μm.

TABLE 3 | Meiotic analysis of hybrid plants containing TB-9Sb-Dp9 and Telo 2-2.

Pairing	No pairing	Total cells
55 (60.43%)	36 (39.56%)	91
Anaphase I (bridge)	**Anaphase I (no bridge)**	**Total cells**
40 (54.79%)	33 (45.21%)	73

Five plants containing B-9Sb-Dp-9 and Telo 2-2 were used to observe meiosis for chromosome pairing and segregation. Pairing denotes when B-9Sb-Dp-9 and Telo 2-2 forms a bivalent and will form a bridge at anaphase I if exchange occurs followed by separation of the two centromeres to opposite during anaphase I.

Meiotic Analysis of TB-9Sb-Dp9 With Telo 6-9 in a Tug of War

Heterozygotes of TB-9Sb-Dp9 and Telo 6-9 were identified as described above for other combinations. The behavior of the two centromeres at various stages is shown (**Figure 4A**). Recombination between the two chromosomes occurred, which produces bridges with a large and small centromere in anaphase I (**Figure 4**).

In this combination, examples of both centromeres progressing to the same pole were observed (**Figures 4C,E,F**) as well as cases in which the two centromeres progressed to opposite poles forming a bridge (**Figure 4D**). If recombination has occurred in those cases proceeding to the same pole, a dicentric would be produced. New dicentric chromosomes were detected in the progeny of these heterozygotes (**Figure 5**) as previously reported for the combination involving Telo 3-5(+) as the misdivision derivative (Han et al., 2009).

Meiotic Analysis of TB-9Sb-Dp9 With Telo 4-4, 4-5 and 4-11

Heterozygotes of TB-9Sb-Dp9 with Telo 4-4, Telo 4-5 or Telo 4-11 were identified using FISH probes as noted above for other combinations (**Figures 6A–I**). Telo 4-4, Telo 4-5 and Telo 4-11 are all further derivatives from misdivision chromosome Iso3 (−) (Kaszas and Birchler, 1998). **Figure 6F** shows an example in which the smaller centromere loses the tug of war and remains attached to the large centromere that has achieved migration to the telophase pole. With these noted exceptions, segregation of the large and small chromosomes occurs regularly.

DISCUSSION

The test of segregation of large versus small centromeres showed a skew toward greater recovery of the larger centromere in all four comparisons but this difference was only significant in two cases. The difference in the amount of centromeric DNA of the assayed examples is much greater than is likely to occur naturally but the segregation skew is not dramatic. Nevertheless, only a small difference in function, compounded over generations, could potentially drive centromere changes.

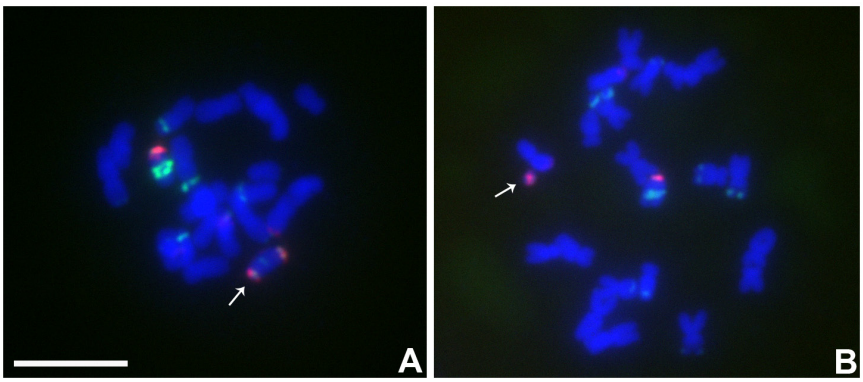

FIGURE 5 | Cytological analysis the progeny from the plants contained TB-9Sb-Dp9 and Telo 6-9. ZmBs is red; knob is labeled in green and chromosomes counterstained with DAPI. **(A)** New dicentric chromosome was formed (arrow). **(B)** Fragment minichromosome with a B centromere in the progeny (arrow). Bar = 10 μm.

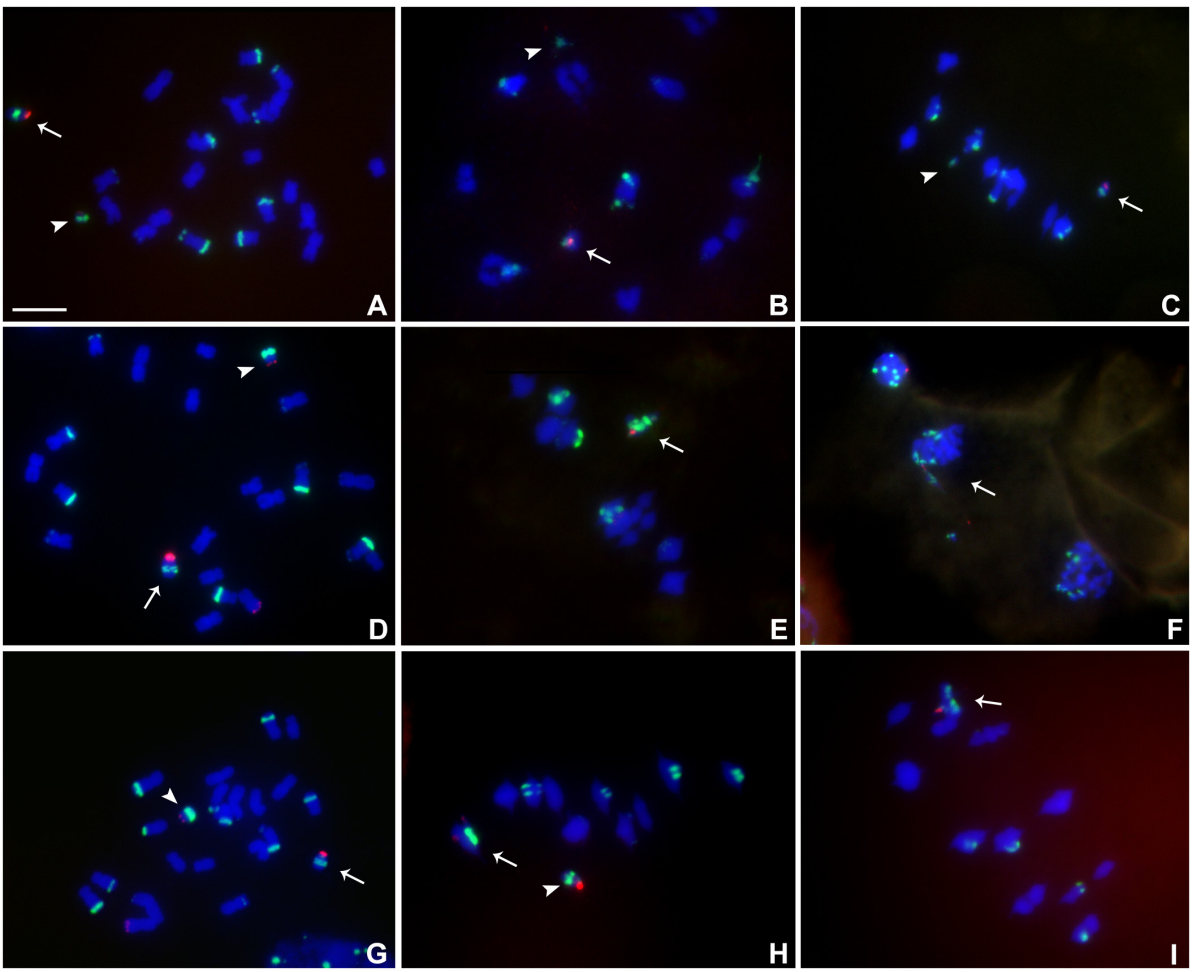

FIGURE 6 | Cytological analysis of plants containing TB-9Sb-Dp9 and Telo 4-4, 4-5 and 4-11. ZmBs is labeled in red. Knob heterochromatin is labeled in green. Chromosomes were counterstained with DAPI in blue. **(A–C)** TB-9Sb-Dp9 (arrow) and Telo 4-4 (arrowhead), Somatic cell **(A)**. Diakinesis **(B)**. Metaphase I **(C)**. **(D)** Somatic cell FISH shows TB-9Sb-Dp9 (arrow) and T4-5 (arrowhead). **(E)** Metaphase I. TB-9Sb-Dp9 paired with Telo 4-5 (arrow). **(F)** Telophase I. A bridge and fragment were produced but the smaller centromere appears to be dragged to the same pole as the larger (arrow). **(G)** Somatic cell of TB-9Sb-Dp9 (arrow) and Telo 4-11(arrowhead). **(H)** Metaphase I. Telo 4-11 paired with chromosome 9 and 9-B forming a trivalent, consisting of the Telo4-11, 9-B and 9 chromosomes. Arrowhead indicates the separate TB-9Sb-Dp9 chromosome. **(I)** Metaphase I. Arrow indicates the TB-9Sb-Dp9 chromosome paired with T4-11(arrow). Bar = 10 μm.

However, as noted, the lower rate of recovery of the small centromeres could potentially be accounted for by non-disjunction if the small centromere entered the same product of meiosis I as the large centromere. While non-disjunction is distinct from meiotic drive, such a regular outcome of large/small centromere segregation could have a potential influence on centromere evolution.

However, such interpretations are complicated by the lack of a relationship of centromere size to the corresponding biochemical features as assayed in this study by determining the signal of phosphorylated histone H2A (Su et al., 2017). The combination (Telo 2-2/TB-9Sb) that produced a segregation that was normal had the greatest difference in H2Aph signal, which was greatly reduced in parallel to the DNA. The two comparisons that were statistically significantly different from a normal segregation (Telo 3-5 and Telo 4-5) had comparable or greater amounts of H2Aph signal associated with the smaller centromeres. Thus, there is not clear support for the concept of conflict between the size of the centromeric DNA and the accumulation of biochemical features of active centromeres (as assayed here by H2AphThr133). As noted, the sizes of the centromere differences are great but the departure from normal segregation rates, even though significant, are small. When coupled with the extensive evidence for epigenetic factors involved with centromeres noted above, a conclusion that there is an antagonism between centromere DNA and the kinetochore proteins is not straightforward.

In the centromere "tug of war" during meiosis, the large and small centromeres are tied together by recombination but they usually progress to opposite poles in anaphase I. Occasionally, they were included in the same anaphase I pole. In still other cases, the large and small centromeres appear to have attached to opposite poles but nevertheless appear destined to be included in the same nucleus. When this occurs, a dicentric is now present that can initiate the BFB cycle in subsequent cell divisions. Indeed, in the TB-9Sb/Telo6-9 combination, dicentrics were recovered in the next generation. In a previous study, one example (Dicentric-15) that was recovered was studied in detail (Han et al., 2009). This chromosome has the large and small centromere together as a structural dicentric. However, only the large centromere was associated with CENH3 and was active, while the small centromere was devoid of CENH3 and was inactive (Han et al., 2009).

In general, the large and small centromeres are effective in progressing to the poles in opposition. In some few cases, the smaller chromosome is extended from the pole with the larger chromosome and likely eventually becomes included in the same nucleus. In the case of Dic-15, the smaller centromere had become inactive. While chromosomes with similar structures were observed in meiosis and in the progeny of some combinations in this study, no determinations of centromere activity were made.

Here, studies of segregation frequency and strength were performed using a unique system in which different versions of a chromosome with varying sizes of centromeric DNA was used. While a slighter lower frequency of recovery of the small centromere was found in two combinations, there was no correlation with the phosphorylated form of histone H2A, which is a mark of active centromeres. When centromeres were placed in opposition to each other, they regularly segregated to opposite poles with minor exceptions.

Previous studies of misdivision derivatives as univalents showed a general correlation between centromere size and transmission frequency (with some exceptions) (Kaszas and Birchler, 1998). In this study, when representatives of this collection were placed in opposition to the progenitor TB-9Sb chromosome, the segregation was close to Mendelian predictions with a slight favor to the larger centromere in some combinations. The presence of a pairing partner appears to improve the transmission rate. Furthermore, the quantities of H2Aph on two of the three small centromeres was equivalent or greater than the progenitor chromosome centromere. This observation suggests that partial deletions of centromere DNA under natural conditions could potentially be of little consequence if the centromeric biochemical domain expands. The epigenetic flexibility of the centromere suggests that lesions to the underling DNA is not necessarily a major factor in centromere evolution.

AUTHOR CONTRIBUTIONS

JB, JL, and FH conceived the experiments. FH, JL, MM, ZG, and NS conducted the experiments. BZ performed the immunolocalizations. JB and FH wrote the paper.

FUNDING

This work was supported by the United States National Science Foundation (DBI 0421671 and IOS-1444514) and National Science Foundation of China (31630049 and 31320203912).

REFERENCES

Alfenito, M. R., and Birchler, J. A. (1993). Molecular characterization of a maize B chromosome centric sequence. *Genetics* 135, 589–597.

Ananiev, E., Phillips, R. L., and Rines, H. (1998). Chromosome-specific molecular organization of maize (*Zea mays* L.) centromeric regions. *Proc. Natl. Acad. Sci. U.S.A.* 95, 13073–13078. doi: 10.1073/pnas.95.22.13073

Carlson, W. R. (1970). Nondisjunction and isochromosome formation in the B chromosome of maize. *Chromosoma* 30, 356–365. doi: 10.1007/BF00306564

Carlson, W. R., and Chou, T. S. (1981). B chromosome nondisjunction in corn: control factors near the centromere. *Genetics* 97, 379–389.

Fu, S., Lv, Z., Gao, Z., Wu, H., Pang, J., Zhang, B., et al. (2013). De novo centromere formation on a chromosome fragment in maize. *Proc. Natl. Acad. Sci. U.S.A.* 110, 6033–6036. doi: 10.1073/pnas.1303944110

Gao, Z., Fu, S., Dong, Q., Han, F., and Birchler, J. A. (2011). Inactivation of a centromere during the formation of a translocation in maize. *Chromosome Res.* 19, 755–761. doi: 10.1007/s10577-011-9240-5

Gao, Z., Han, F., He, M., Ma, Y., and Xin, Z. (1999). Characterization of genomes and chromosomes in a partial amphiploid of wheat-wheatgrass Zhong 2 using

fluorescence in situ hybridization (FISH) and chromosome pairing analysis. *Acta Bot. Sin.* 41, 25–28.

Han, F., Gao, Z., and Birchler, J. A. (2009). Reactivation of an inactive centromere reveals epigenetic and structural components for centromere specification in maize. *Plant Cell* 21, 1929–1939. doi: 10.1105/tpc.109.066662

Han, F., Lamb, J. C., and Birchler, J. A. (2006). High frequency of centromere inactivation resulting in stable dicentric chromosomes of maize. *Proc. Natl. Acad. Sci. U.S.A.* 103, 3238–3243. doi: 10.1073/pnas.0509650103

Henikoff, S., Ahmad, K., and Malik, H. S. (2001). The centromere paradox: stable inheritance with rapidly evolving DNA. *Science* 293, 1098–1102. doi: 10.1126/science.1062939

Jin, W., Lamb, J. C., Vega, J. M., Dawe, R. K., Birchler, J. A., and Jiang, J. (2005). Molecular and functional dissection of the maize B chromosome centromere. *Plant Cell* 17, 1412–1423. doi: 10.1105/tpc.104.030643

Kaszas, E., and Birchler, J. A. (1996). Misdivision analysis of centromere structure in maize. *EMBO J.* 15, 5246–5255.

Kaszas, E., and Birchler, J. A. (1998). Meiotic transmission rates correlate with physical features of rearranged centromeres in maize. *Genetics* 150, 1683–1692.

Kato, A., Lamb, J. C., and Birchler, J. A. (2004). Chromosome painting using repetitive DNA sequences as probes for somatic chromosome identification in maize. *Proc. Natl. Acad. Sci. U.S.A.* 101, 13554–13559. doi: 10.1073/pnas.0403659101

Liu, Y., Su, H., Pang, J., Gao, Z., Wang, X. J., Birchler, J. A., et al. (2015). Sequential de novo centromere formation and inactivation on a chromosomal fragment in maize. *Proc. Natl. Acad. Sci. U.S.A.* 112, E1263–E1271. doi: 10.1073/pnas.1418248112

McClintock, B. (1939). The behavior in successive nuclear divisions of a chromosome broken at meiosis. *Proc. Natl. Acad. Sci. U.S.A.* 25, 405–416. doi: 10.1073/pnas.25.8.405

McClintock, B. (1941). The stability of broken ends of chromosomes in *Zea mays*. *Genetics* 26, 234–282.

Nagaki, K., Song, J., Stupar, R. M., Parokonny, A. S., Yuan, Q., Ouyang, S., et al. (2003). Molecular and cytological analyses of large tracks of centromeric DNA reveal the structure and evolutionary dynamics of maize centromeres. *Genetics* 163, 759–770.

Peacock, W. J., Dennis, E. S., Rhoades, M. M., and Pryor, A. J. (1981). Highly repeated DNA sequence limited to knob heterochromatin in maize. *Proc. Natl. Acad. Sci. U.S.A.* 78, 4490–4494. doi: 10.1073/pnas.78.7.4490

Roman, H. (1947). Mitotic nondisjunction in the case of interchanges involving the B-type chromosome in maize. *Genetics* 32, 391–409.

Roman, H. (1948). Directed fertilization in maize. *Proc. Natl. Acad. Sci. U.S.A.* 34, 36–42. doi: 10.1073/pnas.34.2.36

Schneider, K. L., Xie, Z. D., Wolfgruber, T. K., and Presting, G. G. (2016). Inbreeding drives maize centromere evolution. *Proc. Natl. Acad. Sci. U.S.A.* 113, E987–E996. doi: 10.1073/pnas.1522008113

Su, H., Liu, Y., Dong, Q., Feng, C., Zhang, J., Liu, Y., et al. (2017). Dynamic location changes of Bub1-phosphorylated-H2AThr133 with CENH3 nucleosomes in maize centromeric regions. *New Phytol.* 214, 682–694. doi: 10.1111/nph.14415

Topp, C. N., Okagaki, R. J., Melo, J. R., Kynast, R. G., Phillips, R. L., and Dawe, R. K. (2009). Identification of a maize neocentromere in an oat-maize addition line. *Cytogenet. Genome Res.* 124, 228–238. doi: 10.1159/000218128

Wang, K., Wu, Y., Zhang, W., Dawe, R. K., and Jiang, J. (2014). Maize centromeres expand and adopt a uniform size in the genetic background of oat. *Genome Res.* 24, 107–116. doi: 10.1101/gr.160887.113

Zhang, B., Lv, Z., Pang, J., Liu, Y., Guo, X., Fu, S., et al. (2013). Formation of a functional maize centromere after loss of centromeric sequences and gain of ectopic sequences. *Plant Cell* 25, 1979–1989. doi: 10.1105/tpc.113.110015

Zheng, Y. Z., Roseman, R. R., and Carlson, W. R. (1999). Time course study of the chromosome-type breakage-fusion-bridge cycle in maize. *Genetics* 153, 1435–1444.

Zhong, C. X., Marshall, J. B., Topp, C., Mroczek, R., Kato, A., Nagaki, K., et al. (2002). Centromeric retroelements and satellites interact with maize kinetochore CENH3. *Plant Cell* 14, 2825–2836. doi: 10.1105/tpc.006106

Conflict of Interest Statement: The authors declare that the research was conducted in the absence of any commercial or financial relationships that could be construed as a potential conflict of interest.

frontiers in Plant Science

ORIGINAL RESEARCH
published: 05 February 2018
doi: 10.3389/fpls.2018.00091

Cold-Induced Male Meiotic Restitution in *Arabidopsis thaliana* Is Not Mediated by GA-DELLA Signaling

*Bing Liu[1,2], Nico De Storme[1] and Danny Geelen[1]**

[1] Department of Plant Production, Faculty of Bioscience Engineering, University of Ghent, Ghent, Belgium, [2] School of Integrative Plant Science, Cornell University, Ithaca, NY, United States

Short periods of cold stress induce male meiotic restitution and diploid pollen formation in *Arabidopsis thaliana* by specifically interfering with male meiotic cytokinesis. Similar alterations in male meiotic cell division and gametophytic ploidy stability occur when gibberellic acid (GA) signaling is perturbed in developing anthers. In this study, we found that exogenous application of GA primarily induces second division restitution (SDR)-type pollen in Arabidopsis, similar to what cold does. Driven by the close similarity in cellular defects, we tested the hypothesis that cold-induced meiotic restitution is mediated by GA-DELLA signaling. Using a combination of chemical, genetic and cytological approaches, however, we found that both exogenously and endogenously altered GA signaling do not affect the cold sensitivity of male meiotic cytokinesis. Moreover, *in vivo* localization study using a GFP-tagged version of RGA protein revealed that cold does not affect the expression pattern and abundance of DELLA in Arabidopsis anthers at tetrad stage. Expression study found that transcript of *RGA* appears enhanced in cold-stressed young flower buds. Since our previous work demonstrated that loss of function of DELLA causes irregular male meiotic cytokinesis, we here conclude that cold-induced meiotic restitution is not mediated by DELLA-dependent GA signaling.

Keywords: GA signaling, cold stress, male meiotic restitution, meiotic cytokinesis, diploid pollen

OPEN ACCESS

Edited by:
Changbin Chen,
University of Minnesota, United States

Reviewed by:
Nelson Garcia,
University of Minnesota Twin Cities, United States
Fangpu Han,
State Key Laboratory of Molecular Developmental Biology, Institute of Genetics and Developmental Biology (CAS), China

***Correspondence:**
Danny Geelen
danny.geelen@ugent.be

Specialty section:
This article was submitted to Plant Genetics and Genomics, a section of the journal Frontiers in Plant Science

Received: *31 August 2017*
Accepted: *17 January 2018*
Published: *05 February 2018*

Citation:
Liu B, De Storme N and Geelen D (2018) Cold-Induced Male Meiotic Restitution in Arabidopsis thaliana Is Not Mediated by GA-DELLA Signaling. Front. Plant Sci. 9:91. doi: 10.3389/fpls.2018.00091

INTRODUCTION

The production of viable haploid gametes is vital for the fertility and ploidy stability of flowering plants. Under certain conditions, plants may produce unreduced male gametes through incomplete meiotic cell division, a phenomenon termed 'meiotic restitution' or 'meiotic non-reduction' (Adams and Wendel, 2005;Mason and Pires, 2015). Meiotic restitution can be induced by omission of meiotic cell cycles, defective spindle organization, and/or irregular meiotic cytokinesis (De Storme and Geelen, 2013a; De Storme and Mason, 2014). Meiotic restitution can be classified into either FDR or SDR according to the genetic make-up of the yielded unreduced gametes (Kohler et al., 2010). In FDR-type meiotic restitution, homologous chromosomes fail to separate

Abbreviations: FDR, first division restitution; GA, gibberellic acid; PAC, paclobutrazol; RMAs, radial microtubule arrays; SDR, second division restitution.

whereas sister chromatids successfully disjoin from each other. As a result, FDR-type unreduced gametes maintain parental heterozygosity in genomic regions where meiotic recombination occurs rarely. In contrast, in SDR-type meiotic restitution, homologous chromosomes segregate but sister chromatids are grouped into unreduced gametes, which typically leads to heterozygosity at recombination-free chromatin regions (De Storme and Geelen, 2013b). Meiotic restitution and associated formation of unreduced gametes can be induced either through specific genetic defects or by temperature stress. In *Arabidopsis thaliana*, for example, cold stress causes male meiotic restitution (primarily SDR-type) by specifically disrupting the organization of RMAs at the end of male meiosis, consequently resulting in incomplete meiotic cytokinesis and unreduced gamete formation (De Storme et al., 2012).

The phytohormone GA regulates multiple development processes during male reproduction in plants (Plackett et al., 2011; Kwon and Paek, 2016; Plackett and Wilson, 2016). In most cases, GA regulates plant development by suppressing the activity of DELLAs, a family of transcriptional repressors that operate as negative regulators of GA signaling (Sun, 2010). DELLA proteins negatively regulate the expression of GA-signaling downstream genes and consequently inhibit plant growth and development (Xu et al., 2014). At the molecular level, GA suppresses DELLA activity by promoting DELLA protein destabilization through 26S proteasome. GA-dependent DELLA degradation relies on activity of two F-box proteins SLEEPY1 (SLY1) and SNEEZY (SNE), and the phosphorylation status of DELLA itself (Ariizumi et al., 2011; Ariizumi and Steber, 2011; Qin et al., 2014). In Arabidopsis, there are five DELLA homologs; i.e., RGA, GAI, RGL1, RGL2, and RGL3.

During male reproductive development, programmed degradation of the tapetal cell layer during male gametogenesis and pollen maturation strongly relies on balanced GA signaling and alterations herein lead to defects in tapetal disintegration, eventually causing abortion of microspores or mature pollen grains (Cheng et al., 2004; Aya et al., 2009; Plackett et al., 2014). GA signaling also plays a role in one or more process of microsporogenesis; e.g., meiotic cytokinesis. Ectopic activation of GA signaling in Arabidopsis meiosis-stage anthers, either via exogenous GA treatment or in the DELLA $rga^{-/-}$ $gai^{-/-}$ mutant background, was recently found to cause defects in male meiotic cell wall formation, leading to ectopic events of male meiotic restitution and associated formation of unreduced (2n) spores (Liu et al., 2017b). These findings suggest that balanced GA levels and associated GA signaling in the tapetal cell layer contributes to the progression of male meiotic cell division and is required for gametophytic ploidy stability (i.e., haploid spores). As the cellular mechanism of GA-induced male meiotic restitution highly mimics the meiotic alterations induced by cold (i.e., defects in RMA formation at telophase II and binuclear spore formation), we hypothesized that cold-induced male meiotic restitution in Arabidopsis could be mediated by GA-DELLA signaling. For this hypothesis to be correct, bioactive GA levels would need to increase in response to cold in the Arabidopsis anthers, in contrast to a general notion that low temperature stress causes a reduction in GA level and thereby promoting DELLA accumulation (Colebrook et al., 2014). In Arabidopsis seedlings, cold-induced accumulation of DELLAs is achieved by enhancing the catabolism of endogenous bioactive GA, through the rapid transcriptional activation of *DREB1b*/*C-repeat*/*DRE Binding Factor1* (*CBF1*), a positive regulator of GA-deactivating *GA2OX2* (Achard et al., 2008). Similarly, in rice, low temperature reduces the level of endogenous bioactive GA in developing anthers, where the expression of the GA biosynthesis gene *OsGA3OX1* is down-regulated upon cold stress, whereas the GA signaling repressor *SLR1*/*DELLA* and its upstream cold-responsive factor *CBF1* are up-regulated (Sakata et al., 2014).

Here, in this study, we test the hypothesis that cold-induced meiotic restitution in Arabidopsis male sporogenesis is mediated by alterations in anther GA signaling. In support of our hypothesis, we found that exogenous GA treatment of Arabidopsis primarily induces SDR-type unreduced gametes, in a similar rate and manner as when plants are exposed to cold. However, contrary to the assumption that GA may mediate the cold response of male meiosis, our data indicated that the cold sensitivity of male sporogenesis does not rely on the DELLA-dependent GA signaling. In addition, we found that cold stress does not reduce RGA abundance in the young developing anthers. Together these findings indicate that cold-induced male meiotic restitution in Arabidopsis is not mediated by GA-DELLA signaling.

MATERIALS AND METHODS

Plant Materials and Growth Conditions

Arabidopsis (*Arabidopsis thaliana*) Columbia-0 and Landsberg *erecta* (L*er*) accessions were obtained from the Nottingham Arabidopsis Stock Centre. The GA-insensitive mutant *gai* was kindly shared by Patrick Achard. The DELLA double mutant *rga-24 gai-t6* was previously described (Achard et al., 2006) and were kindly provided by Patrick Achard and Nicholas Harberd. The fluorescent tagged lines (FTLs) in the *qrt1-2*$^{-/-}$ background (FTL1313 and FTL3332), used for genotyping unreduced gametes, were described earlier (Francis et al., 2007; Berchowitz and Copenhaver, 2008). FTL1313 marker is physically located at 11.2 cM on chromosome 1, and FTL3332 is positioned at 10.43 cM on chromosome 3[1] (Supplementary Figure S1A) (Francis et al., 2007; Singh et al., 2017). The *pRGA*::*GFP-RGA* transgenic plants were obtained from Nicholas Harberd. Primers used for mutant genotyping are listed in Supplementary Table S2.

Seeds were germinated on K1 medium for 6–8 days and seedlings were transferred to soil and cultivated in growth chambers at 12 h day/12 h night, 20°C, and less than 70% humidity. To stimulate flowering transition, the photoperiod was changed to a 16-h-day/8-h-night regime. For GA_3 and PAC treatment, flowering plants were sprayed by water (+0.02% Tween), 100 μM GA_3 (+0.02% Tween) and 1 mM PAC (+0.02%

[1]https://www.arabidopsis.org/

Tween), respectively. The chemical concentrations used in this study were chosen based on previous study (Liu et al., 2017b).

Measurement of Cold Sensitivity of Arabidopsis Sporogenesis

Young flowering Arabidopsis plants were treated with cold (4°C–5°C for 48 h) and the unicellular stage microspores were examined at 24–36 h after the cold treatment under microscope. The cold sensitivity of the *rga-24 gai-t6* mutant was analyzed in the *qrt1-2*$^{-/-}$ background. The microspores were released by squashing targeted stage buds on a microscope slide with a drop of orcein staining buffer. The assessment of unreduced microspores was done by comparing the size to the haploid microspores and/or by counting the number of nucleus. The cold sensitivity of sporogenesis was evaluated by quantifying the frequency of enlarged unicellular stage microspores among the haploid microspores in a same flower bud. For each plant individual, more than 500 meiotic products were counted for quantification; and if the total number could not reach 500, then all the meiotic products were counted. More than five biological replicates have been performed, and Student's *t*-test was used for significance analysis at the 5% significance level ($\alpha = 0.05$).

GFP Intensity Quantification

To determine the effect of cold on abundance of GFP-tagged DELLA RGA proteins, Image J software was used for the quantification of GFP intensity. First, Image J was set up by selecting 'SET MEASUREMENTS' in ANALYZE menu with AREA, INTEGRATED DENSITY and MEAN GRAY VALUE being selected. Second, using any of the drawing/selection tools in Image J, the entire anther area of a tetrad stage anther picture taken from a *pRGA::GFP-RGA* plant without cold treatment, was chosen for fluorescence quantification by clicking 'MEASURE.' The value was recorded as integrated density (ID1). Thirdly, a region in the same anther where developing meiocytes were located was chosen as background and the fluorescence intensity was quantified and recorded as mean fluorescence of background readings (FoBR1). Afterward, integrated density in pictures of another four anthers from four non-treated *pRGA::GFP-RGA* plants, and five anthers from five cold-treated (4°C–5°C for 24 h) *pRGA::GFP-RGA* plants was quantified (values are recorded as ID2-10, respectively). The mean background readings were recorded as FoBR2-10, respectively. When all samples were finished, the corrected total cell fluorescence (CTCF) for each sample was calculated using formula: CTCFn = IDn- (area of selected cell × FoBRn). Student's t-test was used for significance analysis with significance level (alpha) = 0.05.

Cytology

Callosic cell wall staining and the analysis of the male meiotic products (tetrad-stage analysis by aniline blue and orcein staining) were performed as described previously (Liu et al., 2017b). Flowering Arabidopsis *qrt1-2*$^{-/-}$ plants segregating for the FTL1313 or FTL3332 pollen fluorescent marker were sprayed with 100 μM GA_3, and the mature pollen grains were observed at 7–9 days following GA treatment. FDR/SDR genotyping of mature pollen grains in the FTL lines (FTL1313 and FTL3332) was performed by releasing mature pollen grains in a drop of pollen extraction buffer (0.5 M EDTA) on a microscope slide, and visualized under fluorescence microscope. Five plant individuals were analyzed for either the FTL1313 or FTL3332 reporter. Meiotic spreads were prepared as described previously (Liu et al., 2017b).

Tubulin Immunolocalization

The alpha-tubulin immunolocalization was performed according to the method of De Storme et al. (2012) with minor modifications. Briefly, the time of the first and second digestions by enzyme mix were adjusted to 3 and 1.5 h, respectively.

Expression Analysis

The young flowering Arabidopsis wild type Columbia-0 plants were treated with cold (4°C–5°C) for 0, 2, and 24 h, respectively, and the total RNA from young flower buds was isolated using the RNeasy Plant Mini Kit with additional on-column DNase I treatment (Qiagen). First-strand cDNA was synthesized using the GoScript^{TM} Reversion Transcription System Kit (Promega). Quantitative gene expression analysis was performed by qRT-PCR on a Stratagene MX3000 real-time PCR system using the GoTaq® qPCR Master Mix (Promega). For each treatment group, young flower buds from ten plant individuals were collected, and mRNA was isolated and pooled for further use. Two more bulks of flower buds (also from ten plants for each bulk) were sampled, for a total of three biological replicates for each treatment. For each bulked mRNA sample, qPCR was performed twice, with three technical replicates for each gene being surveyed (six technical replicates in total). Data from the six assays were pooled and then analyzed. The Arabidopsis *ACTIN2* gene (AT3G18780) was used as the reference gene. The data for each tested gene have been normalized to the value of internal control *AtACTIN2*, and the value of 2 and 24 h cold-treated samples were compared with non-cold treated samples (0 h cold treatment). The relative expression fold-change is presented and was calculated using 2ˆdelta-delta Ct method. Significance analysis was performed on the relative expression fold-change using Wilcoxon rank test. Significance level (alpha) was 0.05. Primers used for specific amplification of targeted gene transcripts are listed in Supplementary Table S3.

Microscopy

The microscopy performed in this study was according to the previous report (Liu et al., 2017b).

RESULTS

GA Primarily Induces SDR-Type Male Meiotic Restitution

In Arabidopsis, recombination hotspots are distributed along entire chromatin except for centromeric regions (Salomé et al., 2011). To determine the type of GA-induced meiotic restitution in Arabidopsis, we analyzed segregation of the hemizygous

centromere-linked FTL markers FTL1313 (dsRed – Chr. 1) and FTL3332 (YFP – Chr. 3) in the *quartet1-2*$^{-/-}$ (*qrt1-2*$^{-/-}$) background. Because we have previously shown that GA treatment may induce around 5% meiotic restitution (Liu et al., 2017b), we here only quantified the number of meiotic restituted products and classified them into either FDR- or SDR-type (Supplementary Table S1). Under control conditions, plants hemizygous for either the FTL1313 or FTL3332 reporter construct produced tetrads in which two out the four pollen grains were GFP fluorescent reflecting regular segregation of these fluorescent markers (Supplementary Figure S1C). At 7–9 days post GA treatment, GA-sprayed plants hemizygous for FTL1313 produced abundant tetrads and, in addition, a small amount of triads with two regular-sized haploid pollen grains and one larger, unreduced pollen grain. When fluorescent expression in these pollen triads was exclusively confined to the unreduced pollen grain or to both haploid pollen grains, the triads most likely originate from SDR-type restitution (Supplementary Figures S1D,E). In contrast, when fluorescent expression in the triads occurred in both a haploid and an unreduced pollen grain, the triads most likely originated from FDR-type restitution (Supplementary Figure S1F). In addition, GA-treated plants also produced dyads in which homologous chromosomes harboring centromere-linked hemizygous FTL markers either segregate both to one single unreduced pollen (Supplementary Figure S1G) or each to one single unreduced pollen (Supplementary Figure S1H), indicating for either SDR- or FDR-type meiotic restitution, respectively. GA-induced dyads and triads in *qrt1-2*$^{-/-}$ plants hemizygous for the FTL1313 reporter were found to contain 75.4% homozygous and 24.6% hemizygous for the locus containing the FTL1313 reporter. For GA-treated *qrt1-2*$^{-/-}$ plants hemizygous for the FTL3332 marker, 92.1% appeared homozygous and 7.9% appeared heterozygous for the FTL3332 locus (Supplementary Figures S1B,I–L). The predominant homozygous status of unreduced microspores of both the FTL1313 and FTL3332 marker lines indicated that GA primarily induced SDR-type meiotic restitution. These results are similar to what has been reported for cold stress-induced male meiotic restitution (De Storme et al., 2012).

Exogenous Modulation of Anther GA Content Does Not Influence the Cold Sensitivity of Arabidopsis Male Sporogenesis

To test whether cold induces meiotic restitution by increasing endogenous GA level in anthers, flowering Arabidopsis plants were sprayed either with 100 μM GA_3 or 1 mM of the GA biosynthesis inhibitor PAC, after which they immediately were transferred to cold conditions (4–5°C) for 48 h. 24–36 h post cold treatment, unicellular stage microspores were examined for indirect quantification of male meiotic restitution (**Figure 1**). Under normal temperature conditions, both mock and PAC-treated plants produced 100% uniformly sized haploid microspores (**Figure 1B**, mock-treated; C, PAC-treated). In contrast, GA_3-sprayed *qrt1-2*$^{-/-}$ plants produced around 3.8% enlarged microspores (**Figures 1A,D,E**). When an additional cold treatment was applied, mock, GA_3 or PAC sprayed plants displayed similar frequency of enlarged unicellular microspores (**Figures 1A,F–K**). These data indicate that cold-induced meiotic restitution is neither enhanced nor reduced by exogenous GA and PAC application, suggesting that GA homeostasis is not critical for evoking a cold response in male meiosis.

Genetic Alteration of GA Signaling Does Not Influence Sensitivity of Male Sporogenesis to Cold

The impact of endogenous genetic alterations in GA signaling on the cold sensitivity of male sporogenesis was investigated by testing the cold response of both dominant and loss of function *della* mutant plants (**Figure 2**). The GA dominant insensitive *gai* mutant produces a non-degradable DELLA GAI protein and thus exhibits a constitutively repressed DELLA-dependent GA signaling (Peng et al., 1997). Under normal temperature conditions, the *gai* mutant produced normal tetrads and haploid microspores (Supplementary Figures S2C,D) as wild type plants (Supplementary Figures S2A,B). Upon exposure to cold (4–5°C for 48 h), *gai* plants exhibited male meiotic restitution with associated unreduced microspore formation at a similar level observed in wild type L*er* plants (**Figures 2A,E,F**), indicating that impaired DELLA-dependent GA signaling does not block the cold sensitivity of Arabidopsis male meiotic cell division. The double *rga-24 gai-t6* mutant plants exhibit constitutively activated GA signaling (Dill and Sun, 2001), and produced 4.8% unreduced male gametes under normal temperature conditions (**Figure 2B**). Cold was found to induce a significantly higher level of enlarged microspores compared to wild type plants (**Figures 2B–D**, wild type L*er*; G and H, *rga-24 gai-t6*), suggesting an additive effect of cold stress on meiotic restitution in the *della* null mutation background. These data demonstrate that the cold sensitivity and response of Arabidopsis male sporogenesis does not rely on RGA- and GAI-dependent GA signaling.

Cold Induces Defective Male Meiotic Cytokinesis in the GA-Insensitive Mutant

We further examined male meiotic chromosome behavior and male meiotic cell wall formation in the GA-insensitive *gai* meiocytes. Cold stress did not disturb male meiotic chromosome segregation in both the *gai* mutant and wild type L*er* plants (Supplementary Figures S3A–C). Under normal conditions, *gai* displayed regular callosic cell wall formation indicating normal meiotic cytokinesis (Supplementary Figures S3D,G). However, at 24 h after cold treatment (4–5°C), meiotic-restituted dyads and triads with incomplete callosic cell walls were observed in both L*er* and the *gai* mutant (Supplementary Figure S3E,F,H,I) manifesting defective male meiotic cytokinesis.

Tubulin immunostaining was performed on the cold-shocked L*er* and *gai* mutant male meiocytes (**Figure 3**). During the stages from prophase I to anaphase II, both the control and cold-stressed meiocytes in either L*er* or *gai* plants displayed regular microtubule configurations (**Figures 3A–E,G–K,M–Q,S–W**). At prophase I, a network of microtubules surrounded the nucleus.

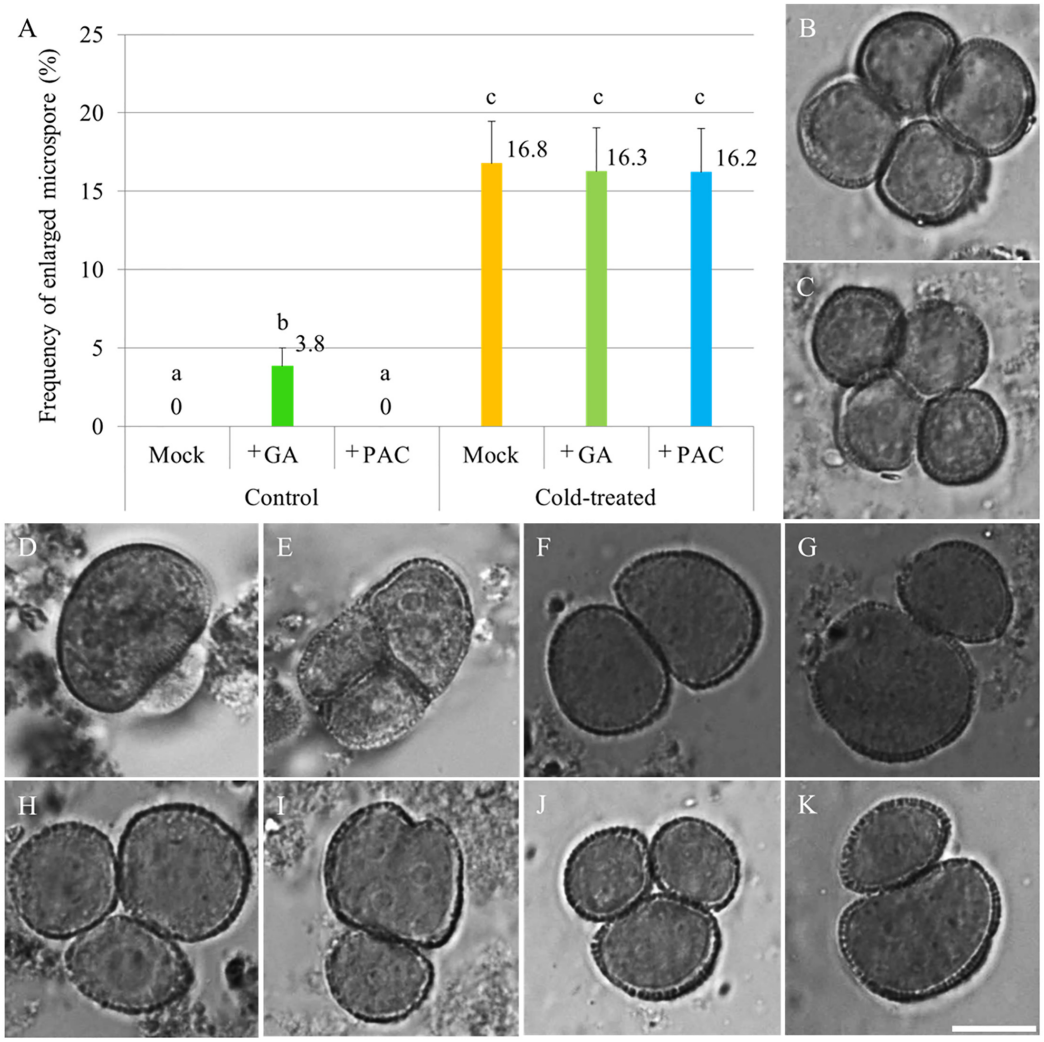

FIGURE 1 | The effect of GA and PAC treatment on cold sensitivity of Arabidopsis male sporogenesis. **(A)** Histogram showing the frequency of enlarged unicellular microspores in *Arabidopsis thaliana* plants with combined chemicals and cold treatment. The numbers indicate mean values of the frequency of the enlarged microspores. For each group, 10 biological replicates were performed and more than 500 microspores have been counted. Student's *t*-test was used for significance analysis. The *qrt1-2*$^{-/-}$ mutant was used for this quantification assay. **(B–E)** Haploid unicellular microspores in control plants **(B)**, plants treated with 1 mM PAC **(C)**, and enlarged unicellular microspores in plants treated with 100 μM GA_3 **(D,E)** under normal temperature conditions. **(F–K)** Enlarged unicellular microspores in flowering plants exposed to a combined treatment of mock and cold **(F,G)**, GA and cold **(H,I)**, and PAC and cold **(J,K)**. Scale bar = 10 μm.

Metaphase I showed formation of a single spindle, while metaphase II showed two perpendicular spindle formations. In contrast, the microtubule network; i.e., RMA, was clearly affected by cold at telophase II. Some of the nuclei in cold-stressed L*er* and *gai* tetrad were adjacent to each other and were not separated by RMA (**Figures 3R,X** and Supplementary Figure S4). These data demonstrate that the cold-sensitivity of meiotic cytokinesis and RMA in male meiocytes does not rely on DELLA-dependent GA signaling.

Cold Does Not Reduce RGA Abundance in Tetrad-Stage Arabidopsis Anthers

To determine the effect of cold stress on abundance of DELLA proteins in developing Arabidopsis anthers, we used an Arabidopsis transgenic line harboring a recombinant *pRGA::GFP-RGA* reporter construct and monitored the *in vivo* GFP fluorescence signals in the developing anthers at 24 h under cold shock (4–5°C for 24 h). The abundance of RGA proteins was determined by quantifying the GFP intensity in the anthers (**Figure 4A**). If cold stress induces defective meiotic cytokinesis by promoting DELLA degradation, the fluorescence signals of GFP-RGA in tetrad stage anthers should be reduced. We observed that the *pRGA::GFP-RGA* was predominantly expressed in the tapetal cell layer and was not affected by 24 h cold stress (**Figures 4B,C**), suggesting that cold induces meiotic restitution in Arabidopsis anthers not by interfering with DELLA protein stability.

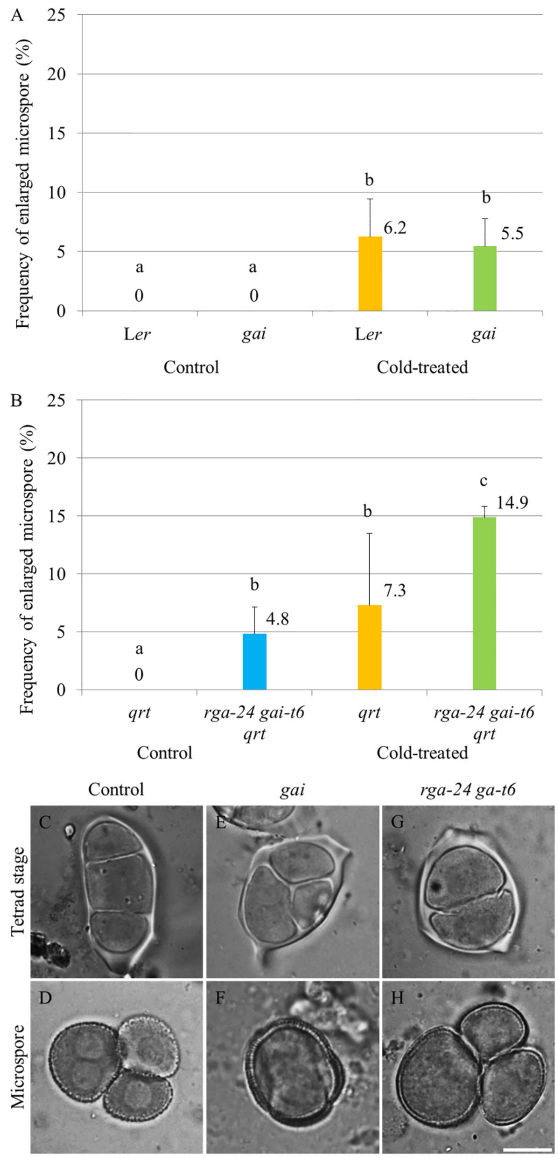

FIGURE 2 | Cold sensitivity of male sporogenesis in Arabidopsis *gai* and *rga-24 gai-t6* mutant plants. **(A,B)** Histograms showing frequencies of cold-induced enlarged unicellular microspores in *gai* **(A)** and *rga-24 gai-t6* **(B)** plants. The numbers indicate mean values of the frequency of the enlarged microspores. For each group, more than five biological replicates were performed and more than 500 microspores have been counted. Student's *t*-test was used for significance. The *rga-24 gai-t6* mutant plants were in *qrt1-2*$^{-/-}$ mutant background. **(C–H)** Cold-induced male meiotic restitution and enlarged unicellular microspores in wild type L*er* **(C,D)**, the *gai* **(E,F)** and *rga-24 gai-t6 qrt1-2*$^{-/-}$ **(G,H)** plants. Scale bar = 10 μm.

The Expression of GA Metabolic and Signaling Genes in Young Arabidopsis Flower Buds Are Influenced by Cold Stress

To determine the effect of cold stress on the expression of GA metabolic and signaling genes in young Arabidopsis flower buds, real-time quantitative PCR of the genes encoding for CBF1, GA biosynthesis GA3OX1, GA 2-oxidases GA2OX2 and GA2OX6, DELLA RGA and GAI proteins was performed (**Figure 5**). In 2 h cold-stressed young flower buds, the *CBF1* and *GA2OX6* transcript levels showed a significant increase and reduction compared to control plants without cold stress, respectively (**Figures 5A,D**), while for *GA3OX1* and *RGA*, no significant alterations were detected (**Figures 5B,E**). The transcripts of *GA2OX2* and *GAI* appeared stable throughout the cold treatment (**Figures 5C,F**). At 24 h under cold stress, the relative expression of *CBF1* and *GA3OX1* declined significantly (**Figures 4A,B**), contrary to *RGA* that showed an elevated expression level (**Figure 5E**). These data suggest that cold stress has an impact on the transcription of both GA synthesis and catabolic genes, and it modulates GA levels in Arabidopsis anthers in a complex manner.

DISCUSSION

Since cold stress and exogenous GA application induce male meiotic restitution using highly similar mechanism in Arabidopsis (De Storme et al., 2012; Liu et al., 2017b), we hypothesized that cold-induced defective male meiotic cytokinesis may be mediated by GA-DELLA signaling. We found that both of these treatments induce SDR-type unreduced pollen grains. This predominant restitution pathway is reminiscent to omission of second division or the elimination of the second meiotic division occurring in mutants defective in *CYCA1;2/TAM* and *OSD1* gene function. In these mutants, the second division is not executed because meiocytes exit the division cycle and immediately pursue with cell wall formation (d'Erfurth et al., 2010; Cromer et al., 2012). Cold and GA-induced restitution are clearly not the result of omission of second division. Instead they cause defects in the organization of the RMAs formed at the end of the second division cycle, with subsequent defects in cell plate formation. Microtubules between the haploid nuclei in tetrad stage meiocytes are poorly developed or maintained, allowing the nuclei to occasionally migrate into close proximity. Adjacent nuclei may then operate as a single unit during cell wall positioning and cytokinesis, establishing triad and dyad formation. Hence it is not likely that cold- and GA-induced cytokinesis defect is mediated by CYCA1;2/TAM and/or OSD1.

Contrary to our hypothesis, both endogenous and exogenous alterations in GA signaling did not influence the cold sensitivity of microsporogenesis, and cold stress did not reduce RGA-GFP abundance in tetrad stage anthers. In addition, the transcript levels of GA biosynthesis gene *GA3OX1* was downregulated and *RGA* was increased upon cold stress in young flower buds. These findings suggest that the cold sensitivity of male meiosis does not rely on a DELLA-dependent GA signaling. Since male meiotic cytokinesis is interfered by a reduced level of DELLAs, and not by an accumulation, we conclude that cold-induced male meiotic restitution in Arabidopsis is not mediated by GA-DELLA signaling.

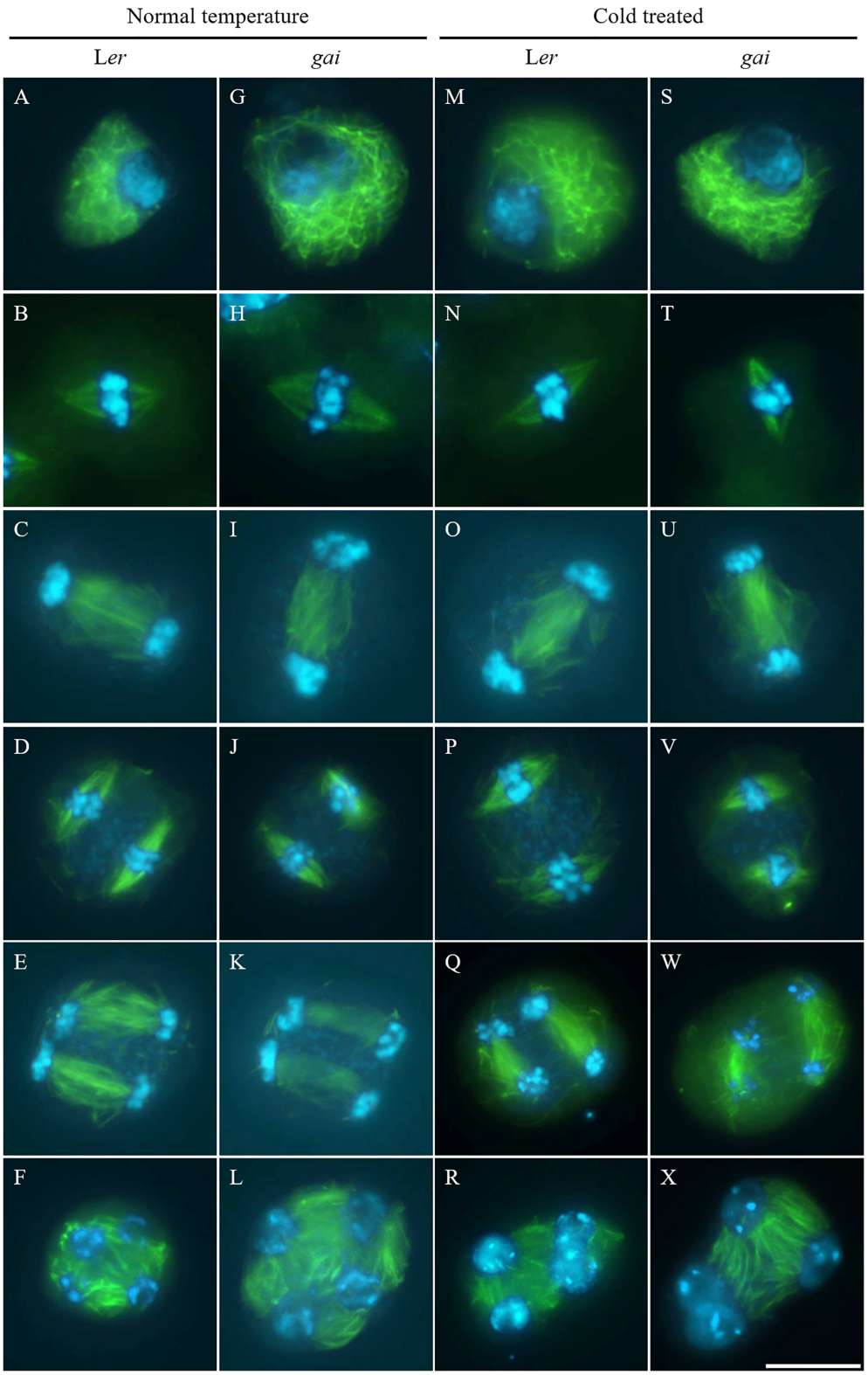

FIGURE 3 | Cold interferes with radial microtubule array (RMA) formation in the *gai* mutant. **(A–L)** Meiotic microtubule structures at prophase **(A,G)**, metaphase I **(B,H)**, interkinesis **(C,I)**, metaphase II **(D,J)**, anaphase II **(E,K)** and telophase II stage **(F,L)** meiocytes in wild type L*er* **(A–F)** and the *gai* mutant **(G–L)** plants under control conditions. **(M–X)** Meiotic microtubule structures at prophase **(M,S)**, metaphase I **(N,T)**, interkinesis **(O,U)**, metaphase II **(P,V)**, anaphase II **(Q,W)** and telophase II stage **(R,X)** meiocytes in cold-stressed wild type L*er* **(M–R)** and the *gai* mutant **(S–X)** plants. Green: α-tubulin, cyan: DAPI. Scale bars = 10 μm.

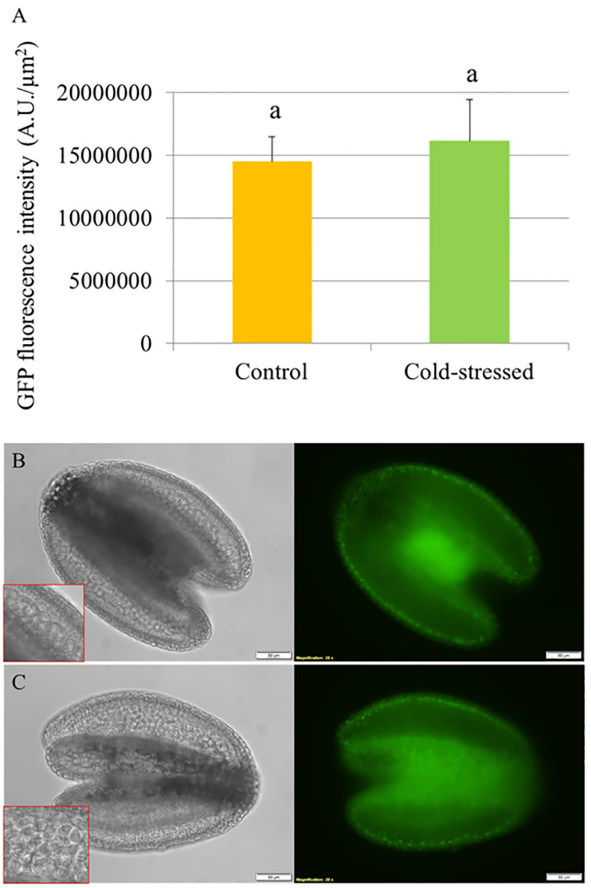

FIGURE 4 | Cold stress does not reduce the abundance of GFP-RGA in tetrad stage Arabidopsis anthers. **(A)** Histogram showing the GFP fluorescence intensity in tetrad stage anthers under cold stress. Five biological replicates were performed and Student's *t*-test was used for significance analysis with significance level (alpha) = 0.05. **(B,C)** Expression of *pRGA::GFP-RGA* in tetrad stage anthers under normal temperature conditions **(B)** and at 24 h under cold stress **(C)**.

Our gene expression analysis shows similarity with the study in rice, where low temperature has been shown to disrupt pollen development by lowering the bioactive GA level and increasing the abundance of DELLA protein in developing anthers, and displays a rapid increase of the *CBF1* transcript (Sakata et al., 2014). At the same time, we observed a negatively regulated expression of GA catabolic factor *GA2OX6* in addition to a downregulated expression of *GA3OX1*, exhibiting a similar situation in rice, in which cold stress reduces the expression of both GA catabolic gene *GA2OX1* and biosynthesis genes *OsGA20OX3* and *OsGA3OX1* (Sakata et al., 2014). These findings hint that reduced temperature modulates GA levels in male reproductive tissues by a complicated mechanism. Whether bioactive GA is reduced or upregulated would depend on a predominant impact of cold stress on GA biosynthesis, or catabolism, and may also depend on which cold-responsive GA metabolism gene plays a major role in the tetrad stage anthers. On the other hand, in Arabidopsis CBF1 and 3 inhibit vegetative development upon cold stress by enhancing the expression of *GA 2-oxidases* and increasing DELLA stability, and negatively regulating GA biosynthesis (Zhou et al., 2017). In both vegetative and reproductive tissues of plants, the expression of *CBF1* is rapidly increased upon cold stress and subsequently declines (Novillo et al., 2004, 2007; Achard et al., 2008; Sakata et al., 2014; Karimi et al., 2015). Our study here revealed a similar expression pattern of *CBF1* as these previous studies. Considering these findings, it is likely that the cold-responsive pattern of CBFs-GA-DELLA module might be conserved in different tissue types of multiple plants species.

Notably, although we observed that cold stress has an additive effect on 2n gamete formation in the *rga-24 gait6* plant background, we did not detect significant difference in plants with combined GA and cold treatment (**Figures 1**, **2**). This may because in the wild type plants, cold offset the effect of GA treatment by lowering GA levels in the anthers somehow, resulting in a non-significant destabilization of DELLAs. At the same time, although the expression of *RGA* increases in 24 h cold-stressed flower buds, we did not observe an elevation of GFP-RGA abundance at this time point under the cold condition (**Figures 4**, **5**). The construct used here may not reflect the endogenous RGA level or alternatively, cold stress differently induces responses of GA signaling in rice and Arabidopsis. Moreover, this fact may also be explained by the observation that although the cold stress reduced the expression level of GA biosynthesis gene *GA3OX1*, it also suppressed the activity of GA catabolic gene *GA2OX6*, which may consequently lead to a minor changed bioactive GA level that cannot significantly alter GFP-RGA abundance in the anthers. To determine a precise cold-responding behavior of bioactive GA levels, further studies should monitor GA gradients in the developing male reproductive tissues *in vivo* (Rizza et al., 2017). An additional difference with the study in rice anther is that whereas GA-insensitive rice mutants were hypersensitive to low temperature, exhibiting severe defects in pollen development and male fertility (Sakata et al., 2014), the Arabidopsis GA-insensitive *gai* mutant was not different from the control wild type and showed a similar cold-induced meiotic restitution. We conclude from these results that the meiotic restitution studied here is distinct from the cold-induced decrease in the number of sporogenous cells and hypertrophy of tapetal cells in rice, and GA signaling preferentially plays a role in later gametogenesis under cold stress.

GA has been shown to regulate cortical microtubule organization in epidermal cells of pea internodes and renders cortical microtubules more susceptible to cold (Akashi and Shibaoka, 1987). A possible mechanism involves the binding of DELLA protein to prefoldin complex, a chaperone required for tubulin folding, and its localization to the cytoplasm (Locascio et al., 2013). Under conditions that reduce GA levels, the prefoldin complex is targeted to the nucleus compromising tubulin heterodimer availability and affecting microtubule dynamics. Rice plant cells have been shown to respond to severe cold shock by modifying the cortical microtubular network and accumulation of microtubules at the nuclear envelope

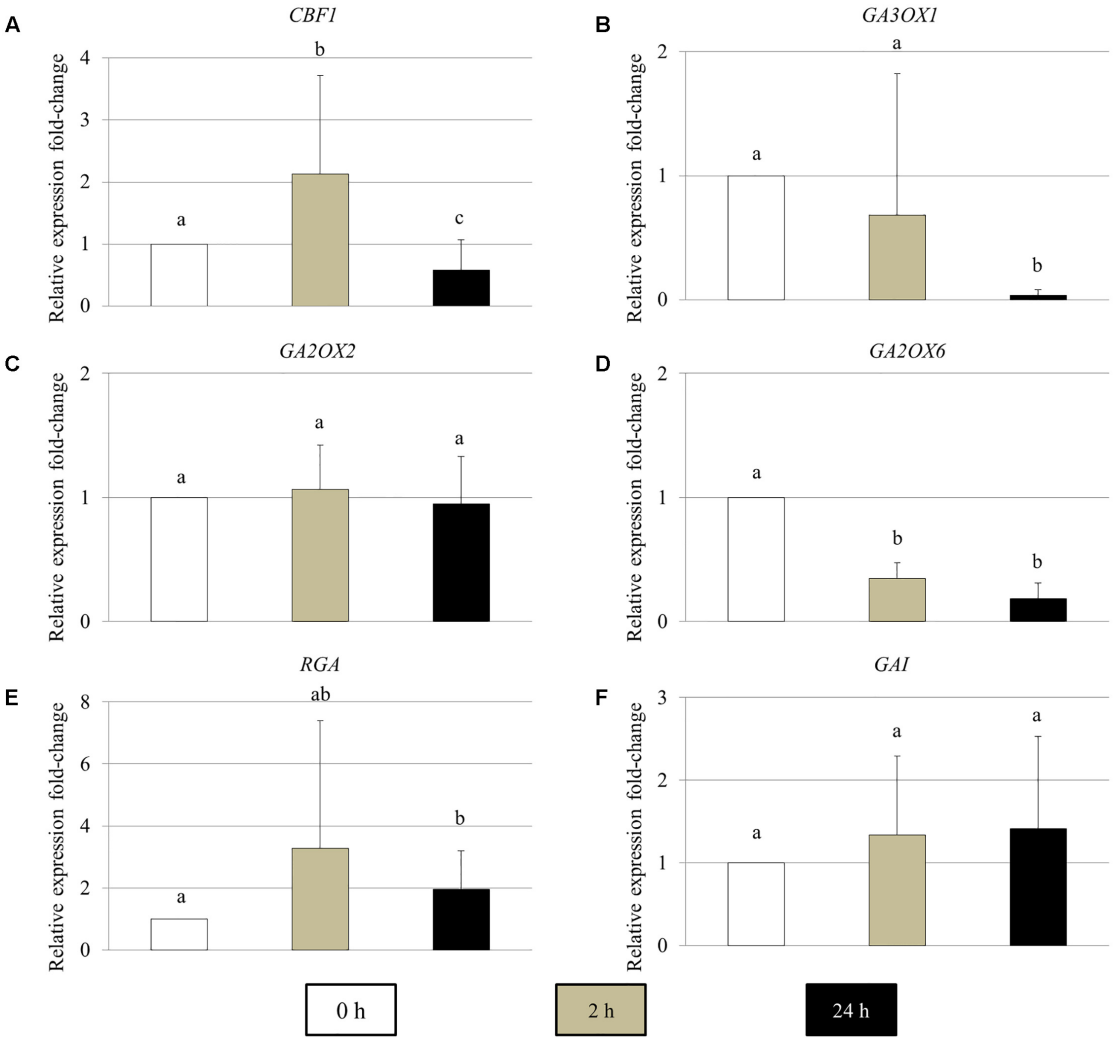

FIGURE 5 | The relative expression fold-change of GA metabolic and signaling genes in Arabidopsis young flower buds under cold stress. **(A–F)** Histograms showing the relative expression fold-change of *CBF1* **(A)**, *GA3OX1* **(B)**, *GA2OX2* **(C)**, *GA2OX6* **(D)**, *RGA* **(E)**, and *GAI* **(F)** in early stage Arabidopsis flower buds under cold stress. *X* axis represents time period under cold treatment; *Y* axis represents relative expression ratio of the genes. Error bars represent standard deviation with significance level (alpha) = 0.05.

(Chen et al., 2011). The growth arrest in rice caused by the 4°C cold shock can be partially rescued by overexpressing OsRAN2 or TaRAN1, members of the small GTPase protein family that plays an important role in nucleo-cytoplasmic transportation of proteins and RNA, mitotic spindle assembly, and nuclear envelope assembly (Chen et al., 2011). The expression of RAN GTPases is subject to environmental stimuli and responds to different levels of exogenously applied plant hormones including GA (Chen et al., 2011; Tian et al., 2015). Hence, RAN protein function may be involved in cold-induced meiotic restitution and future studies should address the possibility that cold affects RAN-mediated re-localization of tubulin heterodimers. The hormone cytokinin also conveys cold responses in plants (Kazan, 2015; Eremina et al., 2016). We previously investigated and reported that the cytokinin signaling module AHK2/3-AHP2/3/5, which plays a role in the cold sensitivity and response of Arabidopsis vegetative development (Jeon et al., 2010; Jeon and Kim, 2013; Liu et al., 2017a), is not involved in cold response of meiotic cytokinesis. Whether cold-induced meiotic restitution is mediated by hormone controlled processes is currently not demonstrated and future studies may need to consider a more direct impact of cold on proteins involved in male meiotic cytokinesis.

AUTHOR CONTRIBUTIONS

BL performed the experiment and wrote the draft manuscript. BL and NDS conceived and designed the project. BL and NDS worked on manuscript edition. DG supervised the project, contributed to the experimental design and to the interpretation of results and edited the manuscript.

FUNDING

This work was supported by China Scholarship Council (No. 201306760005) and FWO PostDoc grant 1293014N.

ACKNOWLEDGMENTS

The authors thank Patrick Achard and Nicholas Harberd for kindly providing the *rga-24 gai-t6* mutant seeds. They thank Burcu Nur Keçeli, Hoang Khai Trinh and Damilola Olatunji for the help with the qPCR experiment.

SUPPLEMENTARY MATERIAL

The Supplementary Material for this article can be found online at: https://www.frontiersin.org/articles/10.3389/fpls.2018.00091/full#supplementary-material

REFERENCES

Achard, P., Cheng, H., De Grauwe, L., Decat, J., Schoutteten, H., Moritz, T., et al. (2006). Integration of plant responses to environmentally activated phytohormonal signals. *Science* 311, 91–94. doi: 10.1126/science.1118642

Achard, P., Gong, F., Cheminant, S., Alioua, M., Hedden, P., and Genschik, P. (2008). The cold-inducible CBF1 factor-dependent signaling pathway modulates the accumulation of the growth-repressing DELLA proteins via its effect on gibberellin metabolism. *Plant Cell* 20, 2117–2129. doi: 10.1105/tpc.108.058941

Adams, K. L., and Wendel, J. F. (2005). Polyploidy and genome evolution in plants. *Curr. Opin. Plant Biol.* 8, 135–141. doi: 10.1016/j.pbi.2005.01.001

Akashi, T., and Shibaoka, H. (1987). Effects of gibberellin on the arrangement and the cold stability of cortical microtubules in epidermal cells of pea internodes. *Plant Cell Physiol.* 28, 339–348.

Ariizumi, T., Lawrence, P. K., and Steber, C. M. (2011). The role of two F-box proteins, SLEEPY1 and SNEEZY, in Arabidopsis gibberellin signaling. *Plant Physiol.* 155, 765–775. doi: 10.1104/pp.110.166272

Ariizumi, T., and Steber, C. M. (2011). Mutations in the F-box gene *SNEEZY* result in decreased Arabidopsis GA signaling. *Plant Signal. Behav.* 6, 831–833. doi: 10.4161/psb.6.6.15164

Aya, K., Ueguchi-Tanaka, M., Kondo, M., Hamada, K., Yano, K., Nishimura, M., et al. (2009). Gibberellin modulates anther development in rice via the transcriptional regulation of GAMYB. *Plant Cell* 21, 1453–1472. doi: 10.1105/tpc.108.062935

Berchowitz, L. E., and Copenhaver, G. P. (2008). Fluorescent *Arabidopsis* tetrads: a visual assay for quickly developing large crossover and crossover interference data sets. *Nat. Protoc.* 3, 41–50. doi: 10.1038/nprot.2007.491

Chen, N. A., Xu, Y., Wang, X. I. N., Du, C., Du, J., Yuan, M., et al. (2011). OsRAN2, essential for mitosis, enhances cold tolerance in rice by promoting export of intranuclear tubulin and maintaining cell division under cold stress. *Plant Cell Environ.* 34, 52–64. doi: 10.1111/j.1365-3040.2010.02225.x

Cheng, H., Qin, L., Lee, S., Fu, X., Richards, D. E., Cao, D., et al. (2004). Gibberellin regulates *Arabidopsis* floral development via suppression of DELLA protein function. *Development* 131, 1055–1064. doi: 10.1242/dev.00992

Colebrook, E. H., Thomas, S. G., Phillips, A. L., and Hedden, P. (2014). The role of gibberellin signalling in plant responses to abiotic stress. *J. Exp. Biol.* 217, 67–75. doi: 10.1242/jeb.089938

Cromer, L., Heyman, J., Touati, S., Harashima, H., Araou, E., Girard, C., et al. (2012). OSD1 promotes meiotic progression via APC/C inhibition and forms a regulatory network with TDM and CYCA1;2/TAM. *PLOS Genet.* 8:e1002865. doi: 10.1371/journal.pgen.1002865

De Storme, N., Copenhaver, G. P., and Geelen, D. (2012). Production of diploid male gametes in Arabidopsis by cold-induced destabilization of postmeiotic radial microtubule arrays. *Plant Physiol.* 160, 1808–1826. doi: 10.1104/pp.112.208611

De Storme, N., and Geelen, D. (2013a). Cytokinesis in plant male meiosis. *Plant Signal. Behav.* 8:e23394. doi: 10.4161/psb.23394

De Storme, N., and Geelen, D. (2013b). Sexual polyploidization in plants – cytological mechanisms and molecular regulation. *New Phytol.* 198, 670–684. doi: 10.1111/nph.12184

De Storme, N., and Mason, A. (2014). Plant speciation through chromosome instability and ploidy change: cellular mechanisms, molecular factors and evolutionary relevance. *Curr. Plant Biol.* 1, 10–33. doi: 10.1016/j.cpb.2014.09.002

d'Erfurth, I., Cromer, L., Jolivet, S., Girard, C., Horlow, C., Sun, Y., et al. (2010). The CYCLIN-A CYCA1;2/TAM is required for the meiosis I to meiosis II transition and cooperates with OSD1 for the prophase to first meiotic division transition. *PLOS Genet.* 6:e1000989. doi: 10.1371/journal.pgen.1000989

Dill, A., and Sun, T.-P. (2001). Synergistic derepression of gibberellin signaling by removing RGA and GAI function in *Arabidopsis thaliana*. *Genetics* 159, 777–785.

Eremina, M., Rozhon, W., and Poppenberger, B. (2016). Hormonal control of cold stress responses in plants. *Cell. Mol. Life Sci.* 73, 797–810. doi: 10.1007/s00018-015-2089-6

Francis, K. E., Lam, S. Y., Harrison, B. D., Bey, A. L., Berchowitz, L. E., and Copenhaver, G. P. (2007). Pollen tetrad-based visual assay for meiotic recombination in *Arabidopsis*. *Proc. Natl. Acad. Sci. U.S.A.* 104, 3913–3918. doi: 10.1073/pnas.0608936104

Jeon, J., and Kim, J. (2013). Arabidopsis response regulator1 and Arabidopsis histidine phosphotransfer protein2 (AHP2), AHP3, and AHP5 function in cold signaling. *Plant Physiol.* 161, 408–424. doi: 10.1104/pp.112.207621

Jeon, J., Kim, N. Y., Kim, S., Kang, N. Y., Novák, O., Ku, S.-J., et al. (2010). A subset of cytokinin two-component signaling system plays a role in cold temperature stress response in *Arabidopsis*. *J. Biol. Chem.* 285, 23371–23386. doi: 10.1074/jbc.M109.096644

Karimi, M., Ebadi, A., Mousavi, S. A., Salami, S. A., and Zarei, A. (2015). Comparison of CBF1, CBF2, CBF3 and CBF4 expression in some grapevine cultivars and species under cold stress. *Sci. Hortic.* 197, 521–526. doi: 10.1016/j.scienta.2015.10.011

Kazan, K. (2015). Diverse roles of jasmonates and ethylene in abiotic stress tolerance. *Trends Plant Sci.* 20, 219–229. doi: 10.1016/j.tplants.2015.02.001

Kohler, C., Mittelsten Scheid, O., and Erilova, A. (2010). The impact of the triploid block on the origin and evolution of polyploid plants. *Trends Genet.* 26, 142–148. doi: 10.1016/j.tig.2009.12.006

Kwon, C.-T., and Paek, N.-C. (2016). Gibberellic acid: a key phytohormone for spikelet fertility in rice grain production. *Int. J. Mol. Sci.* 17:794. doi: 10.3390/ijms17050794

Liu, B., De Storme, N., and Geelen, D. (2017a). Cold interferes with male meiotic cytokinesis in *Arabidopsis thaliana* independently of the AHK2/3-AHP2/3/5 cytokinin signaling module. *Cell Biol. Int.* 41, 879–889. doi: 10.1002/cbin.10805

Liu, B., De Storme, N., and Geelen, D. (2017b). Gibberellin induces diploid pollen formation by interfering with meiotic cytokinesis. *Plant Physiol.* 173, 338–353. doi: 10.1104/pp.16.00480

Locascio, A., Blázquez, M. A., and Alabadí, D. (2013). Dynamic regulation of cortical microtubule organization through prefoldin-DELLA interaction. *Curr. Biol.* 23, 804–809. doi: 10.1016/j.cub.2013.03.053

Mason, A. S., and Pires, J. C. (2015). Unreduced gametes: meiotic mishap or evolutionary mechanism? *Trends Genet.* 31, 5–10. doi: 10.1016/j.tig.2014.09.011

Novillo, F., Alonso, J. M., Ecker, J. R., and Salinas, J. (2004). CBF2/DREB1C is a negative regulator of *CBF1/DREB1B* and *CBF3/DREB1A* expression and plays a central role in stress tolerance in *Arabidopsis*. *Proc. Natl. Acad. Sci. U.S.A.* 101, 3985–3990. doi: 10.1073/pnas.0303029101

Novillo, F., Medina, J., and Salinas, J. (2007). *Arabidopsis* CBF1 and CBF3 have a different function than CBF2 in cold acclimation and define different gene

classes in the CBF regulon. *Proc. Natl. Acad. Sci. U.S.A.* 104, 21002–21007. doi: 10.1073/pnas.0705639105

Peng, J., Carol, P., Richards, D. E., King, K. E., Cowling, R. J., Murphy, G. P., et al. (1997). The *Arabidopsis GAI* gene defines a signaling pathway that negatively regulates gibberellin responses. *Genes Dev.* 11, 3194–3205. doi: 10.1101/gad.11.23.3194

Plackett, A. R., Ferguson, A. C., Powers, S. J., Wanchoo-Kohli, A., Phillips, A. L., Wilson, Z. A., et al. (2014). DELLA activity is required for successful pollen development in the Columbia ecotype of Arabidopsis. *New Phytol.* 201, 825–836. doi: 10.1111/nph.12571

Plackett, A. R. G., Thomas, S. G., Wilson, Z. A., and Hedden, P. (2011). Gibberellin control of stamen development: a fertile field. *Trends Plant Sci.* 16, 568–578. doi: 10.1016/j.tplants.2011.06.007

Plackett, A. R. G., and Wilson, Z. A. (2016). "Gibberellins and plant reproduction," in *Annual Plant Reviews*, Vol. 49, ed. S. Merchant (Hoboken, NJ: John Wiley & Sons), 323–358.

Qin, Q., Wang, W., Guo, X., Yue, J., Huang, Y., Xu, X., et al. (2014). *Arabidopsis* DELLA protein degradation is controlled by a type-one protein phosphatase, TOPP4. *PLOS Genet.* 10:e1004464. doi: 10.1371/journal.pgen.1004464

Rizza, A., Walia, A., Lanquar, V., Frommer, W. B., and Jones, A. M. (2017). In vivo gibberellin gradients visualized in rapidly elongating tissues. *Nat. Plants* 3, 803–813. doi: 10.1038/s41477-017-0021-9

Sakata, T., Oda, S., Tsunaga, Y., Shomura, H., Kawagishi-Kobayashi, M., Aya, K., et al. (2014). Reduction of gibberellin by low temperature disrupts pollen development in rice. *Plant Physiol.* 164, 2011–2019. doi: 10.1104/pp.113.234401

Salomé, P. A., Bomblies, K., Fitz, J., Laitinen, R. A. E., Warthmann, N., Yant, L., et al. (2011). The recombination landscape in *Arabidopsis thaliana* F_2 populations. *Heredity* 108, 447–455. doi: 10.1038/hdy.2011.95

Singh, G., Da Ines, O., Gallego, M. E., and White, C. I. (2017). Analysis of the impact of the absence of RAD51 strand exchange activity in Arabidopsis meiosis. *PLOS ONE* 12:e0183006. doi: 10.1371/journal.pone.0183006

Sun, T.-P. (2010). Gibberellin-GID1-DELLA: a pivotal regulatory module for plant growth and development. *Plant Physiol.* 154, 567–570. doi: 10.1104/pp.110.161554

Tian, Q., Lin, Y., Yang, M., Zhang, D., Lai, R., and Lai, Z. (2015). DlRan3A is involved in hormone, light, and abiotic stress responses in embryogenic callus of *Dimocarpus longan* Lour. *Gene* 569, 267–275. doi: 10.1016/j.gene.2015.06.013

Xu, H., Liu, Q., Yao, T., and Fu, X. (2014). Shedding light on integrative GA signaling. *Curr. Opin. Plant Biol.* 21, 89–95. doi: 10.1016/j.pbi.2014.06.010

Zhou, M., Chen, H., Wei, D., Ma, H., and Lin, J. (2017). *Arabidopsis* CBF3 and DELLAs positively regulate each other in response to low temperature. *Sci. Rep.* 7:39819. doi: 10.1038/srep39819

Conflict of Interest Statement: The authors declare that the research was conducted in the absence of any commercial or financial relationships that could be construed as a potential conflict of interest.

The reviewer NG and handling Editor declared their shared affiliation.

frontiers in Plant Science

REVIEW
published: 28 September 2018
doi: 10.3389/fpls.2018.01429

Anthropogenic Impacts on Meiosis in Plants

*Lorenz K. Fuchs, Glyn Jenkins and Dylan W. Phillips**

Institute of Biological, Environmental and Rural Sciences, Aberystwyth University, Aberystwyth, United Kingdom

As the human population grows and continues to encroach on the natural environment, organisms that form part of such ecosystems are becoming increasingly exposed to exogenous anthropogenic factors capable of changing their meiotic landscape. Meiotic recombination generates much of the genetic variation in sexually reproducing species and is known to be a highly conserved pathway. Environmental stresses, such as variations in temperature, have long been known to change the pattern of recombination in both model and crop plants, but there are other factors capable of causing genome damage, infertility and meiotic abnormalities. Our agrarian expansion and our increasing usage of agrochemicals unintentionally affect plants via groundwater contamination or spray drift; our industrial developments release heavy metals into the environment; pathogens are spread by climate change and a globally mobile population; imperfect waste treatment plants are unable to remove chemical and pharmaceutical residues from sewage leading to the release of xenobiotics, all with potentially deleterious meiotic effects. In this review, we discuss the major classes of exogenous anthropogenic factors known to affect meiosis in plants, namely environmental stresses, agricultural inputs, heavy metals, pharmaceuticals and pathogens. The possible evolutionary fate of plants thrust into their new anthropogenically imposed environments are also considered.

Keywords: anthropogenic, meiosis, recombination, plants, pollution, evolution

OPEN ACCESS

Edited by:
Tomás Naranjo, Complutense University of Madrid, Spain

Reviewed by:
Ahmad Arzani, Isfahan University of Technology, Iran
María-Dolores Rey, Universidad de Córdoba, Spain

***Correspondence:**
Dylan W. Phillips
dwp@aber.ac.uk

Specialty section:
This article was submitted to Plant Cell Biology, a section of the journal Frontiers in Plant Science

Received: *29 June 2018*
Accepted: *07 September 2018*
Published: *28 September 2018*

Citation:
Fuchs LK, Jenkins G and Phillips DW (2018) Anthropogenic Impacts on Meiosis in Plants. Front. Plant Sci. 9:1429. doi: 10.3389/fpls.2018.01429

INTRODUCTION

Humanity's impact on natural ecosystems is well documented and has led to a decline in biodiversity globally (Cardinale et al., 2012; Hautier et al., 2015). The anthropogenic drivers responsible for this are predominantly related to climate change and pollution that stem from the agricultural and industrial demand to support an ever-growing population. These factors are also known to effect cellular processes, meiosis being particularly vulnerable. The meiotic process is key for all sexually reproducing organisms as it is responsible for halving the chromosome number during gametogenesis and for the process of recombination which generates much of the genetic diversity. The biochemical processes underpinning meiosis are highly conserved but can be influenced by both abiotic and biotic stresses (Modliszewski and Copenhaver, 2017).

Atmospheric and terrestrial pollutants, and xenobiotic compounds (defined as any non-biological compounds that have a detrimental effect on the organism) are prevalent in the environment. The actual number of such compounds is difficult to ascertain accurately, but the United States Environmental Protection Agency currently lists over 85,000 substances on their Toxic Substances Control Act Chemical Substance Inventory (Donner et al., 2010; European Psychiatric Association [EPA], 2018[1]). The genotoxicity of such compounds on plants has been assayed using a variety of methods and a range of plants species including *Tradescantia paludosa*,

[1]https://www.epa.gov/tsca-inventory

Allium cepa, and *Vicia faba* (Kristen, 1997). The assays involve exposing plants to a known pollutant and assaying the number of chromosome aberrations induced. Initially, assays utilized root cells undergoing mitosis but it was later realized that meiotic cells were far more sensitive to such compounds (Kristen, 1997). The most widely used assay is the *Tradescantia* Micronucleus-in-Tetrad Assay for Environmental Mutagenesis, commonly referred to as the Trad-MCN assay (Rodrigues et al., 1997). The Trad-MCN assay detects micronuclei formed during meiosis, and has been used for *in situ* and *in vivo* laboratory tests to determine the genotoxicity of pollutants in the air, water and soil. The sensitivity of this assay is staggering; for example, plants exposed to various brands of air fresheners for between to 1–6 h results in a significantly higher number of micronuclei (Ma and Harris, 1987a,b). Such assays emphasize the sensitivity of meiosis to external factors.

In some instances, it is desirable to alter the meiotic process, and there has been a resurgence in interest to modulate the recombination landscape in crop plants in order to increase genetic variability for selection in advanced breeding programs. The benefit to plant breeding is clear, but for non-crop plants such destabilizing factors could be detrimental and could confer selective disadvantage. The aim of this review is to examine anthropogenic factors such as climate, agrochemicals, heavy metals, combustible gasses, pharmaceuticals and pathogens, which are known to influence meiosis in a range of plant species (summarized in **Table 1**).

ENVIRONMENTAL STRESSES

It is now generally accepted that human activity is responsible for climate change (International Plant Protection Convention [IPPC], 2014), which is manifested as a rise in global temperature and carbon dioxide levels, more extreme and unpredictable weather patterns, and a rise in sea levels with its concomitant increased risk of salinisation of ground water. These changes are very likely to challenge our agricultural productivity and threaten global food security. As a consequence, it is imperative that we understand the plant's response to abiotic stresses, as this will inform our strategies of intervention to protect and adapt future crops (Mickelbart et al., 2015). This section focusses upon the effects of environmental stresses on meiosis and recombination in some model, crop and non-crop species. It is pertinent to consider this process in this context, since recombination is fundamental to the fertility, genetic stability and genetic potential of sexually reproducing organisms.

Through exhaustive investigation, we now have a very good idea of how meiosis works (Wang and Copenhaver, 2018), and how external stresses may invoke certain adaptive and ameliorative responses in plants (De Storme and Geelen, 2014; Bomblies et al., 2015; Modliszewski and Copenhaver, 2017). Suboptimal high and low growth temperatures and their effects on modulating crossover (CO) frequency and distribution in plants have received particular attention, and have long been recognized in plants. In most instances, such adjustments in CO landscape have been inferred from observing chiasmata, the cytological equivalents of COs at metaphase I. Elliott (1955) showed that there was a reduction of CO frequency in meiosis in *Endymion nonscriptus* at 20°C but not between 1 and 15°C. These observations are not consistent with a subsequent study, which showed a consistent but gradual decrease in mean chiasma frequency with increasing temperature in this species (Wilson, 1959b). This difference could be explained by genetic and environmental influences beyond temperature. Dowrick (1957) recorded an increase in interstitial chiasmata with increasing temperature in *T. bracteata* and *Uvularia perfoliata*, Elliott (1955) showed a detrimental effect on chiasma frequency at 20°C in *Hyacinthus orientalis*, and Lin (1982) showed that chiasma frequency is reduced at 37°C in *Rhoeo spathacea*. A combination of water and temperature stress in two varieties of *Hemerocallis* induces desynapsis (Karihaloo, 1986, 1994). High temperature induces meiotic irregularities and diploid pollen formation in species of *Rosa* (Pecrix et al., 2011) and *Populus* (Wang et al., 2017; Tian et al., 2018), which is considered to have important implications in terms of adaptation and evolution through polyploidisation. Recombination frequencies in *Arabidopsis thaliana* are positively correlated with temperature over the range 19–28°C (Francis et al., 2007), but this response appears to be part of a U-shaped curve in which chiasma frequencies rise from a low at 18°C to higher values at both 8 and 28°C (Lloyd et al., 2018). The changes involve class I interfering COs only (Modliszewski et al., 2018), in contrast to the observations in barley (*Hordeum vulgare*) described below.

The studies above describe temperature effects on recombination in non-crop species. Whilst these have value in forwarding our knowledge and understanding of fundamental biological processes, they cannot substitute for studying these effects in the crops themselves, especially given the variation in responses of different plants, which confounds direct translation from one species to another. Unfortunately, there is a dearth of systematic studies of this phenomenon in crop plants, but several particular crops stand out. Prakken (1943) showed that high temperature and drought together exacerbated reduced bivalent formation in asynaptic rye, and Saini et al. (1984) showed that temperature and water stress together caused male sterility in wheat, but not through any demonstrable negative effect on meiosis. The latter contrasts with more recent observations, which show that heat stress induces meiotic chromosomal abnormalities in four wheat cultivars, and various changes in meiotic defects in some cereal crops (Rezaei et al., 2010; Omidi et al., 2014). Si et al. (2015) showed that some but not all rice (*Oryza sativa*) plants subjected to heat stress had higher recombination frequencies. Powell and Nilan (1963) described by cytology significantly higher chiasma frequencies at higher temperatures in an inversion heterozygote of barley. In contrast, Jensen (1981) used genetic mapping of barley to show that temperatures of 12, 18, and 24°C had no effect on recombination frequencies. Higgins et al. (2012) later reported that a rise in temperature not only increases the CO frequency, but also redistributes COs to more distal chromosomal locations. Since COs are highly distally localized

TABLE 1 | Summary of anthropogenic factors and their influence on meiosis.

Factor	Species	Phenotype*	Reference
Temperature	*Arabidopsis thaliana*	↑CO	Francis et al., 2007
	Hordeum vulgare	↑CO	Phillips et al., 2015
	Endymion non-scriptus	↓CO	Elliott, 1955
		↓CO	Wilson, 1959b
	Hyacinthus orientalis	↑↓CO	Elliott, 1955
	Oryza sativa	↑CO	Si et al., 2015
	Populus pseudo-simonii	St, L, M, PM, Sp	Wang et al., 2017
	Rhoeo spathacea	↓CO	Lin, 1982
	Rosa spp.	Sp	Pecrix et al., 2011
	Tradescantia bracteata	↑CO	Dowrick, 1957
	Triticum aestivum	PM, L, M	Omidi et al., 2014
	Uvularia perfoliata	↑CO	Dowrick, 1957
Water stress	*Zea Mays*	↑CO	Verde, 2003
	Oryza sativa	U, L, M	Namuco and O'Toole, 1986
	Sesbania cannabina	PM, U, L	Srivastava and Kumar, 2016
	Hemerocallis	M	Karihaloo, 1986
		M	Karihaloo, 1994
Salinity	*Arabidopsis thaliana*	↑CO	Boyko et al., 2006
		↑CO	van Tol et al., 2018
Nutrient solution	*Gilia millefoliata* × *G. achilleaefolia*	↑CO, ↓B	Grant, 1953
	Solanum lycopersicum	↑CO	Griffing and Langridge, 1963
	Triticum aestivum (-Ph1)	↑CO	Martín et al., 2017
Potassium	*Lolium temulentum*	↑CO	Law, 1963
	Pennisetum glaucum	↑CO	Dhesi, 1975
Phosphate	*Secale cereale*	↑CO	Bennett and Rees, 1970
	Hordeum vulgare	↑CO	Fedak, 1973
	Pennisetum glaucum	↑CO	Dhesi, 1975
	Festuca pratensis (2x and 4x)	↓M	Deniz and Tufan, 1998
	Arabidopsis thaliana	↑↓CO	Barth et al., 2000
Nitrogen	*Secale cereale* (4x)	↑Bivalent	Hossain, 1978
Herbicide	*Hordeum vulgare*	St, B, M	Wuu and Grant, 1966
		St, B, F, M	Wuu, 1967
		↓CO	Sharma et al., 1981
	Sorghum vulgare	A, Sp	Liang et al., 1969
		A, Sp, U	Lee et al., 1974
		A, B, L	Soriano, 1984
		Multiple nucleoli, PM	Currie and Liang, 1996
	Vicia faba	St, L, B, M, A	Amer and Ali, 1974
		St	Badr et al., 1987
	Triticum durum	B, L	Razu et al., 2014
Insecticide	*Hordeum vulgare*	St, B, F, M	Wuu, 1967
	Vicia faba	St, B, L	Amer and Ali, 1968
		St, B, L	Amer and Farah, 1968
		St, B, L, Sp	Amer and Farah, 1976
		St, B, F, L, U, Sp, M	Amer and Farah, 1980
		St, L, B	Amer and Farah, 1983
		St, B, F	Amer and Farah, 1987
	Capsicum annuum	St, B, L, Sp, M	Devadas et al., 1986
		St, B, L, M, U	Reddy and Rao, 1981
		↓CO, S, B, L, U, M	Lakshmi et al., 1988
	Allium cepa	St, B, L, PM	Kuchy et al., 2016

(Continued)

TABLE 1 | Continued

Factor	Species	Phenotype*	Reference
Fungicide	*Hordeum vulgare*	St, B, F, M	Wuu, 1967
		↓CO	Bennett, 1971
		↓CO	Sharma et al., 1983
	Allium cepa	St, B, F, M	Mann, 1977
		St, B, L, M	Fisun and Rasgele, 2009
		St, B, L, PM	Kuchy et al., 2016
	Pisum sativum	↑↓CO	Choudhary and Sajid, 1986
	Capsicum annuum	St, B, L, U, multivalents	Prakash et al., 1988
	Lathyrus sativus	S, B, L, F, U	Kumar and Sinha, 1991
Heavy Metals	*Glycine max*	St, L, U, B, PM	Kumar, 2007
	Zea mays	PM, B, L, U, F, M	Kumar and Rai, 2010
	Vicia faba	St, L, B	George, 2000
	Hordeum vulgare	PM, L, B, M	Mittal and Srivastava, 2014
	Lathyrus sativus	U, ↓CO	Kumar and Ritambhara, 2006
		St, Sp, L	Tripathi and Girjesh, 2010
	Capsicum annuum	St, PM, L, B, F, M	Aslam et al., 2017
	Vicia faba	S, St, L, B	George, 2000
Caffeine	*Secale cereale*	L, B, ↓CO	de la Peña et al., 1981
	Trigonella foenum-graecum	L, B, U, St, PM	Anis and Wani, 1997
Pathogen	*Oryza sativa*	↑CO	Si et al., 2015
	Carica papaya	L, B, U	Pandey, 2017
	Datura quercifolia	↓CO, U, L, M	Kaul, 1968
	Solanum lycopersicum	PM, A	Caldwell, 1952
	Capsicum annuum	↓CO, Sp	Swaminathan et al., 1959
	Lycopersicon esculentum	B, PM, M, F	Andronic, 2012
	Hordeum vulgare	B, PM, L	Andronic, 2012
Antibiotics	*Allium cepa*	St, L, P, B, F	Mann, 1978
	Lathyrus sativus	U, St, B	Kumar and Sinha, 1991

**CO, change in crossover rate; St, stickiness; L, laggards; B, bridges; F, fragments; U, univalents; A, aneuploidy; M, micronuclei; PM, precocious movements; Sp, spindle aberrations. ↑ denotes increase, ↓ denotes decrease.*

in this species, this phenomenon has important implications for cracking open tight linkage groups, which are otherwise refractory to recombination events. These observations were confirmed by a subsequent study (Phillips et al., 2015), which went on to show that high temperature increases only class II CO frequency in male meiosis, and also demonstrated that interstitial regions of the genome are more prone to these changes. There is a tantalizing prospect, therefore, that simple heat shocking of barley at vulnerable stages of development could release potentially useful genetic variation for use in advanced breeding programs. However, this is predicated upon a greater understanding of the genetic (see review by Wang and Copenhaver, 2018) and epigenetic processes (reviewed by Yelina et al., 2015) underpinning these effects, which could ultimately enable the precise reprogramming of the crop.

The variation in response to temperature, even within the same species, may indicate that there is plasticity in the mechanisms governing CO control, or may implicate alternative pathways with different mechanisms. A caveat is that these differences may simply reflect discrepancies in the methods used to acquire and compare data, as has been inferred by (Wilson, 1959a; Bomblies et al., 2015; Lloyd et al., 2018).

Whilst temperature effects on recombination are the most widely described in the literature, there is some information describing other abiotic factors of relevance to climate change. Water stress has been shown to cause meiotic chromosome abnormalities in rice, such as laggards, micronuclei, univalents and a partial arrest of meiosis at severe stress levels (Namuco and O'Toole, 1986). In water stressed barley, abnormal chromosomal pairing and segregation during meiosis was found, leading to loss of pollen fertility (Skazkin and Zavadskaya, 1957). Cytological studies in *Sesbania* pea found that waterlogging stress resulted in various chromosomal aberrations and a reduction in pollen fertility (Srivastava and Kumar, 2016). Verde (2003) has also presented evidence that meiotic recombination increases in response to droughting in two genotypes of maize (*Zea mays*). van Tol et al. (2018) detected a 70% increase in recombination frequency between markers in response to salt stress of *Arabidopsis,* and genotyping revealing that CO fluctuation was not limited to the region between the marker genes but occurred throughout the genome. Modliszewski et al. (2018) did not detect the same effect under similar conditions in the same species. Considering that elevated CO_2 levels is one of the most prominent causes of climate change, it is surprising that little research has been conducted to examine its influence

on meiosis. Koti et al. (2005) showed no effect of elevated CO_2 on pollen viability in *Glycine max*, inferring that meiosis was also unaffected.

AGRICULTURAL INPUTS

Innovations that emerged during the 'Green Revolution' led to a steady rise in agricultural output across the globe (Tilman et al., 2002). These gains were driven principally by the development of new crop varieties and through the increased use of inputs, namely synthetic fertilizer and pesticides. The benefits of these inputs to crop productivity are clear and well documented, as are the negative impacts on the adjoining environment. Agricultural pollutants can influence natural non-target plant populations in close proximity via direct contact (e.g., spray drift), or may affect a much larger area via groundwater contamination (Moss, 2008).

FERTILIZER

The global demand for fertilizer nutrients (N, P_2O_5, and K_2O) has increased steadily since the 1960s, and is predicted to increase from 184.02 million tons in 2015 to over 200 million tons in 2020 (Food and Agriculture Organization [FAO], 2017). It has long been recognized that nutrient state influences meiotic processes. One of the first studies used a sterile F_1 hybrid between *Gilia millefoliata* and *G. achilleaefolia,* and observed that plants grown in rich loam had consistently higher bivalent frequencies, more chiasmata per bivalent on average, and fewer anaphase bridges than those grown in sand (Grant, 1953). Later, Griffing and Langridge (1963) determined the optimal growth conditions for elevated levels of recombination in tomato, a key component in commercial breeding programs. They observed that the CO frequency for a known interval decreased from 17 to 6% over a 6 months period during which no additional fertilizer was supplied. Subsequent addition of fertilizer restored the CO frequency to 12%, implying that nutrient-rich conditions enhance the rate of CO (Griffing and Langridge, 1963).

Subsequent investigations used a more systematic approach in order to isolate particular components, which had the greatest influence on meiosis. In an early example of such an approach, Law (1963) determined the influence of high and low concentrations of potassium and calcium on chiasma frequency in *Lolium temulentum* grown at both 20 and 30°C. High potassium increased chiasma frequency at both temperatures, and reduced its variance in the high temperature regime (Law, 1963). Bennett and Rees (1970) observed subsequently the same phenomena in rye (*Secale cereale*) grown under high phosphate conditions, recording higher chiasma frequencies and lower variance compared with controls. One of the most detailed studies of the effects of phosphate was conducted in *Arabidopsis* by comparing the recombination rate between pairs of genes conferring resistance to kanamycin and hygromycin (Barth et al., 2000). Under 10-fold higher levels of phosphate, recombination between loci on chromosomes 1 and 2 was significantly reduced, whilst intervals on chromosomes 4 and 5 showed minor, non-significant increases in recombination.

High phosphate also has a notable effect on a desynaptic barley mutant, enhancing the formation of chiasmata to 10.6 per cell compared to 7.7 for the control (Fedak, 1973). In a subsequent study, Dhesi (1975) noted a significant increase in chiasmata at metaphase I in a desynaptic mutant of pearl millet (*Pennisetum glaucum*) subjected to elevated levels of phosphate or potassium. However, elevated phosphate does not influence recombination in all species, such as soybean (*G. max*) (Hanson, 1961).

All of the studies described above used diploid plant species. However, Grant (1953) reported that bivalent frequency dramatically increases in a neoallotetraploid formed from the hybridisation between *G. millefoliata* and *G. achilleaefolia* when watered with a solution of mineral nutrients. Autotetraploid rye grown in Hoagland's solution II containing nitrogen has a higher quadrivalent frequency, at the expense of bivalent formation, and the same number of chiasmata compared to plants grown without nitrogen (Hossain, 1978). More recently, Hoagland's solution has also been shown the significantly increase CO formation in wheat and wheat-rye hybrids lacking the *Ph1* locus, which suppresses COs between homoeologs (Martín et al., 2017). A subsequent study showed that the magnesium in the Hoagland's solution was responsible for the observed phenotype (Rey et al., 2018).

PESTICIDES

Crop protection agrochemicals are another cornerstone of modern agriculture and are essential for minimizing yield losses. In 2015 alone, a total of 2,752,759 tons of active product was applied to crops globally, predominantly as herbicides, fungicides, and insecticides (Food and Agriculture Organization [FAO], 2018[2]). The influence of each of these pesticides groups on meiosis has been assessed (Sharma and Panneerselvam, 1990) and key examples are highlighted below.

One of the earliest studies to examine the influence of herbicides on meiosis was conducted by Wuu and Grant (1966). Barley seeds were soaked in 3-(3,4-dichlorophenyl)-1-methoxy-1-methylurea for 24 h prior to sowing, and meiocytes collected from the treated plants were analyzed cytologically. The authors documented numerous defects such as chromatin bridges, micronuclei, and asynchronous division. Sharma et al. (1981) examined the influence of three additional herbicides, bromacil, lenacil, and terbacil, all applied to barley seed at various concentrations for 6 h. Treatment with terbacil significantly reduced the chiasma frequency and was as disruptive as ethyl methanesulfonate (EMS), which was included as a control compound. The susceptibility of meiosis in *V. faba* to 2, 4, 5-trichlorophenoxyacetic acid (2,4, 5-T), 2, 4-dichlorophenoxyacetic acid (2, 4-D) and 2, 4-dichlorophenol, an intermediate product in the degradation pathway of 2, 4-D, was assessed by Amer and Ali (1974). The compounds were applied to both seed and sprayed onto 15 and 35 days old plants. Treatment at 35 days with 2, 4, 5-T led to the highest levels of sterile pollen grains resulting from stickiness, lagging chromosomes, and chromosome fragmentation during meiosis.

[2]http://www.fao.org/faostat

Badr et al. (1987) reported terbutryn also induced chromosomal abnormalities in 11.3% of cells undergoing meiosis in *V. faba*.

Liang et al. (1969) sprayed sorghum (*Sorghum vulgare*) plants that ranged between 5 and 20 cm in height with atrazine (2-chloro-4-ethylamino-6-isopropylamino-s-triazine), 2,4-D, alkanolamine salts of 2,4-D, and non-phytotoxic petroleum oil (crop oil), or their combinations. All increased the level of cytological aberrations at meiosis, including inducing aneuploidy and polyploidy. Two further studies assessed the influence of atrazine on meiosis in sorghum. Lee et al. (1974) also found a high degree of meiotic abnormalities in atrazine-treated sorghum, while a subsequent study noted more subtle changes to the meiotic nuclear landscape; additional nucleoli were frequently observed at diplotene and early diakinesis in treated plants (Currie and Liang, 1996). Soriano (1984) also reported the influence of a herbicide, whose active ingredient is N-(butoxymethyl)-2-chloro-2′, 6′-diethyl-acetanilide, applied at concentrations of 0.05–0.20% to sorghum seed. The lowest concentration induces aneuploidy in 2.9% of metaphase I cells, increasing to 8.8% at the highest concentration, compared to 0% in untreated plants. Interchanges, bridges and fragmentation were observed during meiosis I only at the higher concentrations.

The herbicide maleic hydrazine was applied to seed of *Helianthus annuus* at concentrations of 10^{-5} M to 10^{-2} M to determine its meiotic influence (Kaymak, 2005). This study reports not only a significant increase in abnormalities during both the first and second meiotic divisions, even at the lowest concentration tested, but also identifies a significant degree of abnormalities in the subsequent generation. A more recent study by Singh and Srivastava (2014) tested the effect of glyphosate and pendimethalin applied to the foliage of *Vigna mungo* 21 days from the point of sowing. They noted numerous defects, including chromatin bridges, laggards at anaphase I, disturbed spindle formation and binucleate cells in 17% and 21% of pollen mother cells (PMCs) treated with pendimethalin and glyphosate, respectively.

The influence on meiosis of a wide range of insecticides has been assayed in *V. faba* (Amer and Farah, 1968, 1976, 1980, 1983; Amer and Ali, 1983). In one of the earliest studies, Amer and Farah (1968) applied *N*-methyl-1-naphthyl-carbamate over various timeframes. After a single application, 8.7% of PMCs contained an aberration at diakinesis and metaphase I, compared to 1% in the control, rising to 23% if applied daily over a 7-day period. Defects were also later observed at anaphase I, metaphase II, and anaphase II (Amer and Farah, 1968). In *V. faba* both *O*,*O*-dimethyl-*N*-methyl-carbamidomethyl dithiophosphate and *O*-isopropyl-*N*-phenyl carbamate applied to seed prior to planting or sprayed (on day 15 or 35) induced multipolar anaphase II, along with a host of other types of meiotic abnormalities, the effects of which did not influence the yield phenotype of the successive two generations (Amer and Farah, 1976). One of the most profound effects was noted for the organophosphate insecticide chlorpyrifos (0,0-diethyl 0-3, 5, 6-trichloro-2-pyridyl phosphorothioate). When applied as a spray to seedlings or at the flowering stage the result was the same; chromosome stickiness was observed in more than 80% of the abnormal meiocytes (Amer and Farah, 1983). A single application during flowering of another organophosphate, methamidophos (0,*S*-dimethyl phosphoramidothioate), was sufficient to significantly increase the number of abnormal PMCs to 8.4%, compared to 1% in the control (Amer and Farah, 1987). Repeat application exacerbates the effect, causing abnormalities in 21% of PMCs.

The meiotic influence of four organophosphorus insecticides applied to *Capsicum annuum* was assessed by Devadas et al. (1986). The insecticides, namely dimethoate, DDVP, phosphomidon and monocrotophos were applied to seed at concentrations of 0.1, 0.5, and 1.0% for 24 h. Each treatment depressed pollen viability, with the degree of sterility rising with increasing concentration. The sterility is caused by univalents, multivalents, bridges, lagging chromosomes, non-synchronization, multipolar formation, micronuclei, unoriented and unequal disjunction of chromosomes identified in the preceding meiosis. The authors also claim that the insecticides tested are as disruptive as ionizing radiation. Reddy and Rao (1981), also working with *C. annuum*, focused on two different compounds, BHC and Nuvacron, the latter being a organophosphorus systemic and contact insecticide. The compounds were applied at a range of concentrations to both the seed and sprayed on plants at fortnightly intervals. Both were found to induce abnormalities during meiosis, ranging from 3.1 to 5.6% for BHC and 7.7–15.6% for Nuvacron. The authors note that the lowest concentration is favored by Indian farmers at the time of publication. A later study by Lakshmi et al. (1988) examined the influence of Ekalux EC 25 [0-diethyl-o-(quinoxylinyl-2) phosphorothionate] and Metasystox (oxydemeton-methyl = S-(2(ethyl-sulphinyl)-ethyl) & 0, 0-dimethyl phosphorothioate), applied to seed of *C. annuum* followed by four spray applications during growth. This study is one of few to score chiasma frequency, and noted a steady decline in COs with increasing concentration of each insecticide. COs were reduced to the lowest number of 21.08 for Ekalux EC 25 and 20.5 for Metasystox, compared to 23 in the control. Other meiotic defects including laggards, bridges, stickiness and univalents were also noted in this study.

Kuchy et al. (2016) examined the effects on *A. cepa* of an organophosphate insecticide containing dichlorvos (2,2-dichlorovinyl dimethyl phosphate) and a organochlorine insecticide, endosulfan. The organophosphate compound was the most potent at inducing abnormalities, affecting 11–27% of PMCs depending upon which concentration was applied, compared to 3% in the control. Endosulfan also caused numerous meiotic failures, with 9–20% PMCs containing defects, depending upon the concentration used. The most common abnormality observed was stickiness at metaphase I and II.

One of the earliest investigations of the influence of fungicides on meiotic recombination was conducted by Bennett (1971) who tested Ethirimal (5-butyl-2-ethylamino-4-hydroxy-6-methyl pyrimidine), a systemic compound applied as a seed dressing in barley. The mean chiasma frequency in each of three cultivars was significantly reduced to 2–4% lower than the control. A later study in the same species showed that the systemic fungicides fuberidazole, carboxin, and oxycarboxin (but not thiabendazole) all significantly reduced chiasma frequency (Sharma et al., 1983).

Carboxin and oxycarboxin has an effect even at the lowest concentration tested.

The transgenerational effect of the fungicide carbendazim (2-methoxy-carbamoyl benzimidazole), was studied in two different cultivars of *Pisum sativum* (Choudhary and Sajid, 1986). Plants were sprayed four times during development with the recommended dose of 0.2% aqueous solution, and at 0.4%. Both concentrations significantly altered the chiasma frequency, with one cultivar being more susceptible, implying a genotypic interaction with the fungicide. The subsequent two generations of the treated plants, which received no further applications of fungicide, also had a significantly altered CO landscape, one cultivar having fewer COs contrasting with the second which had more. Abnormalities such as stickiness, fragmentation and micronuclei, were also observed in PMCs of *A. cepa* treated with either one of four different Dithane based fungicides or treated with carbendazim (methyl-2-benzimidazole carbamate-MBC) (Mann, 1977; Kuchy et al., 2016). Fisun and Rasgele (2009) treated *A. cepa* bulbs with roots 1.5–2 cm in length with different concentrations (1800–6000 ppm) of the fungicide tebuconazole, for 3–24 h. All treatments resulted in a significant increase in meiotic abnormalities, including a significant increase in the number of quadrivalents, believed to be a result of chromosome translocations.

OTHER ANTHROPOGENIC INFLUENCES

Whilst environmental stresses and agricultural pollutants commonly affect meiosis in plants, there are also a number of other anthropogenic factors that can have a similar effect. As the human population increases and encroaches upon the global natural environment, the trail of anthropogenic influences grows commensurately. Increasing agricultural and industrial developments expose plant populations to new and different chemical and physical agents and places them in environments that can potentially alter their development. There is greater pollution from industrial and automotive combustion, commercially and pharmaceutically used solvents, additives, chemicals and an increase in pathogen prevalence worldwide (Evans et al., 2008; Gaffney and Marley, 2009; Tornero and Hanke, 2016).

HEAVY METALS AND COMBUSTED GASSES

Heavy metal contamination of the environment is increasing due to human activity, with many sources of pollution primarily entering water courses and polluting the land. The accumulation of heavy metals and metalloids in soil also originate from other sources, such as emissions from industrial areas, leaded fuels and paints, sewage sludge, biosolids, animal manures, spillage of petrochemicals and combustion residues (Khan et al., 2008; Zhang et al., 2010).

Samples of agricultural soils from the siling reservoir watershed in Zhejiang Province and an area of north east China that has been of intensively farmed for decades were found to contain high levels of cadmium contamination (Naveedullah et al., 2013; Shan et al., 2013). At some metalliferous sites there can be 100 times elevated metal concentrations in the soil compared with uncontaminated areas (Bert et al., 2002). Soil samples from agricultural areas of Jiaxing, a rapidly industrializing area in the Yangtze Delta of China, has localized hot spots of pollution of copper, zinc, lead, chromium, nickel and cadmium (Xu et al., 2014). The concentrations of the heavy metals lead, copper, cadmium, and zinc can be further increased by urban runoff or combustion sources, and copper, chromium and tin levels even further increased by automobile break and tire wear (Davis et al., 2001; Hulskotte et al., 2007; Shan et al., 2013). Another surprising pollution source are shooting ranges as the soil there often has higher levels of antimony, nickel, lead, copper and zinc and can be used for animal grazing when not in use or decommissioned (Robinson et al., 2008; Bannon et al., 2009).

There may be no cause for concern for some current levels of heavy metal contamination of the soil, and potentially the food chain, as they may often be below the acceptable thresholds for safe human consumption. There is, however, reason to investigate what effects they may have on the recombination landscape of the plants and crops that grow in these areas, as heavy metals are known to effect plant development in a number of ways. *Arabidopsis* plants treated with 50 or 100 mM copper, cadmium or nickel have at least a twofold increase in somatic homologous recombination frequency with successive treated generations exhibiting even higher increases (Rahavi et al., 2011). This study also found that the subsequent generation, which was not exposed to any stress, still possessed significantly higher residual rates of recombination when compared to the non-exposed progeny. Further studies found that chromosomal abnormalities, including chromosomal bridges, scattering and precocious movements occurred in *G. max* and *Z. mays* when treated with cadmium (Kumar, 2007; Kumar and Rai, 2010). Similar results were found when *H. vulgare* was treated with a combination of cadmium and chromium. This combination treatment also resulted in a significant decrease in the number of pollen grains per anther and a significant increase in pollen sterility (Mittal and Srivastava, 2014).

Although the current known levels of heavy metals found in soils due to anthropogenic influences may not be enough to modify the recombination landscape alone, there are other agents, such as anthropogenic gasses, that are known to have detrimental effects on plants. A cytogenetic test based upon quantifying micronuclei resulting from chromosome breakage in meiotic pollen mother cells *T. paludosa* (Trad-MCN) has found that various anthropogenic gasses such as NO_2, SO_2, O_3, HN_3, and EMS have clastogenic effects. Both gaseous HN_3, and EMS were clastogenic after 6 h exposures while SO_2 and NO_2 required 22 and 24 h, respectively (Ma et al., 1982; Rodrigues et al., 1996). Several indoor environments containing pipe and tobacco smoke, and formaldehyde fumes were found by the Trad-MCN assay to cause chromosomal breakage, as well as several outdoor locations such as parking garages, truck and bus stops, agrochemical industrial sites, a P-dichlorobenzene treated

herbarium and an industrial site (Ma et al., 1980, 1982; Ma and Harris, 1987a,b). Although this only shows that *T. paludosa* can be clastogenically affected by anthropogenic environments, it emphasizes the unintended consequences of human activities.

Heavy metals and combusted gasses in the environment are not the only anthropogenic sources that could change the recombination landscape of crops around the world; there are also large amounts of pharmaceutical chemicals that pass into the environment and to the soil.

PHARMACEUTICAL CHEMICALS

As pharmaceutical drug use increases worldwide, there is growing concern for the high level of pharmaceutical residues in aquatic environments (Uslu et al., 2013). Treatment plants are not always able to remove pharmaceutical residues from sewage completely and often release amounts into the receiving waters (Heberer, 2002; Gaw et al., 2014; Küster and Adler, 2014; Zhang et al., 2016). While a large part of the concern comes from the potential of these residues to affect aquatic life and enter the drinking water supply, there is justification to question the effects they could have on plant life when treated biosolids are applied to agricultural land.

Extremely low levels of the anti-cancer drug bleomycin, known to cause an increase in DSBs and increased somatic recombination, have been found at concentrations of 11 – 19 ng/L and <5–17 ng/L in sewage treatment effluent and rivers, respectively (Aherne et al., 1990). Whilst these doses are well below the normal chemotherapeutic doses administered (20–30 mg/m^{-2}), data are sparse concerning the bioaccumulation of bleomycin or the amount that it is used worldwide. Qi et al. (2014) showed that 98 tons of pesticides, 152 tons of pharmaceuticals, 369 tons of polycyclic aromatic hydrocarbons and 273 tons of household and industrial chemicals are flushed annually into the East China Sea by the Yangtze river. This level of pollution could potentially affect meiotic recombination in plants, but virtually no investigations have been undertaken. The recent significant increase in drug-resistant bacterial strains is often attributed to the indiscriminate use of antibiotics by today's society. However, there should perhaps also be concern about the bioactivity of waste antibiotics in the environment. Some antibiotics in water courses and agricultural land are known to affect plants. For example, ciprofloxacin has been found in municipal waste water (Lee et al., 2007) and in soil samples (Golet et al., 2002; Goulas et al., 2016) and is known to cause double strand DNA breaks in *Arabidopsis*, (Rowan et al., 2010). Ciprofloxacin's bactericidal action comes from the inhibition of topoisomerase II (DNA gyrase) and topoisomerase IV, required for various bacterial DNA processes including replication, transcription, repair, strand supercoiling repair, and recombination (Aldred et al., 2014), and a recent study found that ciprofloxacin targets *A. thaliana* gyrase (Evans-Roberts et al., 2016). Tetracycline has been shown to induce meiotic aberrations including stickiness, laggards, bridges, and fragments in *A. cepa* (Mann, 1978), and has been found in soil fertilized with liquid manure and in soil and water near intensive commercial livestock operations (Hamscher et al., 2002; Thiele-Bruhn, 2003).

The increase in anthropogenic chemicals in the environment is not limited to pharmaceuticals, but also applies to chemicals resulting from human consumption. Caffeine can be found in soil due to the reuse of treated wastewater for irrigation (Bruton et al., 2010; Williams and McLain, 2012). Anis and Wani (1997) found that caffeine-treated populations of *Trigonella foenum-graecum* exhibited several meiotic abnormalities including laggards, univalents, bridges, stickiness, and precocious chromosome movements. A 0.1% caffeine solution was administered to *S. cereale* and abnormalities such as laggards, bridges and fragments and decreased chiasma frequency were observed (de la Peña et al., 1981). The widely used chemical bisphenol A (BPA) affects microtubule arrays of meristematic root-tip cells of *P. sativum* resulting in the stalling of cytokinesis, deranged interphase and mitotic microtubule arrays, and abnormal chromosome segregation (Adamakis et al., 2013).

PATHOGENS

The full impact climate change will have on the prevalence and spread of virus disease epidemics in natural vegetation and cultivated plants and crops is still unknown. Research suggests that elevated environmental CO_2 levels can alter hormone production in plants and precipitate the observed shift in susceptibility to insect herbivores and pathogens (Casteel et al., 2012; Zhang et al., 2015). Whilst research to understand the possible effects of some common climate change scenarios is ongoing, reviewed extensively in Jones (2016) and Trebicki et al. (2017), we still do not know what impact climate change may have on the recombination landscape of plants. Climatic changes are compounding the threat of spread of plant pest and diseases. A recent analysis indicated that crop pests are moving 2.7 km poleward annually and that on average, 10% of the major plant pests and disease agents have already infested half of the countries that they potentially could infect (Bebber et al., 2013, 2014). *Carica papaya* infected with papaya ring spot virus exhibited an increase in laggard chromosomes, and had a lower mitotic index and worse pollen viability compared to its healthy counterpart (Kumar Ravindra, 2017). Infection of *Arabidopsis* with the oomycete pathogen *Peronospora parasitica* has been shown to lead to an increase in somatic recombination frequency (Lucht et al., 2002). Interestingly, when Molinier et al. (2006) treated *Arabidopsis* with flagellin, an elicitor of plant defenses, they found that not only did somatic homologous recombination increase in the treated individual but also in successive generations. *Nicotiana tabacum* treated with the tobacco mosaic virus behaves in a similar way; somatic recombination increased in both the subject and its offspring, with one study showing that the offspring even exhibited a delay in symptom development when infected with viruses (Kovalchuk et al., 2003; Kathiria et al., 2010). Si et al. (2015) found that in some of the F_2 generation of *O. sativa* treated with rice blasts spores there was a significantly higher number of CO events compared to the controls. *Datura quercifolia* treated with mosaic virus resulted in a drastic decrease

in chiasma frequency, and the presence of univalents led to many irregularities such as laggards, micronuclei and a significant reduction in pollen and seed fertility (Kaul, 1968). Caldwell (1952) noted that *Solanum lycopersicum* treated with mosaic virus led to the breakdown of meiosis and in some instances cells forming with an irregular number of chromosomes. Yao et al. (2013) found that a local infection of either tobacco mosaic virus or oilseed rape mosaic virus leads to a systematic increase in somatic homologous recombination frequency, with older plants having a higher recombination frequency than younger plants. *Lycopersicon esculentum* and *H. vulgare* infected with barley stripe mosaic virus exhibited an increase in various chromosome abnormalities and a shift in chiasmata toward the interstitial regions (Andronic, 2012). Anthropogenic influences resulting in a changing climate can lead to an increased level of viral vectors and more disease epidemics in plants worldwide, but they could also be enough to change the meiotic recombination landscape forever.

LIMITATIONS OF CURRENT STUDIES

As outlined above, there is a wide range of anthropogenic factors that have been shown to cause various meiotic abnormalities. In the vast majority of cases, the precise biochemical action induced by the treatment during meiosis has not been ascertained; temperature is the notable exception (see earlier section for detail). Many studies reported abnormal meiocytes with chromosome stickiness, bridges, fragmentation and micronuclei. However, it is yet to be determined if the factors themselves are clastogenic and cause DNA damage directly, or whether they interfere with the repair of double strand breaks (DSBs) formed naturally during prophase I. Cytology of fixed meiotic material was by far the most prevalent method of determining the extent of meiotic abnormalities induced by each treatment, and in most studies only gross changes were recorded. More subtle influences, such as changes in chiasma frequency at metaphase I, were recorded in only approximately a third of the studies summarized in **Table 1**. The scoring of chiasmata is not sensitive and cannot detect small changes in recombination frequency, making it likely that more subtle effects at the lower concentration range were not detectable.

The biochemical pathways affected by these treatments may be elucidated by studies in non-plant species. Allard and Colaiacovo (2010) used *Caenorhabditis elegans* to analyze the meiotic molecular pathways affected by BPA. They showed that BPA perturbs both synaptonemal complex and chromosome integrity during pachytene, and also alters DSB repair progression and activation of the DNA damage checkpoint. The effect of the herbicide atrazine on meiosis has been studied in both male and female mice (Gely-Pernot et al., 2015, 2017). In male mice, atrazine reduced sperm count by 68%, caused by a delay in meiotic progression arising from the persistence of unrepaired DSBs (Gely-Pernot et al., 2015). The study also found that the herbicide affects the expression of genes involved in mitochondrial function, steroid-hormone function and GTPase activity, and also altered the pattern of histone H3 trimethylation at lysine 4 (H3K4me3). A subsequent study switched focus to female meiosis and found that atrazine increased the level of oxidative stress in the nuclei of meiotic cells, as measured by the level of 8-oxo-guanine, which affected DBS repair, synapsis and CO frequency (Gely-Pernot et al., 2017).

Another shortcoming of most published studies is that the concentrations of the chemical treatments used cannot be related to those used in agriculture or experienced by plants in natural environments. The biological significance, in terms of potential threat to the meiotic process, is therefore difficult to ascertain. Taking agricultural inputs as an example, a number of agrochemicals have been subsequently banned or their application drastically reduced. The persistence of these substances in the environment also varies, and may have the potential to affect plant communities long after their last application. For example, atrazine was first introduced as a herbicide in 1958 but was subsequently withdrawn from use in most Northern European countries in the early 1990s, and banned from the whole European Union in 2004. Traces of atrazine are still detectable in soil sampled from agricultural land in Germany where the last application was prior to 1991, and in marine sediments of the Mediterranean (Noedler et al., 2013; Vonberg et al., 2014).

In the majority of studies cited, only one treatment was applied to a single plant species that was grown under controlled conditions. This is starkly different to reality where multiple xenobiotics, abiotic and biotic stresses may impact together in one environment. To date, only one published study examines the impact on meiosis of plant species growing in polluted environments. Zohair et al. (2012) sampled 14 species belonging to the Cyperaceae and Poaceae growing in the vicinity of industrial sites and agricultural fields around Karachi, Pakistan, and compared them with their counterparts in unpolluted environments. All of the plant species collected from the contaminated sites had significantly higher numbers of aberrant PMCs with precocious movement, stickiness, aberrant spindles or lagging chromosomes. The prevalence of abnormal PMCs varied greatly between species; the largest effect was observed in *Cyperus arenarius* where 99% of PMCs contained defects, compared to 13% for the control, contrasting with *Ochtochloa compressa* where only 7% of PMCs were defective, compared to 2% in the control. The study also identified an elevated number of unreduced dyads and sterile pollen grains.

Numerous genetic modifiers of recombination have been identified. One of the first studies to note this was Gale and Rees (1970) who observed small but significant differences in chiasma frequencies in five *Hordeum* species, attributed to genotypic variation in the populations. Ziolkowski et al. (2017) identified that 56.9% of CO variation in a F_2 population from a cross between two *Arabidopsis* accessions, Columbia and Landsberg, was caused by semi-dominant polymorphisms in *HEI10*, a conserved ubiquitin E3 ligase. Interaction between such genetic elements and environmental variables has not been extensively studied. Rezaei et al. (2010) noted an interaction between the extent of meiotic irregularities and environmental conditions in *Tritium turgidum*. Zheng et al. (2014) reported that

cyclin-dependent kinase G1 (*CDKG1*) was required for normal levels of synapsis and CO formation in male meiosis in *Arabidopsis*, but only at elevated temperatures.

The range of plant species assessed for their meiotic sensitivity to anthropogenic factors is very narrow and confined to angiosperms, and in most instances only those used in agriculture. Single species are usually examined as targets for agrochemicals, and most non-target species are ignored. The effects on angiosperms in non-agricultural habitats, such as woodlands or estuaries and other plant groups, such as gymnosperms, are less known because of the difficulties of experimenting with such species. One such study by Bykova et al. (2018) found that a 27% reduction in precipitation resulted in a 35% reduction in viable pollen grains compared to the control in male *Quercus ilex*. Most of the studies relate to male meiosis, so the sensitivity of the ovule is largely unknown. Hundreds of xenobiotic compounds have been assessed, including those tested by the *Tradescantia* Trad-MCN assay, but this represents a small fraction of the 10,000s of compounds present in the environment (Donner et al., 2010; European Psychiatric Association [EPA], 2018).

EVOLUTIONARY CONSEQUENCES

Empirical research has shown that both the number and distribution of recombination events are tightly controlled, and such non-random patterns have been shown to be stable through generations (see review by Stapley et al., 2017). In all plant species, there are regions of the genome that have few COs events; such regions are termed cold spots. The result of such linkage-disequilibrium is to maintain supergene groups, co-evolved loci or favorable linkage groups, which are of benefit to the plant. Alternatively, undesirable allele combinations could be maintained. As previously discussed, elevated temperature modulates the meiotic landscape of barley and *Arabidopsis* and disrupts linkage groups (Phillips et al., 2015; Lloyd et al., 2018; Modliszewski et al., 2018), which could alter the evolutionary fitness of the plants subjected to this stress.

Many of the anthropogenic stresses, including temperature, agrochemicals and fungicides were reported to cause spindle aberrations during the first and second meiotic division that in some instances gave rise to unreduced gametes and the potential for polyploidisation (Mason and Pires, 2015). High nutrient conditions aids the stabilization of neopolyploid and could drive the evolution of new polyploidy species. Xenobiotic compounds currently found in the environment have no equivalent in the history of our planet and therefore the long-term effect in terms of promoting polyploidy are unknown. The environmental climate of the planet has fluctuated on numerous occasions, and its impact on ploidy recognized. One such event occurred at the Cretaceous–Tertiary (KT) boundary that caused the mass extinction of many species, including about 60% of plant species, but drove the formation of polyploid species (Fawcett et al., 2009; Vanneste et al., 2014). Polyploidisation is believed to confer better adaptability and tolerance to altered environmental conditions, a trend that may be repeated in the current climate change cycle.

Plant speciation is often associated with structural changes in the genome resulting from aneuploidy, dysploidy, or other chromosome rearrangements such as translocations, inversions, fusions, or fissions (De Storme and Mason, 2014). None of the studies cited in this review report such structural changes, but none specifically set out to identify such morphological changes. Notable abnormal chromosome conformations, such as laggards, bridges, fragments, micronuclei, and aneuploidy are reported in many of the studies, and are capable of altering the genomic landscape of the subsequent generation.

SUMMARY

The influence of the human race on the natural environment is undeniable, ranging from altering climatic conditions globally to the local contamination with a specific xenobiotic compound. The influence of many such factors have been reported in a number of different angiosperms, with effects ranging from altered patterns of recombination to severe chromosome damage originating from stickiness and bridges. In most cases, only basic cytology has been used which has shed little light on the underlying mode of action of the factors. Many of the citations predate the development of the sensitive assays now available, and it would be profitable to use such methods to identify how these factors impinge upon on the biochemical pathways operating during meiosis, using concentrations of xenobiotics of relevance to plant populations. The long-term consequences of destabilizing the genome may have a profound evolutionary legacy.

AUTHOR CONTRIBUTIONS

All authors listed have made a substantial, direct and intellectual contribution to the work, and approved it for publication.

FUNDING

DP was supported through a United Kingdom Biotechnology and Biological Sciences Research Council (BBSRC) Strategic Programme Grant (BBS/E/W/0012843D). LF was supported by a studentship from the Institute of Biological, Environmental and Rural Sciences, Aberystwyth University.

REFERENCES

Adamakis, I. D., Panteris, E., Cherianidou, A., and Eleftheriou, E. P. (2013). Effects of bisphenol A on the microtubule arrays in root meristematic cells of *Pisum sativum*. *Mutat. Res.* 750, 111–120. doi: 10.1016/j.mrgentox.2012.10.012

Aherne, G. W., Hardcastle, A., and Nield, A. H. (1990). Cytotoxic drugs and the aquatic environment: estimation of bleomycin in river and water samples. *J. Pharm. Pharmacol.* 42, 741–742. doi: 10.1111/j.2042-7158.1990.tb06574.x

Aldred, K. J., Kerns, R. J., and Osheroff, N. (2014). Mechanism of quinolone action and resistance. *Biochemistry* 53, 1565–1574. doi: 10.1021/bi5000564

Allard, P., and Colaiacovo, M. P. (2010). Bisphenol A impairs the double-strand break repair machinery in the germline and causes chromosome abnormalities. *Proc. Natl. Acad. Sci. U.S.A.* 2, 20405–20410. doi: 10.1073/pnas.1010386107

Amer, S., and Ali, E. (1983). Cytological effects of pesticides XIV. Effects of the insecticide Difterex "Trichlorophon" V. faba plant. *Cytologia* 48, 761–770. doi: 10.1508/cytologia.48.761

Amer, S. M., and Ali, E. M. (1968). Cytological effects of pesticides: II. Meiotic effects of some phenols. *Cytologia* 33, 21–33. doi: 10.1508/cytologia.33.21

Amer, S. M., and Ali, E. M. (1974). Cytological effects of pesticides V. Effects of some herbicides on *Vicia faba*. *Cytologia* 39, 633–643. doi: 10.1508/cytologia.39.633

Amer, S. M., and Farah, O. R. (1968). Cytological effects of pesticides III. Meiotic effects of N-methyl-1-naphthyl carbamate "Sevin". *Cytologia* 33, 337–344. doi: 10.1508/cytologia.33.337

Amer, S. M., and Farah, O. R. (1976). Cytological effects of pesticides. VIII. Effects of the carbamate pesticides "IPC", "Rogor", and "Duphar" on *Vicia faba*. *Cytologia* 41, 597–606. doi: 10.1508/cytologia.41.597

Amer, S. M., and Farah, O. R. (1980). Cytological effects of pesticides X. Meiotic effects of "Phosvel". *Cytologia* 45, 241–245. doi: 10.1508/cytologia.45.241

Amer, S. M., and Farah, O. R. (1983). Cytological effects of pesticides XIII. Meiotic effects of the insecticide "Dursban". *Cytologia* 48, 557–563. doi: 10.1508/cytologia.48.557

Amer, S. M., and Farah, O. R. (1987). Cytological effect of pesticides VIII Meiotic effects of the insecticide Methamidophos. *Cytologia* 52, 303–307. doi: 10.1508/cytologia.52.303

Andronic, L. (2012). Viruses as triggers of DNA rearrangements in host plants. *Can. J. Plant Sci.* 92, 1083–1091. doi: 10.4141/cjps2011-197

Anis, M., and Wani, A. A. (1997). Caffeine induced morpho-cytological variability in fenugreek, *Trigonella foenum-graecum*. *Cytologia* 62, 343–349. doi: 10.1508/cytologia.62.4_343

Aslam, R., Bhat, T. M., Choudhary, S., and Ansari, M. Y. K. (2017). An overview on genotoxicity of heavy metal in a spice crop (*Capsicum annuum* L.) in respect to cyto-morphological behaviour. *Caryologia* 70, 42–47. doi: 10.1080/00087114.2016.1258884

Badr, A., Hamoud, M., and Haroun, S. (1987). Effect of the herbicide terbutryn on meiosis, yield and mitotic chromosomes in C 2 plants of *Vicia faba* L. *Biol. Plant.* 29, 70–72. doi: 10.1007/BF02902322

Bannon, D. I., Drexler, J. W., Fent, G. M., Casteel, S. W., Hunter, P. J., Brattin, W. J., et al. (2009). Evaluation of small arms range soils for metal contamination and lead bioavailability. *Environ. Sci. Technol.* 43, 9071–9076. doi: 10.1021/es901834h

Barth, S., Melchinger, A. E., Devezi-Savula, B., and Lubberstedt, T. (2000). A high-throughput system for genome-wide measurement of genetic recombination in *Arabidopsis thaliana* based on transgenic markers. *Funct. Integr. Genomics* 1, 200–206. doi: 10.1007/s101420000030

Bebber, D. P., Holmes, T., and Gurr Sarah, J. (2014). The global spread of crop pests and pathogens. *Global Ecol. Biogeogr.* 23, 1398–1407. doi: 10.1111/geb.12214

Bebber, D. P., Ramotowski, M. A. T., and Gurr, S. J. (2013). Crop pests and pathogens move polewards in a warming world. *Nat. Clim. Change* 3, 985–988. doi: 10.1038/nclimate1990

Bennett, M. (1971). Effects of ethirimol on cytological characters in barley. *Nature* 230:406. doi: 10.1038/230406a0

Bennett, M. D., and Rees, H. (1970). Induced variation in chiasma frequency in rye in response to phosphate treatments. *Genet. Res.* 16, 325–331. doi: 10.1017/S0016672300002585

Bert, V., Bonnin, I., Saumitou-Laprade, P., De Laguérie, P., and Petit, D. (2002). Do *Arabidopsis halleri* from nonmetallicolous populations accumulate zinc and cadmium more effectively than those from metallicolous populations? *New Phytol.* 155, 47–57. doi: 10.1046/j.1469-8137.2002.00432.x

Bomblies, K., Higgins, J. D., and Yant, L. (2015). Meiosis evolves: adaptation to external and internal environments. *New Phytol.* 208, 306–323. doi: 10.1111/nph.13499

Boyko, A., Hudson, D., Bhomkar, P., Kathiria, P., and Kovalchuk, I. (2006). Increase of homologous recombination frequency in vascular tissue of Arabidopsis plants exposed to salt stress. *Plant Cell. Physiol.* 47, 736–742. doi: 10.1093/pcp/pcj045

Bruton, T., Alboloushi, A., de la Garza, B., Kim, B.-O., and Halden, R. U. (2010). "Fate of caffeine in the environment and ecotoxicological considerations," in *Proceedings of the Contaminants of Emerging Concern in the Environment: Ecological and Human Health Considerations* (Washington, DC: American Chemical Society), 257.

Bykova, O., Limousin, J. M., Ourcival, J. M., and Chuine, I. (2018). Water deficit disrupts male gametophyte development in *Quercus ilex*. *Plant Biol.* 20, 450–455. doi: 10.1111/plb.12692

Caldwell, J. (1952). Some effects of a plant virus on nuclear division. *Ann. Appl. Biol.* 39, 98–102. doi: 10.1111/j.1744-7348.1952.tb01001.x

Cardinale, B., Duffy, J., Gonzalez, A., Hooper, D., Perrings, C., Venail, P., et al. (2012). Biodiversity loss and its impact on humanity. *Nature* 486, 59–67. doi: 10.1038/nature11148

Casteel, C. L., Segal, L. M., Niziolek, O. K., Berenbaum, M. R., and DeLucia, E. H. (2012). Elevated carbon dioxide increases salicylic acid in *Glycine max*. *Environ. Entomol.* 41, 1435–1442. doi: 10.1603/EN12196

Choudhary, S., and Sajid, S. (1986). The behaviour of meiotic chromosomes as revealed through the use of Bavistin on pea. *Cytologia* 51, 279–288. doi: 10.1508/cytologia.51.279

Currie, R. S., and Liang, G. H. (1996). Cytological and morphological effects of atrazine and propazine application on grain sorghum. *Cytologia* 61, 359–363. doi: 10.1508/cytologia.61.359

Davis, A. P., Shokouhian, M., and Ni, S. (2001). Loading estimates of lead, copper, cadmium, and zinc in urban runoff from specific sources. *Chemosphere* 44, 997–1009. doi: 10.1016/S0045-6535(00)00561-0

de la Peña, A., Puertas, M. J., and Merino, F. (1981). Bimeiosis induced by caffeine. *Chromosoma* 83, 241–248. doi: 10.1007/BF00286792

De Storme, N., and Geelen, D. (2014). The impact of environmental stress on male reproductive development in plants: biological processes and molecular mechanisms. *Plant Cell Environ.* 37, 1–18. doi: 10.1111/pce.12142

De Storme, N., and Mason, A. (2014). Plant speciation through chromosome instability and ploidy change: cellular mechanisms, molecular factors and evolutionary relevance. *Curr. Plant Biol.* 1, 10–33. doi: 10.1016/j.cpb.2014.09.002

Deniz, B., and Tufan, A. (1998). The influence of phosphate treatment on chromosome segregations and tetrad regularity and using tetrads in determination of regular meiosis diploid. *Turk. J. Agric. For.* 22, 381–390.

Devadas, N., Rajam, M. V., and Subhash, K. (1986). Comparative mutagenicity of four organophosphorus insecticides in meiotic system of red pepper. *Cytologia* 51, 645–653. doi: 10.1508/cytologia.51.645

Dhesi, J. (1975). Effect of minerals on the chiasma frequency in desynaptic pearl millet. *Curr. Sci.* 44, 862–863.

Donner, E., Eriksson, E., Holten-Luetzhoft, H.-C., Scholes, L., Revitt, M., and Ledin, A. (2010). "Identifying and classifying the sources and uses of xenobiotics in urban environments," in *Xenobiotics in the Urban Water Cycle: Mass Flows, Environmental Processes, Mitigation and Treatment Strategies*, eds D. Fatta-Kassinos, K. Bester, and K. Kümmerer (Dordrecht: Springer), 27–50. doi: 10.1007/978-90-481-3509-7_2

Dowrick, G. J. (1957). The influence of temperature on meiosis. *Heredity* 11, 37–49. doi: 10.1038/hdy.1957.4

Elliott, C. G. (1955). The effect of temperature on chiasma frequency. *Heredity* 9, 385–398. doi: 10.1038/hdy.1955.39

Evans, N., Baierl, A., Semenov, M. A., Gladders, P., and Fitt, B. D. L. (2008). Range and severity of a plant disease increased by global warming. *J. R. Soc. Interface* 5, 525–531. doi: 10.1098/rsif.2007.1136

Evans-Roberts, K. M., Mitchenall, L. A., Wall, M. K., Leroux, J., Mylne, J. S., and Maxwell, A. (2016). DNA Gyrase is the target for the quinolone drug ciprofloxacin in *Arabidopsis thaliana*. *J. Biol. Chem.* 291, 3136–3144. doi: 10.1074/jbc.M115.689554

Fawcett, J. A., Maere, S., and Van de Peer, Y. (2009). Plants with double genomes might have had a better chance to survive the Cretaceous-Tertiary extinction event. *Proc. Natl. Acad. Sci. U.S.A.* 106, 5737–5742. doi: 10.1073/pnas.0900906106

Fedak, G. (1973). Increased chiasma frequency in desynaptic barley in response to phosphate treatments. *Can. J. Genet. Cytol.* 15, 647–649. doi: 10.1139/g73-076

Fisun, K., and Rasgele, P. G. (2009). Genotoxic effects of raxil on root tips and anthers of *Allium cepa* L. *Caryologia* 62, 1–9. doi: 10.1080/00087114.2004.10589659

Food and Agriculture Organization [FAO] (2017). *World Fertilizer Trends and Outlook to 2020*. Available at: http://www.fao.org/publications

Francis, K. E., Lam, S. Y., Harrison, B., Bey, A. L., Berchowitz, L. E., and Copenhaver, G. P. (2007). Pollen tetrad-based visual assay for meiotic recombination in *Arabidopsis*. *Proc. Natl. Acad. Sci. U.S.A.* 104, 3913–3918. doi: 10.1073/pnas.0608936104

Gaffney, J. S., and Marley, N. A. (2009). The impacts of combustion emissions on air quality and climate – From coal to biofuels and beyond. *Atmos. Environ.* 43, 23–36. doi: 10.1016/j.atmosenv.2008.09.016

Gale, M. D., and Rees, H. (1970). Genes controlling chiasma frequency in *Hordeum*. *Heredity* 25, 393–410. doi: 10.1038/hdy.1970.40

Gaw, S., Thomas, K. V., and Hutchinson, T. H. (2014). Sources, impacts and trends of pharmaceuticals in the marine and coastal environment. *Philos. Trans. R. Soc. B* 369:20130572. doi: 10.1098/rstb.2013.0572

Gely-Pernot, A., Hao, C., Becker, E., Stuparevic, I., Kervarrec, C., Chalmel, F., et al. (2015). The epigenetic processes of meiosis in male mice are broadly affected by the widely used herbicide atrazine. *BMC Genomics* 16:885. doi: 10.1186/s12864-015-2095-y

Gely-Pernot, A., Saci, S., Kernanec, P.-Y., Hao, C., Giton, F., Kervarrec, C., et al. (2017). Embryonic exposure to the widely-used herbicide atrazine disrupts meiosis and normal follicle formation in female mice. *Sci. Rep.* 7:3526. doi: 10.1038/s41598-017-03738-1

George, N. M. (2000). Evaluation on mutagenic effects of the three heavy metals on *Vicia faba* plants. *Cytologia* 65, 75–82. doi: 10.1508/cytologia.65.75

Golet, E. M., Strehler, A., Alder, A. C., and Giger, W. (2002). Determination of fluoroquinolone antibacterial agents in sewage sludge and sludge-treated soil using accelerated solvent extraction followed by solid-phase extraction. *Anal. Chem.* 74, 5455–5462. doi: 10.1021/ac025762m

Goulas, A., Haudin, C. S., Bergheaud, V., Dumeny, V., Ferhi, S., Nelieu, S., et al. (2016). A new extraction method to assess the environmental availability of ciprofloxacin in agricultural soils amended with exogenous organic matter. *Chemosphere* 165, 460–469. doi: 10.1016/j.chemosphere.2016.09.040

Grant, V. (1953). Cytogenetics of the hybrid Gilia millefoliata × achilleaefolia. *Chromosoma* 5, 372–390. doi: 10.1007/BF01271494

Griffing, B., and Langridge, J. (1963). Factors affecting crossing over in the tomato. *Aust. J. Biol. Sci.* 16, 826–837. doi: 10.1071/BI9630826

Hamscher, G., Sczesny, S., Höper, H., and Nau, H. (2002). Determination of persistent tetracycline residues in soil fertilized with liquid manure by high-performance liquid chromatography with electrospray ionization tandem mass spectrometry. *Anal. Chem.* 74, 1509–1518. doi: 10.1021/ac015588m

Hanson, W. (1961). Effect of calcium and phosphorus nutrition on genetic recombination in the soybean. *Crop Sci.* 1, 384–384. doi: 10.2135/cropsci1961.0011183X000100050033x

Hautier, Y., Tilman, D., Isbell, F., Seabloom, E., Borer, E., and Reich, P. (2015). Anthropogenic environmental changes affect ecosystem stability via biodiversity. *Science* 348, 336–340. doi: 10.1126/science.aaa1788

Heberer, T. (2002). Tracking persistent pharmaceutical residues from municipal sewage to drinking water. *J. Hydrol.* 266, 175–189. doi: 10.1016/S0022-1694(02)00165-8

Higgins, J. D., Perry, R. M., Barakate, A., Ramsay, L., Waugh, R., Halpin, C., et al. (2012). Spatiotemporal asymmetry of the meiotic program underlies the predominantly distal distribution of meiotic crossovers in barley. *Plant Cell* 24, 4096–4109. doi: 10.1105/tpc.112.102483

Hossain, M. G. (1978). Effects of external environmental factors on chromosome pairing in autotetraploid rye. *Cytologia* 43, 21–34. doi: 10.1508/cytologia.43.21

Hulskotte, J. H. J., Denier van der Gon, H. A. C., Visschedijk, A. J. H., and Schaap, M. (2007). Brake wear from vehicles as an important source of diffuse copper pollution. *Water Sci. Technol.* 56, 223–231. doi: 10.2166/wst.2007.456

International Plant Protection Convention [IPPC] (2014). *Climate Change 2014: Synthesis Report. Contribution of Working Groups I, II and III to the Fifth Assessment Report of the Intergovernmental Panel on Climate Change*. Geneva: IPCC.

Jensen, J. (1981). Effects of temperature on genetic recombination in barley. *Hereditas* 94, 215–218. doi: 10.1111/j.1601-5223.1981.tb01755.x

Jones, R. A. (2016). Future scenarios for plant virus pathogens as climate change progresses. *Adv. Virus Res.* 95, 87–147. doi: 10.1016/bs.aivir.2016.02.004

Karihaloo, J. L. (1986). Stress induced desynapsis in *Hemerocallis*. *Cytologia* 51, 193–199. doi: 10.1508/cytologia.51.193

Karihaloo, J. L. (1994). Genotype-environment interaction in the desynapsis of a *Hemerocallis* 'Sleeping Beauty' clone and its progeny. *Cytologia* 59, 483–491. doi: 10.1508/cytologia.59.483

Kathiria, P., Sidler, C., Golubov, A., Kalischuk, M., Kawchuk, L. M., and Kovalchuk, I. (2010). Tobacco Mosaic Virus infection results in an increase in recombination frequency and resistance to viral, bacterial, and fungal pathogens in the progeny of infected tobacco plants. *Plant Physiol.* 153, 1859–1870. doi: 10.1104/pp.110.157263

Kaul, B. L. (1968). A study of meiosis in virus infected *Datura quarcifolia*. *Cytologia* 33, 17–20. doi: 10.1508/cytologia.33.17

Kaymak, F. (2005). Cytogenetic effects of maleic hydrazide on *Helianthus annuus* L. *Pak. J. Biol. Sci.* 8, 104–108. doi: 10.3923/pjbs.2005.104.108

Khan, S., Cao, Q., Zheng, Y. M., Huang, Y. Z., and Zhu, Y. G. (2008). Health risks of heavy metals in contaminated soils and food crops irrigated with wastewater in Beijing, China. *Environ. Pollut.* 152, 686–692. doi: 10.1016/j.envpol.2007.06.056

Koti, S., Reddy, K. R., Reddy, V. R., Kakani, V. G., and Zhao, D. (2005). Interactive effects of carbon dioxide, temperature, and ultraviolet-B radiation on soybean (*Glycine max* L.) flower and pollen morphology, pollen production, germination, and tube lengths. *J. Exp. Bot.* 56, 725–736. doi: 10.1093/jxb/eri044

Kovalchuk, I., Kovalchuk, O., Kalck, V., Boyko, V., Filkowski, J., Heinlein, M., et al. (2003). Pathogen-induced systemic plant signal triggers DNA rearrangements. *Nature* 423, 760–762. doi: 10.1038/nature01683

Kristen, U. (1997). Use of higher plants as screens for toxicity assessment. *Toxicol. In Vitro* 11, 181–191. doi: 10.1016/S0887-2333(97)00005-2

Kuchy, A., Wani, A., and Kamili, A. (2016). Cytogenetic effects of three commercially formulated pesticides on somatic and germ cells of *Allium cepa*. *Environ. Sci. Pollut. R.* 23, 6895–6906. doi: 10.1007/s11356-015-5912-6

Kumar, G. (2007). Comparative genotoxic potential of mercury and cadmium in soybean. *Turk. J. Biol.* 31, 13–18.

Kumar, G., and Rai, P. K. (2010). The genotoxic potential of two heavy metals in inbred lines of maize (*Zea mays*). *Turk. J. Bot.* 34, 39–46.

Kumar, G., and Ritambhara, T. (2006). Individual and combined effects of lead and gamma irradiations on genetic recombination in *Lathyrus sativus*. *J. Phytol. Res.* 19, 215–220.

Kumar, U., and Sinha, S. S. N. (1991). Genotoxic effects of two pesticides (Rogor and Bavistin) and an antibiotic (Streptomycin) in meiotic cells of grasspea (*Lathyrus sativus* L.). *Cytologia* 56, 209–214. doi: 10.1508/cytologia.56.209

Kumar Ravindra, P. (2017). Studies on pollen viability of papaya (Carica papaya) infected by Papaya Ring Spot Virus (PRSV). *Int. J. Adv. Res.* 5, 1664–1667. doi: 10.21474/IJAR01/4585

Küster, A., and Adler, N. (2014). Pharmaceuticals in the environment: scientific evidence of risks and its regulation. *Philos. Trans. R. Soc. B* 369:20130587. doi: 10.1098/rstb.2013.0587

Lakshmi, N., Prakash, N., and Harini, I. (1988). Cytological effects of agricultural chemicals I. effects of insecticides "Ekalux and Metasystox" on chilli (*Capsicum annuum* L.). *Cytologia* 53, 703–708. doi: 10.1508/cytologia.53.703

Law, C. (1963). An effect of potassium on chiasma frequency and recombination. *Genetica* 33, 313–329. doi: 10.1007/BF01725768

Lee, H. B., Peart, T. E., and Svoboda, M. L. (2007). Determination of ofloxacin, norfloxacin, and ciprofloxacin in sewage by selective solid-phase extraction, liquid chromatography with fluorescence detection, and liquid chromatography-tandem mass spectrometry. *J. Chromatogr. A* 1139, 45–52. doi: 10.1016/j.chroma.2006.11.068

Lee, K., Rao, G., Barnett, F., and Liang, G. (1974). Further evidence of meiotic instability induced by Atrazine in grain-sorghum. *Cytologia* 39, 697–702. doi: 10.1508/cytologia.39.697

Liang, G. H., Feltner, K., and Russ, O. (1969). Meiotic and morphological response of grain sorghum to atrazine, 2, 4-D, oil, and their combinations. *Weed Sci.* 17, 8–12.

Lin, Y. J. (1982). Temperature and chiasma formation in *Rhoeo spathacea* var. variegata. *Genetica* 60, 25–30. doi: 10.1007/BF00121453

Lloyd, A., Morgan, C., Franklin, C., and Bomblies, K. (2018). Plasticity of meiotic recombination rates in response to temperature in *Arabidopsis*. *Genetics* 208, 1409–1420. doi: 10.1534/genetics.117.300588

Lucht, J. M., Mauch-Mani, B., Steiner, H. Y., Metraux, J. P., Ryals, J., and Hohn, B. (2002). Pathogen stress increases somatic recombination frequency in Arabidopsis. *Nat. Genet.* 30, 311–314. doi: 10.1038/ng846

Ma, T.-H., Anderson, V. A., and Ahmed, I. (1982). "Environmental clastogens detected by meiotic pollen mother cells of Tradescantia," in *Genotoxic Effects of Airborne Agents*, eds Tice, R. Raymond, Daniel, Schaich, and M. Karen (Boston, MA: Springer), 141–157.

Ma, T.-H., and Harris, M. (1987a). Tradescantia micronucleus (Trad-MCN) assay - a potential indoor pollution monitor. *Environ. Mutagen.* 9(Suppl.):8.

Ma, T.-H., and Harris, M. (1987b). "Tradescantia micronucleus (Trad-MCN) bioassay- a promising indoor air pollution monitoring system," in *Proceedings of the 4th International Conference on Indoor Air Quality and Climate*, Berlin, 243–247.

Ma, T.-H., Van Anderson, A., and Sandhu, S. S. (1980). "A preliminary study of the clastogenic effects of diesel exhaust fumes using the tradescantia micronucleus bioassay," in *Short-Term Bioassays in the Analysis of Complex Environmental Mixtures II*, eds M. Waters, S. Nesnow, J. L. Huisingh, S. S. Sandhu, and L. Claxton (Boston, MA: Springer), 351–358.

Mann, S. K. (1977). Cytological and genetic effects of dithane fungicides on *Allium cepa*. *Environ. Exp. Bot.* 1977, 7–12. doi: 10.1016/0098-8472(77)90014-4

Mann, S. K. (1978). Interaction of tetracycline (TC) with chromosomes in *Allium cepa*. *Environ. Exp. Bot.* 18, 201–205. doi: 10.1016/0098-8472(78)90039-4

Martín, A. C., Rey, M.-D., Shaw, P., and Moore, G. (2017). Dual effect of the wheat Ph1 locus on chromosome synapsis and crossover. *Chromosoma* 126, 669–680. doi: 10.1007/s00412-017-0630-0

Mason, A. S., and Pires, J. C. (2015). Unreduced gametes: meiotic mishap or evolutionary mechanism? *Trends Genet.* 31, 5–10. doi: 10.1016/j.tig.2014.09.011

Mickelbart, M. V., Hasegawa, P. M., and Bailey-Serres, J. (2015). Genetic mechanisms of abiotic stress tolerance that translate to crop yield stability. *Nat. Rev. Genet.* 16, 237–251. doi: 10.1038/nrg3901

Mittal, N., and Srivastava, A. K. (2014). Cadmium and chromium induced aberrations in the reproductive biology of *Hordeum vulgare*. *Cytologia* 79, 207–214. doi: 10.1508/cytologia.79.207

Modliszewski, J. L., and Copenhaver, G. P. (2017). Meiotic recombination gets stressed out: CO frequency is plastic under pressure. *Curr. Opin. Plant Biol.* 36, 95–102. doi: 10.1016/j.pbi.2016.11.019

Modliszewski, J. L., Wang, H., Albright, A. R., Lewis, S. M., Bennett, A. R., Huang, J., et al. (2018). Elevated temperature increases meiotic crossover frequency via the interfering (Type I) pathway in *Arabidopsis thaliana*. *PLoS Genet.* 14:e1007384. doi: 10.1371/journal.pgen.1007384

Molinier, J., Ries, G., Zipfel, C., and Hohn, B. (2006). Transgeneration memory of stress in plants. *Nature* 442, 1046–1049. doi: 10.1038/nature05022

Moss, B. (2008). Water pollution by agriculture. *Philos. Trans. R. Soc. Lond. B Biol. Sci.* 363, 659–666. doi: 10.1098/rstb.2007.2176

Namuco, O. S., and O'Toole, J. C. (1986). Reproductive stage water stress and sterility. I. Effect of stress during meiosis I. *Crop Sci.* 26, 317–321. doi: 10.2135/cropsci1986.0011183X002600020022x

Naveedullah, Hashmi, M. Z., Yu, C., Shen, H., Duan, D., Shen, C., et al. (2013). Risk assessment of heavy metals pollution in agricultural soils of siling reservoir watershed in Zhejiang province, China. *Biomed. Res. Int.* 2013:590306. doi: 10.1155/2013/590306

Noedler, K., Licha, T., and Voutsa, D. (2013). Twenty years later - Atrazine concentrations in selected coastal waters of the Mediterranean and the Baltic Sea. *Mar. Pollut. Bull.* 70, 112–118. doi: 10.1016/j.marpolbul.2013.02.018

Omidi, M., Siahpoosh, M. R., Mamghani, R., and Modarresi, M. (2014). The influence of terminal heat stress on meiosis abnormalities in pollen mother cells of wheat. *Cytologia* 79, 49–58. doi: 10.1508/cytologia.79.49

Pandey, R. (2017). Studies on pollen viability of papaya (Carica papaya) infected by papaya ring spot virus (prsv). *Int. J. Adv. Res.* 5, 1664–1667. doi: 10.21474/IJAR01/4585

Pecrix, Y., Rallo, G., Folzer, H., Cigna, M., Gudin, S., and Le Bris, M. (2011). Polyploidization mechanisms: temperature environment can induce diploid gamete formation in *Rosa* sp. *J. Exp. Bot.* 62, 3587–3597. doi: 10.1093/jxb/err052

Phillips, D., Jenkins, G., Macaulay, M., Nibau, C., Wnetrzak, J., Fallding, D., et al. (2015). The effect of temperature on the male and female recombination landscape of barley. *New Phytol.* 208, 421–429. doi: 10.1111/nph.13548

Powell, J. B., and Nilan, R. A. (1963). Influence of temperature on crossing over in an inversion heterozygote in barley. *Crop Sci.* 3, 11–13. doi: 10.2135/cropsci1963.0011183X000300010005x

Prakash, N., Lakshmi, N., and Harini, I. (1988). Cytological effects of agricultural chemicals. II. Effects of fungicides" Bavistin" and" Deltan" on chilli (*Capsicum annuum* L.). *Cytologia* 53, 709–715. doi: 10.1508/cytologia.53.709

Prakken, R. (1943). Studies of asynapsis in rye. *Hereditas* 29, 475–495. doi: 10.1111/j.1601-5223.1943.tb03301.x

Qi, W., Müller, B., Pernet-Coudrier, B., Singer, H., Liu, H., Qu, J., et al. (2014). Organic micropollutants in the Yangtze River: seasonal occurrence and annual loads. *Sci. Total Environ.* 472, 789–799. doi: 10.1016/j.scitotenv.2013.11.019

Rahavi, M. R., Migicovsky, Z., Titov, V., and Kovalchuk, I. (2011). Transgenerational adaptation to heavy metal salts in *Arabidopsis*. *Front. Plant Sci.* 2:91. doi: 10.3389/fpls.2011.00091

Razu, M., Zaman, S., Akhter, R., Rahman, M., Rahaman, M. H., Mazid, M., et al. (2014). Morphological and cytological effects of two herbicides on tetraploid wheat (*Triticum durum* L.). *J. Biosci.* 20, 143–151.

Reddy, S. S., and Rao, G. M. (1981). Cytogenetic effects of agricultural chemicals I. Effects of insecticides" BHC and nuvacron" on chromosomal mechanism in relation to yield and yield components in chilli (*Capsicum annuum* L.). *Cytologia* 46, 699–707. doi: 10.1508/cytologia.46.699

Rey, M. D., Martin, A. C., Smedley, M., Hayta, S., Harwood, W., Shaw, P., et al. (2018). Magnesium increases homoeologous crossover frequency during meiosis in ZIP4 (Ph1 gene) mutant wheat-wild relative hybrids. *Front. Plant Sci.* 9:509. doi: 10.3389/fpls.2018.00509

Rezaei, M., Arzani, A., and Sayed-Tabatabaei, B. E. (2010). Meiotic behaviour of tetraploid wheats (*Triticum turgidum* L.) and their synthetic hexaploid wheat derivates influencedby meiotic restitution and heat stress. *J. Genet.* 89, 401–407. doi: 10.1007/s12041-010-0058-2

Robinson, B. H., Bischofberger, S., Stoll, A., Schroer, D., Furrer, G., Roulier, S., et al. (2008). Plant uptake of trace elements on a Swiss military shooting range: uptake pathways and land management implications. *Environ. Pollut.* 153, 668–676. doi: 10.1016/j.envpol.2007.08.034

Rodrigues, G. S., Ma, T. H., Pimentel, D., and Weinstein, L. H. (1997). Tradescantia bioassays as monitoring systems for environmental mutagenesis: a review. *Crit. Rev. Plant Sci.* 16, 325–359. doi: 10.1080/07352689709701953

Rodrigues, G. S., Madkour, S. A., and Weinstein, L. H. (1996). Genotoxic activity of ozone in *Tradescantia*. *Environ. Exp. Bot.* 36, 45–50. doi: 10.1016/0098-8472(95)00042-9

Rowan, B. A., Oldenburg, D. J., and Bendich, A. J. (2010). RecA maintains the integrity of chloroplast DNA molecules in *Arabidopsis*. *J. Exp. Bot.* 61, 2575–2588. doi: 10.1093/jxb/erq088

Saini, H. S., Sedgley, M., and Aspinall, D. (1984). Developmental anatomy in wheat of male sterility induced by heat stress, water deficit or abscisic acid. *Aust. J. Plant Physiol.* 11, 243–253. doi: 10.1071/PP9840243

Shan, Y., Tysklind, M., Hao, F., Ouyang, W., Chen, S., and Lin, C. (2013). Identification of sources of heavy metals in agricultural soils using multivariate analysis and GIS. *J. Soils Sedim.* 13, 720–729. doi: 10.1007/s11368-012-0637-3

Sharma, C., Behera, B. N., Raju, D. S. S., and Rao, B. G. S. (1983). Effects of some systemic fungicides on the chiasma frequencies in *Hordeum vulgare*. *Cytologia* 48, 749–752. doi: 10.1508/cytologia.48.749

Sharma, C., Patra, B., Raju, D. S. S., and Murty, K. V. (1981). Chiasma variation in *Hordeum vulgare* after exposure to herbicides. *Mutat. Res.* 91, 333–336. doi: 10.1016/0165-7992(81)90010-5

Sharma, C. B. S., and Panneerselvam, N. (1990). Genetic toxicology of pesticides in higher-plant systems. *Crit. Rev. Plant Sci.* 9, 409–442. doi: 10.1016/j.mrfmmm.2016.08.003

Si, W., Yuan, Y., Huang, J., Zhang, X., Zhang, Y., Zhang, Y., et al. (2015). Widely distributed hot and cold spots in meiotic recombination as shown by the sequencing of rice F2 plants. *New Phytol.* 206, 1491–1502. doi: 10.1111/nph.13319

Singh, N., and Srivastava, A. (2014). Biomonitoring of genotoxic effect of glyphosate and pendimethalin in *Vigna mungo* populations. *Cytologia* 79, 173–180. doi: 10.1508/cytologia.79.173

Skazkin, F. D., and Zavadskaya, I. G. (1957). On the influence of soil moisture deficiency and nitrogen nutrition on microsporogenesis in barley. *Dokl Akad Nauk SSSR* 117, 240–242.

Soriano, J. D. (1984). Herbicide-induced chromosomal aberrations and inheritance of a digenic seedling mutation in sorghum. *Cytologia* 49, 201–207. doi: 10.1508/cytologia.49.201

Srivastava, N., and Kumar, G. (2016). Effect of waterlogging stress on meiotic course, tetrad formation and pollen fertility of Sesbania pea. *Cytol. Genet.* 50, 36–39. doi: 10.3103/S0095452716010096

Stapley, J., Feulner, P., Johnston, S., Santure, A., and Smadja, C. (2017). Variation in recombination frequency and distribution across eukaryotes: patterns and processes. *Philos. T. R. Soc. B.* 372:20160455. doi: 10.1098/rstb.2016.0455

Swaminathan, M. S., Ninan, T., and Magoon, M. L. (1959). Cytological effects of mosaic virus in chillis. *Genetica* 30, 63–69. doi: 10.1007/BF01535665

Thiele-Bruhn, S. (2003). Pharmaceutical antibiotic compounds in soils – a review. *J. Plant Nutr. Soil Sci.* 166, 145–167. doi: 10.1002/jpln.200390023

Tian, M., Liu, Y., Zhang, Y., Kang, X., and Zhang, P. (2018). High temperature exposure did not affect induced 2n pollen viability in *Populus*. *Plant Cell Environ.* 41, 1383–1393. doi: 10.1111/pce.13165

Tilman, D., Cassman, K. G., Matson, P. A., Naylor, R., and Polasky, S. (2002). Agricultural sustainability and intensive production practices. *Nature* 418, 671–677. doi: 10.1038/nature01014

Tornero, V., and Hanke, G. (2016). Chemical contaminants entering the marine environment from sea-based sources: a review with a focus on European seas. *Mar. Pollut. Bull.* 112, 17–38. doi: 10.1016/j.marpolbul.2016.06.091

Trebicki, P., Dader, B., Vassiliadis, S., and Fereres, A. (2017). Insect-plant-pathogen interactions as shaped by future climate: effects on biology, distribution, and implications for agriculture. *Insect Sci.* 24, 975–989. doi: 10.1111/1744-7917.12531

Tripathi, R., and Girjesh, K. (2010). Genetic loss through heavy metal induced chromosomal stickiness in grass pea. *Caryologia* 63, 223–228. doi: 10.1080/00087114.2010.10589731

Uslu, M. O., Jasim, S., Arvai, A., Bewtra, J., and Biswas, N. (2013). A survey of occurrence and risk assessment of pharmaceutical substances in the Great Lakes basin. *Ozone Sci. Eng.* 35, 249–262. doi: 10.1080/01919512.2013.793595

van Tol, N., Rolloos, M., van Loon, P., and van der Zaal, B. J. (2018). MeioSeed: a CellProfiler-based program to count fluorescent seeds for crossover frequency analysis in *Arabidopsis thaliana*. *Plant Methods* 18, 14–32. doi: 10.1186/s13007-018-0298-3

Vanneste, K., Baele, G., Maere, S., and Van de Peer, Y. (2014). Analysis of 41 plant genomes supports a wave of successful genome duplications in association with the Cretaceous-Paleogene boundary. *Genome Res.* 24, 1334–1347. doi: 10.1101/gr.168997.113

Verde, L. A. (2003). *The Effect of Stress on Meiotic Recombination in Maize (Zea mays L)*. Ph.D. thesis, Iowa State University, Ames, IA.

Vonberg, D., Hofmann, D., Vanderborght, J., Lelickens, A., Koeppchen, S., Puetz, T., et al. (2014). Atrazine soil core residue analysis from an agricultural field 21 years after its ban. *J. Environ. Qual.* 43, 1450–1459. doi: 10.2134/jeq2013.12.0497

Wang, J., Daili Li, D., Shang, F., and Kang, X. (2017). High temperature-induced production of unreduced pollen and its cytological effects in *Populus*. *Nat. Sci. Rep.* 7:5281. doi: 10.1038/s41598-017-05661-x

Wang, X., and Copenhaver, G. P. (2018). Meiotic recombination: mixing it up in plants. *Annu. Rev. Plant Biol.* 69, 13.11–13.33. doi: 10.1146/annurev-arplant-042817-040431

Williams, C. F., and McLain, J. E. (2012). Soil persistence and fate of carbamazepine, lincomycin, caffeine, and ibuprofen from wastewater reuse. *J. Environ. Qual.* 41, 1473–1480. doi: 10.2134/jeq2011.0353

Wilson, J. Y. (1959a). Chiasma frequency in relation to temperature. *Genetica* 29, 290–303. doi: 10.1007/BF01535715

Wilson, J. Y. (1959b). Temperature effect on chiasma frequency in the bluebell *Endymion nonscriptus*. *Chromosoma* 10, 337–354. doi: 10.1007/BF00396577

Wuu, K. (1967). Chromosomal aberrations induced by pesticides in meiotic cells of barley. *Cytologia* 32, 31–41. doi: 10.1508/cytologia.32.31

Wuu, K., and Grant, W. (1966). Induced abnormal meiotic behavior in a barley plant (*Hordeum vulgare* L) with herbicide Lorox. *Phyton* 23:63.

Xu, X., Zhao, Y., Zhao, X., Wang, Y., and Deng, W. (2014). Sources of heavy metal pollution in agricultural soils of a rapidly industrializing area in the Yangtze Delta of China. *Ecotoxicol. Environ. Saf.* 108, 161–167. doi: 10.1016/j.ecoenv.2014.07.001

Yao, Y., Kathiria, P., and Kovalchuk, I. (2013). A systemic increase in the recombination frequency upon local infection of *Arabidopsis thaliana* plants with oilseed rape mosaic virus depends on plant age, the initial inoculum concentration and the time for virus replication. *Front. Plant Sci.* 4:61. doi: 10.3389/fpls.2013.00061

Yelina, N., Diaz, P., Lambing, C., and Henderson, I. R. (2015). Epigenetic control of meiotic recombination in plants. *Sci. China Life Sci.* 58, 223–231. doi: 10.1007/s11427-015-4811-x

Zhang, H., Zhou, Y., Huang, Y., Wu, L., Liu, X., and Luo, Y. (2016). Residues and risks of veterinary antibiotics in protected vegetable soils following application of different manures. *Chemosphere* 152, 229–237. doi: 10.1016/j.chemosphere.2016.02.111

Zhang, M.-K., Liu, Z.-Y., and Wang, H. (2010). Use of single extraction methods to predict bioavailability of heavy metals in polluted soils to rice. *Commun. Soil Sci. Plant* 41, 820–831. doi: 10.1080/00103621003592341

Zhang, S., Li, X., Sun, Z., Shao, S., Hu, L., Ye, M., et al. (2015). Antagonism between phytohormone signalling underlies the variation in disease susceptibility of tomato plants under elevated CO2. *J. Exp. Bot.* 66, 1951–1963. doi: 10.1093/jxb/eru538

Zheng, T., Nibau, C., Phillips, D. W., Jenkins, G., Armstrong, S. J., and Doonan, J. H. (2014). CDKG1 protein kinase is essential for synapsis and male meiosis at high ambient temperature in *Arabidopsis thaliana*. *Proc. Natl. Acad. Sci. U.S.A.* 111, 2182–2187. doi: 10.1073/pnas.1318460111

Ziolkowski, P. A., Underwood, C. J., Lambing, C., Martinez-Garcia, M., Lawrence, E. J., Ziolkowska, L., et al. (2017). Natural variation and dosage of the HEI10 meiotic E3 ligase control *Arabidopsis* crossover recombination. *Genes Dev.* 31, 306–317. doi: 10.1101/gad.295501.116

Zohair, S., Khatoon, S., and Zaidi, S. (2012). Cytological studies on 14 plant species under polluted conditions. *Pak. J. Bot.* 44, 1977–1982.

Conflict of Interest Statement: The authors declare that the research was conducted in the absence of any commercial or financial relationships that could be construed as a potential conflict of interest.

frontiers in Plant Science

MINI REVIEW
published: 28 June 2018
doi: 10.3389/fpls.2018.00907

Speciation Success of Polyploid Plants Closely Relates to the Regulation of Meiotic Recombination

Alexandre Pelé[1,2], Mathieu Rousseau-Gueutin[2] and Anne-Marie Chèvre[2]**

[1] Plant Breeding, Wageningen University & Research, Wageningen, Netherlands, [2] Institut de Génétique, Environnement et Protection des Plantes, Institut National de la Recherche Agronomique, Agrocampus Ouest, Université de Rennes 1, Rennes, France

Polyploidization is a widespread phenomenon, especially in flowering plants that have all undergone at least one event of whole genome duplication during their evolutionary history. Consequently, a large range of plants, including many of the world's crops, combines more than two sets of chromosomes originating from the same (autopolyploids) or related species (allopolyploids). Depending on the polyploid formation pathway, different patterns of recombination will be promoted, conditioning the level of heterozygosity. A polyploid population harboring a high level of heterozygosity will produce more genetically diverse progenies. Some of these individuals may show a better adaptability to different ecological niches, increasing their chance for successful establishment through natural selection. Another condition for young polyploids to survive corresponds to the formation of well-balanced gametes, assuring a sufficient level of fertility. In this review, we discuss the consequences of polyploid formation pathways, meiotic behavior and recombination regulation on the speciation success and maintenance of polyploid species.

Keywords: polyploidy, genome evolution, diploidization, meiosis, unreduced gametes, recombination, crossover

OPEN ACCESS

Edited by:
Tomás Naranjo, Complutense University of Madrid, Spain

Reviewed by:
Ming Yang, Oklahoma State University, United States
Azahara Carmen Martin, John Innes Centre (JIC), United Kingdom

****Correspondence:***
Alexandre Pelé
alexandre.pele@wur.nl
Anne-Marie Chèvre
anne-marie.chevre@inra.fr

Specialty section:
This article was submitted to Plant Cell Biology, a section of the journal Frontiers in Plant Science

Received: *28 March 2018*
Accepted: *08 June 2018*
Published: *28 June 2018*

Citation:
Pelé A, Rousseau-Gueutin M and Chèvre A-M (2018) Speciation Success of Polyploid Plants Closely Relates to the Regulation of Meiotic Recombination. Front. Plant Sci. 9:907. doi: 10.3389/fpls.2018.00907

INTRODUCTION

Meiosis is the fundamental process by which are formed the gametes in all sexual organisms. Largely investigated in the last decades (for review see Mercier et al., 2015; Zickler and Kleckner, 2015), this process consists in a single phase of DNA replication followed by two divisions, where first, pairs of parental chromosomes (i.e., homologs) and then, sister chromatids separate into four cells of a tetrad. During the first division, occurrence of meiotic recombination is determinant for ensuring both genome stability and generation of diversity, through one of its products: the crossovers. Indeed, in addition to maintain pairs of homologs physically linked at the end of metaphase I (i.e., bivalents), crossovers result in reciprocal exchanges of DNA between non-sister chromatids. At least one crossover is required per bivalent to obtain well-balanced gametes and avoid the formation of aneuploid progenies. However, as a result of the so-called phenomenon of interference, rarely more than three crossovers are formed per bivalent in a meiosis, typically widely spaced from one another and primarily located on chromosome extremities.

In polyploids, which are widespread in plants even in major crops (e.g., cotton, rapeseed, and wheat), the situation is delicate as they combine two genomes or more deriving from the same (autopolyploidy) or related (allopolyploidy) species (Stebbins, 1947). While all Angiosperms have

experienced at least one event of whole genome duplication in their evolutionary history (Jiao et al., 2011), polyploidization remains an active and ongoing process recognized as a major driving force for plants speciation (Comai, 2005; Alix et al., 2017). Indeed, polyploids may occupy new ecological niches (Stebbins, 1985; Blaine Marchant et al., 2016) and often display higher adaptability than their progenitors, as evidenced by their better tolerance to abiotic stresses (McIntyre, 2012; Allario et al., 2013). However, the reasons of such a speciation success are not well-understood given that polyploidization initially results in a depletion of variability, due to the limited number of parental genotypes, and frequently confers instant reproductive isolation (Husband and Schemske, 2000; Husband and Sabara, 2004). In this review, we aim to highlight how meiotic recombination may favor this success by (1) conditioning the genetic variability of newly formed polyploids, (2) expanding the allelic combinatorial possibilities in the following generations, and (3) ensuring the proper segregation of multiple homologs and/or related chromosomes (i.e., homoeologs) in established auto- and allopolyploids, respectively.

THE ROUTES LEADING TO POLYPLOIDY COMBINED WITH THE OCCURRENCE OF MEIOTIC RECOMBINATION CONDITION THE INITIAL ALLELIC VARIABILITY

A novel polyploid individual may form *via* several routes (Ramsey and Schemske, 1998; Tayalé and Parisod, 2013) (**Figure 1**). Depending on the formation pathway, the genetic status (i.e., level of heterozygosity vs. homozygosity) of newly formed polyploids will highly differ and may impact their performance and speciation success, as evidenced by gains recorded in highly heterozygous plants for growth, fertility, and yield (Bingham, 1980; Stebbins, 1980; Werner and Peloquin, 1991). While immediate consequences of polyploidization were mostly investigated by inducing the somatic doubling of chromosomes through chemical treatment (Tamayo-Ordóñez et al., 2016), this path does not fully mimic what happened in nature in terms of occurrence and variability. Indeed, although possible when mitotic non-disjunction of sister-chromatids arises either in meristem tissue of sporophytes, zygote or young embryo, this route remains rarely observed spontaneously and restricts the number of alleles fixed per locus in auto- and allotetraploids (Ramsey and Schemske, 1998).

Nowadays, it is accepted that polyploids predominantly arise sexually, through the generation of gametes having the somatic (2n) rather than the haploid (n) number of chromosomes; a phenomenon referred as 'gametic non-reduction' (Harlan and de Wet, 1975). Indeed, production of unreduced gametes has been observed across widely disparate phyla (Veilleux, 1983; Bretagnolle and Thompson, 1995), at frequencies typically averaging from 0.1 to 2.0% in natural populations (Kreiner et al., 2017). Moreover, polyploidy induction may have been facilitated throughout plants evolutionary history *via* greatly enhanced frequencies of unreduced gametes. For instance, abiotic stresses such as temperature fluctuation often favor the production of unreduced gametes (Mason et al., 2011; Pécrix et al., 2011; De Storme et al., 2012), which is striking in regard to the coincidence of ancient WGD events with adverse climatic events (Vanneste et al., 2014; Van de Peer et al., 2017). On the other hand, mutation of certain genes may also have facilitated polyploidization, especially when promoting unreduced gametes in both male and female meiosis, as observed for *OSD1* and *TAM* in *Arabidopsis thaliana* (d'Erfurth et al., 2009, 2010; Wang et al., 2010). Although a plethora of cytologic mechanisms has been described (De Storme and Geelen, 2013), unreduced gametes commonly arise in plants through First (FDR) or Second Division Restitution (SDR), corresponding to the defect of meiosis I or II, respectively. Thus, depending on their origin, unreduced gametes will display different genetic makeups (Bretagnolle and Thompson, 1995; Brownfield and Köhler, 2011). In the strict sense, the non-disjunction of homologs in FDR is combined with the abolishment of recombination, yielding unreduced gametes retaining the full heterozygosity of the initial individual (**Figure 2**); note however that in some instance a partial loss of variability happens due to the occurrence of recombination, a mechanism referred as FDR-like (Ramanna and Jacobsen, 2003). In contrast, SDR, consisting in the exclusive separation of recombined homologs, always results in partially homozygous unreduced gametes, from the crossover location toward the end of a chromosome arm (**Figure 2**).

Two major routes may lead to the formation of both auto- and allotetraploids, either directly or indirectly *via* a triploid-bridge (**Figure 1**). Theoretically, the highest level of variability is obtained when tetraploids arise directly from the merger of two unreduced gametes provided by different diploid individuals, especially when they belong to the (strict) FDR-type. Indeed, increasing proportions of tri- and tetra-alleles per locus are expected in autotetraploids, while allotetraploids systematically benefit from a full heterozygosity between homologs and homoeologs (Watanabe et al., 1991). Nevertheless, a partial loss of variability may occur between homologs when tetraploids originate from SDR (or FDR-like) unreduced gametes. Except in case of spontaneous mutation preventing the separation of homologs or chromatids in male and female meiosis, two unreduced gametes have relatively low chance to merge in a single step (Ramsey and Schemske, 1998). Therefore, even though a lower variability is expected by this route, it is suggested that tetraploid species are most presumably formed in two steps *via* a triploid bridge (Husband, 2004). Indeed, triploids resulting through the merger of reduced and unreduced gametes are fertile in a large range of plant lineages (Ramanna and Jacobsen, 2003) and may form a tetraploid either by self-fertilization or intercross with one diploid progenitor. From the first path (self-fertilization), two reduced gametes of the triploid individual are required. However, the resulting plants are often aneuploids, decreasing the likelihood of successful speciation (**Figure 2**; Leflon et al., 2006). From the second path (intercross), the triploid must provide an unreduced gamete, likely arising from an indeterminate meiotic restitution (IMR), where FDR and SDR

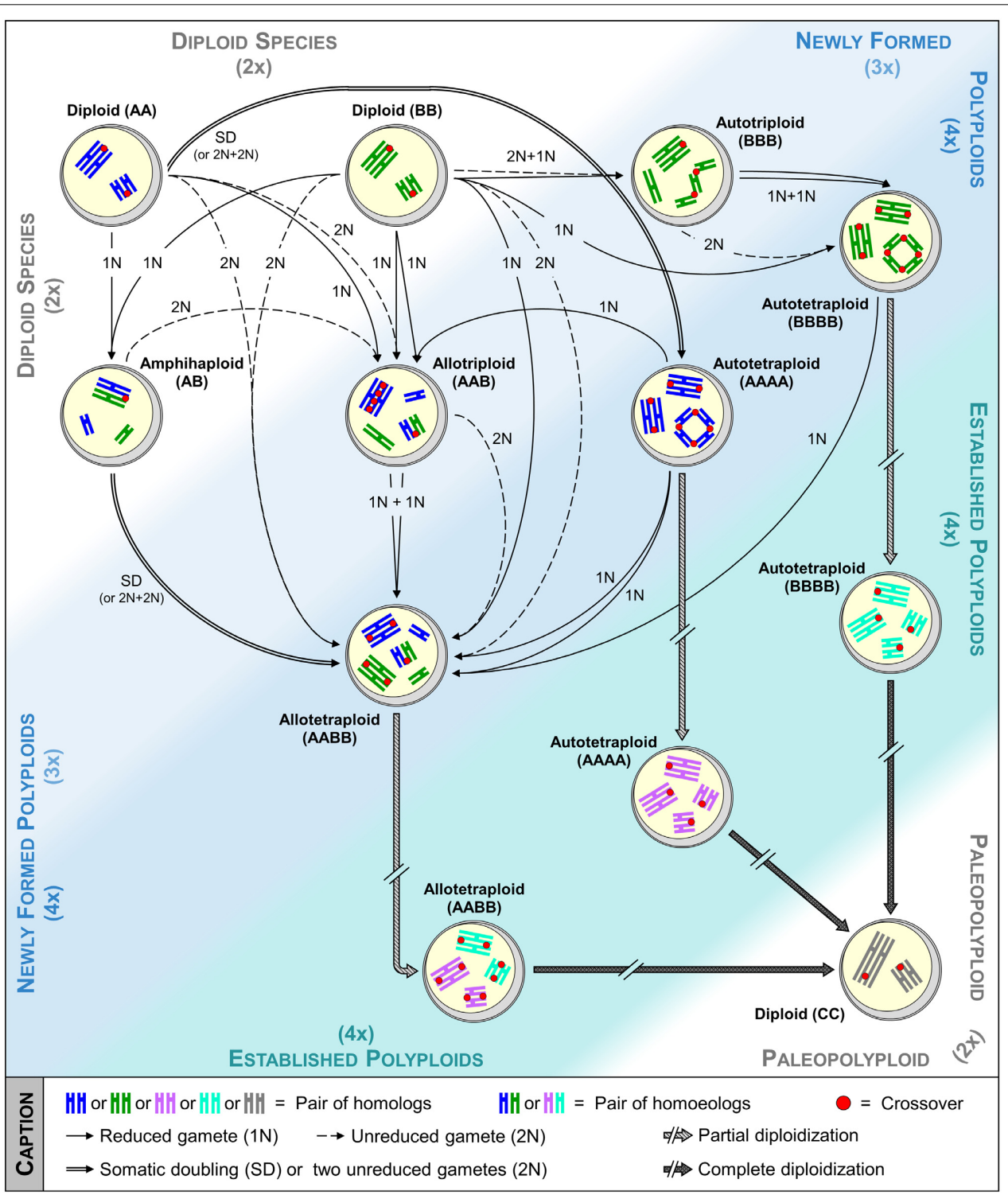

FIGURE 1 | From the formation toward the complete diploidization of polyploids: insights of meiotic pairing and recombination. Auto- and allotetraploids can be formed *via* many routes, which may involve intermediates (e.g., triploids and amphihaploids). While pairing and recombination are initially perturbed, as represented by multiple/illegitimate associations and by increasing number of crossovers, a diploid-like meiosis is setting up through a strict regulation of meiotic recombination, a process referred as partial diploidization. Following millions of years, diploidization becomes complete through a return at a diploid stage resulting in a chromosome number reduction. On this figure, insights of pairing and recombination mostly based on research performed in *Arabidopsis*, *Brassica*, *Lolium,* and *Phlox* genera are presented. Within each pollen mother cell drawn, the chromosomes of the same size and same color derive from the same species, while those of different colors derive from two different species.

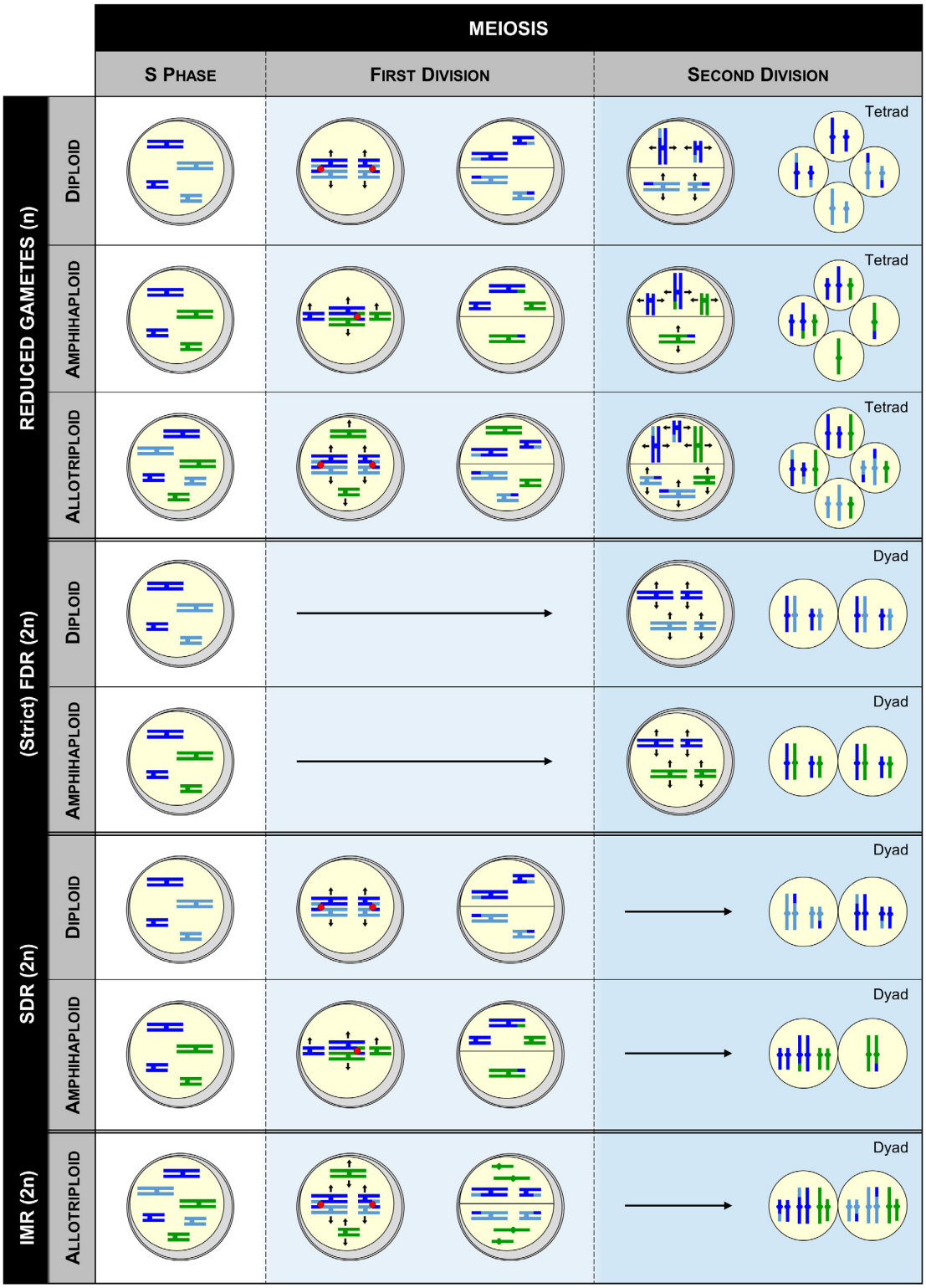

FIGURE 2 | Genotypic outcome of gametes deriving from diploid, amphihaploid and allotriploid heterozygous individuals when meiosis either occurs normally (WT) or undergoes a meiotic restitution (FDR, SDR, or IMR). FDR, SDR, and IMR correspond to first, second, and intermediate meiotic restitution, respectively. Within each pollen mother cell drawn, the chromosomes of the same size colored in light and dark blue derive from the same species (differentiation showing the heterozygosity), while those colored in blue and green derive from two different species. Note that this figure is not exhaustive, as other mechanisms such as FDR-like may occur (see the text).

occur simultaneously for unpaired and paired chromosomes, respectively (**Figure 2**; De Storme and Geelen, 2013).

Allotetraploids may also arise from amphihaploid or autotetraploid intermediates, most presumably in a single step, even though both can first promote an allotriploid bridge (**Figure 1**). However, these paths may have a low natural occurrence. Indeed, while amphihaploids are generally poorly fertile (Mason and Pires, 2015), the success of allotetraploid formation through an autotetraploid closely relates to the ability of this latter to generate well-balanced reduced gametes (see the following sections). The path by which the autotetraploids arose conditions the variability per subgenome of the resulting allotetraploid. On the other hand, the amphihaploid path will provide a lower variability than all routes previously described as only one chromatid of each chromosome is assigned per dyad through (strict) FDR-type, maintaining exclusively the heterozygosity between homoeologs (**Figure 2**). Even more harmful, SDR-type (and FDR-like) may result in unbalanced dyads due to the occurrence of crossovers between homoeologs (Cifuentes et al., 2010).

MANAGING THE VARIABILITY IN NEWLY FORMED POLYPLOIDS THROUGH DISTURBED MEIOTIC RECOMBINATION

Although newly formed polyploids may sometimes successfully establish *via* the main use of vegetative reproduction, as in the young allodecaploid *Spartina anglica* (Ainouche et al., 2004), most favor sexual reproduction (Comai, 2005; Nasrallah, 2017). In addition to harboring a higher variability (**Figure 1**), populations deriving from this latter route will benefit from different patterns of meiotic recombination, increasing their chance of adaptation in new ecological niches and their speciation success through natural selection.

While the generation of diversity is usually hampered, polyploid plants are often able to overcome the limits arising from the tight regulation of meiotic recombination (Mercier et al., 2015). Indeed, as reported in *Arabidopsis*, *Brassica*, *Gossypium*, *Phlox,* and *Zea* genera, newly formed auto- and allotetraploids exhibit higher crossover frequencies between their homologous chromosomes than their diploid progenitors (Bingham et al., 1968; Raghuvanshi and Pathak, 1975; Desai et al., 2006; Leflon et al., 2010; Pecinka et al., 2011). For instance, in allotetraploids *Brassica napus* (AACC, $2n$ = 4x = 38), resulting from the hybridization of *Brassica rapa* (AA, $2n$ = 2x = 20) and *Brassica oleracea* (CC, $2n$ = 2x = 18) (Nagaharu, 1935), about twice as many crossovers were detected between A homologs than in diploid AA plants; whilst both displayed identical A genotypes (Leflon et al., 2010). Similarly, substantial increase of crossover frequencies was found in resynthesized triploids, typically lower than in tetraploids (Gymer and Whittington, 1975; Raghuvanshi and Pathak, 1975), but astonishingly more elevated in *Brassica* AAC allotriploids (Leflon et al., 2010). Moreover, Pelé et al. (2017) have recently pointed out that this crossovers boost occurring within the A genome was strikingly associated with reduced interference and dramatic changes in the shape of recombination landscapes. While the molecular mechanisms remain unknown, observations made in *Brassica* aneuploids suggest that this phenomenon is genetically controlled. Indeed, Suay et al. (2014) demonstrated that the boost of crossovers arising in AAC allotriploids relates to specific additional C chromosomes; the single C09 explaining 50% of the overall variation. Although exceptions have been reported in *Clitoria ternatea* and *Secale cereale* (Hazarika and Rees, 1967; Gandhi and Patil, 1997), enhanced recombination frequencies may have huge repercussions on the speciation success. The wider diversity of resulting gametes may indeed accelerate the elimination of deleterious alleles and facilitate in the long run adaptation of neopolyploids to adverse environmental situations.

In newly formed allopolyploids, meiotic recombination may also occur between the homoeologous chromosomes, as reported in diverse species including *Brassica napus*, *Coffea arabica*, *Nicotiana tabacum,* and *Tragopogon miscellus* (Song et al., 1995; Lim et al., 2004; Gaeta et al., 2007; Gaeta and Chris Pires, 2010; Xiong et al., 2011; Chester et al., 2012; Lashermes et al., 2014). Detected as early as the first meiosis of resynthesized allotetraploids (Szadkowski et al., 2010), homoeologous recombination frequency often correlates with the existing collinearity between homoeologs and varies according to the route of polyploid formation (Szadkowski et al., 2011; Rousseau-Gueutin et al., 2016). For instance, while such events are almost inexistent in the previously described *Brassica* AAC allotriploids (Leflon et al., 2006; Pelé et al., 2017), they commonly occur in ACC allotriploids and AC amphihaploids (Cifuentes et al., 2010; Yang et al., 2017). Moreover, the resulting homoeologous exchanges are smaller and more frequent when arising from unreduced gametes of amphihaploids rather than by somatic doubling (Szadkowski et al., 2011). These homoeologous exchanges deeply impact the variability and gene content of newly formed polyploids. For instance, the young allotetraploid *Coffea arabica* showed about 5% of homoeologous gene loss since its formation (Lashermes et al., 2014). Even more astonishing, up to 10% of genes are impacted after only three generations following the resynthesis of *Brassica napus* (Rousseau-Gueutin et al., 2016), highlighting that homoeologous exchanges are a major cause of gene copy number variation in *Brassica napus* varieties (Hurgobin et al., 2018). In some instances, these structural changes are at the origin of phenotypic variations, such as flowering time divergence, seed quality or disease resistance (Pires et al., 2004; Zhao et al., 2006; Stein et al., 2017), which may have contributed in the ability of allopolyploid species to exploit a wider range of environmental conditions.

ENSURING A DIPLOID-LIKE MEIOSIS TO GET FULLY ESTABLISHED THROUGH OVERALL OR TARGETED DEPLETION OF MEIOTIC CROSSOVERS

The presence of more than one possible partner to pair and recombine with may however lead to the generation of unbalanced gametes and reduced fertility, whenever

illegitimate or multiple associations arise between chromosomes at Metaphase I of meiosis (Ramsey and Schemske, 2002). Nevertheless, while commonly (but not systematically) observed in resynthesized polyploids, such associations unfrequently occur in the established ones (**Figure 1** and Supplementary Table 1). Considering the contrasted examples summarized in Supplementary Table 1, it seems that the mechanisms leading to a diploid-like meiosis (referred as 'partial diploidization') may either already exist in the parental diploids or are set up after the polyploid formation. Indeed, some species show a global genome stasis since their first meiosis (see *Gossypium hirsutum*), while others revealed increasing proportion of bivalents in the following generations (see *Arabidopsis thaliana*, *Pennisetum typhoides*). Although, this may be species-specific, the partial diploidization requires a particular regulation of meiotic recombination that differs according to the polyploids type.

In autopolyploids, multiple copies of every chromosome are true homologs thereby sharing the same chance to pair and recombine with each other. Consequently, when all homologs align in parallel during the Prophase I of meiosis, multiple associations may occur (Lloyd and Bomblies, 2016). However, while these associations are dissolved prior to Metaphase I in established autopolyploids, which primarily form bivalents through a random assortment of homologs into pair (i.e., polysomic inheritance), they are frequently maintained in those resynthesized that exhibit trivalents and/or tetravalents (Supplementary Table 1). Theoretically, a sharp reduction in the overall number of crossovers can overcome this fate, especially by ensuring a single crossover per chromosome (Lloyd and Bomblies, 2016). Although exceptions were reported, this theory has gained concrete support in the autotetraploid *Arabidopsis arenosa*. Indeed, while multivalents and increased crossover rates are observed following polyploidy induction, natural accessions exhibit predominantly bivalents with on average 1.09 crossover (Carvalho et al., 2010; Pecinka et al., 2011; Yant et al., 2013). The molecular basis of the overall crossover number reduction in established autopolyploids remains unknown but it is suggested to result from elevated interference given that the obligatory crossover is maintained per homolog pair (Bomblies et al., 2016). Additionally, genomic comparison of *Arabidopsis arenosa* and its related diploids evidenced the selection of a few meiotic genes involved in the process of crossover formation, thereby providing a list of candidates to test (Yant et al., 2013).

In allopolyploids the situation is even more challenging because of their hybrid origin. Indeed, generation of balanced gametes requires that chromosomes form pairs, instead of multivalents, and that pairs are restricted to homologs (i.e., disomic inheritance). Targeted rather than overall reduction in the number of crossovers is therefore more relevant for dissolving illegitimate associations occurring when homoeologs align in parallel during the Prophase I (Lloyd and Bomblies, 2016). Consistently, allopolyploids seem to maintain elevated crossover rates between their homologs throughout their evolution. Indeed, like resynthesized allotetraploids, cultivars of *Brassica napus* show twice more crossovers than related diploids (Wang et al., 2012; Chalhoub et al., 2014; Cai et al., 2017). Although efficient, homoeologs recognition is not completely error proof as small homoeologous exchanges may be detected in modern allopolyploids (Lloyd et al., 2018), but to a lesser extent than in the resynthesized allopolyploids (Supplementary Table 1). Previously thought to result from the increased divergence between homoeologous genomes (Feldman et al., 1997), it is now considered that this process is more likely genetically controlled (Jenczewski and Alix, 2004). So far, only the *Pairing homoeologous 1* (*Ph1*) locus acting in the hexaploid bread wheat (*Triticum aestivum*, AABBDD, $2n$ = 6x = 42) has been molecularly characterized (Sears, 1976; Griffiths et al., 2006). Briefly, this latter corresponds to a cluster of defective *cyclin dependent kinases*-like (*CDKs*) and methyl-transferase genes, where is inserted a paralog of the major crossover gene *ZIP4* that is responsible for the *Ph1* phenotype (Knight et al., 2010; Greer et al., 2012; Martín et al., 2014, 2017). Indeed, this latter *ZIP4* copy was recently shown to promote homologous recombination while inhibiting the maturation of crossovers between homoeologs (Rey et al., 2017). Moreover, although the underlying gene remains unknown, a *Ph2* locus acting on the synapsis progression has been identified in wheat, likely promoting the *Ph1* efficiency rather than directly suppressing homoeologs crossovers (Martinez et al., 2001; Sutton et al., 2003). Finally, two further genomic regions limiting homoeologous recombination have been mapped in *Arabidopsis suecica* (*BYS*) and *Brassica napus* (*PrBn*) (Liu et al., 2006; Henry et al., 2014). However, while *BYS* explains less than 10% of the variability, the efficiency of *PrBn* in the allotetraploid *Brassica napus* remains unclear as it was detected through a segregating population of amphihaploids and may thereby act exclusively in a single dose (Nicolas et al., 2009; Grandont et al., 2014).

CONCLUSION AND PERSPECTIVE

In this review, we showed that a particular regulation of meiotic recombination may have huge repercussions on the level of genetic diversity and genome stability of polyploids, and thereafter on their speciation success through natural selection. While the molecular basis of meiotic recombination has been strongly investigated in diploid species (for review see Mercier et al., 2015; Zickler and Kleckner, 2015), with recent discoveries of genes and factors (i.e., genomic and epigenetic) controlling formation and frequency of crossovers (Fernandes et al., 2017; Ziolkowski et al., 2017; Serra et al., 2018; Underwood et al., 2018), far less is known in polyploids. However, it has been shown that following polyploidization, duplicated copies of genes regulating meiosis and recombination process are preferentially lost (De Smet et al., 2013; Lloyd et al., 2014). Therefore, with a special attention on meiotic dosage-sensitive genes, and by taking advantage of the increasing number of sequenced polyploid plant genomes as well as of the major advances in NGS and genome editing (Crispr-Cas9) technologies, it will be possible to better understand the molecular mechanisms governing regulation of meiotic recombination in polyploids, from their formation toward their establishment. This increased knowledge on meiotic recombination will thereafter facilitate the growth of genetic diversity or introgression of gene of interest in polyploid crops.

AUTHOR CONTRIBUTIONS

AP organized and prepared the major part of the manuscript. A-MC and MR-G contributed to writing and reviewing the manuscript.

FUNDING

This work was partly supported by BAP INRA Department and ANR CROC: Project ANR-14-CE19-0004. AP was supported by a fellowship from BAP INRA and Conseil Régional de Bretagne.

ACKNOWLEDGMENTS

We thank Dr. Julie Ferreira de Carvalho (UMR IGEPP, France) and Dr. Julia Zinsmeister (Enza Zaden B.V., Netherlands) for their critical review of the manuscript.

SUPPLEMENTARY MATERIAL

The Supplementary Material for this article can be found online at: https://www.frontiersin.org/articles/10.3389/fpls.2018.00907/full#supplementary-material

REFERENCES

Ainouche, M. L., Baumel, A., and Salmon, A. (2004). *Spartina anglica* CE Hubbard: a natural model system for analysing early evolutionary changes that affect allopolyploid genomes. *Biol. J. Linn. Soc.* 82, 475–484. doi: 10.1111/j.1095-8312.2004.00334.x

Alix, K., Gérard, P. R., Schwarzacher, T., and Heslop-Harrison, J. S. (2017). Polyploidy and interspecific hybridization: partners for adaptation, speciation and evolution in plants. *Ann. Bot.* 120, 183–194. doi: 10.1093/aob/mcx079

Allario, T., Brumos, J., Colmenero-Flores, J. M., Iglesias, D. J., Pina, J. A., Navarro, L., et al. (2013). Tetraploid Rangpur lime rootstock increases drought tolerance via enhanced constitutive root abscisic acid production. *Plant Cell Environ.* 36, 856–868. doi: 10.1111/pce.12021

Bingham, E. T. (1980). "Maximizing heterozygosity in autopolyploids," in *Polyploidy*, ed. W. H. Lewis (Boston, MA: Springer), 471–489. doi: 10.1007/978-1-4613-3069-1_24

Bingham, E. T., Burnham, C. R., and Gates, C. E. (1968). Double and single backcross linkage estimates in autotetraploid maize. *Genetics* 59, 399–410.

Blaine Marchant, D., Soltis, D. E., and Soltis, P. S. (2016). Patterns of abiotic niche shifts in allopolyploids relative to their progenitors. *New Phytol.* 212, 708–718. doi: 10.1111/nph.14069

Bomblies, K., Jones, G., Franklin, C., Zickler, D., and Kleckner, N. (2016). The challenge of evolving stable polyploidy: could an increase in "crossover interference distance" play a central role? *Chromosoma* 125, 287–300. doi: 10.1007/s00412-015-0571-4

Bretagnolle, F., and Thompson, J. D. (1995). Gametes with the somatic chromosome number: mechanisms of their formation and role in the evolution of autopolyploid plants. *New Phytol.* 129, 1–22. doi: 10.1111/j.1469-8137.1995.tb03005.x

Brownfield, L., and Köhler, C. (2011). Unreduced gamete formation in plants: mechanisms and prospects. *J. Exp. Bot.* 62, 1659–1668. doi: 10.1093/jxb/erq371

Cai, C., Wang, X., Liu, B., Wu, J., Liang, J., Cui, Y., et al. (2017). *Brassica rapa* genome 2.0: a reference upgrade through sequence re-assembly and gene re-annotation. *Mol. Plant* 10, 649–651. doi: 10.1016/j.molp.2016.11.008

Carvalho, A., Delgado, M., Barão, A., Frescatada, M., Ribeiro, E., Pikaard, C. S., et al. (2010). Chromosome and DNA methylation dynamics during meiosis in the autotetraploid *Arabidopsis arenosa*. *Sex. Plant Reprod.* 23, 29–37. doi: 10.1007/s00497-009-0115-2

Chalhoub, B., Denoeud, F., Liu, S., Parkin, I. A., Tang, H., Wang, X., et al. (2014). Early allopolyploid evolution in the post-Neolithic *Brassica napus* oilseed genome. *Science* 345, 950–953. doi: 10.1126/science.1253435

Chester, M., Gallagher, J. P., Symonds, V. V., da Silva, A. V. C., Mavrodiev, E. V., Leitch, A. R., et al. (2012). Extensive chromosomal variation in a recently formed natural allopolyploid species, *Tragopogon miscellus* (Asteraceae). *Proc. Natl. Acad. Sci. U.S.A.* 109, 1176–1181. doi: 10.1073/pnas.1112041109

Cifuentes, M., Eber, F., Lucas, M. O., Lodé, M., Chèvre, A.-M., and Jenczewski, E. (2010). Repeated polyploidy drove different levels of crossover suppression between homoeologous chromosomes in *Brassica napus* allohaploids. *Plant Cell* 22, 2265–2276. doi: 10.1105/tpc.109.072991

Comai, L. (2005). The advantages and disadvantages of being polyploid. *Nat. Rev. Genet.* 6, 836–846. doi: 10.1038/nrg1711

De Smet, R., Adams, K. L., Vandepoele, K., Van Montagu, M. C., Maere, S., and Van de Peer, Y. (2013). Convergent gene loss following gene and genome duplications creates single-copy families in flowering plants. *Proc. Natl. Acad. Sci. U.S.A.* 110, 2898–2903. doi: 10.1073/pnas.1300127110

De Storme, N., Copenhaver, G. P., and Geelen, D. (2012). Production of diploid male gametes in Arabidopsis by cold-induced destabilization of postmeiotic radial microtubule arrays. *Plant Physiol.* 160, 1808–1826. doi: 10.1104/pp.112.208611

De Storme, N., and Geelen, D. (2013). Sexual polyploidization in plants – cytological mechanisms and molecular regulation. *New Phytol.* 198, 670–684. doi: 10.1111/nph.12184

d'Erfurth, I., Cromer, L., Jolivet, S., Girard, C., Horlow, C., Sun, Y., et al. (2010). The cyclin-A *CYCA1; 2/TAM* is required for the meiosis I to meiosis II transition and cooperates with *OSD1* for the prophase to first meiotic division transition. *PLoS Genet.* 6:e1000989. doi: 10.1371/journal.pgen.1000989

d'Erfurth, I., Jolivet, S., Froger, N., Catrice, O., Novatchkova, M., and Mercier, R. (2009). Turning meiosis into mitosis. *PLoS Biol.* 7:e1000124. doi: 10.1371/journal.pbio.1000124

Desai, A., Chee, P. W., Rong, J., May, O. L., and Paterson, A. H. (2006). Chromosome structural changes in diploid and tetraploid A genomes of *Gossypium*. *Genome* 49, 336–345. doi: 10.1139/g05-116

Feldman, M., Liu, B., Segal, G., Abbo, S., Levy, A. A., and Vega, J. M. (1997). Rapid elimination of low-copy DNA sequences in polyploid wheat: a possible mechanism for differentiation of homoeologous chromosomes. *Genetics* 147, 1381–1387.

Fernandes, J. B., Seguéla-Arnaud, M., Larchevêque, C., Lloyd, A. H., and Mercier, R. (2017). Unleashing meiotic crossovers in hybrid plants. *Proc. Natl. Acad. Sci. U.S.A.* 115, 2431–2436. doi: 10.1073/pnas.1713078114

Gaeta, R. T., and Chris Pires, J. (2010). Homoeologous recombination in allopolyploids: the polyploid ratchet. *New Phytol.* 186, 18–28. doi: 10.1111/j.1469-8137.2009.03089.x

Gaeta, R. T., Pires, J. C., Iniguez-Luy, F., Leon, E., and Osborn, T. C. (2007). Genomic changes in resynthesized *Brassica napus* and their effect on gene expression and phenotype. *Plant Cell* 19, 3403–3417. doi: 10.1105/tpc.107.054346

Gandhi, S., and Patil, V. P. (1997). Colchicine-induced autotetraploidy in *Clitoria ternatea* L. *Cytologia* 62, 13–18. doi: 10.1508/cytologia.62.13

Grandont, L., Cuñado, N., Coriton, O., Huteau, V., Eber, F., Chèvre, A. M., et al. (2014). Homoeologous chromosome sorting and progression of meiotic recombination in *Brassica napus*: ploidy does matter! *Plant Cell* 26, 1448–1463. doi: 10.1105/tpc.114.122788

Greer, E., Martín, A. C., Pendle, A., Colas, I., Jones, A. M., Moore, G., et al. (2012). The *Ph1* locus suppresses Cdk2-type activity during premeiosis and meiosis in wheat. *Plant Cell* 24, 152–162. doi: 10.1105/tpc.111.094771

Griffiths, S., Sharp, R., Foote, T. N., Bertin, I., Wanous, M., Reader, S., et al. (2006). Molecular characterization of *Ph1* as a major chromosome pairing locus in polyploid wheat. *Nature* 439, 749–752. doi: 10.1038/nature04434

Gymer, P. T., and Whittington, W. J. (1975). Hybrids between *Lolium perenne* and *Festuca pratensis*. *New Phytol.* 74, 295–306. doi: 10.1111/j.1469-8137.1975.tb02618.x

Harlan, J. R., and de Wet, J. M. J. (1975). On Ö. Winge and a prayer: the origins of polyploidy. *Bot. Rev.* 41, 361–390. doi: 10.1007/BF02860830

Hazarika, M. H., and Rees, H. (1967). Genotypic control of chromosome behaviour in rye X. Chromosome pairing and fertility in autotetraploids. *Heredity* 22, 317–332. doi: 10.1038/hdy.1967.44

Henry, I. M., Dilkes, B. P., Tyagi, A., Gao, J., Christensen, B., and Comai, L. (2014). The *BOY NAMED SUE* quantitative trait locus confers increased meiotic stability to an adapted natural allopolyploid of *Arabidopsis*. *Plant Cell* 26, 181–194. doi: 10.1105/tpc.113.120626

Hurgobin, B., Golicz, A. A., Bayer, P. E., Chan, C.-K. K., Tirnaz, S., Dolatabadian, A., et al. (2018). Homoeologous exchange is a major cause of gene presence/absence variation in the amphidiploid *Brassica napus*. *Plant Biotechnol. J.* 16, 1265–1274. doi: 10.1111/pbi.12867

Husband, B. C. (2004). The role of triploid hybrids in the evolutionary dynamics of mixed-ploidy populations. *Biol. J. Linn. Soc.* 82, 537–546. doi: 10.1111/j.1095-8312.2004.00339.x

Husband, B. C., and Sabara, H. A. (2004). Reproductive isolation between autotetraploids and their diploid progenitors in fireweed, *Chamerion angustifolium* (Onagraceae). *New Phytol.* 161, 703–713. doi: 10.1046/j.1469-8137.2004.00998.x

Husband, B. C., and Schemske, D. W. (2000). Ecological mechanisms of reproductive isolation between diploid and tetraploid *Chamerion angustifolium*. *J. Ecol.* 88, 689–701. doi: 10.1046/j.1365-2745.2000.00481.x

Jenczewski, E., and Alix, K. (2004). From diploids to allopolyploids: the emergence of efficient pairing control genes in plants. *Crit. Rev. Plant Sci.* 23, 21–45. doi: 10.1080/07352680490273239

Jiao, Y., Wickett, N. J., Ayyampalayam, S., Chanderbali, A. S., Landherr, L., Ralph, P. E., et al. (2011). Ancestral polyploidy in seed plants and angiosperms. *Nature* 473, 97–100. doi: 10.1038/nature09916

Knight, E., Greer, E., Draeger, T., Thole, V., Reader, S., Shaw, P., et al. (2010). Inducing chromosome pairing through premature condensation: analysis of wheat interspecific hybrids. *Funct. Integr. Genomics* 10, 603–608. doi: 10.1007/s10142-010-0185-0

Kreiner, J. M., Kron, P., and Husband, B. C. (2017). Evolutionary dynamics of unreduced gametes. *Trends Genet.* 33, 583–593. doi: 10.1016/j.tig.2017.06.009

Lashermes, P., Combes, M. C., Hueber, Y., Severac, D., and Dereeper, A. (2014). Genome rearrangements derived from homoeologous recombination following allopolyploidy speciation in coffee. *Plant J.* 78, 674–685. doi: 10.1111/tpj.12505

Leflon, M., Eber, F., Letanneur, J. C., Chelysheva, L., Coriton, O., Huteau, V., et al. (2006). Pairing and recombination at meiosis of *Brassica rapa* (AA) × *Brassica napus* (AACC) hybrids. *Theor. Appl. Genet.* 113, 1467–1480. doi: 10.1007/s00122-006-0393-0

Leflon, M., Grandont, L., Eber, F., Huteau, V., Coriton, O., Chelysheva, L., et al. (2010). Crossovers get a boost in *Brassica* allotriploid and allotetraploid hybrids. *Plant Cell* 22, 2253–2264. doi: 10.1105/tpc.110.075986

Lim, K. Y., Matyasek, R., Kovarik, A., and Leitch, A. R. (2004). Genome evolution in allotetraploid *Nicotiana*. *Biol. J. Linn. Soc.* 82, 599–606. doi: 10.1111/j.1095-8312.2004.00344.x

Liu, Z., Adamczyk, K., Manzanares-Dauleux, M., Eber, F., Lucas, M. O., Delourme, R., et al. (2006). Mapping *PrBn* and other quantitative trait loci responsible for the control of homeologous chromosome pairing in oilseed rape (*Brassica napus* L.) *haploids*. *Genetics* 174, 1583–1596. doi: 10.1534/genetics.106.064071

Lloyd, A., Blary, A., Charif, D., Charpentier, C., Tran, J., Balzergue, S., et al. (2018). Homoeologous exchanges cause extensive dosage-dependent gene expression changes in an allopolyploid crop. *New Phytol.* 217, 367–377. doi: 10.1111/nph.14836

Lloyd, A., and Bomblies, K. (2016). Meiosis in autopolyploid and allopolyploid *Arabidopsis*. *Curr. Opin. Plant Biol.* 30, 116–122. doi: 10.1016/j.pbi.2016.02.004

Lloyd, A. H., Ranoux, M., Vautrin, S., Glover, N., Fourment, J., Charif, D., et al. (2014). Meiotic gene evolution: can you teach a new dog new tricks? *Mol. Biol. Evol.* 31, 1724–1727. doi: 10.1093/molbev/msu119

Martín, A. C., Rey, M. D., Shaw, P., and Moore, G. (2017). Dual effect of the wheat *Ph1* locus on chromosome synapsis and crossover. *Chromosoma* 126, 669–680. doi: 10.1007/s00412-017-0630-0

Martín, A. C., Shaw, P., Phillips, D., Reader, S., and Moore, G. (2014). Licensing MLH1 sites for crossover during meiosis. *Nat. Commun.* 5:4580. doi: 10.1038/ncomms5580

Martinez, M., Cuñado, N., Carcelén, N., and Romero, C. (2001). The *Ph1* and P*h2* loci play different roles in the synaptic behaviour of hexaploid wheat *Triticum aestivum*. *Theor. Appl. Genet.* 103, 398–405. doi: 10.1007/s00122-001-0543-3

Mason, A. S., Nelson, M. N., Yan, G., and Cowling, W. A. (2011). Production of viable male unreduced gametes in *Brassica* interspecific hybrids is genotype specific and stimulated by cold temperatures. *BMC Plant Biol.* 11:103. doi: 10.1186/1471-2229-11-103

Mason, A. S., and Pires, J. C. (2015). Unreduced gametes: meiotic mishap or evolutionary mechanism? *Trends Genet.* 31, 5–10. doi: 10.1016/j.tig.2014.09.011

McIntyre, P. J. (2012). Polyploidy associated with altered and broader ecological niches in the *Claytonia perfoliata* (Portulacaceae) species complex. *Am. J. Bot.* 99, 655–662. doi: 10.3732/ajb.1100466

Mercier, R., Mézard, C., Jenczewski, E., Macaisne, N., and Grelon, M. (2015). The molecular biology of meiosis in plants. *Annu. Rev. Plant Biol.* 66, 297–327. doi: 10.1146/annurev-arplant-050213-035923

Nagaharu, U. (1935). Genome analysis in Brassica with special reference to the experimental formation of *B. napus* and peculiar mode of fertilization. *Jpn. J. Bot.* 7, 389–452.

Nasrallah, J. B. (2017). Plant mating systems: self-incompatibility and evolutionary transitions to self-fertility in the mustard family. *Curr. Opin. Genet. Dev.* 47, 54–60. doi: 10.1016/j.gde.2017.08.005

Nicolas, S. D., Leflon, M., Monod, H., Eber, F., Coriton, O., Huteau, V., et al. (2009). Genetic regulation of meiotic cross-overs between related genomes in *Brassica napus* haploids and hybrids. *Plant Cell* 21, 373–385. doi: 10.1105/tpc.108.062273

Pecinka, A., Fang, W., Rehmsmeier, M., Levy, A. A., and Scheid, O. M. (2011). Polyploidization increases meiotic recombination frequency in *Arabidopsis*. *BMC Biol.* 9:24. doi: 10.1186/1741-7007-9-24

Pécrix, Y., Rallo, G., Folzer, H., Cigna, M., Gudin, S., and Le Bris, M. (2011). Polyploidization mechanisms: temperature environment can induce diploid gamete formation in *Rosa* sp. *J. Exp. Bot.* 62, 3587–3597. doi: 10.1093/jxb/err052

Pelé, A., Falque, M., Trotoux, G., Eber, F., Nègre, S., Gilet, M., et al. (2017). Amplifying recombination genome-wide and reshaping crossover landscapes in *Brassicas*. *PLoS Genet.* 13:e1006794. doi: 10.1371/journal.pgen.1006794

Pires, J. C., Zhao, J., Schranz, M. E., Leon, E. J., Quijada, P. A., Lukens, L. N., et al. (2004). Flowering time divergence and genomic rearrangements in resynthesized *Brassica* polyploids (Brassicaceae). *Biol. J. Linn. Soc.* 82, 675–688. doi: 10.1111/j.1095-8312.2004.00350.x

Raghuvanshi, S. S., and Pathak, C. S. (1975). Polyploid breeding and possibility of raising double varieties in *Phlox drummondii*, Hook. *Cytologia* 40, 355–363. doi: 10.1508/cytologia.40.355

Ramanna, M. S., and Jacobsen, E. (2003). Relevance of sexual polyploidization for crop improvement–A review. *Euphytica* 133, 3–8. doi: 10.1023/A:1025600824483

Ramsey, J., and Schemske, D. W. (1998). Pathways, mechanisms, and rates of polyploid formation in flowering plants. *Annu. Rev. Ecol. Syst.* 29, 467–501. doi: 10.1146/annurev.ecolsys.29.1.467

Ramsey, J., and Schemske, D. W. (2002). Neopolyploidy in flowering plants. *Annu. Rev. Ecol. Syst.* 33, 589–639. doi: 10.1146/annurev.ecolsys.33.010802.150437

Rey, M. D., Martín, A. C., Higgins, J., Swarbreck, D., Uauy, C., Shaw, P., et al. (2017). Exploiting the *ZIP4* homologue within the wheat *Ph1* locus has identified two lines exhibiting homoeologous crossover in wheat-wild relative hybrids. *Mol. Breed.* 37:95. doi: 10.1007/s11032-017-0700-2

Rousseau-Gueutin, M., Morice, J., Coriton, O., Huteau, V., Trotoux, G., Nègre, S., et al. (2016). The impact of open pollination on the structural evolutionary dynamics, meiotic behavior and fertility of resynthesized allotetraploid *Brassica napus* L. *G3* 7, 705–717. doi: 10.1534/g3.116.036517

Sears, E. R. (1976). Genetic control of chromosome pairing in wheat. *Annu. Rev. Genet.* 10, 31–51. doi: 10.1146/annurev.ge.10.120176.000335

Serra, H., Lambing, C., Griffin, C. H., Topp, S. D., Nageswaran, D. C., Underwood, C. J., et al. (2018). Massive crossover elevation via combination of *HEI10* and *recq4a recq4b* during *Arabidopsis* meiosis. *Proc. Natl. Acad. Sci. U.S.A.* 115, 2437–2442. doi: 10.1073/pnas.1713071115

Song, K., Lu, P., Tang, K., and Osborn, T. C. (1995). Rapid genome change in synthetic polyploids of Brassica and its implications for polyploid evolution. *Proc. Natl. Acad. Sci. U.S.A.* 92, 7719–7723.

Stebbins, G. L. (1947). Types of polyploids: their classification and significance. *Adv. Genet.* 1, 403–429. doi: 10.1016/S0065-2660(08)60490-3

Stebbins, G. L. (1980). "Polyploidy in plants: unsolved problems and prospects," in *Polyploidy*, ed. W. H. Lewis (Boston, MA: Springer), 495–520. doi: 10.1007/978-1-4613-3069-1_26

Stebbins, G. L. (1985). Polyploidy, hybridization, and the invasion of new habitats. *Ann. Mo. Bot. Gard.* 72, 824–832. doi: 10.2307/2399224

Stein, A., Coriton, O., Rousseau-Gueutin, M., Samans, B., Schiessl, S. V., Obermeier, C., et al. (2017). Mapping of homoeologous chromosome exchanges influencing quantitative trait variation in *Brassica napus*. *Plant Biotechnol. J.* 15, 1478–1489. doi: 10.1111/pbi.12732

Suay, L., Zhang, D., Eber, F., Jouy, H., Lodé, M., Huteau, V., et al. (2014). Crossover rate between homologous chromosomes and interference are regulated by the addition of specific unpaired chromosomes in Brassica. *New Phytol.* 201, 645–656. doi: 10.1111/nph.12534

Sutton, T., Whitford, R., Baumann, U., Dong, C., Able, J. A., and Langridge, P. (2003). The *Ph2* pairing homoeologous locus of wheat (*Triticum aestivum*): identification of candidate meiotic genes using a comparative genetics approach. *Plant J.* 36, 443–456. doi: 10.1046/j.1365-313X.2003.01891.x

Szadkowski, E., Eber, F., Huteau, V., Lodé, M., Coriton, O., Jenczewski, E., et al. (2011). Polyploid formation pathways have an impact on genetic rearrangements in resynthesized *Brassica napus*. *New Phytol.* 191, 884–894. doi: 10.1111/j.1469-8137.2011.03729.x

Szadkowski, E., Eber, F., Huteau, V., Lodé, M., Huneau, C., Belcram, H., et al. (2010). The first meiosis of resynthesized *Brassica napus*, a genome blender. *New Phytol.* 186, 102–112. doi: 10.1111/j.1469-8137.2010.03182.x

Tamayo-Ordóñez, M. C., Espinosa-Barrera, L. A., Tamayo-Ordóñez, Y. J., Ayil-Gutiérrez, B., and Sánchez-Teyer, L. F. (2016). Advances and perspectives in the generation of polyploid plant species. *Euphytica* 209, 1–22. doi: 10.1007/s10681-016-1646-x

Tayalé, A., and Parisod, C. (2013). Natural pathways to polyploidy in plants and consequences for genome reorganization. *Cytogenet. Genome Res.* 140, 79–96. doi: 10.1159/000351318

Underwood, C. J., Choi, K., Lambing, C., Zhao, X., Serra, H., Borges, F., et al. (2018). Epigenetic activation of meiotic recombination near *Arabidopsis thaliana* centromeres via loss of H3K9me2 and non-CG DNA methylation. *Genome Res.* 28, 519–531. doi: 10.1101/gr.227116.117

Van de Peer, Y., Mizrachi, E., and Marchal, K. (2017). The evolutionary significance of polyploidy. *Nat. Rev. Genet.* 18, 411–424. doi: 10.1038/nrg.2017.26

Vanneste, K., Baele, G., Maere, S., and Van de Peer, Y. (2014). Analysis of 41 plant genomes supports a wave of successful genome duplications in association with the Cretaceous–Paleogene boundary. *Genome Res.* 24, 1334–1347. doi: 10.1101/gr.168997.113

Veilleux, R. (1983). Diploid and polyploid gametes in crop plants: mechanisms of formation and utilization in plant breeding. *Plant Breed. Rev.* 3, 253–288. doi: 10.1002/9781118061008.ch6

Wang, W., Huang, S., Liu, Y., Fang, Z., Yang, L., Hua, W., et al. (2012). Construction and analysis of a high-density genetic linkage map in cabbage (*Brassica oleracea* L. var. *capitata*). *BMC Genomics* 13:523. doi: 10.1186/1471-2164-13-523

Wang, Y., Jha, A. K., Chen, R., Doonan, J. H., and Yang, M. (2010). Polyploidy-associated genomic instability in *Arabidopsis thaliana*. *Genesis* 48, 254–263. doi: 10.1002/dvg.20610

Watanabe, K., Peloquin, S. J., and Endo, M. (1991). Genetic significance of mode of polyploidization: somatic doubling or 2n gametes? *Genome* 34, 28–34. doi: 10.1139/g91-005

Werner, J. E., and Peloquin, S. J. (1991). Significance of allelic diversity and 2n gametes for approaching maximum heterozygosity in 4 x potatoes. *Euphytica* 58, 21–29. doi: 10.1007/BF00035336

Xiong, Z., Gaeta, R. T., and Pires, J. C. (2011). Homoeologous shuffling and chromosome compensation maintain genome balance in resynthesized allopolyploid *Brassica napus*. *Proc. Natl. Acad. Sci.* 108, 7908–7913. doi: 10.1073/pnas.1014138108

Yang, Y., Wei, X., Shi, G., Wei, F., Braynen, J., Zhang, J., et al. (2017). Molecular and cytological analyses of A and C genomes at meiosis in synthetic allotriploid *Brassica* hybrids (ACC) between *B. napus* (AACC) and *B. oleracea* (CC). *J. Plant Biol.* 60, 181–188. doi: 10.1007/s12374-016-0221-2

Yant, L., Hollister, J. D., Wright, K. M., Arnold, B. J., Higgins, J. D., Franklin, F. C. H., et al. (2013). Meiotic adaptation to genome duplication in *Arabidopsis arenosa*. *Curr. Biol.* 23, 2151–2156. doi: 10.1016/j.cub.2013.08.059

Zhao, J., Udall, J. A., Quijada, P. A., Grau, C. R., Meng, J., and Osborn, T. C. (2006). Quantitative trait loci for resistance to *Sclerotinia sclerotiorum* and its association with a homeologous non-reciprocal transposition in *Brassica napus* L. *Theor. Appl. Genet.* 112, 509–516. doi: 10.1007/s00122-005-0154-5

Zickler, D., and Kleckner, N. (2015). Recombination, pairing, and synapsis of homologs during meiosis. *Cold Spring Harb. Perspect. Biol.* 7:a016626. doi: 10.1101/cshperspect.a016626

Ziolkowski, P. A., Underwood, C. J., Lambing, C., Martinez-Garcia, M., Lawrence, E. J., Ziolkowska, L., et al. (2017). Natural variation and dosage of the *HEI10* meiotic E3 ligase control *Arabidopsis* crossover recombination. *Genes Dev.* 31, 306–317. doi: 10.1101/gad.295501.116

Conflict of Interest Statement: The authors declare that the research was conducted in the absence of any commercial or financial relationships that could be construed as a potential conflict of interest.

frontiers in Plant Science

REVIEW
published: 05 March 2019
doi: 10.3389/fpls.2019.00074

Meiosis Research in Orphan and Non-orphan Tropical Crops

Pablo Bolaños-Villegas[1] and Orlando Argüello-Miranda[2]*

[1] Laboratory of Molecular and Cell Biology, Fabio Baudrit Agricultural Research Station, University of Costa Rica, Alajuela, Costa Rica, [2] Department of Cell Biology, The University of Texas Southwestern Medical Center, Dallas, TX, United States

Plant breeding is directly linked to the development of crops that can effectively adapt to challenging conditions such as soil nutrient depletion, water pollution, drought, and anthropogenic climate change. These conditions are extremely relevant in developing countries already burdened with population growth and unchecked urban expansion, especially in the tropical global southern hemisphere. Engineering new crops thus has potential to enhance food security, prevent hunger, and spur sustainable agricultural growth. A major tool for the improvement of plant varieties in this context could be the manipulation of homologous recombination and genome haploidization during meiosis. The isolation or the design of mutations in key meiotic genes may facilitate DNA recombination and transmission of important genes quickly and efficiently. Genome haploidization through centromeric histone mutants could be an option to create new crosses rapidly. This review covers technical approaches to engineer key meiotic genes in tropical crops as a blueprint for future work and examples of tropical crops in which such strategies could be applied are given.

Keywords: meiosis, plant breeding, genetic diversity, tropical agriculture, food security, climate change

OPEN ACCESS

Edited by:
Tomás Naranjo, Complutense University of Madrid, Spain

Reviewed by:
Dylan Wyn Phillips, Aberystwyth University, United Kingdom
Veit Schubert, Leibniz-Institut für Pflanzengenetik und Kulturpflanzenforschung (IPK), Germany

****Correspondence:***
Pablo Bolaños-Villegas
pablo.bolanosvillegas@ucr.ac.cr

Specialty section:
This article was submitted to Plant Cell Biology, a section of the journal Frontiers in Plant Science

Received: *06 August 2018*
Accepted: *17 January 2019*
Published: *05 March 2019*

Citation:
Bolaños-Villegas P and Argüello-Miranda O (2019) Meiosis Research in Orphan and Non-orphan Tropical Crops. Front. Plant Sci. 10:74. doi: 10.3389/fpls.2019.00074

INTRODUCTION: CROP YIELDS IN A CHANGING WORLD

Current projections suggest that the world population will increase to 9.6 billion in 2050 and to 10.9–13.2 billion in 2100. Most of this growth may take place in Sub-Saharan Africa, especially Nigeria, followed by Asia (Gerland et al., 2014). Hence, demand for agricultural products is expected to increase by about 50% by 2030 with the increasing global population (Wheeler and Von Braun, 2013), a situation that requires intensifying the food system production (Wheeler and Von Braun, 2013), namely by increasing unit area (yield) (Phalan et al., 2016). This demand is compounded by several problems including (1) insufficient crop yields due to climate change (Zhao et al., 2017) and (2) insufficient crop yield increases with traditional breeding methodologies (Ray et al., 2013).

Furthermore, it is expected that one of the main effects of anthropogenic climate change will be a mean increase of 1.4–5.8°C in the Earth's surface temperature above the pre-industrial temperature, in the range of 1.4–5.8°C by 2050–2080, caused by the greenhouse gasses carbon

dioxide (CO_2), methane (CH_4), nitrous oxide (N_2O), chlorofluorocarbons (CFCs), and ozone (O_3) (El-Sharkawy, 2014). Modeling suggests that the altered pattern of increase in temperatures can have significant adverse effects on crop yields (Zhao et al., 2017). In maize, each increase in 1°C causes a yield reduction of about 7.4%, and 32% in wheat and rice, respectively (Zhao et al., 2017). Estimates vary for mid-latitude countries, especially South America, which are expected to be not as affected as Eastern Europe, Russia, Northeastern China, and Northwest United States and Canada (Iizumi et al., 2017). Low-income countries at low latitudes may experience the worst effects unless intense technological and management mitigation occurs (Iizumi et al., 2017). Future crop yields are believed to become negative in low-income countries with rapidly growing populations (Ray et al., 2013); in countries such as Guatemala, maize yields are already decreasing (Ray et al., 2013). In this scenario, faster and better improvements on crops will be essential to prevent hunger and sustain the future population of the planet.

GENOMICS AND BREEDING OF ORPHAN CROPS

For communities in developing countries, crops such as cassava, sweet potato, yam, plantains, common beans, and millet are of great importance as a food source (Varshney et al., 2012). Most of these crops are not extensively traded, receive little attention in affluent countries, and are grown in marginal environments of Africa, Asia and South America; they are often referred to as "orphan crops" (Varshney et al., 2012). Genomic or bioinformatic resources for orphan crops are usually lacking or underdeveloped (Armstead et al., 2009). Because of lack of access to genotyping, sequencing and computational facilities, scientists have difficulty characterizing these crops (Varshney et al., 2012), and their commonly large, complex and polyploid genomes discourages further research (Kamei et al., 2016).

One viable alternative to study such genomes would be to make use of the available information for model organisms and translate this knowledge to crops (Kamei et al., 2016). Examples of this strategy for applied breeding exist for cassava (Odipio et al., 2017) and for the non-orphan crop cacao (Fister et al., 2018).

Clonal propagation of cassava (*Manihot esculenta*) is thought to have caused a domestication bottleneck, as suggested by the accumulation of deleterious alleles in a heterozygous condition throughout the genome, and may have led to inbreeding depression (Ramu et al., 2017), which is suspected to have reduced yields by 60% (Ramu et al., 2017). The only practical options to purge these mutations is conventional breeding involving sexual reproduction and DNA recombination, perhaps combined with genomic selection and genome editing (Ramu et al., 2017). In cassava (*M. esculenta*), breeding with the wild relative *M. glaziovii* allowed for the transmission of useful traits such as increased water uptake, virus and pest resistance, and apomictic seed development (Nassar and Ortiz, 2010); the latter would be beneficial because it would allow the propagation of hybrids without the need for cuttings that enable viruses and bacteria to contaminate the plants (Nassar and Ortiz, 2010). Introgression of useful traits from wild relatives has also been reported in the breeding of fruit tree papaya (*Carica papaya*) (Coppens d'Eeckenbrugge et al., 2014) and coffee (Herrera et al., 2012) and was proposed in cacao (Dantas and Guerra, 2010). These are tropical cash crops that are not usually considered orphan crops but whose social impact is considerable in developing countries (Myrick et al., 2014; Giuliani et al., 2017; Wickramasuriya and Dunwell, 2018). Therefore, the term orphan crop may not accurately describe scientific and agricultural neglect in all contexts.

MEIOSIS AND PLANT BREEDING

Plant breeding of sexually reproducing species relies on the execution of a specialized form of cell division called meiosis (Wang and Copenhaver, 2018). In this process, two rounds of chromosome segregation occur after a single round of DNA synthesis. In the first meiotic nuclear division, maternal and paternal chromosomes, otherwise known as "homologs," separate, whereas during the second meiotic nuclear division, sister chromatids are segregated (Lambing et al., 2017). The result is the production of recombinant cells, which contain a single copy of the species genome (Lambing et al., 2017; Wang and Copenhaver, 2018).

Meiotic Recombination

The landmark of meiosis is the process of homologous DNA recombination that occurs during the stage of prophase I, before the first meiotic division. The faithful segregation of homologous chromosomes crucially depends on homologous recombination. This process involves the initial formation of DNA double-strand breaks (DNA DSBs) by the conserved endonuclease SPO11 followed by mechanisms that ensure proper DNA repair (Lambing et al., 2017).

In budding yeast, SPO11 is believed to be cleaved and released by the Mre11–Rad50–Xrs2 (MRX) complex and by Sae2/COM1 (Serra et al., 2018). At the same time endonucleases, such as Mre11 and Exo1 create 3′-overhanging single-stranded DNA that may be thousands of nucleotides in length (Serra et al., 2018). Resected single-stranded DNA is then bound by RAD51 and DMC1 RecA-like proteins, which catalyze the invasion of a homologous chromosome and the formation of a displacement loop (D loop) (Serra et al., 2018). Stabilization of the D loop may occur by template-driven DNA synthesis from the invading 3′end (Serra et al., 2018). Strand invasion intermediates may then progress to second-end capture and formation of a double Holliday junction (dHJ), which can be resolved as a crossover (CO) or non-crossover (NCO) or undergo dissolution (Serra et al., 2018). COs can be further categorized as sensitive (Type I) or insensitive (Type II) to a phenomenon called crossover interference, which prevents closely spaced double COs (Wang and Copenhaver, 2018). The formation of Type I COs is believed to be regulated by the MSH4/MSH5 MutS-related heterodimer, MER3 DNA helicase, SHORTAGE OF

CROSSOVERS1 (SHOC1) XPF nuclease, PARTING DANCERS (PTD), ZIP4/SPO22, HEI10 E3 ligase, and MLH1/MLH3 MutL-related heterodimer (Serra et al., 2018). Within this pathway, the HEI10 E3 ligase gene shows dosage sensitivity, which means that copies increase crossovers throughout euchromatin. Type II COs form by a different MUS81-dependent pathway, account for about 15% of crossovers and do not show interference (Serra et al., 2018). NCOs are thought to be generated by an alternate pathway called synthesis-dependent strand annealing (SDSA). SDSA follows the same initial steps as DNA DSB repair until second-end capture, when the invading strand instead dissociates, and the newly synthesized 3′ DNA anneals to the single-strand 3′end on the opposite side of the original break. Gap-filling DNA synthesis and ligation result in an NCO (Wang and Copenhaver, 2018).

The production of viable offspring and the generation of new combinations of traits/alleles in plants crucially depends on the balance of COs/NCOs; for instance, if formation of an obligate CO is absent, there is non-disjunction, whereas the opposite situation of elevated CO level does not lead to inviability (Crismani et al., 2012). Plant breeding also relies on the formation of meiotic crossovers to combine favorable alleles into elite varieties (Mieulet et al., 2018). However, meiotic crossovers are rare, normally 1–3 per chromosome, which limits the efficiency of the breeding process and genetic mapping (Mieulet et al., 2018). Therefore, the manipulation of meiotic recombination to increase the CO/NCO ratio is of capital importance to improve the ability of plant breeders to obtain better combinations of traits and faster.

For instance, *Arabidopsis* has approximately 150–250 DSBs per meiosis, as estimated by immunostaining of DSB markers, such as γH2A.X, RAD51, and DMC1. However, the repair of these DSBs results in the formation of only about 10 COs, which suggests the activity of inhibitory mechanisms, called anticrossover factors, that prevent CO resolution (Wang and Copenhaver, 2018). NCO repair of strand invasion events is believed to be promoted by multiple, non-redundant pathways that may include the proteins FANCONI ANEMIA COMPLEMENTATION GROUP M (FANCM), MHF1, MHF2, FIDGETIN-LIKE1 (FIGL1), RECQ4A, RECQ4B, TOPOISOMERASE3α (TOP3α), and MSH2 (Mercier et al., 2015). The action of these NCO pathways results in repair of about 90% of all initial meiotic DNA DSBs as NCOs (Mercier et al., 2015). As stated earlier, the formation of crossovers is also regulated by activity of the *HEI10* meiotic E3 ligase gene (Ziolkowski et al., 2017), and additional copies of the gene enhance the effectivity of the process (Ziolkowski et al., 2017), especially in the *recq4a/recq4b* mutant background (Serra et al., 2018). An R264G polymorphism in the C-termi-nus of HEI10 is also believed to enhance recombination by promoting protein function or expression timing (Ziolkowski et al., 2017).

Analysis of tomato cv. Micro Tom EMS-mutant lines for the antihelicase RECQ4 indicated a 2.7-fold increase in recombination, and a similar outcome was reported for rice Dongjin/Nipponbare F_1 hybrids, which are *recq4/fancm* mutants; therefore manipulation of the crossover formation in crops is feasible (Mieulet et al., 2018).

Genome Haploidization Using Modified Centromeric Histones/Apomixis

In the model plant *Arabidopsis thaliana*, haploid clonal plants can be obtained from seeds by altering the coding sequence for the centromere-specific histone CENH3 (CENP-A in humans), which is universal in plant species (Ravi and Chan, 2010). On crossing *cenh3* homozygous mutants expressing an altered *CENH3* sequence with the wild-type, chromosomes from the mutant are eliminated in the zygote, which results in haploid progeny. Haploids are then spontaneously converted into fertile diploids via meiotic non-reduction, which allows for propagation of the genotype of choice (Ravi and Chan, 2010). Changes in the naturally hypervariable N-terminal tail of CENH3 cause segregation errors and chromosome elimination (Maheshwari et al., 2015). Comparison of CENH3 protein sequences from more than 50 plant species showed that the N-terminal tail region is highly variable, whereas the C-terminal histone fold domain (HFD) is relatively conserved across species. A key HFD mutation (P82S) caused by a single nucleotide substitution induced haploidy in *Arabidopsis* (Kuppu et al., 2015). This mutation occurs in crops such as cassava, papaya, bananas, soy, maize, and rice and may be exploited for plant breeding purposes (Kuppu et al., 2015). A similar mutation (L130F) causes inactivation of centromere loading in barley (Karimi-Ashtiyani et al., 2015). It has been suggested to combine this approach with the simultaneous inactivation of meiotic genes *OSD1* (*OMISSION OF SECOND DIVISION*, a negative regulator of the *Arabidopsis* APC/C during meiosis), *REC8* (required for proper separation of sister chromatids during meiosis I) and *SPO11*. The inactivation of these three genes leads to the *MiMe* genotype: *Mitosis instead of Meiosis*, and it is believed that a combination with *CENH3* engineering may produce asexual seeds (Ishii et al., 2016). Alternatively, the *MiMe* genotype may be combined with ectopic expression in the egg cell of the *BABY BOOM 1* (*BBM1*) sperm transcription factor to induce parthenogenesis and asexual seed development (apomixis), as shown in rice cultivar Kitaake (*Oryza sativa* L. ssp. *japonica*) (Khanday et al., 2018).

TROPICAL CROPS AMENABLE FOR MEIOTIC GENE MANIPULATION

Cassava (*Manihot esculenta* Crantz)

The cassava genome is 742 Mb in size ($2n = 36$) and to contain 34,483–38,845 functional genes (Wang et al., 2014). Cassava is the main source of starch for 700 million people around the world (Wang et al., 2014; **Figures 1A–C**). Surprisingly, up to 19% of all coding single nucleotide polymorphisms are believed to be deleterious (Ramu et al., 2017), which may explain its poor root yield of only 13.6 tons per hectare (Wang et al., 2014). Meiosis in interspecific hybrids between *Manihot esculenta Crantz* and *Manihot neusana Nassar* lead to the formation of restitution nuclei and micronuclei (Nassar et al., 1995), caused by defects during anaphase I (Nassar et al., 1995). Backcross generations 1–4 were aneuploid and eventually sterile (Nassar et al., 1995). Light

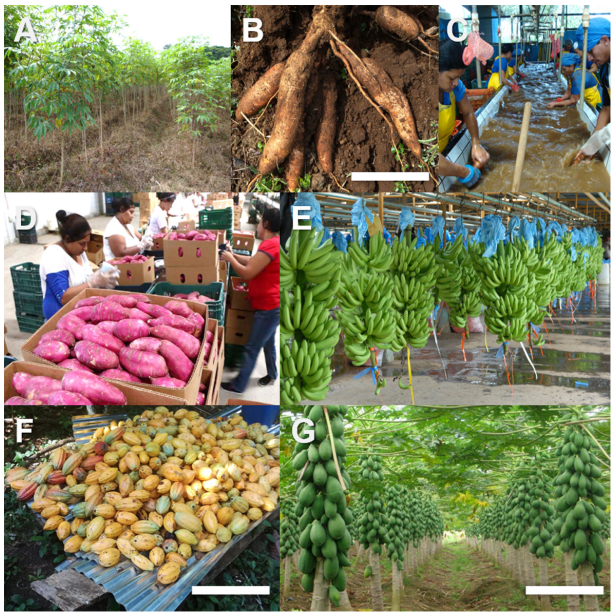

FIGURE 1 | Production of tropical crops in Central America. **(A)** Cassava farm in Northern Costa Rica. **(B)** Cassava tubers being harvested (Costa Rica). **(C)** Cassava processing plant (Costa Rica). **(D)** Sweet potato packaging facility in Honduras. **(E)** Banana processing facility in Costa Rica. **(F)** Papaya farm in Costa Rica. **(G)** Harvest of cacao in Costa Rica. Scale bars: **(B,G)** 25 cm, **(F)** 50 cm. Image credits: **(A)** Alfredo Durán (University of Costa Rica), **(B,C)** Helga Blanco-Metzler (University of Costa Rica), **(D)** La Prensa Newspaper (Honduras), **(E)** Rodríguez Chaparro and Héctor Osvaldo, National Distance University (UNED) image repository, Costa Rica, **(F)** Eric Mora-Newcomer (University of Costa Rica), **(G)** Óscar Brenes, Foundation for Agricultural Research (FITTACORI, Costa Rica).

microscopy analysis of embryo sacs in *M. neusana* suggested that 1.5% of all ovules were apomictic, and F_2 hybrids between *Manihot esculenta* and *M. neusana* appeared to be fully apomictic (Nassar et al., 2000). Gene editing with the CRISPR/Cas9 system in calli of cassava is possible (Odipio et al., 2017), which suggests possible editing of key meiotic genes, especially those related to CO/NCO formation. One possibility in cassava would be to facilitate outcrossing by targeting homologs for *FANCM*, *FIGL1*, *RECQ4A*, and *RECQ4B* as done in tomato and rice (Mieulet et al., 2018). Formation of double haploids by Targeting Induced Local Lesions in Genomes (TILLING) and engineering of *cenh3* mutants has also been suggested for cassava (Kuppu et al., 2015).

Sweet Potato (*Ipomoea batatas* Linn.)

Sweet potato is one of the oldest domesticated crops in the Americas (Kyndt et al., 2015), and is the only cultivated species among the 15 in the section batatas of the family Convolvulaceae (Becerra Lopez-Lavalle, 2002; **Figure 1D**). Cultivated sweet potato is autoallohexaploid ($2n = 90$), although wild tetraploid specimens ($2n = 60$) have been reported (Becerra Lopez-Lavalle, 2002; Kyndt et al., 2015). Most of the world's production is concentrated in China (Wang et al., 2010). The large genome (2205 Mb) contains approximately 56,516 unigenes; 35,051 have been identified (Wang et al., 2010). Sweet potato is one of the most efficient crops in terms of dry-matter productivity and is a model for carbohydrate storage and tuber formation (Wang et al., 2010). Unfortunately, sweet potato is vegetatively propagated, and it is prone to accumulate and disseminate geminiviruses (Paprotka et al., 2010). $2n$ pollen and polyads are formed in tetraploid accessions, so conventional breeding is difficult (Becerra Lopez-Lavalle, 2002). However, work in tetraploid *Arabidopsis arenosa* suggests that meiotic chromosome segregation may be improved by bringing chiasmata number down to one per bivalent because limiting crossovers to one per chromosome prevents multivalent associations (Yant et al., 2013). Results from TILLING and cytological analyses suggest that in polyploid accessions, homoeologous recombination may be reduced by selection of putative specific amino acid sequences in genes involved in sister chromatid cohesion, axis formation, synapsis and recombination, namely *ASY1*, *ASY3*, *SYN1/REC8*, *SMC1*, *PDS5*, *ZYP1a*, and ZYP1b (Wright et al., 2015). In some cases, these changes may reduce DNA binding, and in some cases, they may reduce phosphorylation of the putative protein (Wright et al., 2015). The most notable changes were K40E in the DNA-binding HORMA domain of ASY1; T265I and L268V in ASY3; S242F and S527Y in PDS5; and F595S and Q923K in SMC1 (Wright et al., 2015). Selection of such residues in sweet potato accessions combined with genome editing might help improve meiotic chromosome segregation, viability and facilitate conventional breeding. Alternatively, decreased ASY1 activity in wheat transgenic lines promotes homoeologous pairing (Yant et al., 2013), so overexpression of ASY1 might be useful to reduce CO formation.

Banana (*Musa* sp.)

Banana and plantain are major staple foods and are a source of income for millions in tropical and subtropical regions (Tripathi et al., 2013; **Figure 1E**). Most bananas and plantains grown worldwide are produced by small-scale farmers for home consumption or for sale in local and regional markets. Many pests and diseases significantly affect *Musa* cultivation (Tripathi et al., 2013).

The genome of *M. acuminata* ($2n = 22$) is 523 Mb in size (D'hont et al., 2012). Cultivated bananas are mainly triploids, and breeding mostly involves crossing fertile triploids with diploids to obtain tetraploids, which are then crossed to diploid accessions to obtain triploid cultivars (Muiruri et al., 2017). Modification of *Arabidopsis* CENH3 by replacing the N-terminal tail with that of the variant H3.3 and tagging it with GFP resulted in haploid formation (Muiruri et al., 2017), an outcome that if properly exploited would be useful to breed new bananas (Muiruri et al., 2017). The rationale is as follows, work in barley interspecific hybrids has shown that CENH3 is required for kinetochore function (Sanei et al., 2011); if the CENH3 sequences from both parents are very divergent during early embryogenesis, centromere activity will remain in both parental genomes (Sanei et al., 2011). However, chromosomes of the male will start to lag because of centromere inactivity during anaphase, subsequently forming micronuclei. Finally, micronucleated male

chromatin will degrade, and a haploid maternal embryo will develop (Sanei et al., 2011).

Hypothetically, genotyping banana accessions for divergent *CENH3* alleles could be used to produce natural triploid hybrids (Muiruri et al., 2017). *CENH3* sequences were analyzed in the accessions "Calcutta 4" and "Zebrina GF" from *M. acuminata*, in *M. balbisiana*, and in the commercial interspecific triploids "Sukali Ndiizi," "Pisang Awak" and "Gros Michel" (Muiruri et al., 2017). The genotype "Calcutta 4" and "*M. balbisiana*" have one each, "Gros Michel" and "Pisang Awak" has two, "Zebrina GF" has four and "Sukali Ndiizi" have seven (Muiruri et al., 2017). These sequences are highly variable in the N-terminal tail and show specific P-to-A and G-to-E amino acid substitutions within the HFD that may be used to determine crosses (Muiruri et al., 2017).

Cacao (*Theobroma cacao* Linn.)

Cultivation of *T. cacao*, the tropical tree that produces cocoa beans, is a key export activity for many developing countries, especially from Africa (Fister et al., 2018; **Figure 1F**). Thus, a reliable and sustainable output is important to guarantee the livelihoods of 6 million small-scale cacao farmers around the world (Fister et al., 2018; Wickramasuriya and Dunwell, 2018). Cacao seeds are a rich source of polyphenolic antioxidants that may prevent cancer or delay/slow the progression of cancer and serve as cardioprotective agents (Wickramasuriya and Dunwell, 2018).

The two most serious diseases of cacao are caused by the fungi *Crinipellis perniciosa* (witch's broom disease) and *Moniliophthora roreri* (frosty pod rot) (Aime and Phillips-Mora, 2005). Annual losses are 30% (Argout et al., 2011).

T. cacao L. is a diploid tree species ($2n$ = 20) from the Malvaceae family that is endemic to South American rainforests. It is believed to have been domesticated approximately 3,000 years ago in Central America (Argout et al., 2011). The genome of the Belizean Criollo genotype B97-61/B2 is 430 Mb in size and is rich in retrotransposons (Argout et al., 2011). Cacao displays a late-acting self-incompatibility syndrome, which results in failure of karyogamy after discharge of sperm cells into the embryo sacs (Gibbs, 2014). Selfed pistils in this species abscise 3 days after post-pollination (Gibbs, 2014). Five self-incompatibility genes are proposed to regulate the process, showing dominance and equal effects (in both pollen and pistil) with the sequence of importance $S_1 > S_2 = S_3 > S_4 > S_5$ (Gibbs, 2014); however, no genes have been characterized molecularly. Meiosis has been analyzed in the diploid clones T85/799 (derived from a cross between two Upper Amazon varieties), T28 (a Venezuelan Criollo) and TF6 (from Ghana) (Martinson, 1975). Chromosome segregation at anaphase is regular and laggards are rare. Chiasma frequency was estimated at 9.00–9.35 per cell (Martinson, 1975). These results suggest that the chiasma frequency is less than the basic chromosome number, which implies that during meiosis, univalents are present in most cases and hint at defects in Type I CO formation. Unfortunately, no recent descriptions of cacao meiosis are available.

Development of double haploids is difficult in cacao and has even involved irradiation of pollen at 50 and 100 Gy to induce inhibition of the division of the generative nucleus. The only way to obtain haploid plantlets may be *in vitro* ovary culture (Falque et al., 1992). Cacao is amenable to transformation with CRISPR/Cas9 by using detached leaves (Fister et al., 2018), and haploid clonal plant formation might be possible, as was suggested for banana (Muiruri et al., 2017). Alternatively, deregulation of anticrossover activity by the cacao homologs of *FANCM* and *RECQ4* may facilitate the introgression of wild traits in cacao elite cultivars. Comparison of sequencing results across several accessions in the West Indies and Costa Rica including Criollo, Amelonado and Nacional cultivars suggests that during the process of domestication, there may have been a strong selection for genes involved in the metabolism of protecting anthocyanins and the stimulant theobromine, coupled with a general decrease in population fitness and reproductive success (Cornejo et al., 2018).

Papaya (*Carica papaya* Linn.)

Papaya is a fruit tree cultivated in tropical and subtropical regions and is known for its nutritional benefits and medicinal applications (Ming et al., 2008; **Figure 1G**). Papaya is not considered an orphan crop, but its consumption has a considerable impact on the health and well-being of vulnerable populations. Indeed, consumption of its fruit may prevent vitamin A deficiency, a cause of childhood blindness in tropical and subtropical developing countries (Liao et al., 2017). The largest producers of papaya are Brazil, Indonesia, Ethiopia, Congo, Thailand, Guatemala, and Colombia (Fuentes and Santamaría, 2014).

Papaya belongs to the small family Caricaceae, which contains 6 genera and 35 species (Liao et al., 2017). It is a diploid ($2n$ = 18) with a small genome of 372 Mb and possesses a primitive sex-chromosome system (Ming et al., 2008). In papaya, females are XX while maleness and hermaphroditism are controlled by slightly different sex-specific Y chromosome regions: Y^h (HSY) in hermaphrodites and Y (MSY) in males (VanBuren et al., 2015). Hermaphrodite flowers give rise to oblong fruits that are commercially desirable (Jiménez et al., 2014). Both HSY and MSY loci are 8.1 Mb long and are located on chromosome 1, the largest. Recombination with the X chromosome is suppressed, and any combination of the Y and Y^h loci (YY, YY^h, or Y^hY^h) is inviable (VanBuren et al., 2015).

Hybridization of papaya with the wild relative *Vasconcellea quercifolia* allowed for successful introgression of resistance to Papaya ringspot virus into backcross generations 3 and 4, as determined by serological tests and field evaluation in infested plots (Siar et al., 2011). The process is laborious and requires *in vitro* culture of embryos (Siar et al., 2011). Nonetheless, interspecific hybridization was found an important tool for breeding new papaya cultivars (Siar et al., 2011). In wheat, the *ph1b* deletion line has been exploited in crosses with wild relatives to allow for exchange between chromosomes at meiosis (Rey et al., 2018). The *ph1b* deletion has been shown to correspond to the *ZIP4-B2* gene, a factor that regulates the formation of type I COs (Rey et al., 2018). When this mutation is combined with a nutrition regime rich in Mg^{2+}, the mean number of COs increases to 12 per cell as compared with 1–7 in *ph1b*

mutants and 1 in the wild type (Rey et al., 2018). High phosphate has also a positive effect in barley meiosis, and was shown to increase chiasmata formation from 7,7 per cell in the control to 10,6 (Fuchs et al., 2018). Therefore, gene editing in papaya combined with enhanced nutrition with Mg^{2+} or phosphate might facilitate outcrossing with wild relatives.

CONCLUSION

Tropical crops, considered orphan or not, are the key to preventing hunger, guaranteeing good health and creating economic growth in developing countries (Kamei et al., 2016; Liao et al., 2017). The translation of current knowledge of meiotic processes such as homologous recombination, and CO formation may help produce new varieties that are enriched in desirable wild traits. The application of one particular approach to manipulate meiosis in these crops may depend on factors that go beyond the scope of this review and may vary from what is suggested. However, by first outlining the possibilities, we hope to encourage research into the regulation of meiotic processes in tropical crops and applied translational work.

AUTHOR CONTRIBUTIONS

All authors listed have made a substantial, direct and intellectual contribution to the work, and approved it for publication.

FUNDING

Work by PB-V is supported by the Vicerrectoría de Investigación (University of Costa Rica) intramural grant nos. B6602, B5A52, B5A49, and B7801. PB-V is a TWAS/UNESCO young affiliate in agricultural sciences.

REFERENCES

Aime, M. C., and Phillips-Mora, W. (2005). The causal agents of witches' broom and frosty pod rot of cacao (chocolate, Theobroma cacao) form a new lineage of Marasmiaceae. *Mycologia* 97, 1012–1022. doi: 10.3852/mycologia.97.5.1012

Argout, X., Salse, J., Aury, J. M., Guiltinan, M. J., Droc, G., Gouzy, J., et al. (2011). The genome of Theobroma cacao. *Nat. Genet.* 43, 101–108. doi: 10.1038/ng.736

Armstead, I., Huang, L., Ravagnani, A., Robson, P., and Ougham, H. (2009). Bioinformatics in the orphan crops. *Brief. Bioinform.* 10, 645–653. doi: 10.1093/bib/bbp036

Becerra Lopez-Lavalle, L. A. (2002). Occurrence and cytological mechanism of 2n pollen formation in a tetraploid accession of Ipomoea batatas (sweet potato). *J. Hered.* 93, 185–192. doi: 10.1093/jhered/93.3.185

Coppens d'Eeckenbrugge, G., Drew, R., Kyndt, T., and Scheldeman, X. (2014). "Vasconcellea for papaya improvement," in *Genetics and Genomics of Papaya, Plant Genetics and Genomics: Crops and Models*, Vol. 10, eds R. Ming and P. H. Moore (New York, NY: Springer Science+Business Media), 47–79. doi: 10.1007/978-1-4614-8087-7_4

Cornejo, O. E., Yee, M.-C., Dominguez, V., Andrews, M., Sockell, A., Strandberg, E., et al. (2018). Population genomic analyses of the chocolate tree, Theobroma cacao L., provide insights into its domestication process. *Commun. Biol.* 167, 1–16. doi: 10.1038/s42003-018-0168-6

Crismani, W., Girard, C., Froger, N., Pradillo, M., Santos, J. L., Chelysheva, L., et al. (2012). FANCM limits meiotic crossovers. *Science* 336, 1588–1590. doi: 10.1126/science.1220381

Dantas, L. G., and Guerra, M. (2010). Chromatin differentiation between Theobroma cacao L. and *T. grandiflorum* schum. *Genet. Mol. Biol.* 33, 94–98. doi: 10.1590/S1415-47572009005000103

D'hont, A., Denoeud, F., Aury, J. M., Baurens, F. C., Carreel, F., Garsmeur, O., et al. (2012). The banana (*Musa acuminata*) genome and the evolution of monocotyledonous plants. *Nature* 488, 213–217. doi: 10.1038/nature11241

El-Sharkawy, M. A. (2014). Global warming: causes and impacts on agroecosystems productivity and food security with emphasis on cassava comparative advantage in the tropics/subtropics. *Photosynthetica* 52, 161–178. doi: 10.1007/s11099-014-0028-7

Falque, M., Kodia, A. A., Sounigo, O., Eskes, A. B., and Charrier, A. (1992). Gamma-irradiation of cacao (Theobroma cacao L.) pollen: effect on pollen grain viability, germination and mitosis and on fruit set. *Euphytica* 64, 167–172. doi: 10.1007/BF00046045

Fister, A. S., Landherr, L., Maximova, S. N., and Guiltinan, M. J. (2018). Transient expression of CRISPR/Cas9 machinery targeting TcNPR3 enhances defense response in Theobroma cacao. *Front. Plant Sci.* 9:268. doi: 10.3389/fpls.2018.00268

Fuchs, L. K., Jenkins, G., and Phillips, D. W. (2018). Anthropogenic impacts on meiosis in plants. *Front. Plant Sci.* 9:1429. doi: 10.3389/fpls.2018.01429

Fuentes, G., and Santamaría, J. M. (2014). "Papaya (Carica papaya L.): origin, domestication, and production," in *Genetics and Genomics of Papaya, Plant Genetics and Genomics: Crops and Models*, Vol. 10, eds R. Ming and P. Moore (New York, NY: Springer), 3–16. doi: 10.1007/978-1-4614-8087-7_1

Gerland, P., Raftery, A. E., Ševčíková, H., Li, N., Gu, D., Spoorenberg, T., et al. (2014). World population stabilization unlikely this century. *Science* 346, 234–237. doi: 10.1126/science.1257469

Gibbs, P. E. (2014). Late-acting self-incompatibility - the pariah breeding system in flowering plants. *New Phytol.* 203, 717–734. doi: 10.1111/nph.12874

Giuliani, E., Ciravegna, L., Vezzulli, A., and Kilian, B. (2017). Decoupling standards from practice: the impact of in-house certifications on coffee farms' environmental and social conduct. *World Dev.* 96, 294–314. doi: 10.1016/j.worlddev.2017.03.013

Herrera, J. C., Romero, J. V., Camayo, G. C., Caetano, C. M., and Cortina, H. A. (2012). Evidence of intergenomic relationships in triploid hybrids of coffee (Coffea sp.) as revealed by meiotic behavior and genomic in situ hybridization. *Trop. Plant Biol.* 5, 207–217. doi: 10.1007/s12042-012-9105-x

Iizumi, T., Furuya, J., Shen, Z., Kim, W., Okada, M., Fujimori, S., et al. (2017). Responses of crop yield growth to global temperature and socioeconomic changes. *Sci. Rep.* 7:7800. doi: 10.1038/s41598-017-08214-4

Ishii, T., Karimi-Ashtiyani, R., and Houben, A. (2016). Haploidization via chromosome elimination: means and mechanisms. *Annu. Rev. Plant Biol.* 67, 421–438. doi: 10.1146/annurev-arplant-043014-114714

Jiménez, V. M., Mora-Newcomer, E., and Gutiérrez-Soto, M. V. (2014). "Biology of the papaya plant," in *Genetics and Genomics of Papaya, Plant Genetics and Genomics: Crops and Models*, Vol. 10, eds R. Ming and P. H. Moore (New York, NY: Springer Science+Business Media), 17–33. doi: 10.1007/978-1-4614-8087-7_2

Kamei, C. L. A., Severing, E. I., Dechesne, A., Furrer, H., Dolstra, O., and Trindade, L. M. (2016). Orphan crops browser: a bridge between model and orphan crops. *Mol. Breed.* 36, 1–18. doi: 10.1007/s11032-015-0430-2

Karimi-Ashtiyani, R., Ishii, T., Niessen, M., Stein, N., Heckmann, S., Gurushidze, M., et al. (2015). Point mutation impairs centromeric CENH3 loading and induces haploid plants. *Proc. Natl. Acad. Sci. U.S.A.* 112, 11211–11216. doi: 10.1073/pnas.1504333112

Khanday, I., Skinner, D., Yang, B., Mercier, R., and Sundaresan, V. (2018). A male-expressed rice embryogenic trigger redirected for asexual propagation through seeds. *Nature* 565, 91–95. doi: 10.1038/s41586-018-0785-8

Kuppu, S., Tan, E. H., Nguyen, H., Rodgers, A., Comai, L., Chan, S. W. L., et al. (2015). Point mutations in centromeric histone induce post-zygotic incompatibility and uniparental inheritance. *PLoS Genet.* 11:e1005494. doi: 10.1371/journal.pgen.1005494

Kyndt, T., Quispe, D., Zhai, H., Jarret, R., Ghislain, M., Liu, Q., et al. (2015). The genome of cultivated sweet potato contains *Agrobacterium* T-DNAs with expressed genes: an example of a naturally transgenic food crop. *Proc. Natl. Acad. Sci. U.S.A.* 112, 5844–5849. doi: 10.1073/pnas.1419685112

Lambing, C., Franklin, F. C. H., and Wang, C.-J. R. (2017). Understanding and manipulating meiotic recombination in plants. *Plant Physiol.* 173, 1530–1542. doi: 10.1104/pp.16.01530

Liao, Z., Yu, Q., and Ming, R. (2017). Development of male-specific markers and identification of sex reversal mutants in papaya. *Euphytica* 213:53. doi: 10.1007/s10681-016-1806-z

Maheshwari, S., Tan, E. H., West, A., Franklin, F. C. H., Comai, L., and Chan, S. W. L. (2015). Naturally occurring differences in CENH3 affect chromosome segregation in zygotic mitosis of hybrids. *PLoS Genet.* 11:e1004970. doi: 10.1371/journal.pgen.1004970

Martinson, V. A. (1975). Cytological studies of diploid and tetraploid Theobroma cacao. *Genetica* 45, 341–348. doi: 10.1007/BF01508308

Mercier, R., Mézard, C., Jenczewski, E., Macaisne, N., and Grelon, M. (2015). The molecular biology of meiosis in plants. *Annu. Rev. Plant Biol.* 66, 297–327. doi: 10.1146/annurev-arplant-050213-035923

Mieulet, D., Aubert, G., Bres, C., Klein, A., Droc, G., Vieille, E., et al. (2018). Unleashing meiotic crossovers in crops. *Nat. Plants* 4, 1010–1016. doi: 10.1038/s41477-018-0311-x

Ming, R., Hou, S., Feng, Y., Yu, Q., Dionne-Laporte, A., Saw, J. H., et al. (2008). The draft genome of the transgenic tropical fruit tree papaya (Carica papaya Linnaeus). *Nature* 452, 991–997. doi: 10.1038/nature06856

Muiruri, K. S., Britt, A., Amugune, N. O., Nguu, E. K., Chan, S., and Tripathi, L. (2017). Expressed centromere specific Histone 3 (CENH3) variants in cultivated triploid and wild diploid bananas (Musa spp.). *Front. Plant Sci.* 8:1034. doi: 10.3389/fpls.2017.01034

Myrick, S., Norton, G. W., Selvaraj, K. N., Natarajan, K., and Muniappan, R. (2014). Economic impact of classical biological control of papaya mealybug in India. *Crop Prot.* 56, 82–86. doi: 10.1016/j.cropro.2013.10.023

Nassar, H. N., Nassar, N. M. A., Vieira, C., and Saraiva, L. S. (1995). Cytogenetic behaviour of the interspecific hybrid of *Manihot neusana* Nassar and cassava, *M. esculenta* Crantz, and its backcross progeny. *Can. J. Plant Sci.* 75, 675–678. doi: 10.4141/cjps95-113

Nassar, N., and Ortiz, R. (2010). Breeding cassava to feed the poor. *Sci. Am.* 5, 78–84. doi: 10.1038/scientificamerican0510-78

Nassar, N. M. A., Santos, E., Dos, and David, S. R. O. (2000). The transference of apomixis genes from *Manihot neusana* Nassar to cassava, *M. esculenta* Crantz. *Hereditas* 132, 167–170. doi: 10.1111/j.1601-5223.2000.00167.x

Odipio, J., Alicai, T., Ingelbrecht, I., Nusinow, D., Bart, R., and Taylor, N. J. (2017). Efficient CRISPR/Cas9 genome editing of phytoene desaturase in cassava. *Front. Plant Sci.* 8:1780. doi: 10.3389/fpls.2017.01780

Paprotka, T., Boiteux, L. S., Fonseca, M. E. N., Resende, R. O., Jeske, H., Faria, J. C., et al. (2010). Genomic diversity of sweet potato geminiviruses in a Brazilian germplasm bank. *Virus Res.* 149, 224–233. doi: 10.1016/j.virusres.2010.02.003

Phalan, B., Green, R. E., Dicks, L. V., Dotta, G., Feniuk, C., Lamb, A., et al. (2016). How can higher-yield farming help to spare nature? *Science* 351, 450–451. doi: 10.1126/science.aad0055

Ramu, P., Esuma, W., Kawuki, R., Rabbi, I. Y., Egesi, C., Bredeson, J. V., et al. (2017). Cassava haplotype map highlights fixation of deleterious mutations during clonal propagation. *Nat. Genet.* 49, 959–963. doi: 10.1038/ng.3845

Ravi, M., and Chan, S. W. L. (2010). Haploid plants produced by centromere-mediated genome elimination. *Nature* 464, 615–618. doi: 10.1038/nature08842

Ray, D. K., Mueller, N. D., West, P. C., and Foley, J. A. (2013). Yield trends are insufficient to double global crop production by 2050. *PLoS One* 8:e66428. doi: 10.1371/journal.pone.0066428

Rey, M.-D., Martín, A. C., Smedley, M., Hayta, S., Harwood, W., Shaw, P., et al. (2018). Magnesium increases homoeologous crossover frequency during meiosis in ZIP4 (Ph1 gene) mutant wheat-wild relative hybrids. *Front. Plant Sci.* 9:509. doi: 10.3389/fpls.2018.00509

Sanei, M., Pickering, R., Kumke, K., Nasuda, S., and Houben, A. (2011). Loss of centromeric histone H3 (CENH3) from centromeres precedes uniparental chromosome elimination in interspecific barley hybrids. *Proc. Natl. Acad. Sci. U.S.A.* 108, E498–E505. doi: 10.1073/pnas.1103190108

Serra, H., Lambing, C., Griffin, C. H., Topp, S. D., Seguela-Arnaud, M., Fernandes, J., et al. (2018). Massive crossover elevation via combination of HEI10 and recq4a recq4b during *Arabidopsis* meiosis. *Proc. Natl. Acad. Sci. U.S.A.* 115, 2437–2442. doi: 10.1073/pnas.1713071115

Siar, S. V., Beligan, G. A., Sajise, A. J. C., Villegas, V. N., and Drew, R. A. (2011). Papaya ringspot virus resistance in *Carica papaya* via introgression from *Vasconcellea quercifolia*. *Euphytica* 181, 159–168. doi: 10.1007/s10681-011-0388-z

Tripathi, L., Tripathi, J. N., Roderick, H., and Atkinson, H. J. (2013). Engineering nematode resistant plantains for sub-Saharan Africa. *Acta Hortic.* 974, 99–107. doi: 10.17660/ActaHortic.2013.974.11

VanBuren, R., Zeng, F., Chen, C., Zhang, J., Wai, C. M., Han, J., et al. (2015). Origin and domestication of papaya Yh chromosome. *Genome Res.* 25, 524–533. doi: 10.1101/gr.183905.114

Varshney, R. K., Ribaut, J. M., Buckler, E. S., Tuberosa, R., Rafalski, J. A., and Langridge, P. (2012). Can genomics boost productivity of orphan crops? *Nat. Biotechnol.* 30, 1172–1176. doi: 10.1038/nbt.2440

Wang, W., Feng, B., Xiao, J., Xia, Z., Zhou, X., Li, P., et al. (2014). Cassava genome from a wild ancestor to cultivated varieties. *Nat. Commun.* 5:5110. doi: 10.1038/ncomms6110

Wang, Y., and Copenhaver, G. P. (2018). Meiotic recombination: mixing it up in plants. *Annu. Rev. Plant Biol.* 69, 577–609. doi: 10.1146/annurev-arplant-042817-040431

Wang, Z., Fang, B., Chen, J., Zhang, X., Luo, Z., Huang, L., et al. (2010). De novo assembly and characterization of root transcriptome using Illumina paired-end sequencing and development of cSSR markers in sweetpotato (*Ipomoea batatas*). *BMC Genomics* 11:726. doi: 10.1186/1471-2164-11-726

Wheeler, T., and Von Braun, J. (2013). Climate change impacts on global food security. *Science* 341, 508–513. doi: 10.1126/science.1239402

Wickramasuriya, A. M., and Dunwell, J. M. (2018). Cacao biotechnology: current status and future prospects. *Plant Biotechnol. J.* 16, 4–17. doi: 10.1111/pbi.12848

Wright, K. M., Arnold, B., Xue, K., Surinova, M., O'Connell, J., and Bomblies, K. (2015). Selection on meiosis genes in diploid and tetraploid *Arabidopsis arenosa*. *Mol. Biol. Evol.* 32, 944–955. doi: 10.1093/molbev/msu398

Yant, L., Hollister, J. D., Wright, K. M., Arnold, B. J., Higgins, J. D., Franklin, F. C. H., et al. (2013). Meiotic adaptation to genome duplication in *Arabidopsis arenosa*. *Curr. Biol.* 23, 2151–2156. doi: 10.1016/j.cub.2013.08.059

Zhao, C., Liu, B., Piao, S., Wang, X., Lobell, D. B., Huang, Y., et al. (2017). Temperature increase reduces global yields of major crops in four independent estimates. *Proc. Natl. Acad. Sci. U.S.A.* 114, 9326–9331. doi: 10.1073/pnas.1701762114

Ziolkowski, P. A., Underwood, C. J., Lambing, C., Martinez-Garcia, M., Lawrence, E. J., Ziolkowska, L., et al. (2017). Natural variation and dosage of the HEI10 meiotic E3 ligase control *Arabidopsis* crossover recombination. *Genes Dev.* 31, 306–317. doi: 10.1101/gad.295501.116

Conflict of Interest Statement: The authors declare that the research was conducted in the absence of any commercial or financial relationships that could be construed as a potential conflict of interest.

Advantages of publishing in Frontiers

OPEN ACCESS
Articles are free to read for greatest visibility and readership

FAST PUBLICATION
Around 90 days from submission to decision

HIGH QUALITY PEER-REVIEW
Rigorous, collaborative, and constructive peer-review

TRANSPARENT PEER-REVIEW
Editors and reviewers acknowledged by name on published articles

Frontiers
Avenue du Tribunal-Fédéral 34
1005 Lausanne | Switzerland

Visit us: www.frontiersin.org
Contact us: info@frontiersin.org | +41 21 510 17 00

REPRODUCIBILITY OF RESEARCH
Support open data and methods to enhance research reproducibility

DIGITAL PUBLISHING
Articles designed for optimal readership across devices

FOLLOW US
@frontiersin

IMPACT METRICS
Advanced article metrics track visibility across digital media

EXTENSIVE PROMOTION
Marketing and promotion of impactful research

LOOP RESEARCH NETWORK
Our network increases your article's readership